

مقترح بناء نظام اداري لاختيار اسلوب التعاقد المناسب لاسلوب المقاول العام في قطاع التشييد

د. المهندس حاتم خليفة بريسم العجيلي
مدرس / جامعة بغداد

المستخلص

إن أكثر المشاكل التي تواجهنا هي إشاعة الأساليب القديمة والتعود عليها ، وقد كان الأسلوب التقليدي (المقاول العام) وعقد جدول الكميات الذي يعمل على وفق الشروط العامة لمقاولات اعمال الهندسة المدنية المعتمدة من وزارة التخطيط في العراق ومؤسسة الفيديك هما الأكثر شيوعا واستيعابا لدى الجهات الفنية والإدارية بمختلف مستوياتها ومواقعها ، ولذا أصبح من الضروري البحث عن قواعد تعاقدية معينة يمكن استخدامها كبديل مفضل لجميع الحالات والظروف بعد استخلاص الدروس والعبر من تجارب القطر في حملات الأعمار .

يهدف البحث إلى تحليل موضوع عنصر الزمن والكلفة وتطوير قواعد اختيار اسلوب التعاقد المناسب مع اسلوب التنفيذ التقليدي ومراعاة تأثير كل العوامل المؤثرة على زيادة الكلفة والوقت خلال التنفيذ .

لقد جرى اتباع منهجية علمية في الجانبين النظري والميداني من البحث . تضمن البحث اجراء التحليلات الاحصائية التفصيلية عن طريق اجراء الاستبيان الميداني لغرض تقويم العوامل المؤثرة بصورة مباشرة أو غير مباشرة على اسلوب التعاقد .

في الختام فقد تضمن البحث مجموعة الاستنتاجات والتوصيات التي تم التوصل إليها لغرض تطوير نظام اداري لقواعد اختيار اسلوب التعاقد المناسب .

ABSTRACT

Among the most important problems which faced us is the wide use of old approach , particularly the traditional approach (general contractor) and the bill of quantity contract which works according to the general conditions of civil engineering works contracts sponsored by FIDIC and ministry of planning , so It became necessary to look for certain contract rules to be used as a substitute suited all conditions and cases after concluding lessons from the local experiments in rebuilding issues .

This research aims at analyzing the subject of time and cost factor taking in consideration the effect all the effective factors which leads to increase the cost and time .

A scientific methodology was followed in both theoretical and practical phases of the study . The study concentrated on a detailed statistical analysis of the study was incorporated using questionnaire and interview method to evaluate the effective factors directly or indirectly on contract method

At the end certain conclusions and recommendations were drawn as developing managerial system for selecting satisfy contract method

- مقدمة

ما كان لاختيار اسلوب التعاقد تأثيرا كبيرا على اسلوب التنفيذ في قطاع التشييد من خلال مجموعة كبيرة من المحددات والمتغيرات والعوامل المؤثرة المباشرة وغير المباشرة . لذلك كان الهدف لدى كثير من الباحثين اختيار اسلوب التعاقد الذي يتناسب واسلوب التنفيذ الذي تم اختياره . يهدف البحث الى بناء نظام اداري علمي وكفوء لاختيار اسلوب تعاقدى كفوء يتناسب مع محددات اسلوب المقاول العام التقليدي في التنفيذ ويمكنه من تجاوز المتغيرات واحتضان الخصوصيات والتعامل معها بصيغة ايجابية.

- اساليب التنفيذ :

يقصد باسلوب التنفيذ اسلوب التمويل والتعاقد وكل مايتعلق بعملية التشييد من اختيار المخططس والمصممين والمشرفين والاستشاريين والمقاولين (السنجقلى، 1984) وهو الطريقة التي تنفذ بها المشاريع سواء كان ذلك عن طريق عقد المقاولة والتعاقد مع اطراف خارجية كاسلوب المقاول العام واسلوب الادارة الانشائية او عن طريق اطراف داخلية بدون تعاقدات كالنفيذ المباشر والتنفيذ امانة. يؤثر اسلوب تنفيذ المشروع بصورة مباشرة على كلفة المشروع، ولذلك يتم دراسة العوامل المؤثرة في اختيار اسلوب التنفيذ ومنها طبيعة المشروع وموقعه وحجمه وشكل وعدد الابنية المكونة له وحجم الاعمال المراد احوالها والمحددات في موقع العمل وعلاقة المشروع بالابنية المجاورة ودرجة التعقيد في التصاميم الهندسية ومدى توفر الكفاءات الهندسية والفنية لدى صاحب العمل وتوفر الخبرة والكفاءة لدى الجهة المنفذة ومدى توفر الموارد المطلوبة لتنفيذ العمل وكفاية المساحات المتوفرة لتخزين المواد ومدى توفر وثائق العقد وجداول الكميات لدى عملية الاختيار . كما وتختلف اساليب التنفيذ باختلاف صاحب العمل وظروفه وظروف العمل وحجمه (العاني، 1995).

* اسلوب المقاول العام : General Contractor

ويسمى الطريقة التقليدية او مدخل التصميم والتنفيذ المتعاقبين ، وفيه تتعاقب مراحل المشروع (القرار والتصميم والتنفيذ والاستعمال) دون أن يكون لصاحب العمل أي سلطة فعلية غير دفع الأجور للعاملين في المراحل المختلفة (Hendrickson, 1989). يقوم صاحب العمل باختيار فريق التصميم من داخل تنظيمه او يتعاقد مع جهة تصميمية منفصلة تكون مسؤولة عن تحديد حاجات صاحب العمل وعن جميع الأعمال التصميمية والاستشارية الخاصة بالمشروع واعداد العقد الرئيس بين صاحب العمل والمقاول ليدخل المقاول العام الى المشروع باشراف الاستشاري / المعماري . تتمثل الصورة النموذجية للاسلوب من خلال الكمال البرنامج قبل بداية التصميم واكمال التصميم قبل تسعير المشروع وتحديد الاسعار قبل بداية الانشاء . يتميز اسلوب المقاول العام باحالة المشروع في عقد واحد مباشر بين صاحب العمل ومقاول عام له الحق في الاتفاق مع عدد من المقاولين المختصين كمقاولين ثانويين من الباطن والذين لايملكون أي علاقة مباشرة مع

صاحب العمل (غولدهابر، 1982) بالإضافة إلى امتلاكه حق الأحالة إلى السعر الأوطأ مع الأخذ بنظر الاعتبار النوعية، والسيطرة على كل خطوات العملية الإنشائية التي تحدث بتعاقب من خلال القدرة على المراجعة، والسيطرة على الكلفة التي أسسها المقاول بناء على مجموعة كاملة من وثائق العطاء. أما سلبات استخدام هذا الأسلوب فتتجلى في تتابع مراحل الإنشاء حيث لا يمكن إكمال مرحلة ما قبل الانتهاء من المرحلة السابقة مما يؤدي إلى تأخير العمليات. بالإضافة إلى عدم امتلاك صاحب العمل سلطة فعلية على المشروع.

* أسلوب الإدارة الإنشائية :

موافقة صاحب العمل على صيغة خدمات وأعمال بنسبة مئوية أو اجور ثابتة مع تاهيل عام (Barrie, 1981) ويسمى أسلوب التصميم والتنفيذ المتوازي ويسمح ببدء التنفيذ قبل اتمام التصميم النهائي وباستعمال المرافق التي تنتهي باكراً قبل اتمام المشروع (غولدهابر، 1982). ويعتمد أسلوب الإدارة الإنشائية على نظرية الإدارة الإنشائية التي ترى المشروع نظام إنشاء واحد وذو مراحل مختلفة ومتكاملة، وتعرف الإدارة الإنشائية بأنها طريقة إدارة الإنشاء التي تتيح لصاحب العمل امتلاك خدمات مقاول عام يقوم بإدارة الأعمال المحددة في المشروع ضمن مراحله الثلاث وحتى التشغيل أحياناً مع فريق من الحرفيين الخاصين لكل عمل أو لكل جزء منه وتشكيل فريق ثلاثي يتألف من صاحب العمل والمعماري ومدير الإنشاء يعمل معاً من بداية التفكير بالمشروع إلى انجازه. يتم اختيار المقاول عن طريق التفاوض أو التنافس بناء على أمانته وخبرته وسداد رأيه في تنفيذ المشاريع وعلى أساس مهني يعتمد تقنية المهارة وقابلية الإدارة (الجار الله، 1984). إن هذا الأسلوب يسمح لصاحب العمل بتأخير شراء مواد لاحاجة لاستعمالها إلا عند نهاية التنفيذ مما قد يساعد في إيجاد بدائل أقل سعراً. كما أنه يسمح بإمكانية إعادة النظر في التصميم البديلة وحصول تنافس بين المقاولين وتبادل الآراء المؤثرة ويعطي مرونة كبيرة لأي شيء غير متوقع ويمكن من ضبط الكلفة والسيطرة على المصاريف ويقلل الكلف العالية للإضافات (Ahuja, 1976).

أما مساوئ هذا الأسلوب فتتجلى في صعوبة اختيار الأشخاص الملائمين للعمل، وعدم استحقاق صاحب العمل لفكرة وضع جميع الأمور بيد شخص غيره، وابتعاد بعض الإنشائيين إلى النور التقليدي المطروح، مع صعوبة التنبؤ بالكلفة النهائية (Ahuja, 1976) وينقل هذا الأسلوب الخطر إلى صاحب العمل. ويهدف أسلوب الإدارة الإنشائية إلى السيطرة على الوقت والكلفة في الإنشاء بوسيلة جديدة، ويكون مدخلاً لأسلوب التنفيذ المتسارع عند تجزئة التصميم والإنشاء على شكل مراحل ومجاميع وأجزاء.

* أسلوب التنفيذ المباشر :

هي طريقة بديلة للتنفيذ عن طريق عقد، وتعني قيام صاحب العمل أو أي جهة معينة باستخدام موارده البشرية وممتلكاته ومعداته (أو تأجيرها) لتنفيذ كافة الأعمال اللازمة لانتهاء المشروع وتسليمه إلى الجهة

المستفيدة بدون وسيط او وجود عقد . يتميز اسلوب التنفيذ المباشر بمنح صاحب العمل المرونة . ويعتبر افضل الاساليب واكثرها فعالية في نقل وتطوير التقنيات الحديثة ، وهو الخطوة لصاحب العمل نحو التدخل الكامل في المشروع وتحمل المخاطر حيث يؤدي موظفوه وظائف الإدارة والإشراف والمراقبة والتنفيذ ويقوم بدفع جميع الكلف والمصاريف الحقيقية . ويعتبر انعدام التنافس احد سلبيات هذا الاسلوب بالاضافة الى صعوبة التأكد من مثالية كلفة العمل المنفذ مما يجعل من الصعب التأكد من افضلية استخدامه .

ان الحاجة الملحة لتسريع التنفيذ ، واحجام المقاولين عن تقديم عطاءاتهم بسبب الخطورة التي يتصورونها ، ومحاولة تقليص الكلفة نتيجة حذف الارباح والمبالغ الاضافية التي يضيفها المقاولون ، والحاجة الى تطوير قدرة الفنيين والاداريين في القطاع العام هي اهم الاسباب التي تدعو الى تبني هذا الاسلوب . (العاني، 1995)

* أسلوب التنفيذ أمانة :

وفيه تعهد مسؤولية القيام بتنفيذ الأعمال أمانة إلى لجنة خاصة تقوم بتنفيذ فقرات الأعمال من شراء المواد وتوفير الأيدي العاملة والمعدات المطلوبة على أساس حاجة العمل ، أي إن كلفة التنفيذ هي بالواقع الكلف المباشرة عن مصاريف موارد المشروع الواردة اعلاه بدون أرباح أو مصاريف إدارية . ان اعضاء اللجنة يقومون بالإشراف على سير العمل ماليا وفنيا واداريا ومراقبة العمال وشراء المواد اللازمة مع امكانية الاستعانة بالمقاولين الثانويين . يتطلب هذا الاسلوب توفير فريق عمل فني لديه الخبرة في تبني عملية التنفيذ . كما إنه يحتاج إلى متابعة ودقة في مراقبة اللجنة الخاصة بالتنفيذ والتي توفر نزاهة وأمانة عالية في أفرادها ، (العاني، 1995) ويتحمل صاحب العمل في هذه الصيغة المخاطرة كاملة .

- اساليب التعاقد :

يمكن تقسيم اساليب التعاقد حسب اسلوب الاتفاق على الاسعار الى :

* العقود التنافسية (Competitive Contract)

وتسمى عقود الاسعار الثابتة وتمتاز بامكانية اختيار اوطأ عطاء بسبب الطبيعة التنافسية للعقود والمعاملة العادلة لكل المتنافسين وانعدام المحاباة والامتيازات والضغطات (Haplin, 1998) وتشمل :

* عقد المبلغ الاجمالي : (Lump - Sum Contract)

هو الموافقة على انجاز عمل محدد بمبلغ ثابت قطعي من دون اي زيادة في الكلفة (Barrie, 1981) ، وفيه يوافق المقاول على إنجاز ذلك العمل المحدد بكلفة ثابتة من دون زيادة بغض النظر عن الكلفة الحقيقية للعمل مع تحمل صاحب العمل لمسؤوليته عن التغييرات المفروضة من قبله (Kavanagh, 1978) . ويشترط فيه توفر المخططات والمواصفات مع جميع المعلومات الكافية عن موقع العمل . ويمتاز هذا العقد بضمان المقاول لصاحب العمل اتمام العمل الانشائي بالمدة والنوعية المطلوبتين فتعهد المقاول واجب لاعلاقة له بالصعوبات التي يمكن مواجهتها مع اعطائه كفاءة عالية في التشييد من حيث الكلفة والوقت الاقل بسبب

التنافس الشديد وتحديد الكلفة لصاحب العمل. وتتحصر مساوئ هذه الصيغة في زيادة جدولة المشروع الكلية من خلال فصل تعاقدات التصميم عن التشييد، وتقسيم المسؤولية بين المصمم والمنفذ، ومحدودية المرونة في معالجة اي تغيير للمخططات الاصلية مع تعارض الرغبات للطرفين (Ahuja, 1976) يتم تسديد مستحقات المقاول على شكل دفعات مبرمجة مبنية على تخمين نسبة انجاز العمل. تستخدم هذه الصيغة في الاعمال الصغيرة والمباني المختلفة عندما تكون الوحدات المكونة للمشروع قياسية في طبيعتها وكثيرة في عددها ومختلفة في انواعها ولا يفضل استعمالها في الاعمال غير المحددة والاعمال الترابية والمشاريع الحاوية على فقرات بدائل كثيرة اثناء التنفيذ (Seeley, 1984)

* عقد مقاولات وحدة الاسعار (Unit – Price Contract)

الاتفاق على سعر ثابت لوحدة الكمية المراد تنفيذها وغير المعلومة كميتها بدقة خلال زمن محدد وموقع معين، ويشترط وجود مواصفات متكاملة وتفصيلية تبين طبيعة العمل بدون الحاجة لتحديد كميات الاعمال المتوقعة بدقة وبما يكفي لتخمين حجم العمل واهميته وسعر الفقرة. ويمتاز بالمرونة الممنوحة لصاحب العمل في كميات الاعمال وامكانية المباشرة بها دون معرفة كمياتها الدقيقة (Ahuja, 1976)

تتحصر مساوئ هذه الصيغة في امكانية زيادة الكلفة النهائية عن المبلغ المقرر بشكل كبير مما يحرج صاحب العمل، وامكانية ظهور خلافات بين اطراف التعاقد في تصنيف الفقرات وميل بعض المقاولين لعدم الموازنة في مناقضاتهم لاسباب عدة منها محاولة الحصول على مبالغ كبيرة بشكل مبكر ومن اجل الحصول على كميات اخرى خارج العقد وغيرها (Hendrickson, 1989). يستعمل هذا العقد عند توارد كميات كبيرة من الفقرات الانشائية مع عدد قليل من انواع تلك الفقرات، وعند عدم تحديد حجم العمل قبل توقيع العقد، وفي اعمال الترابيات والاسس والطرق واعمال الصيانة والاعمال التي يتعذر دراستها قبل التعاقد

* عقد مقاولات جدول الكميات والاسعار Bill of Quantities and Rates Contract

هو الاتفاق على تنفيذ العمل بموجب جدول كميات مخمنة بدقة تبين حجم العمل المتوقع ومسعرة بموجب مفردات الفقرات ووحدات التسعير ومعرفة للمواصفات ومقاييس العمل ويرمز له BOQ (Ahuja, 1976) وعليه يتطلب توفير المخططات والمواصفات. وتظهر محاسنه في امكانية معرفة كلفة العمل بوضوح، وتقليل احتمالية الاحتكاك بين الاطراف في حالة التعديل والتحوير. تتحصر مساوئه في وجوب توسيع الاشراف الحقلية لصاحب العمل لقياس الكميات المنفذة وتظهر تطبيقاته في مقاولات المباني ومشاريع الطرق

*** عقد الهدف : Target Contract**

موافقة المقاول على تحديد نسبة مئوية من كلفة العمل المخمّنة لدى صاحب العمل كهدف والحاصل عليها من خلال جدول الكميات المخمن كمية وسعرا . تحدد الاجور او الكلفة التي ستدفع للمقاول على شكل نسبة مئوية اكبر او اقل من الكلفة المخمّنة للمقاول والتخمين لهدف صاحب العمل (Twort,1995) (Haplin,1998)

*** عقد ضمان الحد الاعلى للكلفة (G M P) Guaranteed Maximum Price**

هو الاتفاق على اكمال الاعمال مقابل كلفة محددة بحيث لا تزيد الكلفة عن الحد الاعلى المتفق عليه فاذا زادت الكلفة على الاتفاق يتحمل المقاول ذلك الفرق في الكلفة، اما اذا كانت الكلفة اقل من الحد الاعلى فان هناك فقرة في التعاقد تعالج ذلك وتقسم الفروقات بين الطرفين (الجار الله، 1984).

*** العقود التفاوضية**

تسمى عقود الكلفة زائدا او عقود تعويضات الكلفة وتعني الموافقة على انجاز عمل محدد وتعويض المقاول عنها لقاء عمله على وفق قواعد الكلفة الحقيقية زائدا نسبة مئوية او مبلغ ثابت او اية صيغة اخرى (Barrie, 1981). ويعد من التعاقدات ذات الاسعار غير الثابتة وهو لا يعتمد على التنافس في احالة الاعمال وانما تكون الحالة نتيجة للمناقصة المفتوحة بين المقاولين المؤهلين المنتخبين من صاحب العمل تبنى التعاقدات التفاوضية على اساس تحمل صاحب العمل للكلفة الحقيقية للاعمال المطلوبة في وثائق التعهد مضافا اليها اجور الخدمات والتسهيلات والتقنيات والخبرات مع اجور الادارة المتضمنة النثريرات وكلفة الاشراف والارباح . يحصل المقاول في هذه العقود على تعويضات هي بطبيعتها اجور مهنية اكثر من كونها ارباح مكتسبة من التنفيذ وتكون كلفة التنفيذ على وفق هذه الصيغة غير مثالية. (Ahuja,1976)

يقدم هذا الاسلوب مزايا عديدة منها القدرة على استقدام المقاول في مرحلة مبكرة من العمل واستطاعة المباشرة السريعة في العمل، مع منح صاحب العمل المرونة في احداث تغييرات في المخططات والمواصفات . وتسهل في مشاريع التطوير والمشاريع التي لا يرغب بكشفها للعيان والمشاريع التي تحتاج لجدولة حرجية في الوقت، والمشاريع التي لا يمكن تحديد حجم اعمالها بالضبط وفي المشاريع السريعة وذات الاستراتيجية العالية. ويسجل عليه امكانية زيادة استفادة المقاول من خلال زيادة كلفة العمل وتبذير المواد والاستغلال الردي للعمالة. يعتبر أسلوب تعويض المقاول المصدر الاساس لاختلاف انواع العقود التفاوضية ومنها عقد كلفة زائدا نسبة مئوية من الكلفة وعقد كلفة زائدا اجور ثابتة الذي يظهر باشكال عديدة منها مع بند مشاركة في الارباح ، ومنها مع بند مكافأة ومنها مع ضمان سقف سعري ، واخيرا عقد كلفة زائدا مبالغ متغيرة بأسلوب منزلق (Seeley, 1984)

* عقود مقاولات ذات صيغة خاصة :

ويمكن الوصول اليها عن طريق التفاوض او التنافس او بهما معا ومنها :

* عقد تسليم المفتاح (Turnkey Contract)

هو من مقاولات الجملة وفيه اتفاق صاحب العمل والمقاول على القيام بتنفيذ المنشأ او التصميم والتنفيذ معا وبمبلغ اجمالي محدد لايلزم صاحب العمل بآية مبالغ اضافية عداه نظيرا للتعديلات التي تطرأ على الاعمال ما لم ينتج تغير جذري في التصميم الاصيل بموجب طلب صاحب العمل. ويتطلب هذا العقد توفير المخطط الاولي والمواصفات الفنية ونوع الاداء المطلوب والمخرجات قبل التعاقد ، ويمتاز بتداخل مراحل التصميم والتنفيذ. اما مساوئ هذا العقد فتتمثل في امكانية رفع المقاول للكلفة مع تطلب اكثر صاحب العمل من تدقيق التصميم مما يؤدي الى زيادة اجور فريقه التقني (Ahuja,1976) ويستخدم في انشاء المشاريع الصناعية . اما عقد التصميم والانشاء (Design - Build Contracts) فهو شكل اخر يشابه عقد تسليم المفتاح وفيه يقوم المقاول بمهمتي التصميم والتنفيذ معا لقاء مبلغ مقطوع اجمالي او بناء على جدول كميات مسعر او آية صيغة اخرى . ويتطلب وجود جهاز تصميم جيد لدى المقاول ويعدده البعض احد صيغ عقد تسليم المفتاح وهو لايلائم المشاريع التي تؤسس على اساس فني ومعماري (Haplin, 1998) اي المشاريع ذات الصفة المعمارية مثل النصب والمتاحف

* عقد الاتحاد (Joint Venture Contract)

هو تجمع جهود الشركات المكونة للاتحاد في الامكانيات المالية والادارية والفنية والتقنية لتنفيذ المشروع ويختلف اتحادالشركات عن الشركات الاخرى في انه ينشأ من اجل تنفيذ مشروع واحد وعقد واحد وليس له صفة الاستمرارية ويتم هذا على وفق اتفاقية توقعها الشركات المكونة للاتحاد لتوضيح طريقة التمويل والادارة للمشروع (Ahuja,1976). ويستخدم في المشاريع الكبيرة المنفذة على وفق اسلوب المقاول العام وفي مشاريع السدود وهو شائع التطبيق في الصناعة الانشائية .

* عقد ادارة الانشاء (Construction Management Contract)

هو اسلوب تعاقد لاستخدام رئيس محدد يقوم بادارة الاعمال المحددة في المشروع ضمن مراحلها المختلفة ويتم اختيار المقاول عن طريق التفاوض او التنافس بناءا على خبرته وامانته وتنفيذه لمشاريع مشابهة وعلى اساس مهني يعتمد على تقنية المهارة وقابلية الادارة (Ahuja,1976). ان وظيفة مدير الانشاء تقديم المساعدة لصاحب العمل على اتخاذ القرارات وفقا للوقت والميزانية المحددتين وتحقيق النفع الاقتصادي المطلوب

- العوامل المؤثرة في تحديد نوعية العقد :

يتأثر شكل العقد الهندسي ونوعيته بشكل مباشر أو غير مباشر بعدة عوامل منها نوع المشروع وأهميته و حجم العمل الإنشائي وطبيعته و طول عمر العقد والتحري عن تحقيق مدة إنجاز معينة ، ومدى توفر نطاق المشروع والتصاميم والمواصفات ووثائق المفاولة الأخرى ، ودرجة استيعاب المقاولين المحليين لأنواع التعاقد ، والتحري عن تحقيق نوعية معينة او كلفة معينة ، ووجود جوانب أمنية ، وتحقيق أهداف سياسية أو استراتيجية ، و محدودية البدائل أو فقدانها ، وعدم استقرار السوق ومستوى التنافس المطلوب من عدمه ، وطريقة تمويل المشروع ومدى توفر السيولة النقدية وأسلوب الدفع للمقاول ، ومدى توفر الموارد المطلوبة من المكنائن والمعدات والأيدي العاملة الماهرة والغير ماهرة الدائمة منها والمؤقتة والمواد الأولية والتكميلية لتنفيذ العمل ، والحاجة إلى إنجاز واشغال أجزاء من العمل وتحقيق درجة البرمجة المطلوبة للتنفيذ ، والرغبة في البدء المبكر بالتنفيذ ، ومدى تفضيل صاحب العمل أو استشاريه لنوع وصيغة عقد معينة ، ومدى رغبة صاحب العمل في معرفة الكلفة الكلية للمشروع قبل العقد ، ومقدار الوقت المسموح به لتجهيز العطاء للمناقصة ، والصعوبة في تخمين كلف المشروع، ومدى استقرارية متطلبات صاحب العمل ومقدار المجازفة التي يوافق أن يتحملها ، ودرجة تعقيد التصاميم وصعوبة تنفيذها ، ومدى رغبة صاحب العمل في المشاركة في إدارة العقد ، ودرجة وضوح متطلبات صاحب العمل وإمكانية تطبيقها ، حجم المعلومات المعطاة إلى المناقصين ، وظروف الموقع العامة والخاصة ومدى التقيد في فضاء العمل وتأثير العوامل البيئية مثل الطقس والحرارة والرطوبة وطبيعة التربة، ووضوح العلاقة بين أطراف المشروع وتحديد الوظائف والمسؤوليات

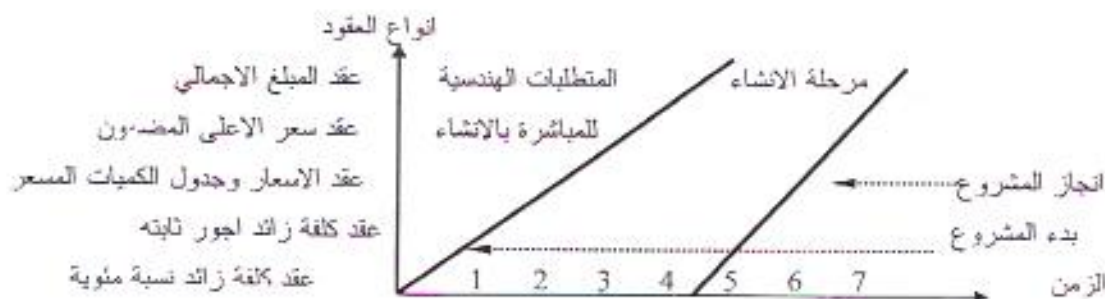
- استراتيجية اختيار نوع العقد المناسب للتنفيذ :

إن إصدار أي قرار بشأن اختيار العقد الملائم يعتمد على الفهم الكامل للاختلافات المبدئية بين أنواع العقود والتحليل المناسب للعوامل المؤثرة المشار إليها في الفقرة (4) اعلاه مع بيان الصفات المميزة للمشروع التي تؤثر على اختيار العقد الأفضل ، ويؤسس قرار الاختيار على نوع مستلزمات التشييد والكفاءة الشخصية للأطراف والشروط القانونية للتعاقد ، وتعتبر عملية اختيار نوع العقد من اختصاص صاحب العمل ، إلا أن الاستشاري يساعده في تقديم النصح لاختيار أكثر الأنواع ملائمة للمشروع واعداد صيغة العقد وشروطه وجداوله ومواصفاته ورسوماته بما يتماشى مع نوع العقد .

تساعد الخبرة في جعل عملية الاختيار لاحد انواع التعاقدات التي يجب ان تجري قبل اعداد وثائق العطاء عملية واضحة ، وبالإضافة الى الخبرة فمن الضروري مقارنة مميزات الانواع المختلفة قبل الاختيار لتقرير شكل العقد الذي سيتم استعماله . فقد يطلب صاحب العمل احيانا معرفة الاسباب التي حددت الاستشاري في اختيار وتفضيل نوعية معينة من العقود على البدائل الأخرى على الرغم من وضوحها بالنسبة للاستشاري. ويتأثر اختيار نوع العقد عادة بتفضيل صاحب العمل أو مستشاريه للنوع الذي يلمون به (Marks,1985) .

يتأثر قرار اختيار الصيغة التعاقدية المناسبة على عدة عوامل تم إيضاحها في الفقرة (4) أعلاه. يمكن أن تعتمد استراتيجية اختيار العقد على نسبة انجاز التصميم في وقت الاختيار والعرض (Thompson, 1981). فتؤسس العروض على عقد الاسعار الثابتة لمعرفة كلف الانشاء الكلية، من خلال اعتماد عقد المبلغ الاجمالي في حالة توفر المخططات والمواصفات بصورة متكاملة مع عدم وجود اعمال اضافية. اما في حالة وجود اعمال اضافية واستخدام للبدائل فيمكن تحقيق ذلك تحت عقد سعر الوحدة او عقد جدول الكميات المسعر اذا كان التخمين المنجز للكميات دقيق. ان التأكيد على كلف المشروع مهم جدا الى صاحب العمل الذي يعمل تحت ميزانية محددة كالقطاع العام الذي يطلب استخدام العقود التنافسية، بالإضافة الى وجوب توفر وقت كافي لاعداد المخططات والمواصفات الفنية وامكانية إجراء تخمينات دقيقة. يتم اختيار العقود التنافسية في حالة ضرورة التنافس للحصول على لوطا عطاء وعند المطالبة بالسيطرة الفعلية على الكلفة وعلى نوعية ومواصفات المقاول. في نفس الوقت يتم اللجوء الى العقود التفاوضية عند وجود رغبة او حاجة لدى صاحب العمل للبدء مبكرا بالتنفيذ قبل الانتهاء من المخططات والوثائق المطلوبة وللتنخلص من الوقت الممنوح لفعاليات اعداد العروض وعند تطلب الإنجاز المبكر للمقاول ولكن ظهور حالة عدم معرفة الكلفة الكلية للانشاء لدى صاحب العمل قبل بدء المشروع يعرضه لمجازفة أكثر من العقود التنافسية مما يدفع باتجاه انواع محددة من عقود الكلفة زائدا التي تحاول تعريف صاحب العمل بحد اعلى للكلفة.

يمثل الشكل (1) العلاقة بين برمجة مدة الانشاء وانواع التعاقدات حيث يمثل المحور الافقي مدة المشروع ويمثل المحور العمودي نوع التعاقد فنلاحظ ان عقد كلفة زائدا نسبة مئوية يبدأ مع بداية مدة المشروع بينما يحتاج عقد المبلغ الاجمالي الى فترة طويلة قبل المباشرة بالمشروع، كما تمثل المساحة المحصورة بين خطي بدء المشروع وانجاز المشروع مرحلة الانشاء التي تزداد في عقد الكلفة زائدا وتنقص في عقد المبلغ الاجمالي، ويمثل الشكل (2) مميزات الانواع المختلفة للتعاقدات الانشائية من حيث المرونة والمعلومات المطلوبة للسيطرة والمعلومات المطلوبة عند تقديم العطاء على المحور العمودي والمجازفة لصاحب العمل والحوافز ومتطلبات السيطرة وحجم سيطرة صاحب العمل على المحور الافقي.



الشكل (1) علاقة مدة تنفيذ المشروع مع انواع التعاقدات (Stone, 1984)



الشكل (2) مميزات الانواع المختلفة من التعاقدات الانشائية

- الاستبيان الميداني :

لغرض تقويم واقع اختيار الأساليب المعتمدة في التعاقدات لأعمال التشييد في العراق وتأثير العوامل المؤثرة في عملية الاختيار فقد تم القيام بمسح ميداني وانتخاب عينة بحث كنموذج مكونة من مجموعة من المهندسين ذوي الخبرة في مجالات عملهم المختلفة الإدارية والهندسية وكان حجم العينة الكلي (30) فردا اعتمادا على نظرية النزعة المركزية التي فحواها عند اخذ عينة بحجم (n) من مجتمع إحصائي يخضع لتوزيع وسطه (μ) وتباينه (σ^2) فان توزيع الوسط الحسابي للعينات (X) يخضع تقريبا لتوزيع طبيعي وسطه (μ) وتباينه (σ^2/n) شرط أن يكون حجم العينة كبيرا نسبيا ($n \geq 30$) } ويعني ذلك انه كلما زاد حجم العينة كلما كانت هنالك دقة عالية من نتائج العينة واقترب توزيع العينة من التوزيع الطبيعي، فإذا كان حجم العينة الكبير أو مساوي إلى (30) فان توزيعها يقترب من التوزيع الطبيعي (عمارة، 1989).

أن أعداد وتنظيم نموذج الاستمارة المعتمدة ضمن الدراسة الميدانية قد تم على مرحلتين هما مرحلة الاستبيان المفتوح ومرحلة الاستبيان المغلق . يمثل الاستبيان المفتوح مرحلة التهيئة والاستعداد للمباشرة في الاستبيان المغلق، ويهدف إلى توسيع قاعدة المناقشة والتحاور مع عينة مختارة بعناية من المهندسين المسؤولين عن إدارة وتنفيذ وتصميم العديد من المشاريع الإنشائية حول نموذج استمارة الاستبيان المطروحة وإمكانية تدعيمها بأسئلة إضافية ناجمة من خبرة المشمولين بالاستبيان المفتوح، وقد تم ذلك عن طريق المقابلات الشخصية. بعد ذلك يأتي دور الاستبيان المغلق، حيث تم توزيع 50 استمارة استبيان على أفراد العينة استلم منها (42) استمارة تم تدقيقها والتأكد من اكتمال الإجابات فيها وقد أهمل بعضها لعدم اكتمال الإجابة ليبقى العدد (38) استمارة وهو عدد مستوف لدقة الاستبيان . وقد كانت هنالك ثلاث محاور للاستبيان هي

1- محور المعلومات الشخصية والعامة ويضم معلومات وبيانات عن أفراد العينة تمثل جهة عملهم

والتحصيل العلمي وسنوات الخدمة والمنصب الوظيفي وكما ورد في الجدول (1)

جدول (1) المعلومات والبيانات الشخصية لأفراد العينة

ت	اسم الدائرة	التخصص العلمي		عدد سنوات الخدمة	الدور المالي في فريق الانشاء						استشاري
		الشهادة	التخصص		مدير دائرة	مدير مشروع	رئيس قسم	مهندس مقيم	مهندس تخطيط	مهندس موقع	
1	جامعة بغداد /	دكتوراة	مدني	34							*
2		ماجستير	ميكانيك	20	*						
3		ماجستير	مدني	35							*
4		ماجستير	مدني	30							*
5		بكالوريوس	مدني	18				*			
6	الشؤون الهندسية	بكالوريوس	مدني	38			*				*
7		بكالوريوس	معماري	29							
8		ماجستير	مدني	19							*
9		ماجستير	مدني	24			*				
10		ماجستير	مدني	23			*				
11	وزارة الاسكان المركز الوطني للاستشارات الهندسية	بكالوريوس	مدني	26							*
12		دبلوم عالي	مدني	20							*
13		بكالوريوس	معماري	29			*				
14		ماجستير	مدني	22							*
15		بكالوريوس	مدني	19							*
16	شركة المعتمد للمقاولات	ماجستير	مدني	25		*					
17		دبلوم عالي	مدني	33		*					
18		بكالوريوس	مدني	31					*		*
19		بكالوريوس	مدني	27					*		*
20	شركة الرشيد للمقاولات	بكالوريوس	مدني	26			*				
21		ماجستير	مدني	18		*					
22		بكالوريوس	مدني	21		*					
23	شركة رمضان	ماجستير	مدني	26		*					
24	شركة المنصور	بكالوريوس	مدني	28		*					
25	شركة انور	ماجستير	مدني	25		*					
26	هيئة التصنيع المتكاملة دائرة المشاريع	ماجستير	مدني	32	*						
27		ماجستير	مدني	23		*					
28		بكالوريوس	مدني	24						*	
29		ماجستير	مدني	32		*					
30		دكتوراة	مدني	26		*					
31		بكالوريوس	مدني	22		*					
32	شركة الفاو الهندسية	ماجستير	مدني	22		*					
33		ماجستير	مدني	22		*					
34		بكالوريوس	مدني	19		*					
35		بكالوريوس	معماري	22		*					
36		دكتوراة	مدني	30							*

37	ماجستير	مذني	31						*
38	ماجستير	مذني	34						*

- محور البيانات التوضيحية ويشمل محاور تهدف الى التعرف على واقع حال احالة الاعمال في العراق وحجم المشاكل الظاهرة وتوحيد تلك المعلومات على وفق أسس ومعايير موحدة متفق عليها
- محور البيانات الاستبائية ويتضمن جمع بيانات تؤدي في تحليلها إلى تقويم العوامل المؤثرة في تحديد نوعية العقد الهندسي المعتمد لتنفيذ العمل على وفق اسلوب المقاول الدائم المعتمد في اغلب المشاريع من خلال استخدام خمس درجات تقويمية في الإجابة ، يمثل الجدول (3) معيار موحد للمقارنة والقياس فيها ولتكون مدخلا لاقتراح نظام اداري لاختيار اسلوب التعاقد المناسب لاسلوب المقاول العام في قطاع التشييد في العراق

* عرض وجدولة نتائج الاستبيان :

تم عرض الإجابات الواردة في الاستبيان باستخدام اسلوب الجداول لعرض المعلومات بغية تحليلها وكمالي :

* التعاقدات الهندسية (واقع الحال) :-

عرض الاستبيان أساليب التعاقدات مستبينا حول الاسلوب الذي يفضل التعامل معه في قطاع التشييد فتبين أن أسلوب (وحدة الأسعار وجدول الكميات) هو الأكثر شيوعا ورغبة وقد بلغت نسبة تدلوله (97,4%) لاسباب تتعلق بسهولة الصيغة والتعود عليها، يتبعه أسلوب (التكلفة زائد نسبة مئوية) بنسبة (36,8%) وهو الأسلوب الوحيد من بين الأساليب التفاوضية الذي كثر استعماله في حملات إعادة الأعمار وتوقف العمل به بعد ذلك ثم أسلوب (المبلغ الإجمالي) بنسبة (34,2%) . ثم بقية الأساليب كما موضح في الجدول (2) حيث رغب (18,4%) باستخدام عقود التصميم والإنشاء وتسليم المفتاح و (10,5%) كان مع استخدام عقود المشاركة ، وأيد (44,7%) تعاقدات الإدارة الإنشائية ، بينما وافق (31,6%) فقط على تعاقدات التصميم والإدارة، ومن الملاحظ إن مجموع النسب المئوية قد تجاوز (100%) بسبب قيام أفراد العينة بتأشير أكثر من صيغة في نفس الوقت لسعة حجم المشاريع وشمولها لاعمال كثيرة .

الجدول (2) يبين الصيغ التعاقدية التي تفضل العينة التعامل معها كطرف تعاقد

ت	الصيغ التعاقدية	العدد	%
1	عقود المبلغ الإجمالي	13	34,2
2	عقود مقاولات سعر الوحدة وجدول الكميات	37	97,4
3	عقود مقاولات الكلفة زائدا - أ - أجور ثابتة	2	5,3
	ب - نسبة مئوية من الكلفة	14	36,8
	د - أجور ثابتة مع ضمان سقف سعري	1	2,6
5	عقود التصميم والإنشاء وتسليم المفتاح	7	18,4



10,5	4	6 عقود المشاركة
31,6	12	8 عقود التصميم والإدارة

الجدول (3) القيم الوزنية لدرجات الأهمية الواردة في إجابات العينة

ت	درجة التقويم في إجابات أفراد العينة	المجال أو (الفترة)	مركز المجال لو (القيمة الوزنية)
1	ضعيف	$0 > - 2$	1
2	متوسط	$2 > - 4$	3
3	جيد	$4 > - 6$	5
4	جيد جدا	$6 > - 8$	7
5	ممتاز	$8 > - 10$	9

العوامل المؤثرة في تحديد نوعية العقد :

في ضوء البيانات الاستبائية المتوفرة بشأن تقويم العوامل المؤثرة في تحديد نوعية العقد الهندسي عند تحليل إجابات أفراد العينة . تم إدخال القيم الوزنية لدرجات الأهمية المحددة في الجدول (3) في إجابات كل عنصر من عناصر أفراد العينة لأمثلة الاستبيان . ومن ثم الاعتماد على المعادلة المرقمة (1) لحساب معدل تكرار الإجابات (العطار ، 1996) (الجميلي ، 2002) .

القيمة الوزنية للفترة × عدد الإجابات للفترة	ن=38
معدل تكرار الإجابات =	ن=1
عدد الإجابات الكلي	(1) ...

يمثل المعدل التكراري تقويما يعادل درجة الأهمية للعامل المؤثر ، فقد حصل العامل الأول في الجدول (4) على معدل تكراري (7.17) وهي تعادل تقويما بدرجة (جيد جدا) لكونه ضمن الفترة (6-8) وهو ما ورد في العمود (التقويم) . ولتحديد العوامل المؤثرة في حسابات النظام المقترح واستخراج درجة الأهمية ، فقد اعتمد التقويم (جيد جدا) كحد أدنى للقبول ، واعتبرت العوامل المؤثرة ذات المعدل التكراري اقل من (6) غير مهمة في حسابات بناء النظام حسب رأي العينة . وأخيرا تم رسم صورة مختصرة مبسطة للنتائج الأولية المأخوذة عن الاستبيان الميداني في الجدول (5)

جدول (5) العوامل المؤثرة في تحديد نوعية العقد مرتبة تنازليا

ت	العوامل المؤثرة في تحديد نوعية العقد	الوزن المعياري	الأهمية
1	الرغبة في البدء المبكر بالتنفيذ والتخلص من وقت صليات المناقصة	5,25	مهم
2	الحاجة إلى إنجاز وإشغال أجزاء من العمل وتحقيق درجة البرمجة المطلوبة للتنفيذ .	4,98	مهم
3	تفضيل صاحب العمل أو استشاريه لنوع وصيغة العقد التي يلزمون بها	4,97	مهم
4	مدى توفر نطاق المشروع والتصاميم والمواصفات ووثائق المقولة الأخرى	4,95	مهم
5	نوع المشروع وأهميته .	4,91	مهم
6	مدى توفر الموارد المطلوبة من المكان والمعدات والأيدي العاملة الماهرة والغير ماهرة الدائمة منها والموقتة والمواد الأولية والتكميلية لتنفيذ العمل .	4,78	مهم
7	مدى رغبة صاحب العمل في معرفة التكلفة الكلية للمشروع قبل العقد	4,76	مهم
8	حجم وطبيعة العمل الإنشائي	4,72	مهم
9	عدم استقرار السوق وحالات عدم التأكد الاقتصادي من العوامل المستقبلية	4,71	مهم
10	الوقت المسموح به لتجهيز العطاء للمنافسة	4,65	مهم
11	التحري عن تحقيق نوعية معينة	4,64	مهم
12	طول عمر العقد والتحري عن تحقيق مدة إنجاز معينة	4,62	مهم
13	الصعوبة في تخمين كلف المشروع	4,51	مهم
14	مدى استقرار متطلبات صاحب العمل وهل هي نهائية وحدود سحدرات	4,39	مهم
15	مقدار المجازفة التي يوافق أن يتحملها صاحب العمل	4,22	مهم
16	درجة تعقيد التصاميم وصعوبة تنفيذها	4,20	مهم
17	مدى رغبة صاحب العمل في المشاركة في إدارة العقد ودرجة تدخله بالعمل	4,13	مهم
18	طريقة تمويل المشروع ومدى توفر السيولة النقدية وأسلوب الدفع للمقاول	4,13	مهم
19	درجة وضوح متطلبات صاحب العمل وإمكانية تطبيقها	4,12	مهم
20	مستوى التنافس المطلوب من عمله .	4,12	مهم
21	التحري عن تحقيق كلفة معينة	4,12	مهم
22	حجم المعلومات المعطاة إلى المنافسين	4,11	مهم
	مجموع الأوزان المعيارية للعوامل	100	

- إقتراح نظام إداري لاختيار أسلوب التعاقد المناسب لاسلوب المقاول العام

يعتبر تسلسل مراحل المشروع من مرحلة القرار إلى مرحلة التصميم فالعطاء ومرحلة التنفيذ مشكلة يصعب تجاوزها في الاسلوب التقليدي بسبب الحاجة إلى تكامل المخططات وإنجاز كل مرحلة قبل المباشرة بالمرحلة التي تليها . لذلك كان الهدف بناء نظام إداري علمي وكفوء يؤدي إلى اختيار أسلوب تعاقدى كفوء يتناسب مع محددات اسلوب المقاول العام التقليدي في التنفيذ ويمكنه من تجاوز المتغيرات واحتضان الخصوصيات والتعامل معها بصيغة إيجابية .

- صياغة هيكلية النظام المقترح :

بعد ان تم تعريف وتحديد المشكلة قيد الدراسة ووضع صياغة واضحة ومحددة لابعادها ونطاقها ، والتي تمحورت حول أسلوب اختيار الأسلوب التعاقدى الذي يتناسب ويتوافق مع أسلوب المقاول العام . وعلى أساس ذلك تم تحديد العوامل المؤثرة في اختيار الصيغة والاسلوب التعاقدى المناسب ، وحساب الوزن المعيارى لها بعد استخدام معيار موحد لدرجات الأهمية كما تم توضيح ذلك وتحويل تلك المعلومات التقويمية إلى أرقام يمكن التعامل معها وفق معيار موحد للمقارنة .

يقوم صاحب العمل ومستشاروه باختيار نوع التعاقد قبل إعداد وثائق العطاء لاعتماد أسلوب إعداد الوثائق على نوع التعاقد وصيغته حيث يجب أن تعد صيغة العقد وشروطه وجدوله ومواصفاته ورسوماته بما يتماشى مع نوع التعاقد ، على أن للخبرة أحيانا دورا فعالا في جعل عملية الاختيار عملية واضحة وسهلة ، ولكن بصورة عامة يجب وضع أسس علمية معتمدة وليس على أساس الخبرة بالرغم من أهمية الخبرة في نجاح كل عمليات أطوار إدارة المشاريع ، ولذلك فمن الضروري تكوين فكرة عامة عن العوامل المؤثرة في عملية اختيار الصيغة التعاقدية، ومن ثم مقارنة وربط محددات صاحب العمل مع متطلبات ومميزات تلك الصيغ التعاقدية وتحديد العوامل التي يجب على صاحب العمل دراستها مع كل الاعتبارات المؤثرة قبل اتخاذ لقرار اختيار الصيغة التعاقدية وهذا ما يهدف إليه البحث، بعد القيام بتحديد درجة المخاطرة التي يمكن أن يتحملها صاحب العمل وتبيان العوامل الخارجية المتغيرة المؤثرة في قرار اختيار صيغة التعاقد والمعتمدة على عدة متغيرات مثل الوقت ونوع العمل والتي قد نجعله لايمتلك الحرية المطلقة في اختيار نوعية العقد . ومن ثم تم طرحها للاستبيان الميداني لتحديد أهميتها وتحديد اتجاه تأثيرها كما ورد في الجدول (4) وقد تم تقسيم تأثيرها إلى مجموعتين :

المجموعة الأولى : وتمثل العوامل المؤثرة فعليا والتي يتجاوز تقويم أهميتها جيد جدا ($6 <$) ، ليتم إعادة تحديد الوزن المعيارى لتلك العوامل في ضوء مجاميع جديدة تشمل العوامل المؤثرة فعليا فقط .

المجموعة الثانية : وتمثل العوامل المؤثرة بصورة عامة والحاصلة على تقويم أهمية دون جيد جدا ($6 >$) والتي تم تأشير انخفاض تأثيرها بموجب المسح والاستبيان الميداني .

بناء نظام اختيار أسلوب التعاقد الملائم لاسلوب التنفيذ التقليدي (المقاول العام) :

يتم دراسة العوامل المؤثرة في تحديد أسلوب التعاقد لاختيار أسلوب تعاقدى يتناسب مع أسلوب التنفيذ وحجم العمل وظروفه . يمكن ان ننظم التعاقدات في صفتين من العقود التي تحمل متغيرات عديدة فيما بينها وهي عقود تعويضات الكلفة وعقود السعر الثابت حيث تعتمد الكثير من الفروقات في تفضيل أحدهما على الآخر مثل مقدار المخاطرة وحجم الحوافز المدفوعة للمقاول وحجم الوقت المختزل ومعيار العلاقة بين الأطراف الثلاثة ومدى المطالبة بتحديد الكلفة النهائية ، وقد تم اجمال عقود مقاولات ذات صيغة خاصة لحاجتها إلى

قرارات خاصة من صاحب العمل . تؤسس العقود على عطاء سعر ثابت أو مبلغ إجمالي عند الحاجة لمعرفة كلف الإنشاء الكلية ، كما يمكن أن يحقق ذلك تحت عطاء سعر الوحدة أو عطاء جدول الكميات إذا كان تخمين الكميات المنجز دقيق ، ويعتبر التأكيد على كلف المشروع مهم جدا إلى صاحب العمل الذي يعمل تحت ميزانية مقيدة ، كما أن المشروع الممول بواسطة القطاع العام يطلب فيه نظام تنافس العطاءات والذي يتم اختياره في حالة وجود وقت كافي لإعداد المخططات والمواصفات الفنية بصورة كاملة مع إمكانية إجراء تخمينات دقيقة ومن أجل السيطرة الفعلية على الكلفة . يتم اللجوء إلى عقود الكلفة زائدا في حالة الحاجة للتخلص من وقت عمليات المناقصة، وعند رغبة صاحب العمل في البدء المبكر بالتنفيذ قبل الانتهاء من المخططات والوثائق المطلوبة وعند نطلب الإنجاز المبكر للمقولة . ولكن في هذه العقود يتحمل صاحب العمل مخاطرة أكثر من بقية العقود لعدم معرفة الكلفة الكلية للإنشاء قبل بدء المشروع . وفي ضوء ذلك يتم تقويم العوامل المؤثرة في تحديد أسلوب التعاقد بأسلوب ينحو باتجاه صيغة عقود الكلفة زائدا بناءً عليها على وفق الأسئلة التالية :

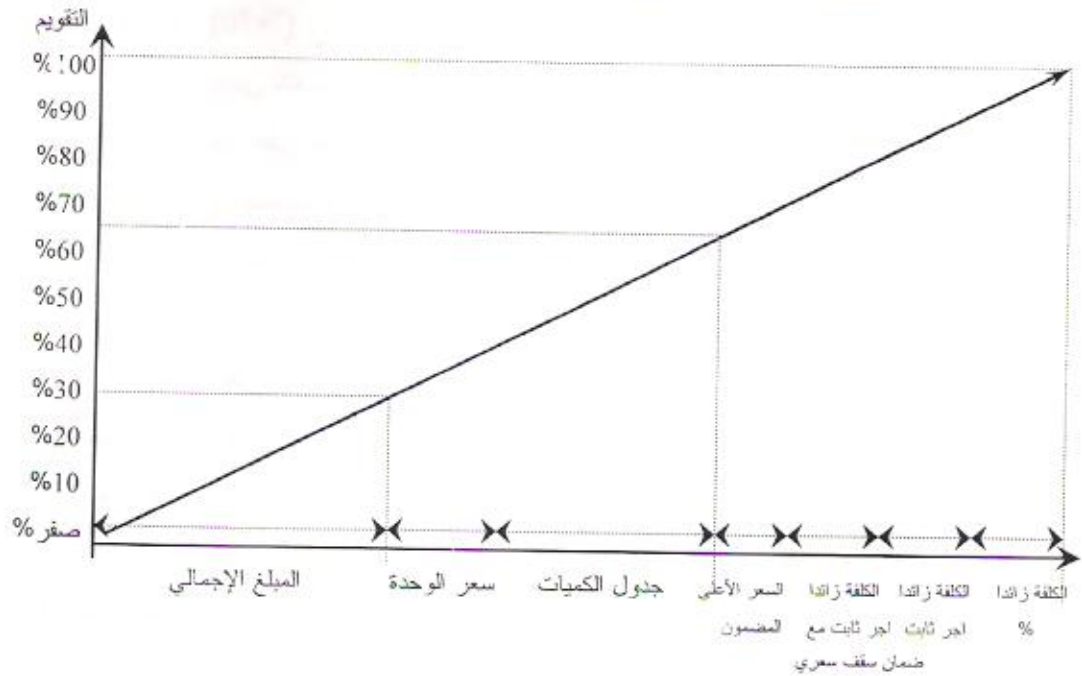
- ما مدى رغبة صاحب العمل في البدء المبكر بالتنفيذ والتخلص من وقت عمليات المناقصة ؟
- ما مدى الحاجة إلى إنجاز واشغال أجزاء من العمل وتحقيق درجة البرمجة المطلوبة للتنفيذ ؟
- ما مدى أهمية المشروع ؟
- هل إن عمر العقد طويل وما حجم التحري المطلوب عن تحقيق مدة إنجاز معينة ؟
- تعتبر هذه المعايير من أولويات العقود لذا تكون الإجابة على هذه الأسئلة بدرجة لا تقل على (70%) وقد تصل إلى (100%) وهي تدفع نحو صيغة الكلفة زائدا .
- ما مدى تفضيل صاحب العمل أو مستشاريه لصيغة الكلفة زائدا التعاقدية لتفهمه لها واستيعابه إياها ؟
- في حالة التفضيل يمنح درجة لا تقل عن (70%) وبعبارة أخرى يمنح درجة لا تزيد عن (30%)
- ما مدى توفر نطاق المشروع والتصاميم والمواصفات ووثائق المقولة الأخرى ؟
- يقوم السؤال بدرجة تعتمد على مدى توفر نطاق المشروع والتصاميم والمواصفات وبقية وثائق المقولة
- ما مدى عدم توفر الموارد المطلوبة لتنفيذ العمل من المكان والمعدات والأيدي العاملة الماهرة والغير ماهرة الدائمة منها والمؤقتة والمواد الأولية والتكميلية ؟
- يقوم السؤال بدرجة تعتمد على درجة عدم توفر الموارد المطلوبة ويمنح في ضوءها درجة تتجاوز (70%) في حالة عدم التوفر لأن ذلك يدفع باتجاه أسلوب الكلفة زائدا .
- ما مدى عدم رغبة صاحب العمل في معرفة الكلفة الكلية للمشروع قبل العقد ؟
- يقوم السؤال بدرجة تعتمد على عدم رغبة صاحب العمل في معرفة الكلفة الكلية للمشروع قبل توقيع العقد حيث يقوم بدرجة لا تقل عن (70%) في حالة عدم رغبته وذلك يدفع باتجاه صيغة الكلفة زائدا .
- ما مدى كبر حجم العمل الإنشائي ؟

- كلما كبر حجم العمل منح درجة تقويمية أعلى ودفع باتجاه صيغة الكلفة زائدا .
- ما مدى عدم استقرار السوق وعدم التأكد الاقتصادي ؟
- يقوم السؤال بدرجة تعتمد على مدى عدم استقرار السوق في العراق وأحيانا في العالم في حالة الحاجة إلى استيراد مواد او تقنية ويمنح في ضوء ذلك تقويم لا يقل عن (70%) في حالة عدم الاستقرار .
- ما درجة عدم توفر الوقت المسموح به لتجهيز العطاء للمناقصة ؟
- يقوم السؤال بدرجة تعتمد على حجم الوقت المطلوب والمسموح به لتجهيز العطاء للمناقصة حيث يقوم بدرجة لا تقل عن (70%) في حالة عدم توفر وقت لتجهيز العطاء لاسباب تتعلق ببرمجة المشروع .
- ما مدى تطلب تحقيق نوعية معينة من مواصفات العمل ؟
- يقوم السؤال بدرجة تعتمد على مطلوبة تحقيق نوعية معينة من المواصفات ، ففي حالة تطلب ذلك يقوم بدرجة لا تقل عن (70%) .
- ما مدى الصعوبة في تخمين كلف المشروع ؟
- يقوم السؤال بدرجة تعتمد على مدى الصعوبة في تخمين كلف المشروع بسبب عدم إكمال المخططات والتصاميم أو بسبب عدم توفر الوقت الكافي لذلك ويقوم بدرجة لا تقل عن (70%) .
- ما مدى عدم استقرارية متطلبات صاحب العمل أو الوصول إلى شكل نهائي لها ودرجة محددهاته ؟
- يقوم السؤال بدرجة تعتمد على متطلبات صاحب العمل حيث يقوم بما لا يقل عن (70%) في حالة عدم استقرار صاحب العمل على متطلبات محددة نهائية وزيادة محددهاته .
- ما مقدار المجازفة التي يوافق أن يتحملها صاحب العمل ؟
- يقوم السؤال بدرجة تعتمد على مقدار المجازفة والمخاطرة التي يوافق صاحب العمل على تحملها .
- ما درجة تعقيد التصاميم وما مدى صعوبة تنفيذها ؟
- يعتمد تقويم السؤال على درجة تعقيد التصاميم وصعوبة تنفيذها فكلما ازداد التعقيد ازداد حجم التقويم
- ما مدى رغبة صاحب العمل في المشاركة في إدارة العقد ودرجة تدخله بالعمل ؟
- يقوم السؤال على مدى رغبة صاحب العمل في المشاركة فكلما ازدادت رغبته ازداد معيار التقويم .
- ما مدى توفر السيولة النقدية ؟
- يقوم السؤال على مدى توفر السيولة النقدية في المشروع فكلما توفرت السيولة ازداد مقدار التقويم .
- ما مدى عدم وضوح متطلبات صاحب العمل وعدم إمكانية تطبيقها ؟
- يعتمد تقويم السؤال اعتمادا على درجة وضوح المتطلبات فكلما كانت غير واضحة ازداد مقدار التقويم .

- ما مدى عدم الحاجة إلى تنافس العطاءات ؟
- يقوم اعتمادا على عدم الحاجة إلى عملية التنافس فكلما كانت الحاجة إلى التنافس قليلة ازداد مقدار التقويم

- ما مدى حجم عدم التحري عن تحقيق كلفة معينة ؟
- يزداد التقويم مع ازدياد عدم الحاجة إلى تحقيق كلفة معينة .
- ما مدى قلة المعلومات المعطاة إلى المقاولين ؟

يقوم السؤال وفقا لحجم المعلومات المعطاة إلى المقاولين فكلما قل حجم المعلومات، ازداد مقدار التقويم في ضوء تلك الإجابات يمكن اختيار صيغة التعاقد المناسبة حيث يتم اختيار إحدى صيغ تعاقد الكلفة زائدا إذا حصل التقويم على معدل عام لا يقل عن (65%) ، وعلى صيغة المبلغ الإجمالي إذا حصل على معدل عام لا يزيد على (30%) وعلى صيغة سعر الوحدة أو صيغة جدول الكميات لما بين هذين التقويمين ، وبموجب الشكل (3) الذي يمثل العلاقة بين التقويم الحاصل من الاجابة على الاسئلة المطلوبة وصيغة التعاقد المقترحة وهو صورة مبسطة للنظام الاداري المقترح



الشكل (3) اختيار صيغة التعاقد المناسبة بموجب درجات التقويم

- الاستنتاجات :

من خلال تحليل البيانات التي تم جمعها خلال اعداد الدراسة فقد تم التوصل الى مجموعة من الاستنتاجات :
* ظهور ضعف واضح في مجال التخطيط لمختلف القطاعات من خلال اعتماد نوع واحد من انواع التخطيط الروتيني والتركيز على مايتعلق بالكلفة واهمال مجالات التخطيط الاخرى مثل تحسين النوعية واستخدام البدائل



- تأثير اساليب التنفيذ نائرا مباشرا بالتضخم المالي والظروف الاقتصادية العامة التي يمر بها البلد مما أدى الى الاعتماد على اساليب محددة
- وجود اكثر من عشرين عاملا مؤثرا بصورة مباشرة او غير مباشرة في تحديد نوع العقد المستعمل
- بالرغم من وجود عدة انواع من التعاقدات الهندسية التي تختلف متطلباتها التعاقدية والفنية والمالية تلائما مع الظروف المحيطة بعملية التعاقد والتنفيذ الا ان عمليات التعاقد تنحصر باساليب محددة بسبب عدم
- 5- وجود قصور في فهم وتقدير اهمية اختيار اسلوب التعاقد بين اصحاب العمل بشكل عام.

- التوصيات

- على ضوء ذلك تم التوصيل الى النقاط الاتية كتوصيات عن البحث :
- وجوب الاهتمام الاوسع بعملية التخطيط بمستوياته ووصول التخطيط الى مستوى مراقب عمل
- استخدام نظام موحد لتبويب المعلومات ، مع ضرورة توثيق ادارات المشاريع لكل المعلومات المتعلقة بمشاريعهم ومهما يكن نوعها لاستخدامها لاحقا للتغذية العكسية وكدليل لمشاريع اخرى
- استخدام الحاسوب بشكل اوسع ووصوله الى مستوى ادارة المشاريع
- اشراك المهندسين والفنيين بدورات دراسية علمية وعملية لتطويرهم ورفع مستوياتهم العلمية والعملية بما يتلائم مع التطور الحاصل في العلوم الهندسية في خارج القطر وخاصة في مجال انواع التعاقدات
- استخدام النظام المقترح في اختيار اسلوب التعاقد الملائم للمشروع المنفذ على وفق اسلوب المقاول العام
- وضع ضوابط وتعليمات خاصة باستخدام اسلوب الكلفة زائدا في التعاقدات
- 7- تجهيز جميع الوثائق التي تم إقرارها بشكل واضح في وقت مناسب قبل المباشرة بالعمل .

- المصادر

- الجار الله . د. محمد ابراهيم & نورة . د. جمال محمد (ادارة المشاريع الانشائية) دار جون وايلي وابنة للطباعة ، انكلترا ، 1984
- العاني . د. راجي (متطلبات تحسين الاساليب المعتمدة في تنفيذ المقاولات الانشائية في العراق) منشورات وزارة الاسكان والتعمير (ندوة حسابات الكلفة) بغداد . 1995
- غولد هابر ، ستانلي & جينا ، شاندراك & ماسيرو . مانويلي (النظم الادارية لهندسة التشييد) ترجمة د. التتير . انيس عبد الله & مجموع . محمد عامر . ط 1 . دار جون وايلي وابنة . انكلترا 1982

- المنجلقي، عادل عزت (عقود الاستشارات الهندسية) مركز البحوث القانونية ، بغداد ، 1984.
- عمارة ، نعمة حمد & توفيق ، سحر شاكر (الإحصاء وتطبيقاته الهندسية) الطبعة الأولى ، الجامعة التكنولوجية ، وزارة التعليم العالي و البحث العلمي ، بغداد ، 1989

REFERENCES

- Ahuja, H.N.(Construction Performance Control By Net Work) John wily ,Inc ,U.S.A. 1976
- Barrie, D. S. (Direction in managing construction) John Wiley & Sons, Inc., USA, 1981
- Haplin, D. W. & Wood Head, R. W. (Construction management) Second Ed. , John Wiley & Sons,Inc, U.S.A . 1998
- Hendrickson , Chris & Au, Tung (Project Management for Construction)First Ed., Prentice- Hall, Inc , Abivision Of Simon & Schuster Englewood Cliffs , New Jersey , U. S. A. 1989
- Kavanagh, T. C. & Muller, F. & Obrien, J. J. (Construction Management Aprofessional Aooroach) McGraw – Hill Book Co. , Inc , USA , 1978
- Marks, R. J. & Marks, R. J. E & Jackson, R. (Aspects of Civil Engineering Contract Procedure) Third Ed. , Pergamon Press Ltd. , Wheaton & Co., Ltd., Exeter , G.B. , 1985
- Twort.A.G. & Rees .J. Gorder (Civil Engineering: Supervision and Management)Third Ed. ,Edward Arnould ,Ltd ,G. B. London , 1995
- Thompson, P. (Organization and Economics of Construction) McGraw-Hill Book Co. , U.K. Limited , England , 1981
- Seely, Ivor (Quantity Surveying Practice) 1st Ed., Macmillan Publishers, G.B., 1984
- Stone, William C. & Carino, N. J. (Investigation of East Chicago Ramp Collapse) ASCE , Management Journal Of Construction Engineering And Management , USA , Vol. 110 , No. 1 , MAR. , 1984

الوزن المعيارى	درجة الأهمية	التقييم	النسبة المئوية لعمل تفرز الأجيال	عدد الأجيال التكرارية بدرجات الأهمية مع السبب السلبي لعمل تفرز الأجيال										ت	
				ممتاز		جيد جدا		جيد		متوسط		ضعيف			
				%	العدد	%	العدد	%	العدد	%	العدد	%	العدد		
4.91	مهم	جيد جدا	7.17	50	18	18.4	7	31.6	12	0	0	0	0	1	نوع الفراغ والهيكلية
4.12	مهم	جيد جدا	6.02	18.4	7	31.6	12	21	8	26.3	10	2.6	1	2	التحري عن تحقيق كافة معايير
4.64	مهم	جيد جدا	6.78	28.9	11	34.2	13	31.6	12	5.3	2	0	0	3	التحري عن تحقيق نوعية معينة
4.62	مهم	جيد جدا	6.74	31.6	12	36.9	14	13.2	5	13.2	5	5.3	2	4	طول عمر العنق والتحري عن تحقيق مدة الحياة معينة ومستوى معين من سرعة تنفيذ العمل
4.13	مهم	جيد جدا	6.03	23.7	9	23.7	9	28.9	11	13.2	5	10.5	4	5	استمرار نموول المشروع ومدى توفر السيولة النقدية واستمرار تدفق للتمويل
		متوسط	3.78	2.6	1	13.2	5	36.9	14	21	8	26.3	10	6	درجة استيفاء المعايير المعايير لأنواع التكاليف
		متوسط	2.47	0	0	0	0	15.8	6	50	19	34.2	13	7	وجود جوانب أمنية
4.13	مهم	جيد جدا	6.03	7.9	3	42.1	16	34.2	13	15.8	6	0	0	8	مدى رعاية صاحب العمل في المشاركة في إدارة العنق ودرجة تعاونه بالأساس
4.76	مهم	جيد جدا	6.94	26.3	10	34.2	13	36.9	14	2.6	1	0	0	9	مدى رعاية صاحب العمل في معرفة كافة التكاليف للمشروع قبل العنق
4.22	مهم	جيد جدا	6.16	28.9	11	26.3	10	18.4	7	23.7	9	2.6	1	10	مقدار المشاركة التي يوافق أن يتحملها صاحب العمل
4.95	مهم	جيد جدا	7.2	44.7	17	21	8	26.3	10	7.9	3	0	0	11	مدى توفر نطاق للمشروع والتكامل والمواصلات ووثائق المشاركة الأخرى
4.34	مهم	جيد جدا	6.4	31.6	12	31.6	12	28.9	11	7.9	3	0	0	12	مدى استمرارية متطلبات صاحب العمل وهل هي نهائية وبعدها محدداة
4.13	مهم	جيد جدا	6.02	26.3	10	23.7	9	21	8	18.4	7	10.5	4	13	درجة وضوح متطلبات صاحب العمل وبشكلية تطبيقها
		جيد	4.61	7.9	3	13.2	5	31.6	12	26.3	10	21	8	14	تحقيق أهداف ميسارية أو استراتيجية
		متوسط	3.93	10.5	4	0	0	52.6	20	15.8	6	21	8	15	مداورة الديال أو فلتاتها
4.71	مهم	جيد جدا	6.87	23.7	9	55.3	21	10.5	4	7.9	3	2.6	1	16	عدم استمرار السوق وحالات عدم توافر الائتماني من العوامل المستقبالية
4.11	مهم	جيد جدا	6.01	18.4	7	42.1	16	18.4	7	21	8	0	0	17	حجم المتطلبات المعطاة إلى المالكين ومدى توفر وثائق الأخطاء
4.20	مهم	جيد جدا	6.14	21	8	28.9	11	28.9	11	21	8	0	0	18	درجة تطبيق التكامل وصعوبة تنفيذها
4.72	مهم	جيد جدا	6.89	36.9	14	31.6	12	26.3	10	0	0	5.3	2	19	حجم وتطبيق العمل الانشائي
4.78	مهم	جيد جدا	6.98	34.2	13	44.7	17	13.2	5	7.9	3	0	0	20	مدى توفر الموارد المطلوبة من المالكين والمعدات والآلات العاملة بالماهرة وقدر ماهرة الدائمة منها والموثقة والمواد الأولية والتكاملية لتنفيذ العمل
6.26	مهم	جيد جدا	7.66	52.6	20	26.3	10	15.8	6	5.3	2	0	0	21	الفرعية في الجهد المبكر بالمتابعة والتواصل من وقت عمليات المناقشة
4.87	مهم	جيد جدا	7.26	55.3	21	15.8	6	13.2	5	15.8	6	0	0	22	تطبيق صاحب العمل أو استثماره لنوع وصيغة العنق التي يتوقع بها
		جيد	6.63	23.7	9	23.7	9	15.8	6	21	8	15.8	6	23	طرق تنفيذ العمل أو الخاصة بمدى تنفيذ في إنشاء العمل ، وتأثير العوامل البيئية على فلتس والعمالة والموثقة ودرجة الجهد وتطبيقه القريبة
4.12	مهم	جيد جدا	6.01	21	8	34.2	13	28.9	11	13.2	5	2.6	1	24	مستوى فلتس المطلوب من عمدة
4.58	مهم	جيد جدا	7.27	34.2	13	39.5	15	21	8	2.6	1	2.6	1	25	المشاركة في الجهد والتواصل الجهد من العمل وتحقيق درجة الفرعية المطلوبة للتنفيذ
4.85	مهم	جيد جدا	6.78	31.6	12	26.3	10	26.3	10	15.8	6	0	0	26	الوقت المسموح به لتجهيز العطاء للمناقشة
4.51	مهم	جيد جدا	6.69	31.6	12	34.2	13	23.7	9	7.9	3	2.6	1	27	التمسوية في تخمين تكاليف المشروع
		جيد	4.74	21	8	7.9	3	47.4	18	13.2	5	10.5	4	28	وضوح العطاء من الأرقام الثلاثة وتحديد الوظائف والمسؤوليات

%100

جدول (4) تحليل إيجابيات أفراد العينة وبينان تقويم وإهمية العوامل المؤثرة في تحديد نوعية العقد وادوارها المعيارية



SPLIT ASSIGNMENT WITH TRANSPORTATION MODEL FOR JOB-SHOP LOADING (CASE STUDY)

Khalil Ibrahim Mahmoud

Electro-Mechanical Engineering Department,
University of Technology, Baghdad, Iraq

ABSTRACT

The aim of this paper, is to analyze the assignment problem in industry where the constraint of allowing to allocate only one job to each machine is relaxed. Thus, splitting the job is permitted and processed by more than one machine. The problem is demonstrated with a real life case study. We solved the problem by splitting the jobs and converting lot of jobs as well as the actual hours of each machine to Standard Machine Hours (SMH). Transportation model is also suggested to overcome the problem, and the optimum solution is obtained by using POM software

KEYWORDS

Assignment problem, splitting, allocate, real life, transportation model.

INTRODUCTION

Loading or shop loading is required to assign specific jobs or teams to specific facilities. Loading is needed for machine shop, hospitals and offices. An important step in production scheduling is to load facilities, which mean taking the actual order and assigning them to designated facilities, loading answers the question which department is going to what work and loading assumes that the material requirement analysis has been done and that order has been properly placed for required material and for needed parts and sub-assemblies.

Specifically, loading assigns the work to divisions, departments, work centers, load centers, stations and people. Whatever names are used in a given organization, orders are assigned to those who will be responsible for performing the work. Loading releases jobs to facilities. In fact, average scheduling use standard hours based on forecasts to determine what resources should be assembled over the planning horizon. Loading takes place in the job shop when the real orders are on hand. If the aggregate scheduling job was done well, then the appropriate kinds and amounts of resources are available for loading. The master production schedule also makes resource assignments that can be modified if capacity is not adequate. A major objective of loading is to spread the load so that waiting time is minimized, the flow is smooth and rapid and congestion is avoided Nahimas, (1989). These objectives are constructed by the fact that not all machines can do all kinds of jobs.

Even though the job uses general purpose equipment, some machines and workers are better suited for specific job than other. Some machines cannot do particular jobs but other machines can do. Some are faster than others and tend to be overloaded. Also, in some situations, planning for actual shop assignments is irregular, where a particular job must be assigned to more machine specially if there is a high request for that job. Thus, let the production manager think about the splitting of jobs assignment and the scheduling objective will be how to smooth the load with balanced work assignments at machines in the flow shop.

In the literature, a great deal and much attention of researchers have been focused on solving the production scheduling problems.

Chan and Wong (2005) developed an assignment and scheduling model to study the impact of machine flexibility on production as a job lateness and machine utilization and presented a genetic algorithm based approach to solve generic machine assignment.

Also, Chan and Wong (2006) addressed the problem from the point of flexible job shop scheduling under resource constraints. They permitted an operation of each job to be processed by more than one machine. Caffrey and Hitchings (1995) considered scheduling of five jobs through a flow shop with five machines. Torres and Centeno (2008) considered a permutation flowshop problem with secondary resources with the objective of minimizing the number of tardy jobs. Recently, Konstantin et. al. (2005) focused on a dynamic generalization of the assignment problem where each task consists of a number of units to be performed by an agent or by a limited number of agents at a time.

ADDRESS THE PROBLEM

In this paper, we deal with the modification of the standard assignment problem where the constraint of allowing to assign only one job to each machine is relaxed. So the splitting the job is permitted to be processed by more than one machine. That means, the job can be divided into a parts, and on the other hand, the machine be allowed to do more jobs without violating the capacity constraint.

The research methodology is to assign operations to machine and determine the processing order of job on machines.

SYMBOLS USED

The following symbols are used throughout the paper:

t_j : Processing Time of Job j

n : Number of jobs to be assigned

m : Number of Machines in the flow shop

M_i : Machine number $i=1,2,\dots,m$

SM : Standard Machine

SMH: Standard Machine Hours

D_u : Demand in units for each kind of job



Pr : Production rate in units per SMH

D_{SMH} : Demand in aggregated standard hours

Pr_{ij} : Production rate in pieces per hour for machine i and job j

PROBLEM FORMULATION

The time minimizing assignment problem is the problem of finding an assignment of n jobs to m facilities, one to each, which minimizes the time for completing all the jobs subject to the assumption that all the jobs are commenced simultaneously Taha, (2007).

The general assignment problem with n jobs and m machines mathematically can be formulated as follows:

$$\text{Minimize } \text{Max} \{ t_{ij} | X_{ij} = 1 \} \quad (1)$$

Subject to

$$\sum_{j=1}^n X_{ij} \text{ for all } i \quad (2)$$

$$\sum_{i=1}^m X_{ij} \text{ for all } j \quad (3)$$

$$X_{ij} = 0 \text{ or } 1 \text{ for } i \text{ and } j.$$

Here, t_{ij} is the time required for completing the i th job if it is assigned to the j th machine and

$$X_{ij} = \begin{cases} 0 & \text{if the } i\text{th job is not assigned to the } j\text{th machine} \\ 1 & \text{if the } i\text{th job is assigned to the } j\text{th machine} \end{cases}$$

In the above formula, the important assumption made is that all the jobs are independent and can be commenced simultaneously.

RELAXING THE ASSUMPTION

The weakness of the classical assignment model is that no more jobs are allowed to one machine and also under certain circumstances, a weakness of the previous assignment model is that the splitting the jobs are not allowed. Moreover, the model assumed that the machine in job shops are identical and each one can do each job but with different time. To review the concept of relaxing the assumption, it can be seen from Table 1 which shows that how three jobs J_1 , J_2 and J_3 are assigned on machines M_1 , M_2 and M_3 . In this case, machine M_1 is assigned three jobs called J_{11} , J_{21} and J_{31} . Also, we can release another type of split prohibited by the classical assignment model is that no job can be divided with that model Starr (2004).

Table 1: Three machines and three jobs

		<i>J1</i>	<i>J2</i>	<i>J3</i>
Machines	<i>M1</i>	J_{11}	J_{21}	J_{31}
	<i>M2</i>			J_{32}
	<i>M3</i>		J_{23}	J_{33}

In the Table 1, job J3 has split into three parts J_{31} , J_{32} and J_{33} .

The above difficulty can be overcome by transportation methods. Although, it has certain restricted assumptions of its own. Particularly, when demand and supply must be in common terms standard units. A convenient common terminology in our case is to express supply and demand in standard hours.

To create standard hours, it is necessary to assume that strict proportionality exists between the productivity rates of the machines. The next section will review this concept.

STANDARD UNITS

Definitions

Standard units are used as the common dominator for aggregated units in the production scheduling problem where jobs are converted from pieces of work (order size) into standard hours on a designated machine called the standard machine. Forecast of specific items such as sweaters of different colors cotton, wool, and mixtures are converted into the standard machine hours required to make each type of sweater. This is referred to as aggregation of the mixed-model product line of the job shop. Aggregating planning is achieved by collecting and lumping all the items to be produced together. The idea is to strip away the specifics while retaining the aggregate properties of the product. The purpose is to match aggregate capacity against aggregate demand. This results in generalized determination of workforce requirements.

Computation of Standard Hours

Standard hours computation is better to know through An example to show how actual hours of work can be changed into standard units of required production capacity.

In Table 2 the standard unit is selected as Standard Machine Hours (SMH) based on using a Standard Machine (SM) for the standard of comparison. The total production capacity consists of four machines. The four machines called M1, M2, M3 and M4, work at different rate. It should be noted that the rate differentials apply across all of the jobs that these machines are assigned. That is M2 is fastest for all of the jobs, and by the same amount in comparison with the other machines. For this reason, it is convenient to choose M2 as the Standard Machine (SM). It will be assigned an index of 100%. Then, all of the other machines will have fractional (SM) index.

**Table 2: Supply of actual and SMH hours available per week**

<i>Machines</i>	<i>SMH Index (%)</i>	<i>SMH per week</i>	<i>Actual Hours</i>
M1	70%	56	80
M2	100%	77	77
M3	60%	90	150
M4	50%	40	80
		263	387

As shown in the above table, M4 is half as fast as M2. The equation for the SMH index is derived in more general terms, as follows:

$$SMH \text{ index of } M(ij) = \frac{\text{Production output of } (M_{ij})}{\text{Production output of } M(SM_j)}$$

For each machine, when SMH index is multiplied by the actual machine hours available per week, the standard machine hours (SMH) available per week are obtained.

Each machine is ranked by an index number that when multiplied by the actual machine hours available per week yields the standard machine hours (SMH) available per week. Thus, Table 2 provides the actual machine hours that are available per week converted by means of the SMH index. There is a total of 263 standard machine hours (SMH) available per week. In fact, there are 387 actual machine hours available per week has no significance for the resolution of the problem. Actual hours must first be converted to standard hours for application to the jobs that need to be done. This will be understood by examining the job requirements. In this department, the following represents a forecast of demand for next week for each job:

Jobs	A	B	C	D
Units	900	480	600	200

On the other hand, the productivity rate (the production output rate) of the standard machine for each of the jobs listed above is as follows:

Jobs	A	B	C	D
Productivity rate of standard machine	9	8	4	8

The computations are guided by the following equation (4) where unit dimensions are shown in parentheses. The dimension of units is the numerator and denominator is cancelled out. The remaining dimension is Standard Machine Hours (SMH). Thus, demand in units has been transformed to demand in standard machine hours for each job.

Input (D) as a unit \longrightarrow Output (D) as SMH

$$D_u \div \Pr \left(\frac{\text{Units}}{\text{SMH}} \right) = D_{SMH} \quad (4)$$

where D_u : Demand in units for each kind of job

\Pr : Production rate in units for SMH

D_{SMH} : Demand in aggregated standard hours.

According to the Equation (4), actual units of demand for Jobs A through D can be converted into standard machine hours (SMH) as follows:

D(SMH)

A: $900/9 = 100$ SM hours

B: $480/8 = 60$ SM hours

C: $600/4 = 150$ SM hours

D: $200/8 = 25$ SM hours

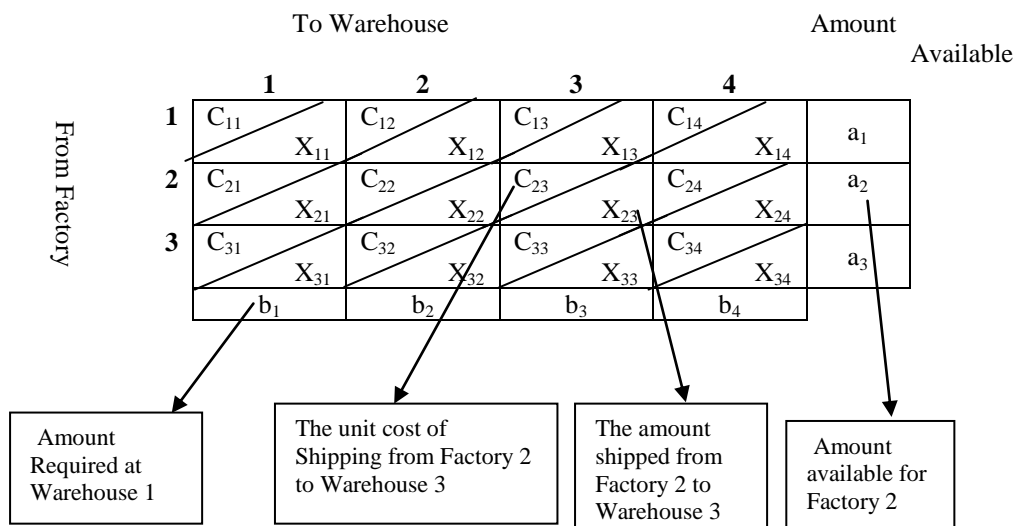
Total = 335 SM hours

Now, both supply (available capacity of machines) and demand (request for the job units) have been converted to the common terms of standard machine hours (SMH). Then this can be solved to find the loading arrangement that uses the resources available in terms of standard machine hours. In this case, the transportation model can be used to get the solution. On the other hand, the above loading problem can be dealt with linear programming. It does not have the constraint of proportionality.

Transportation Technique

Basically, the general transportation model deal with the distribution of goods from one location to another. The general transportation problem can be described in the form of a matrix with shipments from factories to warehouses with factories represented by the rows and warehouses by the columns of the matrix. In Figure 1, there are three factories and warehouses. Each cell in matrix represents a route from a particular factory to a particular warehouse. Listed on the right hand side of the matrix are the amounts available at each factory. Listed on the bottom of the matrix are the amounts required at each warehouse.

Figure 1: Transportation Model (Gillett 1985).



The objective of the transportation problem is to find the shipping routes from factories to warehouses which will minimize the total cost of transportation Russel, (2006). In each cell of the matrix the unit cost of shipping one unit through the cell or route is shown. The total cost of transportation is then the sum of the amounts shipped through each cell multiplied by the unit cost of shipping through that cell.

Mathematically, in this model, if we let

X_{ij} = amount shipped from factory i to warehouse j

C_{ij} = unit cost of shipping from factory i to warehouse j

Thus, the total transportation cost is: (Lockyer and Bestwick 1982).

$$C = \sum_{i=1}^m \sum_{j=1}^n C_{ij} X_{ij} \quad (5)$$

where m is the number of factories and n is the number of warehouses.

We wish to find the values of X_{ij} which will minimize the value of C subject to the constraints

$$\sum_{i=1}^m X_{ij} = b_j \quad (6)$$

The total shipped to each warehouse j must equal the amount required at the warehouse.

$$\sum_{j=1}^n X_{ij} = a_i \quad (7)$$

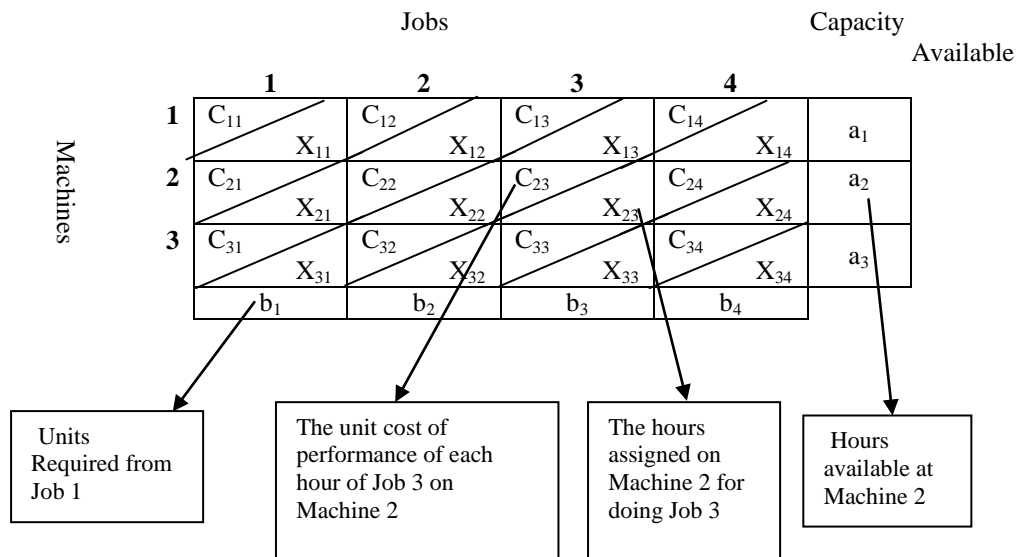
The total amount shipped from factory I must equal the amount available at the factory.

$$X_{ij} \geq 0$$

All shipments must be nonnegative.

To solve a transportation problem, we first find an initial solution (values of X_{ij}), and then improve the initial solution by reducing the cost through successive iterations until the minimum-cost is found. The transportation method is an iterative method, which reduces the solution on each successive iteration Nahimas, (1989).

Consequently, the above model can be modified and used to find the loading arrangement that uses the resources available to minimize the total cost. Then the assignment can be generated using the standard techniques employed to solve the transportation model. Figure 2 represents the equivalent matrix for the assignment model.

Figure 2: Equivalent Matrix for Assignment Model

Softwares are readily available to solve the model involving many variables. i.e. POM software package Natarajan, (2007). To solve the problem, we first find the initial solution and then improve the initial solution by reducing the cost. One way to find an initial solution is to use the North-West-Corner rule or Lowest Cost rule or the Vogel Approximation Method (VAM) Taha (2007). The next step is the evaluation of the solution for optimality of the initial solution. This can be carried out by using the Stepping Stone Method. Finally, the above problem can be solved alternatively by using the linear programming model.

IMPLEMENTATION

To implement the formula and to achieve the objective of this study, a real case study has been taken from the furniture industry. The problem was how to allocate 12 jobs on seven saw machines in cutting department. Any job related to one kind of product are named J1 upto J2 which can be assigned to any saw machine. The specification of each job is defined and the efficiency of each machine has also been defined according to the data collected from the production department. The processing time to complete each task is different. However, one of these machines (number 4) is more efficient than the others, which has been chosen to be the standard machine (SM). Table 3 shows relative productivity and the equivalent SMH index for each machine. Note that Machine 7 is half as fast as Machine 4.

Similarly, Machine 1 is 86% as fast as the standard machine (SM).

Table 3: Relative productivity and the equivalent SM

<i>Machines</i>	<i>SMH Index (%)</i>	<i>Relative Productivity</i>
M1	86%	86% as fast as the SM
M2	75%	75% as fast as the SM
M3	66%	66% as fast as the SM
M4(SM)	100%	Standard Machine
M5	55%	55% as fast as the SM
M6	80%	80% as fast as the SM
M7	50%	50% half as fast as the SM



The restrictive assumption is that the SMH index for each machine applies to all 12 jobs. It is called the presumption of productivity proportionality. Thus, Machine 4 is fastest for all of the jobs by the same amount, in comparison with the other machines. Table 4 provides the actual machine hours that are available per week. These hours are converted by means of the SMH index into standard machine hours available per week as shown in the fourth column. The actual machine hours available per week is 442. Table 4 concludes that total SMH is 324.75. Table 5 provides production rates Pr in pieces per hour for each machine and job. The entries on the matrix are labeled $Pr(ij)$ where i =machine and j =job.

The production rate of the standard machine for the j th job is $Pr(SM,j)$ see the fourth row (Machine 4) in Table 5. Table 6 contains the number of units ordered per job.

Table 4: Actual machine hours per week

<i>Machines</i>	<i>SMH Index (%)</i>	<i>Actual Hours</i>	<i>SMH per week</i>
M1	86%	50	53
M2	75%	60	45
M3	66%	75	49.5
M4	100%	78	78
M5	55%	35	19.25
M6	80%	60	48
M7	50%	84	42
Total		442	324.75

Table 5: Production rate in pieces per hour for each machine and job (Pr_{ij})

Machines	J1	J2	J3	J4	J5	J6	J7	J8	J9	J10	J11	J12
M1	5.16	3.44	2.58	6.88	5.16	6.02	10.32	3.87	10.32	5.16	2.58	6.02
M2	4.5	3	2.25	6	4.5	5.25	9	3.375	9	4.5	2.25	5.25
M3	3.96	2.64	1.98	5.28	3.96	4.62	7.92	2.97	7.92	3.96	1.98	4.62
M4	6	4	3	8	6	7	12	4.5	12	6	3	7
M5	3.3	2.2	1.65	4.4	3.3	3.85	6.6	2.475	6.6	3.3	1.65	3.85
M6	4.8	3.2	2.4	6.4	4.8	5.6	9.6	3.6	9.6	4.8	2.4	5.6
M7	3	2	1.5	4	3	3.5	6	2.25	6	3	1.5	3.5

Table 6: Number of units ordered per job

Jobs	J1	J2	J3	J4	J5	J6	J7	J8	J9	J10	J11	J12
No. of units required	120	108	141	145	150	200	570	100	245	310	120	74
Standard hours of demand	20	27	47	18.13	25	28.6	47.5	22.2	20.4	51.7	40	10.6

As shown in the Table 6, the requests initially stated as the number of units ordered per job. They vary greatly because there are many different types of orders. These quantities have been turned into standard machine hours to match the amount of supply available from machine of type M4.

To accomplish the transformation of all dimensions to standard hours, start by dividing the number of units requested for J1 by the production rate of the standard machine for Ji. This yields demand in standard hours instead of demand in units. The results are shown in the second row of the Table 6.

Now, both capacity available (supply) and the requests for the jobs (demand) have been converted to the common terms of standard machine hours (SMH). There are 324.75 machine hours available per week and 358.13 hours required to complete the orders. Therefore, 33.38 standard machine hours of demand will not be satisfied.

A dummy machine is created to pickup the slack. It is called MD (for machine dummy). By definition, MD has zero output for all jobs. Some part of whichever job is assigned to the dummy will not be done. The balanced capacity available $S(i)$ and request $D(j)$ with the number in standard hours including the output rate per standard hours in the upper right hand corner of each assignment cell is given in Table 7.

As with the assignment model, cost is considered with the transportation model. The cost is calculated for each job j , which is the cost per standard hours of each machine i . The cost per piece (C_{ij}) is independent of the machine used, given in Table 8.

Table 8: Cost C_{ij} per piece (Riyal)

Jobs	J1	J2	J3	J4	J5	J6	J7	J8	J9	J10	J11	J12
Cost per piece (C_{ij})	200	470	550	700	320	150	480	780	100	950	400	100

The product output rates per standard hours have been multiplied by cost per piece to reflect the profit per standard hours ($C_{ij} \cdot P_{ij}$). These are shown in the small boxes in the upper right hand corner of each assignment cell. This information reflects in Table 9 which display the matrix adjusts for cost.

8. Generating the Assignment

After the information is arranged into transportation matrix (Table 9), the solution for assignment can be obtained. Although manual solution of transportation problems is fairly straightforward, computer solutions are generally preferred. The solution is generated by using POM software package. To solve the problem, first we find an initial solution and then improve the initial solution by reducing the cost. One way to find an initial solution is to use the North-West Corner rule or Lowest Cost rule or the Vogel Approximation Method (VAM). The next step in the transportation method is evaluation of the solution for optimality, given a start solution. By using the POM software, the optimal loading schedule is shown in Table 10 in standard machine hours with the minimum total cost (578177.80)

$$\text{Min (Cost) } Z = \left[\begin{array}{l} 20 \times 1032 + 1.4 \times 1419 + 20.4 \times 1032 + 1.2 \times 1032 + \\ 20 \times 1410 + 25 \times 1440 + 4.6 \times 1089 + 18.13 \times 3696 + \\ 22.2 \times 2317 + 4.57 \times 3762 + 28.6 \times 1050 + 38.8 \times 1200 + \\ 10.6 \times 700 + 19.25 \times 3135 + 7 \times 1504 + 41 \times 1320 + \\ 14.12 \times 2880 + 33.38 \times 0 + 27.88 \times 2850 \end{array} \right]$$



There are eight rows and twelve columns which means that $M+N-1=19$ assignments should be made for transportation model. The requisite nineteen are in place. The optimal has been found in terms of standard hours must now be converted back into actual machine hours, and actual job units. Divide the standard hours assignments by the SMH index for each machine. This is shown in Table 11 and Table 12. Table 11 represents the actual assignment in terms of actual units and Table 12 represents the actual assignment in terms of actual hours.

The load is established for each job by consulting Table 10, Table 11, and Table 12 and the calculations as follows:

For Job J1

$20 \text{ SMH} \div \text{SMH index of } 86\% \text{ equal } 23.3 \text{ actual hours assigned on Machine 1 for Job J1.}$
This yields $23.3 \times 5.16 = 120$ units for J1.

For Job J2

$20 \text{ SMH} \div \text{SMH index of } 75\% \text{ equal } 26.3 \text{ actual hours assigned on Machine 2 for Job J2.}$
This yields $26.3 \times 3 = 80$

$7 \text{ SMH} \div \text{SMH index of } 80\% \text{ equal } 8.75 \text{ actual hours assigned on Machine 6 for Job J2.}$
This yields $8.75 \times 3.2 = 28$

Total $80 + 28 = 108$ units as required per J2.

For Job J3

$1.4 \text{ SMH} \div \text{SMH index of } 86\% \text{ equal } 1.63 \text{ actual hours assigned on Machine 1 for Job J3.}$
This yields $1.63 \times 2.58 = 4.2$

$4.6 \text{ SMH} \div \text{SMH index of } 66\% \text{ equal } 7 \text{ actual hours assigned on Machine 3 for Job J3. This}$
yields $7 \times 1.98 = 13.8$

$41 \text{ SMH} \div \text{SMH index of } 80\% \text{ equal } 51.25 \text{ actual hours assigned on Machine 6 for Job J3.}$
This yields $51.25 \times 2.4 = 123$

Total $4.2 + 13.8 + 123 = 141$ units as required per J3.

For Job J4

$18.13 \text{ SMH} \div \text{SMH index of } 66\% \text{ equal } 27.5 \text{ actual hours assigned on Machine 3 for Job J4.}$
This yields $27.5 \times 5.28 = 145$

For Job J5

$25 \text{ SMH} \div \text{SMH index of } 75\% \text{ equal } 33.33 \text{ actual hours assigned on Machine 2 for Job J5.}$
This yields $33.33 \times 4.5 = 150$

For Job J6

$28.6 \text{ SMH} \div \text{SMH index of } 100\% \text{ equal } 28.6 \text{ actual hours assigned on Machine 4 for Job J6.}$
This yields $28.6 \times 7 = 200$

For Job J7

14.12 SMH ÷ SMH index of 50% equal 28.24 actual hours assigned on Machine 7 for Job J7. This yields $28.24 \times 6 = 169.4$

33.38 SMH is assigned to the dummy machine (MD) so Job J7 will be partially completed. This is a shortage of $(570 - 169.4) = 400.6$ units for Job J7.

For Job J8

22.2 SMH ÷ SMH index of 66% equal 33.6 actual hours assigned on Machine 3 for Job J8. This yields $33.6 \times 2.97 = 100$

For Job J9

20.4 SMH ÷ SMH index of 86% equal 23.7 actual hours assigned on Machine 1 for Job J9. This yields $23.7 \times 10.32 = 245$

For Job J10

4.57 SMH ÷ SMH index of 66% equal 6.9 actual hours assigned on Machine 3 for Job J10. This yields $6.9 \times 3.96 = 27.2$

19.25 SMH ÷ SMH index of 55% equal 35 actual hours assigned on Machine 5 for Job J10. This yields $35 \times 3.3 = 115.5$

27.88 SMH ÷ SMH index of 50% equal 55.8 actual hours assigned on Machine 7 for Job J10. This yields $55.8 \times 3 = 167.3$

Total $27.2 + 115.5 + 167.3 = 310$ units as required per J10.

For Job J11

1.2 SMH ÷ SMH index of 86% equal 1.4 actual hours assigned on Machine 1 for Job J11. This yields $1.4 \times 2.58 = 3.6$

38.8 SMH ÷ SMH index of 100% equal 38.8 actual hours assigned on Machine 4 for Job J11. This yields $38.8 \times 3 = 116.4$

Total $3.6 + 116.4 = 120$ units as required per J11.

For Job J12

10.6 SMH ÷ SMH index of 100% equal 10.6 actual hours assigned on Machine 4 for Job J12. This yields $10.6 \times 7 = 74$.



CONCLUSION

- In this research, problem of splitting the jobs among many machines and allow for each machine to perform a lot of jobs is tackled. This problem is mobilized by using standard machine hours (SMH) to convert lot of jobs as well as the actual hours of each machine to Standard Machine Hours (SMH).
- A real case study demonstrates how a production manager can use this model in real life. The problem was how to allocate 12 jobs on seven machines; one of these machines (No 4) has been chosen to be the standard machine (SM).
- The actual machine hours that are available per week were (442). These hours then converted by means of the SMH to 324.75.
- Later on, we suggest any available quantitative techniques, particularly, transportation model which is more convenient to deal when the supply and demand are in common terms which is in our case as SMH. In this case a dummy machine is created to pickup the slack standard machine hours 33.38.
- The optimal solution which has been found in terms of standard hours also converted back into actual machine hours, and actual job units.
- The solution for assignment has been obtained. Therefore splitting the jobs are permitted and processed by more one machine. Thus it can be seen from the results, machine M1 is assigned four jobs: J1, J3, J9, and J11. While job J2 is splited and assigned to machines M2, and M6 as well as other jobs.
- Finally, the optimal loading schedule has been generated in standard machine hours with the minimum total cost (578177.80).

RECOMMENDATION

Based on the empirical findings of this study, following several points can be talked later on which are not discussed in this paper.

- The transportation model have been solved for total cost minimization, it is as simple to use profits and solve for total profit maximization. Total time minimization, productivity maximization, and other goals can be chosen as well.
- The formulation which has been used in this study assumes that costs per piece are the same on machines. If not, it would be necessary to use the cost(C_{ij}) for each cell in the matrix.
- A criterion that must be satisfied for using the transportation approach to shop loading is that reasonable proportionality exists between machines output rates. When the SMH index does not apply, a heuristic modification of the transportation method can be tried. If one machine is especially efficient for J1 and another machine is best for J2, the heuristic could make those assignments more profitable, or less costly. In other words, some assignments would be made a priori based on clear advantages.
- An issue we have not addressed is uncertainty of processing time in practice. It is possible and even likely that the exact completion time of one or more jobs may not be predictable in advance. It is of interest to know whether or not there are some results concerning the optimal assignment when processing time is uncertain

REFERENCES

- Caffrey, J. and Hitchings, G., "Makespan distributions in flow shop scheduling", *International Journal of Operations & Production Management*, 15(3) (1995) 50-58.
- Chan, F.T.S., Wong, T. C. and Chan, L.Y., "A genetic algorithm-based approach to machine assignment problem", *International journal of production research*, 43(12) (2005) 2451-2472.
- Chan, F. T. S., Wong, T. C. and Chan, L. Y., "Flexible job-shop scheduling problem under resource constraints", *International Journal of Production Research*, 44(11) (2006) 2071-2089.
- Gillett, B.E., *Introduction to Operations Research*, (Fourth Edition), Tata, Mc Graw- Hill, Ltd, New Delhi., (1985).
- Konstantin, K., Eugene, K. and Toshihide, I., *Dynamic Generalized Assignment Problems with Stochastic Demands and Multiple Agent--Task Relationships*, *Journal of Global Optimization*, 31(1) (2005) 17-43.
- Lockyer, K. and Bestwick. P.F., *Quantitative Production Management*, (First Edition), Pitman Publishing, New Zealand, Ltd., (1982).
- Nahimas, S., *Production and Operations Analysis*, Irwin, Boston, (1989).
- Natarajan, A.M., Balasubramani, P. and Tamilarasi, A. " *Operations Research (Second Edition)*", Dorling Kindersley (India) Pvt.Ltd, New Delhi., (2007).
- Russel, R.S. and Taylor III, B.W., *Operations Management (Fourth Edition)*, Prentice Hall of India, New Delhi, (2006).
- Starr, M.K., *Production and Operations Management (Second Edition)*, Biztantra, New Delhi, (2004).
- Taha, H.T., *Operations Research: An Introduction*, Eighth Edition, Pearson Prentice Hall, New Delhi, (2007).
- Torres, A.J.R. and Centeno, G. "Minimizing the number of late jobs for the permutation flowshop problem with secondary resources", *Computers and Operations Research*, 35(4) (2008) 1227-1249.

أثر الأغلفة الديناميكية على كفاءة الأداء الحراري لأبنية المناطق الحارة - الجافة

غادة محمد اسماعيل عبد الرزاق كمونة

قسم الهندسة المعمارية - جامعة بغداد

مُستخلص البحث:

يتناول البحث موضوع إيجاد أبنية كفوءة مناخياً تتميز أغلفتها البنائية بديناميكية عالية تمكنها من التفاعل والتكامل بتغير المواسم في منطقتنا الحارة - الجافة، إذ إن إستيراد الأفكار المعمارية وظهور التقنيات الجديدة أفرز توجهاً فكرياً وعمرانياً يتعارض وأدنى خصائص هذه المنطقة بيئياً وعمرانياً، ومن ثم نشوء عمارة غير منتمية للواقع البيئي المحيط بها فوُقت على مفترق طرق بين عدم مراعاة البيئة ومجاراة الفكر الغربي وبين الركون للعمارة التقليدية، ومن هنا وجب على المهندس المعماري أن تكون أفكاره وتصاميمه أساسها التفهم العميق لإمكانيات العصر الذي نعيشه من إختيار المواد المناسبة وإستثمار ما توصل إليه الآخرون من تقدم تقني ومعرفي ملائم مع الإستفادة والإستلهاً من تراثنا المعماري الغني وما يحتويه من فهم شمولي وعميق للمشاكل المناخية، وفي الوقت ذاته تكون هذه الأفكار والتصاميم منتمية لبيئتها ومستفيدة من صفاتها الجغرافية والمناخية وصولاً الى رسم المسارات المستقبلية في إنشاء عمارة متألّفة ومتوازنة مع البيئة المحيطة لتحقيق معادلة التوازن الحراري لأبنيتنا ومن ثم نضع العمارة على دربها البيئي الصحيح.

ويعالج البحث مشكلته من خلال الموازنة بين توظيف التقنيات الحديثة وبصورة مبسطة من جهة، وبين استخدام طرق التصميم المناخي الطبيعي من جهة أخرى لإنشاء أبنية ديناميكية تحاكي التقلبات المناخية القاسية في المناطق الحارة - الجافة على مدار العام، وبالتالي رفع مستوى التصاميم المعمارية المستقبلية للأبنية، لكونها أبنية تستقرئ المستقبل وتحاكيه وتتفاعل معه مسبقاً بمعلومات الحاضر وبنفس الوقت تستلهم من عمارة الماضي وتوظفها بأسلوب معاصر، وصولاً الى تكوين عمارة متكيفة مع الظروف المناخية المحيطة وقادرة على الصمود في المستقبل. وتأتي أهمية موضوع البحث هنا في كونه يدعم الإهتمام العالمي بالتكنولوجيا الحديثة وفي الوقت ذاته يحاكي العمارة التقليدية من خلال انشاء أبنية ديناميكية مستجيبة للتقلبات المناخية المحيطة.

مشكلة البحث:

إنشاء أبنية متكيفة مع الظروف المناخية المحيطة في المناطق الحارة - الجافة من خلال أغلفة بنائية ديناميكية تتجاوب مع المناخ المحيط بتقلبه طوال العام لتخفيض الأحمال الحرارية لأنظمة التكييف ومن ثم خفض إستهلاك الطاقة.

هدف البحث:

تحسين الخصائص الحرارية للمباني لضمان توفير الراحة الحرارية لشاغلها من خلال تأمين التصميم الحراري الكفوء لها، والذي يتم تحقيقه من خلال إنشاء أبنية ذات أغلفة ديناميكية مرنة متكيفة ومستجيبة للظروف المناخية المحيطة في المناطق الحارة – الجافة.

The Influence of Dynamic Envelopes on the Efficiency of Thermal Performance of Hot – Arid Zones Buildings

ABSTRACT:

This research studies the subject of finding efficient climatic buildings whose envelopes are characterized by a high dynamic movement that enables them to react and integrate in accordance with seasons' changing in our hot – arid zones. The importing of architectural thoughts and the emergence of new techniques have led to the evolution of an intellectual and urban trend that disagrees with the least environmentally and urbanly characteristics of these regions, and consequently, the evolution of a kind of architecture that does not belong to its environmental reality, therefore, it has stopped in between the non-considering of the environment and the keeping up with the western intellect and between confining to traditional architecture. Thus, the architect's thought and designs should be based on the deep understanding of the current potentialities of the age concerning choosing the suitable materials and investing what others has reached concerning the suitable technical and epistemic progress along with making use of and inspiring from our rich architectural heritage and all what it contains concerning a comprehensive and deep understanding of the climatic problems, and at the same time, these thoughts and designs belong to its environment and utilizing its surrounding geographical and climatic features to reach to the drawing of futuristic paths in establishing a harmonious and balanced with the surrounding environment to achieve the equation of thermal balance for our buildings and then putting architecture on its right environmental way.

The research takes the problem through balancing between the employment of modern techniques in a simply way on one hand, and the use of the natural climatic design methods on the other hand, in order to establish dynamic buildings that imitate the severe climatic changes in the hot – arid areas during the year, and then by raising the level of the buildings futuristic architectural designs since these buildings explore and imitate the future and already interacting with it by the present information and at the same time inspire from the architecture of the past and make use of it in a contemporary style, in order to reach to the formation of a kind of architecture that is conditioned with the surrounding climatic conditions and is capable of resistance in the future.

The importance of the research's subject is that it supports the worldwide interest of modern technology, and at the same time, it imitates traditional architecture through constructing dynamic buildings responding to the surrounding climatic changes.

كلمات رئيسية: الأغلفة الديناميكية للمباني، المنظومة الحرارية للمبنى، التوازن الحراري، الأحمال الحرارية، الراحة الحرارية.

- المقدمة:

بات التوجه العمراني المعاصر نحو الفكر الوافد الغريب يتعارض مع مفهوم تفاعل المبنى مع البيئة المحيطة به وتأثر كل منهما بالآخر ومن ثم ضعف سلوك المبنى الحراري التفاعلي مع البيئة المؤدي الى إستنزاف عالي لأجهزة التكييف علاوةً على فقدان الطابع والهوية المميزة لمنطقة عن أخرى، إذ ان العمارة المعاصرة أغلقت الأبواب أمام التفاعل مع البيئة المحيطة. ولكون المناطق الحارة - الجافة ومنها العراق تتمتع بمناخ قاسٍ طوال العام وجب على المهندس المعماري التفاعل الإيجابي مع معطيات المناخ من خلال توظيفه لكافة التقنيات الحديثة وطرق التصميم المناخي الطبيعي لإنشاء أغلفة بنائية ديناميكية للمباني لديها القدرة على التفاعل والتغير المستمر تبعاً لتغيرات المناخ طوال العام، حيث تسهم بتوفير بيئة فاعلة وسريعة الإستجابة للظروف المناخية المحيطة لتحقيق أفضل مستويات الراحة الحرارية لشاغلي تلك الأبنية وذلك بتحقيق أعلى كفاءة أداء حراري لأغلفتها البنائية، إذ ان توفير الراحة الحرارية والحماية من المؤثرات المناخية غير المرغوب فيها يُعد من الأهداف الأساسية للتصميم المعماري والعمراني الكفوء مناخياً خصوصاً بعد التغيرات الكبيرة التي شهدتها مدننا الحارة - الجافة من إنشاءات حديثة وتعمير اسمنتي كان له الدور الكبير في ضعف قدرة هذه الأبنية على الموازنة الحرارية، وحاجة أصحابها لإستهلاك كبير للطاقة لتأمين حاجتهم من التدفئة والتبريد. وبالمقارنة مع العمارة التقليدية التي تتصف بقدرتها العالية على الإحتفاظ بجو معتدل طيلة أيام السنة من خلال المواد المستخدمة في إنشاءها وتصاميمها المتكيفة مناخياً وتلاصق ابنيتهما المدروس، أضاف على عاتق المهندس المعماري مهمة معالجة الزيادة الملحوظة في استهلاك الطاقة الكهربائية والوقود في المباني لأغراض التكييف لتخفيض التناهي المتسارع في الطلب على أحمال الطاقة، وحماية البيئة من التلوث الناتج عن إنبعاثات غازات الدفيئة الناتجة عن حرق الوقود الاحفوري، فضلاً عن تحقيق متطلبات الراحة الحرارية داخل المباني، لذا يجب إيجاد تصاميم حرارية كفوءة للمباني تتكيف مع البيئة المحيطة بتغير المواسم وذلك من خلال تطويع أغلفتها البنائية تبعاً للظروف المناخية المحيطة وهو أمر يُدخل مفاهيم وأساليب جديدة لم تكن مألوفة في تصميم وتنفيذ المباني خاصةً في المناطق الحارة - الجافة.

وهنا لسنا بصدد توفير أبنية إقتصادية بتسخير مفاهيم التصميم المناخي الطبيعي في الأبنية أو بصدد إستيراد الفكر التكنولوجي الغريب عن بيئتنا، بل نحن أمام تحدي بيئي طبيعي وتكنولوجي معاً بتوفير أغلفة مباني ديناميكية طيعة ومرنة في تفاعلها مع الظروف المناخية المحيطة لتتمكن من منع تسرب الطاقة خارج المبنى قدر الإمكان، ومن ثم رفع كفاءة أدائه الحراري، وصولاً لأعلى مستويات الراحة الحرارية لشاغليه.

- آلية عمل المنظومة الحرارية للمبنى:

إن ظاهرة الدورة المناخية السنوية والطقس اليومي في المناطق الحارة - الجافة ولدت تبايناً في الخصائص الحرارية، الأمر الذي نجم عنه عدم إستقرار للبيئة الداخلية للمبنى والمستدل عليه من الفرق الحراري داخل المبنى بين النهار الحار والليل البارد، وبين الصيف الحار والشتاء البارد في هذه المناطق، وهو ما يفسر حدوث ظاهرة الإنتقال الحراري، حيث توزع الحرارة نفسها بالتساوي الى أن تحقق حقل حراري منظم منتشر على

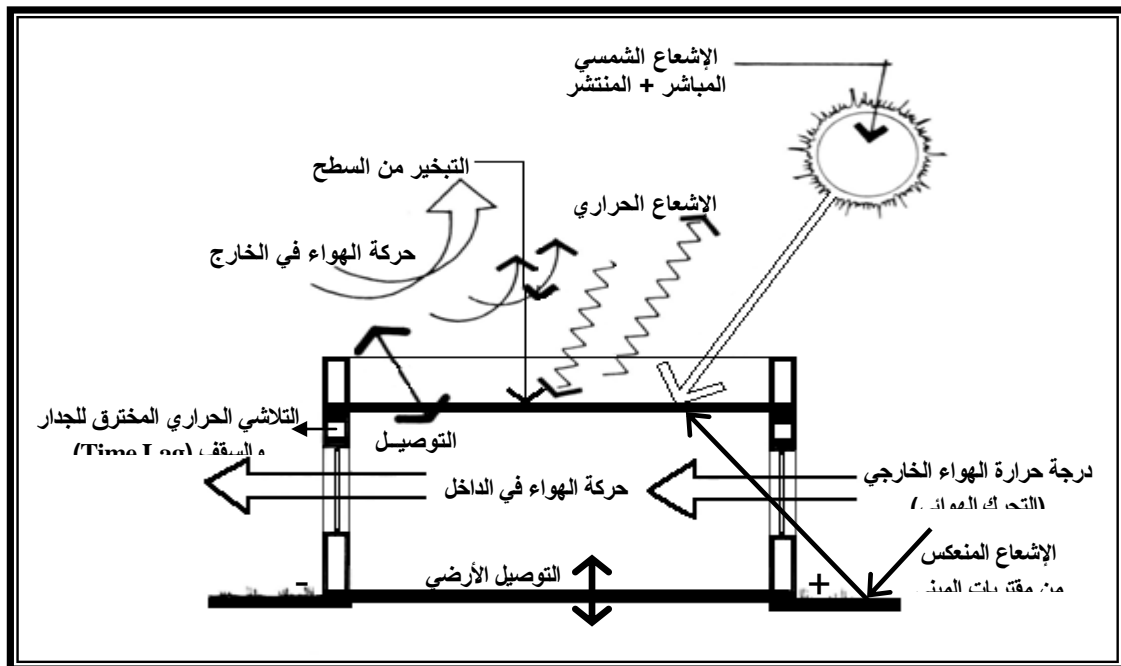
نحو كامل، متجهاً من مناطق ذات درجات حرارة عالية الى مناطق ذات درجات حرارة واطئة (Givoni، 1998، ص 109).

وتتأثر كمية الحرارة المكتسبة الى داخل المبنى صيفاً والمنتسبة خارجه شتاءً بالعوامل الآتية: مساحة الجدار الخارجي للمبنى، طبيعة ونوعية مواد انشاءه، سُمْك الغلاف البنائي، علاقة المبنى مع الشمس، لون الغلاف الخارجي للمبنى، تظليل المبنى بواسطة المنشآت المجاورة، درجة حرارة الفضاءات المحيطة أو البيئة، ودرجة حرارة الفضاء الداخلي (شاهين، 1990، ص 1).

وهنا يجد البحث إن غلاف المبنى يمثل المنظومة الحرارية للمبنى والمعرضة لجميع الأحمال الحرارية الخارجية، فهو يتحكم ويسيطر على جميع أساليب السيطرة الحرارية المنظمة للبيئة الداخلية للمبنى وصولاً الى حدود الراحة الحرارية لشاغليه، إذ تحدث خلاله جميع صيغ إنتقال الحرارة من الداخل للخارج والعكس، ومن خلال كفاءته الأدائية تتم السيطرة المناخية بمستوياتها المختلفة داخل المبنى.

- صيغ إنتقال الحرارة في المباني:

تنتقل الحرارة بين المبنى والبيئة المحيطة به من خلال مختلف عناصر ومكونات الغلاف البنائي، حيث يتعرض المبنى يومياً لكافة أنواع الإنتقال الحراري وبأطواره المعروفة والتي قسمت الى (شكل 1):
أطوار الحرارة المحسوسة (Sensible Heat) وصورها الثلاثة، التوصيل الحراري (Conduction) والحمل الحراري (Convection) والإشعاع الحراري (Radiation).
وأطوار الحرارة الكامنة (Latent Heat) بصيغ تحول المادة وصورها، التبخير (Evaporation) والتكثيف (Condensation).



الشكل (1): يوضح الإجهادات الحرارية المسلطة على الغلاف البنائي.
تنظيم الباحثة بالإستناد الى المصدر (Watson & Labs، 1983، ص 4).

أولاً/ أطوار الحرارة المحسوسة (Sensible Heat):*

- التوصيل الحراري (Conduction): وهو عملية إنتقال الحرارة من الجزيئات ذات درجات حرارة عالية الى الجزيئات ذات درجات حرارة منخفضة بالإيصال، حيث تنتشر الطاقة الحرارية عبر جزيئات المادة الواحدة أو جزيئات المواد المتلاصقة أو جزيئات سطحي مادتين متماسين بشكل مباشر (وبدون إنتقال الكتلة) لوجود فرق في درجات الحرارة.

وتنتقل الحرارة في المباني بطريقة التوصيل عبر الجدران والأسقف من الجهة الحارة الى الجهة الباردة بين عناصر المبنى، ومعدل الإنتقال يعتمد على معامل الموصلة الحرارية (Thermal Conductivity) للمواد، ودرجة سُمك (Thickness) عناصر الغلاف البنائي للمبنى. وأحسن المواد الموصلة للحرارة هي المعادن وأردأها الخشب، الاسبستوس (الحرير الصخري)، الغازات، والسيراميك، وهي تدعى بالعوازل الحرارية (Givoni، 1998، ص 110).

- الحمل الحراري (Convection): وهو عملية إنتقال الحرارة ضمن حركة السوائل والغازات وتحدث بسبب إنتقال الحرارة عبر الجزيئات المتحركة للمادة حاملة الحرارة الى مناطق أبعد وذات درجة حرارة أقل، وتستمر دورة الحمل هذه بمزج المائع لإختلاف درجة الحرارة حتى يصل الى التوازن الحراري.

ويحدث الحمل الحراري في عدة حالات منها، عندما تنتقل الحرارة من السطح الصلب الى الهواء المجاور والعكس، أو إنتقال الحرارة بين سطحين في درجات حرارة مختلفة بواسطة إنتقال الهواء (Air Flow) (D. Roos، 2008، ص 1).

- الإشعاع الحراري (Radiation): وهو عملية تحوّل الطاقة الحرارية لسطح المادة الى طاقة إشعاعية بشكل موجات كهرومغناطيسية بسرعة الضوء تنتقل عبر الفضاء حتى تصدم سطح معتم، فيُمتص جزئياً ويُعكس جزئياً، فتزداد إهتزاز جزيئات السطح وترتفع درجة حرارته بسبب الإشعاع الممتص، ومن ثم يشع السطح الحار طاقة أكثر من إشعاع السطوح الباردة حوله، فتنتقل الحرارة بالإشعاع من السطوح الحارة الى السطوح الباردة ويحدث التبادل الحراري لحين الوصول للموازنة الحرارية بين كميتي الطاقة المنبعثة* * والممتصة (D. Roos، 2008، ص 1).

ثانياً/ أطوار الحرارة الكامنة (Latent Heat):***

- التبخير (Evaporation): وفيه تنتقل الحرارة بتغيّر حالة المادة من السائل الى البخار.
- التكثيف (Condensation): وفيه تنتقل الحرارة بتغيّر حالة المادة من البخار الى السائل.

(*) الحرارة المحسوسة: وتمثل تعبير عن درجة الإهتياج الجزيئي لكتلة معينة والحادث بسبب مصادر عدة مثل التعرض للإشعاع، والإحتكاك بين شيئين، والتفاعل الكيميائي، والتماس المباشر مع شئ حار، وبتغيّر درجة حرارة المادة يتغيّر المحتوى الحراري لذلك الشئ (Bradshaw، 1985، ص 13).

(**) يعتمد الإشعاع المنبعث على معامل إمتصاصية السطح وانبعاثيته (Markus & Morris، 1980، ص 45).

(***) الحرارة الكامنة: وتمثل الحرارة التي تغيّر حالة المادة من الصلبة الى السائلة أو من السائلة الى الغازية وبالعكس. (Bradshaw، 1985، ص 13).

ويؤثر بخار الماء في الجو على طبيعة السلوك الحراري لغلاف المبنى، ومن ثم على درجة حرارة سطحه الخارجي، وبالتالي تأثيره على الخصائص الحرارية للغلاف البنائي.

كما يجب دراسة الحرارة الكامنة في الأبنية لأهميتها في حسابات أحمال التبريد في تكييف هواء الأبنية. وبصورة عامة فإن القوة الباعثة (Motive Force) الانتقال الحراري بأي طريقة من الطرق الآتية الذكر هو إختلاف درجات الحرارة بين منطقتين، وأسرع معدل إنتقال حرارة يتحقق مع أكبر إختلاف في درجات الحرارة (كمونة، 2001، ص 14).

ويشير البحث هنا الى أن تعرض المبنى يومياً لكافة أنواع الإنتقال الحراري من توصيل وحمل وإشعاع حراري يعمل على زيادة محتواه الحراري صيفاً ويخفض محتواه الحراري شتاءً، وتقويم سلوك المبنى الصحيح يتم بتوفير أقل كسب حراري صيفاً وأقل فقدان حراري شتاءً، والمتحقق من خلال التصميم الحراري الديناميكي الفعال لغلاف المبنى والذي يمثل أحد مؤشرات أداء التصميم الحراري الكفوء، ومهارة المصمم الذي إعتده.

- مكونات مقطع الغلاف البنائي للمبنى:

يُعرّف غلاف المبنى على إنه الوسيط بين البيئتين الخارجية (والمتمثلة بالمتغيرات المناخية) والداخلية (والمتمثلة بظروف الراحة الحرارية المطلوبة داخل البيئة المبنية) ويتألف من مجموعة من المواد، العناصر، والمركبات البنائية التي بإجتماعها تكوّن الحيّ الفضائي الإجمالي للفعاليات البشرية القائمة فيه (Bradshaw، 1985، ص 77).

ويمثل مقطع الغلاف البنائي للمبنى بمقطع إنشائي بسيط متكون من أربعة أجزاء رئيسية (كمونة، 2001، ص 28):

- السطح الخارجي (External Surface): وهو الجزء الخارجي من الغلاف البنائي المواجه بصورة مباشرة لجميع الأحمال الحرارية للبيئة الخارجية. ويحدث إنتقال الحرارة من وإلى هذا السطح بواسطة الحمل الحراري للهواء، والإشعاع الشمسي من السماء والإشعاع الحراري من السطوح المحيطة به، وإن توجيه السطح يؤثر في معدل نسبة إنتقال الحرارة الى السطح.

- طبقات المادة البنائية (Individual Layers of Construction): وهي ذلك الجزء من الغلاف البنائي الذي يقع خلف السطح الخارجي مباشرةً بإتجاه القطع الإنشائي في الغلاف للداخل. ويشمل جميع الخصائص الفيزيائية الحرارية لمواد البناء من محتواه المتجانس وغير المتجانس، بطبقة أو مجموعة الطبقات المتتالية الترتيب في مقطعه بما توفر من عازلية وسعة حرارية للغلاف. وهو المسؤول عن طبيعة سرعة وشدة نقل التأثيرات الحرارية للسطح الخارجي نحو الداخل وبالعكس. ويعتمد الإنتقال الحراري عبر طبقات المادة البنائية على خصائص المادة وسُمكها.

- الفضاءات الهوائية (Air Spaces) أو الفجوات (Cavities): وهي عبارة عن فراغات هوائية ضمن طبقات المقطع الإنشائي تستعمل لتخفيض فقدان أو الكسب الحراري للمبنى، وتشابه مقاومتها مقاومة أي مادة في المقطع الإنشائي. وتزيد هذه الفضاءات الهوائية من قابلية ضبط مقدار المقاومة لمقطع الغلاف البنائي وتقلل الحرارة بين الفضاءات عبرها بواسطة الحمل الحراري والإشعاع، وتزداد فاعلية العزل الحراري للفجوة الهوائية كلما قل سُمكها أو تعددت طبقاتها واحتوت جدرانها الداخلية على عاكس حراري مشع كصفائح الألمنيوم.

- السطح الداخلي (Internal Surface): وهو الجزء الداخلي من الغلاف البنائي المواجه بصورة مباشرة تأثيرات التغيرات الحرارية الحاصلة في البيئة الداخلية لفضاءات المبنى والتي تُدعى بدرجة حرارة البيئة الداخلية والمتمثلة بدرجة حرارة الهواء، والرطوبة النسبية، ومعدل درجة حرارة السطوح الداخلية المشعة، والتحرك الهوائي.
- وتؤكد الدراسة هنا الى ان الانتقال الحراري يحدث عبر غلاف المبنى بسبب إختلاف درجات حرارة السطحين الخارجي والداخلي للغلاف، فتنتقل الحرارة من السطح ذي الدرجة الحرارة الأعلى الى الأوطأ، وإعتماداً على الإنتقالية الحرارية بين السطحين (Thermal Transmittance) والتي تأخذ شكلين أساسيين هما الكسب الحراري من خارج المبنى الى داخله والفقْدان الحراري من داخل المبنى الى خارجه وصولاً الى الموازنة الحرارية بين البيئتين الداخلية والخارجية.
- وكفاءة أداء الغلاف البنائي الذي يقوم بدور المنظم والصمام الحراري بين البيئتين الخارجية والداخلية للمبنى تتحقق من خلال تصميمه الصحيح الذي يضمن توفير درجات حرارة ملائمة داخل فضاء المبنى وتقليل الحمل الحراري المرتبط مباشرةً بعمليات الكسب والفقْدان الحراري عبر مكونات الغلاف البنائي.

- استراتيجيات السيطرة المناخية في المباني:

تُستخدم عدة وسائل لأغراض السيطرة الحرارية في التصاميم المناخية وتختلف من حيث التقنية المستعملة التي تخضع جميعها لتصنيف عام يضم: الوسائل الفعّالة (Active Methods) الوسائل الذاتية (المنفعلة) (Passive Methods) بحسب إعتمادها على استحضارات تشغيل المنظومة الحرارية للمبنى، كونها أنظمة مفتوحة تعتمد كلياً أو جزئياً على وجود مصدر طاقة محرك لها وتتشغل بعدم توفره، أو كونها أنظمة مغلقة تعتمد كلياً على ذاتها في إستغلال بعض الظواهر الطبيعية الناجمة عن حدوث الدورة الحرارية للمناخ، كطاقة تتزود بها لغرض التشغيل وهي لا تحتاج غالباً لأعمال الصيانة والمتابعة. ويعتمد كلاهما على استراتيجيات السيطرة المناخية والمتمثلة بمبادئ العمل الأساسية في ترصّد فرص السماح أو المنع للإنتقال الحراري عبر الوسيطين (البيئة الداخلية للمبنى والمحيط الخارجي) وحسب التوقع الزمني للدورة المناخية اليومية والسنوية (كمونة، 2001، ص 20).

ففي موسم الشتاء البارد يكون هدف المهندس المعماري تقليل الفقْدان الحراري (Minimize Heat Loss) من بيئة المبنى الداخلية الى المحيط الخارجي ومحاولة السماح للكسب الحراري (Promote Heat Gain) العكسي من الخارج الى الداخل، وبنعكس الحال في موسم الصيف الحار، فيعمل المعماري على محاولة زيادة الفقْدان الحراري (Promote Heat Loss) من داخل المبنى الى الخارج وتقليل الكسب الحراري (Minimize Heat Gain) المعكوس. وبهذه الفكر الأساسية فإن جميع وسائل السيطرة المناخية تخضع في عملها لتلك القاعدة. ويُطبق نفس المبدأ المذكور في الدورة اليومية للطقس بين ساعات الليل والنهار (Watson & Labs، 1983).

ويؤكد البحث هنا بأنه يمكننا تشبيه المبنى بكائن حي يتفاعل مع البيئة المحيطة من خلال سلوكه الحراري إذ يؤثر فيها وتؤثر فيه، ولتحقيق معادلة التوازن الحراري أعلاه يجب أن يصمم المبنى بطريقة مرنة

ومن خلال غلافه البنائي الذي له الدور الأساس في عمليات السيطرة الحرارية للبيئات الداخلية للمبنى، ويمتاز الغلاف البنائي بديناميكية ومرونة عالية وتغير مستمر والتي تحدث كرد فعل واستجابة للتأثيرات المناخية الخارجية والمتقلبة في المناطق الحارة - الجافة، وصولاً لتخفيض الأحمال الحرارية المسلطة على المبنى، ومن ثم تحقيق أقصى حالات الراحة الحرارية في بيئته الداخلية، وبالتالي يكون إستعمال التكيف الصناعي في المبنى عنصراً مكماً وثانوياً وإقتصادياً عند تطبيقه.

- الغلاف البنائي الديناميكي للمبنى في المناطق الحارة - الجافة:

إن الأبنية عموماً يُنظر إليها كمنشآت ثابتة، في حين يمكن للغلاف البنائي أن يكون ديناميكياً (Dynamic) فهو يتميز بفاعلية مستمرة وحساساً لتغير المتطلبات والظروف البيئية المحيطة به، فيسمح أحياناً بدخول الحرارة، والضوء، والهواء، والصوت، وأحياناً أخرى يحجب هذه المصادر البيئية الخارجية. وكل عنصر في غلاف المبنى يعمل كحاجز مستقر (Static Barrier) (مثل الجدران العادية أو المألوفة) وكعنصر تحوّل أو إنتقال (مثل النوافذ والأبواب)، أو كمنظم معدل (مثل الكاسرات الشمسية والأقنعة المتحركة). وفي أوقات الظروف المزعجة وغير المرغوب بها، فإن غلاف المبنى الملائم يكون بهيئة حاجز مستقر، بينما في الظروف المناخية المرغوبة أحياناً، وغير المرغوبة أحياناً أخرى، يُفترض في الغلاف البنائي أن يكون ديناميكياً يمكن ضبطه والتحكم فيه، فيصبح ببساطة إطار بنائي مفتوح (Open Structural Frame)، فيسمح بالتعديل في درجة الفصل بين البيئتين الخارجية والداخلية، حينها يكون كالصدفة الوقائية. وبهذا فإن أغلفة المباني يُفترض أن تكون ديناميكية، فكلما زادت ديناميكيته زادت ملائمتها للظروف المناخية المختلفة (Bradshaw, 1985، ص 77).

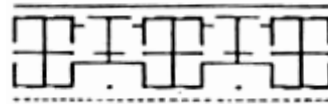
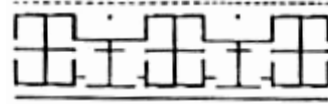
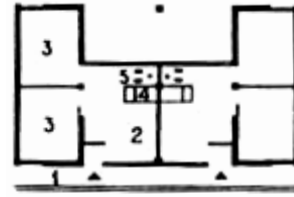
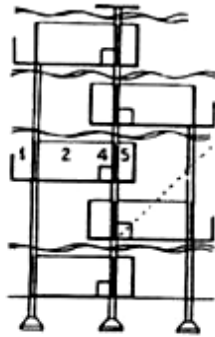
ومن الأمثلة على الأغلفة الديناميكية للمباني في المناطق الحارة - الجافة ما يأتي:-

- **الفضاء الصيفي:** وهي عبارة عن فضاء يتوسط بين خارج المبنى وداخله ويتميز بكونه مرناً ومظللاً وقابلاً للسد والفتح حسب رغبة شاغلي المبنى، ومهمته الأساسية رفع الأداء الوظيفي والمواصفات الصحية لشاغلي المبنى في المناطق الحارة - الجافة. ويعمل هذا الفضاء على شحن البرودة أثناء الليل ليغذي جميع الفضاءات المجاورة له في أوقات الظهيرة الحارة. وقسمت إحدى الدراسات الفضاء الصيفي بدلالة نسبة انفتاحه على الجو الخارجي وعدد الأيام الحارة خلال السنة إلى (شاهين، 1990، ص 1، 3، 7) (شكل 2):
 - أ- النظام المفتوح (المناطق التي تكون فيها عدد الأيام الحارة جداً خلال السنة أقل من 45 يوماً)، وهو الربط الفضائي المباشر مع المحيط الخارجي ومثال عليه الشرف والبالكونات.
 - ب- النظام نصف المفتوح (المناطق التي تكون فيها عدد الأيام الحارة جداً خلال السنة بين 45 - 60 يوماً)، وهنا تكامل تام بين الطرق الطبيعية والطرق الميكانيكية في السيطرة على مايكرومناخ الفضاء الصيفي، فيتم فتح الفضاء الصيفي على الخارج بواجهة أو واجهتين متعامدتين، ويكون عميقاً وأساسياً في الهيكل الإنشائي للمبنى، وجدرانه الداخلية هي نفس جدران الغرف المتاخمة له، والتي يجب أن

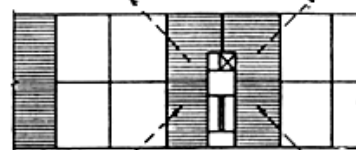
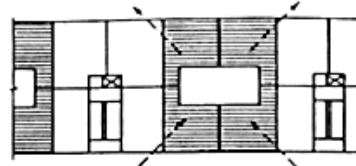
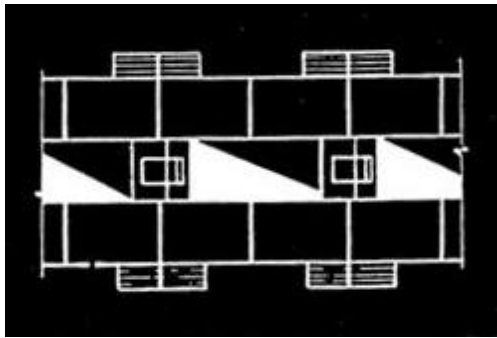
تحمل كافة المواصفات المناسبة للعزل الحراري. وقد يُفَتَّح الفضاء الصيفي من الداخل على فجوة هوائية عمودية لتأمين عملية التهوية في الأوقات المناسبة.

ج- النظام المغلق (المناطق التي تكون فيها عدد الأيام الحارة جداً خلال السنة بين 60 - 100 يوماً)، ويكون الفضاء الصيفي فيه عميقاً ومنغلقاً على نفسه داخل المبنى ومحاطاً بالفضاءات الأخرى، وعادةً ما يُفَتَّح على فجوة هوائية عمودية أو منور داخلي للحصول على التهوية العمودية في الأوقات المرغوب فيها.

ويؤكد البحث هنا إن ما يعنينا هنا هو الفضاء الصيفي ذو النظام نصف المفتوح وذو النظام المغلق على أن تزود هذه الفضاءات بجدار متحرك ذاتي الحركة (أوتوماتيكي) يُغلق في الأوقات المزعجة وغير المرغوب فيها ليحقق الديناميكية المطلوبة لغلّاف المبنى.



(أ) النظام المفتوح للفضاء الصيفي: تصميم مقترح لمبنى سكني في مراكش، حيث احتوت كل وحدة سكنية فيه على شرفة كبيرة يارتفاع طابقين، متصلة مع بعضها عمودياً ومتبادلة في التوجيه ومحاطة بجدران صماء تمنع الشرفية.



(ج) النظام المغلق للفضاء الصيفي.

(ب) النظام نصف المفتوح للفضاء الصيفي.

الشكل (2): أنظمة الفضاء الصيفي.

المصدر: (شاهين، 1990، ص 6، 9).

• الكاسرات والأقنعة المتحركة:

من الحلول المرنة التي توفر ديناميكية عالية للغلاف البنائي للمبنى هو استخدام الكاسرات الشمسية المتحركة التي تغطي النوافذ من الخارج مع ترك مجال هوائي بين الكاسرة والواجهة للحصول على تحرك هوائي ضمن هذا المجال وما يترتب على الكاسرة من تحمل العبء الأكبر من الأشعة الشمسية الساقطة عليها، وبالتالي الطاقة الحرارية العالية، وبهذه الحالة يتم الحصول على إيجابية مناخية في عملية السيطرة على الأشعة الشمسية وحجبها في الأوقات التي تحمل فيها طاقة حرارية عالية إضافة إلى المشاكل الضوئية. وبذلك تتوفر كفاءة عالية في الاستخدام وديناميكية تصميمية عالية (كمونة، 2001، ص 20 - 21).

ويؤكد البحث هنا على ضرورة أن تكون الكاسرات ذاتية الحركة (أوتوماتيكية) تُغلق وتُفتح وفقاً لحركة الشمس والحاجة إليها، ويفضل أن تكون من مواد خفيفة الوزن (سعة حرارية واطئة).

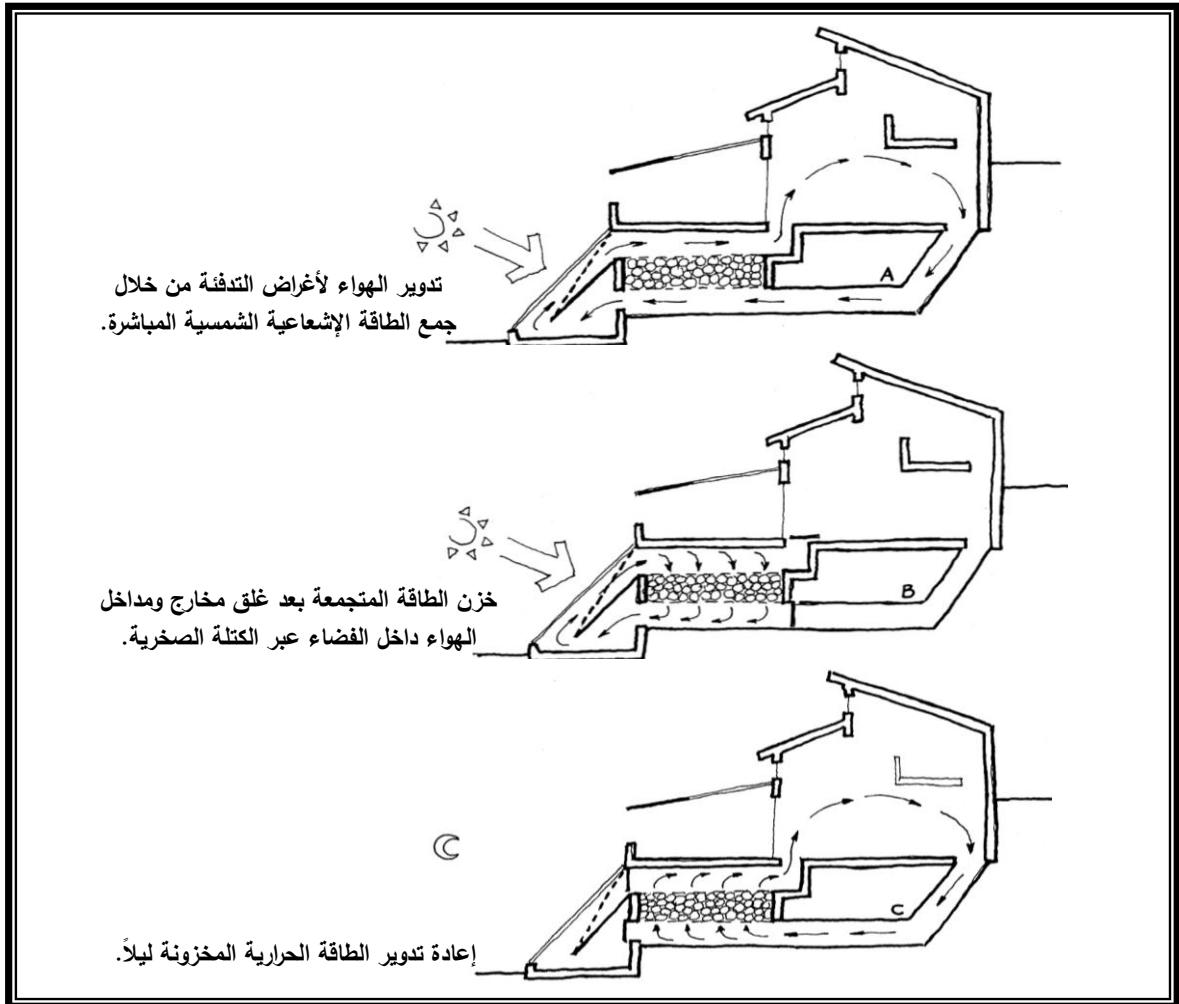
- جدار الحلقات الحَمَلِيَّة (Wall Convective Loops) أو منظومة ستيف باير (Steve Baer System): وتقنيته تعتمد على وجود صندوق صخري أو حصى يخزن الحرارة، ففي الأيام المشمسة يرتفع الهواء الحار خلال المَجْمَع (Collector) ويدخل الى صندوق الحصى ثم يتدفق الى الأعلى عبر أرضية المبنى بواسطة أجهزة تحكم دخول الهواء (Registers)، ثم يرجع الهواء الى المَجْمَع من خلال أنبوب (Duct). وفي الحالات التي لا يحتاج المبنى فيها الى تدفئة ينتقل الهواء للأسفل خلال الصخر فيفقد حرارته عندما يدفئ الصخر، ثم يرجع الهواء لأسفل المَجْمَع. أما في الليل فالمرطب بين الجامع وصندوق الصخر يغلق لمنع التدفق (شكل 3).
- (شكل 4) يوضح مسكن لـ (P. Davis) في ولاية (Albuquerque) الواقعة في نيوميكسيكو، يستخدم منظومة بارا، والمسكن تصميم المعماري (Mark Jones) (Givoni، 1998، ص 167-168).
- (شكل 5) يوضح مثال كحالة دراسية لمسكن في مدينة سانتا في نيوميكسيكو، وهنا يدخل الهواء الى حيز منعزل عن البناء يشبه اللاقط أو المجمع الشمسي بإتجاه الجنوب وينتقل منه الدفء طبيعياً للأعلى ليدخل شبكة القنوات أسفل البناء ثم يصعد عمودياً في جدران الخزانات الحرارية الممتلئة بالحصى، تنتشع بالدفء وتتشع على ما حولها بجدران ذات تشعع عالي. وهذه الطريقة بمجملها تؤمن التدفئة والتهوية وتسخين الماء (في منطقة المجمع الشمسي)، كما يوظف هذا المثال الجدار الترومبي (جدار حراري معتم ففراغ فزجاج) ويمكن استخدام المجمع الكهروضوئي لأغراض تحويل الطاقة الشمسية الى طاقة كهربائية لأغراض التبريد والإنارة، وكذلك أدخل المصمم الحيز الزجاجي الأخضر في التصميم، وبهذا فإنه وظف طرق التصميم الطبيعي أيضاً مع التقنية لجعل التصميم ديناميكياً لتأمين التوازن الحراري (سلقيني، 1997، ص 52 - 53).
- ويعقب البحث هنا الى ان المثال الأخير المذكور يؤكد على ضرورة تواجد البناء قرب منحدر لوضع المجمع الشمسي، ولتوظيف نفس الأسلوب في مناطقتنا الحارة - الجافة التي غالباً ما تخلو من المنحدرات يشير البحث هنا الى أهمية استخدام الأسطح المائلة أو رفع المبنى وتوظيف المجمع الشمسي فيه كأن يكون في مستويات أعلى في المبنى وإتجاه الجنوب.

منظومة بارا (Barra System):

هذه المنظومة تعتمد على توجيه جدار في المبنى نحو الجنوب يحتوي على خازن حراري (Thermosyphonic) وجامع إشعاع شمسي يسخن الهواء. ينشأ الهواء الساخن في جدار جامع معزول يجري الهواء به أفقياً داخل قنوات مطمورة في السقف الكونكريتي (والتي تعمل أيضاً كمخزن حراري). جزء من الحرارة قد تُخزن في السقف الكونكريتي في حين يبقى الهواء الدافئ في القنوات الموجودة في النهاية الشمالية للمبنى، لذا فإن الهواء يُسخن الغرف البعيدة أولاً قبل رجوعه عبر فضاء المبنى الى المداخل الموجودة في الجزء السفلي من الجدار الجامع المواجه للشمس (شكل 6).

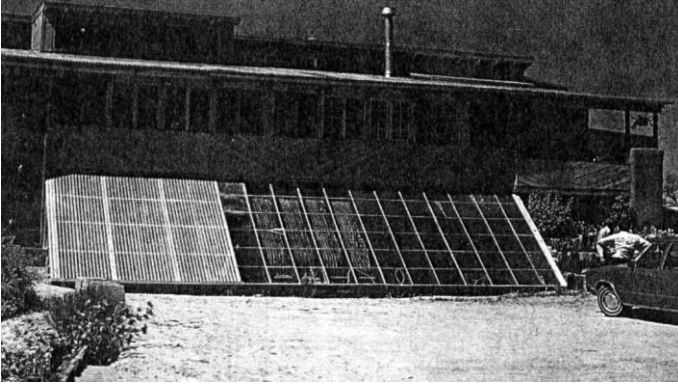
وترجع أهمية هذه المنظومة الى كونها توزع الحرارة خلال كامل المبنى بصورة متساوية، علاوة على إمكانية إستعمالها في المباني المتعددة الطوابق وحتى في المباني التي فضاءاتها الأساسية غير موجهة للشمس وهنا تُستخدم مؤخرة المبنى أو الجهة الجنوبية من المبنى المواجهة لجدار المجمع، لكون الجزء الأساسي من حرارة الشمس تنتقل أولاً بواسطة الحمل الحراري للجهة الشمالية من المبنى (Hardy، 2008، ص 13).

و(شكل 7) يوضح مسكن مؤلف من طابقين للمهندس (Constantini) والواقع في إيطاليا، مستخدماً منظومة بارا (Givoni، 1998، ص 169-171).



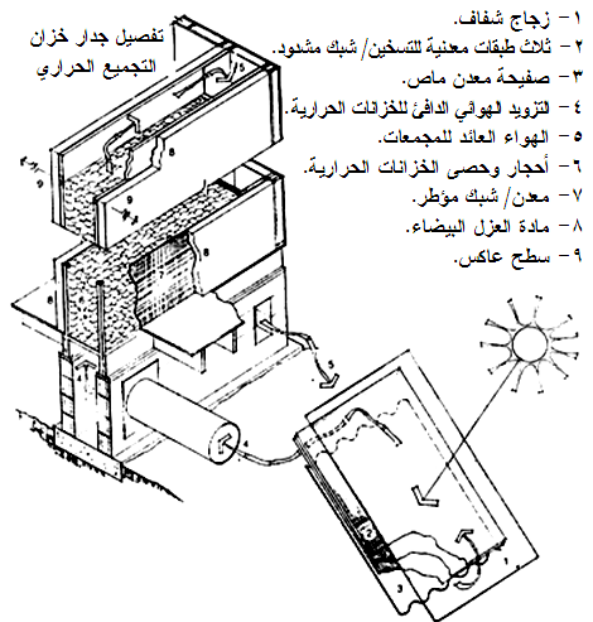
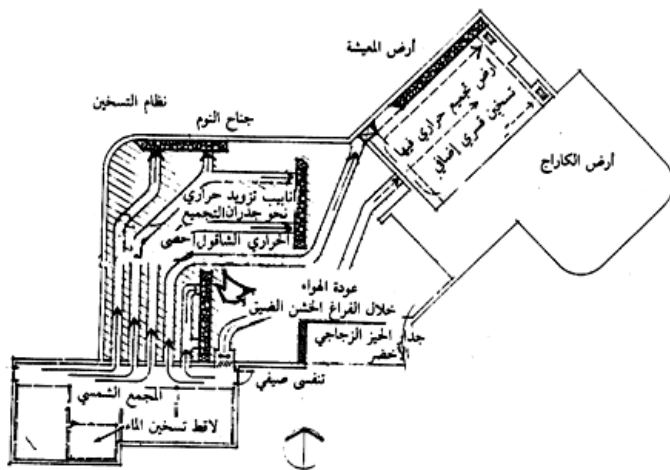
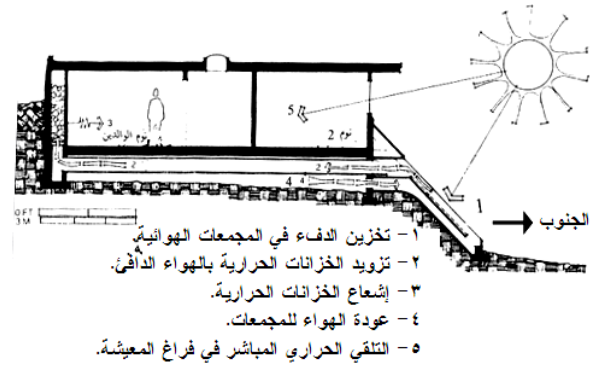
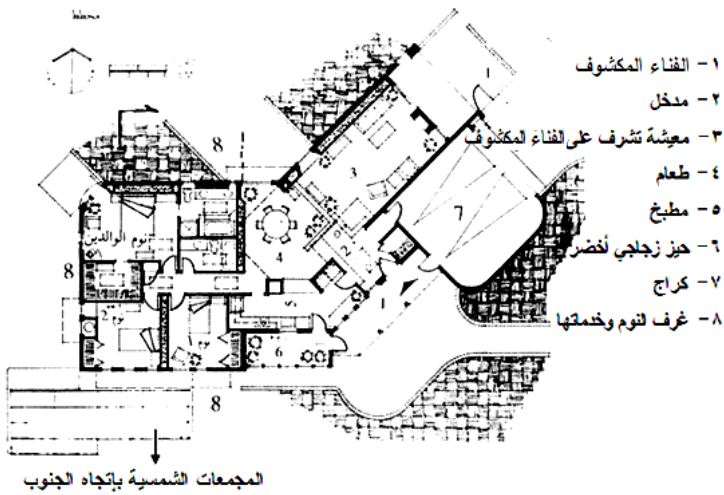
الشكل (3): يوضح منظومة (Steve Baer).

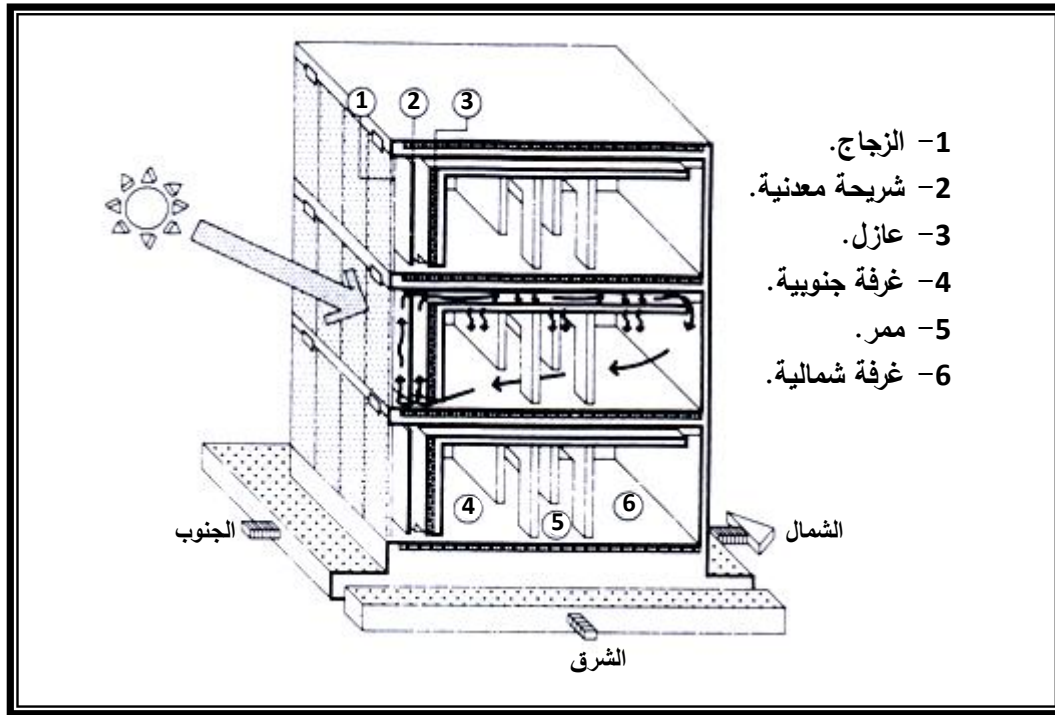
المصدر (Givoni، 1998، ص 166).



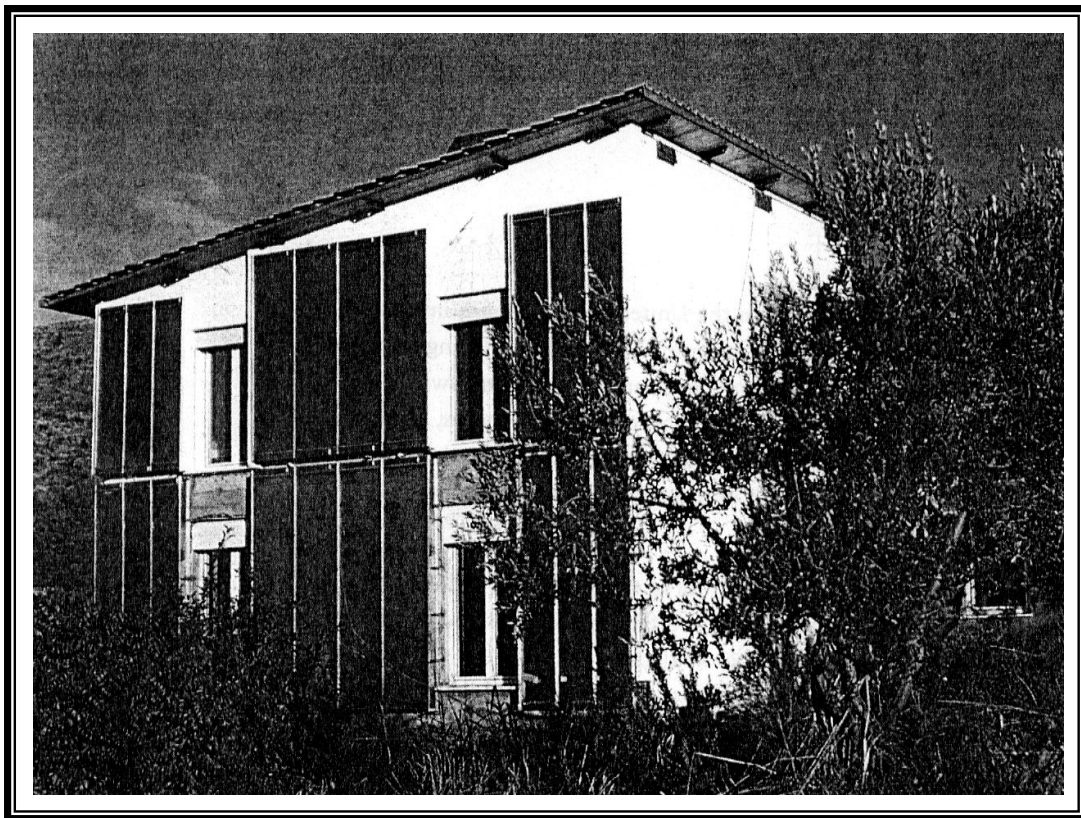
الاسلوب المنفعل في التصميم الشمسي

الشكل (4): مسكن (P. Davis) في (Albuquerque) الواقعة في (New Mexico) والذي يستخدم منظومة (Steve Baer) تصميم المعماري (Mark Jones).
المصدر (Givoni، 1998، ص 167).





الشكل (6): منظومة بارا (Barra System).
المصدر: (Givoni، 1998، ص 169).



الشكل (7): مسكن المهندس (Constantini) في إيطاليا، مستخدماً منظومة بارا (Barra System).
المصدر: (Givoni، 1998، ص 170).

● **السقف المائي:** وهذا الأسلوب يعتمد على وصول الدفء نهار الشتاء، وانتشار الحرارة الى خارج المبنى صيفاً عبر فتح السقف المنزلق والذي يمنع بإغلاقه الدفء من الضياع شتاءً وبصدده عن الدخول صيفاً، ويقوم عامةً بدوران الخزان الحراري المتوازن. وهذه الطريقة تعتمد على السطح المائي تتمتع بدناميكية عالية في التوجيه والتحكم الحراري حسب الطقس مما يجعل منها أسلوباً كفوءاً في مجال التوازن الحراري.

و(شكل 8) يوضح مثلاً لمسكن يحتوي على سقف مائي، يقع المسكن في ولاية أريزونا الحارة - الجافة في الولايات المتحدة الأمريكية والمصمم من قبل المعماري جيلفورد دراند وشركاه. وهنا إتخذ البناء قوامه الخارجي والداخلي ليتلاءم وظروف المناخ الحار - الجاف من خلال إستجابته لعملية الإنسجام المرن مع كل التقلبات المناخية بإيجاده السطوح المتوازنة المتعددة والتي هي عبارة عن:

أ- الجدران: صممت سماكتها الإجمالية لتصل (61 سم) فيها (7,5 سم) طبقة خارجية خشنة أشاعت الظلال الجزئية في السطوح مما رفع من عازليتها للحرارة، مع وجود عازل حراري (7,5 سم)، وهذه الجدران مناسبة لموسمي الشتاء والصيف.

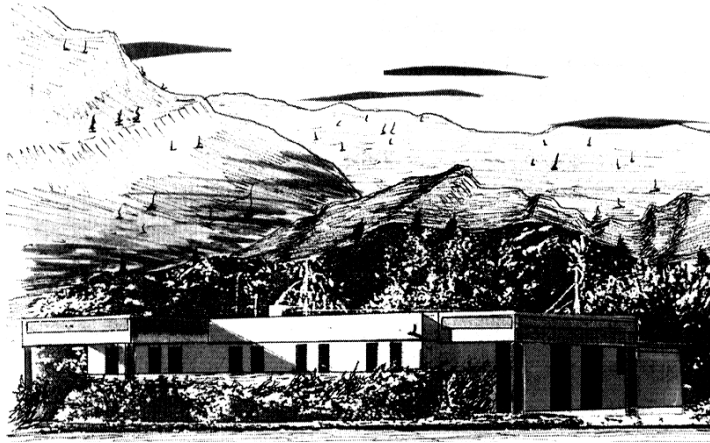
ب- السقف: وسماكته العامة وديناميكيته التي حققها في إنفتاح وإنغلاق السقف العلوي (ذو قطع متزحقة) بواسطة محرك صغير، جعلته يصل الحدود القصوى في مجال تحقيق التوازن الحراري المنشود، حيث يُغلق السقف نهاراً في الأوقات الحارة (صيفاً) ويُفتح ليلاً، بينما يُفتح السقف نهاراً في الأوقات الباردة (شتاءً) ويُغلق ليلاً.

ج- الإجراءات الأخرى: وقد إتبعها المصمم في التفاصيل والمواد والتوزيع الوظيفي، للوصول للتوازن الحراري

وفي هذا المثال تضافرت إجراءات أخرى من طرق التصميم الطبيعي إضافة للتقنيات المستخدمة فيه لرفع مردودية النتائج المناخية كالإقلال من الفتحات وحمايتها وجعلها عميقة في الجدران السميكة، فضلاً عن التوزيع الوظيفي الملائم الواجب أن يصب أيضاً في معادلة التوازن الحراري، حيث ان جناح النوم معزول عن الجهة الغربية بواسطة شريط كامل من الخدمات (سلفيني، 1997، ص 44 - 45).

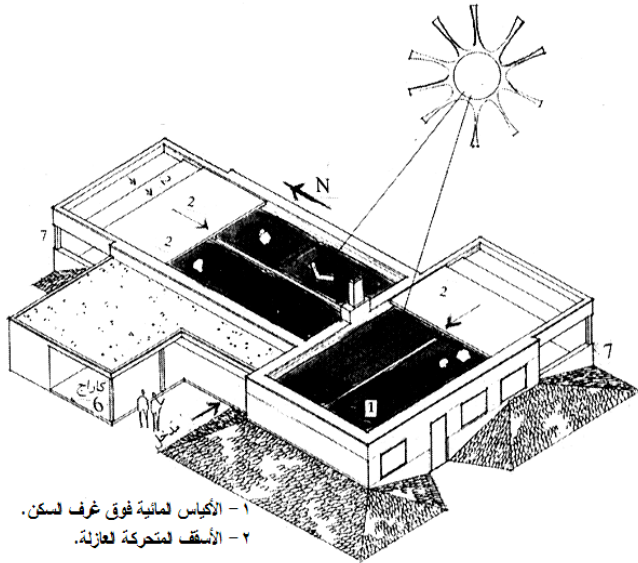
ويُعقب البحث على هذا المثال، انه يشكل خطوة هامة في آفق العمارة الديناميكية لما يتمتع به من حلول وظفت طرق التصميم الطبيعي والتقنيات بأسلوب فعال عبر حلول مرنة وإمكانية تطبيقها تفيد المناطق الحارة - الجافة. ويضيف البحث بعض التحفظات في استخدامات السقف

المائي في ظروف العراق المحلية، وذلك لشحة المياه وسرعة تبخرها فضلاً عن الملوحة العالية فيها.

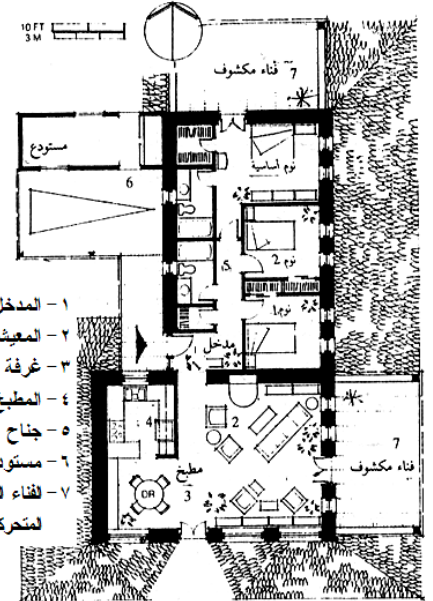


(1)

منظور خارجي للمسكن



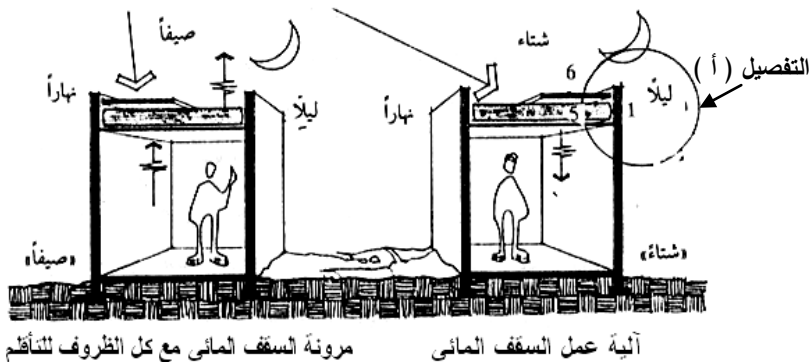
- ١- الأكياس المائية فوق غرف السكن.
- ٢- الأسقف المتحركة لعازلة.



- ١- المدخل.
- ٢- المعيشة.
- ٣- غرفة الطعام.
- ٤- المطبخ.
- ٥- جناح النوم وملحقاته.
- ٦- مستودع وكراج.
- ٧- فناء مكشوف الذي يغطي أحياناً بالأسقف المتحركة شتاءً-نهلاً و صيفاً-ليلاً.

منظور خارجي من الأعلى يوضح السقف المائي

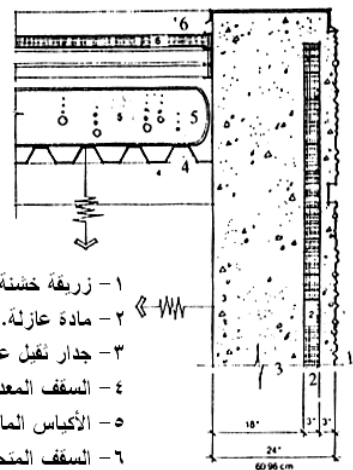
مخطط الطابق الأرضي



مرونة السقف المائي مع كل الظروف للتأقلم

آلية عمل السقف المائي

مقطع



- ١- زريقة خشنة.
- ٢- مادة عازلة.
- ٣- جدار ثقيل عازل.
- ٤- السقف المعدني.
- ٥- الأكياس المائية.
- ٦- السقف المتحرك العازل.

مكبر التفصيل (أ)

ويضيف البحث إمكانية أخرى للأغلفة البنائية الديناميكية للمباني وهي توظيف مفهوم الفناء بأسلوب معاصر، إذ يعيدنا الفناء في العمارة التقليدية الى السلوك الحراري المتوازن للمبنى حيث ينتقل المحتوى الحراري للمبنى من الخارج الى الداخل وبالعكس عبر هذا الفناء وبإختلاف درجات الحرارة اليومية والفصلية في المناطق الحارة - الجافة، إذ يتم هذا الإنتقال وفق قوانين علم الإنتقال الحراري مما يخفض درجات الحرارة داخل المبنى عن الخارج صيفاً والعكس شتاءً، الأمر الذي جعل المبنى أكثر إستقراراً وأقل إستهلاكاً للطاقة، وبالتالي يمكننا إستخدام مفهوم الفناء في العمارة الحالية بأسلوب معاصر فيبقى الفناء مفتوحاً صيفاً ويُغلق شتاءً، ويبقى مفتوحاً خلال ساعات النهار ومغلقاً طوال ساعات الليل لمختلف المواسم، ويتم ذلك بإضافة تقنية السقف المتحرك والتي يمكن إنشاءها من سقف مادته الإنشائية مؤلفة من طبقتين من الزجاج والحديد، وطبقة كاسرات متحركة دائرياً وذلك نظراً لإمكانية الزجاج العالية في نقل الحرارة والتي يمكن زيادة كفاءته أيضاً بإستخدام الزجاج الذي تتغير فيه درجة التعقيم حسب وهج الشمس، فضلاً عن إمكانية استخدام كاسرات شمسية دوراة قابلة للسد والفتح وحسب الحاجة، وبالتالي نحصل على فائدة إضافية في الكفاءة المناخية لسقف الفناء المتحرك هذا.

وهنا يؤكد البحث إن هذا التوجه يولد مفاهيم جديدة للمعماريين والعمارة والتي تؤدي بدورها الى ظهور طرز معمارية جديدة لعصر تفاعلي بين المبنى والبيئة المحيطة به والذي تُقاس فيه العمارة بمدى كفاءة مبانيها وإحترامها لبيئتها المحيطة. هذه العمارة ستعبر عن بيئات متنوعة بحيث تصبح مبانيها تفاعلية متغيرة وليست ثابتة المحددات، حيث ديناميكيته تساعد في التغير بتغير الظروف المناخية على مدار العام، ومن ثم إحترامها لذاتها من خلال توفيرها أقصى حدود الراحة الحرارية لشاغلها، وإحترامها لبيئتها المحيطة من خلال أقل إستنزاف للطاقة وعلاقتها التبادلية المتوازنة حرارياً مع البيئة المحيطة بها.

كما يجد البحث من كل ما قد سبق ذكره، ضرورة الجمع بين طرق التصميم المناخي الطبيعي وبين التقنيات الحديثة (بشكل مبسط) في أغلفة المباني الديناميكية كي تكون الحل الملائم لتقلبات المناخ في المناطق الحارة - الجافة، هذا من ناحية، ومن ناحية أخرى تواكب عمارة الحاضر حيث انها تحمل أصالة الماضي وروح الحاضر وبهذا تضمن لها الاستمرارية والتواصل للمستقبل.

الإستنتاجات:

- إن الأغلفة البنائية الديناميكية للمباني هي الحل الأمثل خصوصاً في المناطق الحارة – الجافة ذات التباين الكبير اليومي والفصلي في درجات الحرارة، إذ تعمل الأغلفة البنائية الديناميكية على تشكيل فائدة إضافية في إيجاد نوع من المرونة للسكان في السيطرة على بيئاتهم الداخلية، لكونها أغلفة طيعة ومتكيفة مع البيئة المناخية المحيطة.
- إن النظرة الشمولية لعملية التوازن الحراري والمتحققة من خلال ديناميكية الأغلفة البنائية لمباني المناطق الحارة – الجافة تمت من خلال إستيعاب مبادئ العمارة التقليدية في تكيفها مع المناخ مع توظيف التكنولوجيا الحديثة، وصولاً الى شمول في الرؤيا لبيتنا العمرانية لضمان استمراريته ومواكبتها للحاضر، ومن ثم تطورها لتعميق دورها الحضاري من خلال أصالة وثبات جذورها فضلاً عن إنفتاحها للتقنيات والعلوم الحديثة.
- أن الأبنية الديناميكية تجمع بين التصميمين الطبيعي والتقانة الذكية ومن ثم تكون كلفة انشائها أقل من الأبنية الذكية العالية الكلفة، وبنفس الوقت توظف التكنولوجيا الحديثة بأسلوب مبسط.
- إن العلاقة بين العوامل المناخية والأغلفة البنائية للمباني هي علاقة تبادلية ديناميكية متوازنة يؤثر ويتأثر كل منهما بالآخر.
- تصميم أغلفة المباني في المناطق الحارة – الجافة يجب أن يكون نابعاً من تحقيق أعلى توازن حراري بين متطلبات الفترة الحارة والفترة الباردة.
- جميع مظاهر الجهد الحراري تشترك بنسب متباينة تبعاً للزمان والمكان في التأثير على درجة حرارة السطح الخارجي للغلاف البنائي للمبنى، ومن ثم التأثير على طبيعة سلوك الانتقال الحراري عبر الغلاف البنائي، وبالتالي فإن اعتماد منهجية التصميم المناخي تُعد من الإعتبارات الأساسية للوصول الى ظروف حرارية ملائمة للبيئة الداخلية للمبنى.
- إن استنباط الأسس والمفاهيم التي تتم بها عملية التوازن الديناميكي للغلاف البنائي وطبيعة سلوكه الحراري مع الظروف المناخية المحيطة هو الأساس لإنشاء أغلفة بنائية كفوءة حرارياً، والمؤدية الى التقليل من استخدام الوسائل الميكانيكية لأغراض التدفئة والتبريد.

المصادر

المصادر العربية:

- سلقيني، د.محي الدين، "العمارة والبيئة"، دار قابس للطباعة والنشر والتوزيع، سوريا، 1997م.
- شاهين، د.بهجت رشاد، "مفهوم الانتقال الحراري عبر القشرة الخارجية للمبنى والجدران الخفيفة المصنعة"، دورة العمارة والمناخ في المناطق الحارة – الجافة، (26 – 28)، شباط، 1990م.
- شاهين، د.بهجت رشاد، "الفضاء الصيفي في السكن متعدد الطوابق"، دورة العمارة والمناخ في المناطق الحارة – الجافة، (26 – 28)، شباط، 1990م.
- كمونة، غادة محمد اسماعيل عبد الرزاق، أثر البيئة الطبيعية على مفهوم التشكيل العمراني في المناطق الحارة – الجافة، رسالة ماجستير مقدمة الى قسم الهندسة المعمارية، جامعة بغداد، 2001.

المصادر الأجنبية:

- Bradshaw, Vaughn, "Building Control System", John Wiley & Sons, 1985.
- D. Roos, Carolyn, "Principles of Heat Transfer", Energy Efficiency Fact Sheet, Extension Energy Program, Washington State University, Washington, U.S.A, Version 1.1, March, 2008.
- Givoni, Baruch, "Climate Consideration in Building and Urban Design", Van Nostrand Reinhold, U. S. A., 1998.
- Hardy, Mike, "A Practical Guide to Free Cooling, Alternative Cooling, Night Cooling and Low Energy Systems for Air Conditioning Systems", Ambthair Services Ltd, 2008.
- Watson, Donald, FAIA & Labs, Kennth, "Climatic Design", Mc Graw-Hill Book Company, 1983.



DOWEL ACTION BETWEEN TWO CONCRETES

Husain M.Husain

Nazar K. Oukaili

. Hakim S. Muhammed

University of Baghdad, Iraq.

University of Baghdad, Iraq.

Najaf, Iraq

ABSTRACT

This paper reports eight tests in which in-plane shear forces are applied across the joint between two different concretes forming a composite action. Shear can be transmitted across the joint either by interlocking of the aggregate particles protruding from each face or by shearing of the reinforcement crossing the joint. Tests are conducted on initially cracked specimens by depending only on dowel action. The results of the tests are compared with theoretical results of the exponential equation presented by Millard and Johnson. The computer program of Al-Shaarbaaf using the nonlinear behavior of concrete is used to perform the analysis with inclusion of the exponential equation for dowel action in the interface layer. The program uses 20-node brick elements with embedded bar elements. This program is also applied to Hofbeck et al. tests. The comparison shows that the experimental and the analytical results give good agreement where the difference between the two is between (2.5-5)% . The use of the exponential equation gives good results when the concrete is assumed to be initially cracked as in construction joints.

الفعل الوتدي بين خرسانتين

الخلاصة

تم إجراء ثمانية فحوص سلطت فيها قوى القص عبر الشق أو الشرخ الموجود بين خرسانتين مختلفتين مكونتين للفعل المركب. يمكن نقل القص عبر الشق أما بتداخل حبيبات الركام البارزة من كل من وجهي الشق أو من خلال التسليح العابر للشق. أجريت الفحوص على نماذج متشققة ومعتمدة فقط على الفعل الوتدي. قورنت نتائج الفحوصات مع نتائج نظرية لمعادلة أسية قدمت من قبل ميلارد وجونسون. ولغرض إجراء التحليل الأنشائي فقد تم استخدام برنامج الشراباف الآخذ بنظر الاعتبار ا

السلوك اللاخطي للكونكريت وبالاعتماد على المعادلة الأسية للفعل الوتدي للطبقة البينية. تم تطبيق البرنامج الذي يستعمل عناصر طابوقية ذات 20 عقدة مع عناصر قضبان مطمورة على فحوصات هوفبك وجماعته. قورنت النتائج التحليلية الحالية مع نتائج فحص هوفبك وجماعته وقد أعطت النتائج العملية والتحليلية مقارنة جيدة. أن أستعمال المعادلة الأسية يعطي نتائج للطبقة البينية يعطي نتائج جيدة فقط حينما تكون الخرسانة متشققة مسبقا كما في المفاصل الإنشائية.

KEYWORDS

Composite construction, Construction joints, Shear transfer, Dowel action.

INTRODUCTION

When two concretes one over the other are cast at different times, a construction joint will exist. The medium which is separating the two dissimilar concretes during the assemblage of precast and cast – in - place

concrete in composite construction is called interface. The highly stressed interface is a potential failure plane, through which shear stress is transferred, and direct shear failure may occur. Therefore an adequate reinforcement across such a plane must be provided to prevent such type of failure. Because of the external tension, shrinkage, or accidental causes a crack may form along such a plane even before shear occurs (13). Therefore the design approach should consider the interface shear capacities for both the initially uncracked and initially cracked concrete. It is commonly believed that a distinct difference exists in shear transfer behavior between initially uncracked and cracked specimens. The present work chooses the initially cracked model of interface because it is well believed that initially cracked specimens are governed largely by the shear- slip characteristics of the cracked plane (14). The interface area between different concretes in composite structures represents an unknown medium especially in shear transfer phenomenon. Therefore so many studies were done in this region especially the tests which were done by Grossfield and Birnstiel (7) on T-beams with precast webs and cast-in-place flanges. The other difficulty is how to model the behavior of concrete under the existence of cracks and the assumption of initially cracked or uncracked specimen. However, Table (1) shows the available models used to represent shear transfer through interfaces in initially cracked or uncracked interfaces.

When load is applied, slip occurs between the two surfaces of concrete especially when there is no enough reinforcement bars connecting them together. The shear transfer is done by two mechanisms: aggregate interlock and dowel action (12). In an initially uncracked model most of the shear force is carried by aggregate interlock (6). In an initially cracked model, the



predominant factor in transferring shear through interface is by dowel action. Therefore the contribution of the bars in shear transfer is by their shear modulus which must be studied and evaluated (18).

Table (1) Models of shear transfer in interfaces

Model or theory used	Author
(1)Shear friction concepts (cracked and uncracked) -(relying on monolithic action)	ACI-code 318-2005 (1)
(2)Increasing roughness and interface-reinforcement Percentage ratio (cracked and uncracked).	Paulay et al.1974 (20) and Patnaik 2000 (19)
(3)Increasing concrete strength (cracked and uncracked)	Walraven et al. 1987 (21)
(4)Strut-and-tie concept (uncracked)	Hwang and Lee 1999 (10)
(5)Softened strut-and-tie concept (uncracked)	Hwang and Lee 2000 (11)
(6)Softened truss theory (cracked)	Hsu et al. 1987 (9)
(7)Shear-slip characteristics (cracked)	Mattock and Hawkins 1972 (14)
(8)Smooth interface model	Patnaik 2001 (17)
(9)Hybrid type finite element model	Barbieri et al. 2003 (3)
(10)Elastic-plastic model (dowel action)	Millard and Johnson 1984,1985 (15) (16)
(11)Two-phase model (aggregate interlock)	Walraven and Reinhardt 1981 (22)
(12) Isoparametric interface element model	Beer G. 1985 (4)

SHEAR MODULUS OF DOWEL BARS

Millard and Jonhson (15, 16) proposed two equations for the dowel force by considering the dowel bar as a beam on an elastic foundation. One of these equations is for linear behavior Fd_1 and the other is Fd_2 for nonlinear behavior of materials, respectively as follows:

$$Fd_1 = 0.166\Delta_s G_f^{0.75} \Phi^{1.75} E_s^{0.25} \quad \dots (1)$$

$$Fd_2 = Fdu_2 \left(1 - e^{\frac{k_i \Delta_s}{Fdu_2}}\right) \quad \dots (2)$$

where the constant term is dimensionless and :

Δ_s is the shear displacement across the interface.

G_f is the foundation modulus for concrete and is given by:

$$G_f = 126.26 \sqrt{f_{cu}} \quad (\text{MPa}) \quad \dots (3)$$

Φ is the diameter of the bar.

E_s is the elastic modulus of steel.

By dividing Eq. (1) by Δ_s , the stiffness of the dowel bar k_i is governed by:

$$k_i = 0.166 G_f^{0.75} \Phi^{1.75} E_s^{0.25} \quad \dots (4)$$

When the two sides of Eq. (1) are divided by $P.B_g$, where P is the pitch or the spacing between the bars and B_g is the width of the upper part of the precast girder which gives the lower face of the interface, the following equation will be obtained:

$$\frac{Fd_1}{P.B_g} = \left[\frac{0.166G_f^{0.75}\Phi^{1.75}E_s^{0.25}}{P.B_g} \right] * \Delta s \quad \dots (5)$$

Multiplying and dividing the right-hand side of Eq. (5) by t_i , the thickness of the interface element, the following expression is obtained:

$$\frac{Fd_1}{P.B_g} = \left[\frac{0.166G_f^{0.75}\Phi^{1.75}E_s^{0.25}t_i}{P.B_g} \right] \left[\frac{\Delta s}{t_i} \right] \quad \dots (6)$$

$$\underbrace{\hspace{1cm}}_{\text{ShearStress } \tau} \quad \underbrace{\hspace{1cm}}_{\text{ShearModulus } G_{DOWEL}} \quad \underbrace{\hspace{1cm}}_{\text{ShearStrain } (\gamma)}$$

$$\text{Therefore, } G_{DOWEL} = \frac{0.166G_f^{0.75}\Phi^{1.75}E_s^{0.25}t_i}{P.B_g} \quad \dots (7)$$

$$\text{Or, } G_{DOWEL} = k_i \frac{t_i}{P.B_g} \quad \dots (8)$$

where $k_i = 0.166G_f^{0.75}\Phi^{1.75}E_s^{0.25}$ as in Eq.(4). However, the high stress concentration in the concrete supporting the bar results in a nonlinear behavior, so that only the initial dowel stiffness can be predicted when using this equation (16). If Eq. (2) is differentiated with respect to Δs , the following equation will be obtained:

$$\frac{dFd_2}{d\Delta s} = -k_i e^{\frac{k_i \Delta s}{Fdu_2}} \quad \dots (9)$$

$\frac{dFd_2}{d\Delta s}$ is the nonlinear stiffness of the dowel bar which will be named k_{in} to distinguish

it from the initial stiffness k_i . Here k_{in} is given by:

$$k_{in} = -k_i e^{\frac{k_i \Delta s}{Fdu_2}} \quad \dots (10)$$

The nonlinear shear modulus of the dowel bar (G_{DOWELN}) can be written as:

$$G_{DOWELN} = k_{in} \frac{t_i}{P.B_g} \quad \dots (11)$$

$$\text{Or, } G_{DOWELN} = -k_i e^{\frac{k_i \Delta s}{Fdu_2}} * \frac{t_i}{P.B_g} \quad \dots (12)$$

where Fdu_2 is the ultimate shear force in the bar at which the ultimate bending moment (Mp) is reached. Failure occurs either by tensile splitting of the concrete or when the bar reaches its ultimate bending moment (Mp).

$$Fdu_2 = 1.3\Phi^2 f_{cu}^{0.5} \sqrt{f_y(1-\alpha^2)} \quad \dots (13)$$

where f_{cu} is the cube compressive strength of concrete, and α is the ratio of the axial stress to the yield stress of reinforcing steel ($\alpha = f_s / f_y$).

EXPERIMENTAL WORK

Millard and Johnson made so many test trials to investigate the effects of aggregate interlock and dowel action. In their study, the governed curves were representing aggregate interlock results, dowel action results and a combination between the two in two papers (15) and (16). They suggested a nonlinear Equation (2) to represent the relationship between shear load transferred through interface and the slip. This equation is used in the present work, and to check its validity an experimental work is conducted in this study through a series of tests.

The presented work is built on the assumption that the model is initially cracked, therefore the tests done are with an initial crack. These tests and the equation used in the program are for the dowel action effect only because as crack initiates aggregate interlock effect will be low or having a value approaching to zero.

TEST SPECIMENS

The samples tested were rectangular concrete prisms having dimensions 200 mm x 200 mm in section and 500 mm length. The prism was divided into three parts through the use of a separation layer of thin polythene sheeting to eliminate aggregate interlock effects.

Four bars were used to represent the effect of dowel action which are erected in positions in the mold at 5 cms from each side. Details of the specimen shape and dimensions are shown in Fig. (1) and Photo (1).

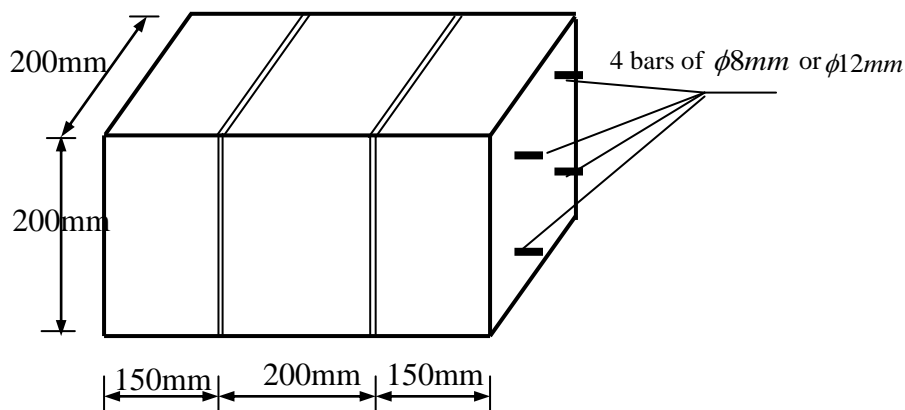


Fig.(1): Push – off test specimen

The middle prism is fabricated with a concrete having a cube compressive strength of 55 MPa (using rapid hardening cement) to simulate or represent the prestressed concrete, while the side prisms are made of concrete with cube compressive strength of 35 MPa for the representation of the slab concrete. The details of mix ratios are shown in Table (2) of Ref.(16). The middle prism is cast after fixing four deformed steel bars throughout the prisms length to represent dowels. The steel bars which are provided used as dowels are of the same bar diameter in each test. Four of the tests are with $\phi 8mm$ bars and other four tests with $\phi 12mm$ bars. After 24 hours, the mold of side parts are removed and replaced by a layer of polythene sheeting to represent the interface layer, then the side prisms are cast.



PHOTO (1) Middle prism and dowel bars used in the test

Table (2): Concrete mix designs (16)

Mix No.	Target strength (N/mm ²)	Cement content (kg/m ³)	Water content (kg/m ³)	Fine aggregate content (kg/m ³)	Coarse aggregate content (kg/m ³)
1	35	300	180	701	1194
2	55	436	205	615	1094

The material properties are shown in Table (3). In 21 days of curing (14 days in water and in 7 days in air curing), the specimens were erected on a prepared frame fixed on a universal testing machine to conduct the test. Details of tests are shown in Fig. (2).

Table (3): Material properties used in the tests (16)

Concrete used	Cube compressive strength f_{cu} (N/mm ²)	Tensile strength f_{ct} $f_{ct} = 2.8 + 0.02f_{cu}$ (N/mm ²)	Steel used			
			$\phi 12mm$		$\phi 8mm$	
			f_y (N/mm ²)	E_s (N/mm ²)	f_y (N/mm ²)	E_s (N/mm ²)
Middle prism	55	3.9	435	196000	485	196000
Edge prisms	35	3.5	-----	-----	-----	-----

The load was applied incrementally to the middle prism from the bottom to push it up while the side prisms were fixed and no movement was allowed for them. The corresponding slip was measured through two dial gauges. The record comprises shear load transferred through the interface and slip.

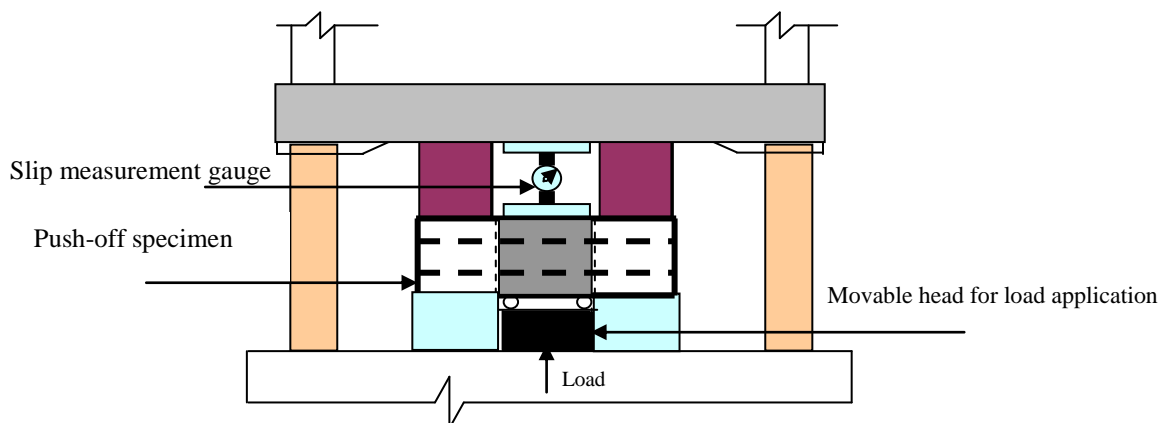


Fig.(2): Instrumentation and test of push-off specimens

RESULTS OF EXPERIMENTAL WORK

The results of the tests are shown in Table (4) for the dowel bars of $\phi 8mm$ and for $\phi 12mm$ and compared with the results of Equation (2).

Figs. (3 and 4) show the relation between the shear force and the slip for two cases of dowel bar diameters selected ($\phi 8mm$) and ($\phi 12mm$). These relationships are represented in terms of shear force and slip for simplicity. It can be represented also by a relationship between the shear stress (which is mentioned also in Table (4)) and the slip.

The shear stress, τ is defined as the total shear load transmitted by the reinforcement divided by the area of the crack. The area of the crack is represented by the area of the adjacent faces of the concrete prisms (200mmx200mm). It can be shown from the figures that increasing the diameter of the bars resulted in a higher shear stiffness and ultimate stress. Failure occurred not by splitting but by crushing of the concrete (Photos 2, 3, and 4). It is likely that the axial tension caused some localized damage and softening to the concrete so that there was a reduction in the splitting stresses below the bar at the crack (joint) face. The shear loading itself will also cause further damage to the concrete. This is likely to reduce the effectiveness of the tensile anchorage of the bar within the concrete and could explain why the crack became wider as shear loading was applied, Photo (4), even though no overriding of the crack faces was expected.

Table (4) Millard-Johnson Eq. (2) and experimental results

Dowel bar diameter (mm)	No. of bars	Shear force F_v (N)	0	4000	6000	8000	8800	9600	10400	10500	10600	10800	10836
8	4	Shear Stress τ (N/mm ²)	0.00	0.10	0.15	0.20	0.22	0.24	0.26	0.2625	0.265	0.270	0.2709
		Millard & Johnson Eq.(2)	0.00	0.262	0.459	0.762	0.950	1.234	1.823	1.970	2.168	3.186	4.483
		Δs (mm)	0.00	0.26	0.50	0.80	1.00	1.25	1.83	1.99	2.20	3.20	4.50
		Experimental	0.00	0.26	0.50	0.80	1.00	1.25	1.83	1.99	2.20	3.20	4.50
12	4	Shear force F_v (N)	0	16000	32000	48000	64000	72000	80000	84000	86000	88000	90000
		Shear Stress τ (N/mm ²)	0.00	0.40	0.80	1.20	1.60	1.80	2.00	2.10	2.15	2.20	2.25
		Millard & Johnson Eq.(2)	0.00	0.113	0.254	0.437	0.704	0.901	1.198	1.430	1.593	1.817	2.179
		Δs (mm)	0.00	0.11	0.26	0.45	0.80	1.00	1.30	1.45	1.65	1.85	2.25
		Experimental	0.00	0.11	0.26	0.45	0.80	1.00	1.30	1.45	1.65	1.85	2.25

Fig. (3) shows a comparison between the experimental and the analytical results governed by eq. (2) for bar of $\phi 8mm$ diameter (shear force transferred by dowel action with slip). At the same time the relationship between shear stress (transferred through

interface by dowel action) and slip is explained in Fig. (5). The results give good comparison where most of the curve points coincided. In Figs. (4 and 6) the experimental and the analytical results of the tests using bar of $\phi 12mm$ diameter are shown. The results here give accurate coincidence with the others compared with the test of $\phi 8mm$ bars. This surely explains the truth that the shear stress transmitted by dowels is increased by increasing the area of dowel bars or the number of these dowel bars. The nonlinear shear stiffness of the dowel action specimens may be attributed to one or both of two causes. The first cause is splitting or crushing of the concrete supporting the bar and the second cause is the plastic yielding of the dowel bars.

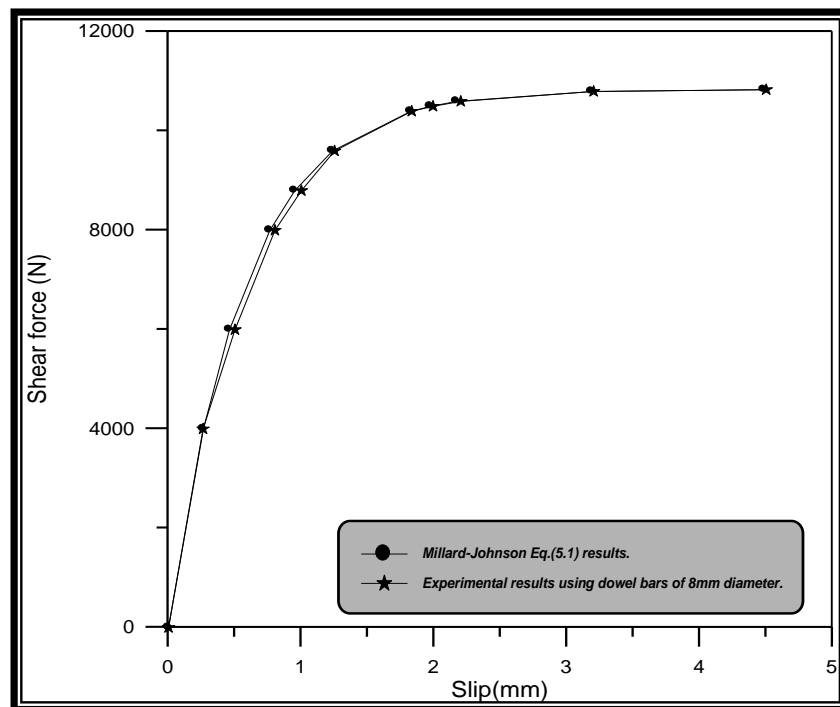


Fig.(3) Comparison between experimental and Millard-Johnson Equation (2) results using dowels of 8mm diameter bars

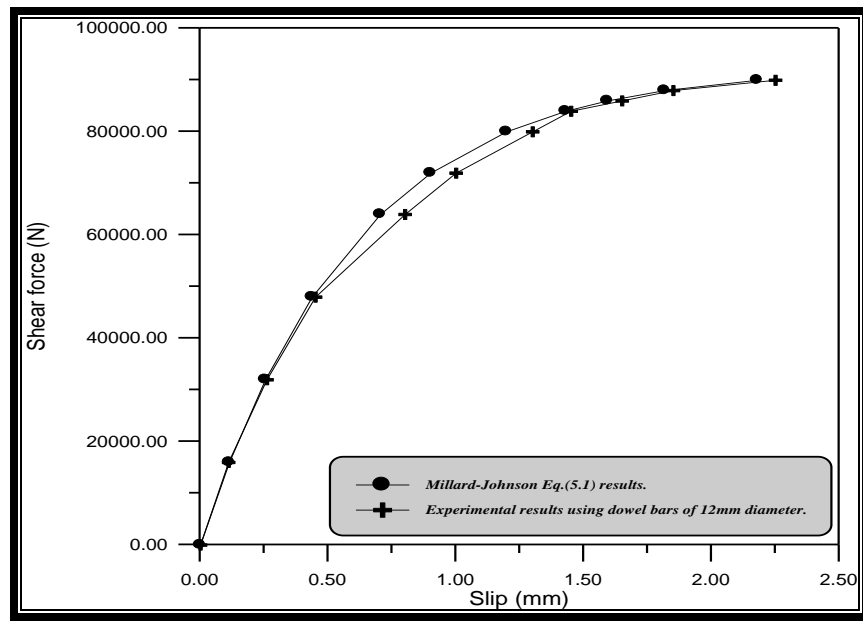


Fig.(4) Comparison between experimental and Millard-Johnson Equation(2) results using dowels of 12mm diameter bars

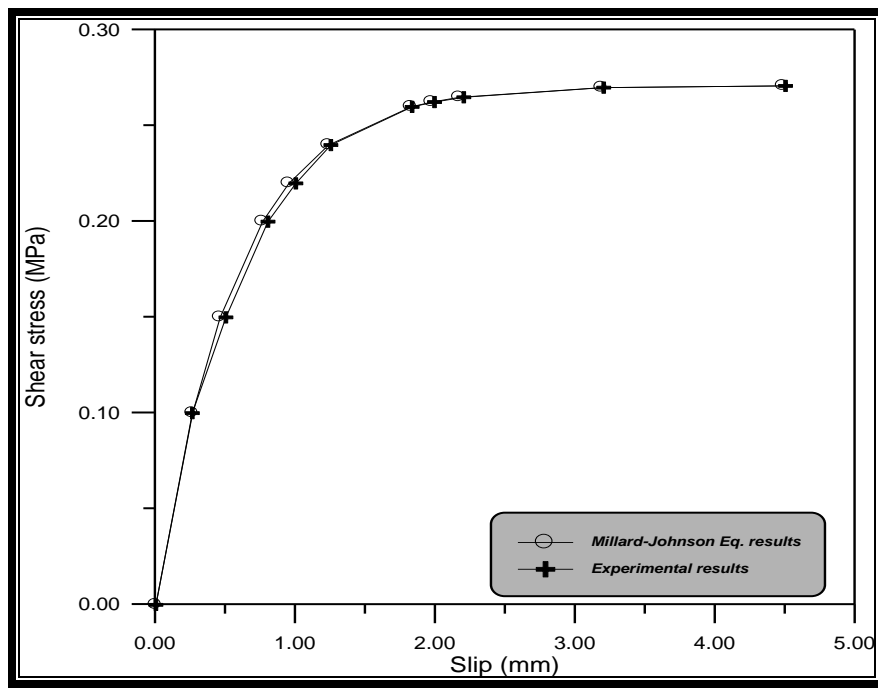


Fig.(5) Comparison between Millard-Johnson Equation results of shear stress-slip and experimental results using dowels of 8mm diameter

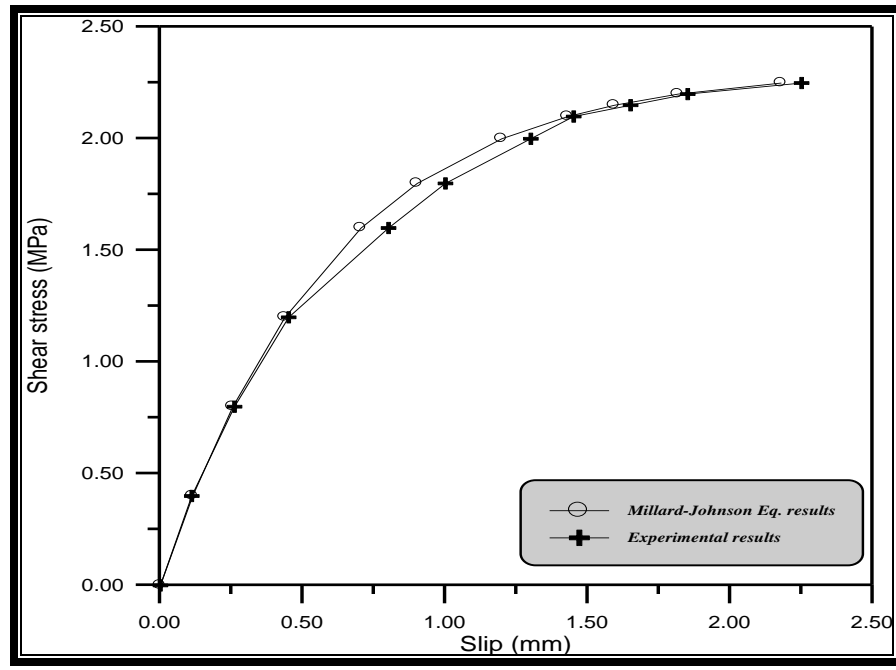


Fig.(6) Comparison between Millard-Johnson Equation results of shear stress-slip and experimental results using dowels of 12mm diameter

Photos (2, 3, and 4) show the failure mode of the specimens using dowel bars of 8mm diameter. It is clear from the pictures that the cracks are due to crushing of concrete near or under the dowel bars because of the reduction in splitting stresses under the bars. Photos (5, 6 and 7) are for dowel bars of 12 mm diameter. In these photos the same type of failure is repeated here with wider and more severe cracks.

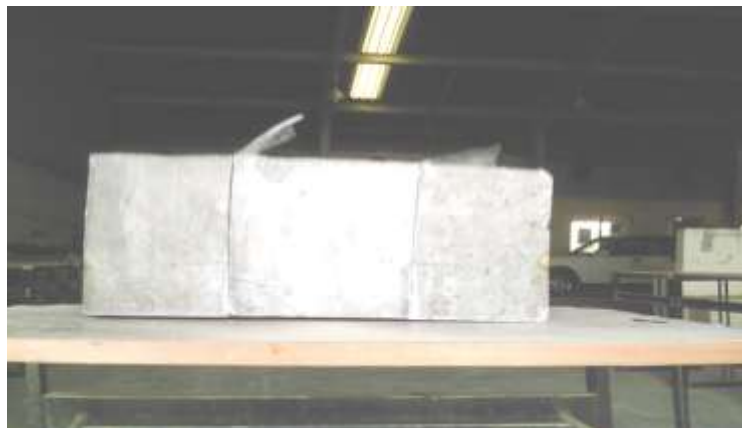


PHOTO (2) Specimen with 8mm dowel bars after test



PHOTO(3) Edge cracks with 8mm bars diameter specimens



PHOTO (4) Cracks in the face with 8mm bars specimens



PHOTO (5) Crushing failure of specimens with 12mm bars.



PHOTO (6) Face cracks with 12mm bars specimens

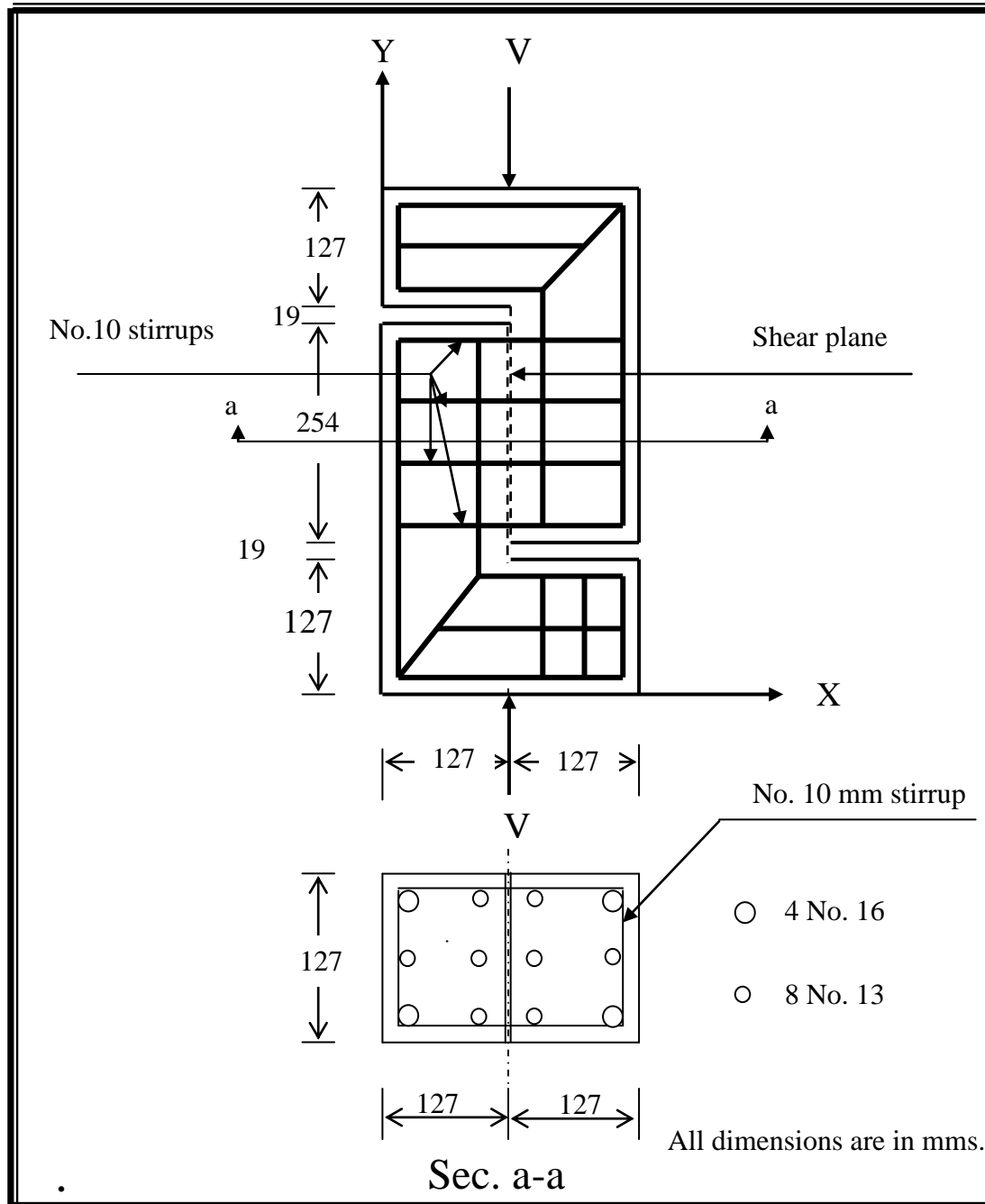


PHOTO (7) Upper and side cracks with 12 bars mm specimens

Finite element analysis of Hofbeck et al. reinforced concrete push-off specimens

The aim of the push-off tests which were done by Hofbeck et al. (8) was to study the transfer of shear across the interface between a precast prestressed girder and a cast -in - place slab. A typical specimen is shown in Fig. (7). Hofbeck et al. (8) tested thirty-eight specimens, some with and some without a pre-existing crack along the shear plane. 20-node brick elements of Al-Shaarbaf (2) for concrete with embedded bar elements were used in the present work. Also the interface was considered as a brick element with an

Material properties and the additional material parameters used in the finite element analysis are listed in Table (5)



specimen



Concrete (interface also included)			
E_c	Young’s modulus (MPa)		25200
f'_c (Hofbeck et al. test) (8)	Compressive strength (MPa)		26.9
f_t	Tensile strength (MPa)		2.7
$\nu *$	Poisson’s ration		0.2
Reinforcing steel			
$E_s *$	Young’s modulus (MPa)		200000
f_y	Yield stress (MPa)	No .10mm	349
		No .13mm	325
		No .16mm	292
Tension stiffening parameters			
α_1	Rate of stress release as the crack widens.		41
α_2	The sudden loss of stress at the instant of cracking.		0.6
Shear retention parameters			
γ_1	Rate of decay of shear stiffness as the crack widens.		10
γ_2	The sudden loss in shear stiffness at the instant of cracking.		0.9
γ_3	Residual shear stiffness due to the dowel action.		0.1

(*) Assumed values

Finite element idealization of push-off specimen of Hofbeck et al.

The specimen which is considered by Hofbeck et al., as an initially cracked specimen is tested here. It is discretized into nine brick elements, one of them is the interface (element N0.5), Fig. (8).

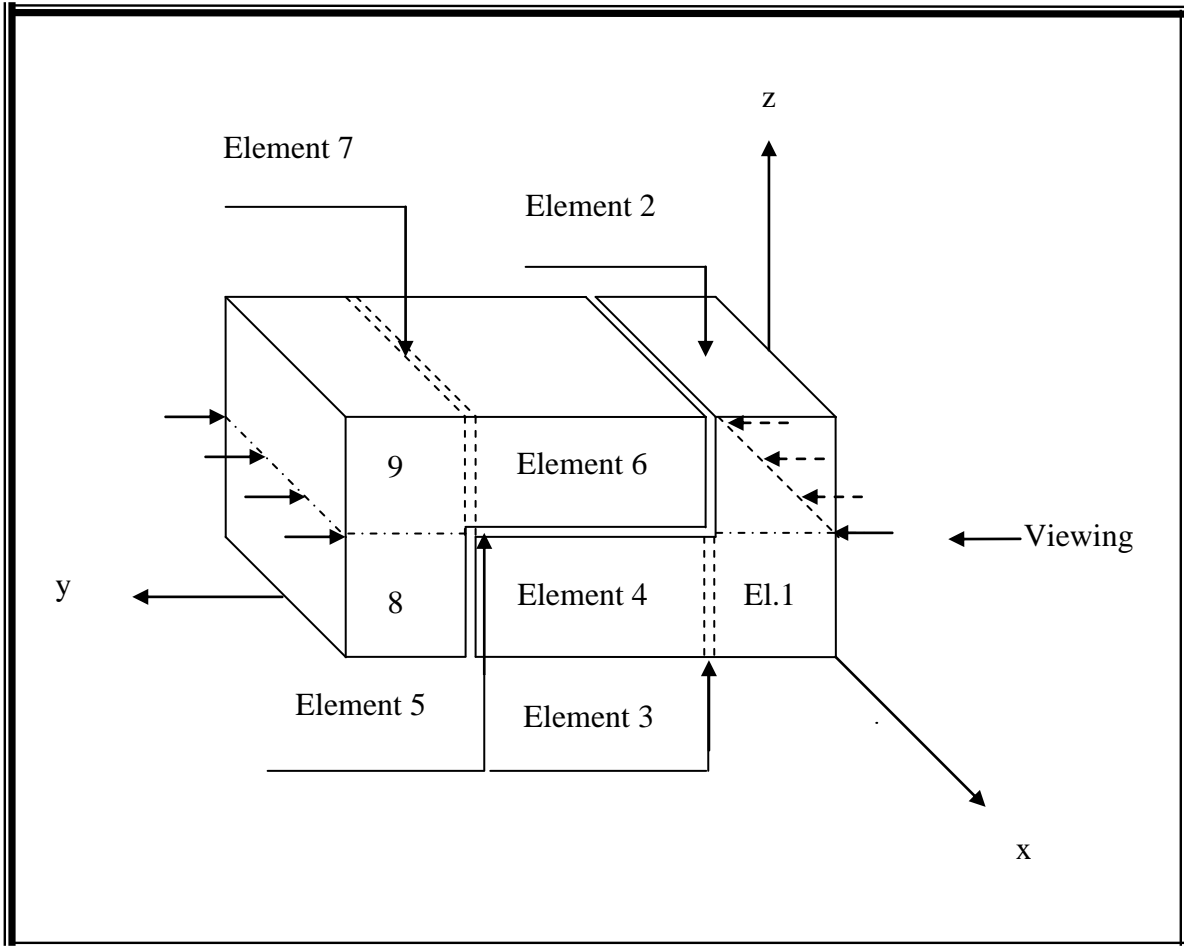


Fig .(8) Finite element mesh used for push-off specimen of Hofbeck et al in the present study

The interface element has a thickness of $(0.01-0.1) b$, where b is the length of the face adjacent to interface, Desai et al. (5). Therefore, depending on the previous assumption the thickness of the interface is taken to be 3mm $(0.1b)$.

The distribution of the nodes in the 20 – noded brick elements is as shown in Fig. (9).

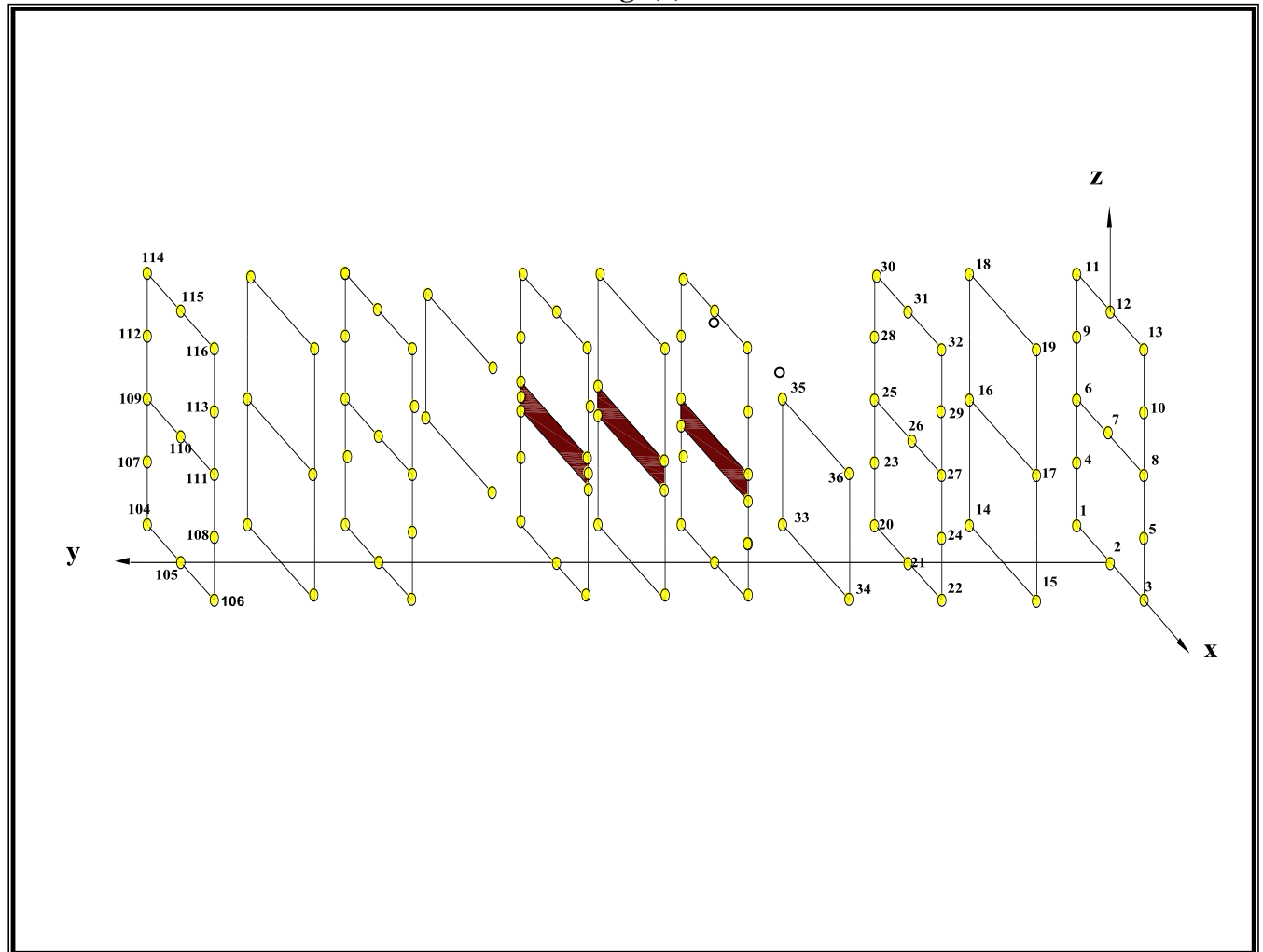


Fig. (9) Distribution of nodes on the 20- noded brick element of the test specimen

RESULTS OF THE ANALYSIS OF PUSH-OFF SPECIMEN.

In the analysis of push-off specimen tested by Hofbeck et al. (9), the interface model used is where dowels are used. The nonlinear Equation (11) of the shear modulus is added and contributed in the constitutive matrix $[D]$. The results of the analytical load-slip relation by finite elements are shown in Fig. (10) which are compared with the experimental results. The figure indicates good agreement throughout the entire range of load – slip behavior. The numerical ultimate load is (222.25 kN), while the experimental ultimate load is (222.3 kN).

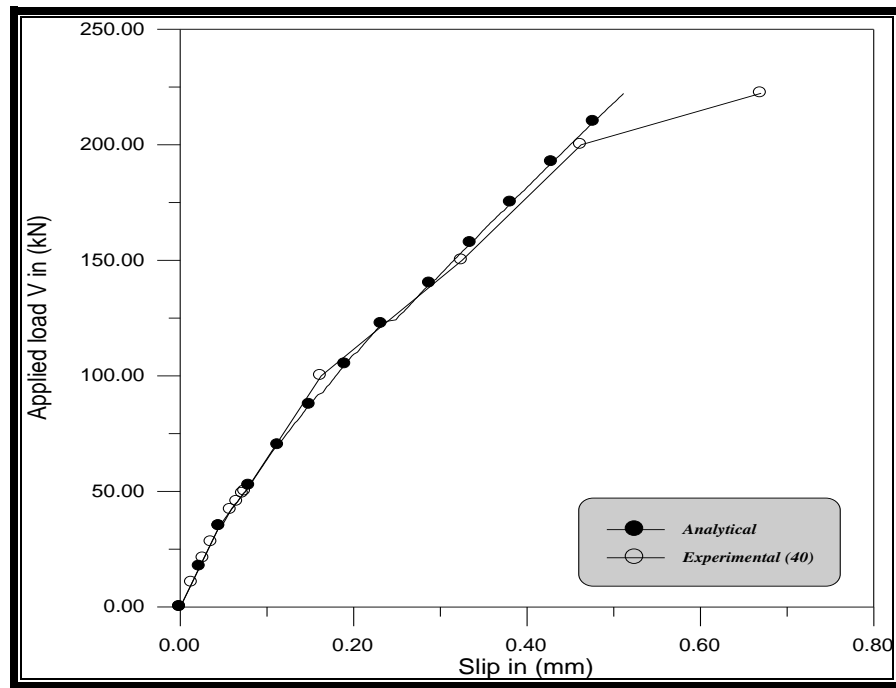


Fig. (10) Experimental and analytical load-slip curves of Hofbeck et al.(8) push-off specimen using Millard-Johnson nonlinear equation of dowel action

Fig. (11) shows the analytical results compared with the experimental results when the model of linear Equation (6), proposed by Millard and Johnson (16), is used. It is clear that there would be a difference larger than that shown in Fig. (10) when Millard-Johnson nonlinear equation is used, where the ultimate analytical load obtained is (224.875 kN). The ratio of the predicted load to the corresponding experimental load is (1.01158). Therefore it is preferable to use the Millard-Johnson nonlinear equation because the ultimate shear values in experimental and analytical results coincide. Besides it is well known that the relation between shear force transmitted through an interface and the slip is always of exponential form which coincides with that of Millard-Johnson equation.

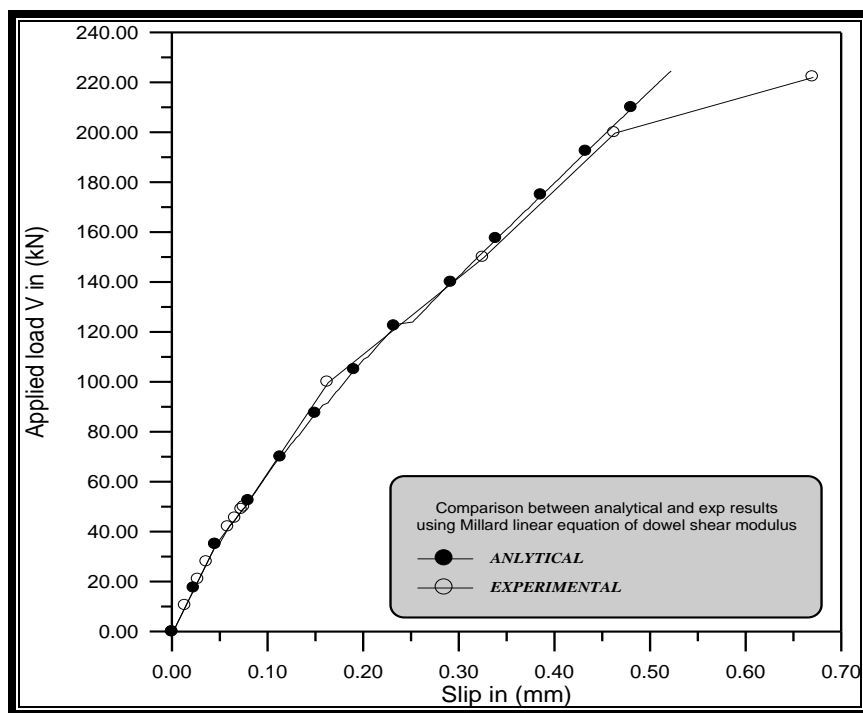


Fig. (11) Experimental and analytical load-slip curves of Hofbeck et al. for push-off specimen using Millard-Johnson linear equation of dowel shear modulus

CONCLUSIONS

The conclusions which can be deduced are listed herein:

- 1- The exponential equation presented by Millard-Johnson to represent the shear transfer through interface with slip by dowel action is sufficiently accurate. When comparing the results of this equation with the results of tests done in the present work and in Hofbeck et al. work, the two give good and reasonable comparison where the difference between analytical and experimental work is between 2.5% and 5% for 8mm ϕ and 12mm ϕ bars respectively.
- 2- The exponential equation is used only for initially cracked specimens because as crack initiates, the transfer of shear is achieved mostly by dowel bars and hardly by aggregate interlock.
- 3- As the area or number of dowels are increased the slip is decreased and that is due to the contribution of the bar stiffness in the overall stiffness of the member.
- 4- It is suggested to reach to a certain equation representing the shear transfer through interface by combined aggregate interlock and dowel action.

REFERENCES

- ACI (2005), Building Code requirements for structural concrete: ACI Committee 318-05. Farmington Hills: American Concrete Institute.
- Al-Shaarbaf, I.A.S., "Three dimensional non-linear finite element analysis of reinforced concrete beams in torsion". Ph.D. Thesis, University of Bradford, U.K., 1990.
- Barbieri R.A., Gastal F.P.S.L. and Filho A.C., "Numerical model of prestressed composite concrete flexural members", J. of Advanced Concrete Technology, Vol. 1, No.2, July 2003, Japan Concrete Institute.
- Beer G., "An isoparametric joint/interface element for finite element analysis", Int. J. for Numerical Methods in Engineering, Vol.21, 1985.
- Desai C.S., Zaman M.M., Lightner J.G. and Siriwardane H.J., "Thin-layer element for interfaces and joints", Int. J. for Numerical and Analytical Methods in Geomechanics, Vol.8, 1984.
- Fardis M.N. and Buyukozturk O., "Shear transfer model for reinforced concrete", J. of the Engineering Mechanics Division, ASCE, Apr.1979.
- Grossfield B. and Birnstiel C., "Tests on T-beams with precast webs and cast-in-place flanges", ACI J., Proceedings, V.59, No.6, June 1962.
- Hofbeck J.A., Ibrahim I.O. and Mattock A.H., "Shear transfer in reinforced concrete", ACI J., Feb.1969.
- Hsu T.T.C., Mau S.T. and Chen B., "Theory of shear transfer strength of reinforced concrete", ACI Struct. J., 84(2), 1987.
- Hwang S.J. and Lee H.J., "Analytical model for predicting shear strengths for exterior reinforced concrete beam-column joints for seismic resistance", ACI Struct. J., 95(5), 1999.
- Hwang S.J. and Lee H.J., "Analytical model for predicting shear strengths for interior reinforced concrete beam-column joints for seismic resistance", ACI Struct. J., 97(1), 2000.
- Looe R.E. and Patnaik A.K., "Horizontal shear strength of composite concrete beams with a rough interface", PCI J., January-February 1994.
- Mast R.F., "Auxiliary reinforcement in concrete connections", J.Struct. Div., Proc., ASCE, 94(6), 1968.



- Mattock A.H. and Hawkins N.M., "Shear transfer in reinforced concrete –recent research", PCI J., March-April 1972.
- Millard S.G. and Johnson R.P., "Shear transfer across cracks in reinforced concrete due to aggregate interlock and to dowel action", Magazine of concrete research, Vol.36, No.126, March 1984.
- Millard S.G. and Johnson R.P., "Shear transfer in cracked reinforced concrete", Magazine of Concrete Research, Vol.37, No.130, March 1985.
- Patnaik A.K., "Behavior of composite concrete beams with smooth interfaces", Journal of Structural Engineering, ASCE, Vol.127, No.4, paper No.22384, April 2001.
- Patnaik A.K., "Longitudinal shear strength of composite beams with a rough interface and no ties", Australian J. Struct. Engrg. 1(3), 1999.
- Patnaik A.K., "Discussion of 'Evaluation of ACI 318-95 shear friction provisions' by R. Valluvan, M.E. Kerger and Jirsa J.O.", ACI J., May-June 2000.
- Paulay T., Park R. and Philips M.H., "Horizontal construction joints in cast-in –place reinforced concrete", Shear in Reinforced Concrete, SP-42, ACI, Farmington Hills, Michigan, 1974.
- Walraven J.C., Frenay J. and Pruijssers A., "Influence of concrete strength and load history on the shear friction capacity of concrete members", PCI J., 21(1), 1987.
- Walraven J.C. and Reinhardt H.W., "Concrete Mechanics-Part A: Theory and experiments on the mechanical behavior of cracks in plain and reinforced concrete subjected to shear loading", Hron. Vol.26, No.1A, 1981, pp 1-68.



STABILITY INDEX OF THE TREATED WATER FROM AL-KARKH AND AL-RASHEED WATER TREATMENT PLANTS IN BAGHDAD CITY

Awatif Soaded Alsaqqar

Dept. of Civil Eng

College of Eng.

University of Baghdad

Mohammed Abdul- Khalek

Dept. of Civil Eng

College of Eng.

Nahrain University

ABSTRACT

An analysis was performed on the treated water from two water treatment plants in Baghdad city. This analysis was used to evaluate the stability of the treated water from these plants and that will flow in the distribution system to consider its corrosivity. The variation in water stability with time and distance from the north to the south of Baghdad was indicated. The analysis showed that the flowing water in the distribution system in Baghdad is corrosive to very corrosive water by calculating Ryznar stability index (RI). In Al- Karkh WTP in the north, RI maximum ranged between 7.958 to 9.403 where RI minimum ranged between 7.03 to 7.915. Where in the south Al-Rasheed WTP, RI maximum ranged between 7.119 to 8.63 and RI minimum ranged 6.679 to 7.994. The corrositivity of water decreased in the water flowing down stream. The water quality parameters affecting RI was discussed which were calcium, alkalinity, total dissolved solids and pH.

الخلاصة

في هذا البحث تم تحليل الماء من محطتين لتنقية المياه في مدينة بغداد. والهدف من هذا التحليل هو لايجاد استقرارية هذه المياه التي تجري داخل شبكة توزيع الماء و معرفة مدى تأكلها. وقد بين البحث مدى تغير هذه الاستقرارية مع الزمن و المسافه بين شمال و جنوب مدينة بغداد. تبين من التحليل بأن المياه الخارجة من محطات التنقية و التي تجري في شبكة التوزيع لمدينة بغداد ذات صفة تأكلية وذلك من حساب معامل الاستقرارية. في محطة الكرخ لتنقية الماء في شمال مدينة بغداد تراوح معامل الاستقرارية الاعظم بين 7.956 - 9.403 و معامل الاستقرارية الادنى 7.03 - 7.915 وفي جنوب بغداد محطة الرشيد لتنقية

المياه كان معامل الاستقرارية الاعظم للماء المعالج 7.119 - 8.63 و تراوح معامل الاستقرارية الادنى بين 6.679-7.994 ومن هذه النتائج نلاحظ بان تآكلية الماء تقل باتجاه الجريان من الشمال الى جنوب من مدينة بغداد اعتمادا على صفات الماء التي تؤثر على معامل الاستقرارية . ومن هذه الصفات والتي تمت مناقشتها تركيز الكالسيوم, القاعديه, الاملاح الكليه الذائبه و درجة الحامضيه .

KEY WORDS

Water Stability, Stability Index, Ryznar Index, Metal Corrosion, Water Quality.

INTRODUCTION

Control of water quality in the distribution system seeks to preserve the basic characteristics of water during its conveyance from the point of production and treatment to the consumers tap. The finished water should be completely stable in its compositional and physical attributes. Also the conveyance system and accessory structures (pipelines, distributing reservoirs, mains and serves pipes) should be reactively inert to the water being conveyed. Most water quality parameters affect the corrosion process to some degree and that each pipe material is affected differently. Altering one parameter to subdue its effect on the corrosivity of water may well change other water quality characteristics, perhaps rendering the water even more corrosive or less likely in some other way to meet drinking water standards (AWWA, 1971). This complex interrelationship of water quality factors that affect corrosion was dictated by many researchers.

Millete et al. (1980) Joined in a national survey covering water supplies serving approximately one fifth of the US population which showed that almost 70% of the representative utilities to have moderately to highly aggressive waters, where 16-18% had highly aggressive waters. The data were analyzed using the Langelier Index (LI) and Ryznar Index (RI). The mean value of LI for the representative utilities was - 1.17 indicating aggressive waters. The data also showed that 20% of the utilities of water supplies had an average RI above 10 indicating very aggressive water. A comparison between the two indices showed good agreement in the results.

Pisigan and Singly (1985) reported the influence of some water quality parameters in particular the LI on the corrosion of galvanized steel using a dynamic circulating water system. Metal pipes (25mm x 50mm) were used in a 40 day experimental run. The corrosion damage was evaluated in terms of weight loss of the metal. Three types of water were tested. The results showed that the greatest corrosion was in the water A of LI = - 0.46 where corrosion in water C of LI= 0.57 was greater than in water B of LI= 0.04. Change in water quality parameter were monitored, hardness and alkalinity exhibited a continuous decline. The rate of decrease of hardness was much greater in water A and C than in water B. The pH dropped initially and then increased slightly at the end of the 40 days.

Pisigan and Singly (1987) dictated from their experimental work that increasing the buffer capacity at a constant water alkalinity of 100mg/l as CaCO₃ in the pH range 6-9 decreased the corrosion rate of mild steel. However an increase in the buffer capacity at various pH by raising the alkalinity did not lower the corrosion rate because of the effects of higher ionic strength and conductivity. Also higher chloride content increased the corrosion rate in some waters of high



buffer capacities. A chlorine residual 1-1.5mg/l as Cl_2 also accelerated the corrosion rate in mild steel and copper during batch studies. The same effect would be observed in distribution systems because of the high oxidation potential of hypochlorous and hypochlorite ion.

Al Stone et al. (1987) studied the corrosion rate of common plumbing materials. Copper and zinc were investigated as a function of physical and chemical water quality characteristics. For the systems studied, changes in dissolved O_2 , conductivity and temperature had a moderate effect on the corrosion rate of both Cu and Zn, whereas pH and chlorine residual affected Cu corrosion rates but not those of Zn. Increases in conductivity up to about 200 $\mu\text{S}/\text{cm}$ increased Cu corrosion rates significantly but generally had less effect at higher values. Zinc corrosion rates increased with conductivity up to 1000 $\mu\text{S}/\text{cm}$. For equal conductivities, corrosion rates were greater in systems with chloride than in systems with HCO_3 , where SO_4 had an effect equivalent to chloride on aged Cu and Zn electrodes but equivalent to HCO_3 on fresh Cu.

Steve et al. (1987) in a 18 month monitoring program, evaluated the relationship between copper plumbing corrosion and variations in delivered water quality in several communities in the Pacific Northwest. Significant relationships were found for copper corrosion rate dependence on pH and free chlorine residual. The data indicated that as the pH increased from 5.8 at the start of the program to 7.7 after 12 months of operation, the corrosion rate decreased from a weekly average of 21.6 $\mu\text{m}/\text{year}$ to 10.2 $\mu\text{m}/\text{year}$ (a 54% decline). The regression equation coefficient indicated that the corrosion rate changes with chlorine residual, approximately 25.6 $\mu\text{m}/\text{year}$ per mg/l chlorine.

WATER STABILITY

Water can exhibit a tendency to either dissolve or deposit certain minerals in pipes, plumbing, and appliance surfaces. This tendency is known as stability. Water that tends to dissolve minerals is considered corrosive. Conversely, water that tends to deposit minerals is considered scaling. The tendency of corrosive water to dissolve minerals can be detrimental to water quality and to the distribution systems. In addition to dissolving calcium and magnesium, corrosive waters can also dissolve harmful metals such as lead and copper from plumbing utilities. The presence of dissolved lead or copper in tap water, require treatment techniques to reduce the corrosiveness of the water. Scaling waters deposit a film of minerals on the pipe wall which reduces and, in some cases, prevents corrosion of metallic surfaces. If the scale deposition is too rapid, however, it can also be harmful. Excessive buildup of scale can damage appliances, such as water heaters, and increase pipe friction coefficients, in extreme cases, scale may clog pipes. Therefore, to prevent corrosion yet but limit scale deposition, the most desirable water is one that is just slightly scaling (Qasim et al., 2000).

OBJECTIVES OF THE STUDY

All WTPs in Iraq are designed as conventional plants. This treatment process does not significantly affect the concentrations of the dissolved constituents, so the characteristics of the raw and treated water are quite the same. The study analyzed the quality of the effluent (treated

water) from the treatment plants in Baghdad. This analyze was performed on the treated water from two chosen plants, Al-Karkh WTP in the north of Baghdad and Al-Rasheed WTP in the south. The data of the water quality were recorded in Amant Baghdad (water sector) for the period between 2000 until 2004 for the maximum and minimum recorded parameters. The analysis is to evaluate the stability of the water flowing from Al-Karkh and Al-Rasheed WTPs to consider its corrosivity. The variation in water stability with time and distance from the north to the south of Baghdad is to be indicated.

COMMON METHODS USED TO MEASURE WATER STABILITY

The most common methods used for calculating the stability of water are Langelier saturation index (LI) and Ryznar stability index (Degremont, 1991; Kawamura, 2000; Millete et al., 1980; MWH, 2005; and Qasim, et al., 2000).

1-Langelier Index (LI)

Describes a saturation index based on determined parameters which have been used in estimating the corrosion potential of water. This index compares the actual pH of the water to the pH of the water if it were saturated with calcium carbonate (Qasim et al., 2000).

The basic equations used for the determination of LI are:

$$LI = \text{pH actual} - \text{pH saturation} \quad \text{eq.1}$$

where pH actual = measured pH of water

$$\text{pH saturation} = (\text{pk}^2 - \text{pk}^s) + \text{pCa}^{+2} + \text{pAlk} + S \quad \text{eq.2}$$

($\text{pk}^2 - \text{pk}^s$) = dissociation constant based on temperature and total dissolved solids or ionic strength.

pk^2 = acidity constant for the dissociation of bicarbonate.

pk^s = mixed solubility constant for CaCO_3

$\text{pCa}^{+2} = -\log(\text{calcium ion in moles / liter})$

$\text{pAlk} = -\log(\text{total alkalinity in equivalent of } \text{CaCO}_3 / \text{liter})$

$$S = \text{salinity correction term} = 2.5 \mu^{1/2} / (1 + 5.3 \mu^{1/2} + 5.5 \mu) \quad \text{eq.3}$$

where μ = ionic strength

For total dissolved solids content less than 500 mg/l, the ionic strength may be estimated by $2.5 \times 10^{-5} \times \text{TDS}$. An alternate approximation of ionic strength can be made using the total hardness and total alkalinity (Millete et al., 1980). Table 1 shows the scale and corrosive tendencies of water at different Langelier index.

**Table 1 Scale and Corrosion Tendencies of Water with Different Langelier Index**

LI /Range	Indication
The index is zero	Water is in equilibrium.
A positive index	Oversaturation and the tendency of water are to lay down a protective coating in the pipe.
A negative index	Under saturation and the tendency of water to be aggressive to the pipe. The greater the value, the greater the aggressiveness.

2-Ryznar Index (RI)

The same parameters in the Langelier saturation index are also used in this index. The Ryznar index is a quantitative index of the amount of calcium carbonate scale that would be formed and to predict the corrosiveness of waters that are non scale forming (REF). The equation for the determination of RI is:

$$RI = 2pH_{\text{saturation}} - pH_{\text{actual}} \quad \text{eq.4}$$

Table 2 lists the scale formation or corrosive tendencies of waters with various Ryznar index values (Qasim et al., 2000).

Table 2 Scale and Corrosion Tendencies of Water with Various Ryznar Index Values

RI/Range	Indication
Less than 5.5	Heavy scale formation
5.5 to 6.2	Some scale will form
6.2 to 6.8	Non-scaling or corrosive
6.8 to 8.5	Corrosive water
More than 8.5	Very corrosive water

RESULTS AND DISCUSSION

The stability of the treated water from the two plants (Karkh and Rasheed) was calculated according to the water quality of the effluents of these plants. In this study the Ryznar Index (RI) was used to evaluate the stability of the effluent from these plants using eq.4. The US Environmental Protection Agency (USEPA) has recommended the use of Langelier index and Ryznar index by utilities to monitor the corrosion potential of water (Pisigan and Singly, 1985). The measured parameters of the treated water that affect the stability index are calcium concentration, alkalinity, total dissolved solids and pH.

CALCIUM (CA)

After bicarbonate, calcium is the second most prevalent constituent in most surface waters of the world and is generally among the most prevalent three or four ions in groundwater. Weathering and soil ion exchange reactions are the main sources of calcium in natural waters. Common minerals forms of calcium are calcite, also known as aragonite (CaCO_3), gypsum ($\text{CaSO}_4 \cdot \text{H}_2\text{O}$) anhydrite (CaSO_4) and fluorite (CaF_2). Calcium is generally present as the free ion Ca^{+2} in natural waters and adsorbed into soil particles calcium concentrations can reach several hundred milligrams per liter in arid regions or under conditions where hydrogen ion activity is higher than under atmospheric equilibrium conditions. Waters with calcium levels between 60 and 100 mg/L are generally considered moderately hard to hard as calcium is a primary constituent of water hardness. Calcium is of importance to industry as a component of scale. The precipitation of CaCO_3 scale on cast iron and steel pipes helps inhibit metallic corrosion but the same precipitate in boilers and heat exchangers adversely affects heat transfer. Water high in calcium have a nuisance value in wash waters both domestic and industrial, as the alkaline environment causes precipitation of the calcium (scale) on fixtures and soap (MWH, 2005). Increasing the Ca concentration will decrease the corrosivity of water, as Ca is important in various roles, including calcium carbonate scales, mixed iron/calcium carbonate solids and the formation of a passivating film on the surface of the pipe, to control corrosion (Schock, 1989). From the recorded data the maximum concentration of Ca ranged between 53 to 143 mg/l in Al-Karkh WTP as shown in Fig.1a. Whereas in Al-Rasheed WTP the maximum concentration was 62 to 146 mg/l. The minimum concentrations shown in Fig.1b ranged 46 to 74 mg/l in Al- Karkh and 62 to 130mg/l in Al- Rasheed .These results indicate that calcium increased from the north to the south in the treated water in Baghdad city. Also a slight increase could be observed with time in Al-Rasheed WTP where the Ca concentrations remain at low and constant values in Al-Karkh WTP in the north of Baghdad.

ALKALINITY (ALK)

Alkalinity is a measure of the ability of water to resist changes in pH. Alkalinity in water is due to the presence of weak acid systems that consume hydrogen ions produced by other reactions or produce hydrogen ions when they are needed by other reactions allowing chemical or biological activities to take place within water without changing the pH. The primary source of alkalinity is the carbonate system, although phosphates, silicates, borates, carboxylates, and other weak acid systems can also contribute. In water treatment plants, alkalinity is required in the coagulation process for the reaction of alum, lime could be added if the natural alkalinity is not enough for this reaction (MWH, 2005).

Fig.2a shows the maximum alkalinity in Al-Karkh WTP ranging from 124 to 161 mg/l as CaCO_3 with a slight difference in Al-Rasheed WTP which was 126 to 169 mg/l as CaCO_3 . The minimum values were 94 to 143 mg/l as CaCO_3 in Al-Karkh and 122 to 158 mg/l as CaCO_3 in Al-Rasheed as shown in Fig.2b. Also indicating that the alkalinity increased in the effluent from the south WTP. Corrosivity of water decreases as the alkalinity increases where it is necessary to



provide a stable pH throughout the distribution system for corrosion control of metal pipes (Schock, 1989). Low iron corrosion rates and iron concentrations in the distribution systems have been associated with higher alkalinities (Pisigan and Singley, 1987). The alkalinity of the treated water from the two plants seems to decrease with time which could be observed from these Figs.

TOTAL DISSOLVED SOLIDS (TDS)

TDS in water are due to inorganic salts. Principally these inorganic constituents are calcium, magnesium, sodium, and potassium salts of bicarbonate, chloride, sulfate, nitrate and phosphate. These compounds originate from weathering and leaching of rocks, soils and sediments. Also some of these compounds are added to the water in the treatment plant (MWH, 2005).

The variation of TDS in the treated water was large from the two plants as shown in Fig.3a and Fig.3b. In Al-Karkh WTP the maximum values ranged between 280 to 680 mg/l and the minimum between 240 to 540 mg/l. The TDS increased in the Al-Rasheed WTP where the maximum concentrations reached 340 to 1020 mg/l and the minimum 330 to 800 mg/l. The conventional treatment process does not affect the dissolved content of the treated water so the high TDS concentrations in Al-Rasheed effluent are due to the raw water quality entering this plant. The increasing amounts of dissolved solids in the Tigris River are due to the discharge of waste water, leaching of fertilizers and the natural weathering of the soil. These concentrations are decreasing with time from the two plants as shown in Figs.3a and 3b.

HYDROGEN ION CONCENTRATION (PH)

pH is a measurement of the acid base properties of a solution. pH is important in water treatment as it directly influences the dosages of chemicals added to reduce hardness and coagulate particles (MWH, 2005). The higher pH of the water in the distribution system will decrease the solubility of the corrosion by products formed in the system (Schock, 1989).

The maximum values of pH ranged between 7.5 to 8 in Al-Karkh WTP and in Al-Rasheed WTP from 7.4 to 7.9. The minimum values varied between 6.9 to 7.6 in Al-Karkh and in Al-Rasheed from 7.1 to 7.9. As shown in Figs.4a, and 4b. This variation in pH of the effluent from the water treatment plants depend on the amount of coagulants added for suspended solids removal and the chlorine dose used for disinfection. The variation of pH with time seems to be stable in the two plants. From these Figs. pH max ranged between 7.6 to 7.9 where the min. ranged 7.2 to 7.8.

RYZNAR INDEX (RI)

The effect of TDS content on water corrosivity is a complex issue. Both the species and the concentration of ions are important factors. Some species such as carbonate and bicarbonate reduce corrosion, whereas chloride, sulfate, bromide and nitrate ions markedly accelerate corrosion. Temperature also affects the corrosion process. Higher water temperatures accelerate the rate of corrosion by increasing the rate of the cathodic reaction. The chemical reaction rate generally is doubled for every 8°C increase in temperature (Kawamura, 2000). Fig.5a and 5b show the variation in the stability index RI of the effluents from the two plants.

In Al-Karkh WTP RI max ranged between 7.958 to 9.403 where RI min ranged between 7.03 to 7.915. In Al-Rasheed WTP RI max ranged between 7.119 to 8.63 and RI min ranged 6.679 to 7.994. According to Table 2 the effluents from these plants are classified corrosive to very corrosive water (RI is more than 6.8). The high RI value in the treated water from Al-Karkh WTP was because of the low Ca and alkalinity content. The RI max. for the two plants remain varying between 8.0-8.5 in Al-karkh and 7.5-8.0 in Al-Rasheed, where RI min. ranged 7.5-7.7 and 7.1-7.3 respectively. This may indicate a constant corrosivity with time. The corrosivity index show that the water is corrosively high in the north part in Baghdad city (Al-karkh WTP) and decreases at the south (Al-Rasheed WTP).

CONCLUSIONS

1-Water quality affects the corrositivity of the treated water flowing from the WTPs to the distribution system in Baghdad city. The parameters most influence the corrosion and leaching the materials of the distribution system are:

a- Calcium (Ca) concentration increased in the treated water from Al-Rasheed WTP that might decrease its corrosivity.

b- Alkalinity (Alk) increased in the effluent of water treatment plant in the south that affects the corrosivity inversely.

c- The increasing amounts of the total dissolved solids (TDS) in the Tigris River are due to the discharge of waste water, leaching of fertilizers and the natural weathering of the soil. These concentrations are high in the flowing water in the south of Baghdad. As mentioned before the treated water also contains high amounts of these contents that will increase the corrosivity of the water.

2- The calculated stability index RI indicated that the treated water from the two plants was corrosive to very corrosive water. The corrosivity index show that the water is highly corrosive in the north part of Baghdad city (Al-karkh WTP) and decreases at the south (Al-Rasheed WTP).

RECOMMENDATIONS

Control of water quality in the distribution system seeks to preserve the basic characteristics of water during its conveyance from the point of production and treatment to the consumers tap. The finished water from the two treatment plants should be completely stable in its compositional and physical attributes. Several methods could be applied in the treatment plants to produce stable water like pH adjustment or adding corrosion inhibitors. The treatment process in Al-karkh plant should be highly adjusted, as the corrosivity index indicates very corrosive water.

**REFERENCES**

- Al Stone, Dimitris Spyridakis, Mark Benjamin, John Ferguson, Steve Reiber, and Stein Osterhus. (1987). The Effects of Short Term Changes in Water Quality on Copper and Zinc Corrosion Rates. AWWA, 79 (2), 75-782.
- AWWA (1971). Water Quality and Treatment (3rd ed.). McGraw Hill Book Company, New York.
- Degremont (1991). Water Treatment Handbook (6th ed.). Lavoisier Publishing, France.
- Kawamura, S. (2000). Integrated Design and Operation of Water Treatment Facilities (2nd ed.). John Wiley & Sons, Inc. New York.
- Millette, J. R., Arthur F. Hammonds, Michael F. Pansing, Edward C. Hansen, and Patrick J. Clark. (1980). Aggressive Water: Assessing the Extent of the Problem. AWWA, 72 (5), 262-266
- MWH (2005). Water Treatment Principles and Design (2nd ed.). John Wiley & Sons, Inc. Hoboken N.J.
- Pisigan, Jr. R. A. and Singley, J. Edward. (1985). Effects of Quality Parameters on the Corrosion of Galvanized Steel. AWWA, 77 (11), 76-82
- Pisigan, Jr. R. A. and Singley, J. Edward. (1987). Influence of Buffer Capacity, Chlorine Residual, and Flow Rate on Corrosion of Mild Steel and Copper. AWWA, 79 (2), 62-70.
- Qasim, S. R., Edward, M. M., and Guany, Z. (2000). Planning, Design, and Operation. Prentice Hall PTR. Upper Saddle River, NJ 07458.
- Schock, M. R. (1989). Understanding Corrosion Control Strategies for Lead. AWWA, 81(7), 88-100.
- Steve H. Reiber, John F. Ferguson, and Mark M. Benjamin. (1987). Corrosion Monitoring and Control in the Pacific Northwest. AWWA, 79 (2), 71-74

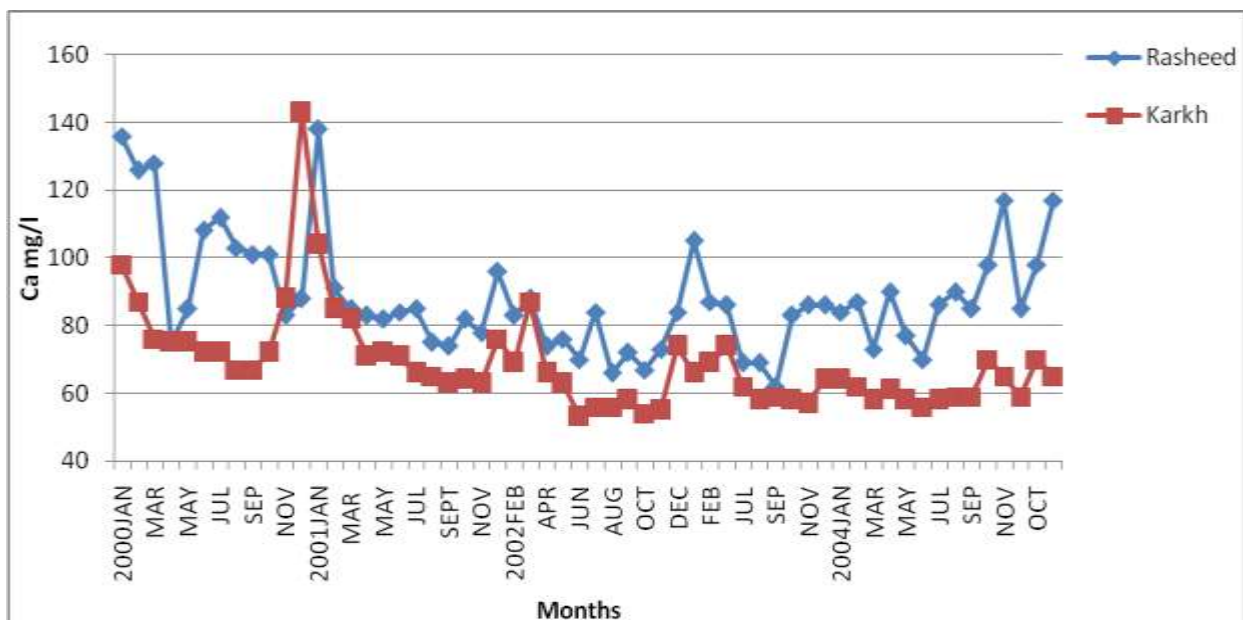


Fig. 1a Max. Ca Concentration

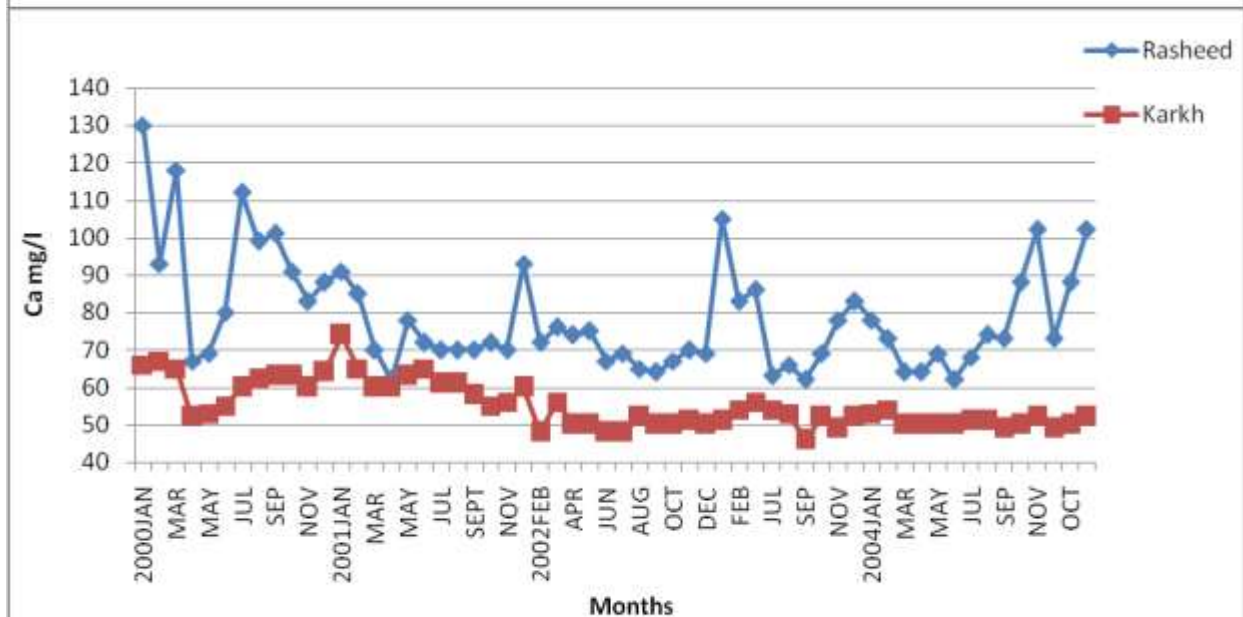
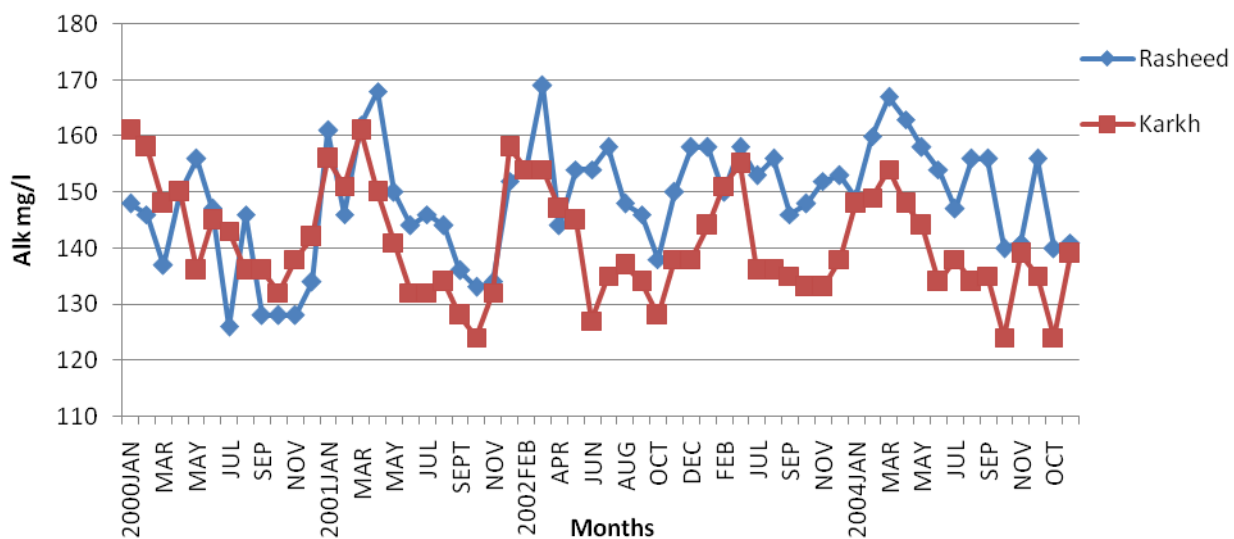
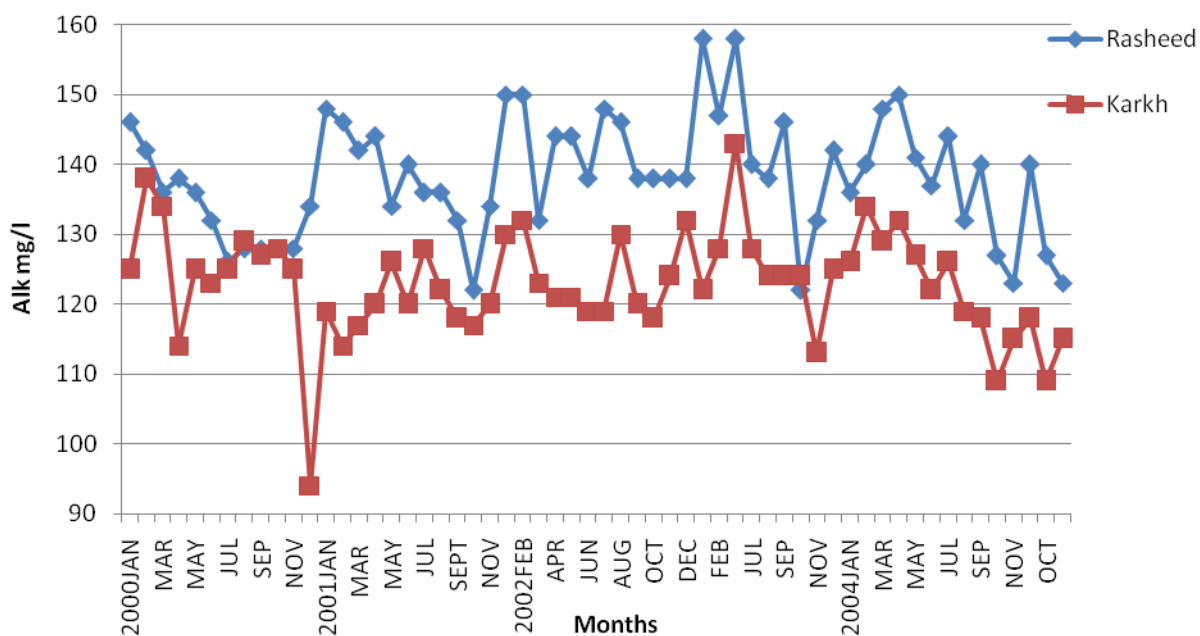


Fig. 1b Min. Ca Concentration

**Fig. 2a Max. Alkalinity****Fig. 2b Min. Alkalinity**

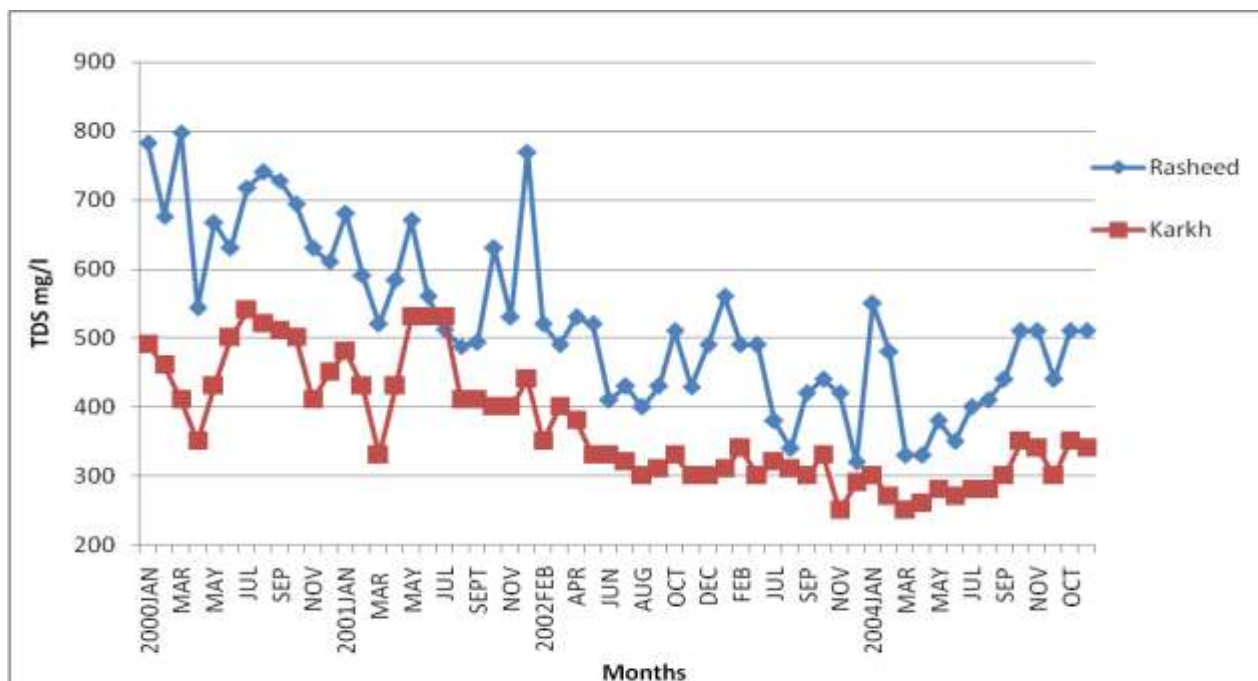


Fig.3b Min.TDS Concentration

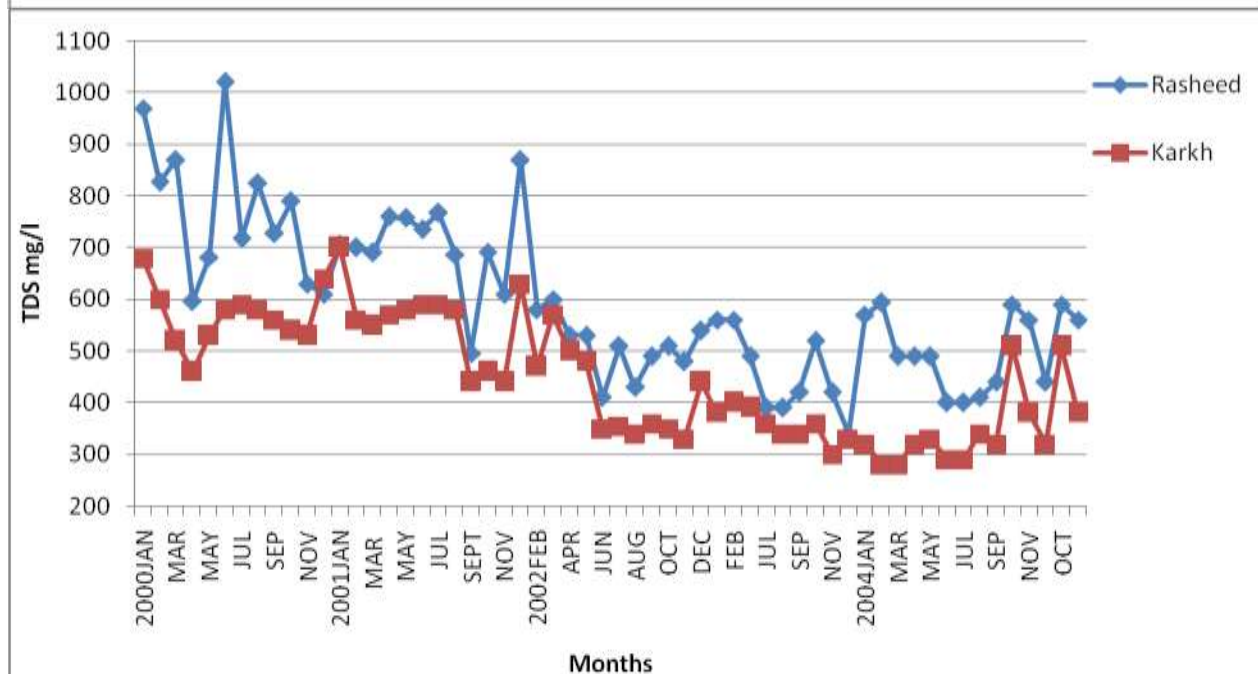


Fig. 3a Max.TDS Concentration

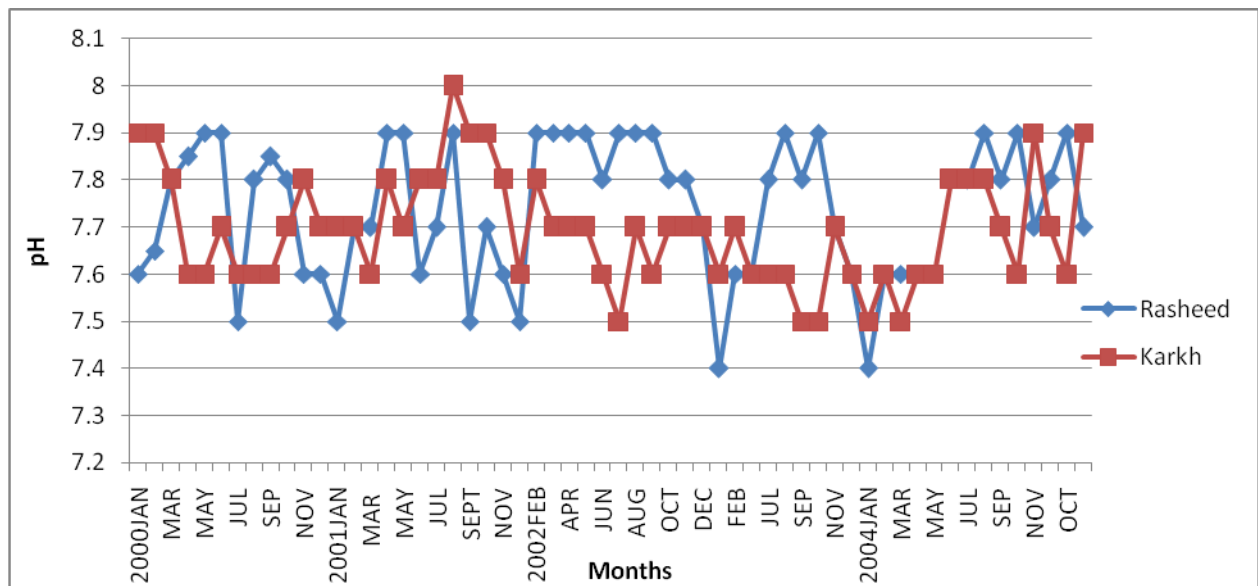


Fig.4a Max. pH

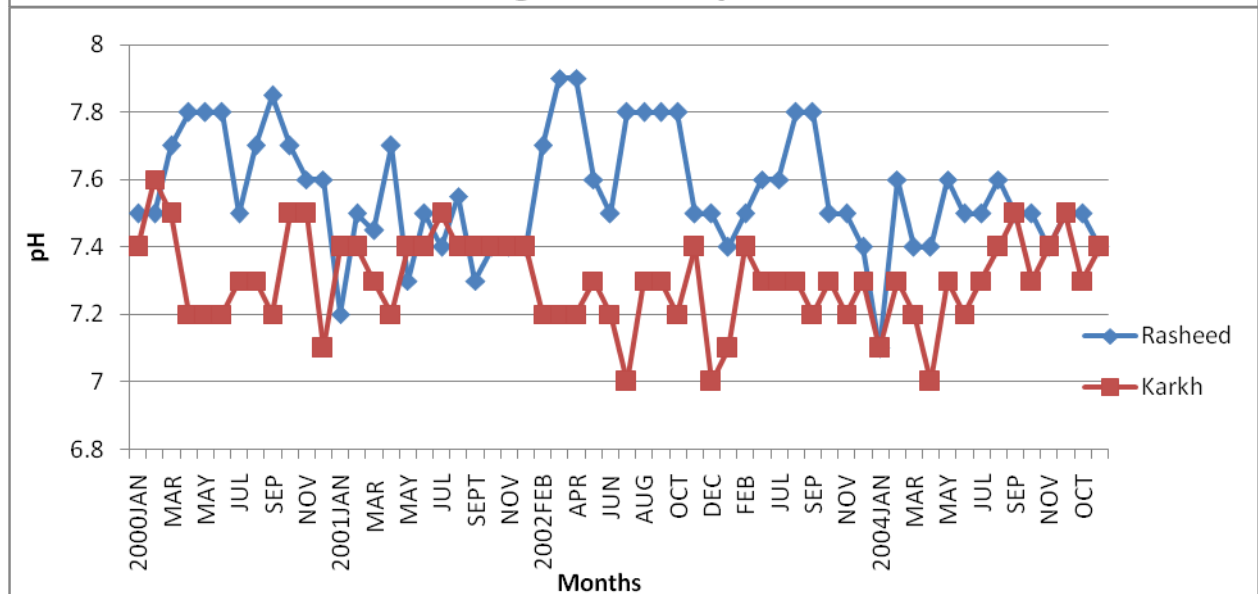
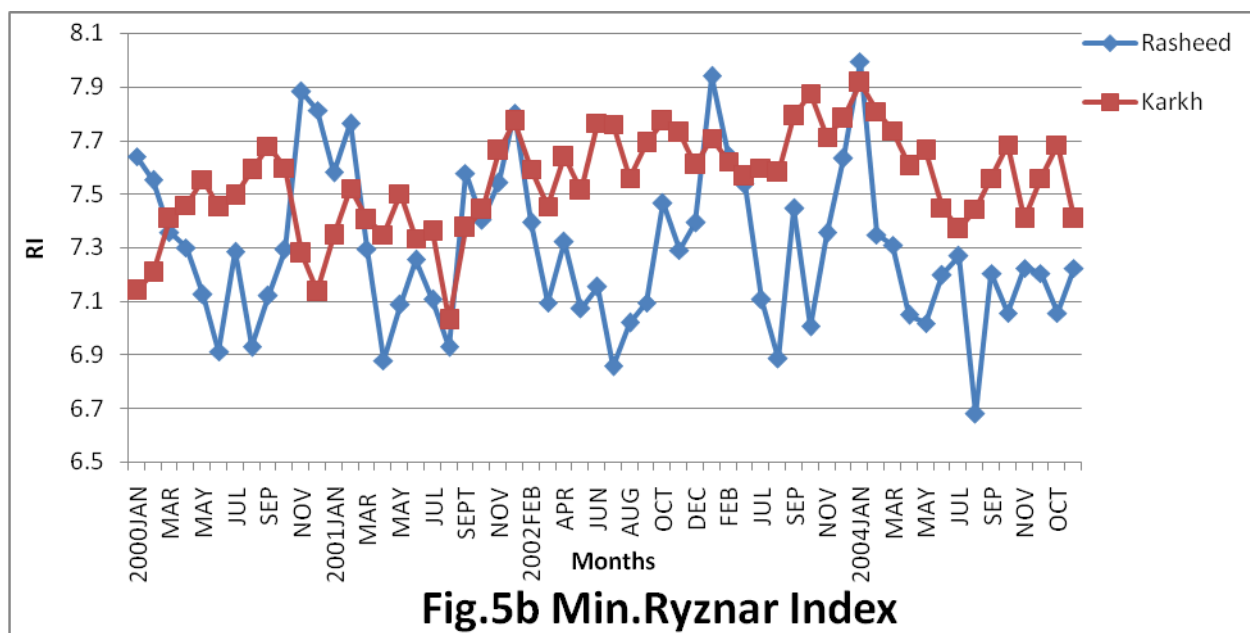
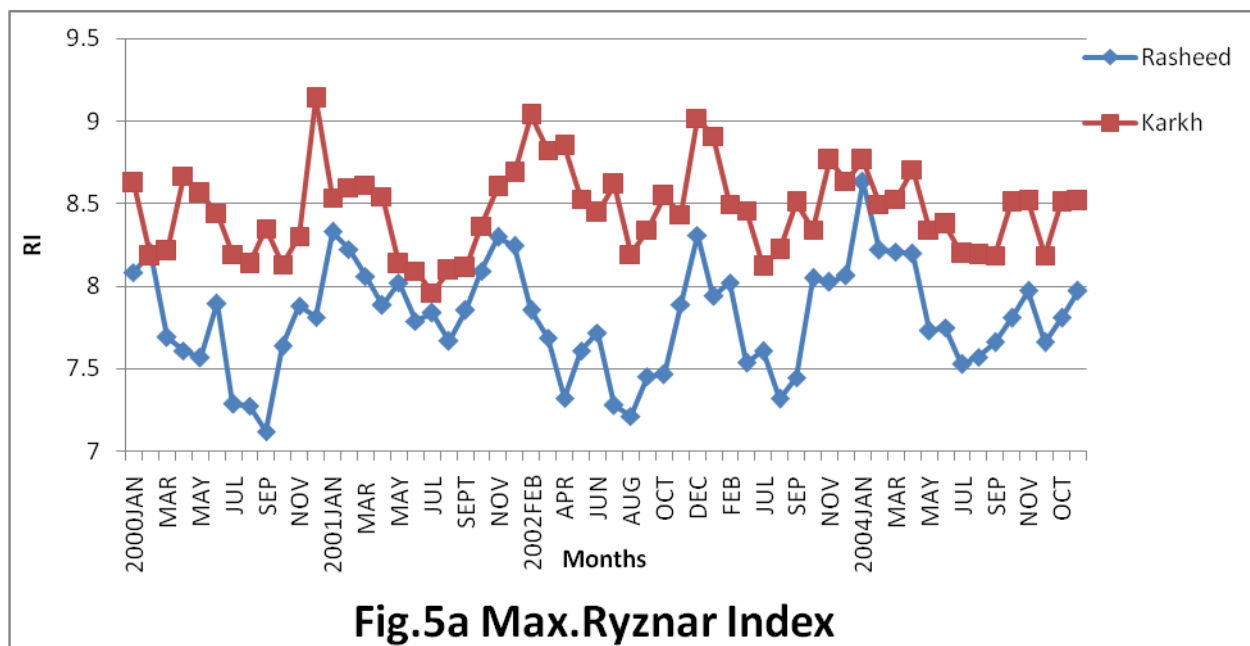


Fig.4b Min. pH



NUMERICAL ANALYSIS OF CONTROLLED MODULUS COLUMN FOUNDATION SYSTEM SUPPORTED EMBANKMENTS

Zainab Ahmed Alkaissi
(Civil Eng. Dep. University
of Al-Mustansiriya)

ABSTRACT

The objective of this research is to present the numerical analysis of deep foundation system namely controlled modulus columns (CMC) for support of embankments. This paper describes the analysis modeling used for CMC foundation system using the finite element method. The elasto-plastic finite element model used to simulate the embankment soil foundation has been verified against field data. The results obtained from this study showed that the effect of CMC could be negligible when the soil strength increased in terms of its angle of internal friction. With low values of internal friction angle, the CMC reduce the potential of surface deformation about 12%. The values of surface deformation decreased with column diameter until it reach constant value at (0.5m) where less than this values the reduction in deformation could be negligible or have insignificant effect. The maximum deformation was observed at the middle of embankment, also the deformation at the embankment foundation reduce by about (17%) when take into consideration the CMC in soil embankment foundation.

الخلاصة:

ان الهدف من هذا البحث هو لتقديم التحليل العددي لنظام اسس التعلبات الترابية المسمى (CMC) لدعم التعلبات الترابية. هذا البحث يصف التمثيل التحليلي المستخدم لـ (CMC) باستخدام طريقة العناصر المحددة. ان نموذج المرونة اللدونة بطريقة العناصر المحددة استخدم لتمثيل نظام التعلبة الترابية وتم مقارنة مع نتائج حقلية. ان النتائج التي تم الحصول عليها من هذه الدراسة اظهرت ان تأثير CMC يمكن اهماله بزيادة مقاومة التربة بدلالة زاوية الاحتكاك الداخلي. ولقيم قليلة لزاوية الاحتكاك الداخلي فان CMC يقلل نسبة التشوه السطحي بحوالي 12%. ان قيم التشوه السطحي تقل مع قطر العمود حتى يصل الي قيمة ثابتة حوالي (0.5 m) حيث ان اقل من هذه القيمة يمكن اهمال النقصان الحاصل بالتشوه او يصبح تأثيره غير ملحوظ. واعلى قيمة للتشوه لوحظت تحت منتصف التعلبة, كذلك ان التشوه في اسس التعلبة يقل بحوالي (17%) عند الاخذ بنظر الاعتبار الـ (CMC) في اسس التعلبة الترابية.

KEY WORDS

Embankment, finite element, (CMC) Controlled Modulus Column, numerical analysis, stress distribution, deformation, Elasto-plastic,

INTRODUCTION

When the embankment is founded on soft soil deposits several problems arises such as settlement or stability problem due to lack of bearing capacity, and or in case of loose saturated fine sand subjected to liquefaction due to ground shaking. To overcome these difficulties, a wide range of deep foundation systems has been developed for construction of embankments on soft soils (*Porbaha et. al, 2002 a*). The objective of this research is to present new deep foundation system namely controlled modulus columns (CMC) for support of embankments.

The behaviour of a test road embankment constructed on soft soil deposits at Haarajoki, Finland is simulated with a multi-laminate constitutive model accounting for structural anisotropy and destructuration effects. Structural anisotropy is achieved by directional distribution of the state variables which are responsible for the bonding of natural soft soil material. The numerical calculations are completed with a finite element method program capable to perform coupled static/consolidation analysis of soils. Problems related to the initiation of in situ stress state, conditions of preconsolidation. Despite simple assumptions concerning field conditions and non-viscous formulation of the constitutive model, the obtained final results are of a sufficient accuracy for geotechnical practice (*Neher and Cudny, 2003*).

The objective of this research is to present the numerical analysis of deep foundation system namely controlled modulus columns (CMC) for support of embankments. This paper describes the numerical modeling used in the analysis of CMC foundation system using the finite element method. Under uniform surcharge traffic load the problem can be studies by plain strain conditions. The approach to the problem allows taking into consideration the settlement tolerance associated with these conditions; and the variability in different soil characteristics.

The Controlled Modulus Column (CMC) as shown in Figure(1), is a ground modification system that reinforces soil by screwing hollow auger into the soft soil and installing a low pressure cement-based grout column through the hollow auger. The combined effect of densification and reinforcement improves characteristics of the soft ground due to composite action. The CMC system uses a displacement auger powered by equipment with very large torque capacity and very high downward thrust, which displays the soil laterally with virtually no spoil or vibration. The auger is screwed to the soil to the required depth and such it increase the density of the surrounding soil and thus increases its load bearing capacity (*Porbaha et. al, 2002 b*).

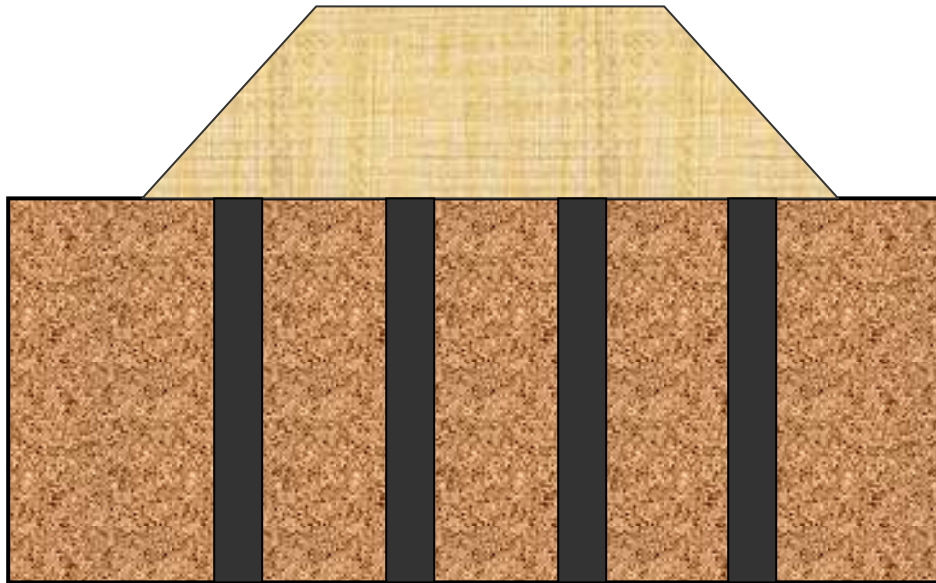


Figure (1): Concept of Column- Supported Embankment.

FINITE ELEMENT ANALYSIS AND MODELING

Work conducted in this part of research aims to numerically analyzing the behaviour of performance embankment structure with CMC system. Numerous researchs used F.E.M to analyze embankments structure over soft soils (*Andrawes et. al. 1980, Han and Gaber 2002, Li and Rowe, 2002*) and embankments with vertical band drains (*Indrartna, et. al. 1992, Hird et. al. 1992*). *Porbaha et. al (2002 a)* simulate the CMC using the axiymmetrical finite difference method to study the behavior of embankment structure with CMC system.

In this paper the method of CMC is described and simulated using finite element numerical analysis as a plane strain conditions with elasto plastic hyperbolic yield criteria. The finite element analysis using the computer program is conducted to discern the stress, strain and surface deformation magnitudes and distribution beneath embankment under varying parameters including column diameter, mesh dimension, soil strength properties. The numerical results are compared with field data.

MODELING OF PROBLEM

The implementation of the model and simulation of embankment soil foundation behavior have been completed using the finite element approach. The finite element mesh and the boundary conditions are shown in Figure (2). Which include 48 elements for soil foundation and 32 elements for embankment. Eight noded rectangular element has been adopted in this study with 263 nodes and the boundary conditions were adopted as follows: vertical boundaries have zero lateral movements, i.e, roller support and the bottom horizontal boundary was restrained both vertically and horizontally.

The finite element program developed in this research is primarily based on the program P6.2 presented by *Smith and Griffiths (1998)* for the analysis of elasto plastic constitutive relations under static loading case. This program is an educational one and has many limitations regarding loading and geometry conditions.

Extensive modifications and newly added subroutines are found necessary to incorporate the initial stress conditions, where the magnitude of insitu stresses in soil embankment layer should be computed at the beginning of the incremental solution, also the embankment layer elements, different properties for different layer, simulation of cement column in embankment soil foundation system

The F.E. program is described, as shown in *Appendix (A)*. The basic finite steps are performed by primary subroutines, which rely on auxiliary subroutines to carry out secondary operations. An auxiliary subroutine may be required by more than subroutine and the order of calling of the primary subroutine is controlled by a main or master routine.

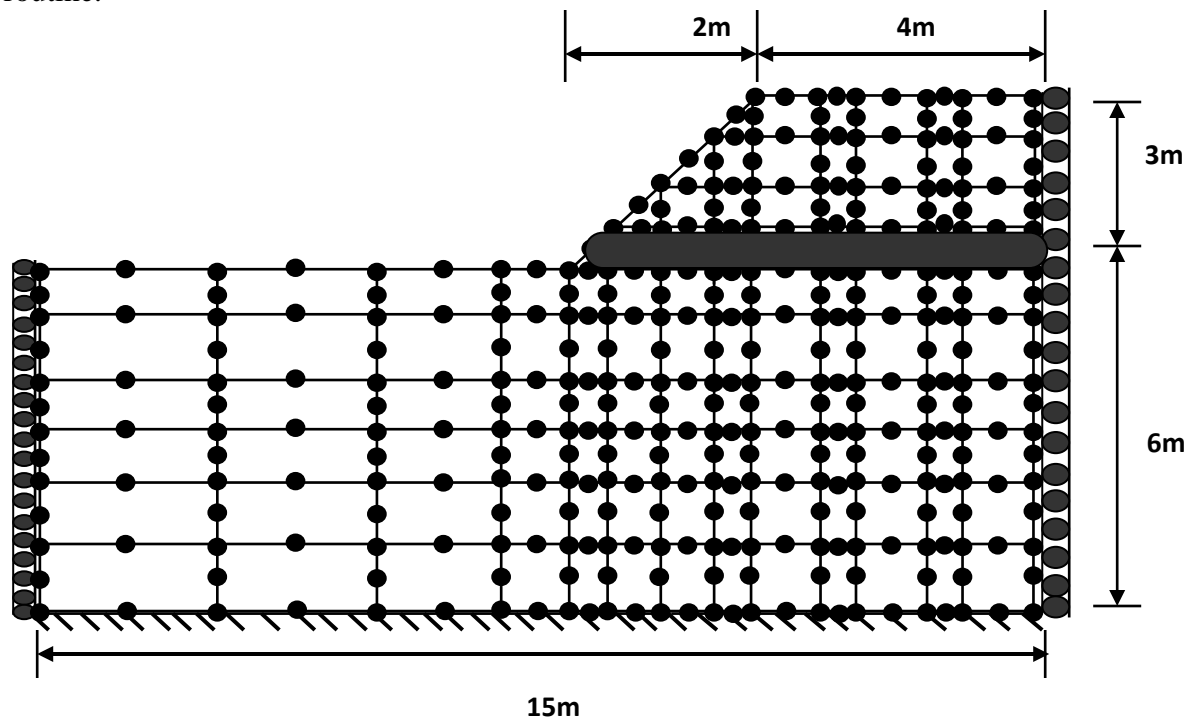


Figure (2): The Finite Element Mesh.

Verification of Computer Program

The results of the finite element program were compared with field data for an embankment section to verify the correct implementation of soil embankment foundation system used in this research. A major instrumented embankment was constructed to 5.5 m elevation above ground level and over soft compressible clay deposit at Leneghan, Newcastle in May 1995 (*Manivannan, 2005*).

The Field and finite element results for predicting performance of this embankment are described. The measured vertical displacement profiles obtained from the HPG reading (horizontal reading profile, based on hydrostatic pressure difference) at the foundation level. The embankment profile used for verification of finite element program is shown in Figure (3). Also the input parameters are shown in Table (1) (*Manivannan, 2005*). The finite element program results have been verified against the field data as shown in Figure (4). The results obtained from finite element analysis are seemed to have reasonable agreement with the observed performance of Leneghans embankment in terms of vertical displacements. The vertical displacement is measured at the toe of embankment and the maximum deformation was observed at middle of embankment profile.

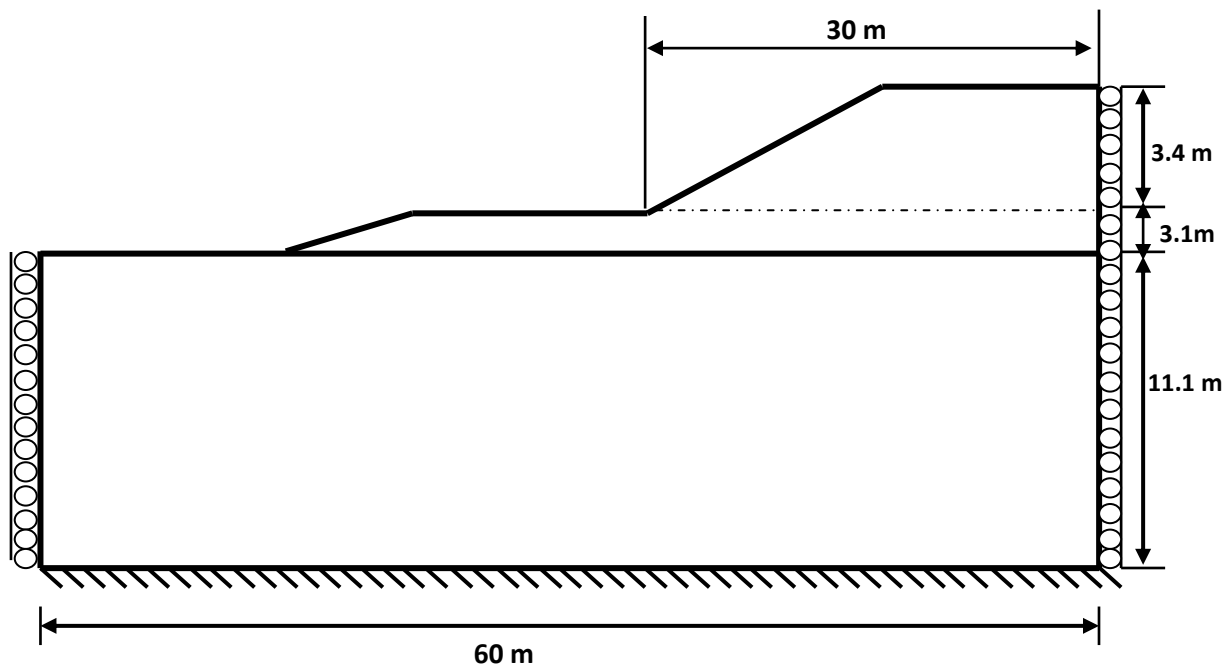
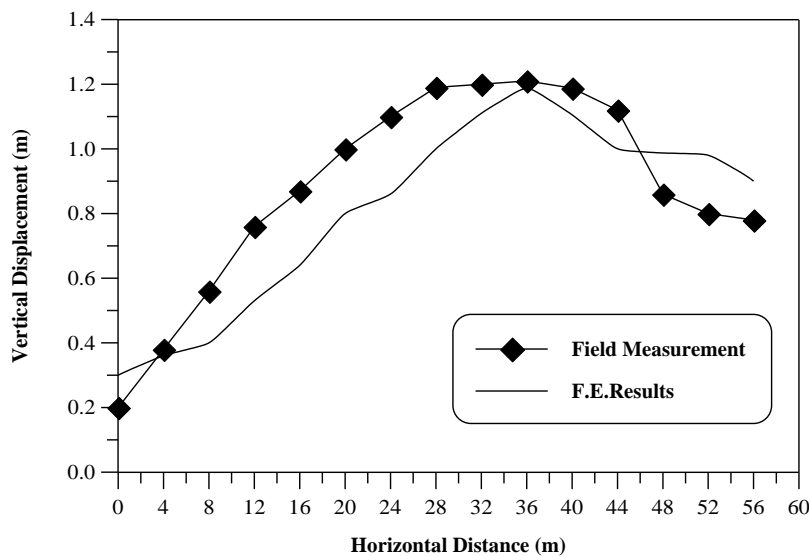


Figure (3): Profile of Cross Section for Test Embankment.

Table (1): Input Parameter for F.E. Program Verification.

Material	Embankment Soil	Foundation Soil (soft soil)
E (kPa)	50	20
Poisons Ratio (ν)	.3	.4
Friction Angle ($^{\circ}$)	28	25
Cohesion (kPa)	5	9.2
Unit weight (kN/m^3)	20	17

**Figure (4): Verification of F.E. Computer Program.**

Also verification of computer program for horizontal and vertical stress distribution with depth have been made. Haarajoki test embankment, which its profile section is shown in Figure (5), has been implemented with finite element program and the material parameters are shown in Table (2) (*Neher and Cudny, 2003*).

The comparison between field and numerical results are presented in Figure (6) and (7) for vertical and horizontal stress distribution respectively and a good agreement is



obtained. But still horizontal stress is overestimated at some location due to the applied isotropic hardening adopted in the finite element program.

Table (2): Input Parameter for F.E. Program Verification (*Neher and Cudny, 2003*).

Material	Embankment Soil	Foundation Soil
E (kPa)	50	20
Poisons Ratio (ν)	.15	.2
Friction Angle ($^{\circ}$)	35	25
Cohesion (kPa)	3.0	5.7
Unit weight (kN/m^3)	21	15

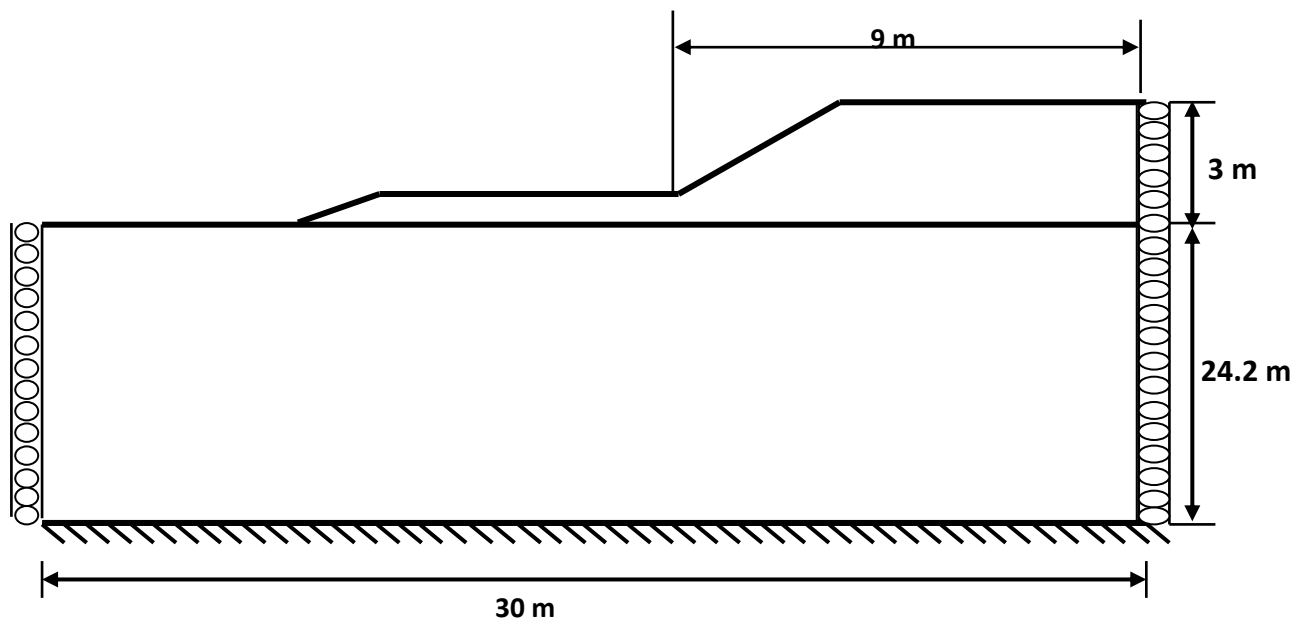


Figure (5): Profile of Cross Section for Haarajoki Test Embankment.

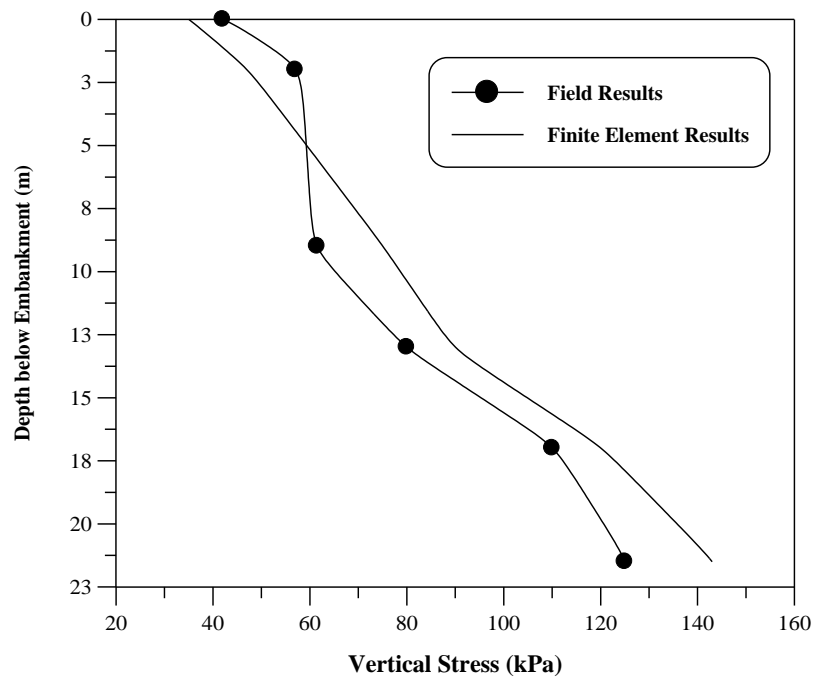


Figure (6): Vertical Stress Distribution below Embankment.

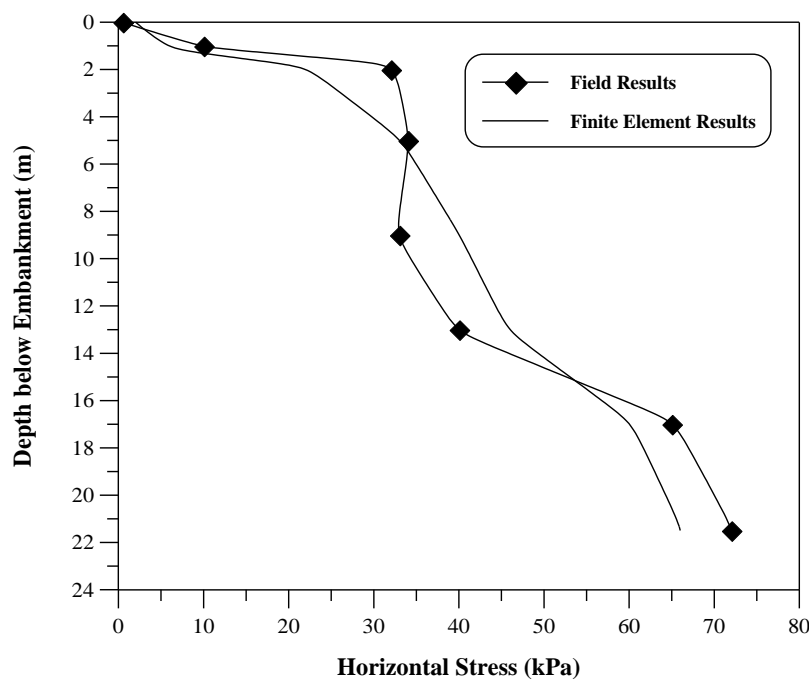


Figure (7): Horizontal Stress Distribution below Embankment.

RESULTS AND DISCUSSIONS

Before the Finite element analysis, the effect of element number on finite element analysis results was checked by comparing the finite element results for two cases with different element number. As shown in Table (3), a check case had four times the foundation elements, four times embankment elements. The F.E.M analysis predicted almost the same maximum surface deformation and maximum foundation stress for both cases.

Table (3): Effect of Element Numbers on Accuracy of Results.

Case	Element Number		Surface Deformation(m)	Foundation Stress (kPa)
	Foundation Element	Embankment Element		
Base case	48	32	0.02044	192.523
Check case	192	128	.02035	191.997

After complete the verification of F.E. program for both model simulation and the accuracy of element numbers, the behaviour of CMC with embankment foundation system has been investigated. The profile section of embankment with CMC is shown in Figure (8) for 1.4 C/C column spacing, and a parametric study was conducted. The input parameter used in the finite element analysis is listed in Table (4) below with traffic load surcharge 20 kPa .

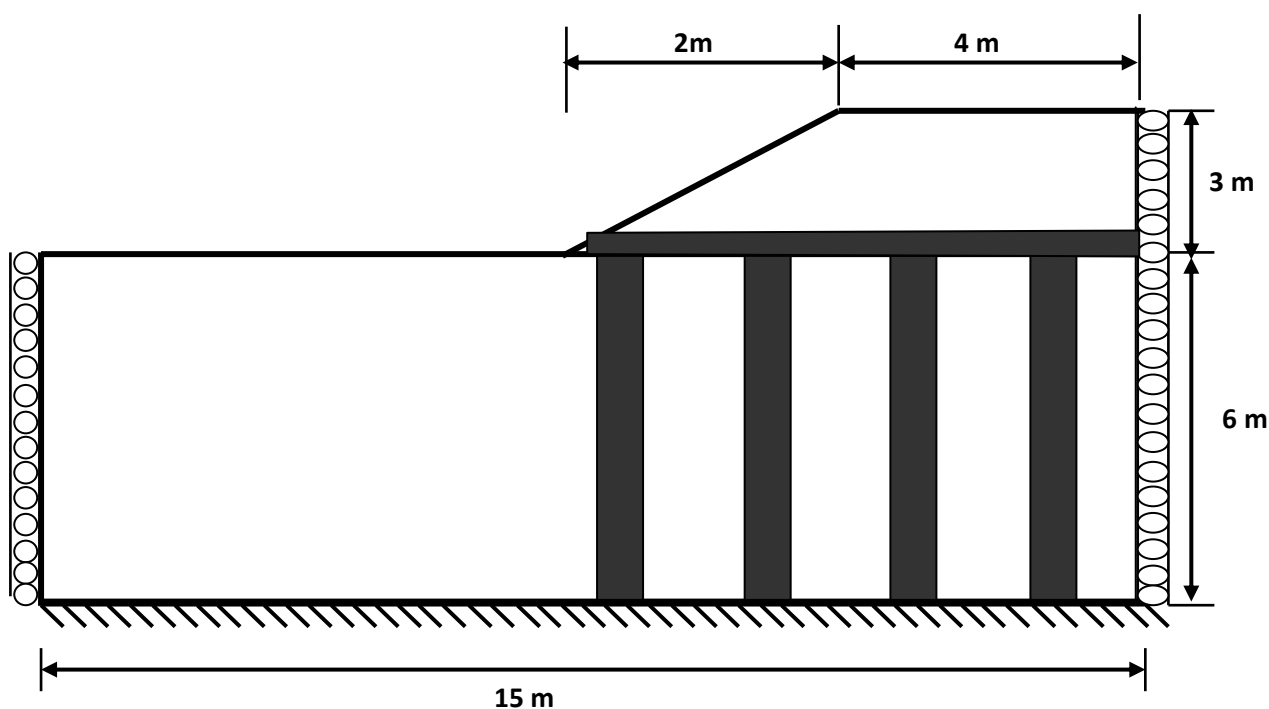


Figure (8): Profile of Cross Section for Studied Embankment.

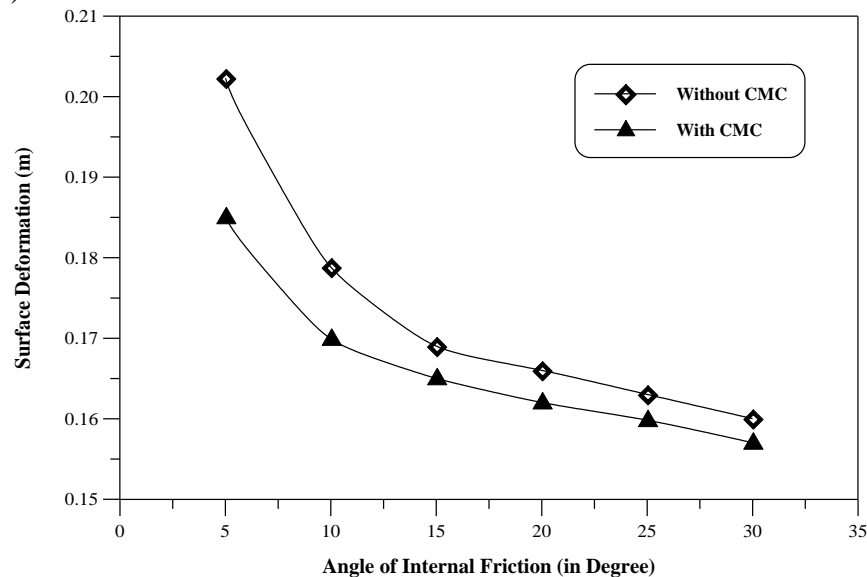
Table (4): Input Parameter for F.E. Analysis.

Material	Embankment Soil	CMC	Transition Layer (Stiff Layer)
E	50 (kPa)	11000 MPa	80
Poisons Ratio (ν)	.4	-	.3
Friction Angle ($^\circ$)	5-30	-	30
Cohesion (kpa)	5	-	20
Diameter (m)	-	0.2 – 1.0	

To consider the effect of soil strength, angle of friction are considered in parametric study. Figures (9) and (10) show the effect of soil properties on surface deformation at the toe of embankment in terms of angle of internal friction and undrained shear strength. It can be concluded that the effect of CMC could be negligible when the soil strength increased in terms of its angle of internal friction. With low values of internal friction angle, the CMC reduce the potential of surface deformation about 12%.

Also Figure (11) show the effect of column diameter on surface deformation. The finite element results indicates that the values of surface deformation decreased with column diameter until it reach constant values at (0.5m) where below this values the reduction in deformation could be negligible or have insignificant effect.

Figure (12) show the variation of surface deformation at the bottom of embankment with radial distance. The maximum deformation as shown in figure is in the middle of the embankment foundation, and the deformation at the embankment foundation reduce by about (17%) when take into consideration the CMC in soil embankment foundation.

**Figure (9): Variation of Surface Deformation with Angle of Internal Friction.**

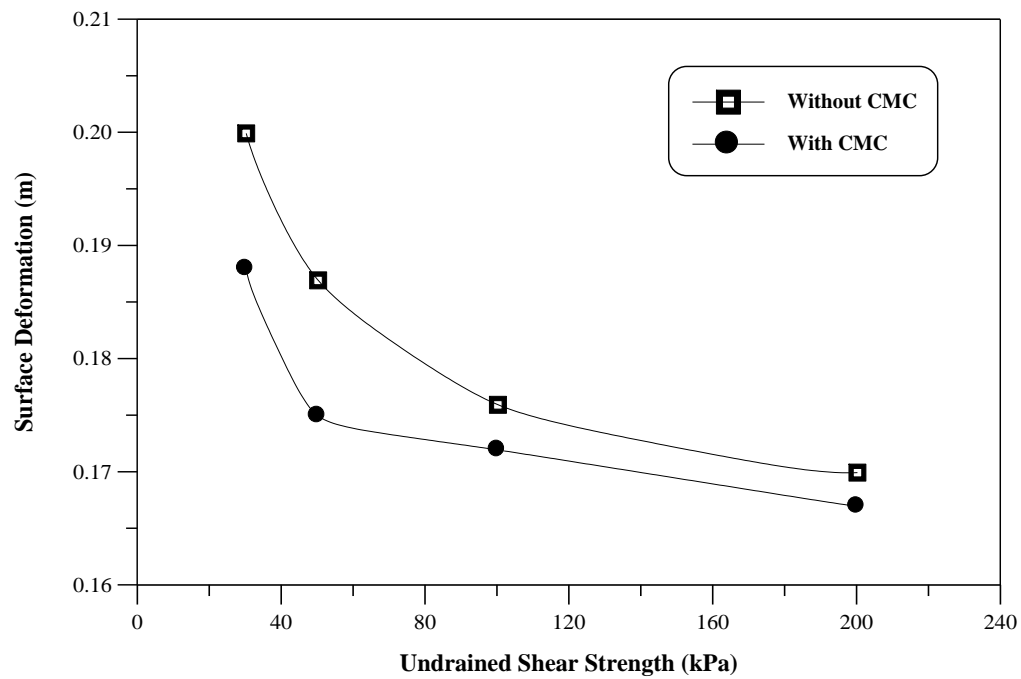


Figure (10): Relation of Undrained Shear Strength with Surface Deformation.

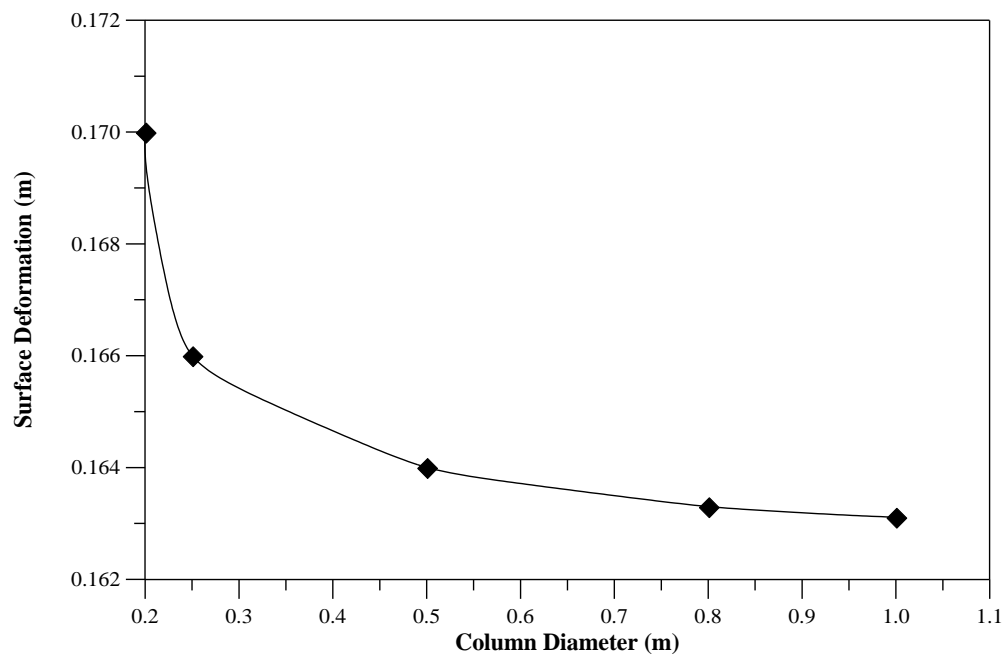


Figure (11): Effect of Column Diameter on Surface Deformation.

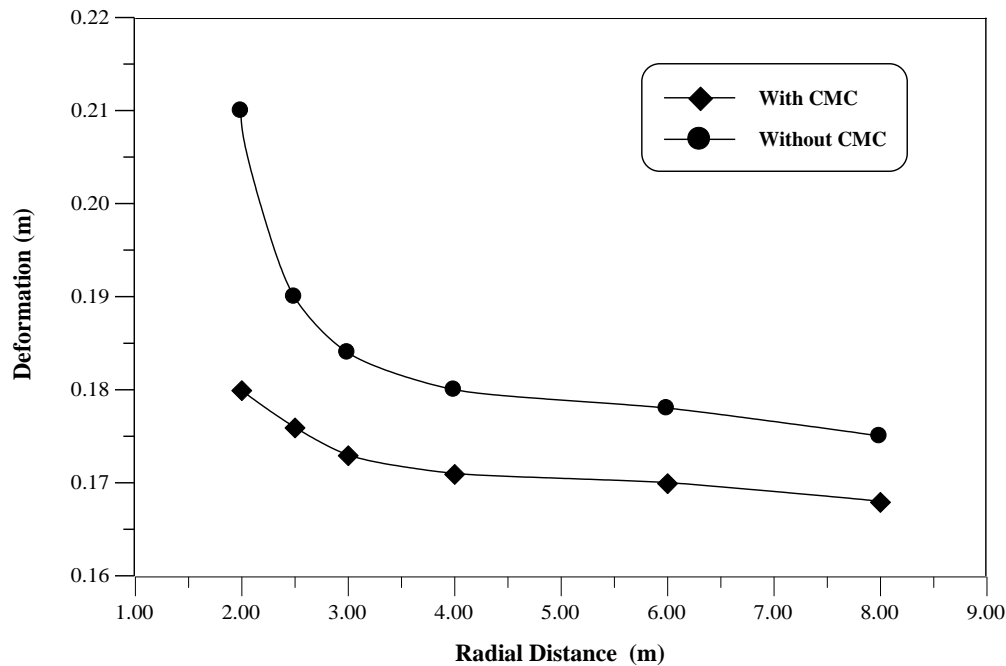


Figure (12): Variation of Bottom Deformation with Radial Distance.

STRESS DISTRIBUTION BENEATH EMBANKMENT

The stress distribution was evaluated using elasto-plastic analysis with the finite element program. And the obtained results were plotted using surfer program to obtain contour lines of horizontal and vertical stress distribution as shown in Figure (13) and (14) respectively. It can be observed from these figure that the horizontal stress increase with depth below embankment.

Figures (15) and (16) represent the 3D surface for horizontal and vertical distribution respectively. According to the stress distribution pattern shown in Figures below for vertical stress, a stiff layer between the embankment and CMC should be applied to ensure that the great part of the generated stress transfer to the head of control modulus column CMC and to study its effect, a transition layer between embankment and soil foundation is applied as shown in Figure (8) with properties of stiff soil as shown in Table (4). Figure (17) and (18) show the horizontal and vertical stress distribution with depth below embankment respectively. Also the 3D-surface for horizontal and vertical stress distribution are shown in Figure (19) and (20) respectively.

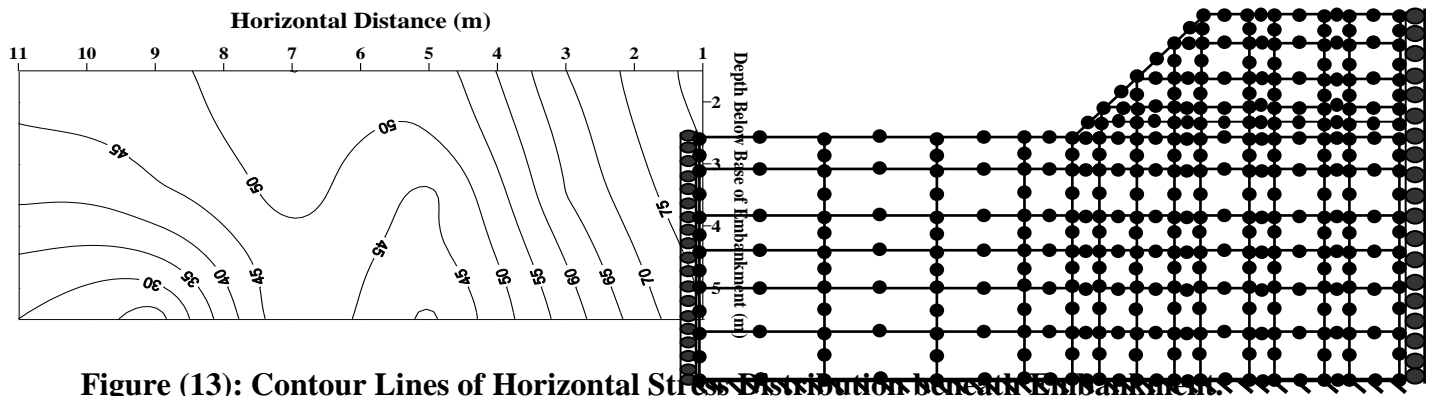


Figure (13): Contour Lines of Horizontal Stress Distribution beneath Embankment.

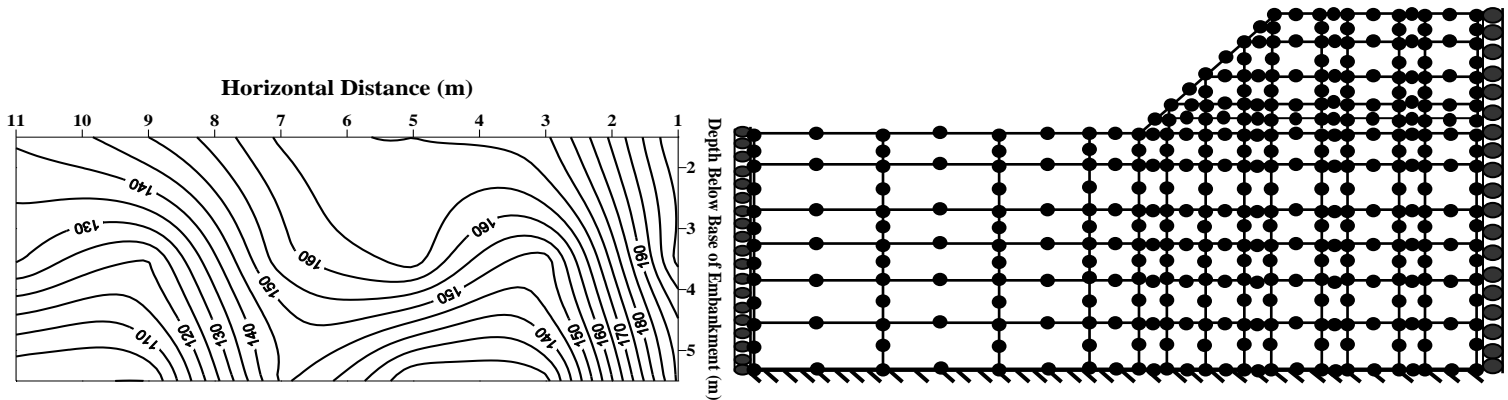


Figure (14): Contour Lines of Vertical Stress Distribution beneath Embankment without transition Layer.

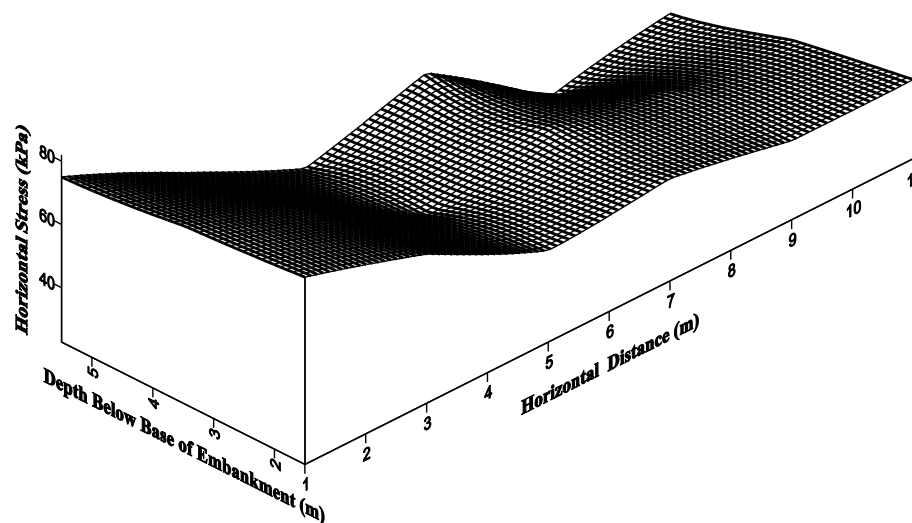


Figure (15): 3D surface of Horizontal Stress Distribution beneath Embankment.

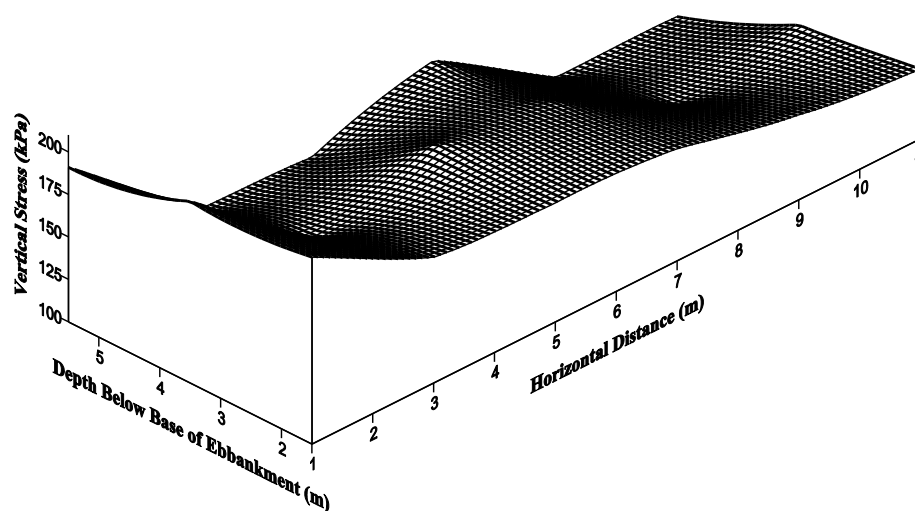


Figure (16): 3D surface of Vertical Stress Distribution beneath Embankment.

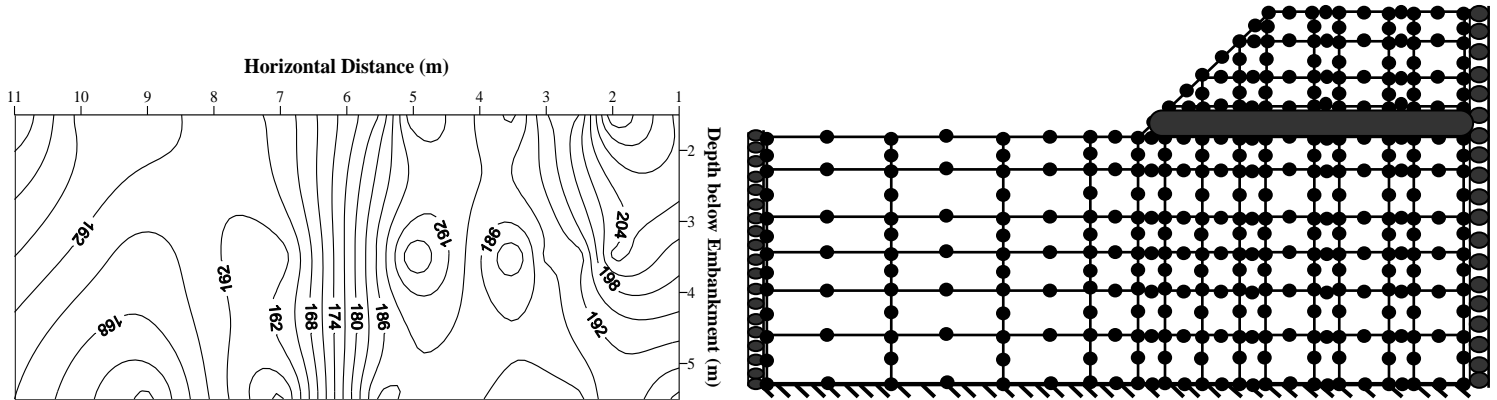
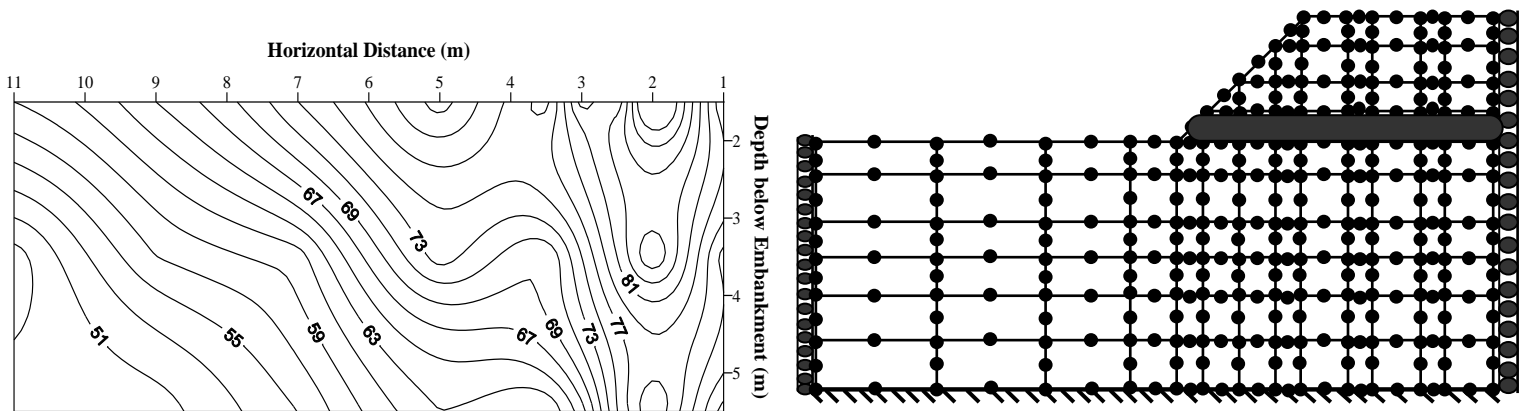


Figure (17): Contour Lines of Horizontal Stress Distribution beneath Embankment with Stiff Layer.



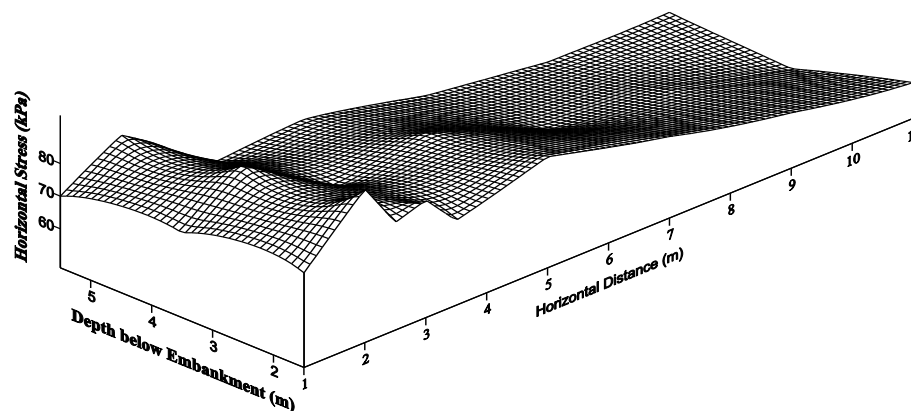


Figure (19): 3D surface of Horizontal Stress Distribution beneath Embankment.

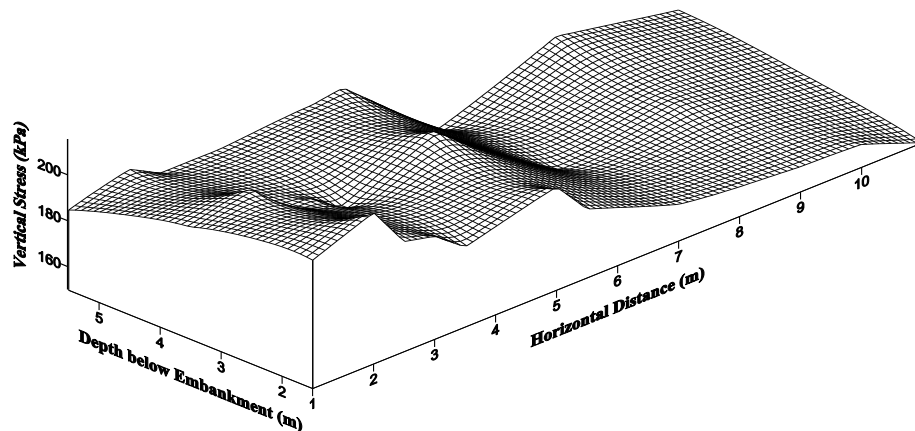


Figure (20): 3D surface of Vertical Stress Distribution beneath Embankment.



CONCLUSIONS

The deformation of embankment supported on controlled column modulus improved foundation soil and can be analyzed using numerical methods. The following conclusions remarks are obtained:

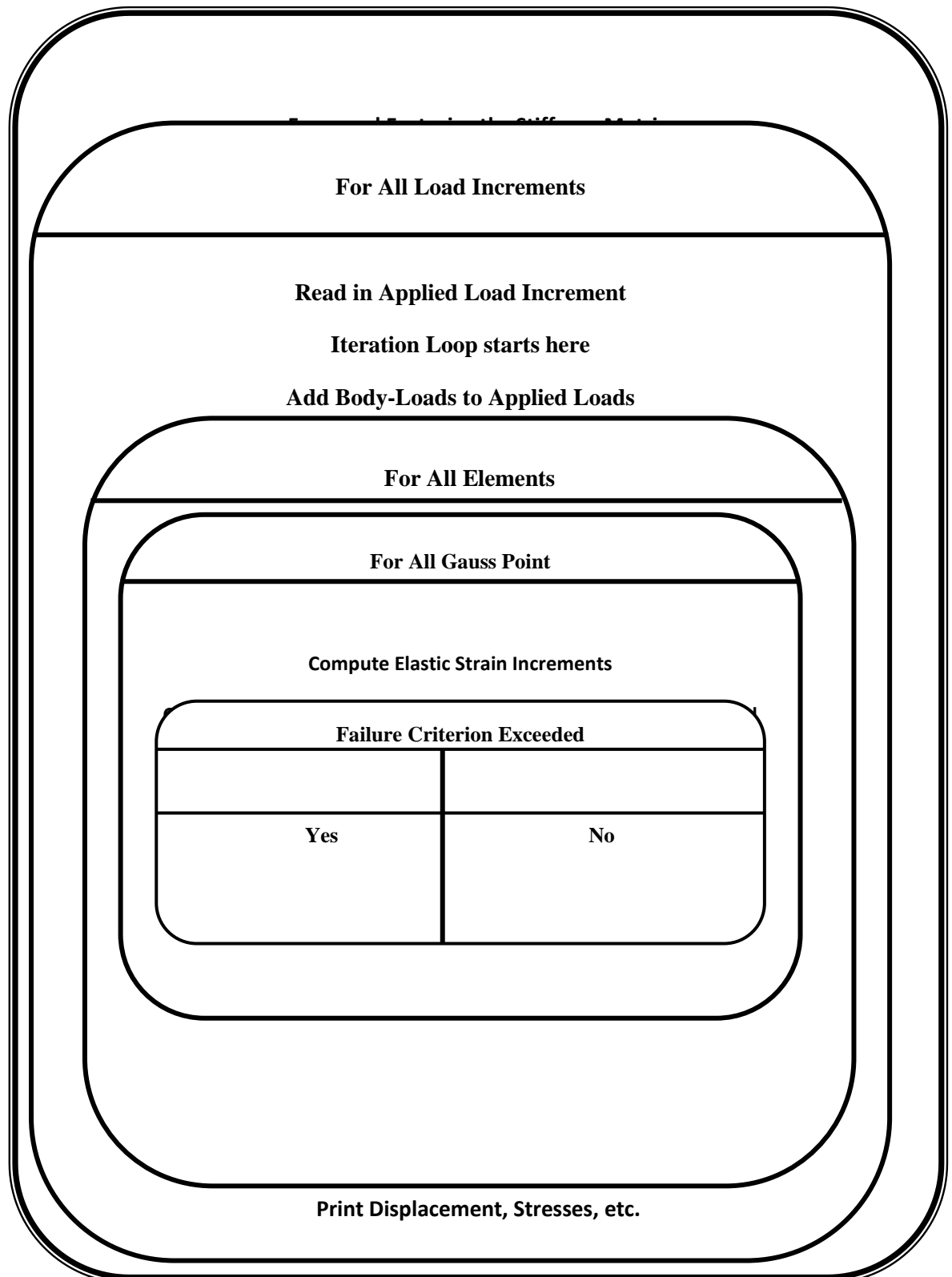
1. The elasto-plastic finite element model used to simulate the embankment soil foundation system including different layer properties and CMC have been verified against field data and seemed to have reasonable agreement with the observed performance of Leneghans embankment in terms of vertical displacements.
2. The effect of CMC could be negligible when the soil strength increased in terms of its angle of internal friction. And with low values of internal friction angle, the CMC reduce the potential of surface deformation about 12%.
3. The values of surface deformation decreased with column diameter until it reach constant values at (0.5m) where below this values the reduction in deformation could be negligible or have insignificant effect. And the maximum deformation was observed at the middle of embankment, also the deformation at the embankment foundation reduce by about (17%) when take into consideration the CMC in soil embankment foundation.
4. The stress distribution pattern for vertical and horizontal stress increases with depth below embankment, and according to the stress distribution pattern a stiff layer between the embankment and CMC should be applied to ensure that the great part of the generated stress transfer to the head of control modulus column CMC.

REFERENCES

- Andrawes, K.Z, McGown, A. , Mashhour, M.M , and Wilson-Fahmy, R.F. (1980): **“Tension Resistance Inclusions in Soils”** . Journal of Geotechnical Engineering Division, ASCE , 106, GT(12):1313-1326.
- Han, J., and Gabr, M.A. (2002): **“Numerical Analysis of Geosynthetic-Reinforced and Pile-Supported Earth Platform over Soft Soil”**. Journal of Geotechnical and Geoenvironmental Engineering, 44-53.
- Hird, C.C, Pyrah , I.C., and Russell, D. (1992): **“Finite Element Modeling of Vertical Drains beneath Embankments on Soft Ground”**. Geotechnique, 42(3):499-511.
- Indraratna, B., Balasubramaniam, A.S. ,and Balachandran, S. (1992): **“Performance on Test Embankment Constructed to Failure on Soft marine Clay”**. ASCE Journal of Geotechnical Engineering, 118(1):12-33.
- Li, A.L., and Rowe, R.K. (2002): **“Design Consideration for Embankmentson Rate Sensitive Soils”**. ASCE Journal of Geotechnical and Geoenvironmental Engineering, 128(11): 885-897.
- Neher, H., and Cudny, M. (2003): **“Numerical Analysis of Test Embankment on Soft Ground using An anistropic Model with Destructuration”** . Institute of Geotechnical Engineering, University of Stuttgart, Germany.
- Porbaha, A., Brown, D., Macnab,A.,Short, R. (2002a): **“Innovative European Technologies to Accelerate Construction of Embankment Foundations- Part 1”** . Proceedings of Time Factor in Design and Construction of Deep Foundations, Deep Foundation Institute, San Diego, C.A., 3-14.
- Porbaha, A., Brown, D., Macnab,A.,Short, R. (2002b): **“Innovative European Technologies to Accelerate Construction of Embankment Foundations- Part 2”** . Proceedings of Time Factor in Design and Construction of Deep Foundations, Deep Foundation Institute, San Diego, C.A., 15-28.
- Smith, I.M., and, Griffiths, D.V. (1998): **“Programming the Finite Element Method”**. Second Edition, John Wiley and Sons Ltd.
- Manivannan, G. (2005): **“Viscoplastic Modeling of Embankment on Soft Soils”**. Ph.D Thesis, University of New South Wales.



Appendix A





ALKYLATION OF BENZENE WITH LONG CHAIN OLEFINS OVER SOLID-ACID CATALYST

Abdul Halim A. K. Mohammed

Department of chemical Engineering,
University of Baghdad

Ali M. Ridha

Department of chemical Engineering,
University of Baghdad

ABSTRACT

This investigation is concerned with the linear alkylbenzene production reaction by the alkylation of benzene with long chain olefins C_{10} - C_{13} over various prepared solid acid catalysts. The alkylation process was studied at different reaction temperature, Weight hourly space velocities and with constant pressure and benzene/olefin ratio. The liquid-phase of alkylation of benzene with olefins carried out over prepared tungstophosphoric acid supported on SiO_2 with 5, 10, 20 and 30 wt. % loading catalysts in a fixed bed reactor. Prepared tungstophosphoric acid supported over silica catalyst with 30 % loading gave the highest conversion of olefin to linear alkylbenzene (94% conversion) at 398K and $5h^{-1}$. The study of the kinetics of benzene alkylation with olefins over these prepared catalysts reveals that the reaction is second order. The value of Thiele modulus for each prepared catalysts is lower than 0.4 which means that diffusion free regime and the surface reaction is the limiting step for the alkylation process.

INTRODUCTION

The alkylation of benzene with higher n-alkenes, basically in the range of C_{10} to C_{13} , is preformed industrially in the manufacture of linear alkylbenzene (LAB), an intermediate used in the production of linear alkylbenzenesulphonate (LAS), the most important biodegradable surfactant in the detergency sector.

LAB is industrially produced by one of three technologies of benzene alkylation from alkenes with hydrofluoric acid or aluminum trichloride as catalysts or from chloroalkanes in the presence of aluminum trichloride as a catalyst ⁽¹⁾. These two Friedel-Crafts catalysts (hydrofluoric acid and aluminum trichloride) give different phenyl isomer distributions in the LAB produced. Alkylation using homogeneous catalysts such as sulphuric acid, hydrofluoric acid and aluminum trichloride has been investigated by Alul ⁽²⁾ and Olson ⁽³⁾.

Since homogeneous acid catalysts are a source of pollution, industrial hazard and equipment corrosion, a good deal of effort has been into research and development to replace hydrofluoric acid HF and aluminum trichloride AlCl₃ by a non-corrosive solid catalyst having acid properties. A Wide variety of heterogeneous catalysts has been investigated so far, such as rare earth X and Y zeolites ⁽⁴⁾, silicotungstic acid supported on alumina and on silica-alumina ⁽⁵⁾, ZSM-4, ZSM-5, ZSM-20, ZSM-38, ZSM-12, mordenite and offertite ⁽⁶⁻¹¹⁾, Ca, NaY ⁽¹²⁾, HNaY zeolites ⁽¹³⁾, MCM-22 ⁽¹⁴⁾ and with aluminum silicate and/ or magnesium silicate ⁽¹⁵⁻¹⁶⁾. Sivasanker and Thangaraj ⁽¹⁷⁾ and Sivasanker et al. ⁽¹⁸⁾ have studied the alkylation of benzene with an industrial mixture of higher alkenes for the production of LAB over β -zeolite, mordenite and ZSM-12 catalysts. Universal Oil Products (UOP/ Petresa) have announced new process in Canada using a solid acid catalyst and the first industrial plant using this solid acid catalyst technology operated in Canada in 1995 ⁽¹⁹⁻²⁰⁾.

To measure how much the reaction rate is lowered because of the resistance to pore diffusion, the quantity ϵ called effectiveness factor must be defined ⁽²¹⁾.

$$\text{Eff. Factor } \epsilon = \frac{\text{(actual mean reaction rate within pore)}}{\text{(rate if not slowed by pore)}} \dots (1)$$

$$= \frac{r_A, \text{ with diffusion}}{r_A, \text{ without diffusion resist.}} \dots (2)$$

Thiele modulus can be estimated for each catalyst type depending on its physical properties and process operation condition. For first order surface reaction Thiele modulus can be estimated in Eqn. (3).



$$M_T = L * \sqrt[2]{k''' / D_e} \quad \dots (3)$$

The aim of this work is the production linear alkylbenzene by alkylation of benzene with long chain olefins over prepared solid acid catalysts such as tungstophosphoric acid supported on silica with 5, 10, 20 and 30 wt. % loading catalysts in a fixed bed reactor. Study the effect of various range of temperature and weight hourly space velocity (WHSV). Then studying the reaction kinetics and developing the mathematical model to describe the rate of reaction and estimate all parameters of this model.

EXPERIMENTAL WORK

Experimental Equipment

The experimental equipment used in this study is shown in the Figure (1). Benzene and olefins were charged in a feed conical vessel. Dosing pump flows the mixture of olefin and benzene to the reactor at volumetric flow rate (0- 1000) cm³/h and discharge pressure 10 bar. The reactor is stainless steel tube with 19 mm inside diameter, 800 mm length and 2mm thickness (Catatest Model BL-2 supplied by Geomecanique, France). The reactor supplied with four heaters (150 mm length for each) and 2 insulators (100 mm length). These heaters were controlled by a temperature indicators and controllers to set the desired temperature for each one automatically. The temperature reading along the full length of reactor was obtained by chromel-alumel thermocouples (K type). For each experiment 10 g of catalyst was charged in the middle zone of the reactor between upper and lower zone filled with inert glass beads.



Fig. (1) Alkylation Reaction Unit (Photographic View)

Process flow diagram of the alkylation process

The alkylation process was examined at reaction temperatures varied from 353-398 K, while the weight hourly space velocities from 5-20h⁻¹. The pressure and benzene/olefin ratio were kept constant at 10 bar and 10/1, respectively. Before the alkylation reaction was started, the catalyst was activated at 423 K and atmospheric pressure in nitrogen flow of (1 liter/h) for 2 h. Then the catalyst bed was cooled to about 333 K and N₂ flow was adjusted at 10 ml /min to keep the system at the required pressure 10 bar. The mixture of benzene and olefins were charged from the conical vessel to the reactor through check valve. The flow rate of reactants was adjusted to the desired value for each particular experiment. The mixture of reactants (Benzene and Olefins) and N₂ is entering the preheating zone and then passed the catalyst bed. As soon as the flow rate of reactants was stabilized, the temperature of the reaction section was adjusted to the desired for each particular experiment. The liquid product was collected in a liquid receiver, which was drained at the end of the run to collection flask.



Preparation of tungstophosphoric acid supported on SiO₂ catalyst

Series of tungstophosphoric acid catalysts supported on silica with different texture properties were prepared by impregnation method. Supports were impregnated with aqueous solutions of the acid using the incipient wetness technique. After impregnation the catalysts were dried at about 393K for 2.5h. The obtained material was then calcined at 523K for 3h, in an electrical furnace.

Test method

The weight percentage of SiO₂ was determined by fusion method ⁽²²⁾. The fusion mixture in this method was (K₂CO₃+Na₂CO₃).

An off-line gas chromatograph (Packard 438A, USA) flame ionization detector (FID) was used to analysis the composition of linear alkylbenzene in the liquid product. The apparatus consists of a stainless steel capillary column with 50m long and 0.25 mm inside diameter. The column was open tube coated (SE-30) name type.

RESULT &DISCUSSION

Effect of temperature

The effect of reaction temperature in the range of 353- 398 K on olefin conversion at different space velocities was studied. As expected, Figure 2 shows that the increasing of temperature will increase the olefin conversion. The olefin conversion at WHSV= 20h⁻¹ was not significantly affected by the increasing of the temperatures from (355- 398K). it was found that no dialkylated product was found even when the temperature was increased from (355-398K). This was because of excess benzene in the reaction mixture. In contrast, at 15, 10 and 5 h⁻¹ the conversion was significantly increased with increasing the temperatures. In addition, high reaction temperature ($\geq 433\text{K}$) can lead to the comparatively quick deactivation of catalyst. It could be expected that the tendency of the polymerization of olefin would be raised by high reaction temperature ($\geq 433\text{K}$)²³.

Effect of WHSV

The effect of weight hourly space velocity between 5-20h⁻¹ on olefin conversion at different reaction temperatures was studied. The results of this investigation were presented in Figure (3). This figure show that the decreasing of WHSV will increase the olefin conversion, because the decreasing in WHSV of the feed results to increasing in the residence time, which leads to a plenty of contact time of the feed (reactants) with the catalyst inside reactor, and this means effective conversions of olefin to linear alkylbenzene. All the results indicate that low WHSV is favored alkylation process.

Kinetic of alkylation process

The kinetic of alkylation process of olefin and benzene was studied. For second order kinetic reaction, the performance equation for reactors containing porous catalyst particles for plug flow type, which represented the solid catalyzed reactions ⁽²¹⁾, the performance equation may be obtained in Eq.(1).

$$k' \cdot C_{A_0} \cdot \tau' = \frac{X_A}{(1 - X_A)} \quad \dots (4)$$

A plot of $\frac{X_A}{1 - X_A}$ vs $\tau' C_{A_0}$ gives straight lines with slopes equal to alkylation rate constant for linear alkylbenzene produced over various types of catalysts. The statistical analysis of these straight lines was computed to identify significant. The correlation coefficients (r^2) for all the straight lines of second order kinetic reaction are > 0.95 which is statistically significant. The alkylation rate constants for linear alkylbenzene tabulated in Table (1). These results indicated that the alkylation rate constant increased with increasing reaction temperature.

Thiele Modulus and Effectiveness factor

For second order kinetic reaction, Thiele modulus was obtained by eqn. (5).

$$M_T = L \cdot \sqrt{\frac{(k''' \cdot C_A)_{obs}}{D_e}} \quad \dots (5)$$



Effective diffusivity for a porous solid can be estimated by using eqn. (6)
(24).

$$D_e = 19400 \frac{\theta^2}{\tau_m \cdot S_g \cdot \rho_p} \sqrt{\frac{T}{M}} \quad \dots (6)$$

The effective diffusivities as well as Thiele modulus values were calculated and presented in Table (2).

The effectiveness factor for all types of catalyst was near to be 1 because Thiele modulus values were very small ($M_T < 0.4$) as mentioned by H.Scott Fogler ⁽²⁵⁾, Levenspiel ⁽²¹⁾ and Hougen and Watson ⁽²⁶⁾ that indicates the concentration of reactant doesn't drop appreciably within the pore, thus pore diffusion offers negligible resistance. This can also be verified by noting that values for M_T means either short pore, slow reaction or rapid diffusion, all three factors tending to lower the resistance to diffusion.

CONCLUSIONS

The liquid-phase of alkylation of benzene with olefins was examined by tungstophosphoric acid supported on S_iO_2 with 5, 10, 20 and 30 wt. % loading catalysts in a fixed bed reactor. Alkylation conversion increased with increasing temperature of reaction 353-398K and decreasing with increasing WHSV 5- 20h⁻¹. Prepared tungstophosphoric acid supported over silica catalyst with 30 % loading gave the highest conversion of olefin to linear alkylbenzene (94% conversion) at 398K and 5h⁻¹. The alkylation reaction of benzene with olefins is well represented by second order performance equation for reactor containing porous catalyst particles as plug type. The values of Thiele modulus for each prepared catalysts are (< 0.4) which means that diffusion free regime and the chemical surface reaction is the limiting step for alkylation process.

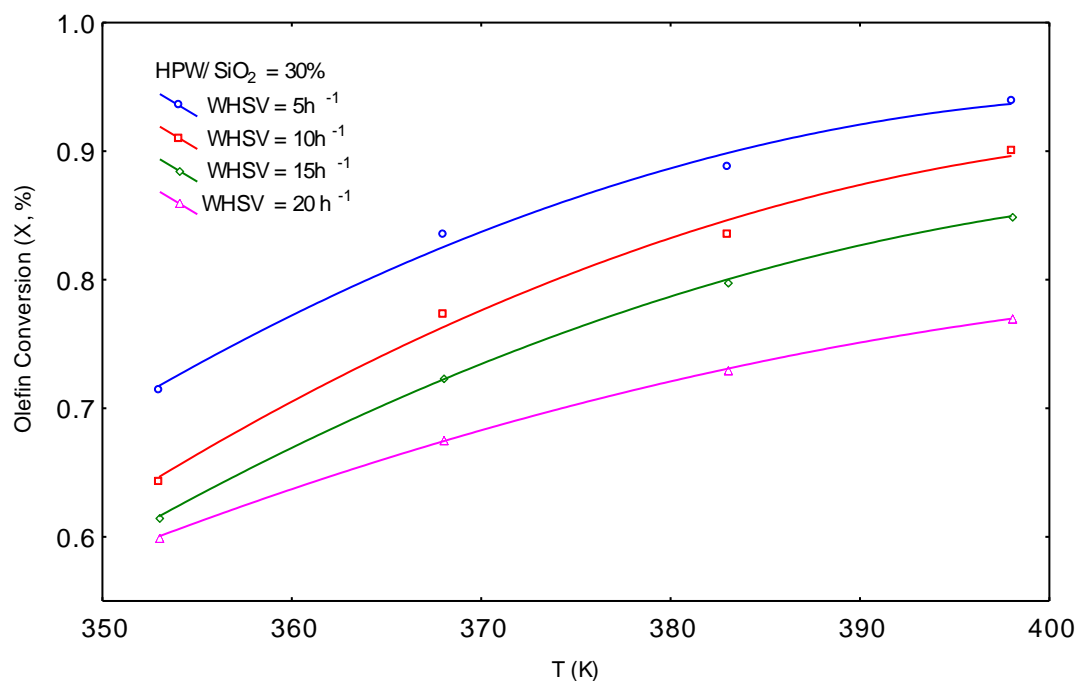


Fig. (2) Effect of Temperatures on the Olefins Conversion at Various WHSV for HPW/SiO₂ = 30 wt. % Catalyst.

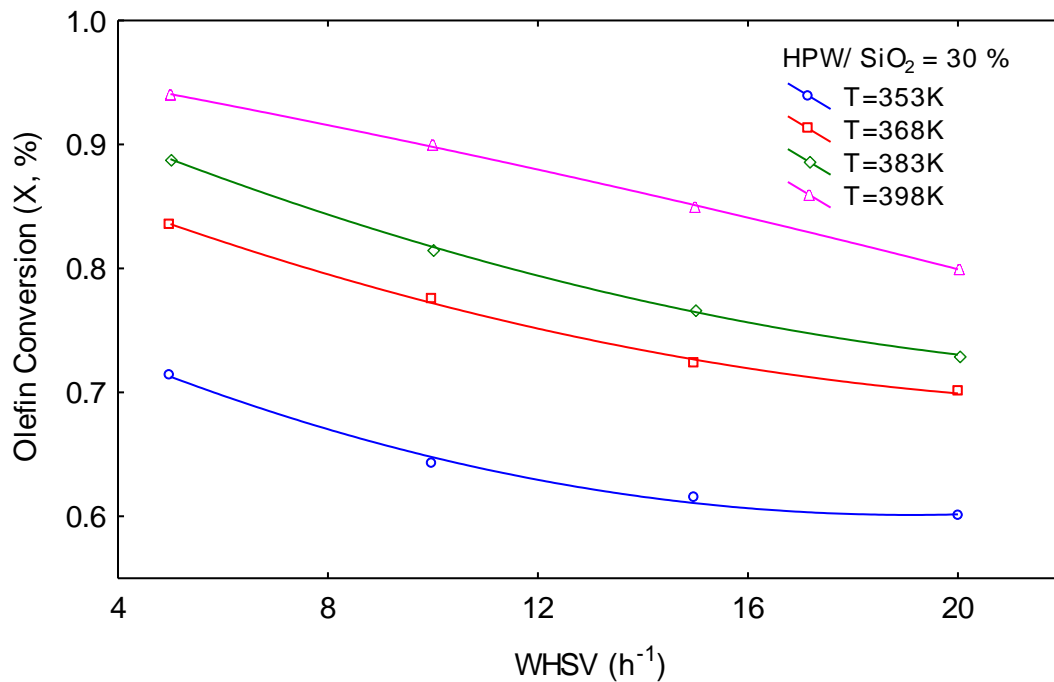


Fig. (3) The Effect of Weight Hourly Space Velocity on the Olefin Conversion at various temperatures for HPW/SiO₂ = 30 wt. % Catalyst.



Table (1) The alkylation rate constants for linear alkylbenzene production

HPW / SiO ₂ - 5 wt.%	
<i>Temperature</i> (K)	<i>k'</i> (lit ² / Kg.mol.h)
353	32.00
368	43.30
383	65.00
398	68.00
HPW / SiO ₂ - 10 wt.%	
<i>Temperature</i> (K)	<i>k'</i> (lit ² / Kg.mol.h)
353	39.87
368	53.50
383	66.20
398	82.00
HPW / SiO ₂ - 20 wt.%	
<i>Temperature</i> (K)	<i>k'</i> (lit ² / Kg.mol.h)
353	59.00
368	117.00
383	172.00
398	228.50
HPW / SiO ₂ - 30 wt.%	
<i>Temperature</i> (K)	<i>k'</i> (lit ² / Kg.mol.h)
353	167.00
368	451.10
383	859.00
398	1806.00

Table (A-6) Thiele Modulus with relative properties

HPW / SiO ₂ - 5 wt.%		
<i>Temperature</i> (K)	$D_e * 10^3$ (cm ² /s)	$M_T * 10^3$
353	1.43	2.88
368	1.46	3.25
383	1.49	3.84
398	1.51	3.82
HPW / SiO ₂ - 10 wt.%		
<i>Temperature</i> (K)	$D_e * 10^3$ (cm ² /s)	$M_T * 10^3$
353	1.47	3.25
368	1.50	3.63
383	1.53	3.78
398	1.56	4.16
HPW / SiO ₂ - 20 wt.%		
<i>Temperature</i> (K)	$D_e * 10^3$ (cm ² /s)	$M_T * 10^3$
353	1.68	3.50
368	1.71	4.50
383	1.74	5.25
398	1.78	5.38
HPW / SiO ₂ - 30 wt.%		
<i>Temperature</i> (K)	$D_e * 10^3$ (cm ² /s)	$M_T * 10^3$
353	1.74	4.47
368	1.78	5.97
383	1.81	7.34
398	1.85	8.29



Nomenclature

D_e	Effective diffusivity	cm^2 / s
k'	Catalytic reaction rate constant	$\text{lit}^2 / \text{mol.kgcat s}$
k'''	Catalytic reaction rate constant.	$\text{lit}^2 / \text{mol.h.m}^3 \text{cat}$
L	Characterization length of catalyst particle	m
M	Molecular weight.	g / mol
M_T	Thiele modulus	
S_g	Surface area of catalyst.	cm^2 / g
T	Temperature	K
X	Olefin conversion.

ABBREVIATION

FID	Flame ionization detector.
GC	Gas chromatography
HPW	Tungstophosphoric acid
LAB	Linear alkylbenzene.
LAS	Linear alkylbenzenesulphonate
UOP	Universal Oil Product.
WHSV	Weight hourly space velocity.
ZSM-12	Zeolite Socony Mobile-12
ZSM-5	Zeolite Socony Mobile-5

GREEK SYMBOLS

ε	Effectiveness factor.	---
θ	Void fraction	---
τ_m	Tortuosity factor	---
ρ^2	Correlation Coefficient	---
ρ_p	Solid density	g/cm^3

REFERENCES

- Cavalli L., Divo C., Giuffrid G., Rodici P., Valtorta L. and Zatta A., "Proceedings 3rd CESIO International Surfactants Congress" London, 1-5 June 1992, P 105.
- Alul H.R., "Ind. Eng. Chem. Prod. Rev. Dev.", 1,7 (1968).
- Olson A.C., "Ind. Eng. Chem.", Vol. 52, No. 10, 833 (1960).
- Moreno A., Cohen L. and Berna J.L., "Surfactant Detergent", 25, 216 (1988).
- Sebuluky R.T. and Henke A. M., "Ind. Eng. Chem. Des. Dev.", 10, 2, 272 (1971).
- Young L. B. and Skillman N.J., US Patent 4 301 316 (1979).
- Young L. B. and Skillman N.J., US Patent 4 301 317 (1981)
- Ming-Yuan H., Zhonghui L. and Enze M., "Catal. Today", 2 , 321 (1988).
- Cao Y., Kessas R., Naccache C. and Y.B., "Appl. Catal. A: Gen." 184, 231 (1999).
- Da Z., Han Z., Magnoux P. and Guisnet M., "Appl. Catal. A: Gen., 215, 45 (2001).
- Da Z., Magnoux P. and Guisnet M., "Appl. Catal. A: Gen.", 182, 407 (1999).
- Wang B., Lee C. W., Tian-Xi C. and Sang-Eon P., "Bull. Korean Chem. Soc.", 22, 9, 1056 (2001).
- Bouncer H. A., Eur. Patent 0 160 144 (1984).
- Le Q. N., Marler D. O., Mc Williams J. P., Rubin M. K., Shim J. and Wong S.S., US Patent 4 962 256 (1990).

R

- Tejero J. L., Danvila A. M., US Patent 5 146 062 (1993).

R'

- Tejero J. L., D. Algeciras A. M., US Patent 5 157 158 (1992).

- Sivasanker S. and Thangaraj A., "J. Catal.", 138, 386 (1992).

R'

- Sivasanker S., Thangaraj A., Abulla R. A. and Ratnasamy P., in Guzzi L., Solymosi F. and Tetenyi P. (Editors), New Frontiers in Catalysis, Proceedings of the 10th International Congress on Catalysis, 19-24 July, 1992, Budapest, Hungary (Studies in Surface Science and Catalysis, Vol. 75), Elsevier, Amsterdam, 1993, 75, P. 397.

- Tanabe K. and Holderich W. A., "Appl. Catal. A: Gen." 181, 399 (1999).

- Imai T., Kocal J. A. and Vora B. V., "Stud. Surf. Sci. Catal.", 92, 339 (1995).

- Levenspiel O., "Chemical Reaction Engineering", 3rd Edition, John-Wiley & Sons, (1999).

- Furman N. H., "Standard Methods of Chemical Analysis", Vol. one, Sixth Edition, USA (1968).

- Xing-Dong Y., Jung-Nam P., Wang J. and Sang-Eon P., "Korean J. Chem. Eng.", 19, 4, 607 (2002).

- Satterfield, "Heterogeneous catalysis in Practice", McGraw-Hill, USA (1980).

- Fogler H. S., "Elements of Chemical Reaction Engineering", Second Edition, Prentice-Hall of India Private Limited, New Delhi (1997).

- Hougen and Watson, "Part Three Kinetics and Catalysis", Eleventh Printing, John Wiley & Sons, INC., New York (1966).

THE EFFECT OF TEMPERATURE AND ACID CONCENTRATION ON POLARIZATION RESISTANCE FOR A CORROSION REACTION UNDER ACTIVATION CONTROL

Aprael Sarguis Yaro

Chemical Engineering Department, College of Engineering, University of Baghdad

ABSTRACT

The effect of temperature (30, 40, 50, and 60°C) on the polarization resistance (R_p) has been analyzed for the corrosion of carbon steel in 1, 3, and 5N HCl solution in absence & presence of phenylthiourea (PHTU) as corrosion inhibitor. The polarization resistance was measured at above mentioned conditions using BETACRUNCH program developed by Green and Gandi [Green, 1982]. i.e; Values of applied current densities at potentials of +20, +10, -10 mv and then -20, +10, -10 mV (SCE) from corrosion potentials were used to obtain corrosion parameters: i_{Corr} , b_a , b_c followed by applying the equation: $R_p = (b_a b_c) / 2.303 \times i_{Corr} (b_a + b_c)$. It is observed that: (i) for a certain acid concentration the polarization resistance decreased with increase in temperature and/or decrease in inhibitor concentration. (ii) for a certain temperature, the polarization resistance decreases with an increase in acid concentration in presence and absence of inhibitor.

KEY WORDS

Inhibition, polarization resistance Betacrunch program, physical adsorption, Chemical adsorption, activation control.

الخلاصة

تم في هذا البحث تحليل تأثير درجة الحرارة (30, 40, 50, و 60 درجة مئوية) على مقاومة الاستقطاب لعملية تآكل الحديد في ثلاث تراكيز مختلفة من حامض الهيدروكلوريك (5 و 31 عيارى) بوجود و عدم وجود فينيل ثايو يوريا كمثبط لعملية التآكل. مقاومة الاستقطاب تم قياسها ضمن الظروف المذكورة باستعمال برنامج (بيتاكرانچ) والتي طورها كرين و غاندى (من منحنيات الاستقطاب التي تم الحصول عليها للظروف المذكورة تؤخذ قيم لكثافة التيارات المسلطة في جهود +20, +10, -10 مللي فولت و -20, -10, +10 مللي فولت بعدا من جهد التآكل) باستعمال هذه الجهود مع كثافة التيارات المقابلة لها سيقوم البرنامج بإيجاد متغيرات التآكل وبالتحديد تيارات التآكل و منحنيات تافل الموجبة و السالبة بطريقة التكرار وصولا الى اقل نسبة خطأ (تعووض متغيرات التآكل في معادلة الاستقطاب الخطى المعروفة للحصول على مقاومة الاستقطاب) عند تحليل النتائج لوحظ ان: (1) لتركيز حامض معين تقل مقاومة الاستقطاب بزيادة درجة الحرارة وتقليل تركيز المثبط (2) لدرجة حرارة معينة, مقاومة الاستقطاب تقل بزيادة تركيز الحامض بوجود و عدم وجود المثبط.

INTRODUCTION & THEORY

The polarization resistance is a measure of the resistance of a metal undergo corrosion in a certain environment. It is defined as the slope of the potential-current (E-i) curve

$$R_p = [\partial E / \partial i]_{E=E_{Corr}} \quad (1)$$

where i , is the current density in A/cm^2 and E_{Corr} is the electrode potential of the corroding metal. Polarization resistance behave like a resistor and can be calculated by taking the inverse of the slope of the current –potential curve at open circuit corrosion potential. During the polarization

of an electrode, the magnitude of the current is controlled by reaction kinetics and diffusion of reactants both toward and away from the electrode. The Butler- Volmer equation is introduced in this case as[Stern,1957]:

$$i = i_{\text{Corr.}} [\exp(2.3 \Delta E / b_a) - \exp(-2.3 \Delta E / b_c)] \quad (2)$$

Where $\Delta E = E - E_{\text{Corr.}}$, b_a , b_c are anodic and cathodic Tafel constants. Equation (2) for small ΔE , i.e; less than 20 mV from $E_{\text{Corr.}}$, can be linearized leading to:

$$i = i_{\text{Corr.}} [1 + 2.3 \Delta E / b_a - (1 - 2.3 \Delta E / b_c)] \quad (3)$$

$$i = i_{\text{Corr.}} [1 + 2.3 \Delta E / b_a - 1 + 2.3 \Delta E / b_c] \quad (4)$$

So,
$$i = i_{\text{Corr.}} [2.3 \Delta E (1 / b_a + 1 / b_c)] \quad (5)$$

Rearranging equation (5) leads to:

$$\Delta E / i = R_p = (b_a b_c) / 2.3 i_{\text{Corr.}} (b_a + b_c) \quad (6)$$

Equation (6) is essentially the original Stern- Geary equation expressed in Tafel slopes of both reaction: $\text{Fe} \longrightarrow \text{Fe}^{+2} + 2e$ (7)



(i.e;the effect of dissolved oxygen concentration is negligible compared with H_2 evolution).Substituting in equation (6) for b_a and b_c as: $b_a = RT / \alpha_a z_a F$; $b_c = RT / \alpha_c z_c F$ (9)

Equation (6) can be expressed in terms of $T, \alpha_a, \alpha_c, z_a, z_c$

$$R_p = RT / 2.3 \times i_{\text{Corr.}} F (\alpha_a z_a + \alpha_c z_c) \quad (10)$$

Equation (10) can be rearranged and put in Logarithmic form :

$$\text{Log}(R_p / T) = - \text{Log}(i_{\text{Corr.}}) + \text{Log}[R / 2.3 F (\alpha_a z_a + \alpha_c z_c)] \quad (11)$$

Accordingly, a Logarithmic plot of (R_p / T) V'S $i_{\text{Corr.}}$, gives a straight line with a slope of (-unity) provided $(\alpha_a z_a)$ and $(\alpha_c z_c)$ are constant. The polarization resistance has been used in corrosion monitoring [Neufeld,1964 & Tamba,1982], determination of corrosion rates [Mahmoud,2005 & Mishra,2007] and inhibitor efficiency[Ashassi,2006].The literature has few references to systematic measurements of the effect of temperature on the polararization resistance and few to a theoretical analysis of this effect[El-Anadouli,1986].But no references to the effect of acid concentration.This is the object of this paper.We have measured the polarization resistance of carbon steel corrosion in three different concentrations of HCl acid,namely, 1,3,and 5N acid solutions at various temperatures in presence of different concentrations of phenylthiourea(PHTU) as corrosion inhibitor using a well-known technique in corrosion field and away from $E_{\text{Corr.}}$ by 20 mV for each condition studied, rather than the plot of potential,E,V'S current density,i,which leads to slopes of straight lines(i.e; $R_p = \Delta E / \Delta i$ at $E = E_{\text{Corr.}}$).

EXPERIMENTAL METHODE

Details of the polarization cell,electrode and electrolyte preparation and experimental techniques are reported elsewhere[Abdul-Hassan,2004]. The electrode was prepared from a carbon steel pipe as cylindrical specimens of chemical composition: Wt.%, C= .041, Mg =.381, P =.05, S = .007,remainder iron. The electrolyte was 1,3, and 5N HCl acid solutions prepared from distilled water and concentrated HCl acid supplied by Al- Furat company for chemical industries: The specifications of acid were as follows:Concentration = 32% Wt., SO_4^{-2} =125.5 ppm, residue = 360 ppm and density = 1.164 gm/ cm^3 . The inhibitor used was phenylthiourea (PHTU) of annular grade, MW =152.2 gm/mole, while acetone and benzene were used for cleaning purposes.

RESULTS & DISCUSSION

From the polarization curves which represent the plots of potential,E, V's Log(current density),i, for the working electrode at different temperatures and in various acid concentrations in absence and presence of PHTU as corrosion inhibitor[Abdul-Hassan,2004], and from the average values of



corrosion parameters: i_{Corr} , b_a , b_c obtained by applying the Betacrunch program by entering two sets of data for each condition as mentioned before. The values of R_p are deduced for the working electrode. These values for the working electrode for each condition are listed in Tables (1) through (4).

Table 1 Polarization resistance(Ωcm^2) of carbon steel in different concentrations of HCl acid containing various concentrations of PHTU as corrosion inhibitor at 30⁰C.

Inhibitor Conc.(Mole/L)	1N	3N	5N
Nil	40.95	17.1	11.8
6.6×10^{-4} M	464.1	117.3	76.4
4.9×10^{-3} M	614.8	172.3	107
6.6×10^{-3} M	792.1	207.4	135

Table 2 Polarization resistance(Ωcm^2) of carbon steel in different concentrations of HCl acid containing various concentrations of PHTU as corrosion inhibitor at 40⁰C

Inhibitor Conc.(Mole/L)	1N	3N	5N
Nil	11.3	12.8	4.9
6.6×10^{-4} M	175.5	79.9	59.3
4.9×10^{-3} M	339	111.2	70.3
6.6×10^{-3} M	243.2	171	84.7

Table 3 Polarization resistance(Ωcm^2) of carbon steel in different concentrations of HCl acid containing various concentrations of PHTU as corrosion inhibitor at 50⁰C

Inhibitor Conc.(Mole/L)	1N	3N	5N
Nil	6.4	3.4	2.3
6.6×10^{-4} M	90	11.4	5.64
4.9×10^{-3} M	151.2	17.2	7.1
6.6×10^{-3} M	191.6	25.8	9.4

Table 4 polarization resistance(Ωcm^2) of carbon steel in different concentrations of HCl acid containing various concentrations of PHTU as corrosion inhibitor at 60°C.

Inhibitor Conc.(Mole/L)	1N	3N	5N
Nil	4.4	2.5	1.64
6.6×10^{-4} M	75	7	5.7
4.9×10^{-3} M	67	12.1	9
6.6×10^{-3} M	108.9	16.6	7.6

At different temperatures and various acid concentration, also, Θ , and I%, can be determined from R_p , obtained by using the following equations, respectively:

$$\Theta = 1 - (R_p)_{\text{free}} / (R_p)_{\text{inhib.}} \quad (12)$$

$$I\% = [1 - (R_p)_{\text{free}} / (R_p)_{\text{inhib.}}] \times 100 \quad (13)$$

where $(R_p)_{\text{free}}$ & $(R_p)_{\text{inhib.}}$ are polarization resistance in absence and presence of inhibitor, respectively, while Θ & I% are surface coverage and inhibition efficiency respectively. Table(5) shows the inhibition efficiency of PHTU under the operating conditions mentioned previously.

Table 5 Inhibition efficiency of PHTU for carbon steel in different HCl acid concentrations and various temperatures.

Temp	30°C			40°C			50°C			60°C		
Acid Conc.	1N	3N	5N	1N	3N	5N	1N	3N	5N	1N	3N	5N
.00066M	91.2	85.5	84.6	93.6	84.0	91.8	93.0	70.2	59.2	94.1	65	71
.0049M	93.3	90.1	89.0	96.7	88.4	93.0	96.0	80.2	67.5	93.4	80	82
.0066M	94.8	91.8	91.3	95.4	92.5	94.2	97.0	87.0	75.5	96.0	85	78
Inhibition Efficiency (I%) at different Temperatures & acid Concentrations												

Figures(1) through (3) show the effect of temperature and inhibitor concentration on the polarization resistance at acid concentrations 1,3,and 5N respectively. It is clear that polarization resistance decreases as the temperature increases and / or the inhibitor concentration decreases. The effect of inhibitor is clearly evident from equation(10). Thus, at constant temperature the increase in inhibitor concentration decreases the corrosion rate, $i_{\text{Corr.}}$, and hence, R_p , increases. (i.e; the corrosion reaction is regarded as a rate process, the rate of which is given by [Potilova,1960] :

$$i_{\text{Corr.}} = A \exp(- E / RT) \quad (14)$$

Thus, as T increases the numerator increases linearly, while the denominator increases exponentially, and hence R_p decreases. The Logarithmic form of equation (10) is given in equation (11), from which a Logarithmic plot of (R_p / T) V's $i_{\text{Corr.}}$ gives a straight line with a slope of [-unity], provided $\alpha_a Z_a$ and $\alpha_c Z_c$ are constants. Figures (4) through (6) show such plot at various temperatures and inhibitor concentrations in HCl acid concentrations 1 ,3, and 5N respectively. The straight lines are the least squares correlation of all the data points at 1,3, & 5N HCL acid, with a correlation coefficient of (.98) and slopes of (1.042) , (1.04 3) , and(.98) respectively,

In satisfactory agreement with the prediction of equation (11). These are taken as confirmation of the validity of this equation, and of constancy of $\alpha_a Z_a$ and $\alpha_c Z_c$ at various temperatures and inhibitor concentrations within the limits of experimental error. Combination of equation (14) and (11) leads to:

$$\text{Log} (R_p / T) = E / 2.3 R T + \text{Constant} \quad (15)$$

where the constant in equation (15) includes $A, R, F, \alpha_a Z_a$, and $\alpha_c Z_c$. Thus a plot of $\text{Log}(R_p / T)$ V's $1/T$ gives a straight line from the slope of which, Activation energy of the corrosion process can be calculated. Figures (7) through (9), illustrate such plots at various concentrations of PHTU in different HCl acid concentrations. The relation between $\text{Log} (R_p / T)$ and $1/T$ is satisfactory straight line under all conditions in agreement with equation (15). Table(6) lists the values of Activation energy obtained in the absence and presence of various inhibitor concentrations of PHTU in different acid concentrations. Since only small differences are observed between the values of activation energy calculated at different concentrations of the same inhibitor in 1N HCl acid, the activation energy is considered to be essentially independent of inhibitor concentration and in this case the inhibitor is physically adsorbed on the mild steel [Ebenso,1998 & Demaskin,1971]. i.e; when the activation energy is less than 80 kJ/mole, the adsorption is considered to be physically. Ideally, a corrosion inhibitor is a substance which greatly increases the activation energy of corrosion and / or adsorbs on the surface and prevents it from corroding. PHTU as corrosion inhibitor increases activation energy pronouncly in 3 and 5N HCl acid solutions and hence the mechanism of its inhibition must not be via simple blocking adsorption. The large values of activation energy in both 3 and 5N acid solutions compared with 1N-HCl system support the fact that PHTU in this case is chemically adsorbed. i.e; Activation energy > 80 KJ/mole [Abiiola,2002 & Barrow,1983].

Table 6 Activation energies of corrosion of carbon steel at various concentrations of PHTU in different concentrations of HCl acid.

Inhibitor Conc.(M/L)	1N	3N	5N
	E (kJ Mole)	E (kJ / Mole)	E (kJ / Mole)
Blank	63.0	61.8	58.2
.00066 M	59.3	84.1	87.1
.0049 M	64.8	89.4	83.7
.0066 M	54.6	81.6	92.7
$E_{\text{mean inhibited}}$	57.8	85.0	87.8

It is important to mention that Betacrunch program [Green,1982] is usually used to obtain the corrosion parameters near the corrosion potential by about +20 to -20 mV. Since the equation(6) is derives with out assumptions and its derivation is completely mathematical, and since Tafel slopes are difficult to estimate. Moreover since the corrosion potential in this study especially at these high concentrations of HCL acid is not near the reversible potentials of one of the half reactions (i.e; The H_2 evolution or the metal dissolution). It is accepted to say: $R_p = f(i_{\text{corr}}, b_a, b_c)$ all at $E = E_{\text{corr}}$. instead of using the reciprocal of the polarization resistance obtained experimentally to represent the corrosion rate for screening purposes: $i_{\text{cor}} = f(R_p, B)$.

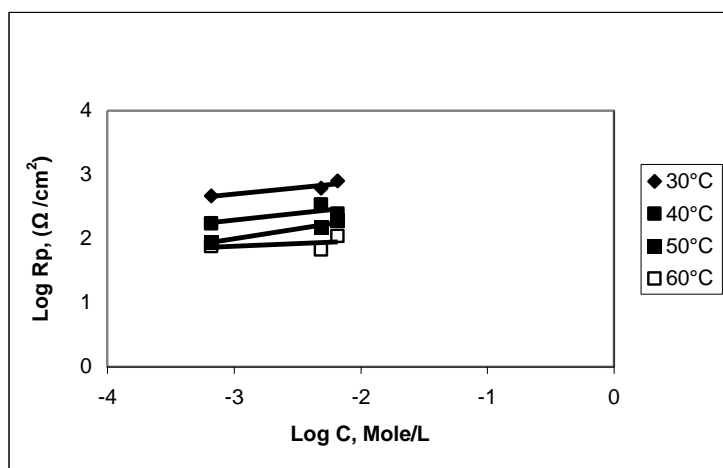


Fig.1 Effect of Temperature and inhibitor concentration on the polarization resistance in 1N HCL acid

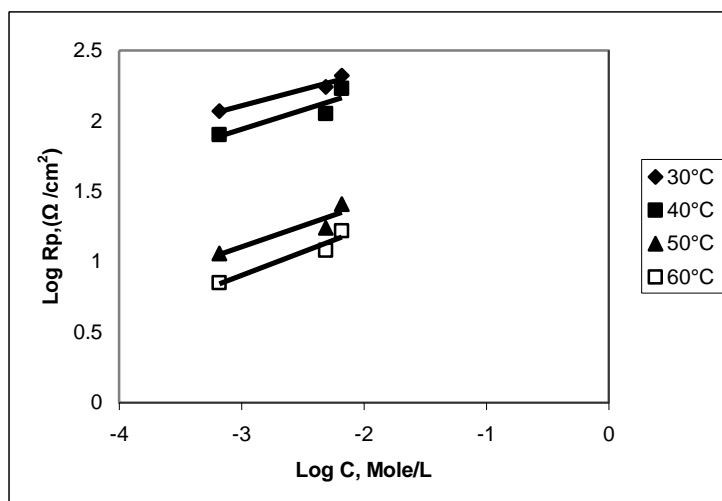


Fig.2 Effect of Temperature and inhibitor concentration on the polarization resistance in 3N HCL acid

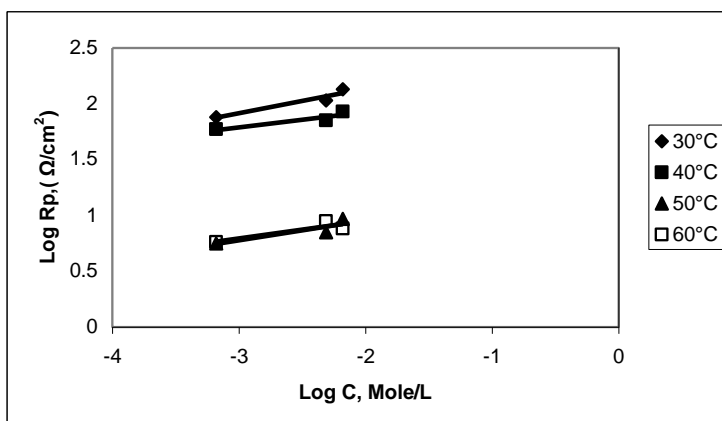


Fig.3 Effect of Temperature and inhibitor concentration on the polarization resistance in 5N HCl acid.

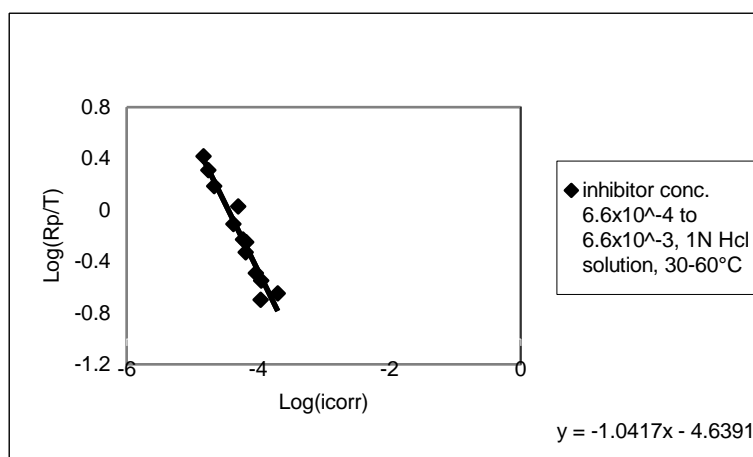


Fig. 4 Plot of polarization resistance data in 1N HCl acid solution.

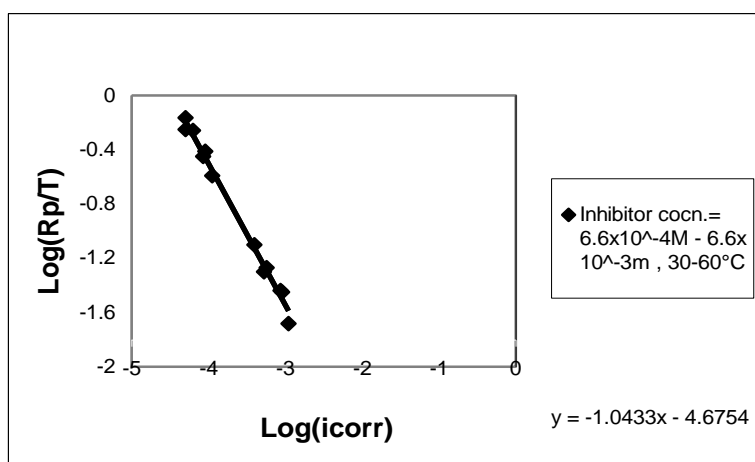


Fig.5 Plot of polarization resistance data in 3N HCl acid solution.

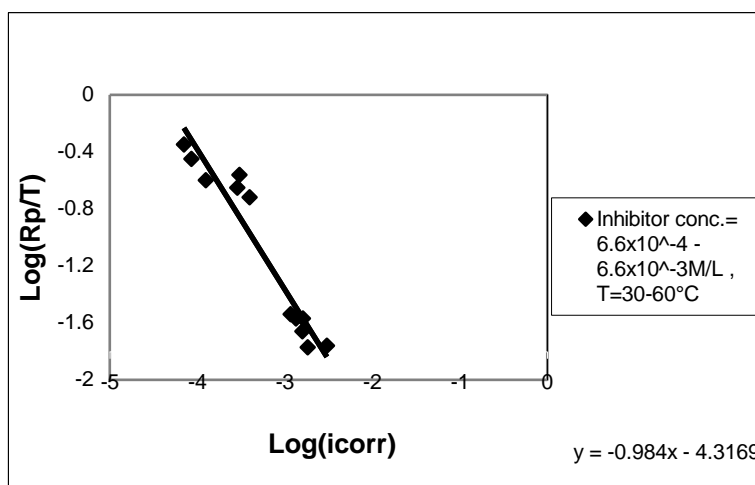


Fig.6 Plot of polarization resistance data in 5N HCl acid solution.

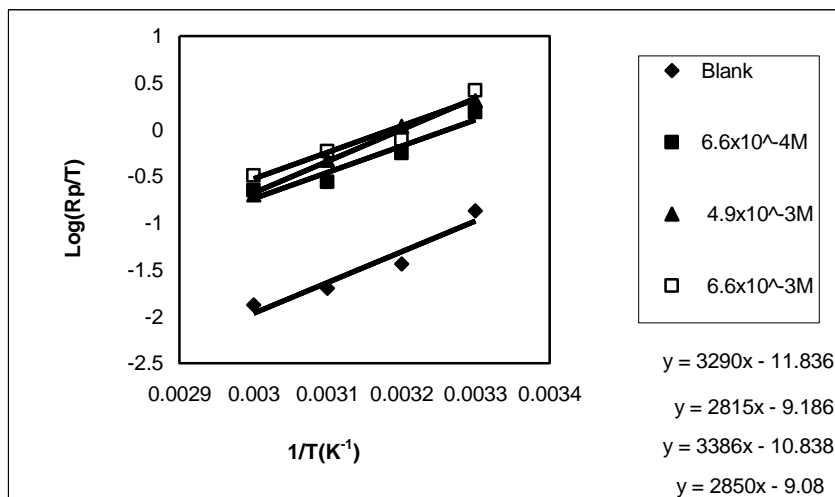


Fig 7 Plots of $\text{Log}(R_p/T)$ V's $1/T$ in absence and presence of various conc. of nhibitor in 1N HCl acid.

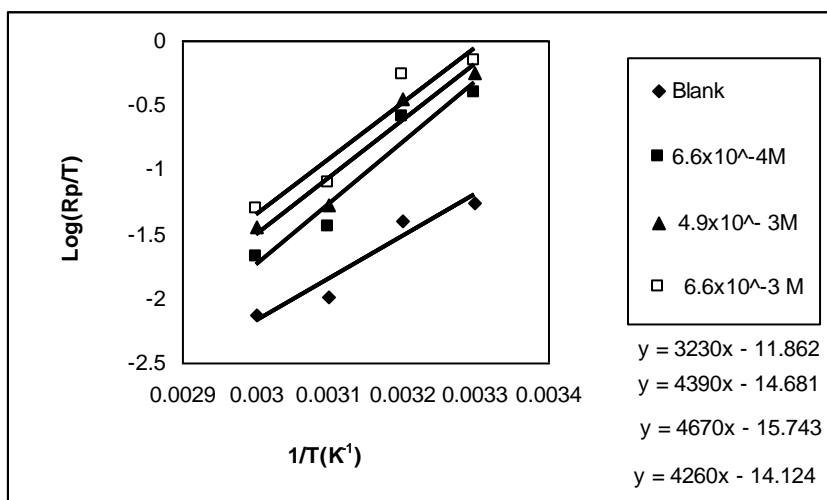


Fig 8 Plots of $\text{Log}(R_p/T)$ V's $1/T$ in absence and presence of various conc. of ibitor in 3N HCl acid.

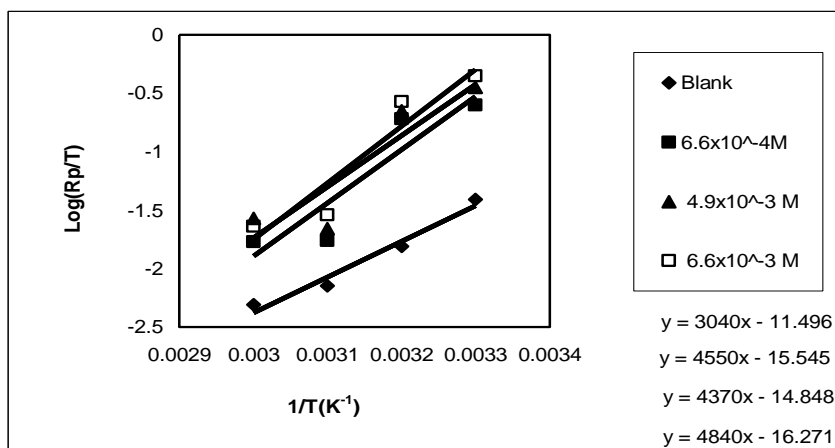


Fig 9 Plots of $\text{Log}(R_p/T)$ V's $1/T$ in absence and presence of various conc. Of inhibitor in 5N HCl acid.



CONCLUSIONS

- PHTU acted as efficient corrosion inhibitor for carbon steel in 1,3, and 5 N HCl acid concentrations.
- The results obtained by Betacrunch technique are thought to be in good agreement with those if obtained experimentally since corrosion potential is far from the equilibrium potentials of both H_2 evolution and metal dissolution reactions.
- For a certain temperature the polarization resistance decreases with acid concentration increase, while increases with inhibitor concentration increase.
- For a certain acid concentration, the polarization resistance decreases with temperature increase in absence and presence of inhibitor.
- The inspection of data in Table(6) reveal that the activation energy of the corrosion reaction in absence of inhibitor(PHTU) is approximately the same and is acid concentration independent.
- The average activation energy value of (57.8 kJ/mole) for 1 N- HCl inhibitor system support the fact that the inhibitor is physically adsorbed on the metal surface, although the increase in inhibition efficiency is not so pronounced.
- The experimental result indicates generally that the energy barrier of corrosion reaction in 3 , and 5 N- HCL inhibitor system increase as the concentration of PHTU is increased, since the value of activation energy increase with an increase in PHTU. This suggests that the process is activation controlled and the mechanism of the inhibitor adsorption in this case is chemical adsorption. i.e; 85 and 87.8 kJ/mole is > than 80 kJ /mole

REFERENCES

- Abdul-Hassan, A.S., Msc. Thesis, University of Baghdad, Sep. (2004).
- Abiiola, O.K., Oforka, N.C., " Corrosion science Engineering", 3, 21 (2002), [http://www2.umist.ac.uk/corrosion/JCSE/Volum/paper 21/v3P21.htm](http://www2.umist.ac.uk/corrosion/JCSE/Volum/paper%2021/v3P21.htm)
- El-Anadoul, B.E., Ateya, B.G., and EL-Nizamy, F.M., "Corrosion Sci." Vol. 26, No. 6, P. 419-424 (1986).
- Ashassi-Sorkhabi, H., and Seifzadeh, D., "Int. J. Electrochem. Sci." 1, P. 92-98 (2006)
- Barrow, G.M., Physical Chemistry, McGraw- Hill, New York, P. 739 (1983).
- Demaskin, B.B., " Adsorption of organic compounds on electrodes", Plenum press, New York, P. 221 (1971).
- Ebenso, E.E., Nig. Corrosion J. I., 1, 29 (1998).
- EL-Anadoul, B.E., Ateya, B.G., and EL-Nizamy, F.M., "Corrosion Sci.", Vol. 26, 6, p. 419-424 (1986).
- Mishra, A.K., and Balasubramanian, R., "Corrosion", Vol. 63, 3 (2007)
- Mahmoud, S.S., "Corrosion" Vol. 61, 12 (2005)
- Neufeld, R., " Corrosion Sci.", 4, 245 (1964)
- Putilova, I.N., Balezin, S.A., and Baranik, V.P., "Metallic corrosion inhibitor" pergamon press, Oxford (1960).
- Stern, M., and Geary, R.L., " Electrochem. Soc." Vol. 104 (1957). Tamba, A., " Br. Corrosion J.", 17, 29 (1982)

TRANSMISSION OF A MULTIPLEXED EIGHT CHANNELS SUBCARRIER OPTICALLY INTENSITY MODULATED BASED ON MICROCONTROLLER.

Husam A. Mohammed
Baghdad University\ College of
Engineering\ Elec. & Comm. Dep.

Hani J. Kbashi
Baghdad University\ College of
Science\
Physics Department.

ABSTRACT

An optical fiber communication system for transmitting eight time division multiplexed analog signals each of bandwidth of 500 Hz was designed and implemented. The system utilizes the 8051 microcontroller as a parallel to serial converter in the transmitter side and parallel to serial converter in the receiver side in addition to the control process of the multiplexer and demultiplexer in both sides and for serial transmission via its RS232. The transmitted signal is subcarrier intensity modulated using the Amplitude Shift Keying (ASK) modulation technique with a carrier of 20 MHz. A laser diode of the type HFCT-5205 at 1300 nm wavelength was used as an optical carrier generator with an emitted optical power of -10 dBm, and a HFCT-S205 InGaAs/InP PIN Photodiode with responsivity of 0.36 A/W at the receiver side. A single mode fiber of (42 km) length was used as a transmission channel. This system can be utilized in the TDM fiber telephone lines often operating at higher rates such as T3 (44.7 Mbps), T3C (91 Mbps) and above.

إرسال ثمان قنوات ممتزجة بطريقة تضمين الشدة للناقل الثانوي مستنداً على المسيطر الدقيق

الخلاصة

تم تصميم و بناء منظومة اتصالات الليف البصري لارسال ثمان اشارات تماثلية باستخدام تقنية التجميع بالتقسيم الزمني (TDM). المنظومة تستفيد من المسيطر الدقيق 8051 كمحول من التوازي الى التوالي في جهة المرسل و محول توالي الى التوازي في جهة المستلم بالاضافة الى عملية السيطرة على الجمع (multiplexer) و الموزع (demultiplexer) في الجهتين و للارسال التوالي عبر RS232.

تم تضمين الاشارة المرسله بواسطة تضمين ازاحة السعة (ASK) مع تردد حامل 20 MHz. استعمل ليزر داوود من النوع HFCT-5205 ذو طول موجي 1300 nm و قدرة ضوئية مشعة -10 dBm في المرسل و كاشف

ضوئي من النوع InGaAs/InP HFCT-s205 ذو استجابة 0.3 A/W في المستلم. استعمل الليف البصري احادي النمط بطول 42km كقناة ارسال. يتم الاستفادة من المنظومة في بدالات الهاتف الضوئية و عادة تعمل بمعدلات اعلى مثل T3 (44.7 MHz) و T3c (91 MHz) وفوق.

KEY WORD

Optical communication system, Microcontroller, Subcarrier optical Intensity modulation.

INTRODUCTION

Everywhere on this planet hair-thin optical fibers carry vast quantities of information from place to place. The use of light as communication methods can date back to antiquity if we define optical communications in a broader way [Govind 2002]. People had used mirrors, fire beacons, or smoke signals to convey a single piece of information. The modern fiber-optic communications started around 1970s when GaAs semiconductor laser was invented and the optical fiber loss could be reduced to 20 dB/km in the wavelength region near $1\mu\text{m}$ [Govind 2002]. Since then, fiber-optic communication has rapidly developed. The enormous progress of lightwave systems can be grouped into several generations. A widely used figure of merit is the bit rate-distance product, BL , where B is the bit rate and L is the repeater spacing [Govind 2002].

The digital optical fiber link mainly consists of a transmitter, fiber transmission medium, and receiver [Govind 2005]. The transmitter converts incoming binary data to on-off light pulses, which are launched into the fiber. At the receiver, the optical stream is detected and converted back into electrical signal.

The laser diode is a preferred source for moderate band to wideband systems. It offers a fast response time (typically less than 1 ns), has a narrow optical bandwidth (as a rule less than 1 nm) and can couple high levels of useful optical power (usually several milliwatts) into an optical fiber with small core and small numerical aperture [Donald & Gerd 1985, Paul 1985].

Generally only the photodetector and its load which usually form the first stage of the gain are uniquely related to the fiber optics, the remaining portion of the receiver is conventional electronics [Donald & Gerd 1985].

Before 1970, such a link could not have been used for transmission over distances greater than a few hundred meters, because of rapid signal attenuation in the fiber [Donald & Gerd 1985]. In that year however, Corning Glass achieved a breakthrough by producing a fused silica (SiO_2) fiber with loss low enough (20 dB/km) to make transmission lengths of a few kilometers commercially practical. This events coupled with the development of semiconductor light sources at about the same time, stimulates a worldwide building of lightwave research and development continues today. Attenuation coefficients of 0.15 dB/km at 1550 nm [Tatsuya1988] and 0.6 dB/km at 1300 nm have been achieved.

In virtually all optical fiber systems only two types of devices are employed for detection. These are either PIN photodiode or Avalanche PhotoDiode (APD). The PIN detector is preferred because it requests no complicated control circuitry, uses much lower DC bias voltage, and has no excess noise mechanism when compared to an APD [Donald&Gerd 1985].

The optical link can operate at an acceptable low error rate only if the optical power at the receiver exceeds some minimum level P_R called the receiver sensitivity. The maximum loss limited transmission distance L_{\max} is given by [Govind 2002, Max & Kang 1996]

$$L_{\max} \alpha = P_T - P_R - L_c - \text{splice loss} - \text{margin} \quad [1]$$

Where P_T is the transmitted power, α is the fiber attenuation expressed in dB/km, L_c is the connector losses usually taken as 1 dB, and the system margin usually taken between 3-10 dB.

This relationship implies that L_{\max} is relatively sensitive to change in the fiber attenuation, but is only weakly dependent on the transmitted power and receiver power. So increasing the transmitter power by order of magnitude, increases L_{\max} by only about 20 percent [Donald & Gerd 1985].

In designing an optical communication system it is necessary to consider the limits on the performance of the system set by the Signal to Noise Ratio SNR [1, Paul 1985]. The main noise sources that affect the performance of the optical fiber communication system are:

1. the thermal noise which results due to the load resistance R_L . It may be calculated as follows [Govind 2002, Max & Kang 1996]

$$i_{th} = \sqrt{\frac{4KT\Delta f}{R_L}} \quad [2]$$

where K is the Boltzman constant, T is the temperature in Kelvin, and Δf is the bandwidth.

2. the shot noise which is a combination of the dark current noise i_d and the quantum noise current, it is given by [Govind 2002, Max & Kang 1996]:

$$i_{shot} = [q\Delta f(i_s + i_d)]^{1/2} \quad [3]$$

where q is the electron charge, and i_s is the signal current generated due to the incident optical power in the optical detector which is equal to:

$$i_s = p_i R \quad [4]$$

where p_i is the incident optical power and R is the responsivity of the optical detector.

The SNR for the PIN photodiode receiver may be calculated as in below [Max & Kang 1996]

$$SNR(dB) = 20 \log \left(\frac{i_s}{i_{th} + i_{shot}} \right) \quad [5]$$

The performance criterion for digital receiver is governed by the bit error rate BER, defined as the probability of incorrect identification of a bit by the decision circuit of the receiver [Govind 2002]. A commonly optical receiver requires $BER \leq 1 * 10^{-9}$ [Donald & Gerd 1985].

The BER with the optimum setting of the decision threshold is obtained as in follows [Max & Kang 1996]:

$$BER = \frac{\exp(-SNR)}{\sqrt{2\pi SNR}} \quad [6]$$

The receiver sensitivity is then defined as the minimum average received power P_{rec} required by the receiver to operate at a BER of 10^{-9} .

SYSTEM DESCRIPTION

A block diagram of the implemented system is shown in Figure1. Eight analog signals are generated each at 500 Hz frequency. These signals are time division multiplexed. Multiplexing provides a mechanism to share the use of a common channel by two or more users. TDM interleaves bits or groups of bits (word or characters) belonging to different messages prior to transmission. As such, its original development was based on economics. The advantages in the use of pulse modulation with the Time Division Multiplexing TDM include the fact that the circuitry required is digital. Thus, offering high reliability and efficient operation.

The selection of the required channel is accomplished under the control of the microcontroller (8051) by the software. The sampling rate is about 8 kHz which is the Nyquist rate (Eight channels each with 500 Hz $(8 \times 0.5) \times 2 = 8\text{kHz}$). The selected sample then converted into a digital signal by the Analog to Digital Converter (ADC). The ADC action is controlled by the software of the microcontroller. The generated data is then fetched by the microcontroller for further process.

The microcontroller controls the whole operation of multiplexing and analog to digital data conversion. In addition, it acts as a parallel to serial converter. It converts the data generated by the ADC into a serial stream and transmitting it through the RS-232 of the microcontroller asynchronously, so that, there is no need for encoding the data stream for the clock and data recovery at the receiver side. By this, the complexity of the system is reduced and the system becomes more flexible. The flow chart of the program of the microcontroller used in the transmitter is shown in the Figure (2).

The transmission of data over the RS 232 of the microcontroller was 100 kbaud. The serial stream then was amplitude shift keying modulated (ASK) with a carrier of 20 MHz.

The ASK modulated signal is used to modulate a laser diode with intensity modulation type. The laser diode was with an operating wavelength of $1.3 \mu\text{m}$, a power of 0.1 mW is launched into the fiber at the high level voltage. The fiber used for guidance of the optical signal is a single mode fiber with attenuation of 0.6 dB/km and length of 42 km that consists of ten pieces of optical fiber each with 4.2 km length. So the length was changed from 4.2 km to 42 km with a 4.2 km step. Each piece was connected with the neighboring one by a splice. The loss of each splice was 0.03 dB and measured by using the Optical Time Domine Reflectrometer (OTDR).

The optical signal at the receiver is detected and converted into electrical signal. A block diagram of the optical receiver is shown in the Figure (4). A PIN photodiode is used in the work with a responsivity of 0.36 A/W at $1.3 \mu\text{m}$.

The detected signal is then demodulated. The reconstructed signal is then passed to the microcontroller serially via its RS-232 port. Here the microcontroller first converts the serially received bit stream into a parallel fashion and controls the



operation of demultiplexing and digital to analog conversion by the software of the receiver which is shown in the Figure (3). Then the pulses belonging to the individual messages are separated and routed to their appropriate destinations.

RESULTS AND DISCUSSION

The main test achieved on the implemented system was measuring the received optical power for different fiber length from which the calculations of the bit error rate were done. A plot which relates the SNR to the BER is shown in the Figure (6). BER was calculated using equation 6. The power budget calculations showed that the maximum length of the optical fiber can be 78.2 km. Where the safety margin was taken to be equal to 6 dB.

CONCLUSION

The suggested system operates properly with acceptable BER. The BER varies with SNR parameter. The BER improves as SNR increases and becomes lower than 10^{-9} for SNR >14.

REFERENCES

- Donald H. Rice, Gerd E. Keiser, 1985, "Applications of fiber optics to tactical communication systems", IEEE Communication Magazine, May, V-23, N-5.
- Govind P Agrawal, 2002, "Fiber Optic Communication Systems", third edition, Willy interscience.
- Govind P. Agrawal, 2005, "Light Wave Technology Telecommunication Systems", Willy interscience.
- James M.R. 1997. "Microcontrollers Cookbook PIC & 8051", first edition, Newnes.
- Max Ming-Kang Lu, 1996, "Principles and Applications of Optical Communication", IRWIN.
- Paul S. Henry, 1985, "Introduction to Lightwave Transmission", IEEE Communication Magazine, May, V-23, N-5.
- Tatsuya Kimura, 1988, "Factors Affecting Fiber Optic Transmission Quality", Journals of Lightwave Technology, May, V-6, N-5.

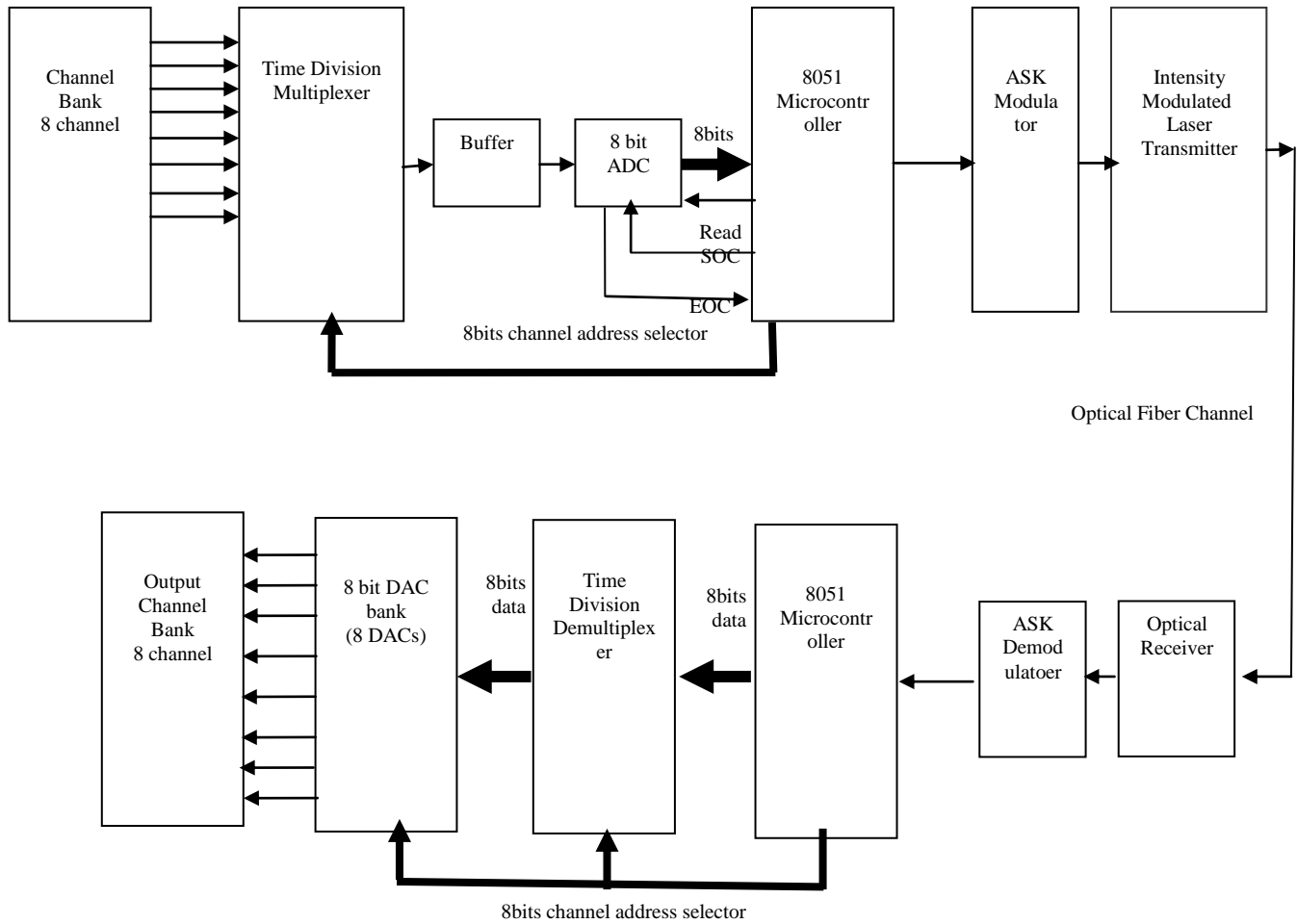


Figure (1): A block diagram of the 8 channel time division multiplexed ASK subcarrier intensity modulated optical fiber communication system

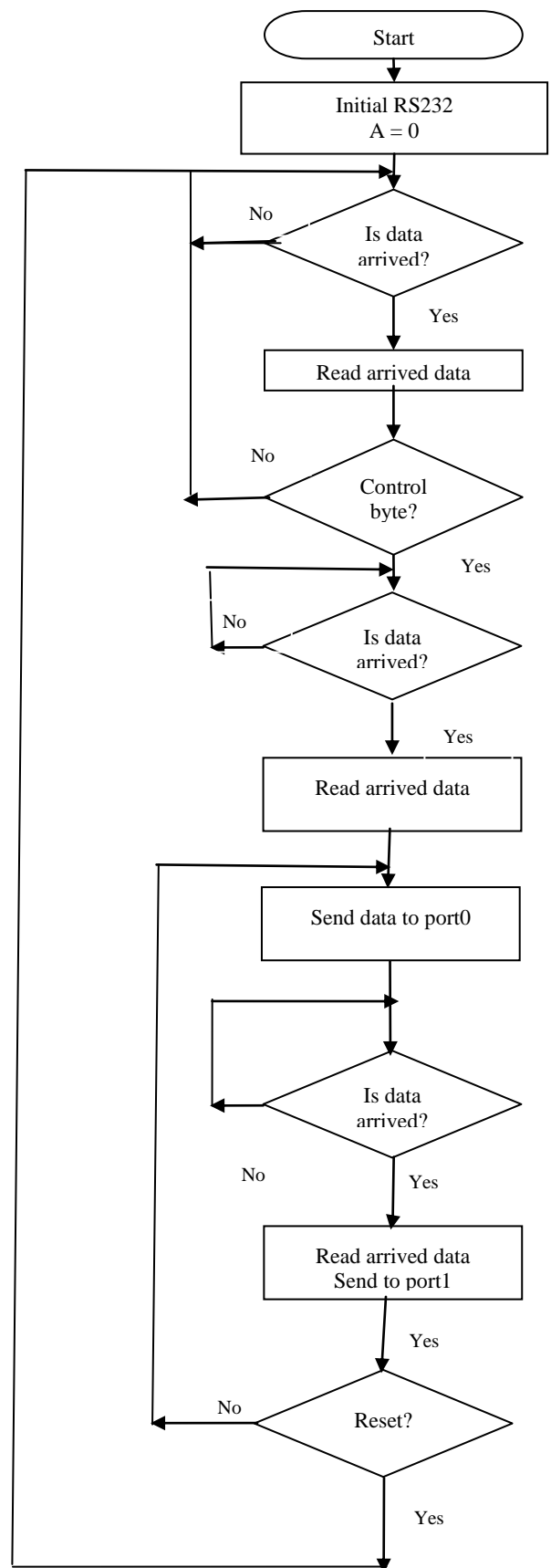
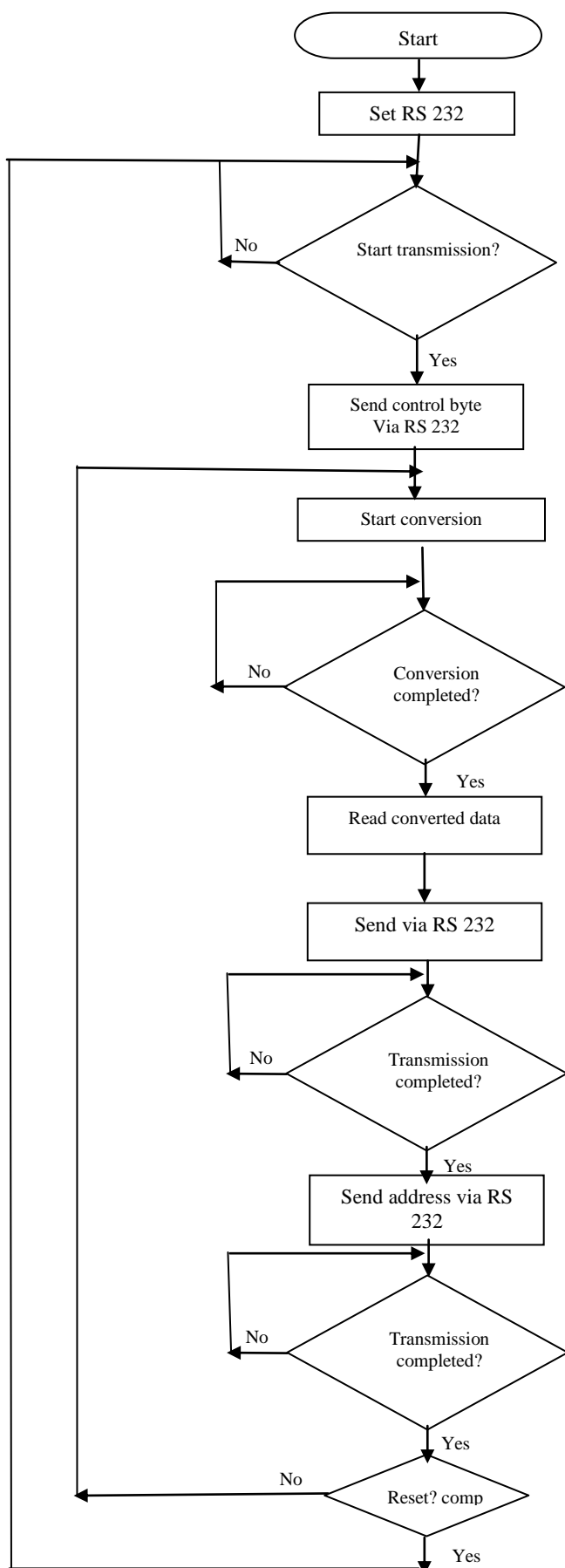


Figure (2): the software program of the transmitter unit

Figure(3): the software program of the receiver unit

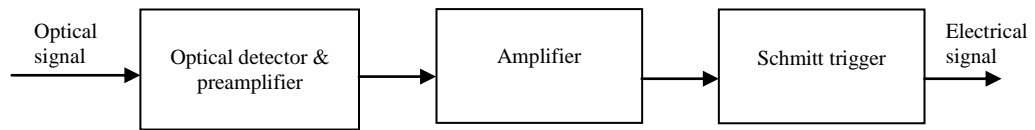


Figure (4): A block diagram of the optical receiver

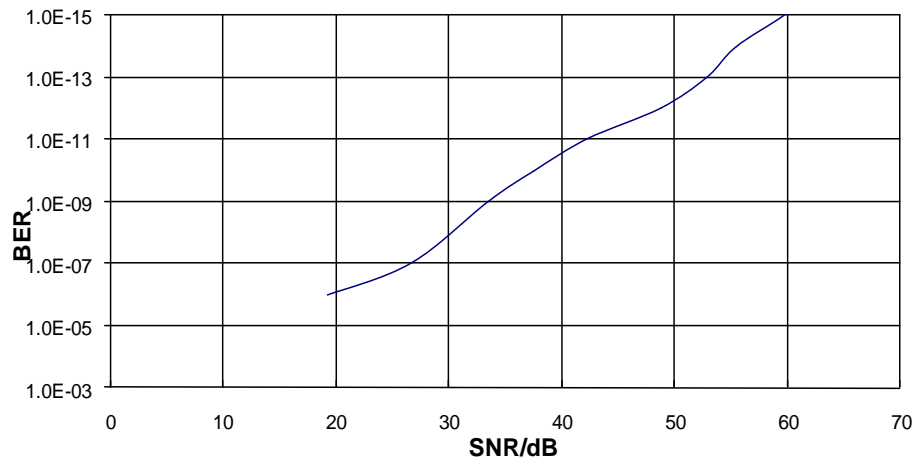


Figure (5): BER versus SNR



RADAR PARAMETER GENERATION TO IDENTIFY THE TARGET

W.A. Mahmoud , A.K. Sharief and F.D.Umara

**University of Baghdad
Baghdad , Iraq**

ABSTRACT

Due to the popularity of radar , receive often “ hear “ a great number of other transmitters in addition to their own return merely in noise . The dealing with the problem of identify and / or separating a sum of tens of such pulse trains from a number of different sources are often received on the one communication channel. It is then of interest to identify which pulses are from which source , based on the assumption that the different sources have different characteristics .This search deals with a graphical user interface (GUI) to generate the radar pulse in order to use the required radar signal in any specified location .

الخلاصة :

بسبب شعبية الرادار , المستقبلات غالبا تسمع عدد كبير من مراسلات اخرى بالاضافة الى الضوضاء الراجعة فقط منها . التعامل مع مشكلة تعريف او فصل جمع من عشرات من هذه الحزم النبضية من عدد مختلف المصادر غالبا يتم استلامه في قناة اتصال واحدة . وهذا الاهتمام منصب لتعريف اي نبضات من اي مصدر على اساس افتراض كون المصادر المختلفة لها خصائص مختلفة . هذا البحث يستخدم GUI لتوليد النبضة الرادارية لغرض توليد الاشارة الرادارية المطلوبة في اي موقع محدد .

KEY WORDS

Identification : Target ; Electronic ; Warfare ; Radar Pulse ; graphical User Interface(GUI).

INTRODUCTION

The continuous growth of air traffic increase demand to determine reliable algorithms and systems to tell where , on what altitude and how fast an aircraft is moving , as well as whether that aircraft of interest is friendly . foe or neutral . In general , this is referred to as a tracking . When something is under tracking , it implies that the current object is a target . In the sequel , tracking can be defined more precisely “ as processing measurements obtained from a target in order to maintain an estimate of its current state , which typically consists of kinematics components (such as position , velocity , acceleration etc.) and other components (radiated signal strength m spectral characteristic , feature information etc.) Emphasis of the word “state “ implies that scientists in tracking field are mainly concentrated in estimating the trajectory of the target .The use of the word ‘state ‘ is ambiguous , exact meaning depend always on the context [Hau00].

Defense systems dealing with tracking are important in the warfare because the present aircraft and vessels may be quick and destructive . Therefore m tracking systems are required to be as highly intelligent as possible .Software package presented in this paper comprehends GUI[Alb03] to achieve more reliability in tracking system in order to solve a given problem e.g. the identification problem .

This paper is organized as follows : The principles of the target tracking and the electronic warfare system are presented in section 2 , and section 3, respectively . While the receiving system and the radar signal description are presented in section 4 and section 5 . respectively. The parameters to be identified and the simulated results are presented in section 6and section 7. Respectively, finally the conclusion is represented in section 8 followed by the references.

TARGET TRACKING

In the civilian aviation the target’s velocity , height , position and heading can be easily solved . because all targets are cooperative by default . When dealing with defense applications, qualities listed above are not enough . In fact , they are not even considered first . In the military field , the most urgent is to know whether the targer of interest is friendly or hostile . After then questions as “What is the type of the target ?” and “What is the target threatening ?” rise .Problem that deals with the type of the target is referred to as an identification problem . An example of tracking system , with using

identification network (Bayesian network) in association , is illustrated in Fig.(1) [Vac93]

The identification procedure is as follows ; Targets emit signals, which can be detected sensors , when a sensor has detected a signal , it will be modified and transmitted to the identification system .Then identification system processes all observations and results a type probability function , which is returned to the operator. An example of the identification system is illustrated in Fig.(2).

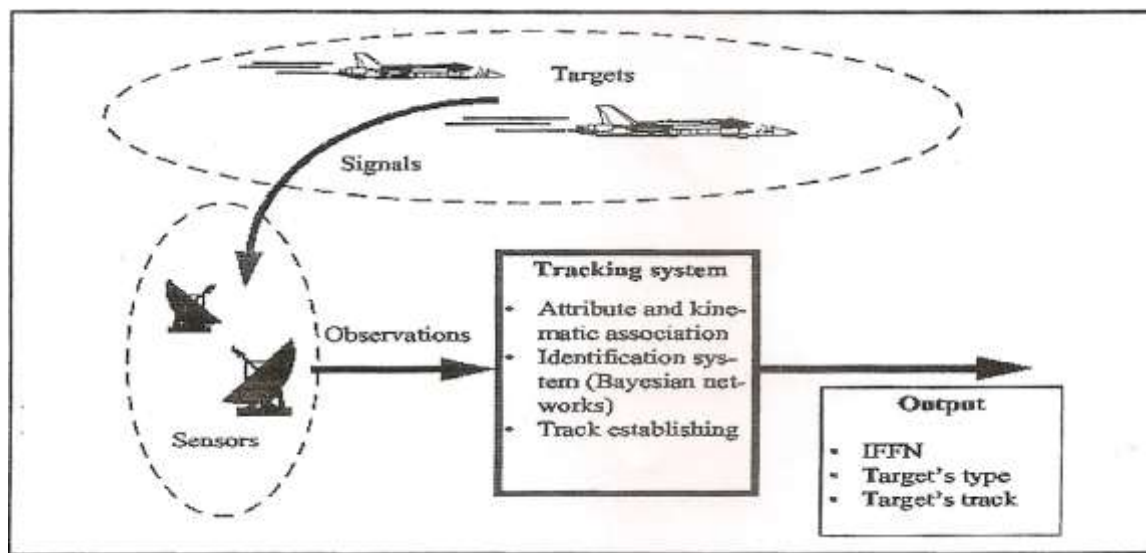


Fig (1) : Illustration of a tracking system

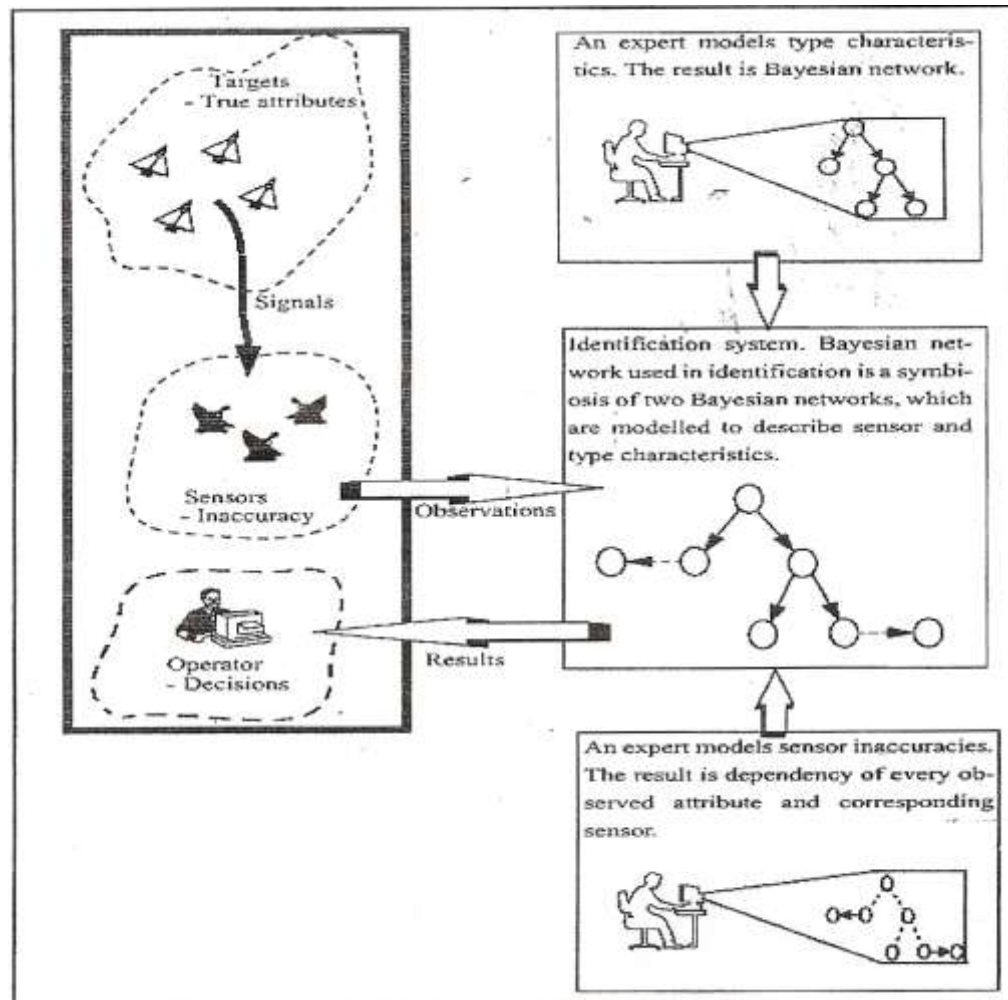


Fig. (2) illustration of the identification procedure .

ELECTRONIC WARFARE SYSTEM

Electronic warfare (EW) receivers will be the assumed approach . It takes many distinct forms , such as detecting and degrading the performance of a hostile radar , intercepting and disrupting enemy communications , decoying aircraft and ordinance and confusing the enemy's perception of the tactical area . It represents a necessary investment to protect friendly weapon platforms [Tsu86].

The basic concept of EW , is to exploit the enemy's electromagnetic emission in all parts of the electromagnetic spectrum in order to provide intelligence on the enemy's order of battle, intentions and capabilities , and to use countermeasures to deny effective use of communications and weapons system while protecting one's own effective use of the same spectrum [Tsu86] .

The modern concept of EW as a vital and basic elements of military strategy , which when used in concert with other military assets , provides a method of neutralizing an enemy force (force divider effect) while simultaneously enhancing the power of a friendly force(force multiplier effect). Thus EW is defined as a military action involving the use of electromagnetic energy to determine, exploit , reduce , or prevent hostile use of the electromagnetic spectrum and action which retains friendly use of the electromagnetic spectrum .FIG. (3) illustrates the functions performed in a modern tactical EW system .

Electronic warfare systems are used in military actions to protect resources from enemy threats . In EW , as in other electronic system , simulation plays a vital role in training the operators to become proficient in using the equipment and recognizing threats . These systems can be organized into the three major categories or divided into three parts:

- Electronic Support Measure (ESM) , which collects information on the electronic environment .
- Electronic Countermeasures (ECM) , trying to disturb enemy systems .
- Electronic Counter-Countermeasures (ECCM) , trying to disturb the enemies ECM [Tsu86].

The ESM and ECCM are referred to as passive systems because they do not radiate electromagnetic energy , while the ECM is energy , EW encompasses the two major areas : ESM and ECM s [Fan01].

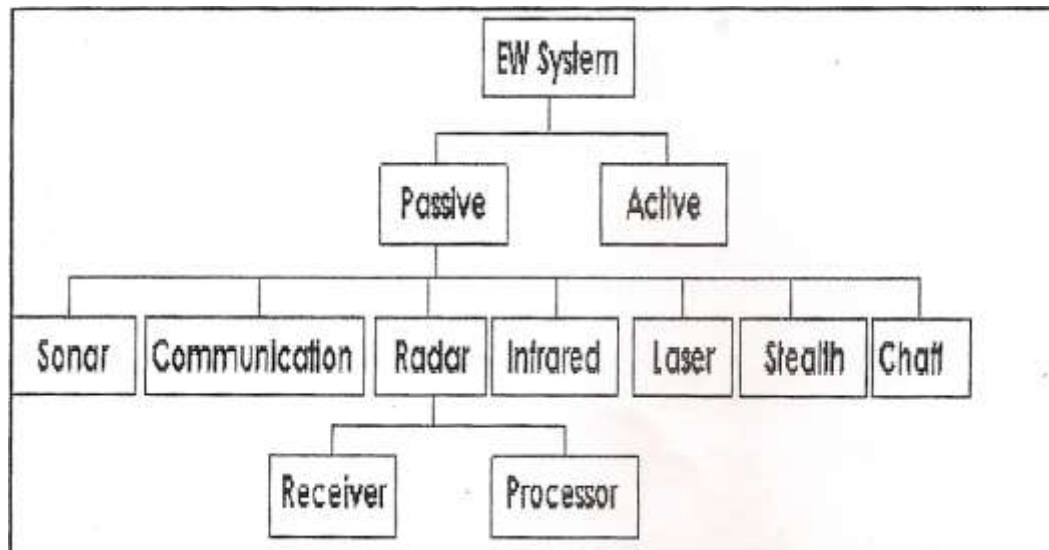


Fig. (3) Functional structure of EW system.

ELECTRONIC WARFARE RECEIVING SYSTEM

A Simplified Block Diagram Of An Ew Receiving System Is Shown In Fig. (4). The First Block Is The Feature Extractor , Which Represents The Radio Frequency Receiver Hardware , The Parameter Measurement And Encoding Circuitry .

Figure(5) Shows A Diagram Of The Digital Receiver . The Output Of The Feather Extractor Is A Pulse Descriptor Word (Pdw) , Which Contains Of Feather Values Of The Intercepted Signal (I.E., Frequency , Amplitude , Pulse Width , Time Of Arrival (In Some Cases) The Signal's Azimuth And Elevation Bearing).

The Pdw For Each Intercepted Signal Is Stored In A Pulse Buffer For Further Processing . Modern Ew Receiving System Must Operate In An Increasingly Dense Signal Environment. . Hence , A Large Quantity And Jumble Of Signals Are Intercepted That Must Somehow Be Stored In A Timely And Efficient Manner So That Subsequent Actions , Such As Identifying The Signal's Origin , Can Be Taken . The Third Block Performs The Sorting Or Deinterleaving Function By Clustering The Incoming Radar Pulses In To Groups . In Principle , Each Group Or Cluster Should Represent A Single Radar Or Emitter .

However , The Task Of Isolating A Particular Signal From A Specific Emitter Can Be Different To Accomplish , Since The Parameter Boundaries Between Different Signals May Overlap , And Since Factors Such As Measurement Error Can Cause The Measured Characteristics Of The Signal To Become Inexact Or “ Fuzzy “ . A Proper Choice Of The Signal Parameters That Are Used For Sorting As Well As A Proper Assignment Of Their Relative Importance In The Decision Process Can Minimize Some Of The Problems Caused By Inexact Or Ambiguous Signal Characteristics . For Example , One Example , One Signal Parameter That Can Be Very Useful For Signal Sorting Or Deinterleaving Purposes Is The Direction Of Arrival (Doa) Of The Intercepted Signal . Unfortunately , This Parameter May Not Always Be Available , Since Many Ew Systems Cannot Measure A Signal's Doa . Moreover , In Highly Dynamic Situations , Signal's Doa May Be Changing Too Rapidly To Be Of Practical Use .

Consequently , Many Ew Systems Must Rely On Other Parameters , Such As Frequency Or Pulse Width , To Sort The Received Signals . Therefore , The Problem Of Making Decisions Based On Inexact Or Ambiguous Evidence Will Always Be Present To Some Degree .

Intercepting and then isolating the signal (s) of interest is (are) not the end goal of a large array of EW receiving system . In many cases , the intercepted signal must also be ascribed to a specific radar or class of radar in the environment . For example , ECM systems must determine the identity of a victim radar or threat before the appropriate jamming technique can be selected . The task of determining the identity of an intercepted signal is laden with uncertainty , since the evidence (data cluster) itself

contains uncertainty , and since each stage in the identification process introduces additional uncertainties . Nevertheless , an accurate identification must be made ; in some cases , an error can be fatal.

The final two blocks support the task of identifying and classifying the intercepted signals . The fourth block , the pattern extractor and tracker (PET) , uses the stored information from the deinterleaver to compute any patterns . (e.g., the pulse repetition interval (PRI) pattern) that may be contained in each data cluster (emitter) by using the appropriate data item from the PDWs stored in a cluster . The final and fifth block is the classifier , which describes each data cluster in the PET to a particular emitter .

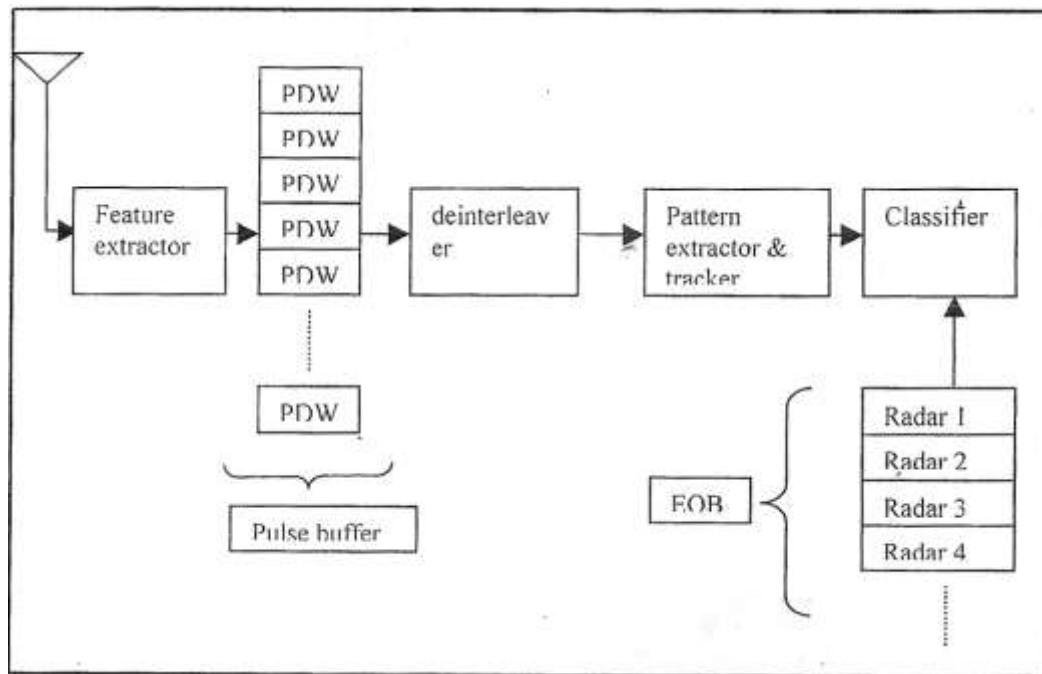


Fig. (4) : General block diagram of an EW receiving system

The identity of a particular signal is usually inferred by correlating the observed characteristics of that signal with those that are stored in the electronic order of battle (EOB) , which is a list that contains the identity and signal characteristics of all known radars or those likely to be encountered [Vac93] .

Major applications of EW receivers serve three purposes in EW system : they warn of enemy radar (radar warning receiver (RWR)) , they support electronic jammers (electronic countermeasures (ECM) receiver) , and they aid reconnaissance (electronic intelligence (ELINT) receiver) . The requirements for each of these functions are different , and so in most situations they are supported by different receives [Sch86].

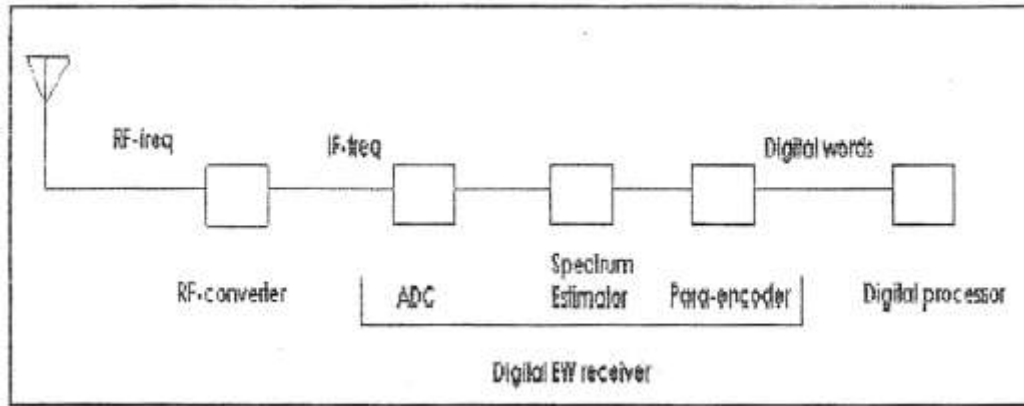


Fig. (5): Functional block scheme of digital EW receive.

RADAR SIGNALS : CW PULSE ,RF PULSE TRAIN AND CHIRPED TYPE SIGNALS

Most radars are designed to transmit a continuous train of RF pulses in order to perform target detection . These RF pulses have the same power , and share a common antenna for transmitting and receiving signals . For Continuous –Wave (CW) radars , the pulse is transmitted continuously , often through a separate transmitting and receiving antenna . Both of these radar designing operate mainly at a single frequency . For a high- resolution modern radar , see eq. (1) , it requires a wide radar bandwidth to increase the information about the location and the identity of target .

$$\text{Radar resolution } (\Delta r) = \frac{\text{Propagation velocity}}{2 \times \text{bandwidth}}$$

Pulsed radar signals ,are predominantly pulsed with widths varying between 0. micros and tens of microseconds . so they are transmitted as periodic pulse trains.

A chirped pulse is a RF pulse consisting of a sine wave that is phase modulated in such a way that linear frequency modulation results across the pulse duration . By statistical definition , a linear chirped sinusoidal signal is a non – stationary signal and is described as :

$$S(n) = \sqrt{P_x} \exp j(2\pi f n + \psi n^2 / 2 \cdot \Phi) \quad (2) \text{ [Hau00]}$$

Where Ψ is the chirp rate of the signal f is the center frequency, n is the time period and Φ is the constant phase of the signal . The signal amplitude \sqrt{p} x is constant but the signal is non-stationary due to the chirping of the frequency that sweeps linearly with time . The input signal $x(n)$ is given by :

$$x(n) = s(n) + \eta(n) \quad (3)$$

[Hau00].

Where $\eta(n)$ is a zero mean white noise (Gaussian) signal with noise power of P_{π} . Different radar signal properties are graphically illustrated in Fig.(6) [Bro79.Tin01].

PARAMETERS TO DETECT

A radar receiving system is generally used to extract the features of each input pulse , including RF, amplitude (Amp), pulse width (Pw). Angle of arrival (AOA) , time of arrival (TOA) , and modulation of pulse (MOP). Other parameters measured are pulse repetition interval (PRI) and burst repetition interval (BRI) .PRI indicates how often pulses arrive and BRI indicates how often groups of pulses arrive . For detailed discussion about the quantities that an EW receivers receive, one should refer to chapter three into [Sch86].

According to these features , the deinterleaver wants to cluster pulses which are emitted from distinct emitters into distinct groups . The ability of a radar system to determine and resolve these important target parameters depends on the characteristics of the transmitted radar signal.

Fig. (7) illustrates (a) CW pulse train signal with its time – frequency representation (b) CW chirped train signal with it time – frequency representation [Bro79].

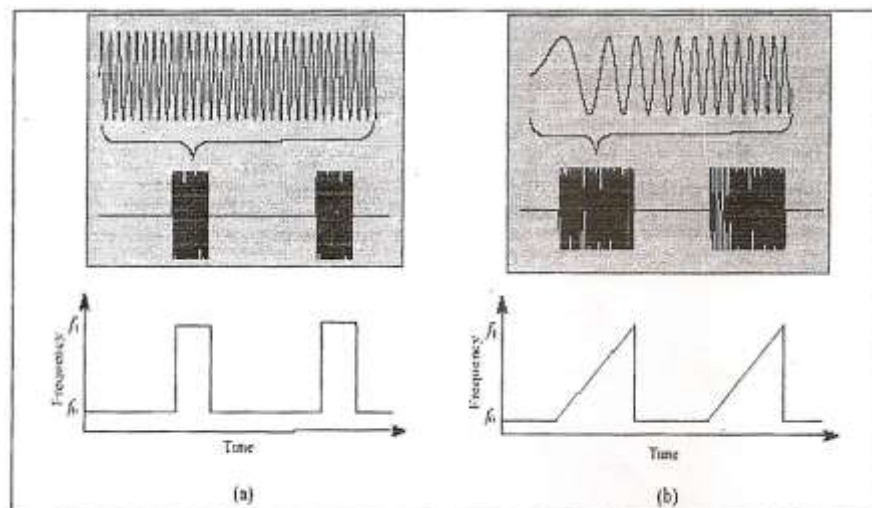
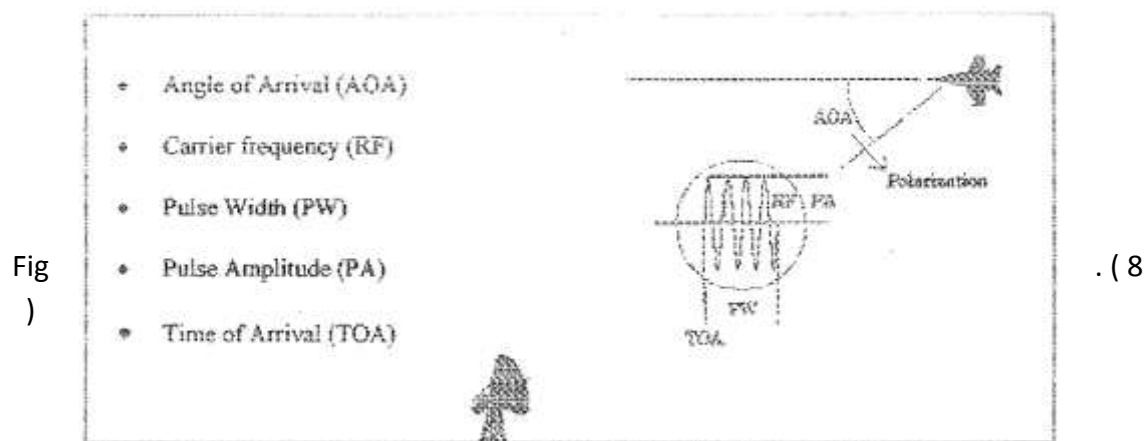


Fig. (7) : Pulse train signal with its time frequency

The train of interleaved pulses is processed in the ESM receiver to identify for each pulse the center frequency ,amplitude , PW ,TOA and bearing (or AOA), see fig. (8) The information is then input to a pulse sort processor , which deinterleaves it into the PRI appropriate to each emitter .

Further comparison against a store of known radar types permits the generation of an emitter list, classified with threat significance . Depending on the detected radar signal the pilot of an airplane gets information of the threat he is exposed to :



Parameters measured by receiver .

The receiver subsystem detects the radar pulses and measure the individual parameter , (the digital words a receiver generates and passes to a digital processor). The availability , resolution and accuracy of these measurements must all be taken into account when designing the deinterleaveing system . Obviously , the better the resolution and accuracy of any parameter measurement , the more efficiently the preprocessor can carry out its task . However , there are limitation on the measurement process from outside the ESM system (e.g. noise , jamming , and multipath), inside the system (e.g. timing requirement)and from cost- effectiveness considerations.

SIMULATION RESULTS

In the following section different types of the radar signals will be evaluated by the radar-parameter- generation GUI package , from the applied signal flowgraph shown in Fig. (9) the signal shown in Fig. (10), some other samples of generated signals from there applied simulink shown in Fig.(11) , are shown in Fig.(12)and (13).

As a short summary ,the following individual units are used in Fig.(9) : they are further divided into different modules and sub modules in order to manipulate different types of input data.

The Input Unit.

The Digital Signal Processing Unit.

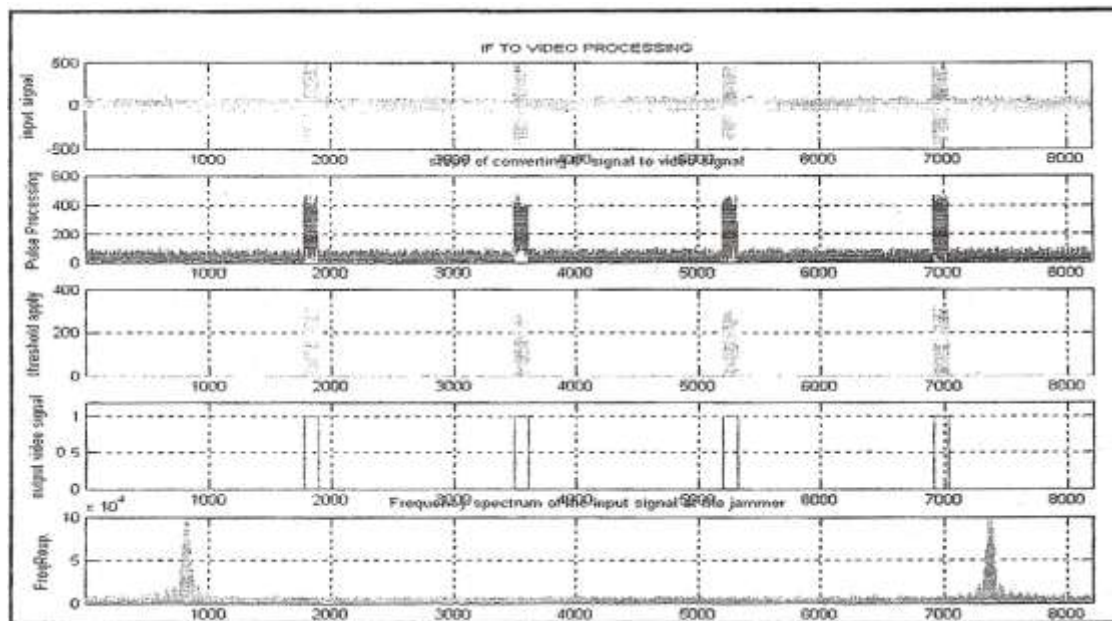
The EA Strategy Unit.

The Human Computer Interface Unit.

The Output Unit.

The Control and Management Unit and

The Power Calculation and Evaluation Unit.



(10) Simulated sample of Radar signal.

Matlab-Simulink ,the processing and analyzing phases applied onto the received IF signals .It has the function of reading out the data samples of the digitized IF signal of constant , chirp , or nonlinear frequency modulation , converting the digitized IF into video signal measuring processed video pulse parameters and displaying time and frequency drawings of input and video signals. Fig. (11) shows the implemented model.



Fig.(11) :The simulink to generate a signal.

Fig. (11): Second sample of the radar signal

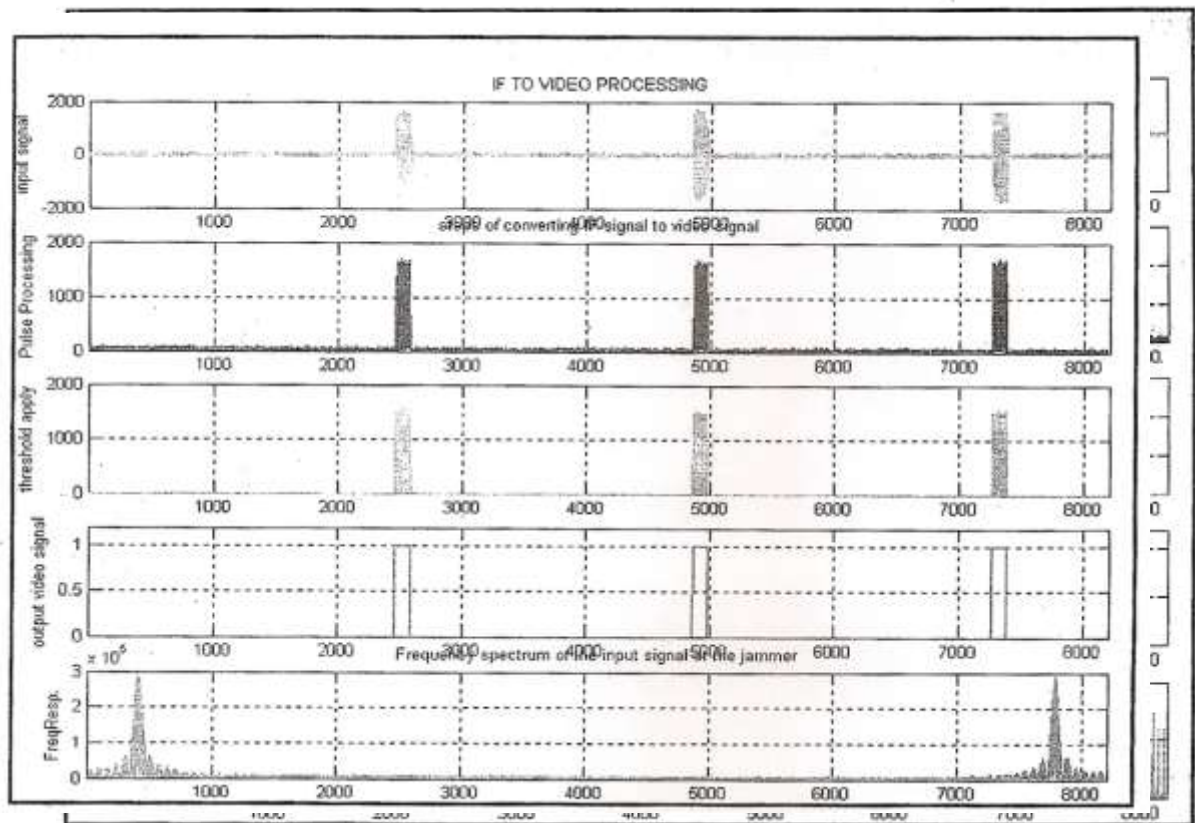


Fig.(12): Third sample of the radar signal

CONCLUSION



From the above results the generated electronic order of battle can be obtained m hence, in order to identify any target the only requirement is to compare it with the available standard table.

REFERENCES

- Albaky B.M.,2003.”Interference Analysis and Generation in Radar System”, M.Sc. Thesis Electrical Eng. Dep. University of Baghdad.
- Fanden P., 2001, “Evaluation of Xilinx System Generator “ , M.Sc. Thesis, Linkping University Sweden.
- Ting L.K.,2001” Algorithm and FPGA Implementation of Adaptive LMS-Based Predictors for Radar Pulse Deinterleaving “ , Ph.D. Thesis Queen’s University Belfast.
- Hautaniemi S., 2000 “ Target Identification with Bayesian Networks”, M.Sc. Thesis Tampere University of Technology , Finland.
- Vaccaro D.D. , 1993, “Electronic Warfare Receiving System “ Artech House .
- Schleher D.C.,1986, “ Introduction to Electronic Warfare “, Artech House.
- Tsui J.B. , 1986 “ Microwave Receivers with Electronic Warfare Application “ John Wiley and Sons.
- Brookner E. “Radar Technology “ Artech House.

COLOR SATELLITE IMAGES DENOISING USING WAVELETS

Hawrra H.Abbas Al-Rubiae
Computer Engineering. The University of Kerbala

ABSTRACT

The satellite image is multi band image, the first three bands have the largest wavelength and image information and usually contain noise due to different reason such as image band acquisition or transmission.

In this paper an adaptive method implemented to denoising the satellite image by using the Haar wavelet transform applied to the principle components bands of the satellite image.

The image denoising by Haar wavelet transform is applied on the first band(PC1). This band has found contain about 90% of the image information, in this case the time required for processing and storage size are reduced, and the image appearance are more suitable than the processing the image bands directly.

الخلاصة

تعتبر صورة الأقمار الصناعية صورة متعددة الحزم، الحزم الثلاث الأولى لها الطول الموجي الأكبر والجزء الأكبر من معلومات الصورة. هذه الحزم تحتوي نسبة عالية من الضوضاء نتيجة لعملية استحصال المعلومات أو إرسالها.

في هذا البحث استخدمت Haar wavelet لاستخلاص الضوضاء من حزم الصور الفضائية وتم مقارنة النتائج من خلال قياس نسبة الضوضاء ومقارنتها مع الطرق التقليدية. من خلال دراسة توزيع المعلومات وجد أن الحزمة الأولى تحتوي تقريبا على 90 % من معلومات الصورة ولهذا تم استخدام Haar wavelet على هذه الحزمة فقط، وبهذا تم تقليل الوقت المستغرق والمساحة التخزينية المطلوبة في حالة معالجة الصور الفضائية.

KEYWORDS

satellite image, principle component, Wavelet transform

INTRODUCTION

Satellite images are multi band, i.e. the image is consisting from three bands or more according to satellite sensor used to capture these images. But usually only the first three bands used to represent these images as true color images with RGB bands, and contain noise due to image acquisition, transmission error or compression side effects. The noise causes great problems to image processing algorithms. Only when the image de-noising is effective the edge detection is proper. In other case the edge detection is significantly noised [Scoott E Umbaugh(1998)].

De-noising is typically handled by smoothed filters applied to the image three bands. But smoothing can delete useful information or distort the input image [Gomies(1997)].

The main steps of the proposed strategy are (1) transform the image to its principle components bands, (2) image denoising using wavelet transformation implemented on the first principal component only, (3) extract back the new image band from its principle components bands.

PRINCIPAL COMPONENTS TRANSFORM (PCT)

Some of the images processing techniques applied on two or all the bands of an image. If there are many bands, it becomes difficult to visualize as well as expensive to process all the bands. The principal components transform is based on statistical properties of the image, it can be applied to any n-dimensional mathematical space to collapse any multiband image down to fewer bands. In this paper, the PCT is applied to the three-dimensional color space. Each pixel in the (n)-spaced image may be considered as a point in (n) dimensional pixel space. The set of all pixels in the image becomes a distribution of points in this space.

The effect of computing the principal components of a distribution is to determine a new set of axes with two related properties [R. Wilson 1988].

1- The axes may be ordered by their "information content", thus using only the first axis, the best one dimensional representation of the data is obtained, by using the first two, the best two dimensional representation, and so on.

2- The data expressed in the new axes are uncorrected .

The PCT is easily explained graphically with an example of data in two bands. Figure (1-a) shows the relationships of data file values in two bands. The values of one band are plotted against those of the other. If both bands have normal distribution, an ellipse shape results, (for three band ellipsoid shape results).

To perform principal component analysis, the axes of the spectral space are rotated, changing the coordinates of each pixel in spectral space, and the data file values as well. The new axes are parallel to the axes of the ellipse, major (longest) axis of the ellipse, is called the first principal component of the data, a new axis of the spectral space is defined by this first principal component as shown in Figure (1-b), and since in spectral space, the coordinates of the points are the data file values, new data file values are derived from this process. These values are stored in the first principal component band of a new data file. The second principal component is the widest transect of the ellipse that is orthogonal (perpendicular) to the first principal component as shown in Figure (1-c). The second principal component describes the largest amount of variance in the data that is not already described by the first principal component . The eigenvectors and eigenvalues represent the lengths and directories of the principal axes. [ERDAS Inc(1995)]. Figure (2) represent the implemented block diagram to explain the process of extract the pinciple bands from RGB (multiband) satellite image.

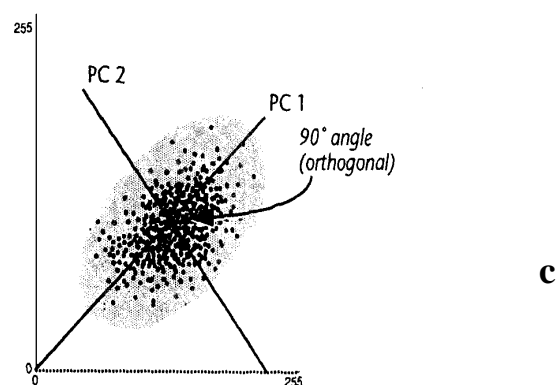
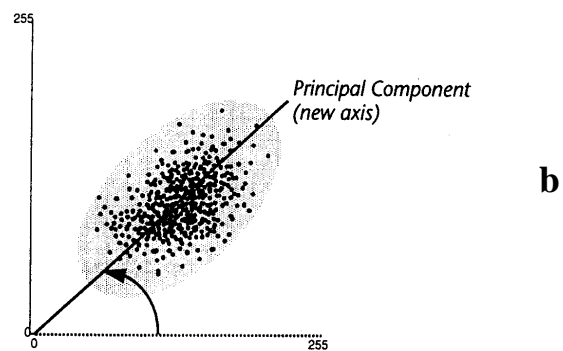
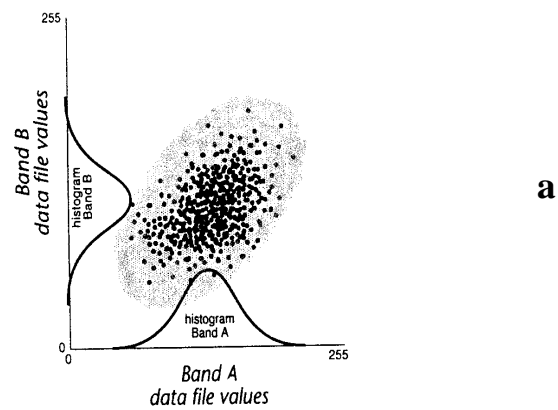
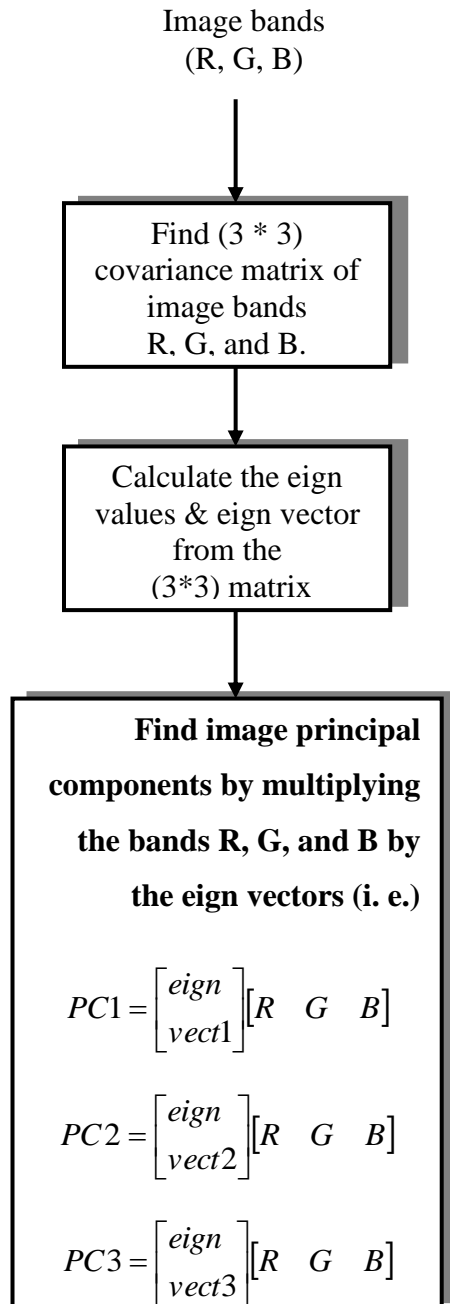


Figure (1-a, b ,c) Transformation of the two bands by PCT



**Figure (2) PCT
block diagram**

$$PC_j = \sum_i^3 e_{ij} b_i$$

IMAGE DE-NOISING USING WAVELET TRANSFORM

Wavelet transforms used to represent signals with a high degree of sparsity. This is the principle behind a non linear wavelet based signal estimation technique known as wavelet denoising. A precise explanation of the wavelet denoising procedure can be given as follows. Assume that the observed data is

$$X(t) = S(t) + N(t)$$

Where $S(t)$ is the uncorrupted signal with additive noise $N(t)$ [R.Gonzalez and P.Wintz(2001)]. Let $W(.)$ and \hat{w} denote the forward and the inverse wavelet transformation operators. Let $D(.,\lambda)$ denote the denoising operator with threshold λ . This paper intends to denoise $X(t)$ to recover $\hat{S}(t)$ as an estimate of $S(t)$. The procedure can be summarized in three steps

$$Y = W(X)$$

$$Z = D(Y, \lambda)$$

$$\hat{S} = \hat{w}(Z)$$

So the basic method of image denoising is thresholding. By choosing a correct threshold, it is possible to remove most of the random noise [Jonathan Y. Stein(2000)].

- The Haar Wavelet Transformation Algorithm

The Haar wavelet transform is one of the simplest and basic transformations from the space domain to a local frequency domain. Haar wavelets are being used for the image transformation technique proposed here. To get an idea about the implementation of this wavelet, a simple example used to illustrate this, assume a one dimensional image with an eight pixel resolution, where the pixels have the following values : 7 5 3 9 3 7 5 3

By applying the Haar wavelet transform this image can be represented in terms of a low resolution image and a set of details coefficients. The transformed data coefficients are obtained by averaging two consecutive pixels, while the detail coefficients represent the difference between the average and one of the two consecutive pixels. So the above image will be represented as follows after the first cycle:

Transformed coefficients : 6 6 5 4

Detail coefficients: 1 -3 -2 1

Now the original image can be represented by a four pixel transformed image $((a+b)/2)$ after the first cycle and a four pixel image containing the detail coefficients

((a-b)/2). Recursively iterating this algorithm leads to an image that is reduced by a factor of two for each cycle. The detail coefficients are required to reconstruct the image. Reconstruction of the original image involves adding and subtracting the detail coefficients to and from the subsequent transformation coefficients for each cycle. During Reconstruction of the original image of the previous example, adding and subtracting the transformation and detail coefficients obtain the first pair of pixels [Colm Mulcahy(2004)].

In 2D wavelet transformation, structures are defined in 2-D and the transformation algorithm is applied in x direction first and then in the y -axis

- Thresholding

Threshold determination is an important question for denoising process. Small Threshold may yield a result close to the input, but the result may still be noisy. A large threshold on the other hand, produces an output with large number of zero coefficients. This leads to a smooth image. Paying too much attention to smoothness, however, destroys details and in image processing may cause blur and artifacts [Pujita Pinnamaneni(2003)].

The plot in fig (3) shows a noisy signal, for this signal replacing noisy coefficients (small coefficients below a certain threshold value) by zero and an inverse wavelet transform may lead to reconstruction that has denoised. Stated more precisely, the thresholding idea based on the following assumptions [Gabriel Cristobal 1996]:

- The decorrelating property of a wavelet transform creates a sparse signal: most untouched coefficients are zero or close to zero.
- Noise is spread out equally along all coefficients
- The noise level is not too high so that the signal wavelet coefficients from the noisy ones can be distinguished [Martin Vetterli S Grace Chang, Bin Yu(2000)].

- Hard and Soft Thresholding

Hard and soft thresholding with threshold λ are defined as follows

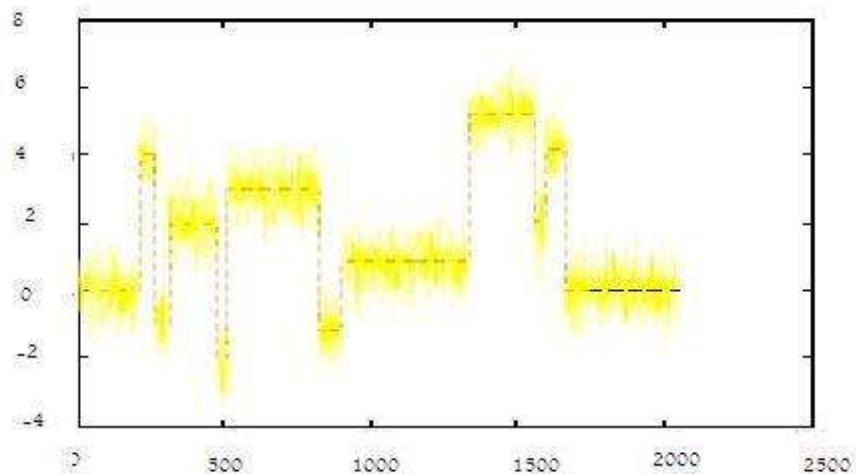
The hard thresholding operator is defined as

$$D(U, \lambda) = U \text{ for all } |U| > \lambda \\ = 0 \text{ otherwise}$$

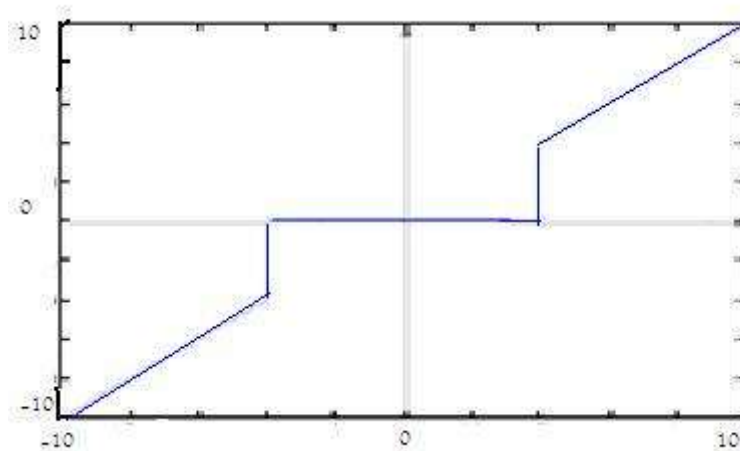
The soft thresholding operator on the other hand is defined as

$$D(U, \lambda) = \text{sgn}(U) \max(0, |U| - \lambda)$$

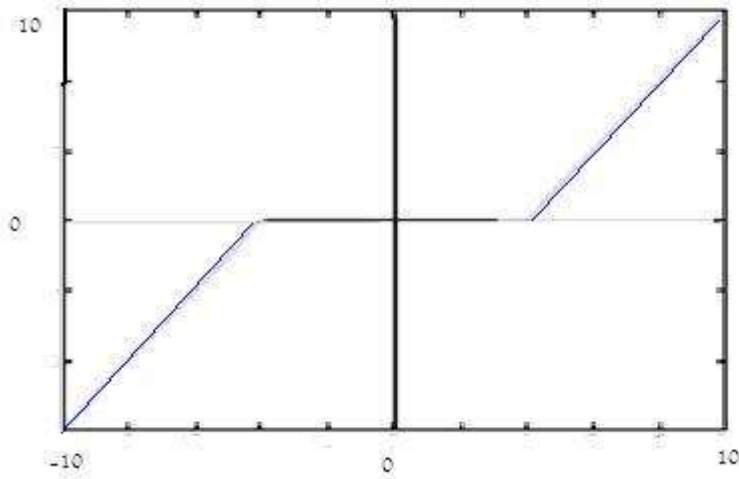
Hard threshold is a "keep or kill" procedure and is more intuitively appealing. The transform function is shown in fig (4). The alternative, soft thresholding (whose transfer function is shown in fig(5)), shrinks coefficients above the threshold in absolute value. While at first sight hard thresholding may seem to be natural, the continuity of soft thresholding has some advantages. It makes algorithms mathematically more tractable. Moreover, hard thresholding does not even work with some algorithms, sometimes, pure noise coefficients may pass the hard threshold and appear as annoying 'blips' in the output. Soft thresholding shrinks these false structures [Maarten Jansen(2001)].



Fig(3) Noisy signal



Fig(4) Hard threshold



Fig(5) Soft threshod

IMPLEMENTATION and RESULTS

In this paper the(Matlab 7) program used to for image denoising according to following steps:

- Read RGB image
- Used the flowchat in Fig (2) to extact PC bands
- Define the throshold value, two type of throshold value used the hard throshold and the soft throshold
- The Haar transform matrix used to handle the PC1 using the block process operation that found in the Matlab
- Get RGB band from the PC bands from following

$$\begin{bmatrix} R' \\ G' \\ B' \end{bmatrix} = E_{(i,j)}^{-1} * \begin{bmatrix} PC1' \\ PC2 \\ PC3 \end{bmatrix}$$

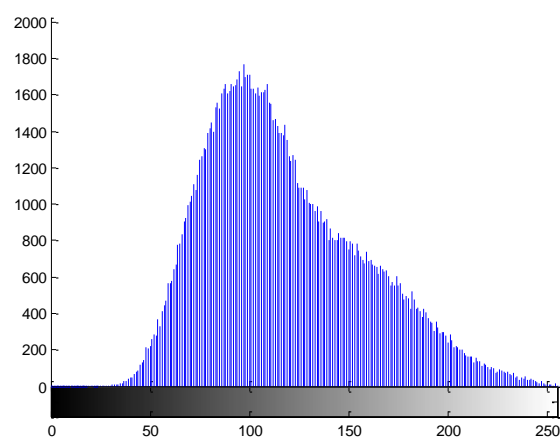
Where $PC1'$ is the processed band

$E_{(i,j)}^{-1}$ is the (3*3) eign vector matrix inverse

Fig(6) shows the result obtained when denoising sheme(Haar Wavelet)is applied to the noisy sattelite image(PC1 only)fig(5) using the hard threshold(zero threshold) and soft threshold (this threshold represent the stander deviation and the mean of image PC1 gray values).



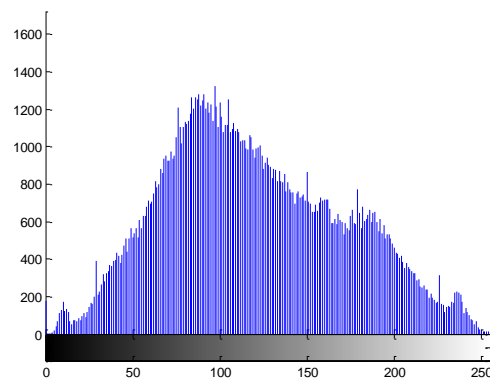
Fig(5-a) the original image



Fig(5-b)Original image histogram(PC1 only)



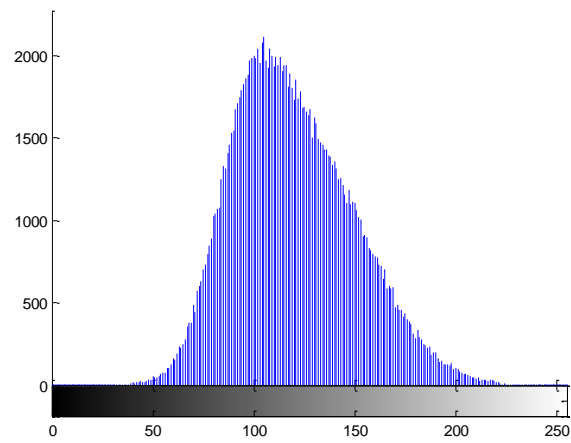
Fig(5-c) The noisy image



Fig(5-d)Noisy image histogram(PC1 only)



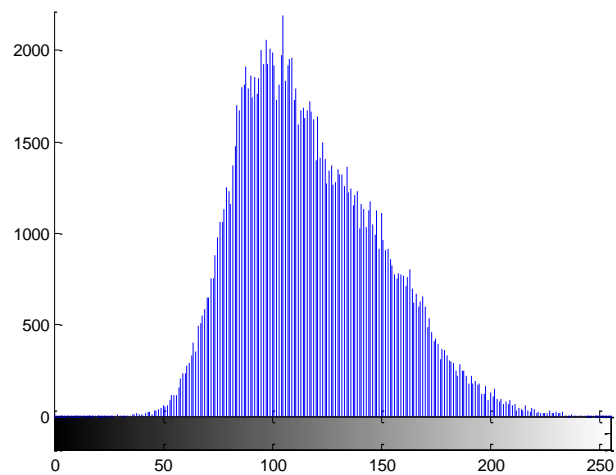
Fig(6-a)Denoising image using standard deviation threshold



Fig(6-b)The Histogram of image (6-a)



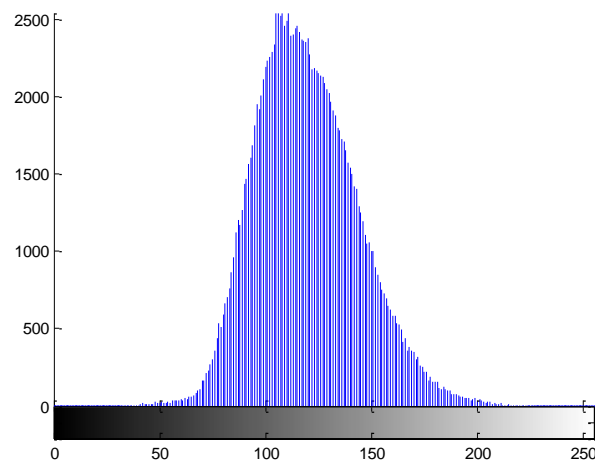
Fig(6-c)Denoising image using mean threshold



Fig(6-d)The Histogram of image (6-c)



Fig(6-e)Denoising image using Hard threshold



Fig(6-f)The Histogram of image (6-e)

The effect of using wavelet denoising is clear ,by comparing the result images histograms with the original image histogram ,for example ,fig(6-f) shows the information losses (using hard threshold)comparing to fig(5-b), also the PSNR(Peak Signal to Noise Ratio) used to analysis and compare the Wavelet performance with standered method (a daptive wiener filter) .The PSNR defiend as folow

$$PSNR= 20\log_{10}\left(\frac{b}{rms}\right)$$

where b is the largest possible value of the signal (typically 255 or 1), and rms is the root mean square difference between two images. So by applying the a above equation the following result obtained

Image	PSNR
Noisy Image	20.24 dB
Wavelet denoising (standard devation threshold)	26.71 dB
Wavelet denoising (mean threshold)	26.78 dB
Wavelet denoising (hard threshold)	26.55 dB
Adaptive filter	25.87 dB

CONCLUSION and FUTURE WORK

Experimental results shown above(the PSNR values) indicates that wavelet transform is an effective method of denoising noisy images and the most important feature is the transform threshold choicing by investigating Soft threshold schemes virses the Hard threshold shemes.

The principal component transformation, is applied to the color image. The data histogram for the PC1 band is studied and compare with the one of the origional histogram and was found that approixamtly 90% of image information found in this band ,so by process the first component (PC1) only the time and storage need for color image processing can be reduced.

In future handle the same process using another methods of threshold technique such as SureShrink,VisuShrink and BayesShrink[Raghuram Rangarajan(2002)].



REFERENCES

- Scoott E Umbaugh(1998), "Computer Vision and Image Processing", Prentice Hall.
- ERDAS Inc(1995).,"Graphical models reference guide", ERDAS Inc., Atlanta, Georgia.
- Gomies(1997) "Image Processing and Computer Graphics ",Springer.
- R.Gonzalez and P.Wintz(2001),," Digital Image Processing"second Edition , Addison – Wesley, Pub Comp.
- Maarten Jansen(2001). "Noise Reduction by Wavelet Thresholding", volume 161. Springer Verlag,United States of America, 1 edition.
- Martin Vetterli S Grace Chang, Bin Yu(2000). "Adaptive wavelet thresholding for image denoising and compression". *IEEE Transactions on Image Processing*, 9(9):1532–1546.
- Jonathan Y. Stein(2000)," *Digital Signal Processing: A Computer Science Perspective*",John Wiley & Sons, Inc.
- Pujita Pinnamaneni(2003),"3-D Wavelet Transformation in Java", Dept of Computer Science,Mississippi State University.
- Colm Mulcahy(2004),"Image Compression using the Haar Wavelet transform", Spelman Science and Math Journal.
- Raghuram Rangarajan(2002)," Image Denoising Using Wavelets".
- Gabriel Cristobal, Monica Chagoyen, Boris Escalante-Ramirez, Juan R Lopez, "Wavelet-based denoising methods, A comparative study with applications in microscopy", *Proc. SPIE's International Symposium on Optical Science, Engineering and Instrumentation, Wavelet Applications in Signal and Image Processing IV*,Vol. 2825, 1996.
- R. Wilson and A.D. Calway. A general multiresolution signal descriptor and its application to image analysis. In *Signal Processing*, pages 663{666. EURASIP, 1988.



VARIABLE VOLTAGE - FREQUENCY CONTROL OF A SINGLE PHASE INDUCTION MOTOR DRIVEN BY SHEPWM INVERTER

Ali Hussein Abdul-Jabbar
Al-Mustansiriyah University
College of Engineering
Electrical Engineering Department

ABSTRACT

Single phase AC induction motors are one of the widely used motors in the world, yet relatively little work has been done in the applications of power electronic converter to these motors to achieve variable speed operation. When variable speed is required, it is usually achieved either by using auto transformer or by switching between two or more fixed winding configurations. The motor is analyzed as an unbalanced two phase system to determine the torque that can be expected under variable frequency control.

The performance of capacitor-run single phase induction motor used in SHEPWM adjustable speed drives in the steady-state is investigated. The supply voltage-frequency law for the motor is selected in such a way as to insure a correct operation of the motor over the whole speed range.

السيطرة على مسوق محرك حثي أحادي الطور مغذى من عاكس يعمل بتقنية SHPWM باستخدام طريقة التردد و الجهد المتغيرين

الخلاصة

المحرك الحثي أحادي الطور هو أحد المحركات الأكثر شيوعاً في العالم. حتى الآن توجد أعمال قليلة نسبياً تم إنجازها حول تطبيقات محولات الكترولنيات القدرة التي تغذي هذه المحركات لتحقيق عملية تغيير السرعة. عندما يكون المطلوب تغيير السرعة فإن ذلك يتم عادةً أما باستخدام المحولة الذاتية أو بواسطة التحويل بين اثنين أو أكثر من التشكيلات الثابتة للملف. تم تحليل المحرك كمنظومة ثنائية الطور غير متزنة لحساب العزم الذي يمكن توقعه تحت سيطرة التردد المتغير.

تم التحقق من أداء المحرك الحثي أحادي الطور ذو المتسعة الدائمية وعند الحالة المستقرة والمستخدم في مسوقات السرعة القابلة للتنظيم والتي تعمل بتضمين عرض النبضة بحذف التوافقيات الانتقائي. يتم اختيار قانون الفولتية- تردد للمحرك بطريقة ما ليضمن الاشتغال الصحيح للمحرك عبر المدى الكامل للسرعة.

INTRODUCTION

Single phase induction motors are one of the most widely used types of low power motors in the world, especially for domestic or commercial applications where a three-phase power supply is not available. These are inherently single and comparatively constant speed machines. In the case of applications requiring variable speed operation, a supply with variable frequency and voltage is needed. Variable frequency-voltage supplies can be available in the form of inverter [M.Ozdemir 1999, D.G.Holmes 1993].

However, speed modulation of a single-phase motor is usually achieved either by some electrical means, such as reducing supply voltage by auto-transformer, or by switching windings to change the number of motor poles for different operating condition as required.

Up to date only a few alternatives to variable frequency converters have been reported used to achieve variable speed single phase motor operation. One of these approaches uses a single phase converter to control the phase angle of the voltage applied to the motor auxiliary winding, while the main winding remains connected to the AC supply [E.R. Collins 1988]. Other work have proposed a continuous variable speed control of single phase motor, using a standard three phase voltage source inverter [M.Ozdemir 1999].

Voltage control is a simple method for changing the speed of capacitor-run motor shown in Fig.1, but it allows only a very limited speed range to be obtained. Nowadays the frequency control acts as an interesting alternative to voltage control [P.C.Sen 1997]. The capacitor-run motor seems to be one of the most appropriate actuators for variable speed drives [Twin City 2000]. In this paper frequency control in a range below the rated frequency is investigated. The current study provides a performance analysis of capacitor-run single phase induction motor fed from variable frequency variable voltage supply involved steady-state equivalent circuit of the machine.

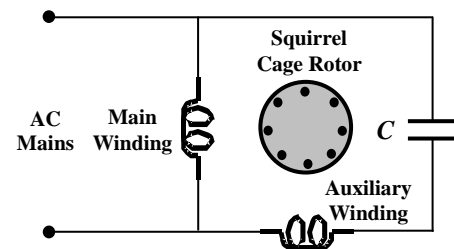


Fig. 1: Capacitor-run Single Phase Induction Motor

SINGLE PHASE INDUCTION MOTOR MODEL

Single winding single phase motors are most effectively analyzed using the Double Revolving Field Theory, which splits the oscillating single magnetic field produced by a current flowing through the winding into two contra-rotating magnetic fields, each of which can be analyzed using normal three phase rotating field theory. The equivalent circuit for a single winding motor under these conditions is shown in Fig.2 [D.G.Holmes 1993].

The rotor impedance referred to the stator has been separated into two halves, with one half influenced by the forward rotating field and the other influenced by the backward rotating field.

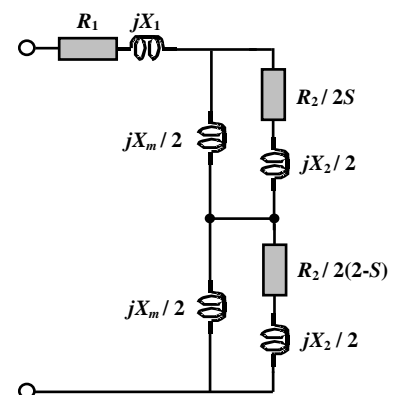


Fig. 2: Equivalent Circuit of Single Winding Single Phase Induction Motor

For a two winding motor, with the windings arranged in space quadrature on the stator, this analysis can be extended to develop a similar single phase equivalent circuit for each winding, with an additional speed voltage in each winding representing the voltage induced in the winding from the other winding's flux. The total equivalent circuit for this arrangement is shown in Fig.3, for two

unbalanced windings with a turns ratio of " $1:a_s$ " between the main and the auxiliary winding. Note that the parallel branches for each winding equivalent circuit have been converted into equivalent series impedances.

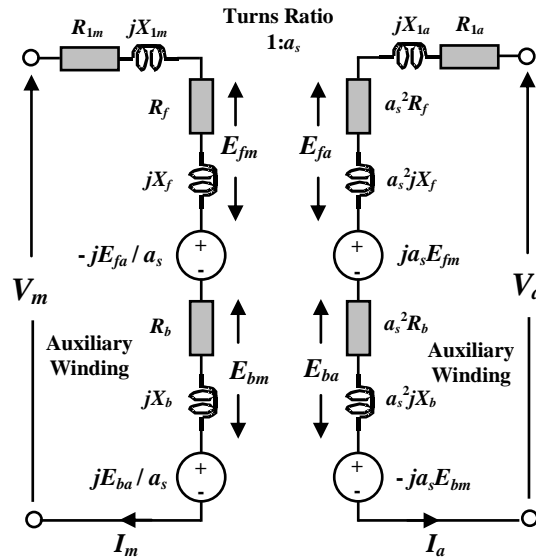


Fig. 3: Equivalent Circuit of Unbalanced Two Winding Induction Motor

The impedances for this equivalent circuit are defined as:

R_{1m} , X_{1m} = Main winding resistance and leakage reactance.

R_{1a} , X_{1a} = Auxiliary winding resistance and leakage reactance.

X_m = Main winding magnetizing reactance.

$a_s^2 X_m$ = Auxiliary winding magnetizing reactance.

R_2 , X_2 = Rotor resistance and leakage reactance referred to main winding.

$a_s^2 R_2$, $a_s^2 X_2$ = Rotor resistance and leakage reactance referred to auxiliary winding.

$1:a_s$ = Turns ratio between main and auxiliary winding.

No attempt has been made to include a core loss representation into the model.

Using these definitions, the series equivalent forward and backward impedances shown in Fig. 3 become:

$$R_f = \frac{X_m^2 R_2 / S}{(R_2 / S)^2 + (X_2 + X_m)^2} \quad (1)$$

$$X_f = \frac{X_m [(R_2 / S)^2 + X_2 (X_2 + X_m)]}{(R_2 / S)^2 + (X_2 + X_m)^2} \quad (2)$$

$$R_b = \frac{X_m^2 R_2 / (2 - S)}{(R_2 / (2 - S))^2 + (X_2 + X_m)^2} \quad (3)$$

$$X_b = \frac{X_m [(R_2 / (2 - S))^2 + X_2 (X_2 + X_m)]}{(R_2 / (2 - S))^2 + (X_2 + X_m)^2} \quad (4)$$

where S is the motor slip.

As shown in [D. G. Holmes 1993], the average motor torque developed using this model is given by:

$$T_{av} = \frac{1}{\omega_1} \left[\frac{(I_m^2 + a_s^2 I_a^2)(R_f - R_b)}{+ 2a_s(I_m I_a \sin \varphi)(R_f + R_b)} \right] \quad (5)$$

, and the pulsating torque is:

$$T_{puls} = \frac{1}{\omega_1} \left\{ \left[\frac{I_m^4 + (a_s I_a)^4 + 2(a_s I_m I_a)^2 \cos(2\varphi)}{*(R_f - R_b)^2 + (X_f - X_b)^2} \right] \right\}^{1/2} \quad (6)$$

where φ is the Phase angle between the main winding current I_m and auxiliary winding current I_a and ω_1 is the angular synchronous speed.

SPEED CONTROL OF INDUCTION MOTORS

There are really only two techniques by which the speed of an induction motor can be controlled. One is to vary the synchronous speed, and the other is to vary the slip of the motor for a given load. The synchronous speed (N_1) of an induction motor is given as:

$$N_1 = 60 f_1 / P \quad (7)$$

So only two ways in which N_1 can be varied: (i) by changing the electrical frequency (f_1) and (ii) by changing the number of poles ($2P$) on the machine. Slip control may be accomplished by varying either the rotor resistance or terminal voltage of the motor.

There are two major approaches to changing the number of poles: (i) the method of consequent poles, and (ii) multiple stator windings.

For the first method, the speeds will be in ratio of 2:1. With combining the two methods it is possible to build a four-speed induction motor only (could be accomplished for three phase induction motor only).

The speed may be controlled over limited voltage by varying line voltage. This method is sometimes used on small motors driving fans. The torque developed by the motor is proportional to the square of the applied voltage.

In the wound rotor induction motors, it is possible to change the shape of torque-speed curve by inserting extra resistances into the rotor circuit machine. The more popular speed control technique is by changing the line frequency [S.J. Chapmen 1999].

A. (V/f) Speed control Strategy

Nowadays the rotary-converter method is being supplanted on a wide scale by static converter methods in which performance and reliability of variable speed AC systems are improved.

If the electrical frequency applied to the stator of an induction motor is changed, the rate of rotation of its magnetic fields N_1 will change in direct proportion to the change in electric frequency, and the no-load point on the torque-speed characteristic curve will change with it. The synchronous speed of the motor at rated conditions is known as the base speed. By using variable frequency control, it is possible to adjust the speed either above or below the base speed. A properly designed variable-frequency

induction motor drive can be very flexible. It can control the speed of the motor over a range from as little as 5% of base speed up to about twice base speed. However it is important to maintain certain voltage and torque limits on the motor as the frequency is varied, to ensure safe operation.

When running at speed below the base speed of the motor, it is necessary to reduce the terminal voltage applied to the stator linearly with decreasing stator frequency. This process is called (derating). If it is not done, the steel in the core of the motor will saturate and excessive magnetization currents will flow in the machine.

The starting current drawn by an induction motor with a fixed frequency during direct-on-line start is normally about six times its rated value. This current can be reduced by reduction of supply voltage magnitude which leads to reducing the starting torque. However, when variable frequency is used it is possible to use a low starting frequency and voltage and then raise it as the motor accelerates to maintain constant air gap flux, and constant (V/f) [A. Jalil 1980].

The method of choice today for induction motor speed control is the solid-state variable-frequency induction motor drive. The output voltage and frequency control is achieved by using PWM techniques.

B. Choice of Voltage and Frequency Patterns

Some loads such as fans require little torque when starting (or running at low speeds) and have torques, which increases, as the square of the speed. Other loads might be harder to start, requiring more than the rated full-load torque of the motor just to get the load moving. This drive provides a variety of voltage-versus-frequency patterns, which can be selected by its load. Fig. 4.a shows the general-purpose pattern, and Fig.4.b shows fan torque pattern (with low starting torques) when the output voltage changes parabolically with changes in output frequency for speeds below base speed (f_1).

For any given frequency below the base frequency, the output voltage will be lower than it was with the general pattern, providing a slow, smooth start for low torque loads [S.J. Chapmen 1999] for this work the selected voltage values will increase by 10% for the low order frequency (5-15Hz) to improve the starting torque.

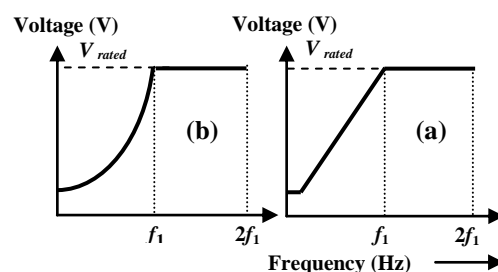


Fig. 4: Voltage versus Frequency Patterns:
(a) General Purpose, (b) Fan Torque.

C. Speed Control of Capacitor-run Single Phase Induction Motor

Fractional horsepower single phase motors were estimated to constitute about 80 % of the motors used in the industrial and commercial sectors. Therefore, the intensive exists to improving the efficiency and power factor and harmonic contents of single phase motor applications [Y. Baghzouz 1988].

The capacitor-run single phase motor seems to be one of the most appropriate actuators for variable speed fractional-horse-power drives. Voltage control is a simple method for changing the capacitor-run

motor speed. The supply voltage may be varied by an autotransformer, as in the past, or by semiconductor switching elements. However, voltage control of standard capacitor motors allows only a very limited speed range to be obtained.

Nowadays the development of less expensive electronic power devices makes frequency control an interesting alternative to voltage control. Recently some authors have proposed to change the speed of single phase motors using cycloconverters, or inverters. The most advantageous of this kind of control seems to be the possibility of obtaining satisfactory speed regulation with standard motors [Twin City 2000, U. Raghzouz 1988].

Adjustable speed is needed in various single phase motor drives. At speed lower than the rated value, the motor current increases considerably. The resulting heat dissipation, in addition to sufficient motor torque development, sets a lower limit to the operating speed range. It is well known that line power factor improvement and minimum current distortion can be achieved by using PWM inverters which have been successfully applied to adjustable-speed three phase induction motor drives where motor voltage and frequency are simultaneously controlled. It is feasible to apply the variable-voltage variable-frequency control strategy to a PWM inverter-fed single phase motor [Twin City 2000, U. Raghzouz 1988]. In this paper, frequency control in a range below rated frequency is investigated.

With the same number of pulses per cycle, the optimized Selective Harmonic Elimination PWM technique tends to produce currents of higher quality than do other PWM techniques [Jamal A. 2002]. In this paper, the feasibility of applying the variable-voltage variable-frequency control strategy to a HEPWM inverter-fed single-phase motor is studied.

torque-speed characteristic of a single phase motor will first be analyzed for the frequency range of interest, followed by a simulation of the drive in steady-state condition.

SIMULATION RESULTS

The operation of a single phase induction motor under the proposed variable-speed control strategy has been extensively tested in simulation using a four pole, 1275 rpm, 220V, 175W, capacitor-run single phase induction motor, and the applied voltage rose by 10% for the frequencies (5, 10 and 15) to improve the starting torque. The parameters of this motor are listed in the Table A.1 in the Appendix A.

Simulation of this motor was developed using the MATLAB program on a PC, using the model topology shown in Fig. 3, but with all reactance's replaced with equivalent inductance values, to allow the effects of the variable supply frequency to be investigated.

The performance of capacitor-run single phase induction motor used in adjustable speed drives is investigated by applying the optimal SHEPWM technique [Dariusz 2002] for two different values of switching angles ($sw=3$ and 7 or eliminating of the first two and six harmonics respectively). Fig. 5 shows the comparison of the motor performance at these two cases. It can be seen from the curves that the rated, starting and maximum motor currents with $sw=7$ are less than that with $sw=3$ for the most frequency range. It can be seen that decreasing of frequency causes decreasing of these currents, since the voltage decreases with frequency at the same time. It should be noted that for 5Hz; the starting and maximum torque to rated torque (T_s/Tr and $T_m/Tr=9.5$) with $sw=7$, while they are equal to (8.5 to 9) for $sw=3$. Therefore the torque ratios with $sw=7$ are larger than that with $sw=3$ by (11.2%) at the low frequency. So that the motor will start with higher starting torque with $sw=7$ than that with $sw=3$. From the same figure we can also see that the motor rated and maximum currents, losses, additional losses, input power, pulsating torque, and additional pulsating torque with $sw=7$ is less than that with $sw=3$.

Since the switching angles with $sw=7$ is higher than that with $sw=3$, therefore the switching losses will be higher with $sw=7$. The drive switching losses can be neglected with respect to the motor losses. As a

result the overall efficiency (η) will be higher with $sw=7$ than that with $sw=3$. It can be seen from the Fig. (5) that the performance of the motor fed by SHEPWM inverter with $sw=7$ is better than that with $sw=3$. In other word increasing the switching angles (or harmonics to be eliminated) in the output voltage of the inverter will improve the performance of the motor. As a result the 7-switching angles SHEPWM technique is more suitable to be used with the motor adjustable speed drive.

Table 1 illustrates the performance of the motor with different frequencies with $sw=3$ and 7 to get speed control of motor with smooth start.

Fig. 6 shows the performance curves of the proposed motor fed by 7-switching angles SHEPWM inverter adjustable speed drive. The figure shows that the maximum slip are equal to unity (standstill) at low frequency 5 Hz, and will decrease with increasing frequency, therefore the motor starts at maximum torque. In this case, the starting with frequency more than 5 Hz is suitable for speed control. As a result, the motor torques (starting and maximum) are very low at low frequencies and they increase with increasing frequency. It can be seen from the same figure that the starting and maximum to rated currents (I_s/I_r and $I_m/I_r \approx 1$) at lower frequency (5 Hz) and equal to (1.91 and 1.35 respectively) at (50 Hz). Therefore the starting current with $f=5\text{Hz}$, reduces by approximately (91%) of that with base frequency. Therefore the frequency 5Hz is suitable for smooth starting.

It can also be seen that the current ratios approximately (equal to 1.6) in the range of (5-15) Hz, which is more than the rated (due to voltage increasing) and that might cause heating the motor over the rated due to increases.

Studying the curves in Fig. 6 is very important for improving the performance of the proposed motor. As a result it is feasible to apply the variable-voltage-frequency control strategy to SHEPWM inverter fed single phase capacitor-run induction motor.

The mechanical and electrical characteristics of the proposed motor fed by 7-switching angles SHEPWM adjustable speed drive are shown in Fig.7. It can be seen from the mechanical characteristic, that the speed range for fixed load (T_c) will be limited to 50 Hz curve only, since this curve intersects the straight line T_c at the point Q_{50} , while the fan load line (T_L) will pass through all the operating points ($>5\text{Hz}$). As a result, the speed control of motors with fan load is more effective than with fixed load.

The electrical characteristic in Fig. 7 shows how the motor will be started smoothly at 5 Hz drawn 1.5A, and increases with frequency increase till it reach 2.355 at (50Hz). While the motor will drawn four to five times of its rated if starts directly with 50 Hz (220volt) main supply

At low frequency operation the torque reduced due to increasing the effect of the capacitor reactance which lead to torque reduction, increasing the applied voltage for low frequencies will cause starting torque increasing as well as the losses.

CONCLUSIONS

At speed lower than the rated speed the motor current increases considerably for constant voltage. The resulting heat dissipation, in addition to insufficient motor torque development, sets a lower limit to the operating speed.

The current study has shown that the variable-voltage variable-frequency method can be effectively applied to control the speed of a single phase induction motor through a SHEPWM inverter. Note that not only the motor performance is improved, but also the speed range is much wider.

Increasing the voltage for low frequencies is a good solution to improve the starting torque but might cause extra heating.

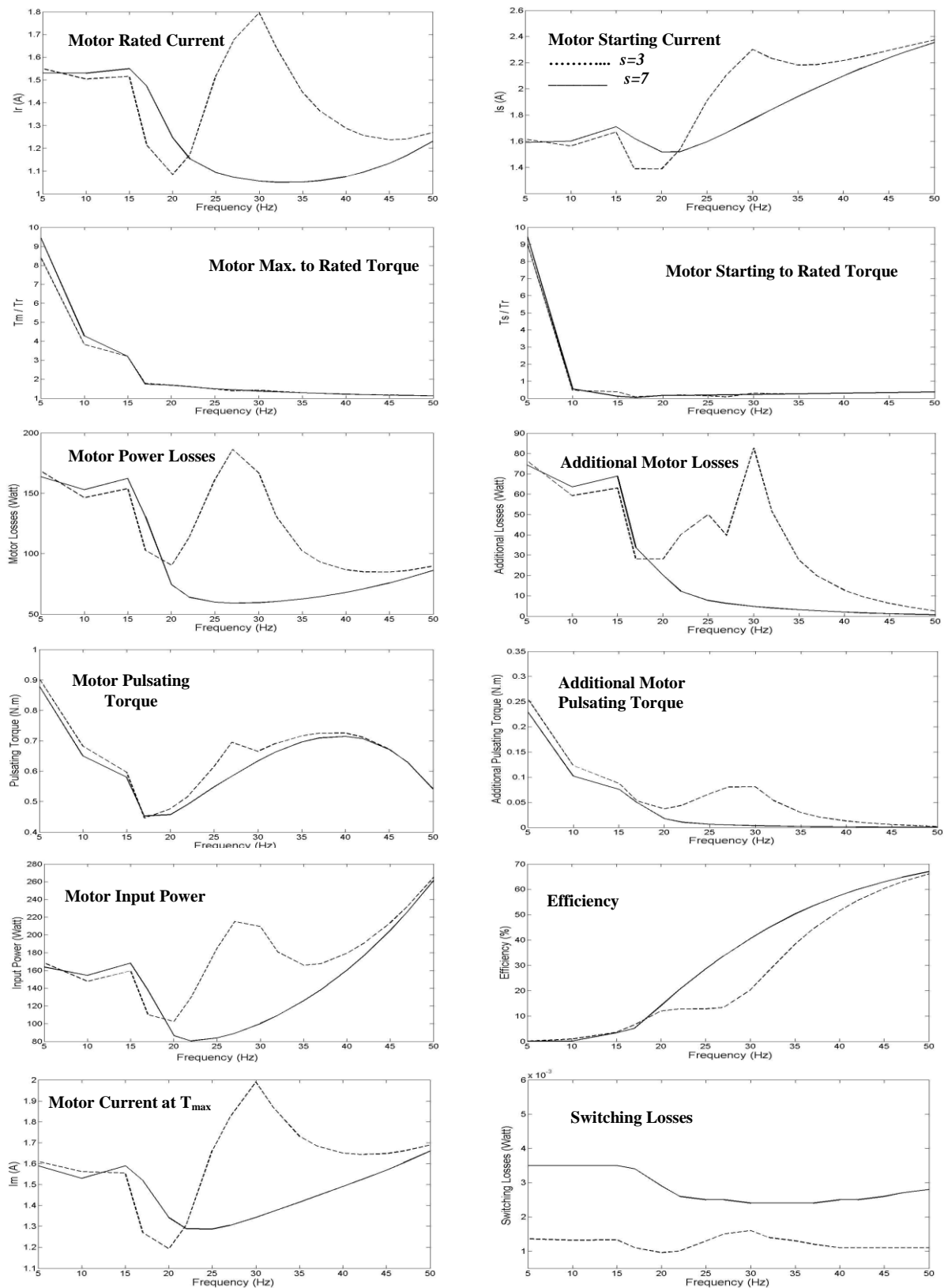
Smooth starting of the motor prevents the excessive current from occurring at starting time, which causes heat generation and may destroy the motor insulation and decrease the motor lifetime. As a result smooth starting improves the motor performance.

Single phase motor can only be effectively applied for adjustable-speed drives with fan-type loads for constant (v/f) but it can be effective for general purpose when starting torque improved.

Increasing the switching in the output voltage of the inverter will improve the performance of the motor but increasing the switching losses

REFERENCES

- A. Jalal. B. , 1980 **“Two-Phase Inverter Supplied Two-Phase Induction Motor”**, M.Sc. Thesis, Baghdad University.
- Dariusz Czarkowski, David V. Chudnovsky, Gregory V. Chudnovsky, and Ivan W. Selesnick, ,April 2002 **“Solving the Optimal PWM Problem for Single-Phase Inverters,”** IEEE Trans. on Circuits and Sys., Vol.49, No.4, pp.465-475.
- D. G. Holmes, and A. Kotsopoulos, , October 1993 **“Variable speed control of single and two phase induction motors using a three phase voltage source inverter,”** in IEEE/IAS Annual Meeting Conference Record, pp. 613-620.
- E.R. Collins Jr., H.B. Puttgen, W.E. Sayle, , 1988 **“Single Phase Induction Motor Adjustable Speed Drive: Direct Phase Angle Control of the Auxiliary Winding Supply,”** 11, IEEE IAS-88, Pittsburgh, pp246-252.
- K.S. Krikor and Jamal A. Mohammed, 2002 **“PWM Strategies for Inverter-Fed Induction Motors - A Comparative Study,”** University of Technology, Vo. 21, No. 11.
- M. Özdemir, S. ünter and B. Yurtseven, 1999 **“Modeling and Simulation of a Split Phase Induction Motor Fed by Single-Phase AC-AC Converter,”** Inter. Journal for Eng. Modeling, Vol. 12, No. 1-4, pp. 17-23.
- P.C. Sen, 1997 **“Principles of Electric Machines and Power Electronics”**, 2nd Edition, John Wiley and Sons, Inc.
- S. J. Chapman, 1999 **“Electric Machinery Fundamental”**, 3rd Edition, McGraw-Hill, New York.
- Twin City Fan Companies, 2000 **“Speed Control for Fractional Horse Power Motors”**, Engineering Data, Ltd. ED-1000.
- U. Reggiani, C. Tassoni and G. Figalli, 1983 **“Analysis of an Inverter-Fed Single-Phase Induction Motor Drive,”** IFAC Control in Power Electronic and Electric Drives, Lausanne, Switzerland.
- Y. Baghzouz, and O. T. Tan, 1988 **“PWM Inverter-fed Single-phase Induction Motor Drives,”** Journal of Energy System, Vol. 8, No. 3.



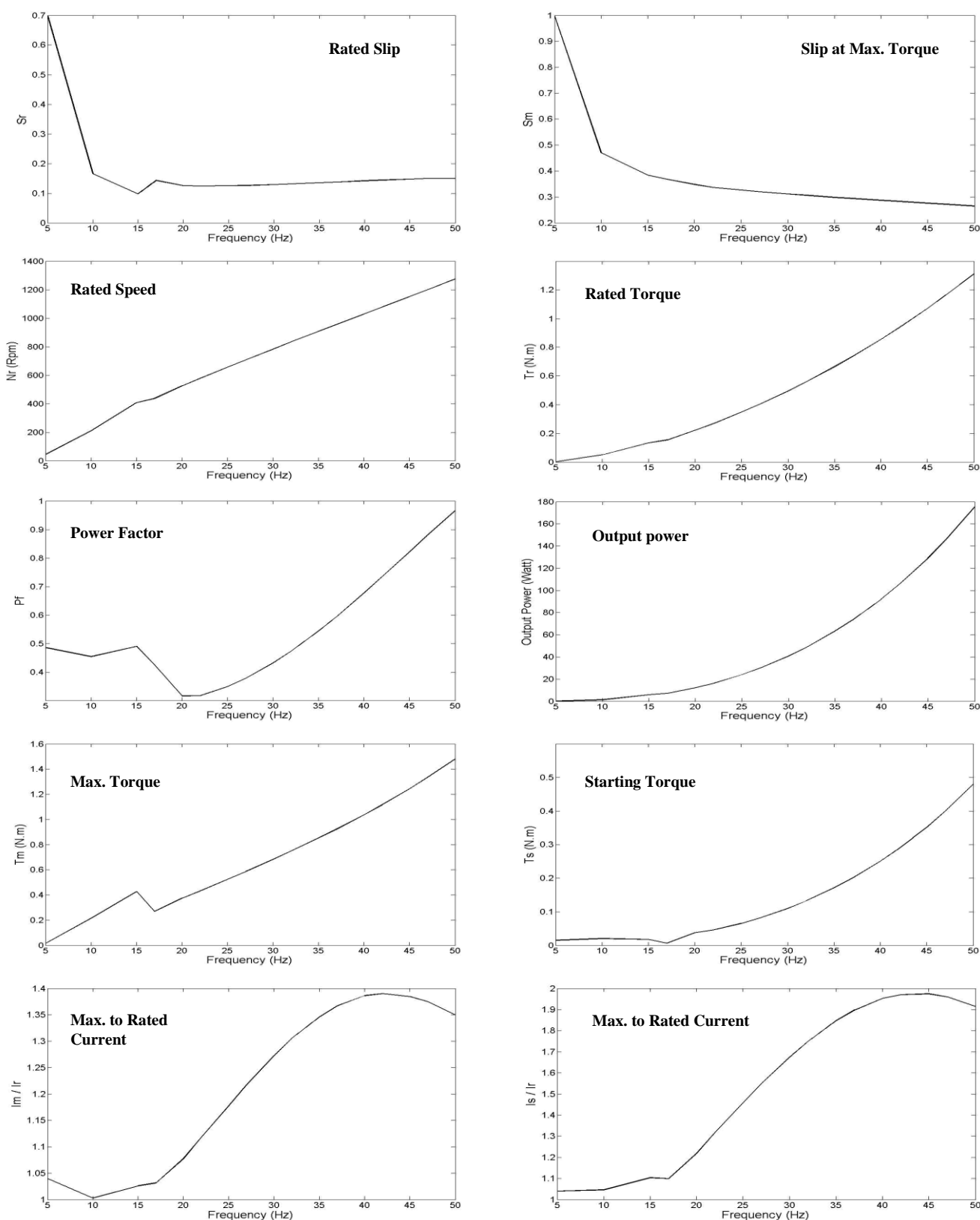


Fig. 6: the performance of the proposed motor fed by 7-Switching Angles SHEPWM Inverter Adjustable Speed Drive

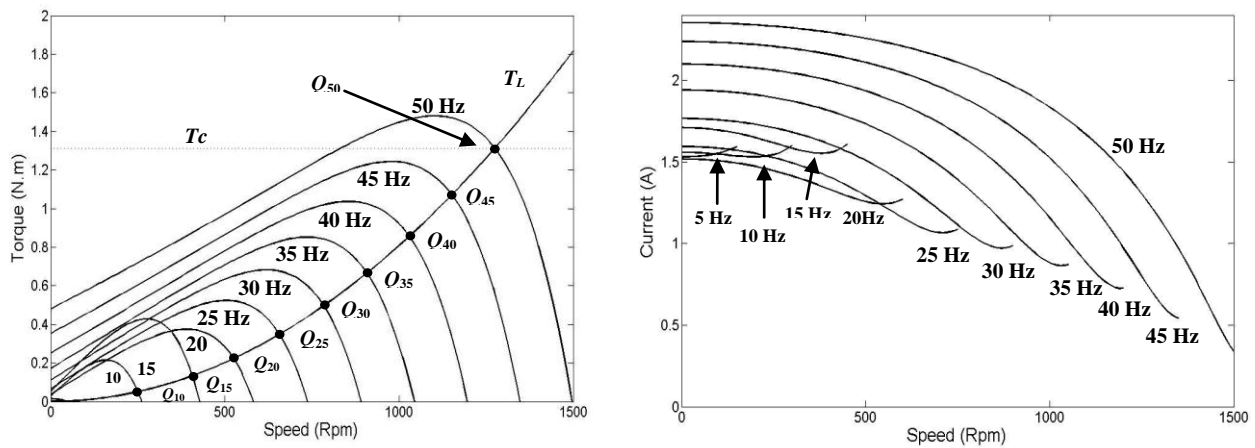


Fig. 7: Mechanical and Electrical Characteristics of the Proposed Motor Fed by 7-Sw. Angles SHEPWM Adjustable Speed Drive

Table 1: Motor Speed Control by Using Variable-Voltage, Variable-frequency Method Using SHPWM Technique

<i>s</i>		3							7					
<i>f</i> (Hz)	<i>V₁</i> (V)	<i>N_r</i> (Rpm)	<i>I_r</i> (A)	<i>I_s</i> (A)	<i>T_r</i> (N.m)	<i>T_s</i> (N.m)	<i>η</i> (%)		<i>N_r</i> (Rpm)	<i>I_r</i> (A)	<i>I_s</i> (A)	<i>T_r</i> (N.m)	<i>T_s</i> (N.m)	<i>η</i> (%)
5	24.2	45	1.55	1.56	1.66e-3	.015	4.6e-3		44	1.5	1.59	1.5e-3	.0147	2.5e-3
10	48.4	250	1.54	1.6	.056	.0215	.9		208	1.53	1.6	.05	.027	.8
15	72.6	406	1.51	1.67	.1334	.049	3.6		406	1.5	1.7	.1335	.0174	3.4
20	88	525	1.0837	1.3872	.2234	.0347	11.96		525	1.246	1.5178	.222	.0372	14.1
25	110	654	1.5185	1.9115	.3461	.0468	12.79		656	1.0932	1.5946	.3491	.065	28.62
30	132	796	1.7963	2.3013	.5095	.1506	20.29		784	1.0554	1.7666	.4953	.1098	40.59
35	154	910	1.4454	2.1826	.6681	.1771	38.39		908	1.0514	1.9407	.6642	.1709	50.25
40	176	1030	1.287	2.2156	.8574	.2519	51.57		1030	1.0751	2.0994	.8548	.2505	57.61
45	198	1152	1.2371	2.2933	1.0694	.3523	60.35		1151	1.1332	2.2374	1.0709	.352	63
50	220	1275	1.2692	2.3747	1.3122	.48	66.13		1275	1.2299	2.3539	1.312	.4799	67.04

Appendix (A)

Table A. 1: Parameters and Specifications of the Proposed Motor

Turn ratio	<i>a_s</i>	1.066	
Number of pole pair	<i>P</i>	2	
Main winding resistance	<i>R_{1m}</i>	33.5	Ω
Main winding leakage reactance	<i>X_{1m}</i>	27	Ω
Auxiliary winding resistance	<i>R_{1a}</i>	34.5	Ω
Auxiliary winding leakage reactance	<i>X_{1a}</i>	28	Ω
Rotor resistance	<i>R₂</i>	20	Ω
Rotor leakage reactance	<i>X₂</i>	12.5	Ω
Magnetization reactance	<i>X_m</i>	173	Ω
Rated supply voltage	<i>V₁</i>	220	V
Rated current	<i>I</i>	1.215	A
Total Power losses	<i>ΣP</i>	85	W
Output power	<i>P₂</i>	175	W
Efficiency	<i>η</i>	67.38	%
Power factor	<i>P_f</i>	0.9726	
Rated speed	<i>N_r</i>	1275	Rpm
Capacitance	<i>C</i>	6	μF

MODELING THE DISTRIBUTION OF (BOD) AND (TDS) IN PART OF TIGRIS RIVER WITHIN BAGHDAD

Ibtihaj A. Abdul Razzak , Abbas H. Sulaymon and Abdul Jabbar R. Al-Zoubaidy

الخلاصة:

تم تطبيق نموذج الخلايا المتعددة لغرض معرفة انتشار الملوثات والمتمثلة في (الأكسجين الحيوي الممتص (BOD_5)) ، المواد الذائبة الكلية (TDS) على نوعية مياه نهر دجلة في المنطقة الواقعة بين جسر الأئمة وجسر الجمهورية والممتدة على طول (9 كم) ضمن مدينة بغداد ، والتي تحتوي على اربعة محطات للصرف الصحي تصرف مباشرة الى النهر . قسمت منطقة الدراسة الى احدى عشر خلية ذات احجام مختلفة ، وتم تشغيل البرنامج بعد تزويده بالبيانات الحقلية التي تم الحصول عليها من نتائج تحليل النماذج التي جمعت من اثني عشر موقعا من النهر ومن اربعة محطات للصرف الصحي الموجودة ضمن منطقة الدراسة تم جمعها كل اسبوعين للفترة من 2005/11/15 الى 2006/4/30 ، أنجز التحقق من النموذج وذلك بتطبيقه لاستنباط التراكيز للمتغيرات التي تم فحصها بصورة دورية ضمن منطقة البحث . تم تطبيق برنامج جاهز يعتمد على طريقة الفروقات لغرض تقدير تراكيز المتغيرات ونمذجة نوعية المياه ، وتم ملاحظة ان تراكيز الملوثات في النهر يزداد خاصة في المناطق التي يتم فيها الصرف مباشرة الى النهر حيث ان تراكيز BOD_5 بلغت (140ppm) على بعد 1.4km من بداية منطقة الدراسة و 170ppm على بعد 5km و 160ppm على بعد 6.5km و 155ppm على بعد 7.5km ثم تتخفض في المناطق البعيدة عن نقاط الصرف حيث انها تصل الى الحدود المسموحة بعد 300m من اخر نقطة صرف اي بعد 7.8km من بداية منطقة الدراسة ، بينما قيم TDS كانت ضمن الحدود المسموحة على طول منطقة الدراسة ما عدا عند البعد 5km فانها تصل الى 1100ppm ، ومن الضروري السيطرة على تصاريص محطات الصرف الصحي لجعل تراكيز الملوثات في مياه نهر دجلة ضمن الحدود المسموح بها حيث لوحظ عند تشغيل هذه المحطات بطاقتها القصوى (12 ساعة يوميا) فأن تراكيز الملوثات يزداد خصوصا عندما يكون تصريف نهر دجلة قليل (250 م³/ثا). بتطبيق برنامج (Surfer) فانه تم توضيح انتشار الملوثات في النهر بالنسبة لنتائج النموذج (التي تم الحصول عليها من البرنامج السابق) وكذلك بالنسبة للنتائج الحقلية (التي تم الحصول عليها من الفحوصات المختبرية) وأجريت المقارنة بينهما .

ABSTRACT:

A multi-cells in serial model was developed to simulate the distribution of pollutants (which are BOD_5 and TDS) in Tigris river between Al-A'imma bridge and Al-Jumhuriya bridge, a reach which is about (9 km) length within Baghdad city; this includes four sewage pumping stations untreated discharged to the river.

This region was divided into eleven cells of different volumes. The model was operated using the field data, which were obtained from the results of laboratory test of samples which were collected from twelve stations in the river and four sewage pumping stations located within the study region twice a month from 15/11/2005 to 30/4/2006. Verification of the simulation model was accomplished by its application to predict the substances concentrations observed.

A package program of differential equation were applied to obtain the concentrations of parameters and modeling the water quality, it was concluded that the concentrations of pollutants were increased at the discharge points in the river, the concentration of BOD_5 reached 140ppm at 1.4km from the beginning of the study region, 170ppm at 5km, 160ppm at 6.5km and 155ppm at 7.5km, then BOD_5 became within the acceptable values in the other regions and finally it reaches the acceptable value after the last discharge point (7.8km) from the beginning of the study region, TDS was within the acceptable range except at 5km it reaches 1100ppm. sewage pumping stations shouldn't set at high discharge rate (12 hr/day) to decrease the pollutants concentrations in Tigris river in order to keep these concentrations within the acceptable values specially at low flow of the river (250 m³/sec).

By using Surfer program to show the distribution of model results (obtained from the previous program) and the field results (which were obtained from the laboratory tests) and to compute the comparison between them.

INTRODUCTION:

Fresh waters are facing an increasing load of the disposal of polluted waters due to rapid growth of industrial and municipal activities as well as the increase of land drainage due to agricultural activities. Outfalls effluents with high pollutant concentrations are discharged to fresh water without treatment causing near field and far field pollution conditions in rivers (Petrus,1990).

The quantitative and qualitative study of water resources, their development and management become one of the major concerns of the society. The escalating demands on limited water resources, needs for maintaining suitable water quality for human, agricultural, and industrial uses and complex interactions of numerous elements of the man-water environment have necessitated the use of more sophisticated forecasting techniques. Such forecasting is essential in the planning, designing, and management of water resources system. [Hikmat , 2005]

Water quality studies have focused on cases where sever pollution problems are arises, especially in heavily populated urban areas. Baghdad city is over populated and produced a huge amount of wastewater from different sources which are disposed into Tigris River directly or after treatment. In the last few years, an increase of wastewater directly disposed in the river using pump stations of storm sewer network have caused high pollution levels in the river water.(Dahr,2004).

Most potential negative environmental impacts from the application of recycled water to the environment come from recycled water's origin as wastewater. These impacts include other water resources, potential contamination of surface and groundwater sources. Public health hazards, and other environmental impacts that may directly or indirectly affect the public. Fortunately, very few significant negative impacts have ever occurred. It is important that all public water systems serve water of the best possible quality to their customers(William,2001).

Water quality characteristics fall into the following four broad categories:

- 1- Physical.
- 2- Chemical.
- 3- Biological.
- 4- Radiological.

The concentration of pollutant in the river is affected by water discharges, velocities and the dispersion coefficient values which is continuously changes with time.

The estimation of the velocities which is the major factor affecting the pollutant movement, is often based on physical models or actual measurements. Both are time-consuming and relatively expensive.

Tigris river facing the effect of conservative pollution due to the discharge of wastewater in it.

The present research is to study the effect of pollution sources between Al-A'imma bridge and Al-Jumhuriya bridge on Tigris river water quality, the pollution sources include four sewage pumping stations: Fig.(1).

- 1- (RQ) sewage pumping station. (S1)
- 2- (T1) sewage pumping station. (S2)
- 3- (M112) sewage pumping station. (S3)
- 4- (M108) sewage pumping station. (S4)

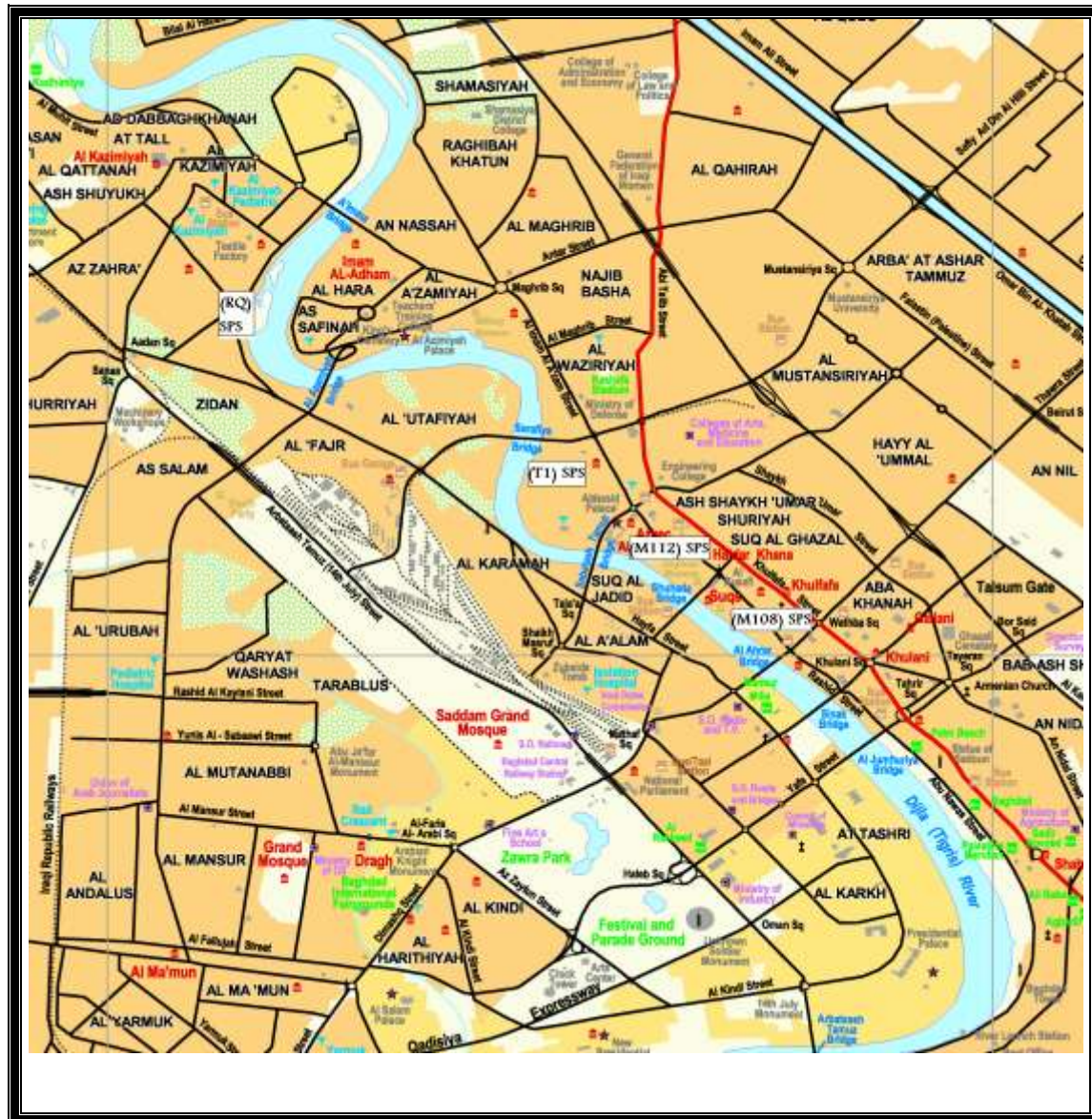


Figure (1) Tigris river between Al A'imma bridge and Al-Jumhuriya bridge. [Tourist map of Baghdad 2004]

EXPERIMENTAL WORK

The experimental work, in this study, can be divided into two parts; field work and laboratory work. In the following sections a brief description of the procedures and equipment were used.

FIELD WORK

Spot samples were collected in order to study the effect of discharge of wastewater from the sewage stations to Tigris river between Al-A'imma bridge and Al-Jumhuriya bridge on Tigris river water quality.

Twelve stations were chosen in the study region, which includes four discharge points as shown in Fig. (2), and four samples from the sewage pumping stations which were discharge directly to the river within the study region.

The samples were collected from the same stations twice a month from 15/11/2005 to 30/4/2006. Table (1) shows the location and distances of these stations.

RIVER-CROSS SECTIONS

An updating of the cross-sections measured in May 2000 for the Tigris river in Baghdad city which were conducted by the Ministry of Water Resources was utilized. Twelve cross-sections were surveyed along different selected stations on the river reach involved in the present study.

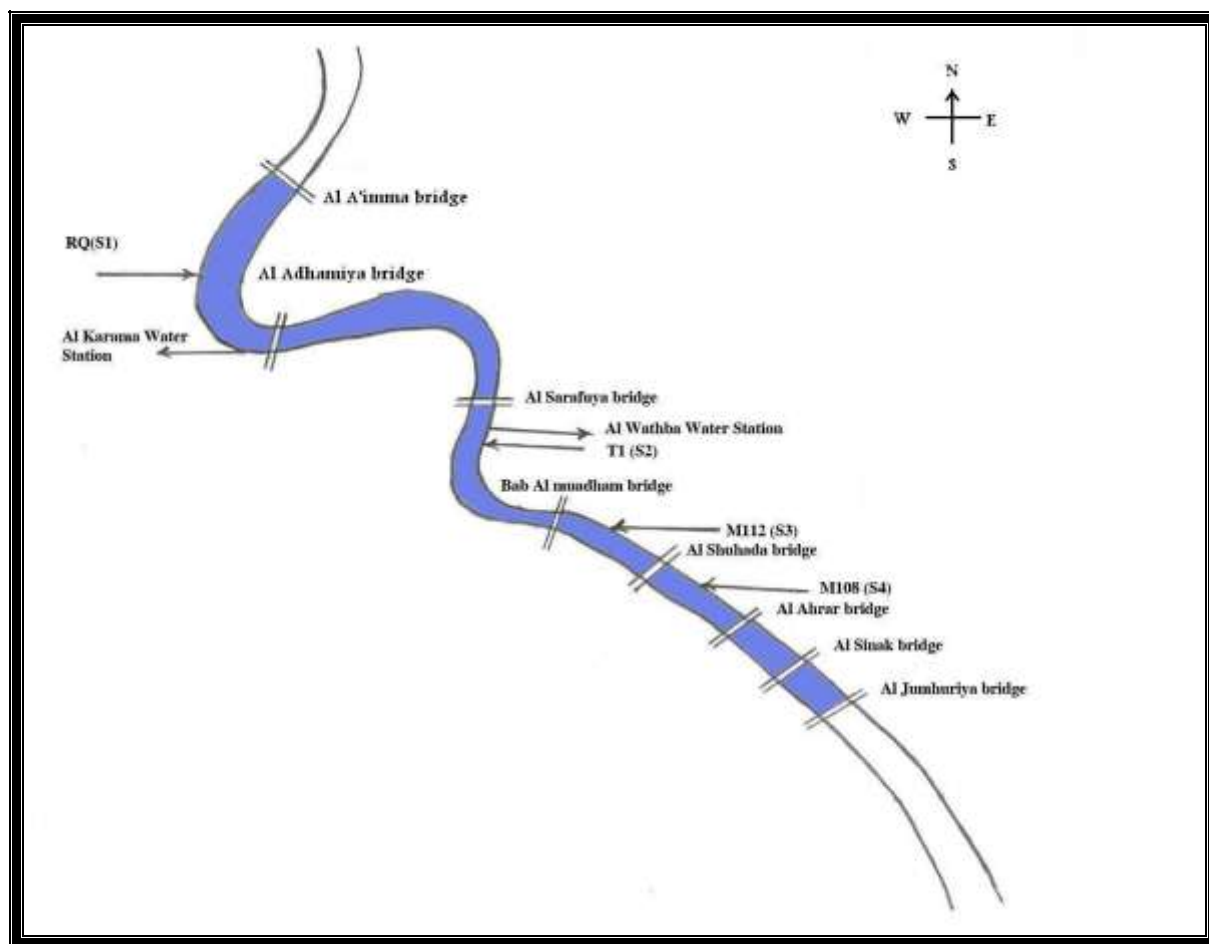


Figure (2) General layouts of the study region

**Table (1) The locations and distances of the sampling stations on Tigris river.**

St. No.	Distance(Km)	Locations	Coordinates	
1	0.0	At Al-A'imma bridge	33°22'29".82N	44°21'19".22E
2	1.2	At (RQ) pumping station	33°21'55".54N	44°20'54".82E
3	2.0	At Al-Adhamiya bridge	33°21'33".71N	44°21'14".30E
4	4.0	At Al-Sarafiya bridge	33°21'27".50N	44°22'21".12E
5	5.0	At (T1) pumping station	33°21'02".14N	44°22'17".30E
6	6.0	At Bab Almuadham bridge	33°20'33".20N	44°22'44".99E
7	6.5	At (M112) pumping station	33°20'26".12N	44°23'03".80E
8	7.0	At Al-Shuhada bridge	33°20'17".03N	44°23'16".52E
9	7.5	At (M108) pumping station	33°20'09".70N	44°23'26".01E
10	7.9	At Al-Ahrar bridge	33°19'55".80N	44°23'43".17E
11	8.5	At Al-Sinak bridge	33°19'42".22N	44°24'00".99E
12	9.0	At Al-Jumhuriya bridge	33°19'28".46N	44°24'15".05E

The relationship between water level and flow of Tigris river was plotted as Rating Curve Fig.(3).

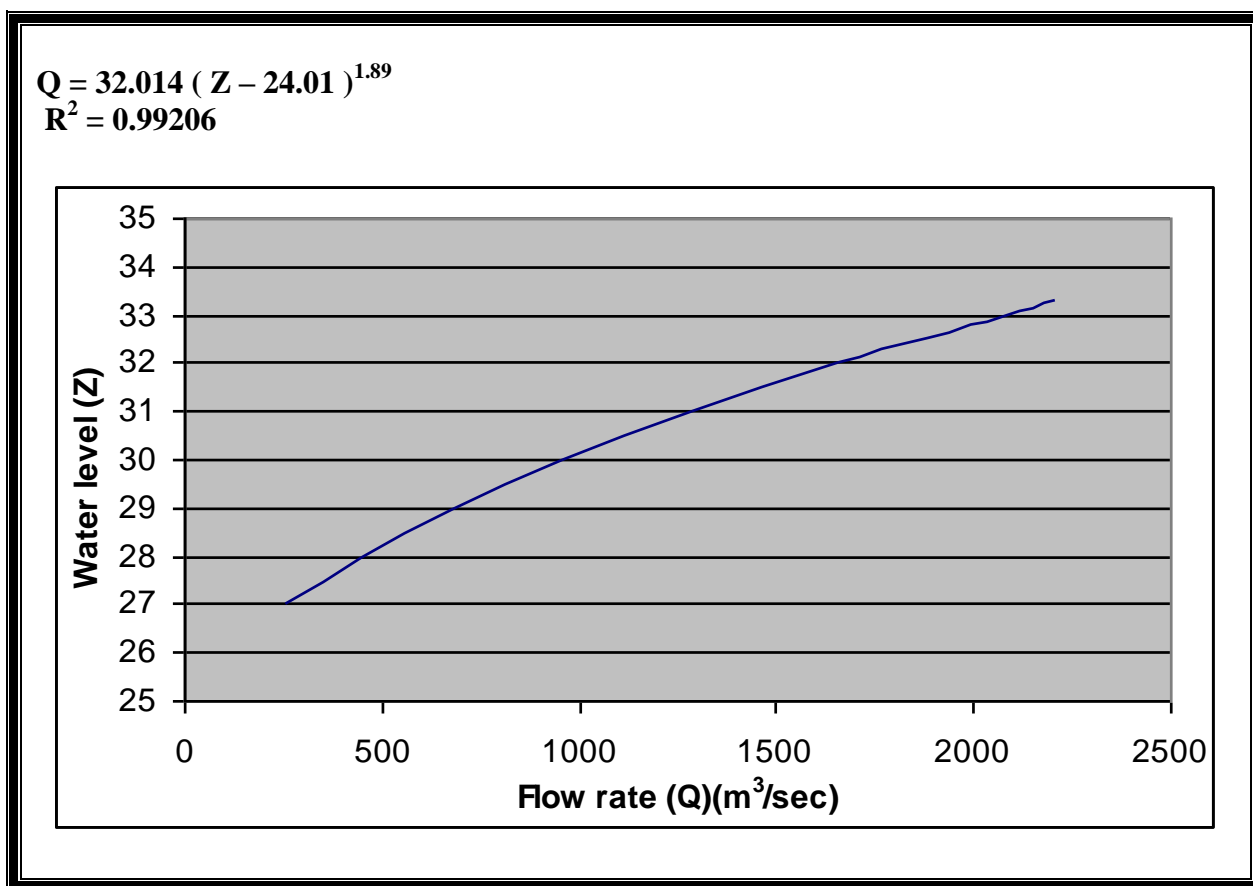


Fig.(3) Rating Curve at Sarai Baghdad Gauging Station.

The water level of Tigris river for the days when the samples collected were measured at Sarai Baghdad Gauging Station then the values of flow of the river were founded from the rating curve Fig. (3) and the results were tabulated in table (2).

Table (2) Water Level and Flow of Tigris river at Sarai Baghdad Gauging Station.

Date	W.L.(m) Sarai Baghdad	Flow (Q _{in}) (m3/sec)
15/11/2005	29.72	875
30/11/2005	29.08	698
15/12/2005	28.96	667
30/12/2005	28.90	652
15/01/2006	28.88	647
30/01/2006	28.94	660
15/02/2006	28.79	625
28/02/2006	28.72	607
15/03/2006	29.36	770
30/03/2006	29.20	730
15/04/2006	28.92	655
30/04/2006	28.88	645



LABORATORY WORK

River stream and outfalls sewage pumping stations samples were collected using bottles of one-liter capacity from the middle of the river at the depth of (0.5m), and the samples which collected twice a month were tested.

Two constituents were involved in the present work, Biological Oxygen Demand (BOD₅), Total Dissolved Solid (TDS).

BOD₅ TEST BY ELECTROMETER METHOD

The instrument used In this method is BOD meter. The electrode placed in (250 ml) diluted sample in order to measure the initial dissolved oxygen (D₁), and after 5 days the final dissolved oxygen was measured (D₂) (YOUNG,1981)

then BOD₅ was calculated by:

$$BOD_5, (ppm) = \frac{D_1 - D_2}{P}$$

Where:

D₁= DO of diluted sample immediately after preparation, mg/l

D₂= DO of diluted sample after 5 days incubation at 20°C, mg/l

P = decimal volumetric fraction of sample used (dilution factor).

TDS TEST BY FILTRATION FOLLOWED BY OVEN DRYING

200 ml (V) of sample was filtered by filter paper to separate the suspended solid, then the beaker was weighted (A) and filled by the filtered sample ,the sample was dried in the oven at105°C for 5 hours ,the beaker with the dissolved solid was weighted again (B) (Clesceri,1998).

Then TDS was calculated by :

$$TDS(ppm) = \frac{B - A}{V}$$

Figures (4) and (5) show the contaminants distribution of the average values of the field results.

The allowable limit of (BOD₅) according to the Iraqi standards is (40 ppm) and for (TDS) is (1000 ppm)

According to the Iraqi standards No.417 (2001), the allowable limit of (BOD_5) is (40 ppm) and for (TDS) is (1000 ppm).

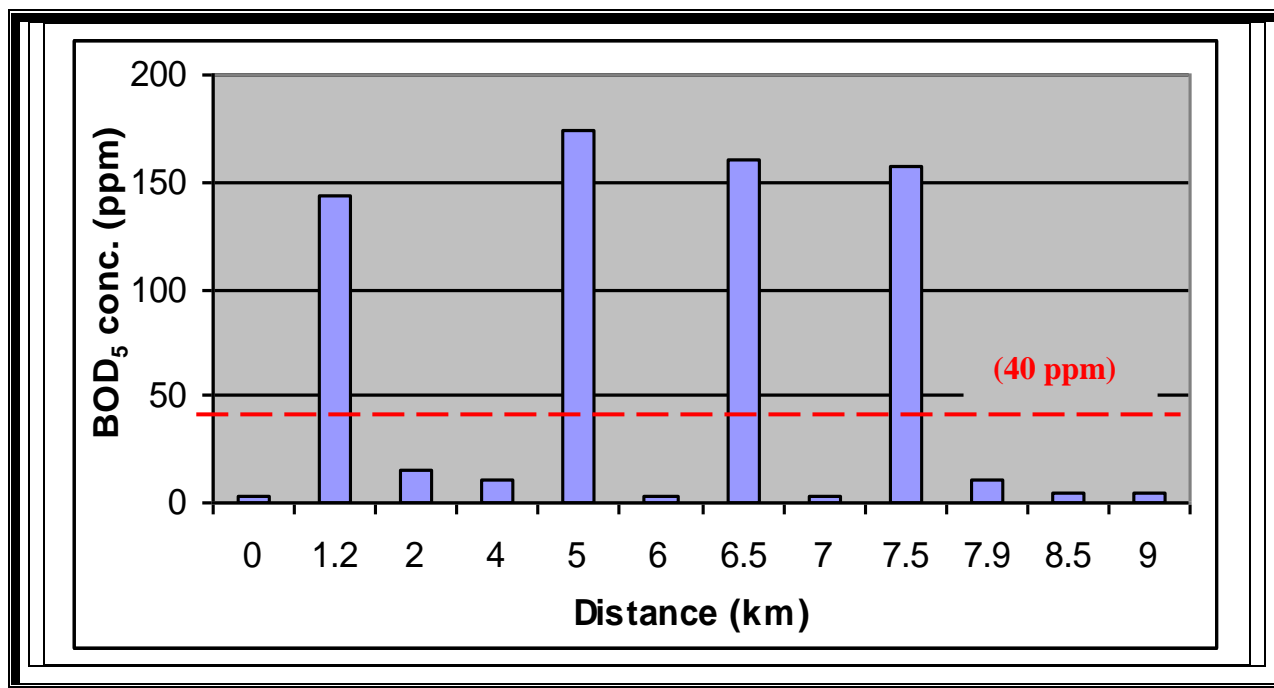


Figure (4) BOD_5 variation along the study region.

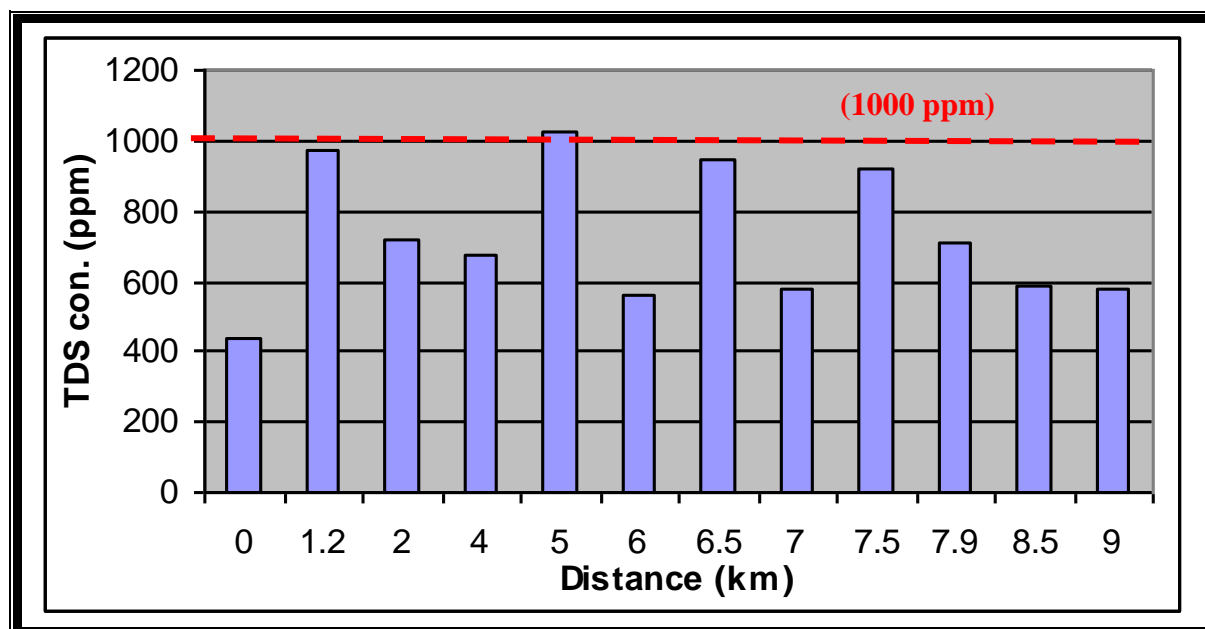


Figure (5) TDS variation along the study region.

MODEL, RESULTS, AND DISCUSION:

The model operation will be tested and compared, separately as quality part, with field results.

Input Data

In order to prepare the input data needed to operate the model and runs the computer program the following steps were followed:-

- The study region was limited from AL-A'imma bridge to AL- Jumhuriya bridge on Tigris river which is about (9) kilometers length within Baghdad city.
- The study region was divided into eleven cells as shown in Fig.(6).

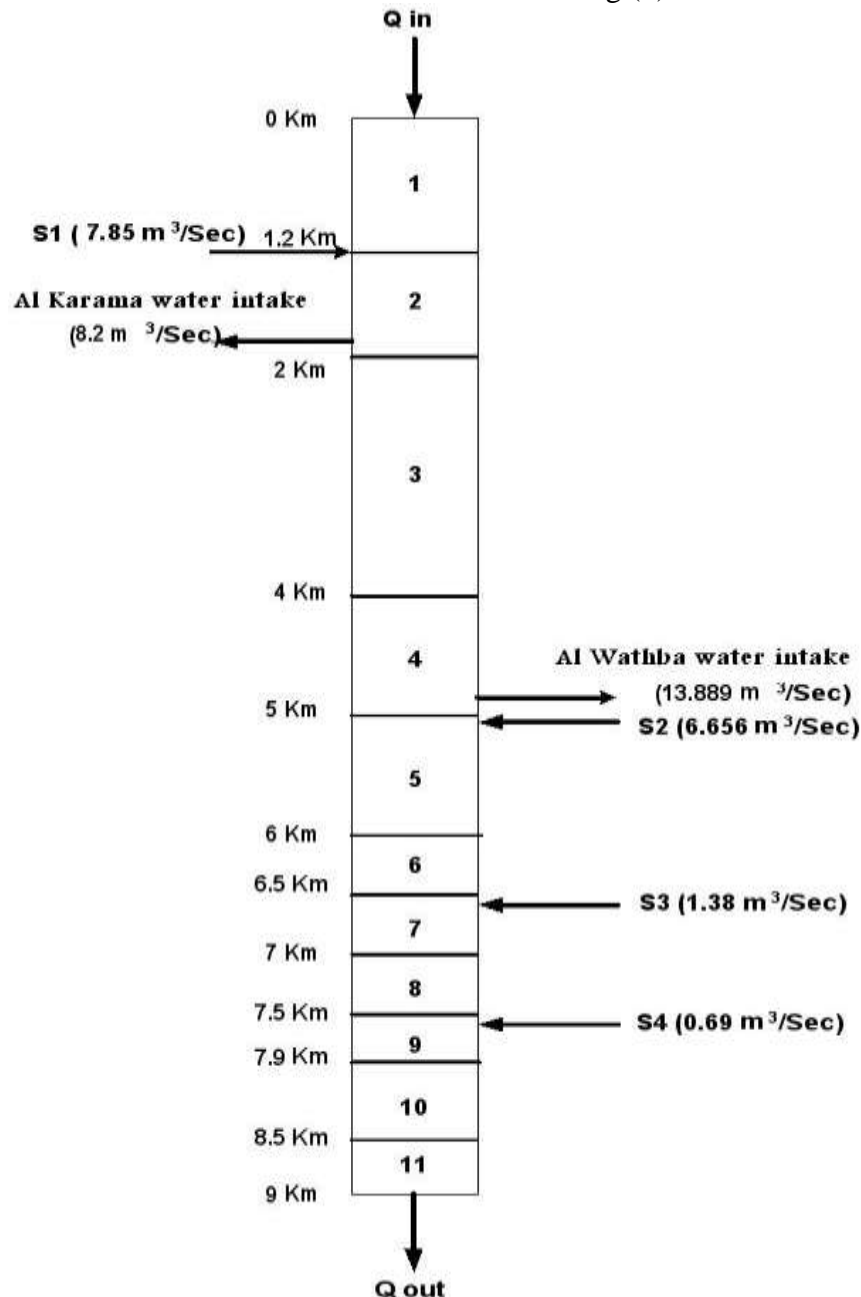


Figure (6) Sketch of the study region (AL-A'imma bridge to AL-Jumhuriya bridge)

- The cross sectional area of each cell (A_1) was calculated with the help of the cross sectional areas of the river (water resources ministry, 2000) .

To calculate the slope of the river within the study region the following steps followed:-

- The water level at Sarai Baghdad gauging station (6800 m from Al'Aimma bridge) (WL_1) was 28.88 m .
- The water level at Al-Jumhuriya bridge (9000 m from Al'Aimma bridge) (WL_2) was 28.73 m .

$$Y = WL_1 - WL_2 \\ = 28.88 - 28.73 = 0.15 \text{ m}$$

$$D = 9000 - 6800 = 2200 \text{ m}$$

$$\text{Slope} = Y/D \\ = 0.15/2200 = 6.82 \times 10^{-5} = 6.82 \text{ cm/km}$$

While:

Y = The different of water levels between two stations.

D = The distance between the two stations.

- The surface area of each cell (A_2) was calculated by multiplying the length by the width.

$$A_2 = L * W$$

While:

L = the length of the cell

W = the width of the cell

- The distance between each two neighboring cells (from center to center) (C_3) was setted.
- The volume of cells were calculated (V) .

$$V = A_1 * L$$

- The concentration of the pollutant in the river (C) and from the sewage pumping stations (C_2) were taken from the laboratory tests.

- The flow rate of water into the cell was measured (Q_{in}) (Table (2))

- The flow rate of the sewage pumping stations discharge (Q_2) are listed In table (3) :-

**Table(3)The flow rate of the sewage pumping stations
(Baghdad sewage authority, 2006).**

SPS	Q_2 (m^3/sec)
S1	7.85
S2	6.656
S3	1.38
S4	0.69

- The withdraw flow of water pumping stations were shown in table (4) :-

**Table (4) Withdraw flow of water intake stations
(Baghdad water authority, 2006).**

Water stations	Q_w (m^3/sec)
Al Karama	8.2
Al Wathba	13.889



-The monthly rainfall and evaporation rate are tabulated in table (5) which used in the equation:-

$$Q_{out} = Q_{in} + Q_2 - Q_w + Q_P - Q_E$$

Table (5) The monthly rainfall and evaporation rate (Iraq Climate, 2006)

Months	Rain fall (P) (mm)	Evaporation (E') (mm)
11	9.9	113
12	13.4	89
1	11.9	45
2	10.8	67
3	20.5	112
4	24.7	154

- The dimensions of the cells are tabulated in table (6):-

Table (6) Some dimensions of the cells in the study region

Cell number	W(m)	L(m)	C ₃ (m)	A ₁ (m ²)	A ₂ (m ²)	V (m ³)
1	230	1200	1000	1084.7	276000	1301640
2	240	800	1400	580.3	192000	464240
3	130	2000	1500	924.2	260000	1848400
4	230	1000	1000	793.6	230000	793600
5	175	1000	750	532.9	175000	532900
6	150	500	500	527.9	75000	263950
7	150	500	500	879.0	75000	439500
8	175	500	450	903.2	87500	451600
9	200	400	500	1479.4	80000	591760
10	230	600	550	157.9	138000	945540
11	260	500	/	1467.2	130000	733600

- To compute the longitudinal dispersion-coefficient there are several empirical and analytical equations have been recommended by various investigators. Elder (1959), derived a formula for the dispersion coefficient for an infinitely wide two-dimensional flow down a plane as follows:-

$$D_L = 5.93 H U \quad (1)$$

Where:

D_L is the longitudinal dispersion coefficient (m²/sec.).

H is the depth of flow (m).

U is the velocity of flow (m/sec.) ($U = Q / A_1$).

SIMULATION MODEL

The computer program is an essential research tool used for performing computation of simulation model, it was mainly consists of two parts, the first part was used to perform the out flow rate of each cell by applying a water flow balance for each cell

$$Q_{out} = Q_{in} + Q_2 - Q_w + Q_p - Q_E \quad (2)$$

The second part of the computer program was used to perform the computations of water quality model by applying multi-cells in serial by substitute the results of eq. (2) in the following equation: (Shanahan and Harleman, 1984).

An increase in the dispersion coefficient would make the peak concentration reach the outlet at a shorter time, and reduce the variation of the cells concentrations.

$$V \frac{dC}{dt} = \sum \left[Q_2 C_2 - Q_{out} C + \frac{D_L A_1}{C_3} (C_2 - C) \right] \quad (3)$$

In order to keep the stability of the model , the calculation of pollutants of every record was done by divided the step into multi steps and calculate the concentration in each step , then the results were used as an initial concentration to the following step , and the computer program was calculated the concentration in the second cell in the same way by using the final step concentration from the first cell as an input concentration to the second cell and so on for all cells and records the results .

This method depends on many assumptions, the main ones of which are:

- 1- The water enters the cell or leaves it as a pulse at the start of the simulation time step.
- 2- The resultant of inflow and outflow of cell across its boundary is uniformly distributed, so it would be at the same level in the cell at the start of the simulation time step.
- 3- The cells volumes were remain constant.
- 4- The concentration of pollutants in dropped rain and evaporated water are equal to zero.

RESULTS AND DISCUSSION

1- The concentrations of the contaminants increase at the discharge points in the river and decrease in the other regions, due to the mixing with the river's water.

2- From the results of laboratory tests, the concentrations of the samples at stations 2, 5, 7, and 9 were very high compared with the other stations, because they were collected from the stations at the river at the discharge of the sewage pumping stations (S1, S2, S3, and S4).

3- The BOD₅ and TDS concentrations at station (5) were higher than the other stations (2, 7, and 9) because of the higher concentrations of the discharge sewage from (S2) than those from (S1, S3, and S4).

4- The BOD₅ concentration levels increase at the river at the discharge points, Fig. (4) and (5), so they increase at distance 1.2 km by 350% of the acceptable limit , at distance 5 km by 420% of the acceptable limit, at distance 6.5km by 400% of the acceptable limit, and at distance 7.5 km by 380% of the acceptable limit, then they decrease at the other regions, and at (7.8 km) they reach the allowable values.

5- The TDS concentrations increase at the discharge points , these values were between (400 ppm - 1100 ppm) so they were within the acceptable values (1000 ppm) except at station (5) it was reached (1100) ppm due to high TDS concentration in the discharge sewage from (S2) at (5 km).

6- Al-Karama water intake locate at (1.8 km) on the study region and Al-Wathba water intake locate at (4.8 km) on the study region,, at these stations BOD₅, TDS are acceptable according to the allowable Iraqi standard .

7-The results which obtained from that computer program were plotted as a model results, and the field results which obtained from the laboratory test were plotted as a field results in order to compare between the two results

8- There are perfect results and a good agreement between measured and predicted results especially in November and March, due to the operation of the pumping stations with the designed discharge rate (Q_2) during sampling period, while in some days the stations set at low discharge rate, so the field results were less than the model results on these days especially in February and April.

Surfer program was applied to explain the contour map and vector map for model results, field results, and the comparison between them as a residual Fig. (7 & 8) .

A contour map is a two-dimensional representation of three-dimensional data; the first two dimensions are the XY coordinates which refer to the cell number and the collecting time, while the third dimension Z is represented by lines of equal value which refer to the concentration.

A vector map shows the direction and magnitude of data at points on a map; they are automatically generated from a single grid by computing the gradient of the concentration. At any given grid node on the map, the arrow points in the direction of the steepest ascent, the magnitude of the arrow changes depending on the steepness of the ascent.

CONCLUSIONS

1- Results of laboratory tests the concentrations of the samples at stations (2, 5, 7, and 9) were very high (about six times for BOD₅ and double for TDS) compared with the other stations, because they were collected from the stations in the river at the discharge of the sewage pumping stations (S1, S2, S3, and S4).

2-There are good agreement between measured and predicted results, which confirms the validity of the selection of the pertinent specified.

3-Field measurements on laboratory tests present that:

* BOD₅ concentration level are exceed the allowable Iraqi standards (40 ppm) in the river at the discharge points then they return to the acceptable values in the other points, and they reach the allowable Iraqi standard at (7.8 km) due to the mixing in the river.

* TDS are within the allowable standard (1000 ppm) except in the position (5) at (5 km) it reached (1100 ppm) because of high TDS concentrations in (S2).

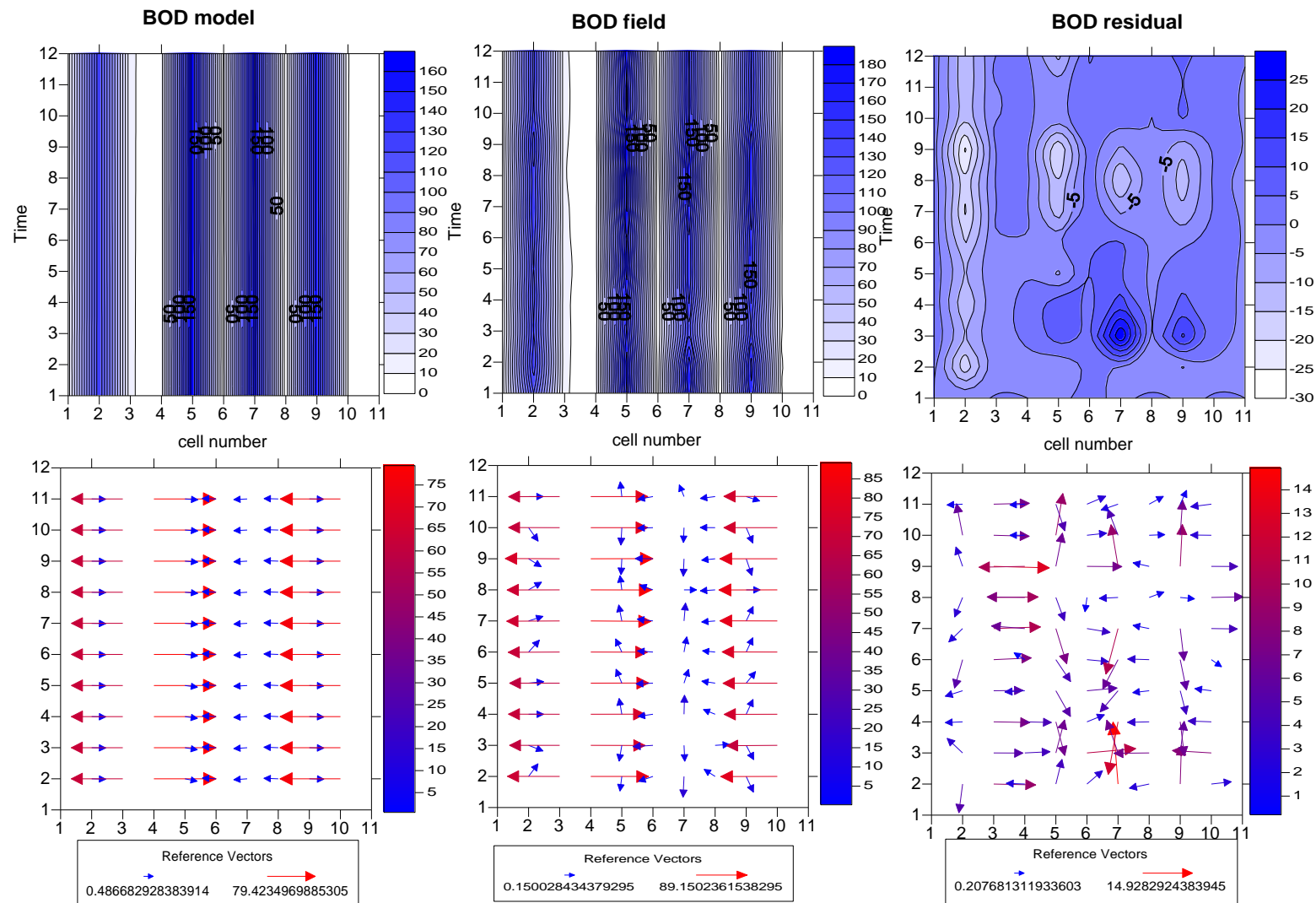
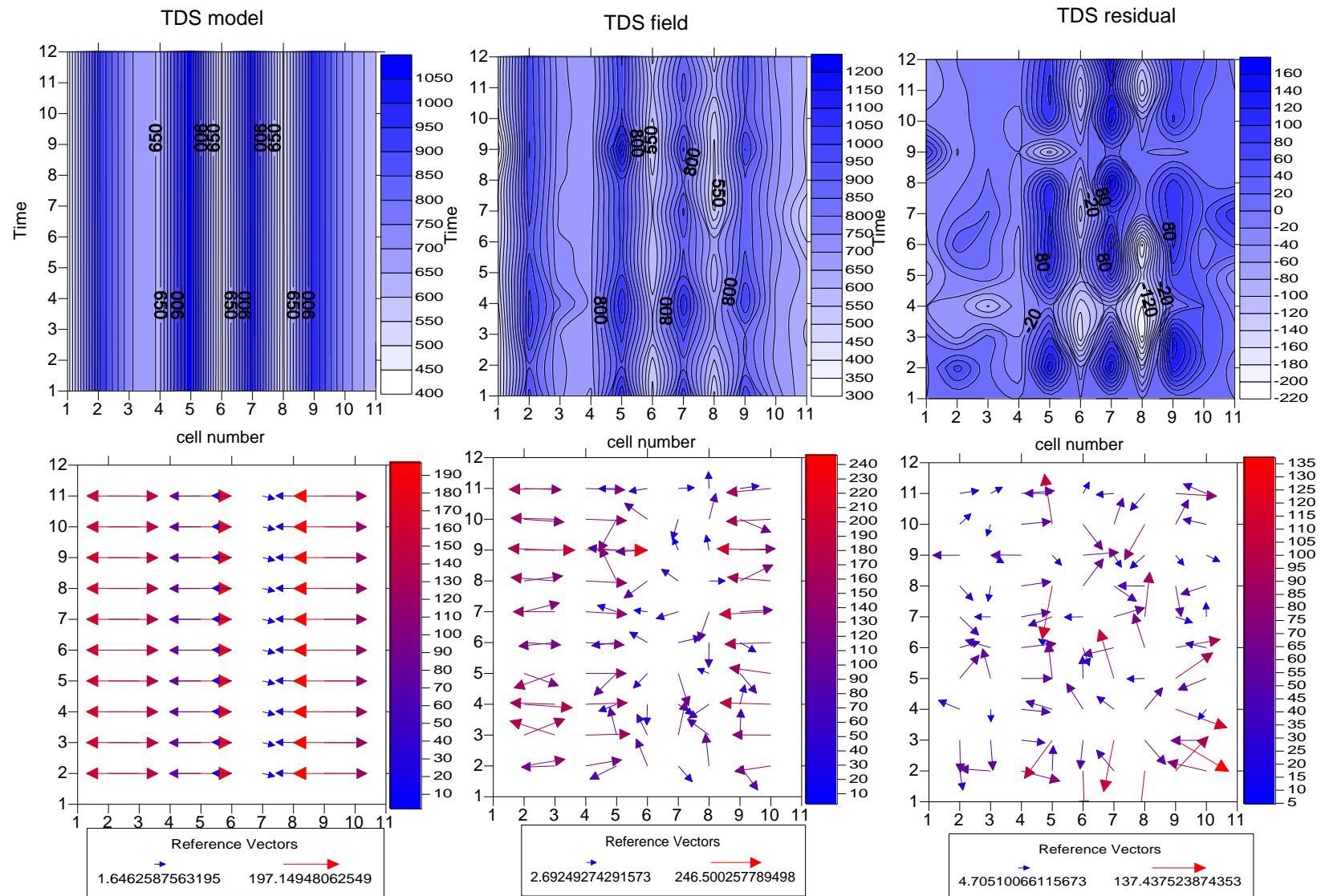


Fig.(7) BOD distribution

**Fig.(8) TDS distribution**

REFERENCES

- **Abed, B. SH.**, (1998), "*Development of Dynamic Water Quality Model for Tigris River within Baghdad City*", Ph.D. Thesis, College of Engineering, University of Baghdad.
- **Clesceri, L.S.**, (1998), "*Flow Injection Analysis for The Orthophosphate*", Standard Methods for The Examination of Water and Wastewater, 20th Edition.
- **Dahr, J.**, (2004), "*Pollution Chokes The Tigris; A Main Source of Baghdad's Drinking Water*".
<http://www.newstandardnews.net/content/action=showitem&itemid>
- **Elder, J.W.**, (1959), "*The Dispersion of Marked Fluid in Turbulent Shear Flow*", Journal of Fluid Mechanics, vol.5.
- **Hikmat, M.A.**, (2005), "*Two Dimensional numerical model for The Distribution OF Pollutants in Tigris River Downstream of Tharthar- Tigri Channel*", M.Sc. Thesis, College of Engineering, University of Baghdad.
- **Shanahan, P. & Harleman, D.R.F.**, (1984), "*Transport in Lake water quality modeling*", Journal of Environmental Engineering division, ASCE, Vol.110, No.EE1, Paper 18551, Feb. 1984, pp.42-57.
- **William, O. Maddous**, (2001), "*Water Resources Planning*", First Edition, p.98.
- **Young, J.C., G.N., Mcdermott & D.Jenkins**, (1981), "*Alterations in BOD Procedure for The 15th Edition of Standard Methods for The Examination of Water and Wastewater*", Journal of Water Pollution Control, vol.15.
- **Young, J.C.**, (1973), "*Chemical Methods for Nitrification Control*", Journal of Water Pollution Control, vol.3.

**List of Abbreviations**

<i>Abbreviate</i>	<i>Description</i>
BOD	Biological Oxygen Demand
Conc.	Concentration
DO	Dissolved Oxygen
E	East
Eq.	Equation
Fig.	Figure
N	North
ppm	Part Per Million
P.S.	Pumping Station
SPS	Sewage Pumping Station
St.no.	Station number
S1	(RQ) sewage pumping station
S2	(T1) sewage pumping station
S3	(M112) sewage pumping station
S4	(M108) sewage pumping station
T.D.S	Total Dissolved Solids
WL	Water Level

Symbol	Description	Units
A_1	The cross sectional area of the cell.	m^2
A_2	The surface area of the cell.	m^2
C	Constituent concentration	mg/l
C_2	The concentration of completely mixing water at the final time step	mg/l
C_3	Distance from center of the cell to the center of the neighbor cell	m
E'	Rate of evaporation from the cell surface	mm
P	Rate of rain fall on the cell surface	mm
Q_2	Flow rate of the pumping sewage station	m^3/sec

List of Symbols



Q_E	The flow of evaporation	m^3/sec
Q_{in}	The in flow of water into the cell .	m^3/sec
Q_{out}	The out flow of water from the cell .	m^3/sec
Q_p	The flow of rain	m^3/sec
Q_w	Withdraw flow of water pumping station	m^3/sec
t	Time	sec.
V	The volume of the cell.	m^3

SITE ASSESSMENT GUIDANCE A CASE STUDY (OUIREEJ SCRAP YARD)

Jathwa A. Ibraheem

الخلاصة:

اصبحت عمليات التقطيع والتفكيك (صناعة السكراب (Scrap industry) من العمليات الرائجة في الصناعة العراقية مؤخرا فهناك مجاميع متخصصة من الافراد تخصصت في مثل هذا النوع من الصناعة ولاسيما صناعة تقطيع وتفكيك او تفصيح الاحزمة الصناعية والاليات المدنية والعسكرية لاعادة استخدامها اما كماهي او كمواد اولية تدخل في صناعات اخرى من خلال عمليات بيع رائجة وصلت اعمالها عبر الحدود العراقية.

ومما يزيد من مخاطر تلوث البيئة هو خلط الاليات العسكرية المحترقة والمهشمة وما تحمله من ذخائر واسلحة مع السيارات المدنية المحطمة والمحترقة وبقياتها من عمليات التفخيخ واجهزة ومعدات لمنشات التصنيع العسكري وما تحويه من مواد كيميائية تاهت اسمائها ومناشئها واختلطت انواعها في خضم المجموع الهائل من المخلفات الملقاة في الساحات المفتوحة. وفي ضوء الصعوبات الراهنة واقتتاد الامن ولاسيما في مناطق اطراف بغداد اصبح التركيز مقصورا على توفير المتطلبات القصيرة والمتوسطة المدى فقط كالسيطرة على استخدام المواقع نفسها، أو تحديد استخدام الارض، أو منح اجازة مرخصة لاشخاص محددين للتصرف بالمخلفات من تقطيع او بيع او غيرها من الفعاليات المشابهة. ان عملية بيع المخلفات والاليات بالجملة بانواعها المختلفة بعد تجميعها في ساحات خاصة وعلى الرغم من فائدتها في تنظيف البيئة سيما وان تم اعادة استخدامها تبقى عمليا محدودة ولا يمكن تحقيقها محليا لا على المدى القريب ولا المتوسط لصعوبة السيطرة على المواقع كما ان عملية تنظيف كافة ساحات تجميع المخلفات (السكراب) مثل ساحة تجميع السكراب في منطقة عويريج قد تكون غير ممكنة ايضا في الوقت الحاضر .

تم اجراء تقييم بيئي لاحد مواقع تجميع المخلفات والاليات المدنية والعسكرية وضمن محافظة بغداد وظهرت نتائج فحص عينات الماء والترربة المأخوذة من الموقع ، ان الموقع ملوث بدرجة متوسطة بPCBs و الزيوت المعدنية وبشكل اساسي النحاس و الرصاص والانتيمون والزنك وان عملية خلط المخلفات والاليات العسكرية مع المدنية ادت الى ارتفاع معدلات التلوث والخطورة .

اظهرت نتائج الفحوصات ان مستويات التلوث في الموقع واطنة نسبيا، غير ان التلوث بPCBs كان واسع الانتشار فقد تم اكتشافه في ثمان مواقع من اصل اثنتي عشر موقع وبلغ اعلى تركيز له $23 \mu\text{g/kg}$ وكذلك اظهرت التحاليل تلوث المياه السطحية في الموقع تلوث طفيف بالمعادن الثقيلة والزيوت المعدنية.

ABSTRACT

Scrap metal export is currently one of the few thriving industries in Iraq. Looters and legitimate operators are together effectively demolishing many of the old industrial facilities in order to retrieve the metal contained in buildings, processes and storage equipments and vehicles.

The mixing of civilian and military scrapping operations such as that occurring at Ouireej is exacerbating the problem. The situation is particularly difficult for Iraq, given the rapid growth of the scrap industry and the lack of security.

In view of the current difficulties, the focus was on practical short to medium term improvements such as controlling access to sites, land use zoning, licensing and export controls. The wholesale reform of the scrap metal industry to improve environmental practices, whilst desirable, is also probably not feasible in the short to medium term. The remediation of working scrap sites, such as Ouireej is also probably unfeasible at present. Laboratory analysis of shallow

soil detected contamination by PCBs, mineral oil and heavy metals, principally copper, lead, antimony and Zinc.

The detected levels of all contaminants were relatively low. But PCB contamination was relatively widespread, being detected in eight soil samples with a maximum concentration of 23 µg/kg. Laboratory analysis of rainwater ponds on the site indicated marginal contamination by heavy metals and mineral oils

KEYWORD

Scrap, Military scrap, Ouireej, Site assessment, Contamination, Weapons of Mass Destruction (WMD), Risk. PCB

INTRODUCTION

Iraq has significant legacy of contaminated and derelict industrial and military sites. Many facilities are unlikely to re-start operation but apportion of the sites in urban areas may be developed for other uses.

These sites have major problems with hazardous wastes but generally lesser problems with contaminated soil and water. In a minority of cases, the sites represent a severe risk to human health, specifically to site workers and trespassers (UNEP, 2005).

The background of conflict in Iraq since 1980 has also contributed to the environmental problems. As Iraq is a relatively industrialized country, with tens of thousands of industrial sites, it is considered too large and costly to address in a uniform manner, i.e. by assessing and cleaning up every site.

International experience (UNEP, 2005) indicates that whilst a large percentage of industrial sites may have ground contamination or problems with hazardous waste management, only a very small fraction represent such an immediate and grave threat to human health or to the environment that urgent action is warranted. To be most effective, efforts in Iraq should be focused on first identifying and addressing the most urgent cases.

Iraq is unique in that its industrial sites have been under some form of international monitoring and assessment since 1991, for military reasons. The 15-year search for weapons of mass destruction (WMD) covered potential chemical, biological and nuclear weapons research and manufacturing programs across Iraq.

The hundreds of contaminated sites through Iraq require characterization and assessment before remediation systems are designed and implemented. In some cases, no clean up maybe the best alternative to protect public health and the environment. Nonetheless, the complexity of contaminated sites requires a multiphase assessment process in which the sites are identified, screened, and characterized.

SCRAP METAL INDUSTRIES

Although scrap yards are recognized worldwide as important source of water pollution, land contamination and hazardous waste (Watts, 1997), yet military scrap and scrap yards in Iraq present a number of additional hazards (ISEPI, 1994) including:

- Explosion and fire risks from munitions
- Unusual concentration of toxic chemicals (e.g. each T72 tank contains up to 150 liters of pure polychlorinated biphenyls PCB)
- Asbestos (again from tanks and military vehicles)
- Depleted uranium (DU) fragments in destroyed tanks and vehicles

Separation of military and civilian scrap operation could reduce the scale of the problem. The great majority of scrap metal generated is linked to civilian vehicles and derelict industries.



Within the military scrap category, a large amount (such as trucks, building materials) does not represent any additional hazard over civilian scrap. These materials could be left to the civilian scrap industry.

SITE ASSESSMENT GUIDANCE

Assessment strategy

The assessment strategy for the scrap yard industry needs to address the issues of location and prioritization (ISO/IEC 17025, 1999).

- **Location.** The number and position of all scrap yards in Iraq dealing with military equipment is unknown. There is no central register and many operations are small and temporary in nature.
- **Prioritization.** The list of physical and chemical hazards associated with scrap yards is long. It can be assumed that environmental conditions within the scrap yards are very poor and likely to remain so until an organized system of environmental regulation is implemented. Before this occurs, any comprehensive assessment and cleanup work is likely to be wasted effort as ongoing scrap yard operations will simply continue to contaminate the areas in which they work.

The recommended activities for scrap yards site assessments are as follows:

Site mapping project: The objective of site-mapping project is to broadly understand the contamination situation within and immediately surrounding the site. Detailed assessment of the surface waters, soil, and groundwater over all of the sites is excluded on the grounds of scale. Enquiries and escorted site visits should be able to establish the overall location and pattern of contamination sources on the site. In particular, the number and types of military vehicles should be estimated and counted. The density of vehicles/scrap should be estimated, by counting the number within defined areas say 50m by 50m. The results of the survey should be developed as a series of maps with accompanying notes on the activities and materials involved. Some very limited general sampling of soil and water is recommended to obtain a general idea of the composition and peak concentrations of the contamination.

Military vehicle area survey: The objective of the survey is to obtain detailed data on the actual environmental conditions immediately surrounding stored and dismantled military vehicles. The survey should focus on the ground surface within 25m of the target vehicle. Scrapped military vehicles, particularly tanks, should not be entered due to the multiple risks from depleted uranium (DU), unexploded ordnance (UXO), asbestos, and chemicals.

Local watercourse survey: Watercourses on or very close to the major scrap yards should be assessed for contamination migrating offsite. In this case, sediment sampling is as important as water sampling as PCBs will mainly be found in the sediments.

GENERAL GUIDANCE

Investigation techniques: Efforts should be focused on non-intrusive sampling (i.e. avoid extensive digging). Surface soil samples can be taken by hand. Open watercourses can be sampled by hand. For intermittent watercourses such as storm water drains, sediment sampling may be useful (Watts, 1997).

Sample analysis techniques: The wide range of chemicals potentially present means that sample analysis should also be wide ranging. The following laboratory analyses and analyses suites are recommended (ASTEM, 2004):

- pH and alkalinity
- Aluminum
- Heavy metals including Vanadium
- Uranium
- Volatile Organic Compounds (VOCs) by GC MS
- Total Petroleum Hydrocarbons by GC and IR (both methods)
- Nitrogen compounds - Total Nitrogen, Oxides of Nitrogen , Ammonium,
- Inorganic ions - Chloride, phosphate, sulfate, calcium, magnesium, salinity, conductivity
- Polar organics - alcohols and glycols and poly chlorinated biphenyls (PCBs).

On site, testing is suitable for pH, surface water parameters, and volatile organics. VOCs such as toluene can be tested onsite using a Photo-ionization Detector.

Hazardous material sampling: The main objective of the hazardous material sampling programme is to obtain an accurate assessment of the type of hazardous waste disposed at the site. In particular, visible oils and oily stains should be sampled to test for PCBs from the scrapping of military vehicles (watts, 1997).

Water monitoring and sampling: The objectives of the water monitoring and sampling is to obtain an indication of the mobility of the contamination in the water phase in any standing water on site or in drains leading from the site (ISO/IEC 17025, 1999)..

Water monitoring and sampling will be located using the list of Assessment Target Areas. For monitoring, use the Troll 9000 for all samples. Avoid putting the Troll 9000 into any pools of chemicals, as this will damage it (UNEP, 2005).

CASE STUDY (SCRAP YARD OF OUIREEJ):

Ouireej is one of the largest military scrap yards in Baghdad. Its location is about 20 km to the west of Baghdad, in the alluvial plain southwest of the River Tigris. The region is under the responsibility of Al-Rasheed municipality (figure 1). It used to be an open land intended to be distributed to create a living zone. After the conflict, the land turned to be an open landfill, or a scrap yard collecting solid waste and hazardous wastes

The site was allocated as one of the main dumping and processing sites for military scrap arising from the conflict of the subsequent destruction of the Iraq arsenal, scrapped in an uncontrolled manner, resulting in localized contamination, potential to affect surface and shallow soils, surface water (drainage ditches flow to Tigris) and shallow groundwater.

The principal source of hazards is the open dumping of highly toxic chemical wastes and the dispersal of such wastes by looting, demolition, or weather.

The site was damaged or in an environmentally poor condition due to either looting, fire, conflict or poor operating practices. At the peak of activity, the site held hundreds of items of potentially hazardous military hardware including tanks missiles, yet it still containing unexploded ordnance and hazardous chemicals.

Two people were reportedly killed, by explosions and by poisoning, in the uncontrolled scrap metal recovery operations that occurred over the period mid 2003- early 2005 (UNEP, 2005). The surrounding land use is a mixture of industrial residential and agricultural. There are some houses on and adjacent to the site. The margins of the site also appear to be used for



dumping of construction debris. The site is very sparsely occupied and there is a great deal of vacant or unused land.

Site assessment strategy: The work was carried out over the period January 2004 to July 2005 in Iraq, with support activities in Jordan, Switzerland, and United Kingdom. The assessment strategy for the site was as the assessment of the whole site in moderate detail, with detailed assessment of the numerous hotspots and any standing water.

Assessment target areas and contaminants: The key assessment targets approach was to divide the site into 9 general zones as follows:

North

1. Northwest	2. North	3. North East
4. West	5. Central	6. East
7. SouthWest	8. South	9. SouthEast

South

In addition to the 9 general zones there were three items which required individual assessment:

10. The new housing onsite
11. The standing water (ponds)
12. External control points.

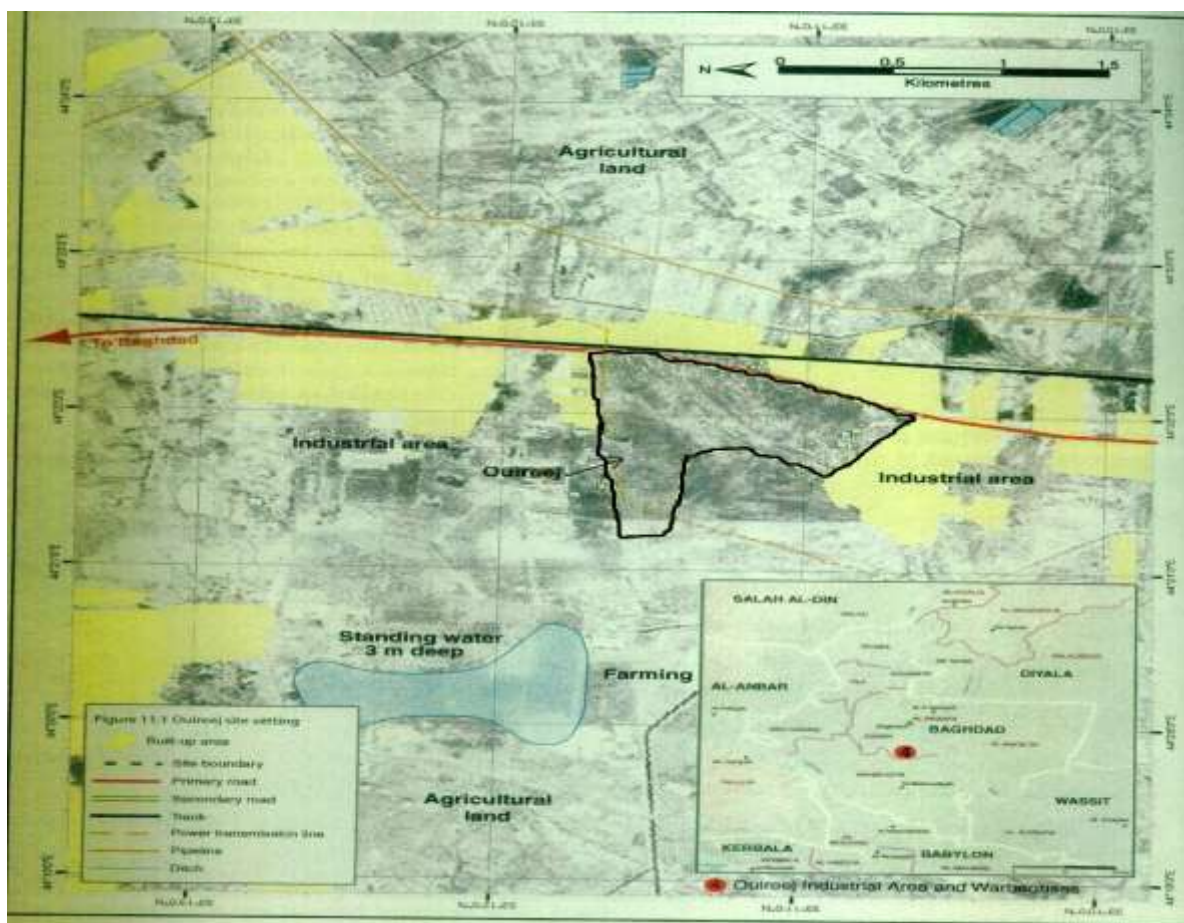


Fig. 1 Ouireej yard location (UNEP, 2005)

Overview of techniques: The following techniques were used on the site;

1. Soil sampling
2. Hazardous material sampling
3. Water sampling

Sampling on site was of soils, hazardous materials, and waters from wells and ponds where applicable. Hand auger equipment and hand tools such as trowels were used to collect soil and hazardous material samples. Drum keys, grounding wires, hand pumps, disposable bailers and a flap gouge auger was used, to take representative samples of the contents of barrels and containers for identification through off-site laboratory chemical analysis. Disposable bailers were used to sample groundwater from wells, and disposable plastic containers were used, where appropriate, to take samples from standing water bodies, sumps, and tanks, logged, and packed for export by air freight to the international laboratories.

Water quality was tested onsite with the Troll 9000. Probes were used to measure pH, temperature, dissolved oxygen, and oxygen-reduction potential. Soil vapor was measured using Photo Ionization Detector (PID) for detection of volatile organic compounds.

Chemical analysis: Samples were exported via airfreight and analyzed at three commercial analytical laboratories in the United Kingdom. Alcontrol laboratory in Chester, united Kingdom, carried out the standard analysis and coordinated the specialist analyses (Tables 1a, 2a, 3a and 4a in appendix A). Alcontrol is accredited to the ISO 17027 standard (ISO/ IEC 17025, 1999).



There is no Iraqi legislation or guidance material regarding acceptable levels of risk from hazardous waste or contaminated land. Existing formal standards from the UK (ASTEM, 2004), USA, Australia and the Netherlands were considered suitable as initial guidelines but are also considered to be generally too stringent and therefore too costly to be implemented in Iraq at present. International standards such as the WHO drinking water standards (WHO 1998) are relevant mainly as end –user standards rather than directly applicable to contaminated land.

For safety reasons samples with potentially high concentrations of cyanide or organic mercury were unsuitable for the standard process of quartering grinding and acid digestion.

Hazardous samples were dispatched to London Scandinavian Metallurgical Company Ltd. for elemental analysis by x-Ray Fluorescence spectroscopy (XRF) and X-Ray Diffraction (XRD). Samples for organic mercury were dispatched to Mountain Heath Service laboratory for specialized treatment and analysis.

Iraq has no screening system so an appropriate substitute was needed. The systems used for this project were the current (National Environmental Protection Australian Council Schedule B1 and B7a, 1999) and Dutch (Netherlands Government Gazette, 2000) standards and accompanying guidance. For the Australian system, the Health Investigation Limits A were used for soil screening and the ground water Investigation Limits (drinking water) were used for waters. These values represent the levels above which contamination is considered significant enough to warrant further investigation and assessment. For the Dutch system, the soil remediation intervention values were used as terms of references

More general terms (A. Richard and P.E. Conway, 1982) are used as follow:

1. Uncontaminated- Any contamination, if detected, is below the selected international standards
2. Slightly contaminated- Contamination is present, but in limited volumes and at concentrations limited to 1-10 times the selected international standards
3. Moderately contaminated- Contamination is present, in limited volumes and at concentrations 1-100 times the selected international standards
4. Heavily contaminated- Contamination is present in large volumes and over large areas and at concentrations, which can exceed 100 times the selected international standards.

Site Assessment activities: Ouireej site was visited for general fact-findings, Table 1 details sampling and monitoring activities of the April and May 2005 site visits.

Table 1 Site assessment activities

Sample type/ activity	Number of samples or points
Soil	148
Waste chemicals	10
Surface water	3
Ground water	6

FINDINGS

Although hazardous wastes are present on the site, they are not present as large discrete stockpiles, but scattered as fragments, barrels, and small piles. The most common type of waste appears to be scattered burnt residues from uncontrolled burning of the non-metallic parts of the scrapped vehicles.

Shallow soil contamination is present at numerous points throughout the site, as evidenced by encrustations of metal oxides, oil stains and discolored ground. Laboratory

analysis of shallow soil detected contamination by PCBs, mineral oil and heavy metals, principally copper, lead, antimony and Zinc.

The detected levels of all contaminants were relatively low. PCB contamination was relatively widespread, being detected in eight soil samples with a maximum concentration of 23 µg/kg. Laboratory analysis of rainwater ponds on the site indicated marginal contamination by heavy metals and mineral oils. In summary, the limited sampling indicates that:

1. The site in its current state represents a moderate risk to human health, primarily to site workers, and to site residents.
2. The principal toxicity risk was from direct contact with, and inhalation of chemicals in the process of transporting, cutting, sorting and burning the scrap.
3. Explosion and fire risks from UXO present on the site were expected but could not be quantified.
4. The mixing of civilian and military scrapping activities increased the scale of the problem
5. The observed house building on a working military scrap yard site with UXO risks is creating new risks and issues.

CONCLUSIONS

The scrap operations on site reached a peak in late 2003 and throughout 2004 and that the amount of scrap on site at time of investigation (June 2005) represents only 25% of the original volume. The scrapping operations apparently closed down due to a combination of dwindling economic return and pressure from the municipalities. The site in its current state represents a **moderate** risk to human health, principally to site workers, but also to site residents, and the mixing of civilian and military scrapping activities is increasing the scale of the problem.

RECOMMENDATIONS

The recommendations, in summary, are :

1. To separate the military and civilian operations and the residential development to mitigate the obvious risks of combining all these land uses. **Separation of the hazardous military scrap from other material by relocation.**
2. **Secure fencing** would be a simple but cost effective method for reducing the risk of exposure for most site workers and all of the nearby residents.
3. Maintenance of this separation would need to be enforced by commercial means, e.g. **only one contractor is allowed to deal with military scrap and is paid to manage the issue.**
4. The current building of new houses in the scrap yard area should be stopped or managed to include **land re-zoning** and **site cleanup** prior to redevelopment.
5. In the longer term, national, strategies, policies, **legislation, and enforcement are needed for hazardous waste management and contaminated land.** There is currently no specialist technical capacity in Iraq to take any quick corrective action on highly hazardous waste. This would need to be developed prior to conducting any such works. A new hazardous waste treatment and disposal facility should be built for mainly inorganic wastes with most organic chemical wastes being incinerated in a nominated cement plant furnace.



REFERENCES

- Richard and P.E. Conway, (1982), "Environmental Risk Analysis for Chemicals", Van Nostrand Reinhold Company.
- American Society for Testing and Materials (ASTM) 2004. Standard guide For Risk-Based Corrective Action [E-2081-00 Reapproved 2004].
- International Standards Organization 1999. ISO/IEC 17025: 1999 Standard: General requirements for the competence of testing and calibration laboratories. 1999.
- Iraqi Society for Environment Protection and Improvement (ISEPI), "The international Scientific Symposium on Post War Environmental Problems in Iraq", Baghdad, December 10-12, 1994
- National Environmental Protection Council (Australia) 1999. Assessment of site contamination. Schedule B (1) Guideline on the investigation Level for Soil and Ground water.
- [http:// www.ephc.gov.au/php/list_documents .php?pdfType=cs](http://www.ephc.gov.au/php/list_documents.php?pdfType=cs)
- National Environmental Protection Council (Australia) 1999. Assessment of site contamination. Schedule B (7a) Guideline on health-Based Investigation Levels, 1999.
- [http:// www.ephc.gov.au/php/list_documents .php?pdfType=cs](http://www.ephc.gov.au/php/list_documents.php?pdfType=cs)
- Netherlands Government Gazette 24th February 2000, No 39 English translation. Circular on target values and intervention values for soil remediation.
- [http:// www2.minvrom.nl/Docs/international/S_I2000.pdf](http://www2.minvrom.nl/Docs/international/S_I2000.pdf)
- Richard Watts, "Hazardous Wastes, Sources, Pathways and receptors" 1997
- UNEP (2005). Assessment of Environmental Hot Spots in Iraq - UNEP Technical Report. Geneva, Switzerland, United Nations Environment Programme:
- UNEP "Assessment of Environmental hot spots in Iraq" 2005.
- WHO Guidelines for Drinking Water Standards. 3rd Edition.
- http://www.who.int/water_sanitation_health/dwq/gdwq3/en/index.html

ACRONYMS

BTEX: Benzene, Toluene, Methylbenzene, and Xylem

DRO: Diesel Range Organics

DU: Depleted Uranium

EPH: Extractable Petroleum Hydrocarbons

GCMS: Gas Chromatography Mass Spectrometer

GRO: Gasoline Range Organics

IR: Infra Red

ISO: International Standards

PCBs: Poly Chlorinated Biphenyls

PID: Photo Ionization Detector

SVOCs: Semi Volatile Organic Compounds

UXO: Unexploded Ordinance

VOCs: Volatile Organic Compound

WMD: Weapon of Mass Destruction

XRD: X-Ray Diffraction

XRF: X-Ray Fluorescence spectroscopy



Appendix 1

Table 1a Summary of Laboratory analyses for soils

Metals (all results in mg/kg)	No. of samples analyzed	No. detected above MDL	All concentration mg/kg	
			Minimum detected concentrations	Maximum detected concentrations
Arsenic	50	50	4	19
Beryllium	50	0	<	<
Cadmium	50	3	3	11
Chromium	50	50	49	138
Copper	50	50	13	1738
Mercury	50	0	<	<
Nickel	50	50	65	209
Lead	50	50	6	1291
Antimony	50	50	3	55
Selenium	50	0	<	<
Silver	50	0	<	<
Thallium	50	0	<	<
Zinc	50	50	41	1381
Hydrocarbons and VOCS (µg/kg unless stated)				
EPH (DRO)(C10-C40)(mg/kg)	49	42	7	118679
GRO (C4-C10)	13	1	<	44
GRO (C10-C12)	13	0	<	<
Benzene	13	0	<	<
Toluene	13	2	4	44
Ethyl benzene	13	1	<	2
M & P xylene	13	1	<	10
O xylene	13	1	<	3
MTBE	13	0	<	<
PCBs (all results in µg/kg)				
Total of 7 congener PCBs	29	8	1	23
SVOCs (all results in µg/kg)				
Anthracene	18	2	121	352
Benzo(a)anthracene	18	1	<	326
Benzo(a)pyrene	18	0	<	<
Benzo(ghi)perlyene	18	0	<	<
Benzo(k)fluranthene	18	0	<	<
Chrysene	18	1	<	1841
Fluranthene	18	2	185	233
Indeno(1/2/3-cd)pyrene	18	0	<	<
Naphthalene	18	2	215	1400
Phenathrene	18	4	271	2096
Pyrene	18	3	145	890
2-methylnaphthalene	18	1	<	2025
Bis(2-ethylhexyl)phthalate	18	6	919	13118

DNn-butyl phthalate	18	2	3192	7209
SVOC TICs (all results in mg/kg)				
C14-c24 Hydrocarbons	5	3	13.2	93.3
C12-C30 Hydrocarbons	5	1	<	60778.4
C14-C30 Hydrocarbons	5	1	<	6341.5
Other parameters (mg/kg unless stated)				
Calcium	14	14	37530	66630
Magnesium	14	14	9330	16300
Potassium	14	14	1579	10619
Sodium	14	14	3614	22317
Bicarbonate alkalinity as CaCO ₃	14	14	89	874
Sulphate SO ₄ (mg/l)	14	14	3126	115500
Acid soluble sulphide	5	0	<	<
Chloride	13	13	2100	43908
Acid soluble carbonate (%)	14	14	18.47	35.23
pH	17	17	7.21	8.38
Total sulphur (%)	5	5	0.12	1.38
Asbestos	17	0	<	<

Table 2a Screening process for soils

Metals (all results in mg/kg)	Dutch criteria for soils	No. of samples exceeding Dutch criteria		
			Australian criteria for soils	No. of samples exceeding Australian criteria
Arsenic	55	0	100	0
Beryllium	30	0	20	0
Cadmium	12	0	20	0
Chromium	380	0	Nc	0
Copper	190	2	1000	1
Mercury	10	0	15	0
Nickel	210	0	600	0
Lead	530	3	300	2
Antimony	15	2	Nc	0
Selenium	100	0	Nc	0
Silver	15	0	Nc	0
Thallium	15	0	Nc	0
Zinc	720	3	7000	0
Hydrocarbons and VOCS (µg/kg unless stated)				
EPH (DRO)(C10-C40)(mg/kg)	5000	5	5600	5
GRO (C4-C10)	nc	0	nc	0
GRO (C10-C12)	nc	0	nc	0
Benzene	1	0	nc	0
Toluene	130	0	nc	0
Ethyl benzene	50	0	nc	0



M & P xylene	25	0	nc	0
O xylene	nc	0	nc	0
MTBE	nc	0	nc	0
PCBs (mg/kg)				
Total of 7 congener PCBs	1	8	10	3
SVOCs (all results in µg/kg)				
PAH sum of 10	40	0	nc	0
Chlorophenols	10	0	nc	0
Chlorobenzenes	30	0	nc	0
Phthalates	60	0	nc	0
SVOC TICs (all results in mg/kg)				
C14-c24 Hydrocarbons	Nc	0	nc	0
C12-C30 Hydrocarbons	Nc	0	nc	0
C14-C30 Hydrocarbons	nc	0	nc	0
Other parameters (mg/kg unless stated)				
Sulphate SO ₄ (mg/l)	nc	0	2000	14
Acid soluble sulphide	nc	0	nc	0
Asbestos	nc	0	nc	0

Table 3a Summary of laboratory analyses for waters

Metals (all results in µg/l)	No. of samples analyzed	No. detected above MDL		
			Minimum detected concentrations	Maximum detected concentrations
Arsenic	3	3	20	83
Beryllium	3	0	<	<
Cadmium	3	1	<	6.3
Chromium	3	3	3	11
Copper	3	3	4	27
Mercury	3	0	<	<
Nickel	3	3	17	62
Lead	3	2	3	38
Antimony	3	2	13	13
Selenium	3	3	38	203
Silver	3	0	<	<
Thallium	3	1	<	2
Zinc	3	3	21	7258
Hydrocarbons and VOCs (µg/l unless stated)				
EPH (DRO)(C10-C40)(mg/kg)	3	2	898	1950
GRO (C4-C10)	2	0	<	<
GRO (C10-C12)	2	0	<	<
Benzene	2	0	<	<
Toluene	2	0	<	<
Ethyl benzene	2	0	<	<
M & P xylene	2	0	<	<
O xylene	2	0	<	<

MTBE	2	0	<	<
SVOCs (all results in µg/l)				
Anthracene	3	0	<	<
Benzo(a)anthracene	3	0	<	<
Benzo(a)pyrene	3	0	<	<
Benzo(ghi)perylene	3	0	<	<
Benzo(k)fluranthene	3	0	<	<
Chrysene	3	0	<	<
Fluranthene	3	0	<	<
Indeno(1/2/3-cd)pyrene	3	0	<	<
Naphthalene	3	0	<	<
Phenathrene	3	0	<	<
Other parameters (mg/l unless stated)				
Calcium	3	3	852	1868
Magnesium	3	3	1051	5869
Potassium	3	3	93	690
Sodium	3	3	12188	18375
Carbonate alkalinity as CaCO ₃	3	0	<	<
Bicarbonate alkalinity as CaCO ₃	3	3	160	370
Sulphate SO ₄ (mg/l)	3	3	4307	15019
Chloride	3	3	6489	>40000
pH	3	3	7.73	8.14

Table 4a Screening Process for waters

Metals (all results in µg/l)	Dutch criteria for ground water	No. of samples exceeding Dutch criteria		
			Australian criteria for ground waters	No. of samples exceeding Australian criteria
Arsenic	60	1	7	3
Beryllium	15	0	nc	0
Cadmium	6	1	2	1
Chromium	30	0	nc	0
Copper	75	0	2000	0
Mercury	0.3	0	1	0
Nickel	75	0	20	1
Lead	75	0	10	1
Antimony	20	0	3	2
Selenium	160	1	10	3
Silver	40	0	100	0
Thallium	7	0	nc	0
Zinc	800	1	3000	1
Hydrocarbons and VOCs (µg/l unless stated)				
EPH (DRO)(C10-C40)(mg/kg)	600	2	nc	0
GRO (C4-C10)	nc	0	nc	0



GRO (C10-C12)	nc	0	nc	0
Benzene	30	0	1	0
Toluene	1000	0	800	0
Ethyl benzene	150	0	300	0
M & P xylene	70	0	600	0
O xylene	nc	0	nc	0
MTBE	nc	0	nc	0
SVOCs (all results in µg/l)				
Anthracene	5	0	nc	0
Benzo(a)anthracene	0.5	0	nc	0
Benzo(a)pyrene	0.05	0	nc	0
Benzo(ghi)perlyene	0.05	0	nc	0
Benzo(k)fluranthene	0.05	0	nc	0
Chrysene	0.2	0	nc	0
Fluoranthene	1	0	nc	0
Indeno(1/2/3-cd)pyrene	0.05	0	nc	0
Naphthalene	70	0	nc	0
Phenathrene	5	0	nc	0
Other parameters (mg/l unless stated)				
Chloride	nc	0	250000	0

nc:Not detected.



PERFORMANCE EVALUATION OF THERMAL STORAGE POROUS WALL WITH VENTS USING PASSIVE SOLAR ENERGY

Saad M. Saleh

Mechanical Eng. Dept.

University of Baghdad

Hussein K. Saleem

Mechanical Eng. Dept.

University of Baghdad

ABSTRACT

The performance of thermal storage porous wall with vents (gravel material) is analyzed for passive solar heating system under Baghdad climatic conditions by comparing it with conventional wall (Concrete wall) for a variety of control strategies. The variation has been calculated during a period of heating season for three months from December (1999) to February (2000) by using computer simulation with **MATLAB** language (Ver.6.5). A mathematical model containing the governing differential equations of heat transfer through the wall and glazing under unsteady heat flow was performed by using "control volume" technique to obtain the temperature distribution within the wall. The study was carried out for a south facing vertical wall and the effect of different thicknesses, porosities, effect of insulation and glazing layers and effect of vents was also investigated.

الخلاصة

تم تحليل أداء جدار الخزن الحراري المسامي ذو تهوية (مادة الحصى) بالاستخدام السلبي للطاقة الشمسية تحت الظروف المناخية لمدينة بغداد بمقارنته بجدار تقليدي مصنوع من الكونكريت لعدد من الإستراتيجيات المسيطر عليها. تم حساب التغيرات أثناء موسم التسخين ولثلاث شهور من كانون الأول (١٩٩٩) إلى غاية شباط (٢٠٠٠) باستخدام الحاسوب وبمساعدة لغة **MATLAB** (النسخة 6.5). تم تكوين المعادلات التفاضلية الحاكمة لانتقال الحرارة خلال الجدار و الزجاج باعتبار أن سريان الحرارة متغيرة مع الزمن وذلك باستعمال طريقة تدعى "الحجم المسيطر" للحصول على توزيع درجات الحرارة خلال الجدار. تمت الدراسة على جدار عمودي وأخذ بنظر الاعتبار أسماك وقيم للمسامية مختلفة، إضافة إلى تأثير وضع عازل ليلي وتأثير وجود التهوية خلال الجدار.

KEYWORD

Thermal storage, Passive solar, Trombe wall, Porous wall

INTRODUCTION

Passive solar heating systems , collect and utilize solar energy by natural means and generally exclude the use of mechanical power or electric controls to regulate the flow of heat.

The thermal energy is transferred in and out of the structure, in and out of the storage medium and around it, and through the conditioned space by natural means.

A passive solar heating system has four features that distinguishes it from a conventionally heated one, since the sun is a primary source of heat, a passive solar design includes (Ralph 1980) :

- A method to collect solar energy.
- A way to store that energy.
- A system to release energy in the form of heat to the living space "room".
- A means for controlling the heat that reaches the living spaces.

(Nayak 1983) developed a mathematical model to analyze the thermal performance of some typical passive heating concepts, mainly the Trombe wall. The model yields analytical expression for the time dependent heat flux entering the living space. (Aung 1972) investigate the effect of asymmetric heating on the free convection heat transfer in parallel plates vertical channel. The average Nusselt number was found to be related to the Rayleigh number very nearly by a universal curve for all temperature difference ratios. The theoretical results were verified by experimental measurement.

(Ohanessian 1978) perform a comparative analysis between Trombe wall and conventional heated house over atypical 28 day Melbourne winter period. Saving of 40 percent interims of energy of energy costs was obtained. (Casperson 1979) provided experimental information regarding the heat transfer characteristic of the collector wall system. The data collected provided some useful information and interested trends.

THERMAL STORAGE BY POROUS WALL

The type of thermal storage wall can be divided into three kinds:

1. Masonry wall.
2. Water wall.
3. Porous wall.

To formulate the mathematical model of this problem, one dimensional heat flow has been considered, and homogeneous layer with constant properties has been assumed (Al Mashat S M 1999).

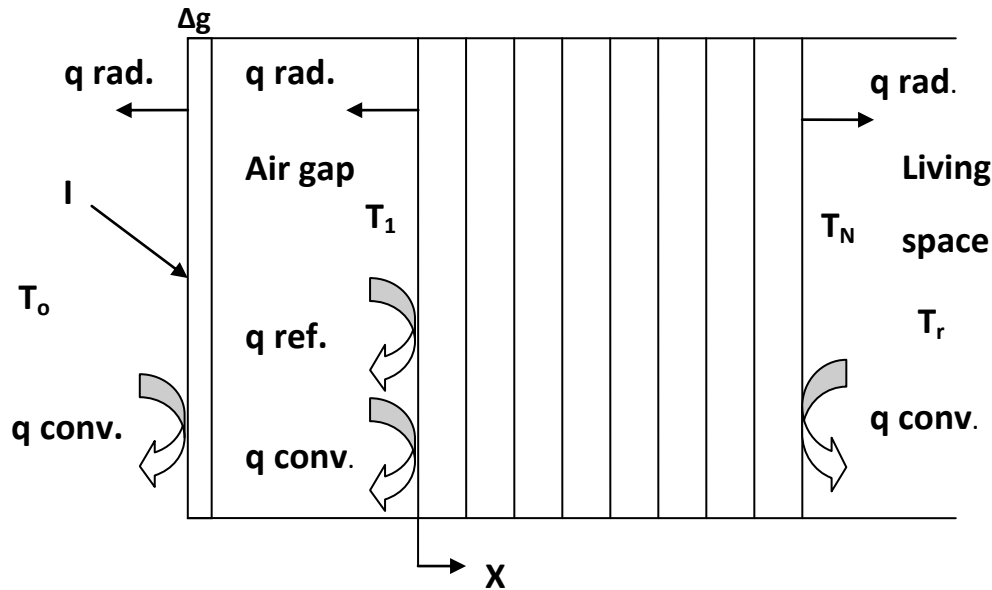


Fig. 1. Schematic of Wall Energy Balance

The energy equation through the porous wall layers shown in Fig. (1) Can be written as (Warren 1973)

$$\frac{\partial}{\partial x} \left(K_e \frac{\partial T}{\partial x} \right) = [\phi(\rho C)_f + (1 - \phi)(\rho C)_s] \frac{\partial T}{\partial t} \quad (1)$$

Where K_e is the thermal conductivity of thermal storage porous wall.

The differential equations can be changed to discretization equations by using a numerical method called “Control Volume Technique”. Details of this method explained by reference (Patanker 1980). This by integrating equation (1) over a control volume as shown in Fig. (2) and over a time interval from t to $t + \Delta t$, yield to discretization equation.

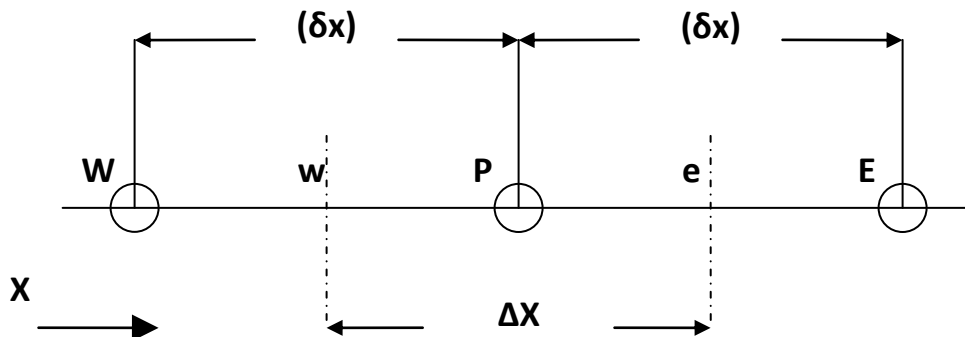


Fig. 2. Grid point cluster for one dimensional problem

Equation (1) can transfer to the following discretization equation by which the temperature of point P the center of the control volume as in Fig. (2) at time $t+\Delta t$ can be calculate in term of temperature at time t in the adjacent points.

$$a_p T_p^1 = a_e T_e^\circ + a_w T_w^\circ + (a_p - a_e - a_w) T_p^\circ \quad (2)$$

Where

$$a_p = \frac{(\rho C)_t \Delta x}{\Delta t}, \quad (\rho C)_t = [\phi(\rho C)_f + (1-\phi)(\rho C)_s]$$

$$a_e = \frac{K_e}{(\delta x)_e}, \quad a_w = \frac{K_e}{(\delta x)_w}$$

For the outside surface of the porous wall as shown in Fig. (1), the discretization equation of energy balance:

$$a_1 T_1^1 = [a_1 - a_a - a_R - a_2] T_1^\circ + a_a T_a^\circ + a_R T_g^\circ + a_2 T_2^\circ + b \quad (3)$$

Where

$$a_1 = \frac{(\rho C)_t \Delta x}{\Delta t}, \quad a_a = h_a, \quad a_2 = \frac{K_e}{\Delta x}$$

$$a_R = \frac{\sigma(T_1^{\circ^2} + T_g^{\circ^2})(T_1^\circ + T_g^\circ)}{\frac{1}{\epsilon_g} + \frac{1}{\epsilon_w} - 1}, \quad b = \tau_g \alpha_w I$$

For the inside surface of the wall shown in Fig. (1), the discretization equation of energy balance can be written as:

$$a_N T_N^1 = [a_N - a_{N-1} - a_1 - a_R] T_N^\circ + a_{N-1} T_{N-1}^\circ + a_1 T_r^\circ + a_R T_r^\circ \quad (4)$$

Where

$$a_N = \frac{(\rho C)_t \Delta x}{\Delta t}, \quad a_{N-1} = \frac{K_e}{\Delta x}$$

$$a_1 = h_i, \quad a_R = \sigma \epsilon_w (T_N^{\circ^2} + T_r^{\circ^2})(T_N^\circ + T_r^\circ)$$

The discretization equation for the glass layer can be written as follows:

$$a_g T_g^1 = [a_g - a_o - a_{Ro} - a_a - a_{Rw}] T_g^\circ + a_o T_o^\circ + a_{Ro} T_{sky}^\circ + a_a T_A^\circ + b \quad (5)$$

Where



$$a_g = \rho_g C_g \frac{\Delta g}{\Delta t}, \quad a_o = h_o$$

$$a_a = h_a, \quad a_{Ro} = \sigma \epsilon_g (T_g^{\circ 2} + T_{sky}^{\circ 2})(T_g^{\circ} + T_{sky}^{\circ})$$

$$a_{Rw} = h_{Rw} = \frac{\sigma(T_g^{\circ 2} + T_1^{\circ 2})(T_g^{\circ} + T_1^{\circ})}{\frac{1}{\epsilon_g} + \frac{1}{\epsilon_w} - 1}, \quad b = [\alpha_g + \tau_g(1 - \alpha_w)]I$$

The average air temperature in the gap T_a can be computed from the energy balance on air in the gap (Akbarzadeh 1982):

$$T_a = T_{in} + \left(\frac{2T_{in} - T_1 - T_g}{2} \right) \times \left[-\frac{\dot{m}C_a}{2h_a A_p} \left(\exp - \left\{ \frac{2h_a A_p}{\dot{m}C_a} \right\} - 1 \right) - 1 \right] \quad (6)$$

And the exit air temperature from the air gap can be computed from the following equation :

$$T_{out} = T_{in} + \left(\frac{2T_{in} - T_1 - T_g}{2} \right) \times \left(\exp - \left\{ \frac{2h_a A_p}{\dot{m}C_a} \right\} - 1 \right) \quad (7)$$

It is necessary to estimate the air mass flow rate (\dot{m}). The mass flow rate can be calculated by the following equation:

$$\dot{m} = \rho_a \bar{V} A_v \quad (8)$$

The mean air velocity in the gap (\bar{V}) has been estimated (Duffie 1980) by a solution of Bernoulli's equation. This based on the assumption that density and air temperature in the gap vary linearly with height of the wall (\bar{H}). So the average velocity through the gap can be determined from the following equation (Akbarzadeh 1982):

$$\bar{V} = \sqrt{\frac{2g\bar{H}}{C_1 \left(\frac{A_p}{A_v} \right)^2 + C_2} \times \frac{T_m - T_r}{T_m}} \quad (9)$$

Where T_m is the mean air temperature in the gap= T_a

The wall layers are divided to strips, each strip equal to 1 cm ($\Delta x=0.01m$). The time step is equal to 100 s to satisfy the criteria of stability (Patanker 1980). The discretization equations (2-5) are solved for each time step. Hour by hour calculation for a period of heating for three months (Dec.1999 to Feb2000) under Baghdad climatic conditions.

The heat transfer to the room for vented thermal storage porous wall is calculated from the following equation:

$$Q = Q_C + Q_R + Q_{CR} \quad (10)$$

Where Q_C and Q_R are heat flux due to convection and radiation respectively:

$$Q_C = h_i(T_N - T_r) \quad (11)$$

$$Q_R = \sigma \epsilon_w (T_N^4 - T_r^4) \quad (12)$$

The rate of heat flux that enters the room due to air circulation (Q_{CR})

can be computed as:

$$Q_{CR} = \frac{\dot{m} C_a}{A_p} (T_{out} - T_{in}) \quad (13)$$

The rate of heat per unit area stored in the wall (Q_{SR}) can be calculated from:

$$Q_{SR} = \tau_g I - \frac{\sigma(T_1^4 - T_g^4)}{\frac{1}{\epsilon_w} + \frac{1}{\epsilon_g} - 1} - h_a(T_1 - T_a) - Q \quad (14)$$

RESULTS AND DISCUSSION

The results of the mathematical model that is derived in the previous section will be presented and discussed. The hourly variation for solar intensity on the south facing vertical wall and ambient temperature data are taken from the solar energy research center, Jaderia-Baghdad. The porous wall having dimension equal to 2.8m height and 2.5m width, 0.04 vent area to the wall area ratio. The air gap width equal to 0.1 m. The solar intensity for clear and cloudy day on the wall is shown in Fig. (3). The 9th and 26th February was chosen to represent the cloud and clear days respectively in this study. Fig. (4) and (5) show the hourly variation of the rate of heat flux transferred to the living space “room” during a selected clear and cloudy day. The living space assumed to be at a constant temperature equal to 20 °C. The hourly variation of the rate heat flux studied for the following cases:

1. Vented porous wall without night insulation (VPORWN).
2. Unvented porous wall without night insulation (NVPORWN).
3. Vented Concrete wall without night insulation (VCONWN).
4. Unvented Concrete wall without night insulation (NVCONWN).

For clear day Fig. (4), for Concrete wall, there is a positive heat flux to the room during the day. But for unvented wall the heat flux due to heat conduction through the wall starts to increase at (9 A.M.) till it reach the maximum value at (5 P.M.) which have the value equal to 192 W/m². While for a vented wall system, the heat flux is due to conduction through the wall in addition to thermo-circulation, so it start rising from (8 A.M.) till (3 P.M.) where its maximum value is about 225 W/m². So in the case of vented system there is about 23% increase in heat gain through the heat period over



that of unvented system. It is therefore evident that wall with natural air circulation construction is only useful when immediate heat transfer, i.e. without delay required.

For wall that is constructed from porous material (gravel), its behavior is the same as that of Concrete wall .but its values of heat flux are relatively small than the Concrete wall. For unvented wall the heat starts to increase in (9 A.M.) and reach its maximum value at (5 P.M.) and its value equal to 177 W/m^2 . And for vented wall start to increase at (8 A.M.) and reach the maximum value at (3 P.M.) which equal to 210 W/m^2 . So there is an increase for vented system to unvented one by a 20%. And the Concrete wall is 7% higher than porous wall in transferring heat flux, this is because the porous wall having specific heat value greater than that for Concrete wall, so the porous wall having the ability to store the heat instead of transfer the heat to the living space.

For cloudy day, Fig. (5) illustrates the hourly variation of heat flux coming into the room. For all compared systems, there is a negative heat flux transfer to the room during most of the day hours. This is means that there is a heat loss from the room to the ambient. So it causes more auxiliary heat required during cloudy whether to compensate the energy loss. There is a positive value of heat flux coming to the room at the beginning of the day, i.e. in the morning hours, from (0 A.M.) to (7 A.M.) hour for unvented systems (Concrete and porous wall), this is because the heat store in the wall from the last day discharged to the room in the beginning of the present day. And to (10 A.M.) for vented systems, this is due to additional heat from the thermo-circulation which delays the negative value of heat flux. The Concrete wall appears a relatively increase in heat flux coming to the room than that of porous wall.

The rate of heat storage in the wall is equal the difference between heat received by the wall from the sun and heat transfer out of the wall from both side by convection, radiation and by thermo-circulation for vented wall system. The storage heat depends mainly on the material and thickness of the wall. So three different thicknesses for porous wall of 0.1m, 0.15m and 0.2m are compared with 0.2m thickness of Concrete wall,

Figs. (6) to (7) illustrate the variation of heat stored in the walls for different thicknesses for vented and for clear and cloudy day. Fig.(6) shows the hourly variation of heat stored through different wall systems, for clear day with walls having vents, Fig. (6) shows that Concrete with thickness 0.2m having approximately the same behavior and the values of heat stored in porous wall with thickness 0.1m. For other porous wall thicknesses, the heat stored in 0.15m is a 3-9% greater than porous wall with thickness 0.1m and Concrete wall with thickness 0.2m. The wall which having a thickness of 0.2m is 8-15% greater than that of porous wall with 0.1m thickness and Concrete wall with thickness 0.2m. This is because the specific heat for gravel is greater than that for Concrete. The behavior of storage heat is the same for all systems. The wall starts to be charged with heat. I.e. becomes positive at about (7 A.M.) for all system except that for 0.2m porous wall which starts to charges at (6 A.M.). The system still charged until reach the maximum value at (2 P.M.) which equal to 470 W/m^2 for porous wall with thickness 0.2m. and then begin to discharge heat to the ambient through the sunset until reach the minus value.

CONCLUSIONS

1. The heat flux that enters the room for concrete wall is greater than that in the case of using a porous wall.
2. The heat stored in the case of porous wall is greater than that of concrete wall.
3. The heat stored in the wall increases with increasing thickness of the porous wall.

REFERENCES:

- Akbarzadeh, A.; Charter, W.W.S.; Lesslie, D.A. (1982) "Thermocirculation characteristic of Trombe wall passive test cell", J. Solar Energy, Vol. 28, PP 461,
- Al Mashat, S.M. (1999) " Free convection laminar flow in the heated vertical duct application to Trombe wall" Sci. J Tikrit University, Vol.6, No. 1 pp 97.
- Aung, W. (1972) "Fully developed laminar free convection between vertical plates heated asymmetrically" Int.J. Heat and Mass Transfer. Vol. 84 pp1577.
- Casperrson, R.L.; Hocevar, C.J. (1979) "Experimental investigation of the Trombe wall passive solar system" In the proceeding of the third national passive solar conference. Vol. 3 pp231.
- Duffie, J.A.; Beckman, W.A. (1980) "Solar Eng. Of Thermal Process" Wiley N.Y.
- Nayak, J.K.; Baval, N.K.; Sodha, M.S. (1983) "Analysis of passive heating concept" J. Solar Energy, Vol.30, No 1, pp51.
- Ohanessian, P.; Chartars, W.W.S. (1978) "Thermal simulation of passive solar house using Trombe- Michel wall structure" J. Solar Energy, Vol. 20 pp 275.
- Patanker, S.V. (1980) "Numerical heat transfer and fluid flow" McGraw Hill.
- Ralph M.L. (1980) "Passive solar heating design" Applied science
- Warren, M.R.; Hartnett, J.P. (1973) "Handbook of heat transfer" McGraw Hill

NUMENCLATURES:

A	Area (m^2)
A_P	Projected area (m^2)
A_V	Vent area (m^2)
C	Specific heat (J/kg.K)
g	Acceleration of gravity (m/s^2)
H	Wall height (m)



$\bar{H} = H_m$	Distance between vents (m)
h	Heat transfer coefficient ($W/m^2.K$)
I	Solar intensity (W/m^2)
K	Thermal conductivity ($W/m.K$)
L	Wall thickness (Air mass flow rate in the gap (kg/s)
Q_C	Rate of heat flux due to convection (W/m^2)
Q_{CR}	Rate of heat flux due to thermo circulation (W/m^2)
Q_R	Rate of heat flux due to radiation (W/m^2)
Q_{SR}	Rate of heat stored in the wall (W/m^2)
q	Rate of heat flux (W/m^2)
T	Temperature (K)
T°	Temperature at time t (K)
T^1	Temperature at time $t+\Delta t$ (K)
T_m	Mean air temperature in the gap (K)
\bar{V}	Mean air velocity in the gap (m/s)
w	Width of the wall (m)
x,y	Coordinates

GREEK SYMBOLS

α	Absorbitivity
ρ	Density (kg/m^3)
ϕ	Porosity
ε	Emmisivity
σ	Stefan-Boltzman constant ($W/m^2.K^4$)
τ	Transmissivity

SUBSCRIPTS

A	Air
Cond	Conduction
Conv	Convection
f	Fluid
g	Glass
i	Inside
in	Inlet
N	Inside wall face
o	Outside
out	Outlet
P	Center point
r	Room
rad	Radiation
s	Solid
v	vent
w	Wall
1	outside wall face

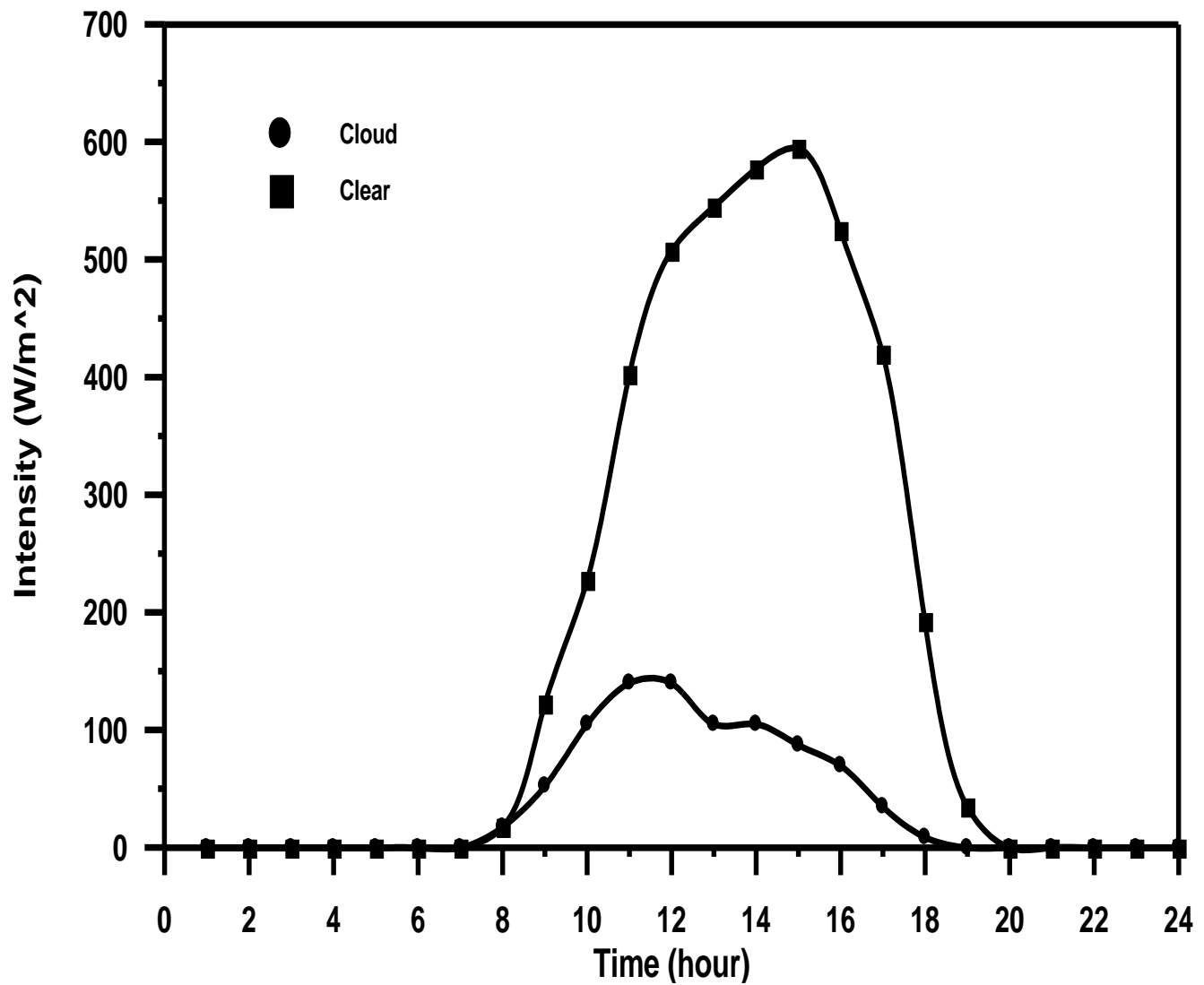


Fig. 3. Solar intensity on wall for clear and cloudy day.

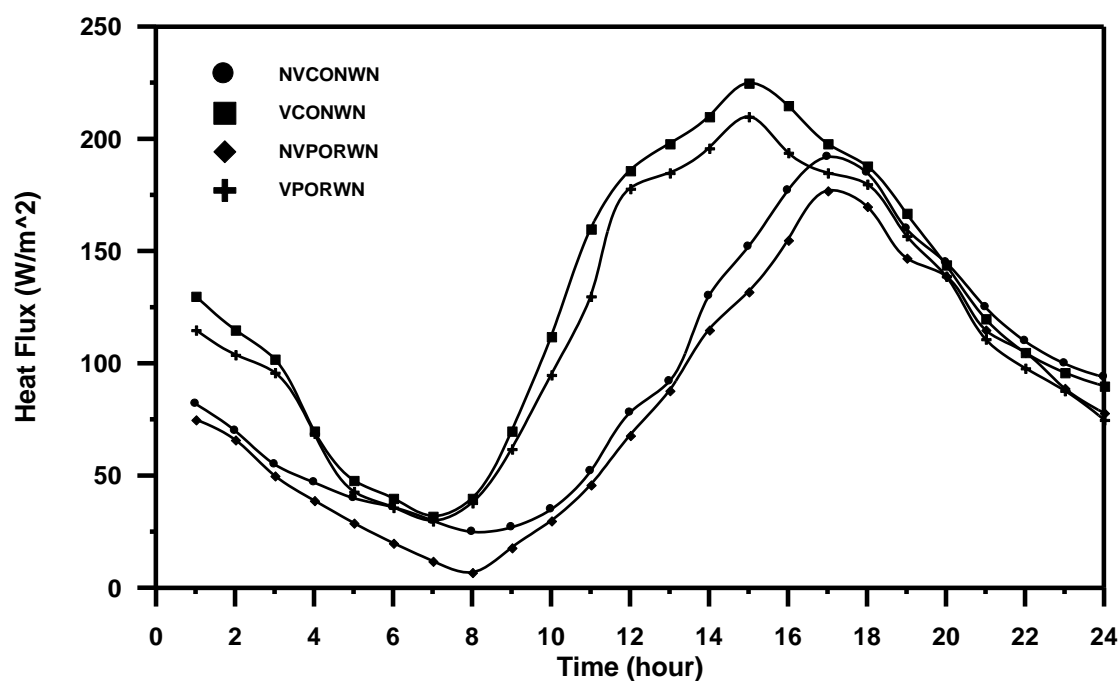


Fig. 4. Heat flux for Concrete and porous wall without night insulation (clear day).

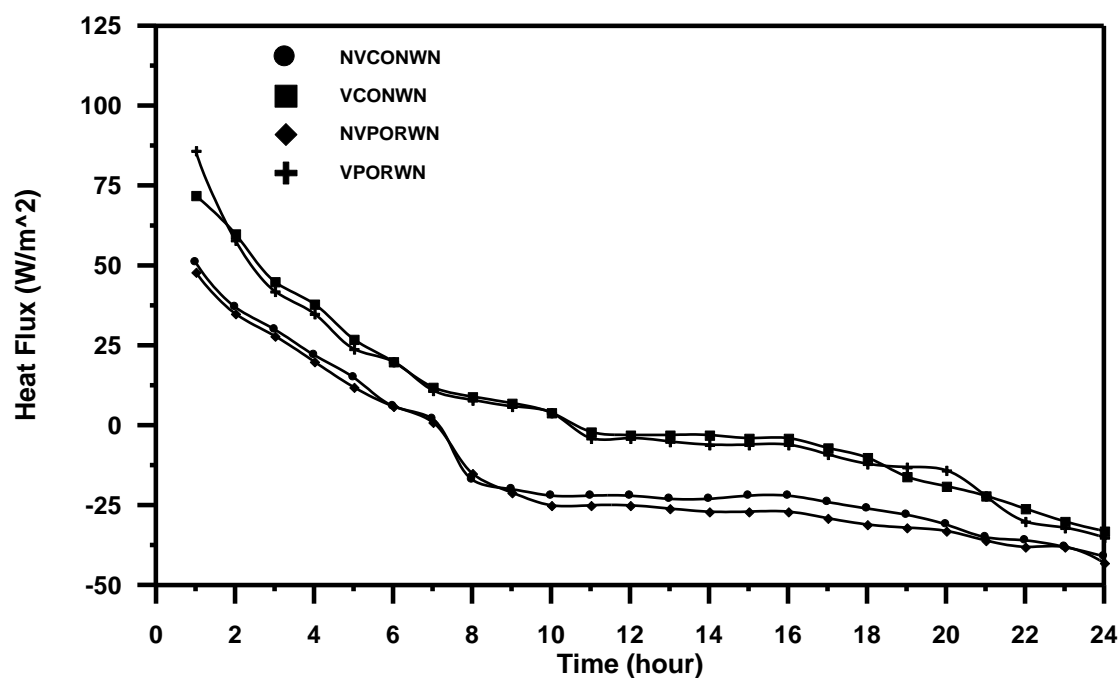


Fig. 5. Heat flux for Concrete and porous wall without night insulation (cloud day).

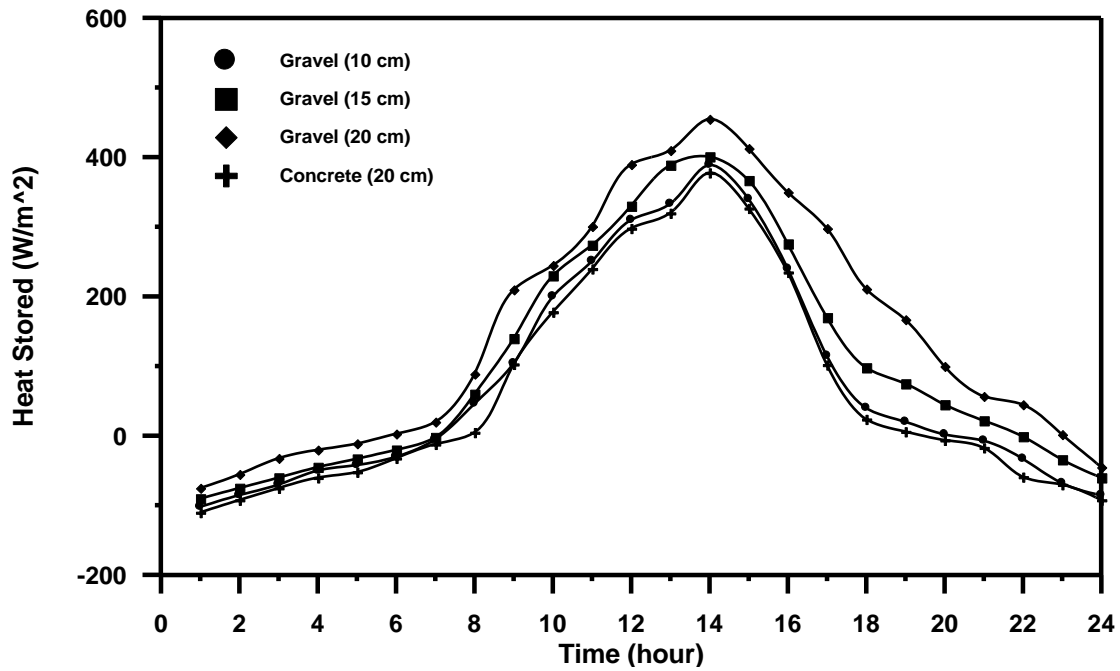


Fig. 6. Comparison between Concrete wall and different thicknesses porous wall heat stored with vents (clear day).

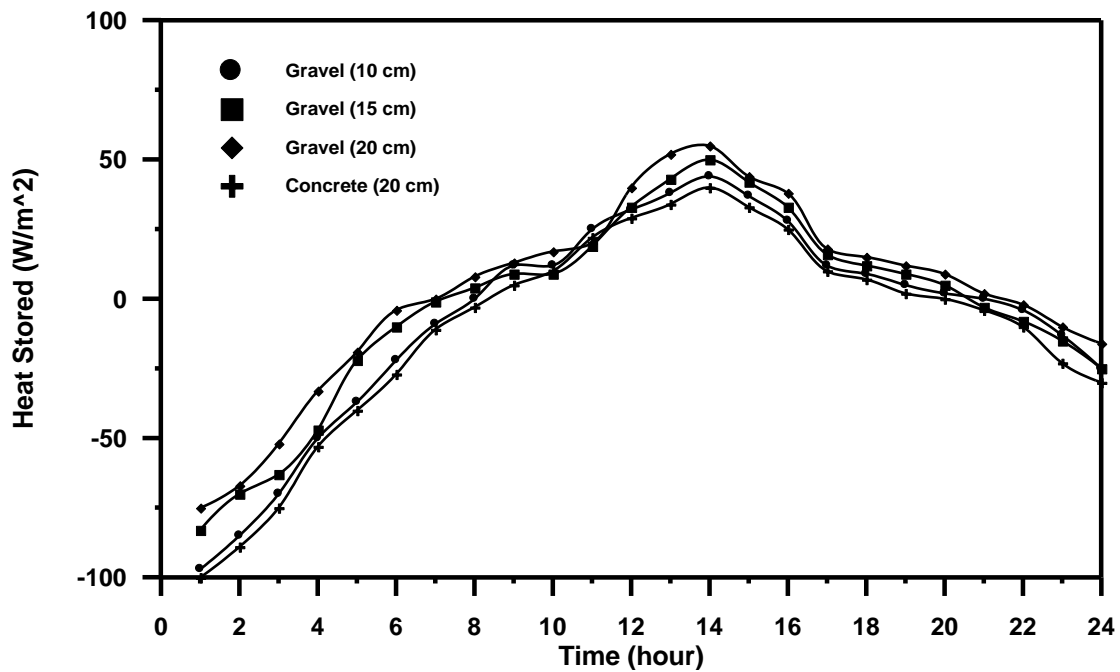


Fig. 7. Comparison between Concrete wall and different thicknesses porous wall heat stored with vents (cloud day).



GENERATION AND SIMULATION OF MESHING FOR INVOLUTE HELICAL GEARS

Mohammad Qasim Abdullah

University of Baghdad/college of Engineering
Mechanical Engineering Department.

Mansour Ali Ismael

University of Baghdad/college of Engineering
Mechanical Engineering Department.

ABSTRACT

A new method for generation and simulation of meshing for involute helical gears is presented. The approaches proposed for generation are based on the imaginary application of two rack-cutters one for pinion and the other for gear generation. The proposed simulation of meshing of aligned and misaligned helical gears gives (i) the shift of the bearing contact (real contact path) on pinion and gear tooth surfaces, (ii) the function of transmission errors.

الخلاصة

طريقة جديدة لتوليد و محاكاة التعشيق للتروس الحلزونية ذات الجانبية العدلة قد تم عرضها التقريبات المقترحة للتوليد أستندت على تطبيق أدواتي قطع تخيليتين واحدة للترس الصغير و الأخرى للترس الكبير محاكاة التعشيق المقترحة للتروس الحلزونية المنتظمة و غير المنتظمة تعطي (أ) الانتقال في موقع التماس (مسار التماس الحقيقي) على سطح سن الترس الصغير و الترس الكبير (ب) دالة الأخطاء المنقولة.

KEYWORDS

Helical gear; Gear generation; Gears Meshing; Simulation of Gears; Bearing Contact.

INTRODUCTION

A review of the history of the development of involute gears shows that the involute was introduced as a profile for gear tooth on account of the simplicity in design and manufacture of gears having these profiles, also the involute teeth not sensitive to slight errors in profile and center distance (Avinash et. al., 2003). (Kubo, 1988) presented a general calculation method of load sharing to every tooth pair in meshing, load distribution, and contact pattern on tooth flank of helical gears

with manufacturing and alignment error, for which some parts of tooth flanks on the geometrical line of contact can separate from each other due to the errors. For such gears, stiffness of meshing tooth pair, exciting force of gear vibration, and total composite error under loaded conditions was derived. (Litvin et. al, 1995) described the design and generation of modified involute helical gears that have a localized and stable bearing contact, and reduced noise and vibration characteristics.

(Litvin and Fan, 2001) covered the data on involute helical gears manufactured by shaving. Modification of geometry of helical gear with parallel axis was proposed. The finishing process of gear generation is shaving. (Litvin and Ignacio, 2003) covered design, generation, simulation of meshing and stress analysis of modified involute helical gears. The approach developed for modification of the conventional involute helical gears was based on conjugation of double-crowned pinion with a conventional helical involute gear. The bearing contact was localized and oriented longitudinally, and edge contact was avoided. Also, the influence of misalignment on the shift of bearing contact, noise and vibration were reduced.

In order to drive in a given direction and to transmit power or motion smoothly and with a minimum loss of energy, the contacting surfaces on the mating gears must have the following properties (Dudley, 1962):-

1. The height and the lengthwise shape of the active profiles of the teeth must be such that, before one pair of teeth goes out of contact during meshing, a second pair will have picked up its share of load.
2. The shape of the contacting surfaces of the teeth (active profile) must be such that the angular velocity of the driving member of the pair is smoothly imparted to the driven member in the proper ratio.
3. The spacing between the successive teeth must be such that a second pair of tooth-contacting surfaces (active profiles) is in the proper positions to receive the load before the first leave mesh.

BASIC PRINCIPLES OF GENERATION

The process for gear generation is based on the followings (Litvin et. al, 1997):-

1. The generation of tooth surfaces is based on the imaginary derivation of conjugate surfaces by application of two rack-cutters. The surfaces of the two rack-cutters are rigidly connected each to other in the process of the imaginary generation, and they are in tangency along one straight line as shown in **Fig. (1)**. This line and axes of the gears form a helix angle (β).

2. In the process for the generation, the two rigidly connected rack cutters perform translational motion, while the pinion and gear perform rotational motions about their axes, O_1 and O_2 .
3. Surfaces of gear and pinion (Σ_1 and Σ_2) determined as the envelope to the family of rack cutter surfaces.
4. When the generated surfaces Σ_1 and Σ_2 are in mesh, their will be one contact point at every instant. The path of contact on surfaces Σ_i ($i = 1, 2$) is the set of points of Σ_i where Σ_1 and Σ_2 contact each other. Such a path of contact is a helix, and the contact point moves in the process of meshing along the helix on Σ_i .

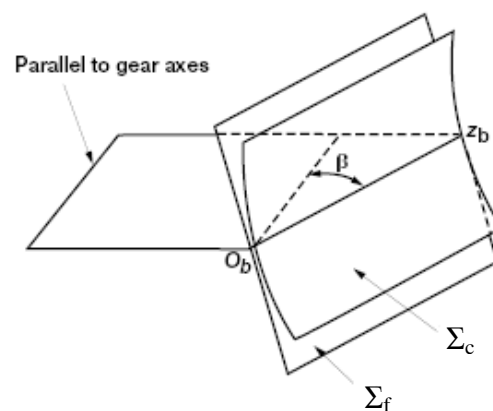


Fig. (1):- Rack cutter surfaces for involute helical gears.

DERIVATION OF PINION TOOTH SURFACE:-

The normal section of pinion rack cutter is shown in **Fig. (2)** The profile of the basic tooth of the rack cutter in the normal section is symmetric about x_{cp} .

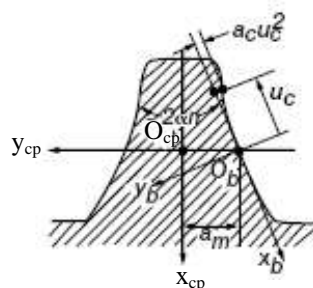


Fig.(2):- Normal section of pinion rack cutter.

The normal section of the pinion rack cutter is represented in the coordinate system S_{cp} by the equations (Litvin et. al, 1997):-

$$r_{cp}(u_c) = \begin{bmatrix} x_{cp} \\ y_{cp} \\ z_{cp} \\ 1 \end{bmatrix} = \begin{bmatrix} -u_c \cos \alpha_n - a_c u_c^2 \sin \alpha_n \\ u_c \sin \alpha_n - a_c u_c^2 \cos \alpha_n - a_m \\ 0 \\ 1 \end{bmatrix} = M_{cpb} r_b(u_c) \quad (1)$$

where $r_b(u_c) = [-u_c \quad -a_c u_c^2 \quad 0 \quad 1]^T$, $a_m = \frac{\pi}{4p_n}$, (a_c) is the parabolic coefficient

and

$$M_{cpb} = \begin{bmatrix} \cos \alpha_n & \sin \alpha_n & 0 & 0 \\ -\sin \alpha_n & \cos \alpha_n & 0 & -a_m \\ 0 & 0 & 1 & 0 \\ 0 & 0 & 0 & 1 \end{bmatrix}$$

The rack cutter tooth in the three dimensional system can be defined by S_c coordinate system as

$$r_c(u_c, \iota_c) = \begin{bmatrix} x_c \\ y_c \\ z_c \\ 1 \end{bmatrix} = \begin{bmatrix} -u_c \cos \alpha_n - a_c u_c^2 \sin \alpha_n \\ (u_c \sin \alpha_n - a_c u_c^2 \cos \alpha_n - a_m) \cos \beta - \iota_c \sin \beta \\ (-u_c \sin \alpha_n + a_c u_c^2 \cos \alpha_n + a_m) \sin \beta + \iota_c \cos \beta \\ 1 \end{bmatrix} \quad (2)$$

where

$$M_{ccp} = \begin{bmatrix} 1 & 0 & 0 & 0 \\ 0 & \cos \beta & -\sin \beta & -\iota_c \sin \beta \\ 0 & -\sin \beta & \cos \beta & \iota_c \cos \beta \\ 0 & 0 & 0 & 1 \end{bmatrix}$$

The unit normal to the pinion rack cutter surface is represented as:

$$n_c = \frac{N_c}{|N_c|}, \quad N_c = \frac{\partial r_c}{\partial \iota_c} \times \frac{\partial r_c}{\partial u_c} \quad (3)$$

Thus,

$$n_c(u_c) = \begin{bmatrix} n_{xc} \\ n_{yc} \\ n_{zc} \end{bmatrix} = \frac{1}{\sqrt{1 + 4a_c^2 u_c^2}} \begin{bmatrix} -\sin \alpha_n + 2a_c u_c \cos \alpha_n \\ -(\cos \alpha_n + 2a_c u_c \sin \alpha_n) \cos \beta \\ -(\cos \alpha_n + 2a_c u_c \sin \alpha_n) \sin \beta \end{bmatrix} \quad (4)$$

To derive the equation of meshing between pinion rack cutter and pinion tooth surfaces, it is considered that the movable coordinate systems S_c and S_1 are rigidly connected to the tool (pinion rack cutter) and the pinion, respectively. The fixed coordinate system S_n is rigidly connected to the frame of the cutting machine. The derivation of equation of meshing is based on the theorem that the common normal to Σ_c and Σ_1 must pass through the instantaneous axis of rotation (Litvin, 1989). Thus

$$\frac{X_c - x_c}{n_{xc}} = \frac{Y_c - y_c}{n_{yc}} = \frac{Z_c - z_c}{n_{zc}} \quad (5)$$

where $X_c = 0$ and $Y_c = -R_{p1}\psi_1$

Using Eq. (5) the equation of meshing can be represented as:

$$f(u_c, t_c, \psi_1) = 0 \quad (6)$$

where ψ_1 is the angle of rotation of the pinion in the process for generation.

After transformation, the following equation of meshing can be obtained

$$f(u_c, t_c, \psi_1) = R_{p1}\psi_1 - t_c \sin \beta - a_m \cos \beta + \frac{u_c(1 + 2a_c u_c^2) \cos \beta}{\sin \beta - 2a_c u_c \cos \alpha_n} = 0 \quad (7)$$

Finally, the generated surface of the pinion Σ_1 is represented by the family of lines of contact between the rack cutter surface Σ_c and the pinion tooth surface Σ_1 being generated. Surface Σ_1 is represented in coordinate system S_1 by the equations:

$$r_1(u_c, l_c, \psi_1) = M_{1n} M_{nc} r_c(u_c, l_c), \quad f(u_c, l_c, \psi_1) = 0 \quad (8)$$

where

$$M_{nc} = \begin{bmatrix} 1 & 0 & 0 & R_{p1} \\ 0 & 1 & 0 & R_{p1}\psi_1 \\ 0 & 0 & 1 & 0 \\ 0 & 0 & 0 & 1 \end{bmatrix} \quad \text{and} \quad M_{1n} = \begin{bmatrix} \cos \psi_1 & \sin \psi_1 & 0 & 0 \\ -\sin \psi_1 & \cos \psi_1 & 0 & 0 \\ 0 & 0 & 1 & 0 \\ 0 & 0 & 0 & 1 \end{bmatrix}$$

Thus

$$r_1 = \begin{bmatrix} (-u_c \cos \alpha_n a_c u_c^2 \sin \alpha_n) \cos \psi_1 + \{(u_c \sin \alpha_n - a_c u_c^2 \cos \alpha_n - a_m) \cos \beta \\ - l_c \sin \beta\} \sin \psi_1 + (\cos \psi_1 + \psi_1 \sin \psi_1) R_{p1} \\ (u_c \cos \alpha_n + a_c u_c^2 \sin \alpha_n) \sin \psi_1 + \{(u_c \sin \alpha_n - a_c u_c^2 \cos \alpha_n - a_m) \cos \beta \\ - l_c \sin \beta\} \cos \psi_1 + (-\sin \psi_1 + \psi_1 \cos \psi_1) R_{p1} \\ (-u_c \sin \alpha_n + a_c u_c^2 \cos \alpha_n + a_m) \sin \beta + l_c \cos \beta \end{bmatrix} \quad (9)$$

DERIVATION OF GEAR TOOTH SURFACE:

The normal section of gear rack-cutter is shown in **Fig. (3)**. The profile of the basic tooth of the rack-cutter in the normal section is symmetric about x_{cf} .

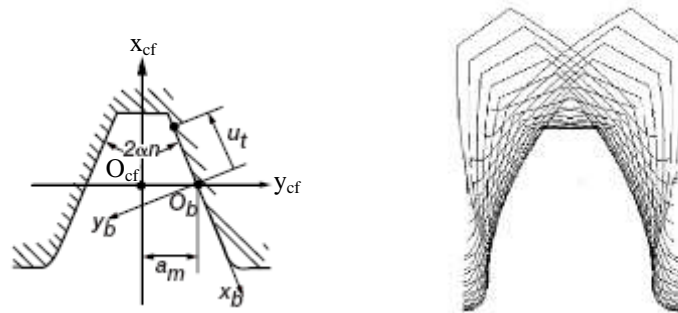


Fig. (3):- Normal sections of gear rack cutter.

By using coordinate system S_{cf} , the normal section of gear rack-cutter can be represented by the following equations (**Litvin et. al, 1997**):-

$$r_{cf} = M_{cfb} r_b(u_f)$$

$$\text{Or } r_{cf}(u_f) = \begin{bmatrix} x_{cf} \\ y_{cf} \\ z_{cf} \\ 1 \end{bmatrix} = \begin{bmatrix} u_f \cos \alpha_n \\ a_m - u_f \sin \alpha_n \\ 0 \\ 1 \end{bmatrix} \quad (10)$$

Hence, $r_b(u_f) = [-u_f \ 0 \ 0 \ 1]^T$, u_f is the variable parameter and M_{cfb} is the matrix of coordinate transformation from S_b to S_{cf} that is

$$M_{cfb} = \begin{bmatrix} -\cos \alpha_n & \sin \alpha_n & 0 & 0 \\ \sin \alpha_n & \cos \alpha_n & 0 & 0 \\ 0 & 0 & 1 & a_m \\ 0 & 0 & 0 & 1 \end{bmatrix}$$

The derivation of gear rack-cutter tooth surface in the three dimensional system may be accomplish similarly to that for pinion rack-cutter, and the following vector equations in S_f coordinate system can be obtained:

$$r_f(u_f, l_f) = M_{fcf} r_{cf}(u_f)$$

Where

$$M_{fcf} = \begin{bmatrix} 1 & 0 & 0 & 0 \\ 0 & \cos \beta & \sin \beta & l_f \sin \beta \\ 0 & -\sin \beta & \cos \beta & l_f \cos \beta \\ 0 & 0 & 0 & 1 \end{bmatrix}$$

Thus,

$$r_f(u_f, l_f) = \begin{bmatrix} x_f \\ y_f \\ z_f \\ 1 \end{bmatrix} = \begin{bmatrix} u_f \cos \alpha_n \\ (a_m - u_f \sin \alpha_n) \cos \beta + l_f \sin \beta \\ (u_f \sin \alpha_n - a_m) \sin \beta + l_f \cos \beta \\ 1 \end{bmatrix} \quad (11)$$

The unit normal to the gear rack-cutter surface Σ_f is:

$$n_f(u_f) = \begin{bmatrix} n_{xf} \\ n_{yf} \\ n_{zf} \end{bmatrix} = \begin{bmatrix} \sin \alpha_n \\ \cos \alpha_n \cos \beta \\ -\cos \alpha_n \sin \beta \end{bmatrix} \quad (12)$$

The equation of meshing can be derived in similar manner to that of **Eqs. (5) and (7)**, thus

$$\frac{X_f - x_f}{n_{xf}} = \frac{Y_f - y_f}{n_{yf}} = \frac{Z_f - z_f}{n_{zf}} \quad (13)$$

Where $X_f = 0$ and $Y_f = R_{p1} \psi_1$

After transformations, the following equation of meshing between Σ_f and Σ_2 can be obtained

$$f(u_f, l_f, \psi_2) = R_{p2} \psi_2 - l_f \sin \beta - a_m \cos \beta + \frac{u_f \cos \beta}{\sin \alpha_n} = 0 \quad (14)$$

Finally ,the generated gear tooth surface Σ_2 is determined as the envelope to the family of rack-cutter surfaces Σ_f and is represented in coordinate system S_2 as

$$r_2(u_f, l_f, \psi_2) = M_{2m} M_{mf} r_f(u_f, l_f)$$

where

$$M_{2m} = \begin{bmatrix} \cos \psi_2 & -\sin \psi_2 & 0 & 0 \\ \sin \psi_2 & \cos \psi_2 & 0 & 0 \\ 0 & 0 & 1 & 0 \\ 0 & 0 & 0 & 1 \end{bmatrix}$$

and

$$M_{mf} = \begin{bmatrix} 1 & 0 & 0 & R_{p2} \\ 0 & 1 & 0 & -R_{p2}\psi_2 \\ 0 & 0 & 1 & 0 \\ 0 & 0 & 0 & 1 \end{bmatrix}$$

Thus

$$r_2 = \begin{bmatrix} u_f \cos \alpha_n \cos \psi_2 - \{a_m - u_f \sin \alpha_n\} \cos \beta + l_f \sin \beta \sin \psi_2 \\ + (\cos \psi_2 + \psi_2 \sin \psi_2) R_{p2} \\ u_f \cos \alpha_n \sin \psi_2 - \{(a_m - u_f \sin \alpha_n) \cos \beta + l_f \sin \beta\} \cos \psi_2 \\ + (\sin \psi_2 - \psi_2 \cos \psi_2) R_{p2} \\ (u_f \sin \alpha_n - a_m) \sin \beta + l_f \cos \beta \end{bmatrix} \quad (15)$$

Fig. (4) shows a sample of three teeth generated by the equations mentioned above using Ansys computer program.

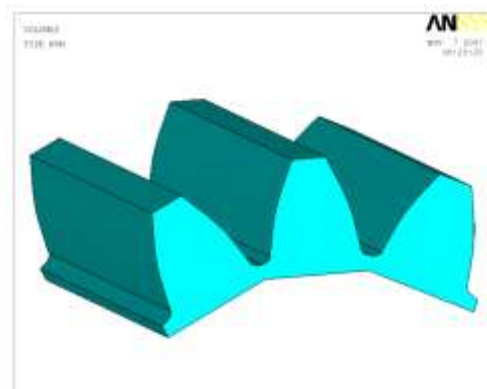


Fig. (4):- Sample of three teeth generated.

SIMULATION OF MESHING:

Computerized simulation of meshing is applied to discover the influence of misalignment on the shift of the bearing contact and transmission errors. The misalignment of the gear drive is simulated by the error of installation and orientation of the gear with respect to the pinion.

The theoretically correct tooth form is defined by the parameters tooth alignment, tooth profile, tooth spacing and center distance.

SIMULATION OF MESHING FOR INVOLUTE HELICAL GEARS:-

Consider that surfaces Σ_1 and Σ_2 and their unit normals n_1 and n_2 are represented in coordinate systems S_1 and S_2 , which are connected to the pinion and gear, respectively. The meshing of the gear tooth surfaces is considered in the fixed coordinate system S_f that is rigidly connected to the frame. The auxiliary coordinate systems S_q and S_p are used for simplification of coordinate transformation.

The simulation of meshing is based on the following procedure (**Litvin and Ignacio, 2003**) and (**Litvin et. al, 1997**):-

Step1: Using coordinate transformation, we represent Σ_1 , Σ_2 , n_1 and n_2 in the fixed coordinate system S_f as following **Fig. (5)**.

$$r_f^{(1)}(u_c, \psi_1, \phi_1) = M_{f1} r_1(u_c, \psi_1) \quad (16)$$

$$r_f^{(2)}(u_f, \psi_2, \phi_2) = M_{fp} M_{pq} M_{q2} r_2(u_f, \psi_2) \quad (17)$$

Where

$$M_{f1} = \begin{bmatrix} \cos \phi_1 & \sin \phi_1 & 0 & 0 \\ -\sin \phi_1 & \cos \phi_1 & 0 & 0 \\ 0 & 0 & 1 & 0 \\ 0 & 0 & 0 & 1 \end{bmatrix}$$

$$M_{q2} = \begin{bmatrix} \cos \phi_2 & \sin \phi_2 & 0 & 0 \\ -\sin \phi_2 & \cos \phi_2 & 0 & 0 \\ 0 & 0 & 1 & 0 \\ 0 & 0 & 0 & 1 \end{bmatrix}$$

$$M_{pq} = \begin{bmatrix} 1 & 0 & 0 & 0 \\ 0 & \cos \Delta\gamma & \sin \Delta\gamma & 0 \\ 0 & -\sin \Delta\gamma & \cos \Delta\gamma & 0 \\ 0 & 0 & 0 & 1 \end{bmatrix}$$

$$M_{fp} = \begin{bmatrix} -1 & 0 & 0 & E' \\ 0 & -1 & 0 & 0 \\ 0 & 0 & 1 & 0 \\ 0 & 0 & 0 & 1 \end{bmatrix}$$

$$E' = R_{p1} + R_{p2} + \Delta E$$

$$n_f^{(1)}(u_c, \psi_1, \phi_1) = L_{f1} n_1(u_c, \psi_1) \quad (18)$$

$$n_f^{(2)}(u_f, \psi_2, \phi_2) = L_{fq} L_{pq} L_{q2} n_2(u_f, \psi_2) \quad (19)$$

$$L_{f1} = \begin{bmatrix} \cos \phi_1 & \sin \phi_1 & 0 \\ -\sin \phi_1 & \cos \phi_1 & 0 \\ 0 & 0 & 1 \end{bmatrix}$$

$$L_{q2} = \begin{bmatrix} \cos \phi_2 & \sin \phi_2 & 0 \\ -\sin \phi_2 & \cos \phi_2 & 0 \\ 0 & 0 & 1 \end{bmatrix}$$

$$L_{pq} = \begin{bmatrix} 1 & 0 & 0 \\ 0 & \cos \Delta\gamma & \sin \Delta\gamma \\ 0 & -\sin \Delta\gamma & \cos \Delta\gamma \end{bmatrix}$$

$$L_{fp} = \begin{bmatrix} -1 & 0 & 0 \\ 0 & -1 & 0 \\ 0 & 0 & 1 \end{bmatrix}$$

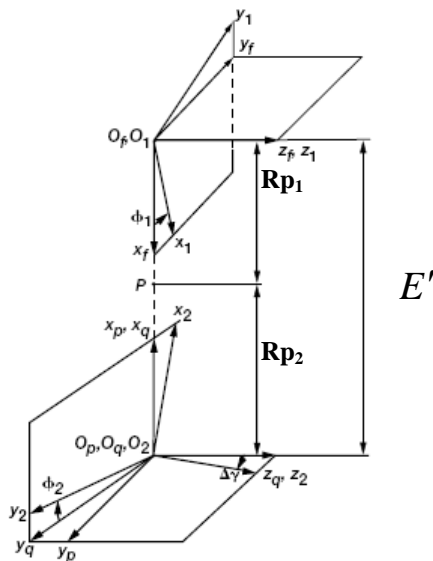


Fig. (5):- Applied coordinate system for simulation of meshing.

Step2: By using S_f coordinate system, the condition of continuous tangency of gear tooth surfaces can be represented by the following vector equations (see Fig. (6)):-

$$r_f^{(1)}(u_c, \psi_1, \phi_1) = r_f^{(2)}(u_f, \psi_2, \phi_2) \quad (20)$$

$$n_f^{(1)}(u_c, \psi_1, \phi_1) = n_f^{(2)}(u_f, \psi_2, \phi_2) \quad (21)$$

Step3: Vector Eq. (21) yields only two independent equations since $|n_f^{(1)}| = |n_f^{(2)}| = 1$. So, Eqs. (20) and (21) provide a system of five independent equations represented as

$$f_i(u_c, \psi_1, \phi_1, u_f, \psi_2, \phi_2) = 0 \quad (22)$$

Eq. (22) contains six unknowns but the theorem of Implicit Function System Existence yields that one parameter, say ϕ_1 , may be chosen as input and obtain the solution to equation system (22) by functions

$$\{u_c(\phi_1), \psi_1(\phi_1), u_f(\phi_1), \psi_2(\phi_1), \phi_2(\phi_1)\} \in C^1 \quad (23)$$

The gear tooth surfaces are in point contact, and so that it is suppose that the Jacobian of the fifth order differs from zero. Thus,

$$\left| \frac{\partial f_i}{\partial u_c} \frac{\partial f_i}{\partial \psi_1} \frac{\partial f_i}{\partial u_f} \frac{\partial f_i}{\partial \psi_2} \frac{\partial f_i}{\partial \phi_2} \right| \neq 0 \quad (24)$$

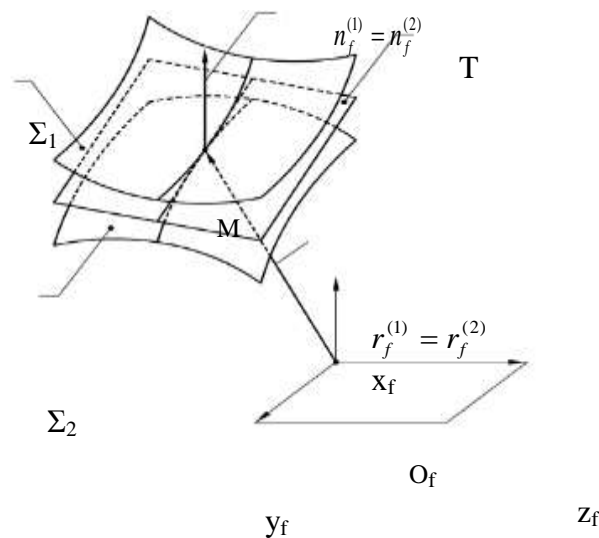


Fig. (6):- Tangency of contacting tooth surfaces in ideal gear.

If Eqs. (24) are satisfied then, using functions (23) we are able to determine:

- (i) the path of contact on surfaces Σ_1 and Σ_2 represented as

$$r_i(u_t, \psi_i), u_t(\phi_1), \psi_i(\phi_1) \quad (25)$$

where (i = 1, 2 and t = c, f) for pinion and gear, respectively.

- (ii) the transmission errors determined as

$$\Delta\phi_2(\phi_1) = \phi_2(\phi_1) - \frac{N_1}{N_2}\phi_1 \quad (26)$$

CONCLUSIONS:

1. Generation procedure based on equations of tooth surfaces has been conducted.
2. Algorithms for simulation of meshing indicates that such gear drives are sensitive to misalignment.
3. Simulation of meshing permits one to determine the shift of the bearing contact and transmission errors.

NOMENCLATURES:

- a_c Parabolic coefficient of profile of pinion rack cutter.
- C^1 Denote that the functions have continuous derivatives to the first order, at least.
- E' Center distance between gear and pinion (m).
- f Equation of meshing between tooth surface and rack-cutter surface.
- l_j, u_j Parameters of surface (j = c, f) (m).
- m_n Module in normal plane (m).
- N_i Number of teeth on pinion (i=1) or for gear (i = 2).
- n_j, n_f^j, N_j unit normal and normal to surface j (j = c, f).
- P_n Normal diametral pitch (1/m).
- r_i Position vector of a point in coordinate system S_i (mm).
- R_{pi} Radius of pitch circle of pinion (i = 1) or for gear (i = 2) (m).
- S_i Coordinate system (i = c_p, b, c, n, 1, 2, c_f, p, f).
- (x_i, y_i, z_i) Coordinates (i = c_p, c, 1, 2, c_f, f, p) (mm).



α_n	Normal pressure angle (deg).
β	Helix angle (deg).
$\Delta\gamma$	Error of shaft angle (deg).
$\Delta\phi_2$	Function of transmission errors (deg).
\in	Denotes that the element belongs to the set.
Ψ_i	Angle of rotation of pinion ($i = 1$) or the gear ($i = 2$) in the process of generation (deg).
Σ_i	Surfaces ($i = c, f, 1, 2$).
ϕ_i	Function of transmission errors (deg) ($i = 1, 2$).

REFERENCES:

- A. Kubo, (Stress Condition, Vibration Exciting Force, and Contact Pattern of Helical Gears with Manufacturing and Alignment Error), Transaction of the ASME, Journal of Mechanical Design, Vol. 100, PP. 77-84, January 1978.
- Darle W. Dudley, (Gear Hand Book), First Edition, McGRAW-HILL Book Company, INC, 1962.
- F .L. Litvin, (Theory of Gearing), NASA RP-1212 (AVSCOM 88-C-035), 1989.
- Faydor L. Litvin, Ningxin Chen and Jain Lu, (Generation and Computerized Simulation of Meshing and Contact of Modified Involute Helical Gears), Illinios Unv., Chicago Circle, Jan. 1995.
- F. L. Litvin, D. P. Townsend and M. Hawkins,(Computerized Simulation of Meshing of Conventional Helical Involute Gears and Modification of Geometry), NASA TM-10741, July 1997.
- Faydor L. Litvin, Qi Fan, Daniele Vecchiato and Alberto Demenego, (Computerized Generation and Simulation of Meshing of Modified Spur and Helical Gears Manufactured by Shaving), NASA/CR-2001-210893 (ARL-CR-468), May 2001.
- F. L. Litvin, Ignacio G. P., Luca C. and Kazumasa K., (Modified Involute Helical Gears: Computerized Design, Simulation of Meshing, and Stress Analysis), NASA CR-2003-212229, 2003.
- M. Avinash P., Mahader P. and M. Hussain, (Analysis of Wildhaber-Novikov Circular Arc Gears), Project, R.V. Collage of Eng., Bangalore, India, 2002-2003.



EXPERIMENTAL PERSPECTIVE ASSESSMENTS FOR A PROPER REFRIGERANT ALTERNATIVE TO R-22 IN A WINDOW-TYPE AIR CONDITIONING UNIT

Ali Hussain Tarrad

Al-Mustansiriya University

College of Engineering

Mech. Eng. Department

Baghdad-Iraq

Ameera Yaseen Salim

Al-Mustansiriya University

College of Engineering

Mech. Eng. Department

Baghdad-Iraq

ABSTRACT

The present research is concerned with the future phase-out of halocarbon types of refrigerants used in the vapor compression refrigeration systems. A window-type air conditioner is selected for the tests to be conducted with two different refrigerants. It is well known that these cooling units are wide spread in their applications and are circulating **R-22** as a refrigerant. It is intended to replace this type of refrigerant by another type which is considered to be as environmental friendly refrigerant for smooth operation. The refrigerant selected for this object was **R-407C** for its favorable thermal properties and acceptable pressure and temperature ranges. The effect of replacing this refrigerant as a substitute on the performance of the cooling unit was studied. The performance characteristics comprise of cooling capacity (\dot{Q}_{evap}), power consumed by the compressor (\dot{W}_{cons}) and the coefficient of performance (**COP**) of the air conditioning unit were obtained. The results showed that the pressure ratio of the **R-407C** for a proper operation was higher than that of the **R-22** by a mean value of (13) %. The power consumed per ton of refrigeration by the unit when circulating **R-407C** was about (19) % greater than the **R-22** values for the whole range of tests. Further, the experimental work has revealed that the actual **COP** of the unit was reduced by (17) % when circulating the alternative **R-407C** for the test conditions. The results also showed that this alternative for the present refrigerant with existing cooling unit requires the attention to the mass flow rate of refrigerant circulated and the pressure and temperature ranges throughout the system.

KEY WORDS

Refrigeration, Alternatives, R-22, Window Type, Air Conditioning, R-407C

وجهة نظر لتقييم تجريبي لاستخدام مائع تثليج مناسب بديلاً لـ R-22 في وحدة تبريد هواء من النوع الشبكي

الخلاصة

يهتم البحث الحالي بالإيقاف المستقبلي لاستخدام موائع التثليج الهالوكاربونية والتي يدخل في تركيبها الكيميائي الغازات الهالوجينية في منظومات التبريد الانضغاطية. لقد تم اختيار مكيف هواء من النوع الشبكي لإجراء التجارب العملية ولمائعي تثليج مختلفين. ومن المعروف إن هذه الوحدات واسعة الانتشار بالاستخدام وتعمل بواسطة تدوير (Freon-22) كوسيط للتبريد. لقد كانت الرغبة باستخدام مائع تثليج قليل التأثير السلبي على البيئة وله القابلية على تشغيل الوحدة بصورة طبيعية. لقد وقع الاختيار على (Freon-407C) كبديل مناسب خلال البحث الحالي نظراً لما يتميز به من مواصفات حرارية مفضلة وله القابلية للعمل بمديات مقبولة من حيث درجة الحرارة والضغط. تم دراسة التأثير الناتج من استخدام هذا المائع على أداء وحدة تكييف الهواء موضوع البحث. إن دراسة الأداء لوحدة التبريد تتضمن حساب كلاً من حمل التبريد (\dot{Q}_{evap}) الطاقة المستهلكة من قبل الضاغط (\dot{W}_{comp}) ومعامل الأداء (COP).

لقد بينت النتائج لهذه الدراسة إن نسبة الضغط بين جانب الدفع والسحب للضاغط لمائع التثليج (Freon-407C) ولعمل مستقر ومناسب للوحدة كان أعلى مما عليه في حالة استخدام (Freon-22) كمائع للتثليج وبمعدل (13 %). الطاقة المستهلكة لكل طن تثليج باستخدام (Freon-407C) كانت أعلى بمقدار (19 %) من مثيلتها لحالة (Freon-22) ولكل مدى التجارب الحالية. بالإضافة لذلك فإن النتائج العملية قد بينت بأن معامل الأداء لوحدة التكييف قل بمقدار (17 %) عند تدوير (Freon-407C) عبر منظومة التبريد. كما وبينت الدراسة الحالية بأن البديل المقترح عند استخدامه في منظومات التبريد يتطلب الاهتمام بمعدل التدفق ومديات الضغط التشغيلي ودرجة الحرارة عبر المنظومة.

INTRODUCTION

For nearly sixty years, chlorofluorocarbons (CFCs), have been widely used as solvent, foam blowing agents, aerosols and specially refrigerants due to their preeminent properties such as stability, non-toxicity, non-flammability, good thermodynamic properties and so on. However, they also have some disadvantages of harmful effect on the Earth's protective ozone layer known as ozone depletion potential (ODP). Subsequently, it was discovered that (CFCs) also contributed significantly to the global warming potential (GWP). The reputation, reliability and maintainability of equipment normally improves with age, but this has not been true when it comes to refrigeration field. The (1990) Clean Air Act amendments imposed new regulations with landmark dates that industry was unable to meet. So stop gap solutions and lack of time to do research and development have resulted in a lack of standards and poor information.

The direct replacement of **R-12** with the pure refrigerant **R-134a** has been experienced much earlier and an excellent knowledge has been performed in the retrofit for the old machines. The phase out of **R-22** as working medium in refrigerating equipments and heat pumps began in the late of 1990s with terminating of their new installation and manufacturing throughout Europe. The new working fluids for the alternative of **R-22** are zeotropic refrigerants introducing further difficulties for the prediction of the cooling unit characteristics behavior during smooth operation.

The most attractive thermal properties of refrigerant that have significant effect on the performance of the vapor compression refrigeration system are the critical temperature and the

molar heat capacity as pointed out by (McLinden, 1987) and (Domanski, 1999). (Meurer et al., 1999) compared the performance of *R-22* and *R-410A* for elevated condensing temperature up to (60) °C. They have found that the variation of the (*COP*) of the system depends on the level of the condensing operating temperature of the refrigerant circulated. (Lee et al., 2000) investigated the performance of mixture refrigerants alternatives for the *R-22*. They compared the coefficient of performance, *COP*, the volumetric capacity of refrigeration, *VCR* and capacity for the alternatives *R-407C* and *R-410A* with those of *R-22*. Their results showed that *R-410A* exhibited very close *COP* to that of the *R-22* within (3%) for the same pressure ratio. *R-407C* gave lower *COP* than that of the *R-22* by (9%). Motta and (Domanski, 2000) simulated a number of binary and ternary mixtures as alternatives for the use of *R-22* when working in elevated outdoor temperatures. Their results showed that fluids with a low critical temperature experience a large degradation of cooling capacity, while rate of compressor power increase is similar for all fluids. Johansson and (Lundqvist, 2003) presented a qualitative and quantitative literature survey for the alternatives for *R-12* and *R-22* used in Sweden refrigeration industry.

Other trend of investigations was devoted to study the effect of replacing the alternatives on the working components of the existing system. For this category, the reader is referred to the work published by (Kuelh, 1987), (Kim, 1993), (Wolf et al., 1995), (Sami and coworkers, 1998 and 2000). (Sami et al., 2005) studied the use of *R-407C*, *R-410A* and *R-410B* in addition to the *R-22* for a good range of pressure and mass flow rate for three different sizes of capillary tubes. Their results showed that the pressure drop across the capillary tube is significantly influenced by the diameter of the capillary tube and the entering refrigerant conditions. Further, the pressure drop decreases with the increase of the capillary diameter and that alternatives in general experience higher pressure drop than that of *R-22*.

EXPERIMENTAL APPARATUS:

The test apparatus selected for this project was a two refrigeration tons window-type air conditioner cooling unit manufactured by (*LG*) commercial company. The overall physical external dimensions of the cooling unit are (62 × 72 × 41) cm, (*LG Company Manual, 1999*). The overall dimensions and characteristic specification of the evaporator and condenser are shown in **Table 1**. The air conditioner is using a capillary tube as expansion component made of copper tubing having four equally length paths of refrigerant with a geometrical dimensions of diameter of (3) mm and length of (80) cm each. A typical tube circuiting for the refrigerant circulating path through the evaporator and condenser for a window type air conditioner is shown in **Fig. 1**. The tube layout arrangement for the test evaporator and condenser of the air conditioning unit is shown in **Fig. 2**.

The experimental rig is shown schematically in **Fig. 3**. Two (6) mm stainless steel sheath thermocouples of (*J*) type are installed at the entering and leaving sides of the capillary tube. These temperature sensors are used to measure the temperature at the exit and inlet lines of the evaporator and condenser refrigerant paths respectively. The temperatures at the suction and discharge sides of the compressor were measured by fixing a temperature sensor at the pipe surface delivering the refrigerant. The pressure throughout the air conditioner was measured by the application of two pressure gauges in the range of (-1 to 18) bar for the low side and (-1 to 38) bar for the high pressure side. These gauges were installed at the inlet and exit sides of the all of the components of

A. H. Tarrad	Experimental Perspective Assessments for a Proper
A.Y. Salim	Refrigerant Alternative to R-22 in a Window-Type
	Air Conditioning Unit

the cooling unit. The manufacturer equipped the air conditioner unit with a single reciprocating compressor.

In the present work, the pressure drop of the refrigerant flowing through the evaporator and condenser heat exchangers were also considered. The air side measurements were only conducted for the dry and wet bulb temperatures at the inlet and exit sides of both heat exchangers. The air dry bulb temperatures were measured by using a digital thermometer of the (*K*) type and the wet bulb values measured using the wet cotton wick at the bulb of a mercury glass thermometer. The thermocouples for the temperature measurements were calibrated against a mercury glass thermometer and showed an accuracy of about (0.1%). Further, the refrigerant side pressure gauges were also calibrated and exhibited an accuracy of about (0.2%).

TEST PROCEDURE:

On commencing of the tests, the air conditioner was allowed to operate for at least (10) minutes, which is the time required to approach the steady state conditions. The steady state was considered to be established when the temperature and pressure all around the cooling unit to be stable with time. This was achieved by the reading indications of the temperature sensors and pressure gauges for the refrigerant circulated. After that establishments, the temperature and pressure measurements were recorded all around the selected ports in the cooling unit. The data was collected for different operating conditions to assure the reproducibility of the measurements and to detect any variation in the environment effects. These tests were carried out for different ambient conditions concerning the air dry bulb and wet bulb temperatures. This was done to show the effect of ambient condition variation on the performance of the air conditioning unit.

After, finishing the tests with ***R-22***, the unit was discharged, cleaned, evacuated, and kept under (2) bar vacuum followed by recharging with the suggested alternative ***R-407C***. The proper amount of refrigerant required for circulation was limited by the allowable pressure of the cooling unit. Since, the alternative is assumed to work with the same heat exchangers and compressor, then the allowed volumetric flow rate of refrigerant that passing through the unit will be limited by that of the ***R-22*** value. This refrigerant amount was limited by the suction pressure of the compressor corresponds to a value close to (70) psig. The expansion component of the cooling unit comprises of copper capillary tube was used with the same length and inner diameter.

DATA REDUCTION

The measured operating conditions were used for the prediction of the air conditioner performance including the power consumed, refrigerating effect and condenser load calculated per unit mass of refrigerant for both tested refrigerants. Further the measure for the performance characteristics, the ***COP*** was predicted from the above parameters. The refrigerant thermal properties for both fluids were obtained from the published tables presented by (***ASHRAE Handbook, 1997***).

The refrigerating effect achieved by the cooling unit through the evaporator can be expressed as:

$$\dot{q}_{evap} = h_1 - h_4 \quad (1)$$

The amount of the *R-22* refrigerant circulated through the air conditioner was obtained from the known cooling capacity of the unit in the form:

$$\dot{m}_r = \frac{\dot{Q}_{evap}}{\dot{q}_{evap}} \quad (2)$$

Where

$$\dot{Q}_{evap} = \dot{m}_{air} (h_{ai} - h_{ao}) \quad (3)$$

Equation (2) was also used to predict the *R-407C* refrigerant mass flow rate circulated through the unit. The volumetric flow rate of air circulated through the cooling coil, evaporator is the same as that of the *R-22* circulating case.

It is worthwhile to mention here that the air conditioner capacity is not necessary to have the same value as that of the manufacturer for *R-22*. However, the air mass flow rate passing through the evaporator and condenser coils are still constants and having the same values as those provided for the *R-22* case. The manufacturer manual reveals that the maximum indoor and outdoor circulating air rates are (12) m³/min and (26) m³/min respectively.

The work rate done by the reciprocating compressor may be estimated per unit mass of refrigerant from:

$$\dot{w}_{comp} = (h_2 - h_1) \quad (4)$$

The air conditioner condenser load is estimated by:

$$\dot{q}_{cond} = (h_2 - h_3) \quad (5)$$

At the exit of the condenser, the liquid enthalpy was calculated from the knowledge of the pressure and temperature as measured during the experiments. This liquid may be at sub-cooled condition depending on the measured condition. The enthalpy of the refrigerant mixture leaving the capillary tube was considered to be equal to that of the entering liquid to capillary tube. Here, the process was assumed to be isenthalpic through the capillary tube as deduced from the first law of thermodynamics.

Finally, the coefficient of performance of the cooling unit was obtained from:

$$COP = \frac{\dot{q}_{evap}}{\dot{w}_{comp}} \quad (6)$$

For the purpose of comparison between the refrigerants performance used in the present work a new parameter is suggested to be used having the expression:

$$WRR = \frac{(\dot{w}_{comp})_{R-407C}}{(\dot{w}_{comp})_{R-22}} \quad (7)$$

This parameter represents the ratio of the work rate between the alternative **R-407C** and the original circulating refrigerant **R-22**. The parameters predicted from eq. (7) are to be based on the physical values required per ton of refrigeration. Another parameter can be defined for the **COP** comparison, that is the coefficient of performance ratio, **COPR**. This represents the ratio of **COP** of the **R-407C** to that of the **R-22** in the form:

$$COPR = \frac{COP_{R-407C}}{COP_{R-22}} \quad (8)$$

This expression may be estimated for both of the isentropic compression and actual cycles.

EXPERIMENTAL RESULTS AND DISCUSSION:

It is of the beneficial object to highlight some important aspects of the present work in this category. The following points should be considered:

- i- The same air conditioner was used which means that the heat exchangers and compressor capacities are limited to those of the **R-22** case. This will limit the heat transfer area, pressure ratio and power consumed for the alternative to those available of the existing equipments.
- ii- The tube circuiting for the evaporator and condenser were unaltered. Therefore, the thermal characteristic parameter, (**UA**), is limited to that of the **R-22** refrigerant condition. In other words, the **R-22** characteristic value will be the controller of the operation for the alternative performance.

The above will impose some restrictions for the allowable mass flow rate of the alternative refrigerant **R-407C** circulating through the air conditioning unit and operating conditions. The pressure ratio of the compressor and its volumetric displacement are the controller for the charging amount of the refrigerant **R-407C**. Further, the physical geometry of the available heat exchangers control the heat transfer rate through the air conditioner.

A typical measured results of the tests conducted during the circulation of **R-22** and **R-407C** are shown in **Tables 2** and **3** respectively. The data presented in these tables show the temperature and pressure measurements at the selected points through the cooling unit. The final results for the tests when circulating the refrigerants **R-22** and **R-407C** are shown in **Tables 4** and **5** respectively for the test conditions considered in the present study. In these tables the followings were considered to exist:

- a- The (**IMPC**) represents the cycle in which the suction and discharge pressures were considered to be the mean value at the entering and leaving sides of the evaporator and condenser respectively. The condenser load and the compression work rate were calculated for the case of the isentropic compression for the refrigerant.
- b- The (**AMPC**) represents the cycle at which the calculation of the performance was based on the actual measured pressure for all of the selected ports throughout the cycle.

The actual and isentropic (p - h) diagrams for the **R-22** and **R-407C** circulating refrigerants are shown in **Fig. 4**. Here, the dotted lines represents the isentropic mean pressure cycle (**IMPC**), whereas the solid lines express the actual measured pressures cycle (**AMPC**). The actual measured air side conditions for both of the evaporator and condenser of the cooling unit obtained during the tests are shown schematically on the psychrometric chart in **Fig. 5**. All the performance assessment of the present work was based on a (12) m³/min of indoor air circulation, (**LG Company Manual, 1999**).

REFRIGERANT R-22 TESTS:

It is clear that the actual apparent compression of the compressor is lower than that of the isentropic value due to the friction losses and heat losses during the operation of the compression process. The final results for the actual measured data obtained for the cycle ($abcd$), **Fig. 4.a**, are shown in **Table 4.b**. In this table, the power consumption, \dot{W}_{cons} , during the operation of the unit was estimated from the measured values of the current and voltage of the power supply. During the steady state conditions, the current was ranged between (11.2) and (11.4) amperes while the voltage was almost constant at (220) volts.

$$\dot{W}_{cons} = I \times V \times \cos \varphi \quad (9)$$

In which the power factor ($\cos \varphi$) was assumed to be (0.94) according to the manufacturer manual.

The isentropic compression through the compressor is higher than that of the actual compression for all of the tests conducted in the present work. The ratio of the actual to that of the isentropic compression, \dot{W}_{ratio} , expressed mathematically as:

$$\dot{W}_{ratio} = \frac{\dot{W}_{meas}}{\dot{W}_{cs}} \quad (10.a)$$

is ranged between (69) and (91) % for the whole range of the test conditions as shown in **Table 4.b**. The efficiency of the actual compression is defined as:

$$\eta_{ca} = \frac{\dot{W}_{meas}}{\dot{W}_{cons}} \quad (10.b)$$

This parameter shows the ability of the unit to make advantage of the power input to the compressor. This parameter revealed that the actual useful work of the unit was ranged between (41) and (52) %. These values were lower than those of the isentropic compression where (η_{cs}) was ranged between (53) and (65) %. Clearly, this was due to the irreversibility of the compression process where it has a deviation from the ideal behavior.

The measured pressure ratios (p_r) of **R-22** tests were ranged between (3.73) and (3.84) as shown in **Table 2.a** and the **COP** of the cooling unit was ranged between (3.8) and (4.3) when the calculation based on the (**IMPC**) mode, **Table 4.a**. The corresponding actual values based on the consumed power (**AMPC**) was ranged between (2.2) and (2.5), **Table 4.b**, as estimated from:

$$COP_{cons} = \frac{Q_{evap}}{\dot{W}_{cons}} \quad (10.c)$$

A. H. Tarrad	Experimental Perspective Assessments for a Proper
A.Y. Salim	Refrigerant Alternative to R-22 in a Window-Type
	Air Conditioning Unit

It is obvious that the (*IMPC*) has higher coefficient of performance than that of the (*AMPC*) for the whole range of the test conditions to be within the range of (36-47) %. This reveals that the actual compression operating process follows a path different from that of the constant entropy process on the (*p-h*) diagram. Further, the useful work for compression in the latter mode of calculation was lower than that of the former mode which represents the expected behavior for the irreversible process mode through the compressor.

The measured parameters for the air side of test number (1) are shown schematically on the psychrometric chart in **Fig. 5.a**. Here, the process throughout the evaporator exhibited almost a straight horizontal line revealing a major part of the cooling load to be a sensible heat only, process line no. (2). As the usual operation process through the condenser in which it exhibits a sensible load only, line no. (2) represents the air side process on the psychrometric of test no. (1).

Fig. 6 shows the (*IMPC*) and (*AMPC*) performance variables variation with the cooling unit capacity. These variables include, the power consumption per ton of refrigeration, *COP*, condenser load, power consumed and the calculated work rate of the compressor. The last column of **Table 4** represents the estimated condenser air flow rate for both of the modes of calculations. It is obvious that the actual required air flow rate for (*AMPC*), **Table 4.b**, was higher than that of the ideal (*IMPC*) cycle, **Table 4.a**, by a range of (10-15) %. This was due to the increasing load required for the condenser as a result of the higher power required to run the compression unit.

Refrigerant R-407C Tests:

All of the above parameters were calculated for the alternative refrigerant *R-407C* applying the same relations and modes of the considered category of the estimation procedure. The (*p-h*) diagram of both of the (*IMPC*) and the (*AMPC*) results are shown in **Fig. 4.b** for test number (1) presented in **Table 3.a** for the refrigerant side of the cycle. The air side processes are presented schematically on the psychrometric chart in **Fig. 5.b** for both of the evaporator and condenser heat exchanger sides of test no. (1).

For all of the tested pressure ratio conducted using this refrigerant, the isentropic useful work was higher than that of the actual compression due to the irreversibility of the compression process. The (η_{ca}) values were ranged between (44) % and (55) %, **Table 5.a**, whereas, the corresponding values of the (η_{cs}) were within the range of (47 - 56) %, **Table 5.b**. The isentropic coefficient of the performance exhibited a range of (3.8 – 3.9) with a mean value of (3.86). The corresponding values for the actual cycle (*AMPC*) were in the range of (1.60) to (2.16) having a mean value of (1.79) which lower than that of the (*IMPC*) by (53) %. The trend of the data showed almost constant power consumption for the tested cooling load capacity in this work, **Fig. 7.a**. The actual *COP* showed an increase when the cooling unit load was increased, **Fig. 7.b**. It was observed that the power consumption per ton increases with load reduction. This was also noticed during the tests when circulating *R-22* as shown in **Table 4.b**.



RESULTS ASSESSMENT:

For the purpose of comparison of the results, **Table 6** was prepared for the ratios presented in eqs. (7 & 8) for the (*AMPC*) and the (*IMPC*) cycles. These results based on a mean values of the predicted variables of **Tables 4 & 5**. It is useful to construct the following argument about the experimental assessments of the present work:

- i- The data showed that the coefficient of performance of the *R-407C* refrigerant was lower than that of the *R-22* results for both modes of calculations. Moreover, the *COPR* was ranged between (0.94) and (0.83) for the (*IMPC*) and (*AMPC*) modes respectively. This means that the *COP* of the unit was lower for the *R-407C* than that of the *R-22* circulating refrigerant.
- ii- Accordingly, the power consumed per ton of refrigeration, WRR_{cons} , for the *R-407C* was higher than that of the *R-22* by (19) % although the useful work rate of the latter was lower than that of the former by (5) %. This is partly due to the higher working pressure range of the *R-407C* than that of the *R-22* during the steady state conditions, **Table 6**.
- iii- For all tests of both refrigerants, the air mass flow rate for the (*IMPC*) and (*AMPC*) modes to pass through the condenser showed an increase with cooling capacity of the unit due to the increase of the condenser load.
- iv- The circulated refrigerant per ton of refrigeration for the *R-407C* refrigerant was in the range between (81-88) kg/hr. This was greater than that of the *R-22* case which has the range of (79 – 82) kg/hr. This is related to the physical properties of both refrigerants and essentially is not dependent on the operating pressure ratios.
- v- The experimental data shown in **Tables 4 and 5** reveals that the work rate ratios (\dot{W}_{ratio}) for the *R-407C* tests were higher than those of the *R-22* results. In other words, the calculated useful work rate (\dot{W}_{meas}) was closer to the isentropic (\dot{W}_{cs}) condition for *R-407C* than that of the *R-22* circulating case.

CONCLUSIONS:

The experimental work conducted in the present work revealed the following findings:

- i- The suggested alternative refrigerant *R-407C* is one of the promising substitute for the *R-22* in the air conditioning cooling systems. This object can be targeted without a major alteration in the geometrical and physical dimensions of the existing unit.
- ii- Higher pressure ratio has been experienced during this work for the *R-407C* than that of the present circulating refrigerant *R-22* for the object of system operation with the existing geometrical cooling unit design.
- iii- The power consumed per ton of refrigeration was higher for the present alternative than that of the *R-22* by about (19) % calculated as a ratio of power consumed with respect to the base refrigerant *R-22*..
- iv- The above was accompanied by a reduction of the actual *COP* of the air conditioning unit by (17) % and an increase in the circulated mass flow rate of refrigerant per ton.

A. H. Tarrad	Experimental Perspective Assessments for a Proper
A.Y. Salim	Refrigerant Alternative to R-22 in a Window-Type
	Air Conditioning Unit

- v- The assessment formulated in the present work recommends to use **R-407C** as a direct alternative for the refrigerant **R-22** in this type of air conditioning equipments.

ACKNOWLEDGEMENT:

The authors would like to express their sincere thanks to Mr. Wahhab Abdul-Razzak for his valuable participation in the workshop work for the preparing of the experimental rig.

REFERENCES:

- **ASHRAE Refrigeration Handbook**, (1997), American Society of Heating, Refrigerating, and Air Conditioning Engineers, Chapter 19.
- **Domanski, P. A. and Didion, D. A.**, (1993), NIST Report prepared for ARTI.
- **Johansson, A. and Lundqvist, P.**, (2003), "Replacement of R-22 in Existing Installations: Experiences from the Swedish Phase Out", Royal Institute of Technology, Department of Energy Technology, Stockholm, Sweden.
- **Kim, R. H.**, (1993), "A Numerical Analysis of a Capillary tube Expansion Valve in a Vapor Compression Refrigeration System with Alternative Refrigerants", ASME 1993, HTD-Vol. 243, Heat Transfer with Alternate Refrigerants.
- **Kuelh, S.**, (1987), "Study, Validation and Improvement of a Model for Sizing a Capillary Tube for an Air Conditioning/Heat Pump System", M.S.M.E. Thesis, Purdue University.
- **Lee, B. J., Park, J. Y., Kim, J. D. and Lim, J. S.**, (2000), "A Study on the Performance of Alternative Refrigerant Mixtures for HCFC-22", Korea Institute of Science and Technology (KIST), Seoul, South Korea.
- **McLinden, M. and Radermacher, R.**, (1987), Int. J. Refrg., Vol. 10, pp. 318.
- **Meurer, C., Buyle, O. and Paulus-Lanckrier, M.**, (1999), "Comparison of R-22 and R-410A at elevated Condensing Temperatures", 20th International Congress of Refrigeration, IIR/IIF, Sydney.
- **Motta, S. F. Y. and Domanski, P. A.**, July (2000), "Performance of R-22 and its Alternatives Working at High Outdoor Temperatures", Eighth International Refrigeration Conference, Purdue University, West Lafayette, IN, USA, pp. 47-54.
- **Sami, S. M. and Maltais, H.**, (2000), "Experimental Analysis of Capillary Tube Behavior with some HCFC-22 Alternative Refrigerants", Int. J. Energy Research.
- **Sami, S. M., Maltais, H. and Desjardins, D. E.**, (2005), "Influence of Geometrical Parameters on Capillary Behavior with New Alternative", Int. J. Energy Research.



- **Sami, S. M. and Tribes, C.**, (1998), "Numerical Prediction of Capillary Tube Behavior with Pure and Binary Alternative Refrigerants", Jl. Of Applied Thermal Engineering, Vol. 18, No. 6, pp. 491-502.
- **Technical Guide Book I**, (1999), LG Air conditioner, LG Electronics Inc.
- **Wolf, D. A., et al.**, (1995), " Adiabatic Capillary Tube Performance with Alternative Refrigerants", ASHRAE Research Project RP-762.

NOMENCLATURE:

COP : Coefficient of Performance defined by eq.(7)

COPR : Coefficient of Performance Ratio

h : Enthalpy, (kJ/kg)

\dot{m} : Mass Flow Rate, (kg/s)

p : Pressure, (bar)

p_r : Pressure Ratio

P : Work rate per ton of refrigeration, (kW/TR)

\dot{Q} : Heat Transfer Rate, (kW)

\dot{q} : Heat Transfer per Unit Mass, (kJ/kg)

T : Temperature, (°C or K)

WRR: Work Rate Ratio

\dot{W} : Work Rate, (kW)

Greek Letters:

Δp : Pressure Difference, (bar)

η : Efficiency

Subscript:

a : Air

ca : Actual Compression Value

cond : Condenser

comp : Compressor

cons : Consumed Value

cs : Isentropic Compression Value

d : Dry Bulb

evap : Evaporator

i : Inlet

o : Outlet Value

r : Refrigerant

w : Wet Bulb

A. H. Tarrad	Experimental Perspective Assessments for a Proper
A.Y. Salim	Refrigerant Alternative to R-22 in a Window-Type
	Air Conditioning Unit

Table (1): The Characteristic Physical Dimensions of the Evaporator and Condenser Geometry.

Dimension specification	Evaporator	Condenser
Tube Length (mm)	390	570
Inner Tube Diameter (mm)	7.93	6.34
Outer Tube Diameter (mm)	9.52	7.94
Transverse Tube Pitch (mm)	19.25	17.32
Longitudinal Tube Pitch (mm)	28	20
Number of Tube Circuits	4	3
Number of Tubes per Circuit	11	23
Total Number of Tubes	44	76
Number of Tube Rows	3	4
Tube Metal	Copper	Copper
Tube Metal Thermal Conductivity (W/m.K)	386	386
Inner Tube Surface	Smooth	Smooth
Fin Thickness (mm)	0.2	0.2
Fin Pitch (mm)	1.5	1.5
Number of Fins per Inch (FPI)	17	17
Fin Type	Flat Plate	Flat Plate
Fin Metal	Aluminum	Aluminum
Fin Thermal Conductivity (W/m.K)	202	202

Table (2): Experimental Data of Air Conditioning Unit Circulating R-22.

Table (2.a): Refrigerant Side Measured Operating Conditions.

Test No.	Δp_{cond} (bar)	Δp_{evap} (bar)	P_1 bara	P_2 Bara	P_3 bara	P_4 bara	T_1 (°C)	T_2 (°C)	T_3 (°C)	T_4 (°C)	p_r (---)
1	0.3	0.1	5.71	22.51	21.81	5.81	10.0	81.0	43.6	9.0	3.846
2	0.7	0.3	5.71	22.71	22.01	6.01	11.0	82.0	42.0	8.5	3.814
3	0.7	0.1	5.61	21.51	20.81	5.71	9.0	82.0	42.0	9.0	3.737
4	0.8	0.1	5.51	21.31	20.51	5.61	9.0	81.0	42	9.0	3.76

**Table (2.b): Air Side Measured Operating Conditions.**

Test No.	Heat Exchanger Type	T _{di} (°C)	T _{wi} (°C)	T _{do} (°C)	T _{wo} (°C)
1	Evaporator	30.8	16	9.3	5.8
	Condenser	35.2	22	58.5	28
2	Evaporator	31.2	18	10.2	9.0
	Condenser	34.5	22	60.0	28.5
3	Evaporator	29.7	15	8.2	5.5
	Condenser	31.8	25	52.2	30
4	Evaporator	28.2	14	8	5.0
	Condenser	32.4	18	57.4	25
5	Evaporator				
	Condenser				

Table (3): Experimental Data of Air Conditioning Unit Circulating R-407C.**Table (3.a): Refrigerant Side Measured Operating Conditions.**

Test No.	Δp_{cond} (bar)	Δp_{evap} (bar)	P ₁ bara	P ₂ bara	P ₃ Bara	P ₄ bara	T ₁ (°C)	T ₂ (°C)	T ₃ (°C)	T ₄ (°C)	p _r (---)
1	0.3	0.1	5.51	24.31	24.01	5.61	18.0	89	45	9.7	4.34
2	0.5	0.1	5.21	23.51	23.01	5.31	16	89	49	12	4.42
3	0.5	0.2	5.31	24.01	23.51	5.51	15	90	50	12	4.31
4	0.6	0.15	5.66	25.11	24.51	5.81	15.6	89	53	11	4.32

A. H. Tarrad	Experimental Perspective Assessments for a Proper
A.Y. Salim	Refrigerant Alternative to R-22 in a Window-Type
	Air Conditioning Unit

Table (3.b): Air Side Measured Operating Conditions.

Test No.	Heat Exchanger Type	T _{di} (°C)	T _{wi} (°C)	T _{do} (°C)	T _{wo} (°C)
1	Evaporator	25.0	13	6.6	5.0
	Condenser	30.6	16	54.6	23.5
2	Evaporator	25	12	6	3.0
	Condenser	28	16	54	24
3	Evaporator	26	13	6	3.0
	Condenser	29	16	55	24
4	Evaporator	26	13	6.1	3.0
	Condenser	32	17	57	24.5

Table (4.a): The Performance Criteria of (IMPC) Mode Circulating R-22.

Test No.	\dot{Q}_{evap} (kW)	\dot{W}_{cs} (kW)	\dot{Q}_{cond} (kW)	COP _s (----)	\dot{m}_r (kg/h)	\dot{W}_{cons} (kW)	P_s (Kw/TR)	η_{cs} (%)	\dot{m}_{acs} (kg/h)
1	5.796	1.533	7.330	3.84	134.6	2.358	0.930	65.0	1082
2	5.520	1.314	6.834	4.20	124.5	2.316	0.837	56.7	846.1
3	5.324	1.226	6.55	4.34	119.32	2.296	0.810	53.4	1126
4	4.913	1.231	6.144	3.99	110.8	2.275	0.881	54.1	864.6

**Table (4.b): The Performance Criteria of (AMPC) Mode Circulating R-22.**

Test No.	\dot{Q}_{evap} (kW)	\dot{W}_{cons} (kW)	\dot{Q}_{cond} (kW)	COP_{cons} (----)	\dot{W}_{meas} (kW)	\dot{W}_{ratio} (%)	P_{cons} (kW/TR)	\dot{m}_r (kg/h)	η_{ca} (%)	\dot{m}_{ac} (kg/h)
1	5.796	2.358	8.154	2.460	1.060	69.1	1.408	131.64	45.0	1203.2
2	5.520	2.316	7.840	2.383	1.195	91.0	1.475	123.6	51.6	971.6
3	5.324	2.296	7.620	2.319	1.041	85.0	1.516	119.0	45.4	1310.4
4	4.913	2.275	7.188	2.160	0.936	76.0	1.628	110.45	41.1	1012.0

Table (5.a): The Performance Criteria of (IMPC) Mode Circulating R-407C.

Test No.	\dot{Q}_{evap} (kW)	\dot{W}_{cs} (kW)	\dot{Q}_{cond} (kW)	COP_s (----)	\dot{m}_r (kg/h)	\dot{W}_{cons} (kW)	P_s (kW/TR)	η_{cs} (%)	\dot{m}_{acs} (kg/h)
1	4.235	1.111	5.346	3.811	97.57	2.378	0.922	46.7	740.2
2	4.471	1.141	5.61	3.92	105.3	2.399	0.898	47.6	734.4
3	5.17	1.352	6.523	3.823	124.83	2.399	0.920	56.4	869.7
4	5.20	1.337	6.583	3.890	130.1	2.440	0.903	54.8	923

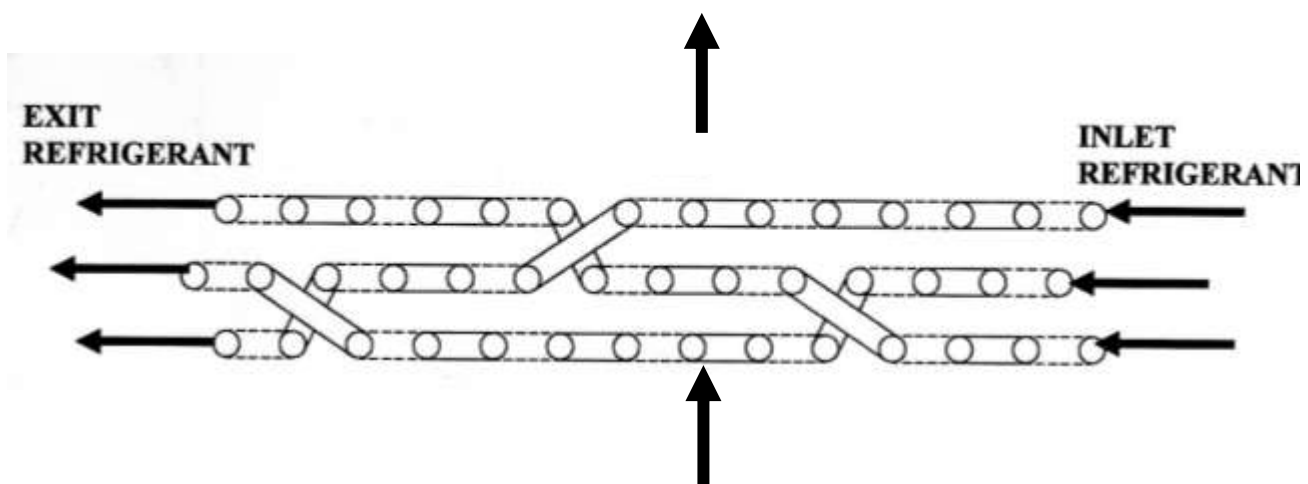
Table (5.b): The Performance Criteria of (AMPC) Mode Circulating R-407C.

Test No.	\dot{Q}_{evap} (kW)	\dot{W}_{cons} (kW)	\dot{Q}_{cond} (kW)	COP_{cons} (----)	\dot{W}_{meas} (kW)	\dot{W}_{ratio} (%)	P_{cons} (kW/TR)	\dot{m}_r (kg/h)	η_{ca} (%)	\dot{m}_{ac} (kg/h)
1	4.235	2.378	6.613	1.580	1.051	94.6	1.973	97.50	44.2	915.7
2	4.471	2.399	6.870	1.864	1.063	93.2	1.889	104.8	44.3	899.3
3	5.17	2.399	7.570	2.160	1.310	97.0	1.631	124.7	54.6	1009.3
4	5.20	2.44	7.640	2.131	1.147	85.8	1.649	129.9	47.0	1078.6

Table (6): A Comparison for the Work Rate and (*COP*) Ratios of *R-22* and *R-407C*.

Refrigerant Type	p_r (----	$COPR_s$ (----	$COPR_{cons}$ (----	WRR_s (----	WRR_{cons} (-----)
<i>R-22</i>	3.73 ---3.84	1.00	1.00	1.00	1.00
<i>R-407C</i>	4.31--- 4.42	0.94	0.830	1.05	1.19

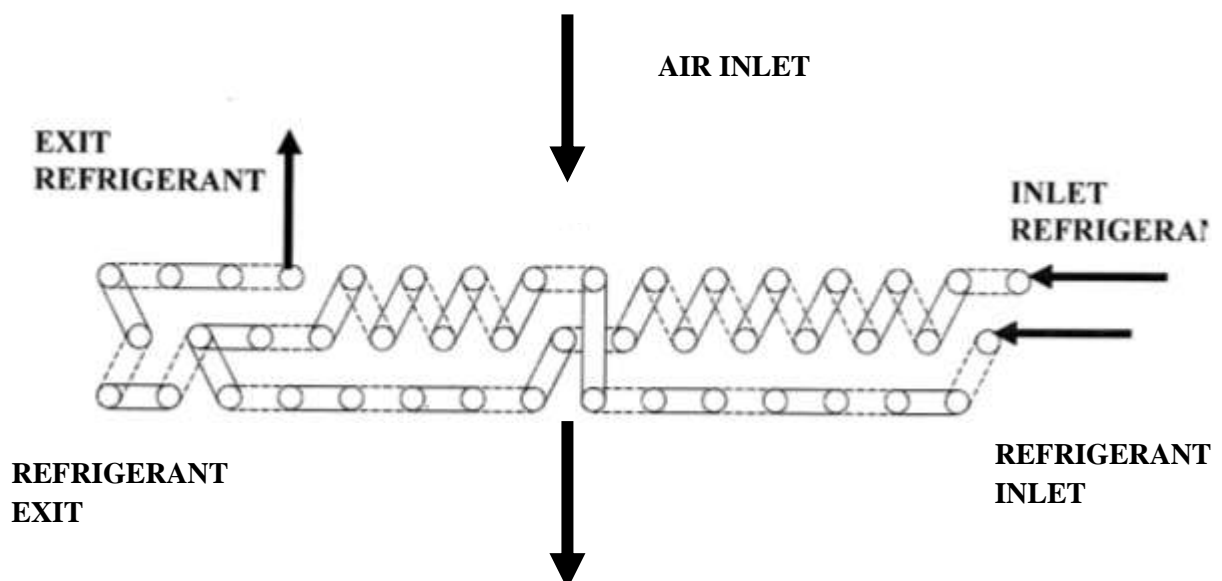
AIR EXIT



(1.a): Evaporator Tube Circuiting

Inlet Air

AIR INLET



(1.b): Condenser Tube Circuiting

Exit Air

Figure (1): A Typical Heat Exchangers Tube Circuiting of an Air Conditioner.

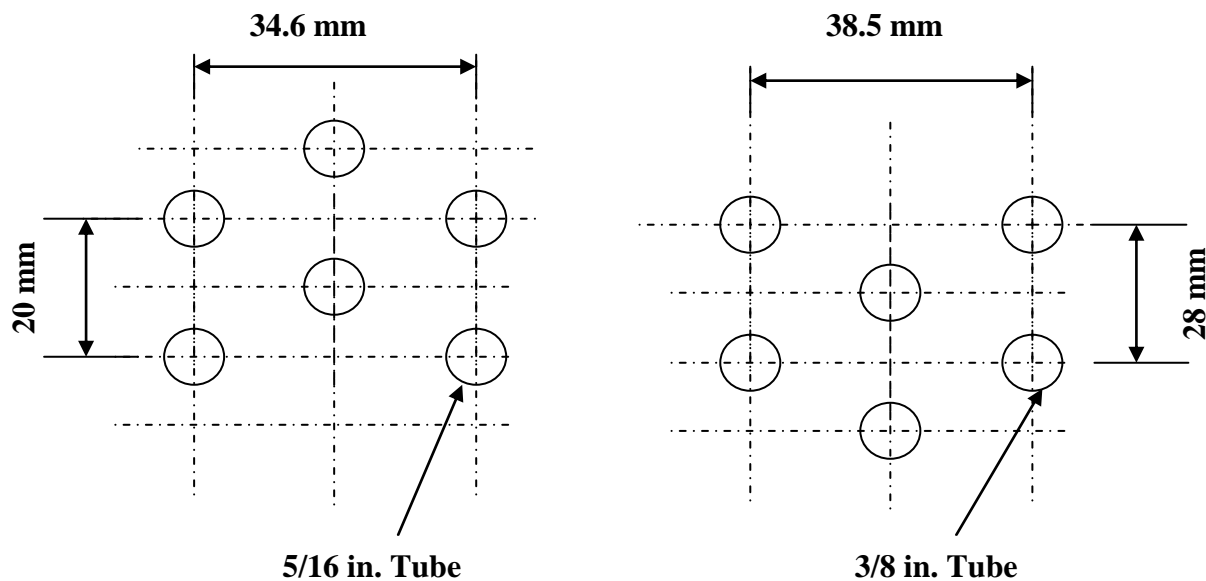


Figure (2.a): Condenser Tube Arrangement Figure (2.b): Evaporator Tube Arrangement

Figure (2): The Tube Layout Arrangement of the Test Air Conditioner.

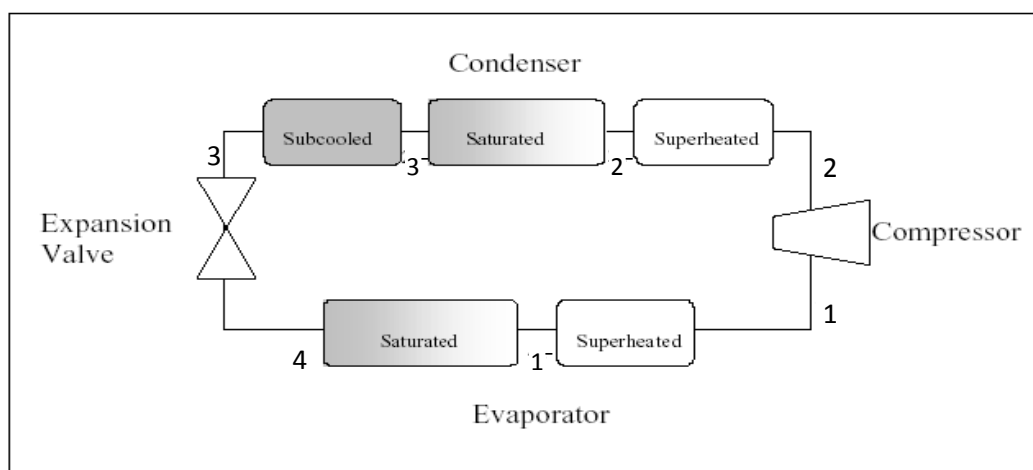


Figure (3.a): A Schematic Diagram for a Vapor Compression Refrigeration System.

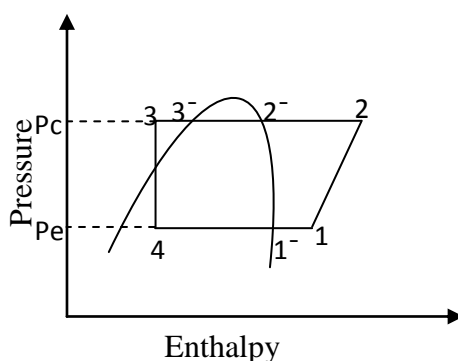
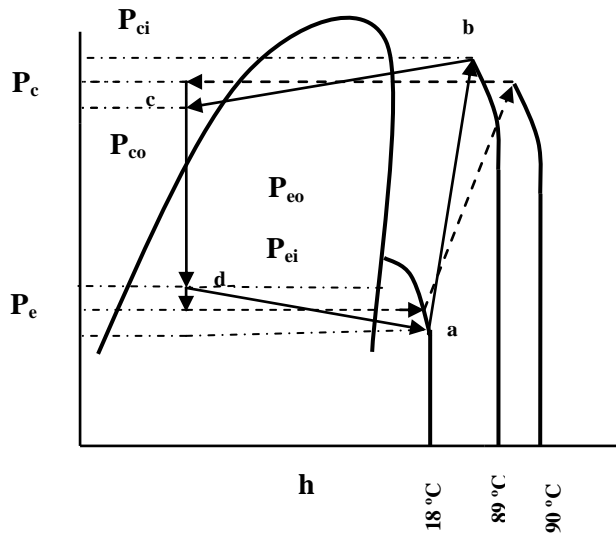
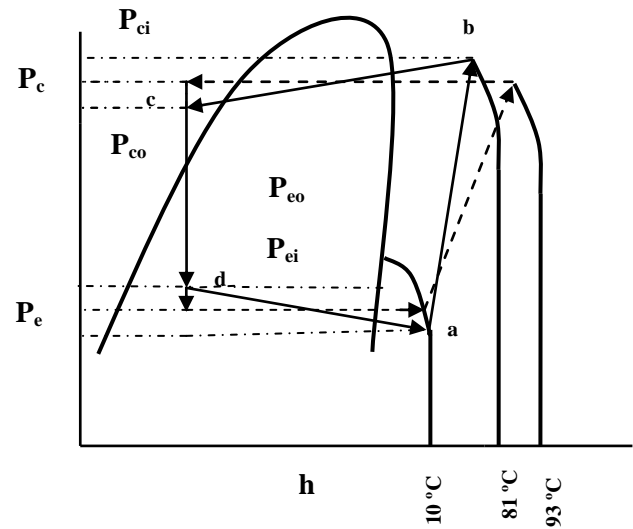
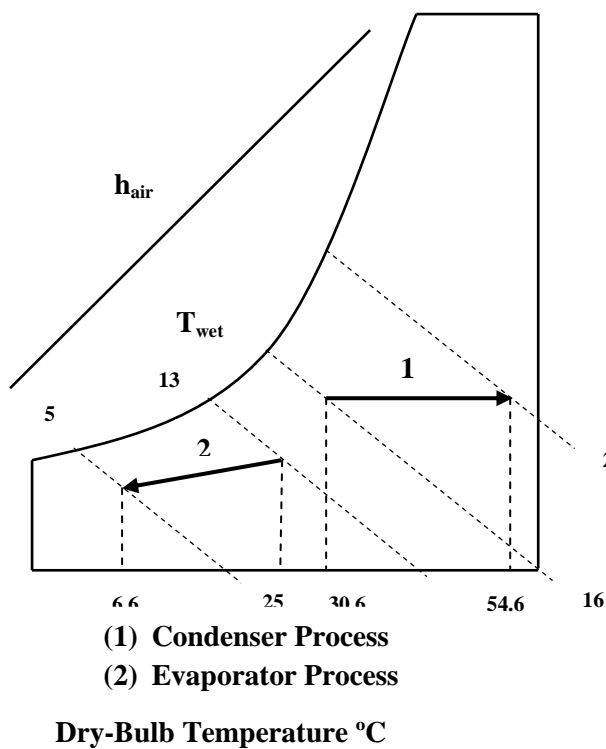
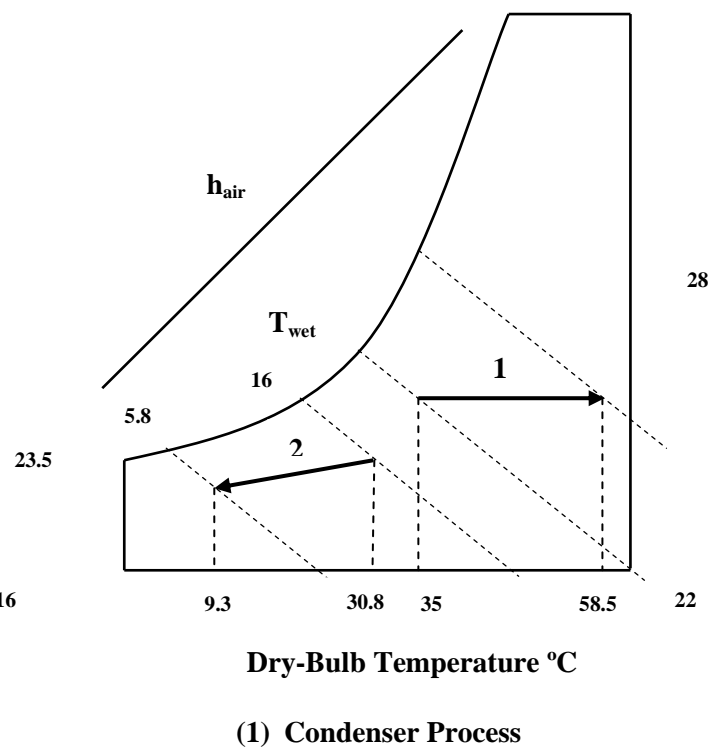


Figure (3.b): A Standard Vapor Compression Cycle Considering Superheating and Sub-cooling.

Figure (4.b): Test Number (1) for *R-407C*Figure (4.a): Test Number (1) for *R-22*Figure (4): A Typical (p-h) Diagram of the *R-22* and *R-407C* Refrigerants Tests.Figure (5.b) Test No. (1), *R-407C*Figure (5.a) Test No. (1), *R-22*Figure (5): A Typical Psychrometric Process Chart of the *R-22* and *R-407C* Refrigerants Tests.

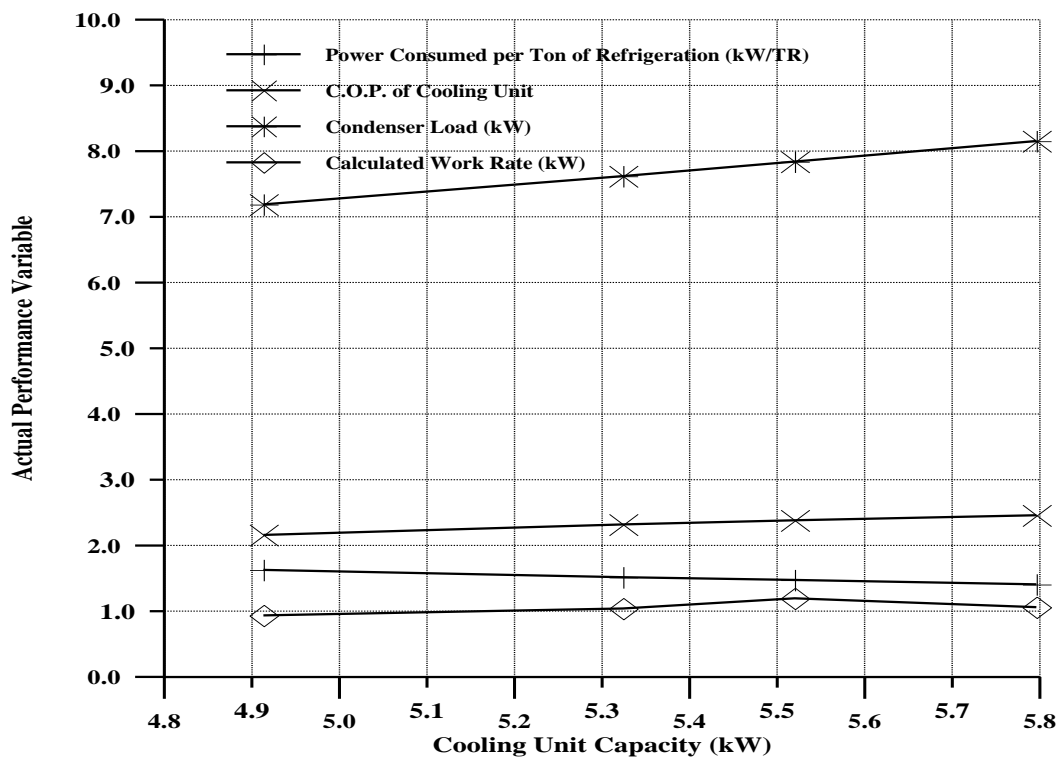


Figure (6.a): IMPC Cycle, R-22.

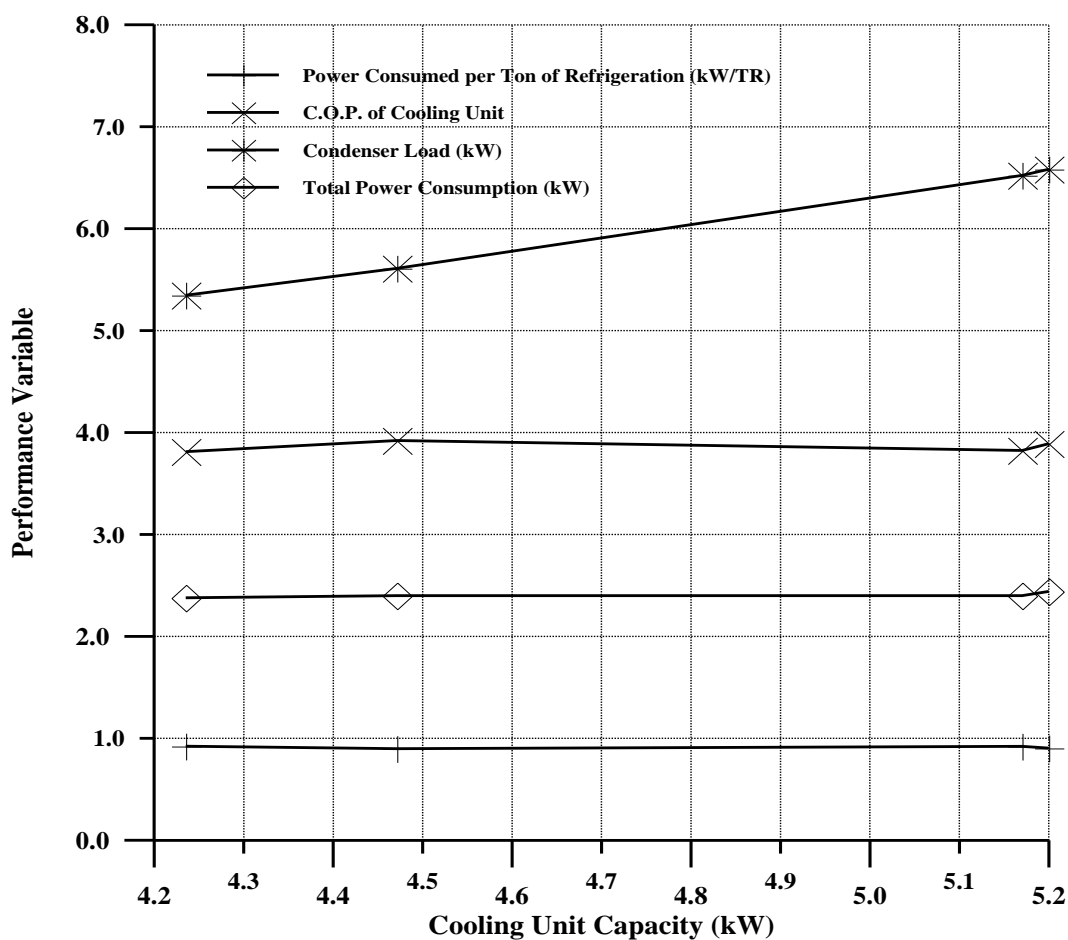


Figure (6.b): AMPC Cycle, R-22.

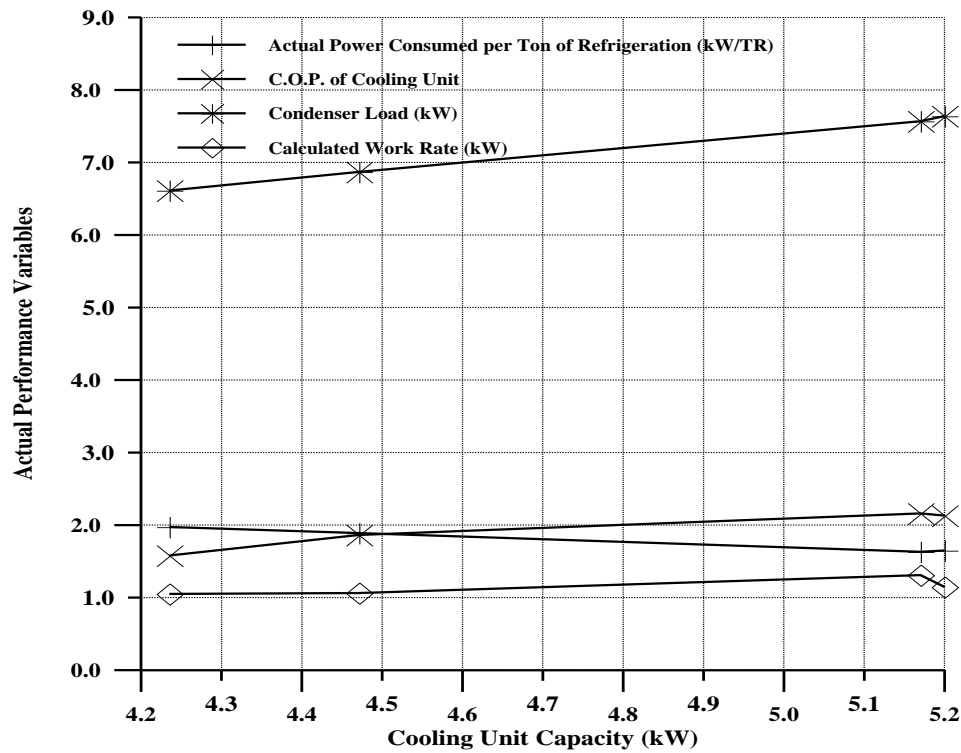


Figure (7.a): IMPC Cycle, R-407C.

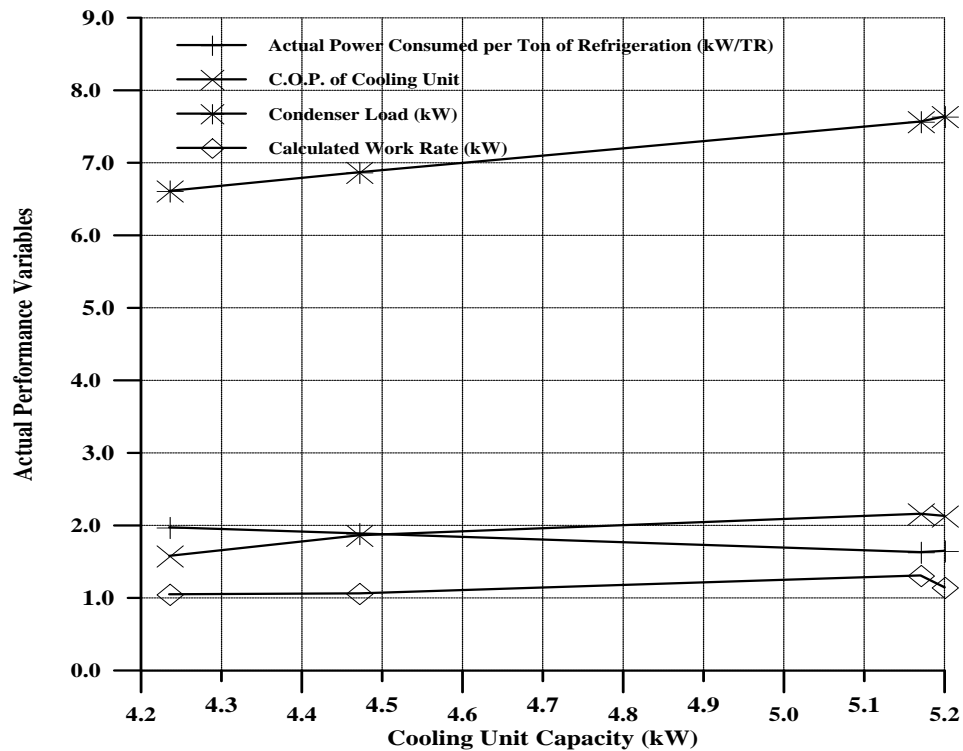


Figure (7.b): AMPC Cycle, R-407C.

PARAMETRIC STUDY OF LAMINAR NATURAL CONVECTION IN GLAZING ENCLOSURE

Karima E. Amori

Ahmed Mohammed Toima

Mech. Eng. Dept. College Of Engineering, University of Baghdad

ABSTRACT

This work includes a numerical investigation of steady two dimensional laminar natural convection heat transfer in glazed rectangular enclosure at different tilt angles ranged from (0° to 90°) for Rayleigh number (10^3 - 10^6), aspect ratios (4,5, and 8), and Prandtl number (0.7). The study considers the effect of different boundary conditions on the heat transfer within the enclosure. The continuity equation, Navier-Stokes equations and the energy equation are solved by developing a numerical model based on finite volume method using SIMPLE algorithm with hybrid scheme to compute the velocity vectors, temperature, pressure, and Nusselt No. (local and average). Results show an increase in heat transfer rate with increasing of Rayleigh number, and for low Rayleigh numbers, the conduction is the dominant heat transfer mode. At $Ra = 10^3$, the mean Nusselt number remains constant around unity for all cases. The tilt angle has the major effect on the heat transfer for Rayleigh number larger than 10^4 . A comparison of the present results with previously published data is conducted, and good agreement is seen to indicate the effectiveness and flexibility of the developed numerical procedure.

الخلاصة

يتناول هذا البحث دراسة عددية لجريان الهواء وانتقال الحرارة بواسطة الحمل الحر الطبقي في حيز زجاجي مستطيل ذو زوايا ميل تتراوح بين (0° - 90°) وحالة مستقرة ثنائية البعد. الدراسة تغطي المدى لرقم رايلي من 10^3 الى 10^6 ولنسب باعية (4,5,8) ولعدد برانتل ($Pr=0.7$). تم حل معادلات الاستمرارية , معادلات نافير- ستوكس ومعادلة الطاقة ببناء نموذج عددي باستخدام طريقة الحجم المحدد وأتباع خطوات (SIMPLE) بالطريقة الهجينة لحساب قيم كل من , مركبات السرعة ودرجة الحرارة والضغط ورقم نسلت (الموضعي والمعدل). بينت النتائج ان معدل انتقال الحرارة يزداد مع زيادة رقم رايلي , وان انتقال الحرارة بالتوصيل يظهر بشكل واضح عند رقم رايلي منخفض, في حين ان رقم نسلت المتوسط يبقى ثابتا بقيمة واحدة عند رقم رايلي 10^3 . وأن زاوية ميل الحيز لها التأثير الأكبر على انتقال الحرارة لقيم رايلي أكبر من 10^4 . تمت مقارنة النتائج المستحصلة في هذه الدراسة مع المنشورة سابقا ووجد تقارب جيد بينهما للدلالة على فعالية ومرونة الحل العددي الذي تم ببناءه.

KEYWORDS

natural convection; rectangular enclosure; uniform and non-uniform heating

INTRODUCTION

The number of heat transfer applications in which the natural convection is a dominant phenomenon within enclosures is large, and better understanding of this phenomenon has even increased the number of applications and has led to a number of sophisticated industrial and environmental designs. Natural convection flows in enclosures such as double pane systems have received a great interest in engineering applications. Windows have always been a significant part of building design, and provide many functions and play a significant role in daily building operations. **Hiroyuki Ozoe (1973)** , studied (numerically using FDM and experimentally) two dimensional natural circulations in an inclined, confined box heated on one side and cooled on the opposing side. The angle of inclination was varied from (0° to 180°) for four aspect ratios. The study assumed $Pr=0.7$ and Rayleigh number ranged from 10^3 to 10^6 . The preferred mode of fluid circulation was observed to change with the angle of inclination and the aspect ratio. He found that a minimum in the heat flux occurred at the point of transition (merging of the circulation cells), while the maximum occurred as the angle was further increased. **Ivan Catton (1973)**, studied numerically natural convection flow in a finite, two-dimensional rectangular slot arbitrarily oriented with respect to the gravity vector for aspect ratios (0.1 to 20), and tilt angles from -30° to $+75^\circ$ and Rayleigh numbers up to 2×10^6 . It was found that the flow structure and heat transport were dependent on aspect ratio, angle of tilt and Rayleigh number. **Mayer, Mitchell, and El-Wakil(1979)** studied experimentally the effect of natural convection in moderate aspect ratio (0.25-4) enclosures using an interferometric technique. The slat enclosure is represented as an array of cells which are essentially contiguous enclosures each having a small aspect ratio. The Rayleigh number range tested was up to 7×10^4 and the angles were from 45° to 90° . They showed that the convective heat transfer is a strong function of the aspect ratio (less than 4). Also slat angles less than 90° (i.e., oriented downward) reduce convective heat transfer. **Elsherbiny et al. (1982)**, studied experimentally the effect of thermal boundary conditions on natural convection in vertical and inclined air layers between two isothermal plates of different temperature depends on the side and end walls boundary conditions. These walls are usually assumed to be perfectly conducting or adiabatic. The study has qualitatively described the wall conduction, radiation and fluid convection interactions. **Wang and Hamed (1980)**, investigated numerically steady two-dimensional natural convection in air filled, rectangular enclosure using finite volume approach. The effect of various configurations of bidirectional temperature gradients on mode transition of thermal convection inside the cavity has been investigated. Simulations have been carried out for Rayleigh numbers ($10^3 < Ra < 10^6$), aspect ratio=4 and angle of inclination from (0° to 90°) . They showed that it is quite possible to alter the resulted heat transfer rates by adjusting the thermal conditions; by varying cavity angle of inclination, or by modifying initial conditions of fluid inside the cavity.

In this work, laminar flow in inclined glazing enclosure is adopted for various heating cases to study the effect of different boundary conditions and different effective parameters on flow field and heat transfer within it.

MATHEMATICAL MODEL AND BOUNDARY CONDITIONS

Figure.(1) depicts the schematic of the rectangular enclosure considered here. The enclosure has a length of (L) along the x-axis and a width of (W) along the y-axis. The two side walls of the enclosure are insulated, the others perfectly conducting walls are considered isothermal and are maintained at constant temperatures T_h and T_c , respectively. The tilt angle γ , is the angle of inclination of the enclosure with respect to the horizontal.

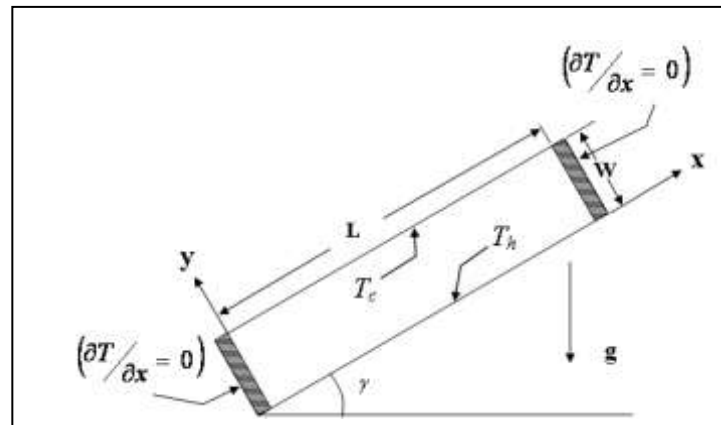


Fig. (1): Two-Dimensional Enclosure Geometry.

The following assumptions accompanied to the adopted mathematical model: Steady, two-dimensional natural convection flow inside the enclosure, assuming constant and employing the Boussinesq approximation for the gravity term. The governing equations for natural convection flow using conservation of mass, momentum and energy can be written as:

$$\frac{\partial u}{\partial x} + \frac{\partial v}{\partial y} = 0 \quad (1)$$

$$\left. \begin{aligned} u \frac{\partial u}{\partial x} + v \frac{\partial u}{\partial y} &= -\frac{1}{\rho} \frac{\partial P}{\partial x} + \nu \left(\frac{\partial^2 u}{\partial x^2} + \frac{\partial^2 u}{\partial y^2} \right) - \beta g (T - T_c) \sin \gamma \\ u \frac{\partial v}{\partial x} + v \frac{\partial v}{\partial y} &= -\frac{1}{\rho} \frac{\partial P}{\partial y} + \nu \left(\frac{\partial^2 v}{\partial x^2} + \frac{\partial^2 v}{\partial y^2} \right) - \beta g (T - T_c) \cos \gamma \end{aligned} \right\} \quad (2)$$

$$u \frac{\partial T}{\partial x} + v \frac{\partial T}{\partial y} = \alpha \left(\frac{\partial^2 T}{\partial x^2} + \frac{\partial^2 T}{\partial y^2} \right) \quad (3)$$

Using the following change of variables:

$$Y = \frac{y}{W}, X = \frac{x}{L}, V = \frac{vW}{\alpha}, U = \frac{uW}{\alpha}, \theta = \frac{T - T_c}{T_h - T_c} \quad (4)$$

$$\text{Pr} = \frac{\nu}{\alpha}, P = \frac{pW^2}{\rho\alpha^2}, \text{Ra} = \frac{\text{Pr} g \beta (T_h - T_c) W^3}{\nu^2}$$

The governing equations (1)-(3) reduced to the following set of dimensionless equations:

$$\frac{\partial U}{\partial X} + \frac{\partial V}{\partial Y} = 0 \quad (5)$$

$$\left. \begin{aligned} U \frac{\partial U}{\partial X} + V \frac{\partial U}{\partial Y} &= -\frac{\partial P}{\partial X} + \text{Pr} \left(\frac{\partial^2 U}{\partial X^2} + \frac{\partial^2 U}{\partial Y^2} \right) - \text{Ra Pr} \theta \sin(\gamma) \\ U \frac{\partial V}{\partial X} + V \frac{\partial V}{\partial Y} &= -\frac{\partial P}{\partial Y} + \text{Pr} \left(\frac{\partial^2 V}{\partial X^2} + \frac{\partial^2 V}{\partial Y^2} \right) - \text{Ra Pr} \theta \cos(\gamma) \end{aligned} \right\}$$

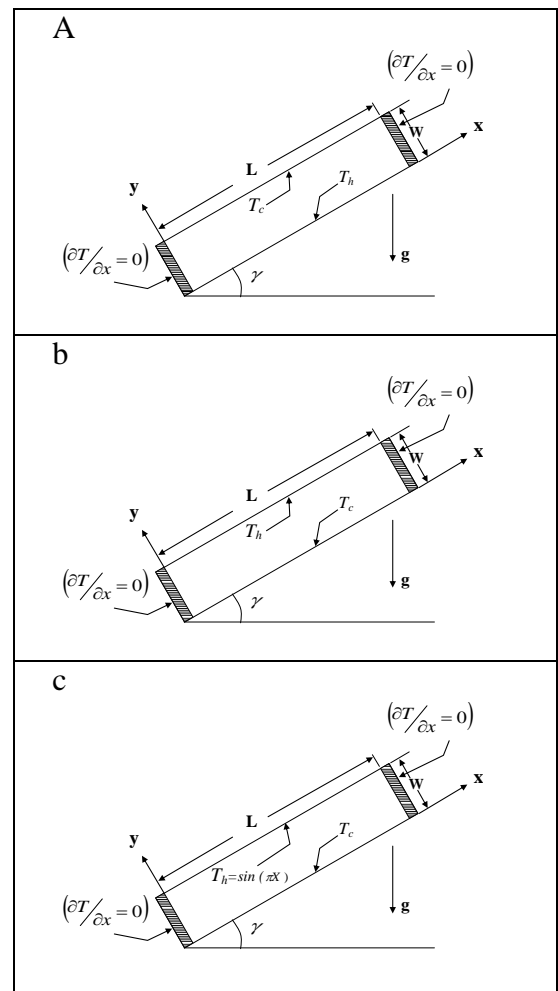


Fig.(2): Enclosure Geometry And Coordinate System For The Studying Cases

$$U \frac{\partial V}{\partial X} + V \frac{\partial V}{\partial Y} = -\frac{\partial P}{\partial Y} + \text{Pr} \left(\frac{\partial^2 V}{\partial X^2} + \frac{\partial^2 V}{\partial Y^2} \right) - Ra \text{Pr} \theta \cos(\gamma) \quad (6)$$

$$U \frac{\partial \theta}{\partial X} + V \frac{\partial \theta}{\partial Y} = \left(\frac{\partial^2 \theta}{\partial X^2} + \frac{\partial^2 \theta}{\partial Y^2} \right) \quad (7)$$

The Boussinesq approximation is introduced in the present study, which treat the density as a constant variable in the continuity equation and in the inertia term of the momentum equation, but allow it to change with temperature in the buoyancy terms, such that:

$$\rho = \rho_\infty (1 - \beta [T - T_\infty]) \quad (8)$$

The no-slip boundary condition is applied at all four boundaries.

$$U(X,0)=U(X,1)=U(0,Y)=U(I,Y)=0 \quad (\text{where } I = L/W)$$

$$V(X,0)=V(X,1)=V(0,Y)=V(I,Y)=0$$

Thermal boundary conditions adopted in the present work are related to the cases considered shown in Fig (2). These cases are:

- I. Enclosure which has a lower wall heated and upper wall cooled with two insulated sidewalls as shown in Fig (2a). i.e.:

$$\theta(X,0) = 1$$

$$\theta(X,1) = 0 \quad (\text{Constant wall temperature})$$

$$\frac{\partial \theta}{\partial X}(0,Y) = \frac{\partial \theta}{\partial X}(I,Y) = 0 \quad (\text{Insulated sidewalls})$$

- II. Enclosure which has a lower wall cooled and upper wall heated with two insulated sidewalls as shown in Fig (2b). i.e.:

$$\theta(X,0) = 0$$

$$\theta(X,1) = 1 \quad (\text{Constant wall temperature})$$

$$\frac{\partial \theta}{\partial X}(0,Y) = \frac{\partial \theta}{\partial X}(I,Y) = 0 \quad (\text{Insulated sidewalls})$$

- III. Enclosure with upper wall is subjected to non-uniform temperature (sinusoidal) distribution in space coordinate while the lower wall is cooled and the sidewalls are kept insulated as shown in Fig (2c).

i.e.:

$$\theta(X,0) = 0 \quad (\text{Constant wall temperature})$$

$$\theta(X,1) = \sin(\pi X') \quad (\text{Sinusoidal temperature distribution and } X' = Xw/L)$$

$$\frac{\partial \theta}{\partial X}(0,Y) = \frac{\partial \theta}{\partial X}(I,Y) = 0 \quad (\text{Insulated sidewalls})$$

The Nusselt number was calculated using the following equation:

$$Nu_{ave} = \frac{1}{W} \int_0^W \frac{q}{k(T_h - T_c)} dx \quad (9)$$

NUMERICAL ALGORITHM AND RESULTS VALIDITY

Eqs. (5) to (8) are solved using FVM and the SIMPLE algorithm. The procedure was regarded converged when maximum difference of all independent variables (U , V , P , and θ) and maximum change in calculated average Nusselt number between two successive iterations were less than 10^{-4} .

These governing differential equations can be rewritten in the general form as: **Patankar** (1980)

$$\frac{\partial}{\partial x}(\rho u \Phi) + \frac{\partial}{\partial y}(\rho v \Phi) = \frac{\partial}{\partial x} \left[\Gamma_{\Phi} \frac{\partial \Phi}{\partial x} \right] + \frac{\partial}{\partial y} \left[\Gamma_{\Phi} \frac{\partial \Phi}{\partial y} \right] + S_{\Phi} \quad (10)$$

Where the left hand side represents the convective terms, the right hand side represents the diffusion and source terms. The physical domain is divided into elements as shown in Fig.(3), and a Fortran 90 computer program is developed with the structure chart shown in Fig. (4).

RESULTS AND DISCUSSION

Verification of the Numerical Discussion

In order to check the accuracy of the results obtained using the present numerical algorithm, results were compared with those available in the literature. The computed and the reference Nusselt No. values of **Wang** (2005) and **Yao** (1999) along with the percentage deviation, are presented in table (1). **Wang** and **Yao** studied an enclosure at ($\gamma = 0^\circ$) with insulated upper and lower walls and isothermal side walls. Table (1) shows that the minimum and maximum deviations are (0.0007%) and (2.288%) respectively.

$$\text{Where: Deviation \%} = \frac{Nu_{ref} - Nu_{comp}}{Nu_{ref}} \times 100$$

Table.1. Verification of the Mean Nusselt number

Ar	Pr	Ra	Nu			Deviation %
			Present Study	Wang	Huafu Yao	
4	0.7	1000	1.000003	1.00001	-	0.0007
4	0.7	3000	1.554243	1.57002	-	1.004
4	0.7	5000	2.000682	2.0022	-	0.075
4	0.7	10^4	2.507354	2.55	-	1.672
1	0.71	10^4	2.294327	-	2.243	2.288
1	0.71	10^5	4.520762	-	4.519	0.039
1	0.71	10^6	8.774747	-	8.9693	2.169

Glazing Enclosure Heated From Lower Surface - (Case I)

The effect of inclination angle is studied by varying (γ) from 0° to 90° on flow and temperature fields for $Ra=10^4$ are shown in Fig. (5) for ($Ar = 4$ and 8), respectively. At ($Ar=4$), the multi-cells begin to coalesce into one. A pronounced one-cell motion was observed between $30^\circ < \gamma < 90^\circ$ while multicellular form could be observed for ($Ar=8$) at

($\gamma=0^\circ$). At an angle of 60° hot wall produces an acceleration to the flow along the top and bottom walls, causes the velocity vectors in the core region to stretch toward the top right and bottom left corner of the enclosure. The number of circulation cells for $Ar=8$ is larger than that for $Ar=4$ due to the effect of shallow effect of the enclosure. The circulation cells tends to merge and move to the upper end of the inclosure with increasing of the inclination angle as shown in Fig. (6) due to the gravity effect. Fig.(7) illustrates the velocity vectors and isotherm contours for $Ra=10^3, 10^4, 10^5$, and 10^6 for Aspect ratio of (4 and 8) at $\gamma = 0^\circ$. As Ra increased slightly, the upslope temperature gradient causes a change in the number of cells from four to two for ($Ar=4$), and from six cells to four cells for ($Ar=8$). Fig.(8) shows the relation between the Nu_{ave} vs. Ra for various aspect ratios and inclination angle. Results show that Nu_{ave} increases as increasing the Ra No. and at $Ra=1000$ the value of Nu_{ave} was unity which indicate that the conduction and convection effect is the same. Also it can be shown that the specified values of inclination angle the circulation fluid cells merged and cause a decrease in Nu number, while a slight effect of Ar is shown.

Glazing Enclosure Heated From Upper Surface - (Case II)

The effect of the inclination angle is studied by varying γ from 0° to 90° for the case of $Ra=10^4$. The Isotherms and Velocity vectors at Aspect ratios (4, 5, and 8) was studied and found to be so similar in trend as that for case II, therefore only $Ar=4$ is presented in Fig. (9) in this section to avoid repetition.. This figure shows that for ($\gamma = 0^\circ$), two fluid cells are formed, while they are merged for higher tilt angles, also a weak convection heat transfer exist tending the fluid to move towards the enclosure ends at the upper heated wall. This fluid movement increases with increasing of γ noting that the fluid moves upward near the heated side due to decreasing the fluid density, and moves downward near the colder wall to form one flow cell for ($\gamma = 30^\circ, 60^\circ, \& 90^\circ$). Effect of Ra No. on the vertical velocity distribution and the isothermal contour along enclosure centerline is shown in Fig. (10) where the fluid flows is clock-wise unicellular, except for ($Ar=4, Ra=10^5, \gamma=0^\circ$) where twin in opposite direction circulation fluid cells are formed, also it shows that increasing of Rayleigh number leads to increase the circulation strength due to the increase in temperature difference. As Ra increases to 10^5 and 10^6 , the thermal boundary layer gets intensive and thinner. Compressed isotherms extend longer along the y-axis and the isotherms are further distorted due to the stronger convection, this is also shown in Fig.(11).

Fig.(12) shows the effect inclination angle on the averaged Nu for ($Ar=4$ and 8). It can be concluded that increasing γ leads to increasing the heat transfer and the effect of increasing the aspect ratio has larger effect, due to the confirmation effect to fluid circulations in shallow enclosure. Also it can be shown that for $\gamma=0^\circ$ all values of Nu_{avg} is equal to one i.e convection effect is the same as conduction.

Glazing Enclosure with Non-Uniform Heating of Upper Surface - (Case III)

The effect of the inclination angle is studied by varying γ from 0° to 90° and $Ra=10^4$ for the case(III) as shown in Fig.(13). The Isotherms and Velocity vectors at Aspect ratios (4, 5, and 8) was found to be so similar in trend, therefore only ($Ar=4$) is presented in this section to avoid repetition. It can be seen from velocity plot at $\gamma=0^\circ$, two circulating fluid cells are formed inside the enclosure. Further increase in the tilt angle to $\gamma=30^\circ$ and $\gamma=60^\circ$ leads to merge to a unicellular pattern with the tendency to increase the rotational velocity with the tilt angle. At the vertical position $\gamma=90^\circ$, where the gravitational field is parallel to the boundary layer the circulation cell is squeezed towards the upper section of the enclosure.

The effect of Rayleigh number on the heat transfer and fluid motion is investigated for ranges of $10^3, 10^4, 10^5$, and 10^6 as shown in Fig.(14).

For small Ra , the fluid is almost stagnant and pure conduction through adjacent fluid layers dominates the heat transfer as it is confirmed by the temperature distribution. It also noted for horizontal position that the temperature at the top wall is non –uniform and a maximum temperature is located at the center. At $Ra=10^5$, the circulation pattern is qualitatively similar to the uniform upper surface heating as shown in Fig.(15). Fig.(16) shows the effect of Ra No. on the vertical velocity distribution along the enclosure centerline. Fig. (17) shows the combined effect of inclination angle and aspect ratio and Ra No. on the averaged Nu No. The same trend in case II is presented with the exception that the conduction is dominated at $\gamma=0$ than convection .

CONCLUSION

Steady, two-dimensional, natural convection in an air-filled rectangular enclosure has been numerically investigated using the finite –volume based SIMPLE numerical algorithm. Based on the obtained results, conclusions can be listed as follows. When $Ra \leq 10^3$, the inclination of the enclosure does not have any influence on \overline{Nu} for all aspect ratios $Ar=4, 5$ and 8 . And for $5 \cdot 10^3 \leq Ra \leq 10^4$, the Nusselt number tends to increase when the cavity inclination increases and then drops to minimum value when transition mode occurs. Heat transfer is increased with the increasing of Rayleigh number for all parameters which affect on flow and temperature field. Inclination angle is the dominant parameter on fluid flow and heat transfer and has a big effect on the cellular fluid form.

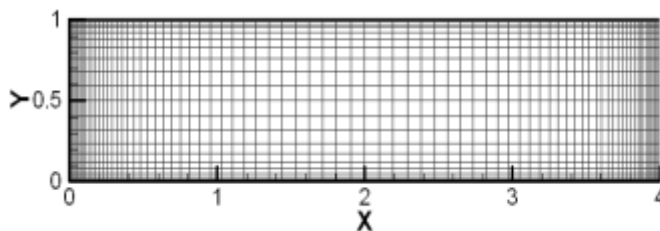


Fig.(3):The Computational Domain of the Enclosure

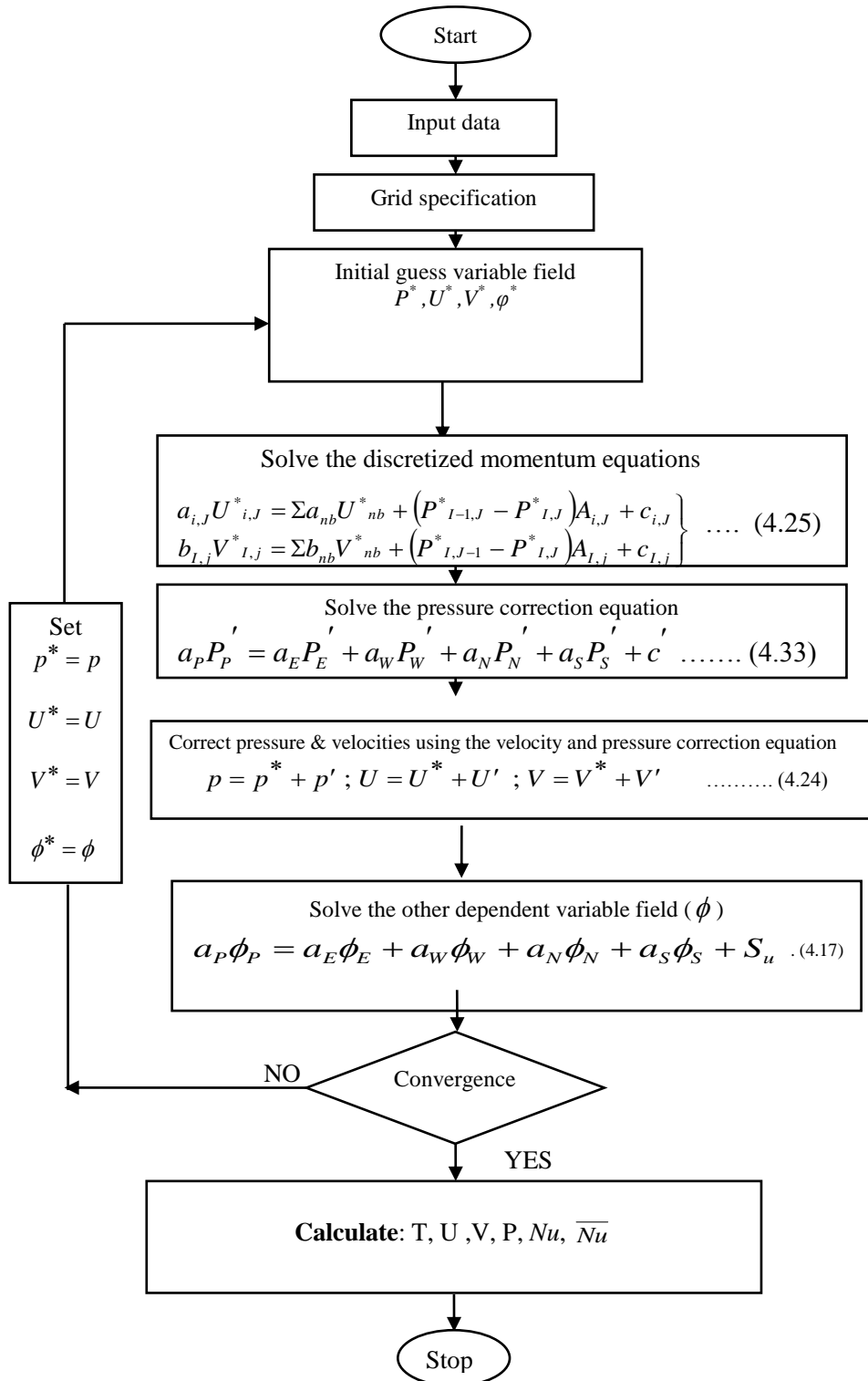
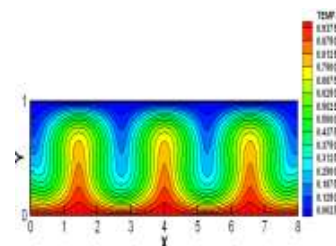
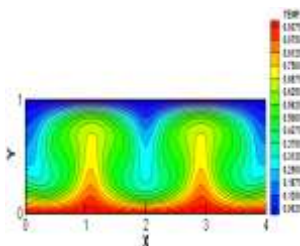


Fig.(4): Flow Chart of the Computer Program.



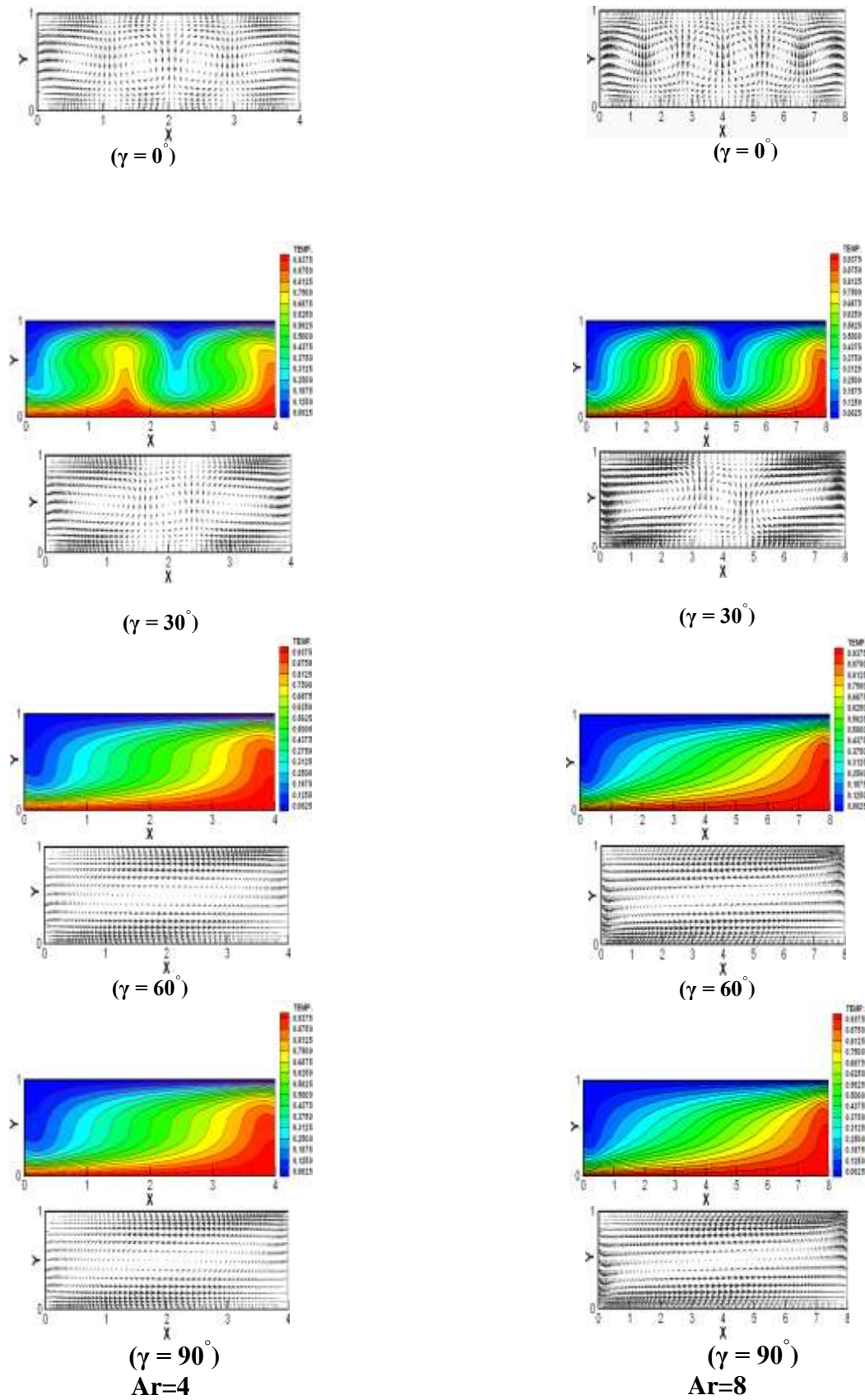
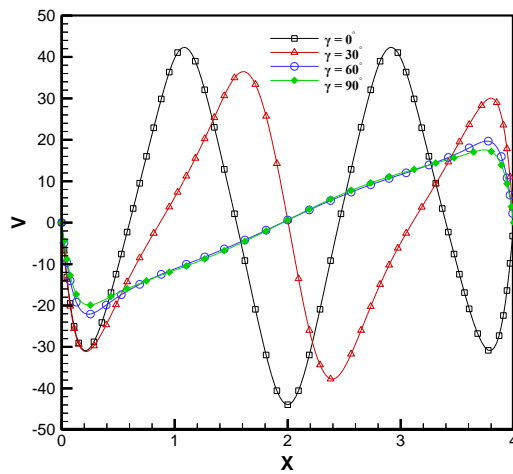
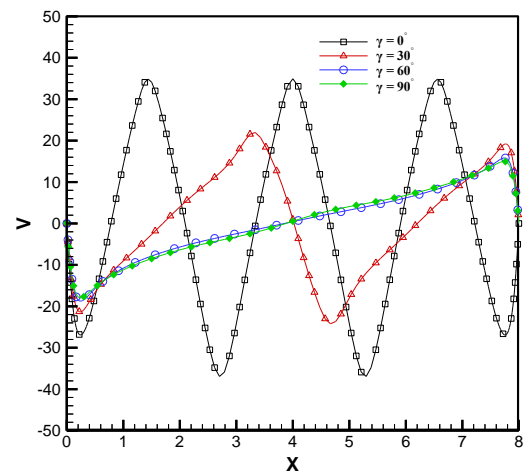


Fig (5) Effect of Inclination Angle on Temperature Contours and Velocity Vectors for (Case I), [Ar= 4 and 8, Ra=10⁴]

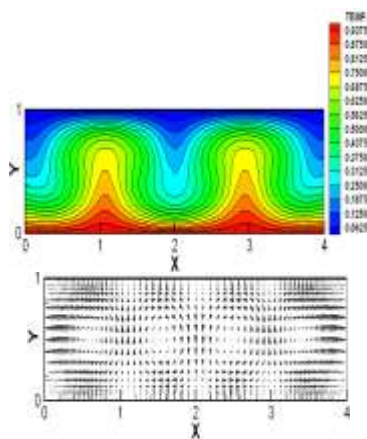


Ar=4

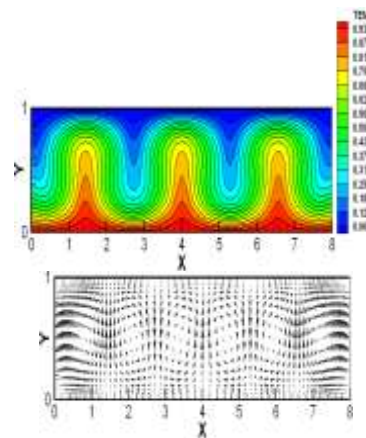


Ar=8

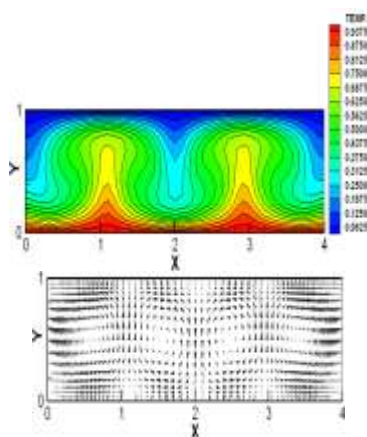
Fig (6): Effect of Inclination Angle on Vertical Velocity Distribution along Enclosure Centerline for (Case I), [Ar = 4 and 8, Ra =10⁴]



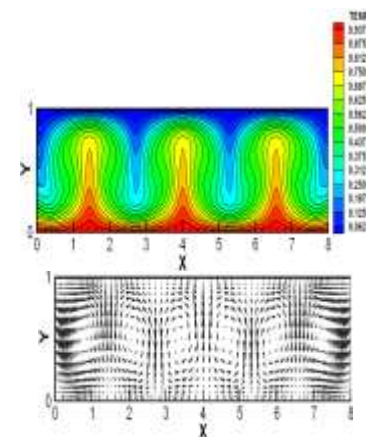
(Ra = 10³)



(Ra = 10³)



(Ra = 10⁴)



(Ra = 10⁴)

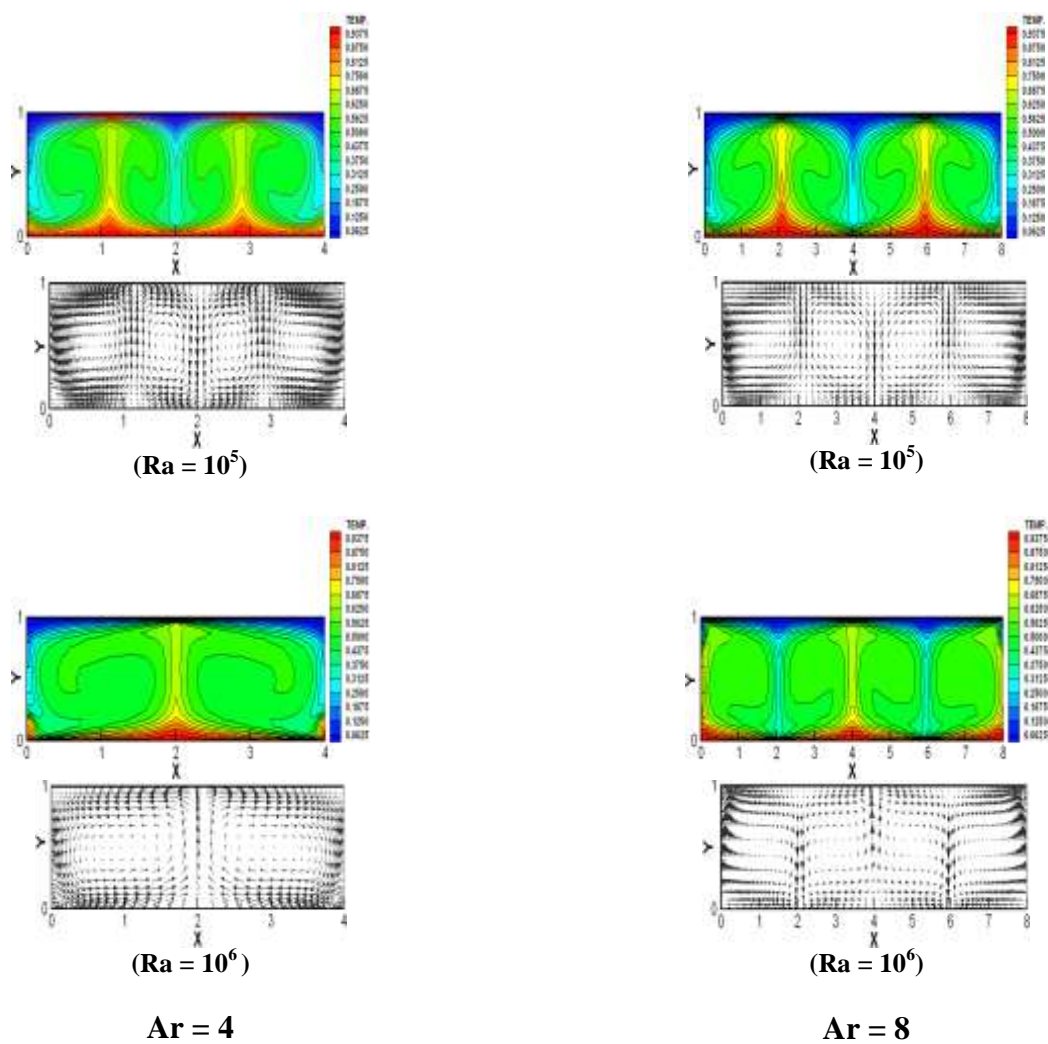


Fig (7): Effect of Rayleigh Number on Temperature Contours and Velocity Vectors for (Case I), [Ar = 4 and 8, $\gamma = 0^\circ$]

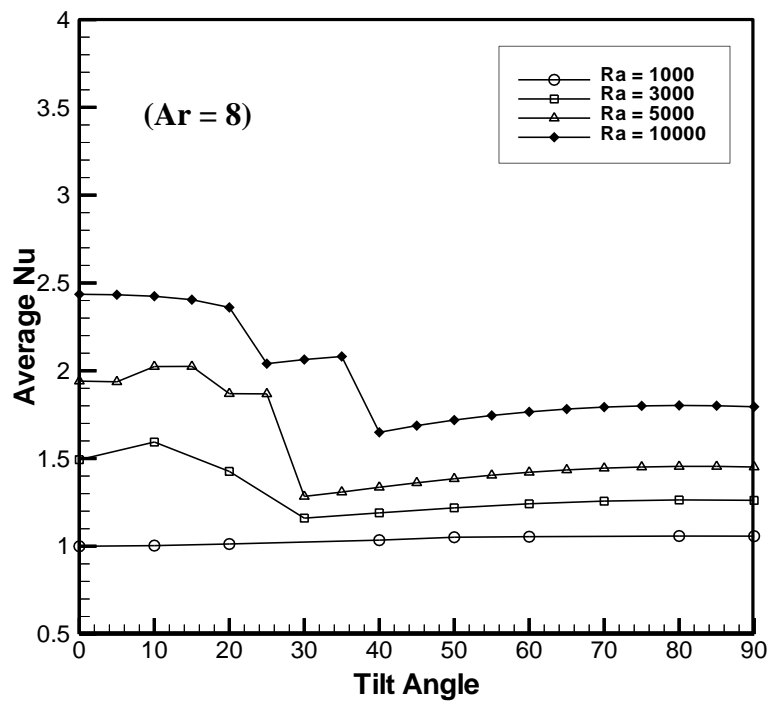
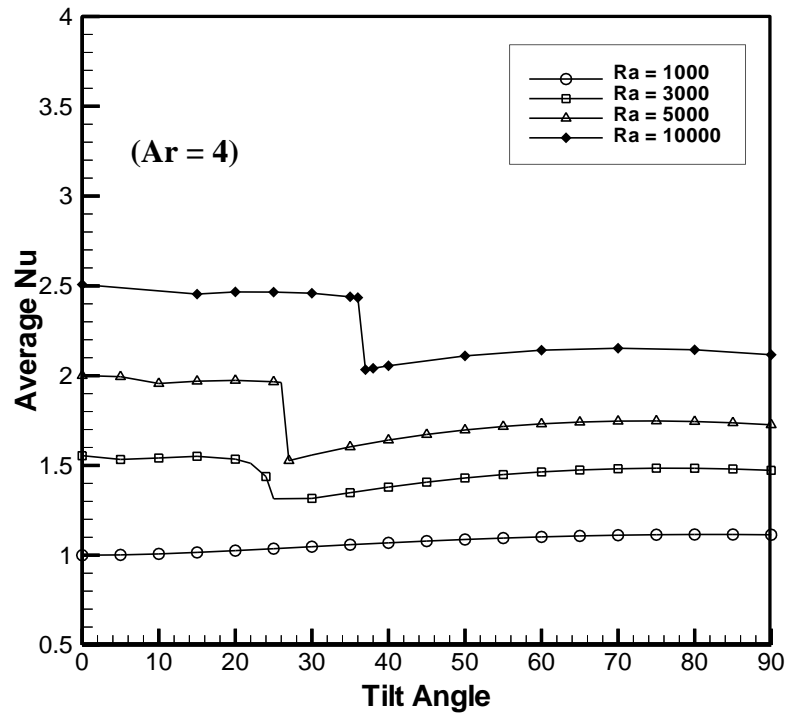
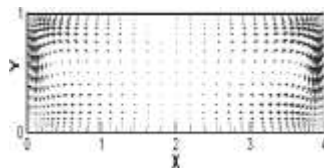
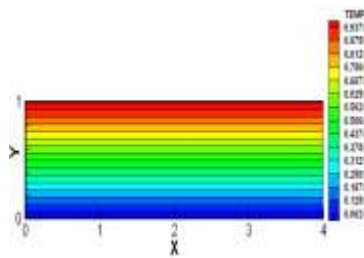
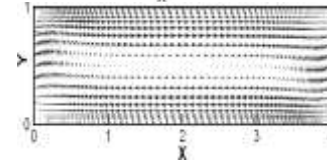
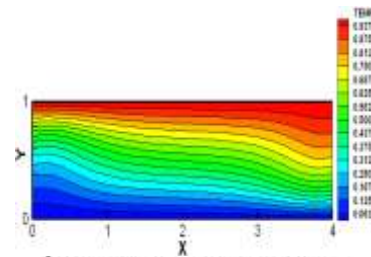
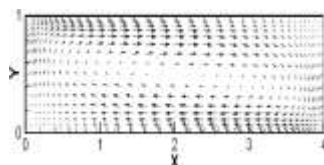
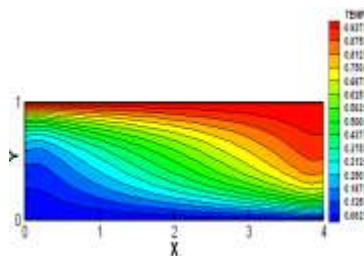
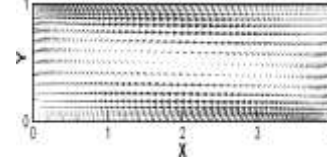
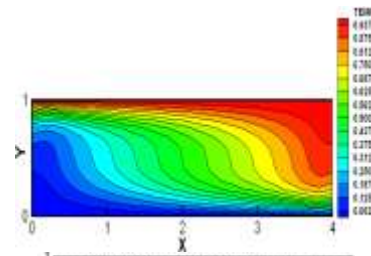
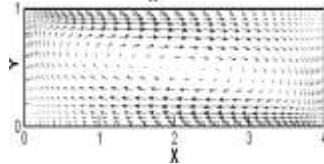
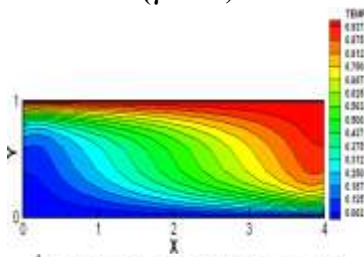
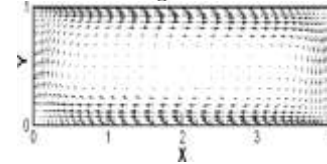
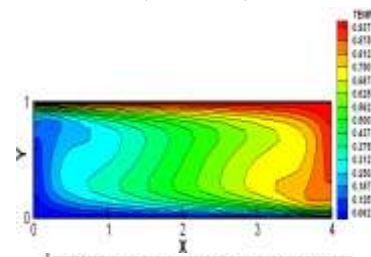


Fig (8); Effect of Aspect Ratio on Average Nusselt Number at Different Inclination Angles for (Case I).

 $(\gamma = 0^\circ)$  $(Ra = 10^3)$  $(\gamma = 30^\circ)$  $(Ra = 10^4)$  $(\gamma = 60^\circ)$  $(Ra = 10^5)$

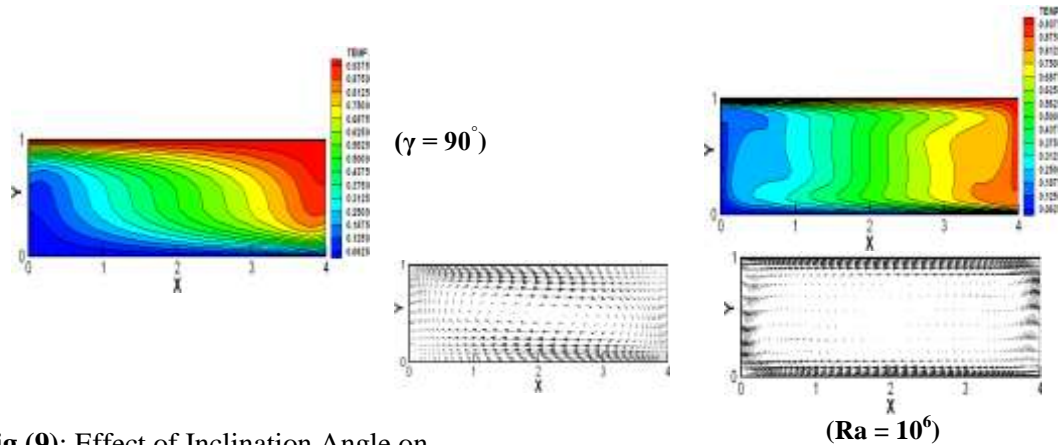


Fig (9): Effect of Inclination Angle on Temperature Contours and Velocity Vectors for (Case II), $[Ar = 4, Ra = 10^4]$

Fig (10): Effect of Rayleigh Number on Temperature Contours and Velocity Vectors for (Case II), $[Ar = 4, \text{ and } \gamma = 90^\circ]$

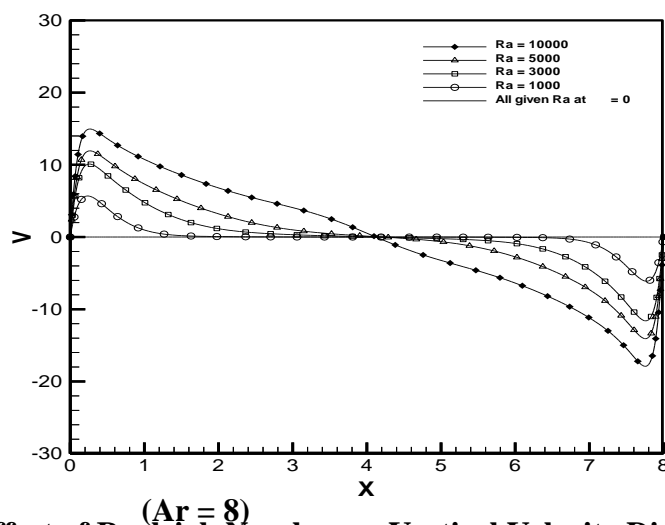
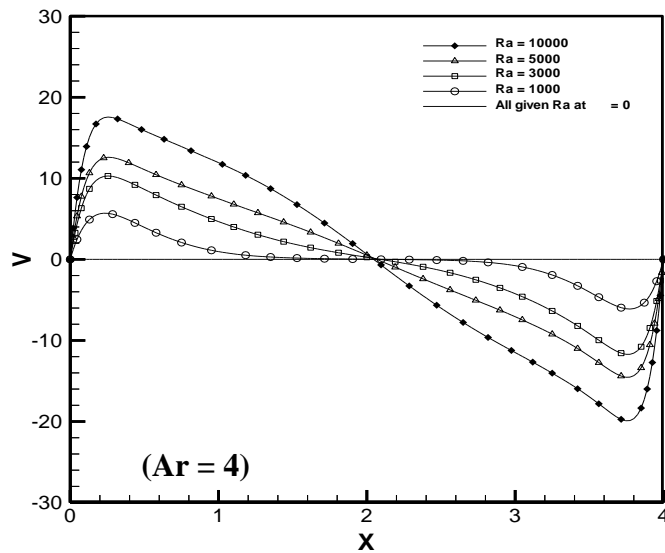


Fig (11): Effect of Rayleigh Number on Vertical Velocity Distribution along Enclosure Centerline for (Case II), $[Ar = 4, \text{ and } \gamma = 90^\circ]$

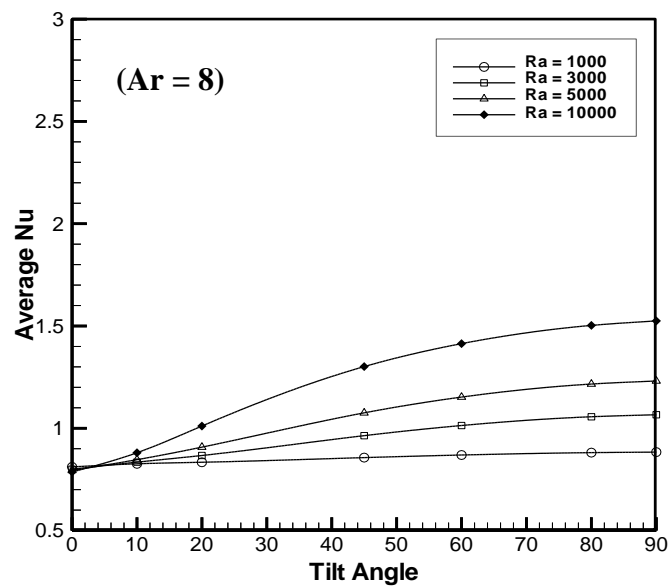
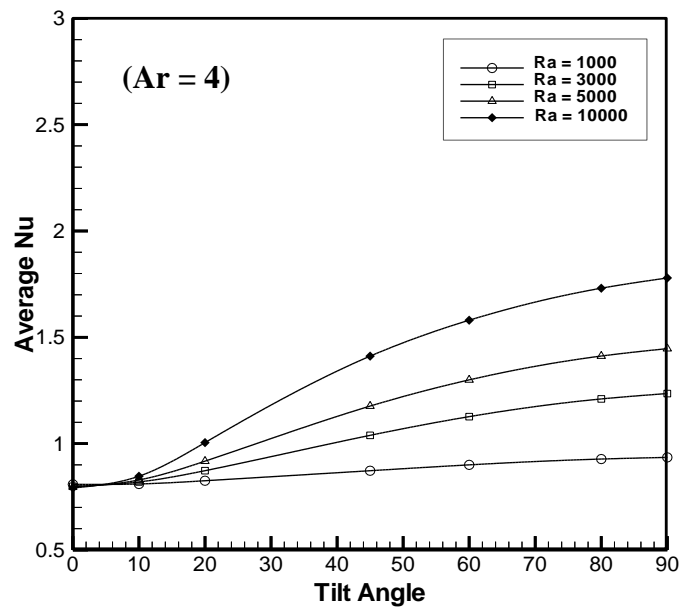


Fig (12) Effect of Aspect Ratio on Average Nusselt Number at Different Inclination Angles for (Case II).

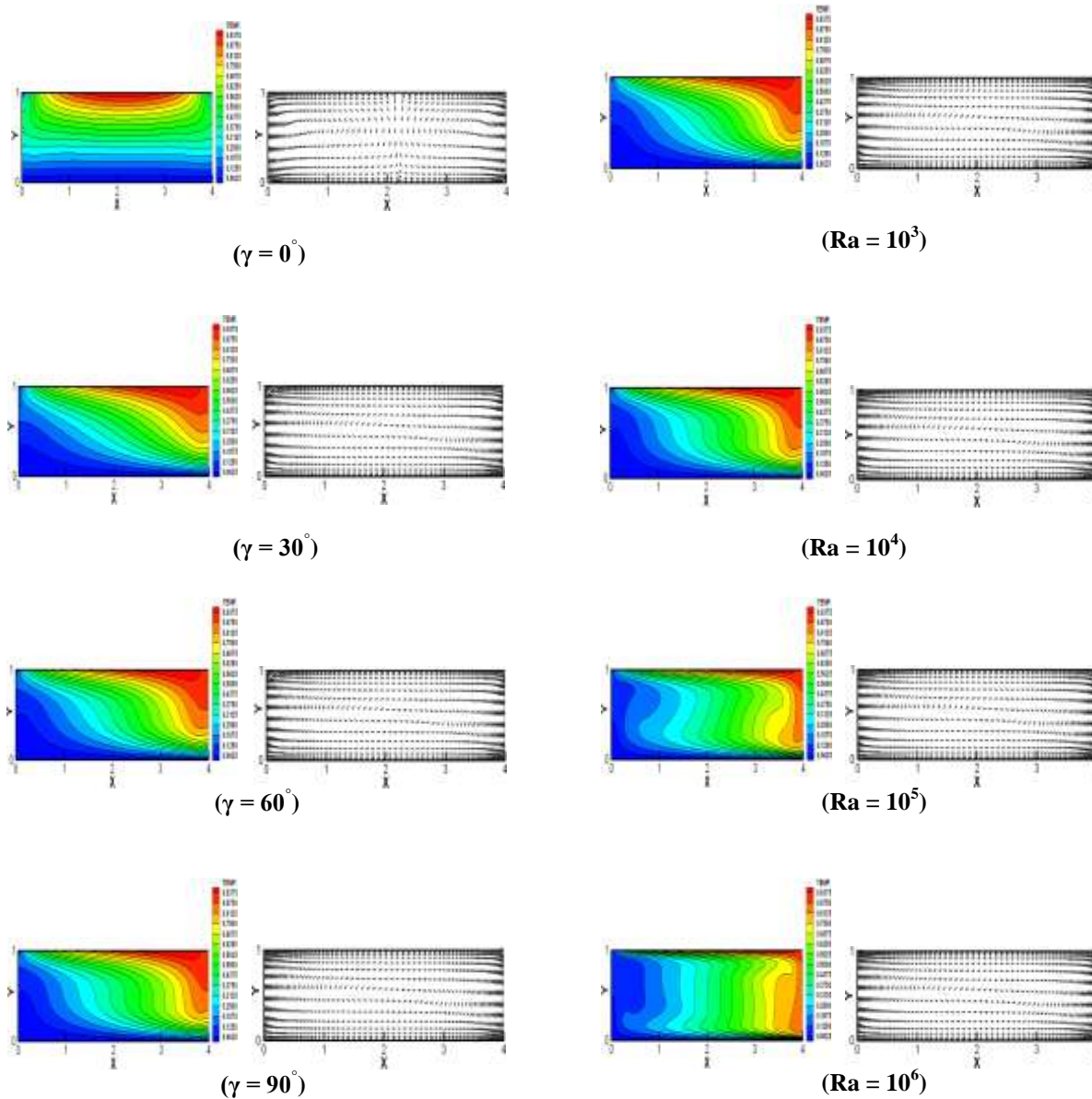


Fig (13): Effect of Inclination Angle on Temperature Contours and Velocity Vectors for (Case III), [Ar = 4 , Ra = 10^4]

Fig (14) Effect of Rayleigh Number on Temperature Contours and Velocity Vectors for (Case III), [Ar = 4, and $\gamma = 90^\circ$]

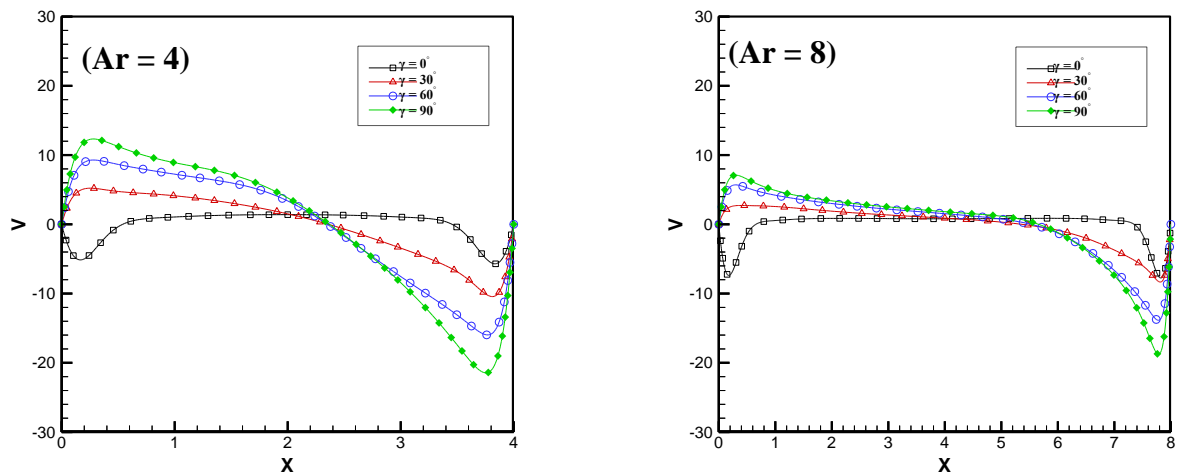


Fig.(15): Effect of Inclination Angle on Vertical Velocity Distribution along Enclosure Centerline for (Case III), [Ar = 4 and 8, Ra = 10^4]

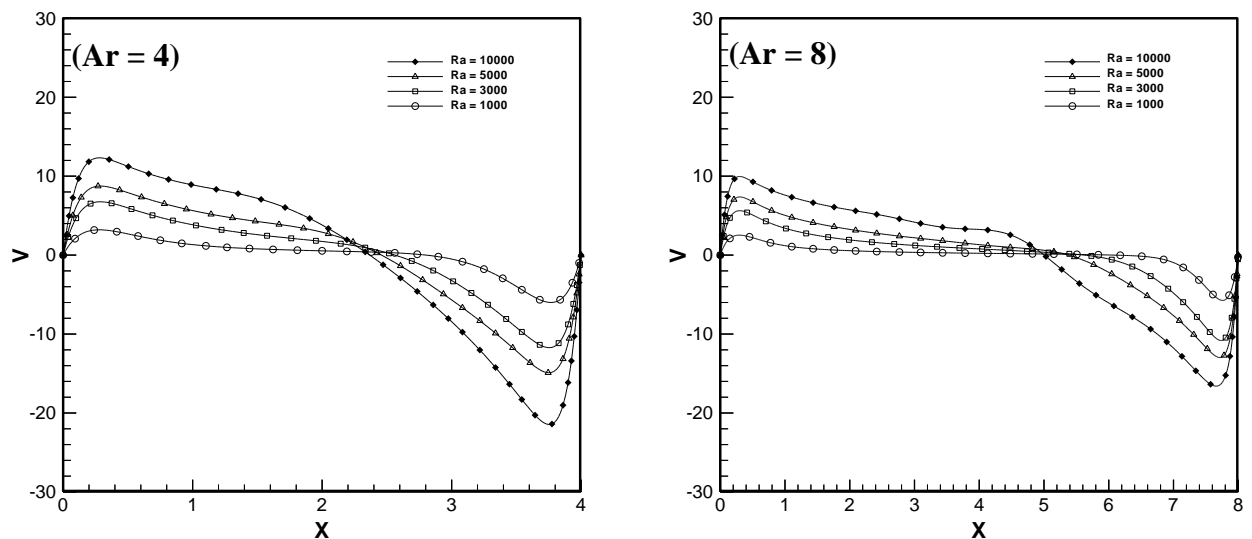


Fig (16): Effect of Rayleigh Number on Vertical Velocity Distribution along Enclosure Centerline for (Case III), [Ar = 4, and $\gamma = 90^\circ$]

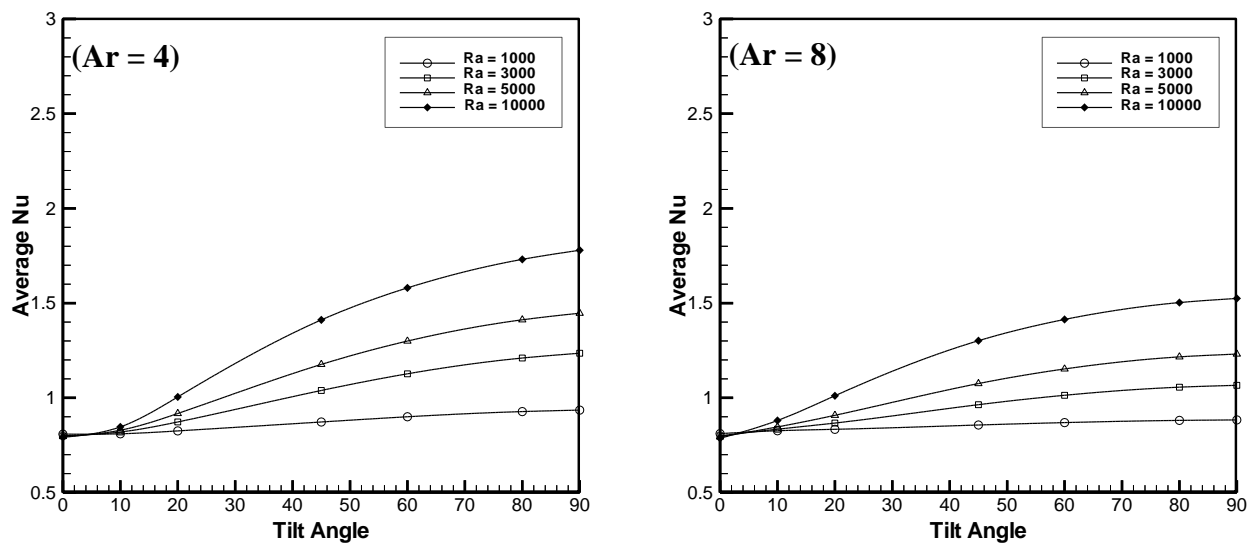


Fig (17) Effect of Aspect Ratio on Average Nusselt Number at Different Inclination Angles for (Case III).

REFERENCES

- Hiroyuki Ozoe, "Natural Circulation in an Inclined Rectangular Channel Heated on One Side and Cooled on the Opposing Side", International Journal of Heat & Mass Transfer, Vol.17, pp.1209-1217, (1973).
- Ivan Catton "Natural Convection Flow In A Finite Rectangular Slot Arbitrarily Oriented With Respect To The Gravity Vector" International Journal of Heat & Mass Transfer, Vol.17, pp.173-184, June (1973).
- Mayer B.A and Mitchel J.W., "Natural Convection Heat Transfer in Moderate Aspect Ratio Enclosures", International Journal of Heat Transfer, Vol. 101, pp.655-659, Nov (1979).
- Elsherbiny S.M.; Raithby G.D and Hollands K. G. T., "Heat Transfer by Natural Convection across Vertical and Incline Air Layers ", Transactions of the ASME, Vol. 104, pp. 96-102, (1982).
- Patankar, S. V., "Numerical Heat Transfer and Fluid Flow", Hemisphere Publishing Corporation, Taylor & Francis Group, (1980).
- Wang.H.; and Hamed M.S., "Flow Mode-Transition Of Natural Convection In Inclined Rectangular Enclosures Subjected To Bidirectional Temperature Gradients", International Journal of Thermal Science, Vol.45, pp.782-795, (2005).
- Huaifu Yao., "Studies Of Natural Convection In Enclosures Using The Finite Volume Method", PhD. Thesis, Mechanical Engineering Department, University of York, Ontario,(Canada) (1999).



- Toima, A.M., “An Investigation of Heat Transfer in Glazing Enclosure at Different Orientation Angles”, M.Sc. Thesis, Mechanical Engineering Department, University of Baghdad, (2008).

• **NOMENCLATURE**

LATIN SYMBOLS

A_r	L/W Dimensionless aspect ratio	S	Source term
g	Gravitational acceleration	u	Velocity component in x-direction m/s
h	Convective heat transfer coefficient $W/m^2\ ^\circ C$	U	Dimensionless velocity in x-direction
K	Thermal conductivity $W/m.\ ^\circ C$	v	Velocity component in y-direction
Nu_{ave}	Average Nusselt number	V	Dimensionless velocity in y-direction
P	Pressure (Pa)	T	Temperature $^\circ C$
Pr	Prandtl number, $\square\square\square\square\square\square\square$	W	Dimensionless width of enclosure
Q	Heat flux per unit area (W/m^2)	x,y	Cartesian coordinate
Ra	Rayleigh number	X,Y	Dimensionless Cartesian coordinate

GREEK SYMBOLS

α	Thermal diffusivity
β	Thermal expansion coefficient
Γ	Diffusion coefficient
ϕ	General dependent variable
γ	Inclination angle
ν	Kinematics viscosity

ρ	Density
θ	Dimensionless Temperature

Superscripts & Subscripts

-	Average
C	Cold
h	Hot



ANALYSIS OF APPROXIMATED CURVED CRACKS IN HOMOGENEOUS AND GRADED MATERIALS

HAYDER FANOOS NEAMAH
Mechanical Engg. Dept., Baghdad University,

ABSTRACT

In this paper two stages of analysis are studied. In stage I, the influence of crack shape on the crack-tip stresses, critical loads and subsequent propagation direction is investigated via a simple analytical model for cracks in homogeneous materials. This model is verified through finite element simulations using ANSYS. It is demonstrated that accurate predictions of mechanical energy release rate and crack deflection angle may be obtained from a smaller number of crack shape parameters.

In stage II, this concept is extended to curved cracks in functionally graded materials (FGMs). It is common that analytical and computational models of fracture in FGMs have focused almost extensively on straight cracks. If it can be demonstrated that straight cracks give an adequate approximation of curved cracks in graded materials, then the existing solutions for straight cracks provide a sufficient foundation for fracture analysis of FGMs. On the other hand, if straight cracks do not adequately approximate curved cracks in FGMs, then the development of solutions for non straight cracks in graded materials is priority. Three cracks shapes approximations are performed to compare with the actual crack in isotropic and graded materials. The crack propagation and the SIFs were simulated using finite element method. It was concluded that piecewise linear crack shapes provide a significantly better approximation than straight crack shapes. Accordingly, analytical solutions for piecewise linear cracks in graded materials would be very useful, and should be a focus of future work in this area.

KEY WORDS

SIF, FGM, Fracture mechanics, FEA, ANSYS

الخلاصة:

في هذا البحث تم دراسة مرحلتين من التحليل. في المرحلة الاولى , دُرس تحليلياً تأثير شكل الكسر على جهودات القمة عند الكسر في المواد المتجانسة. وتم الحصول على نتائج مقارنة من خلال استخدام برنامج العناصر المحددة ANSYS. في المرحلة الثانية هذا التحليل توسع لدراسة تأثير شكل الكسر في المواد الطباقية. من الشائع في النموذج الحسابي و النظري للكسر في المواد الطباقية (المتدرجة في معامل المرونة) استخدام الكسر الخطي لتمثيله. اذا تم اثبات انه الكسر الخطي يعطي نتائج تقريبية للكسر الحقيقي, فان الحلول المتوفرة

للكرس الخطي تعطي صورة كافية للكرس الحقيقي. اما اذا ثبت العكس فانه الكسور الخطية هي الاساس في التحليل. ثلاثة اشكال تقريبية من الكسر تم أستقصاؤها لمقارنة الاجهادات عند القمه لمواد متجانسة ومواد طبقية . أنتشار الكسر والمقارنة تمت باستخدام العناصر المحددة. لوحظ أنه شكل الكسر الخطي المتدرج يعطي نتائج تقريبية من الاشكال التقريبية الاخرى بالمقارنة مع الشكل الحقيقي للكرس. وعليه الدراسة النظرية للكرس الخطي المتدرج في المواد الطبقية هي الاكثر صحة لدراسة ميكانيك الكسر في المواد الطبقية.

INTRODUCTION

FGMs (functionally graded materials) are “functionally graded” to provide the exact combination of characteristics desired, and in these materials or structures the material properties vary with location in such a way as to optimize some function of the overall FGM. The metal, the ceramic, the volume, shape, location of the ceramic, and the fabrication method can all be tailored to achieve particular desired properties. The design of FGMs requires an explicit understanding of the material behavior at each location and over all these length scales. There has been quite considerable work on the manufacturing methods of metal/ceramic FGMs. Advanced manufacturing techniques are used to process FGMs, among which we may mention spark plasma sintering (SPS), 3D-printing, electrophoretic deposition and high-temperature infiltration (Jin et al., 2001). Due to the brittle nature of the ceramic components in ceramic/metal FGMs, fracture mechanics of graded materials is also studied quite extensively. A detailed literature review of the fracture mechanics of graded materials is given by Dag (2004). Functionally graded microstructure in a ceramic/metal composite has been found to reduce the otherwise thermal stress field at the interface between ceramic and metal plates (Taya et al., 2005). Chatterjee et al. (2006) have developed a multi-layered rainbow type actuator with graded piezoelectric properties through the thickness.

The criteria for crack propagation should take into consideration the account of the influences of material property gradient along with crack geometry and applied loading, on the applied stress intensity factor (Erdogan, 2006). Furthermore, it should be include the effects of intrinsic toughness variation (Jin & Batra, 2007). Although a crack shape may be quite complicated, several researches have suggested that the stress intensity factor may be approximated by a function of several simple crack-shape parameters, or indeed by approximating the curved crack to an equivalent straight crack. The relevance of these types of approximation has been demonstrated for particular crack-shapes and loading configurations, although reasons were not given for why this is so (Kitagawa et al., 1975, Leever et al., 1980, Noda et al., 1994). Approximations to an equivalent straight crack, or other simplified crack-shape, simplifies calculation appreciably and may often sufficiently accurate. In fact, this approximation is made when treating any macroscopically straight crack as being perfectly straight, despite the fairly ubiquitous presence of crack deflection at a microscopic level. The validity of the approximation in this case is generally not questioned. For macroscopically deflecting cracks, this approximation is clearly useful for simply estimating fracture parameters, and thus warrants further investigation.

It is proposed that the shape of a crack may be described by several parameters, from which an approximate SIF value may be predicted. For an edge crack, a common configuration in experiment fracture mechanics, the proposed parameters, shown in Fig. 1. are:

- Crack length perpendicular to the edge, a ;
- Transverse deviation parallel to the edge, d ;
- Crack-tip orientation relative to loading direction, ϕ .

In this paper, the influence of crack shape on crack tip stresses in homogeneous materials is investigated via a simple analytical model. This model is verified through finite element simulations. Second, the curved cracks of graded materials were simulated by FE program ANSYS.

MATERIALS AND METHODS

Analytical Model(For Homogeneous Material)

A simplified approach given by Ashby and Jones (1996), for calculating the mechanical energy release rate, based on the assumption of an elliptical region of stress relaxation around the crack and the increase in this region with the crack extension. For a straight crack of length, $2a$, as in Fig.2, the rate of energy release, G , associated with a crack extension was determined as:

$$G = \frac{k\pi\sigma^2 a}{2E'} \quad (1)$$

Where E' is the effective Young's modulus, and k describes the aspect ratio of the relaxation volume. It can be shown that k is 2, for a through-thickness straight crack in an infinite medium.

Mechanical Energy Release Rate

The mechanical energy release rate is calculated from the following formula (Noda et al., 1994):

$$G = \frac{\pi\gamma\sigma^2}{4E'} [2a(\cos \eta + d \sin \eta) \cos(\phi - \eta)] \quad (2)$$

To estimate the value of γ , the simple case of a straight crack under tensile loading is considered. In this case, parameter d , θ and η are zero, and:

$$G = \frac{\pi\gamma\sigma^2 a}{2E'} \quad (3)$$

This may be compared with the known expression for an edge crack (Broek, 1991):

$$G = \frac{1.12^2 \pi\sigma^2 a}{E'} \quad (4)$$

And the geometrical constant is thus determined as $\gamma = 2(1.12)^2 \approx 2.5$.

Deflection Angle

Whilst a number of different criteria have been used to predict deflection angle, the focus of the current analysis is strain energy release rate. Accordingly, the maximum energy release rate criterion is most appropriate. Considering a kink extending at angle from the tip of a particular curved crack the mechanical energy release rate is estimated from Eq. (2) as:

$$G(\theta) = \frac{\pi\gamma\sigma^2}{4E'} [2a(\cos \eta + d \sin \eta) \cos(\phi - \eta + \theta)] \quad (5)$$

This is maximized for:

$$\frac{dG(\theta)}{d\theta} = 0 \quad (6)$$

After simple sequence of calculations, the optimum value of the kink angle, :

$$\theta_k = \eta - \theta \quad (7)$$

This implies that mechanical energy release rate will be maximized for crack growth perpendicular to the loading direction, which is understood to be the case.

This simple analytical model may not be applied to FGMs, as the elastic property gradient, leads to a spatial variation in strain energy density. It was assumed, however, that curved cracks in FGMs, by analogy with those in homogeneous materials, may also be approximated by simple-shaped cracks. This was investigated with FE simulation, using several different crack-shape approximations.

FINITE ELEMENT SIMULATIONS (FOR BOTH FGMS AND HOMOGENEOUS MATERIALS)

Geometric Modeling

Specimens were modeled in two dimensions under plane stress conditions. Generally, compositionally symmetrical samples, consisting of two graded sections situated between materials 1 and 2, as in Fig. 2. A tensile load is applied to the edge of the plate and the other is clamped. Crack propagation was assumed to initiate from a notch in the graded section, oriented perpendicular to the gradient section. The material gradient was described by the magnitude of elastic property mismatch, $R_E = E_2/E_1$, the width, w , and the shape of the elastic property profile, defined by the exponent, n , in a power-law expression. Continuous and stepped gradients respectively, as shown in Fig. 3, were defined by

$$E(\xi) = E_1(1 + (R_E - 1)\xi^n) \quad (\text{Continuous}) \quad (8)$$

$$E(\xi) = E_1(1 + (R_E - 1)(\text{Int}[N_s \xi] / N_s)^n) \quad (\text{Stepped}) \quad (9)$$

Where N_s is the number of steps across the gradient and $\text{Int}[N_s \xi]$ represents the operation of rounding to the nearest integer. Stepped gradients with smoothing of effective properties at step interfaces were also considered.

In linear elastic problems, it is known that the displacements near the crack tip (or crack front) vary as \sqrt{r} , where r is the distance from the crack tip. The stresses and strains are singular at the crack tip, varying as $1/\sqrt{r}$. To resolve the singularity in strain, the crack faces should be coincident, and the elements around the crack tip (or crack front) should be quadratic, with the midside nodes placed at the quarter points. Such elements are called singular elements. Fig. shows 2D singular element. Meshing was conducted under free meshing conditions using the AMESH command, with isoparametric quadrilateral PLANE 82 elements which have 8 nodes: 4 vortex nodes and 4 midside nodes. The crack tip singularity were modeled using degenerate triangular quarter point elements, which enabled crack tip fields and fracture parameters to obtained. An example of meshing is given in Fig. 4. To improve solution accuracy, the mesh was refined around the crack and the crack tip in particular, with crack tip element size $(a_o/1000)$ where a_o is initial crack length, as shown in Fig. 3. approximately 3500 elements were used in total.

Simulation Of Crack Propagation

Crack propagation was simulated incrementally. Fig. 5 shows a schematic diagram explaining the sequence of events in simulation of crack propagation.

SUMMARY

These were conducted in two stages. In stage I, stationary cracks with a range of shapes in homogeneous specimens were modeled to obtain values for mechanical energy release rate and deflection angle. In stage II, propagation of cracks in homogeneous and graded specimens was simulated, and crack paths and SIF profiles were obtained.

The general specimen configuration for stage I, an edge-cracked size with stresses applied to edge of plate, and a representative mesh, are shown in Fig. 4. Deflection angle was predicting using the maximum energy release rate criterion for consistency with the analytical model.

To investigate a range of crack shapes, a degree of variability within the constraints of the set parameter scheme was introduced by varying the curvature of the cracks, whilst keeping the defined parameters constant. Three different general crack shapes were considered, A, B and C, as shown in Fig. 6. By using each of these for each set of values of a , d , and, the sensitivity to curvature could be examined. It should be noted that, in the geometrical scheme used, the radius of curvature, r , is proportional to a and d , so that when d is varied, the relative curvature, i.e. r/a varies also.

When the entire crack shape was used, the finite extension per increment resulted in a path made up of numerous small line segments. As the propagation direction did not change abruptly, these formed a smooth path. The effect of using approximated crack shapes on predictions of crack-path and stress concentrations was examined. When simplified crack-shapes, as shown in Fig. 7(a), were used, the crack was extended in the same way; however, after each crack extension, a new approximated crack-shape was defined and meshed. This approximated crack shape was used for calculation of the propagation direction for the subsequent increment. This is illustrated schematically in Fig. 7(b). The crack-shape geometry and surrounding mesh was deleted and refined between each increment of the propagation. The crack paths presented here are essentially plots of the variation of crack-tip location, as calculated using a variety of crack-shape approximations.

It should be emphasized that the use of approximated crack shapes in this manner did not improve simulation efficiency, except for simplifying the mesh pattern around the crack which could slightly reduce the number of elements and hence the computation time. Rather, the efficiency of analytical solutions would be improved notably if a simplified crack shape could be used. Establishing the validity of this was a principal aim of this study.

This approach was applied to several different material configurations. The general specimen geometry, an edge-cracked plate in tension, is depicted in Fig. 3. Specimens containing the following material interface configurations were examined:

- (1) No interface (asymmetrically-notched homogeneous specimen), with the notch situated 36 mm from the load line (center of specimen).
- (2) Step interface (biomaterial specimen), with crack initially 8 mm from the interface;
- (3) Continuously-graded interfaces, with parabolic spatial variation in material properties across a 10 mm wide gradient region, and crack initially situated 8 mm from the interface between the gradient region and material 1;
- (4) Continuously graded interface, with parabolic spatial variation in material properties across a 10 mm in wide gradient region, and crack initially situated 8 mm from the interface between the gradient region and material 1;
- (5) Discontinuously-graded interface, with stepped-linear (3 steps) spatial variation in material properties across a 10 mm wide gradient region, and crack initially situated 8 mm from the interface between the gradient region and material 1.

The assumed properties of material 1 were $E_1=3.4$, $\nu_1=0.25$. Properties of material 2 were assumed as $E_2=340$ and $\nu_2=0.25$ for all cases except the homogeneous specimen, which material 1 and 2 were identical (Matthew T.Tillbrook, 2005). The large disparity in elastic properties was assumed so that deflection angles would be high, thereby amplifying the differences which may arise between predictions from different crack-shape approximations.

RESULTS & DISCUSSION

Curved Cracks In Homogeneous Materials

The predictions from this analytical model are shown in Figures 8 to 10, along with results obtained from finite element analysis. The FE results are shown as dots or triangles, with a degree of scatter between results obtained for different shape types, A, B and C, whilst analytical model results are shown as solid lines. Mechanical energy release rate values are normalized with respect to effective Young's modulus, E' , and applied stress, σ , so that the effect of crack geometry may be examined directly. However, as applied stress and effective Young's modulus were held constant for all cases examined, the absolute and normalized values for mechanical energy release rate are directly proportional.

The effect of variation in relative deviation, d , is illustrated in Figs.8a and b for cracks with loading angles of $\eta = 0^\circ$ & 30° respectively. There is a systematic influence of d on the deflection angle. Although the difference is larger for larger values of d , the influence of d seems to be greater for smaller d values, as the slope of the variation of θ with d is greater in that region. Variation in d leads to a variation in the curvature at the crack tip, so the influence of d is likely to be attributable to curvature.

The effect of variation in crack-tip angle, ϕ , is illustrated in Fig. 9(a and b) for cracks with loading angles of $\eta = 0^\circ$ & 30° respectively. Crack-tip orientation is seen to influence fracture parameters significantly. Increasing the crack-tip angles leads to an increase in deflection angle, and a decrease in mechanical energy release rate. Very close agreement is observed between the model and FE predictions for both energy release rate and deflection angle.

The effect of variation in crack shape is illustrated in Fig.10 (a and b) for cracks with loading angle of $\eta = 0^\circ$ & 30° respectively. In these cases, the key shape parameters remain constant whilst the shape of the crack is varied. This was achieved by varying the radius of curvature in the circular arc section of the crack shape. Crack curvature has only a minor influence on fracture parameters, as anticipated in the original hypothesis. This implies that a wide range of cracks may be simulated reasonably accurately by analogy with simplified crack shapes. Crack curvature does seem to have a slight effect, especially when the radius of curvature near the crack tip is small. This is in agreement with the findings of (Kitagawa et al., 1975).

Curved Crack In Graded Materials

Crack paths and SIF magnitude profiles obtained using each of the approximated crack shapes are compared with those obtained using the entire crack-path shape, in Figs 11 to 15. SIF magnitude has been normalized with respect to the SIF for straight crack of the same length in a homogeneous specimen of the same dimensions and loading. This allows the influence of material property variation to be examined independent of the effects of crack length, which would otherwise dominate the variation of SIF magnitude. The normalized SIF magnitude profiles are plotted against crack-tip position in the horizontal direction so that variation across the interface region may be compared between the different crack-shape approximations.

Fig. 11 shows results for the asymmetrically-notched homogeneous specimen. Path predictions and SIF magnitudes obtained using crack-shape approximations show very good agreement with those obtained using the entire crack-path. In the homogeneous material specimen in Fig.11, the use of an approximated crack shape appears to have almost no effect at all on SIF magnitude predictions. Results for the bimaterial specimen are presented in Fig. 12. Deviation between results from approximated crack shapes and the entire crack path is more significant in this case. Fig. 12 and 14 show the results for the two continuously graded specimens with different gradient steepness. Results for the discontinuously graded (step graded) specimen, which contained three steps, are shown in Fig. 15.

The presence of material inhomogeneity, in Figs 12 to 15, seems to cause greater deviations between results from approximated crack shapes and those obtained using the entire crack path. In

inhomogeneous specimens, the results predicted using straight deviated significantly from the results for exact crack shape. Those approximations tended to result in less deflection. This could be attributed to a slight skewing of the crack tip stress field, caused by the difference in crack tip orientation of the approximated and exact crack shapes. The piecewise linear approximation gave good predictions for all the configurations examined.

The crack path shows a cumulative deviation effect. In the first increments of crack growth, before any deflection has occurred, the exact and approximated crack shapes are identical, and then they become progressively more different as the crack propagate, as was shown schematically in Fig. 7(b). Concordant with this, differences in the crack propagation direction, due to the use of a crack shape approximation, are initially very small then these increase as the crack extends. Furthermore, the differences accumulate, and the differences between crack paths lead to further divergence.

For cracks in the specimen with some material inhomogeneity, the SIF magnitude varied significantly across the interface region. In Fig. 12, it increases sharply as the biomaterial interface is approached. A similar effect is observed as the crack approaches the two interfaces in the step graded specimen in Fig. 15. A more continuous variation in SIF magnitude is observed for the continuously graded specimens, though these still exhibit notable variation with crack tip position. The contrast between the results for linear property variation in Fig. 13 and those for parabolic variation in Fig. 14 highlights the importance of material property distribution in influencing crack tip stresses.

For the crack approaching the biomaterial interface in Fig. 12, SIF magnitudes varied significantly between simulations using different crack shape approximations. For a crack with tip situated 1 mm from the biomaterial interface, for instance, the relative SIF magnitude calculated for using exact crack shape is 1.8 times that calculated using the straight crack approximation. This means that using the straight crack approximation would lead to an overestimate of critical load by a factor of 1.8. Similar comparisons may be made for crack in continuously graded and step graded specimens. These also show significant differences between SIF magnitudes obtained from different crack shape approximations.

CONCLUSIONS

From this analysis, the following concluding points can be deduced,

1. Curved cracks in homogeneous materials may be reasonably approximated by equivalent straight cracks for the calculation of mechanical energy release rates and deflection angles.
2. Piecewise linear crack shapes provide a significantly better approximation than straight crack shapes. Accordingly, analytical solutions for piecewise linear cracks in graded materials would be very useful, and should be a focus of further work in this area.

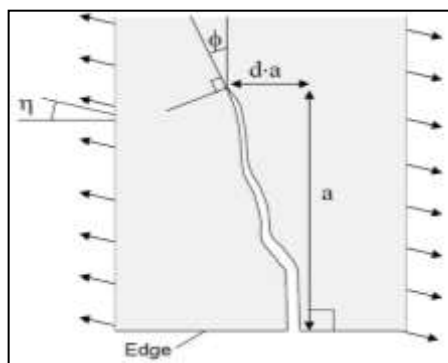


Fig. 1 Example of deviating crack showing key parameters

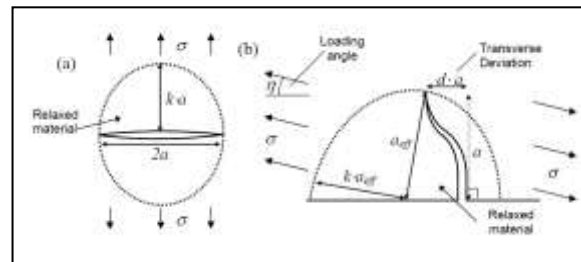


Fig. 2 Stress relaxation volume around (a) a straight internal crack under tensile loading (b) a curved edge crack under mixed mode loading

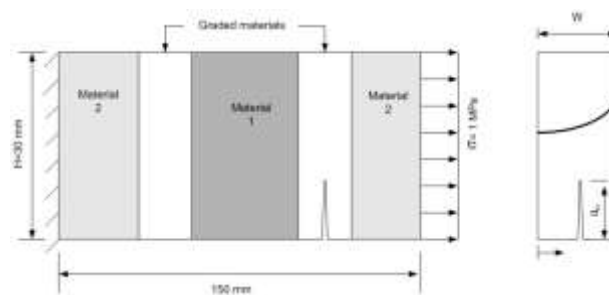


Fig. 3 Graded material specimen used in simulation

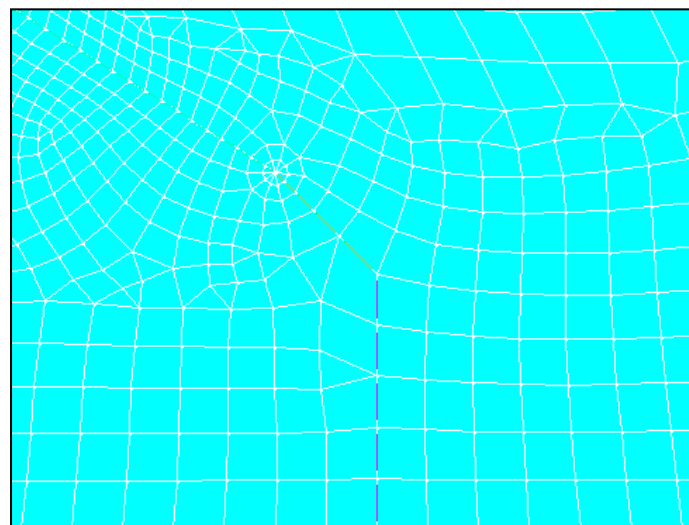


Fig. 4 Representative meshing of finite element modeling around the crack tip and crack front

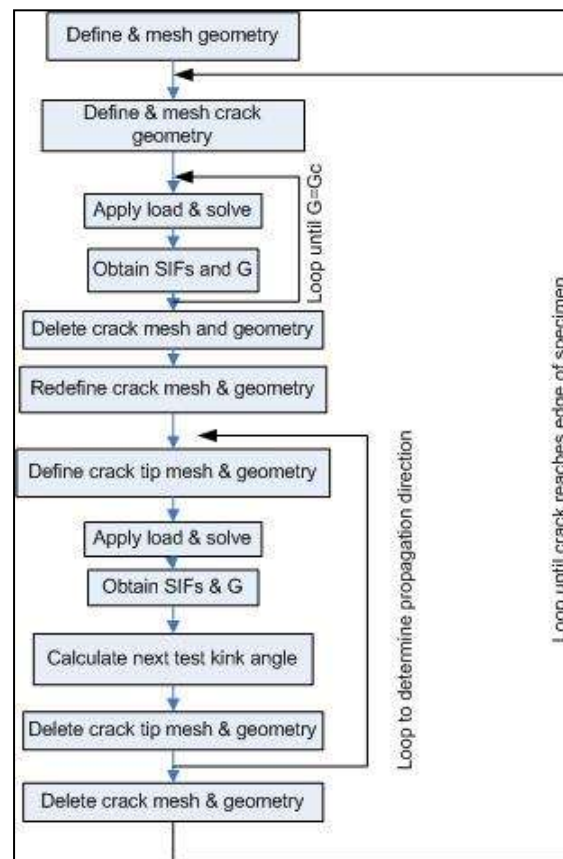


Fig. 5 schematic diagram shows the sequence of procedure of crack propagation using ANSYS

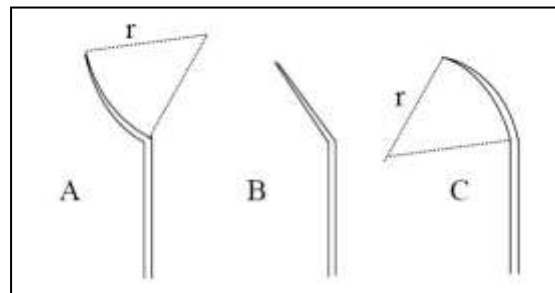


Fig. 6 Generic crack shapes used in FE validation (Stage I):A-Concave, B-Piecewise linear, C-Convex(Stage I)

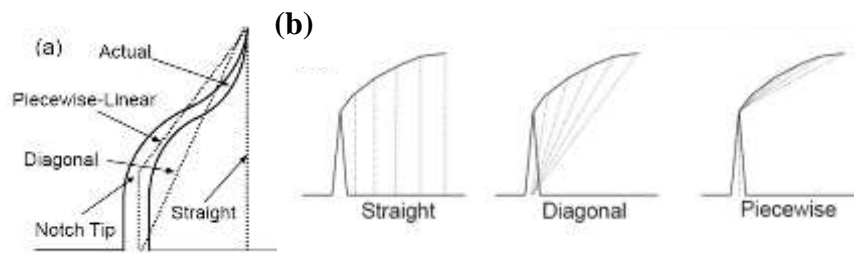
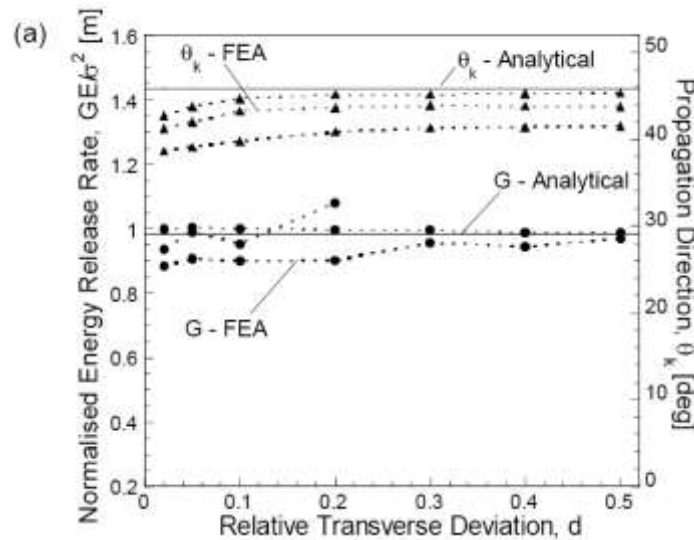
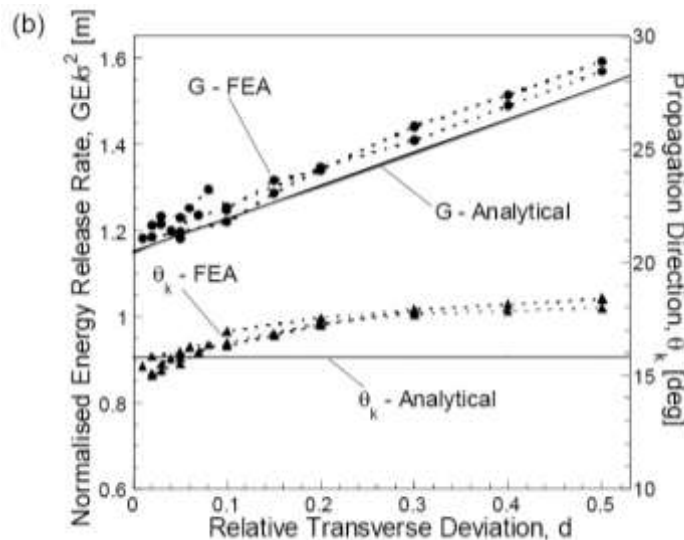


Fig. 7 Illustration of crack approximation (Stage II)

Fig. 8a Effect of transverse deviation, d , on mechanical energy release rate and propagation direction under tensile loading ($\eta=0^\circ$)Fig. 8b Effect of transverse deviation, d , on mechanical energy release rate and propagation direction under tensile loading ($\eta=30^\circ$)

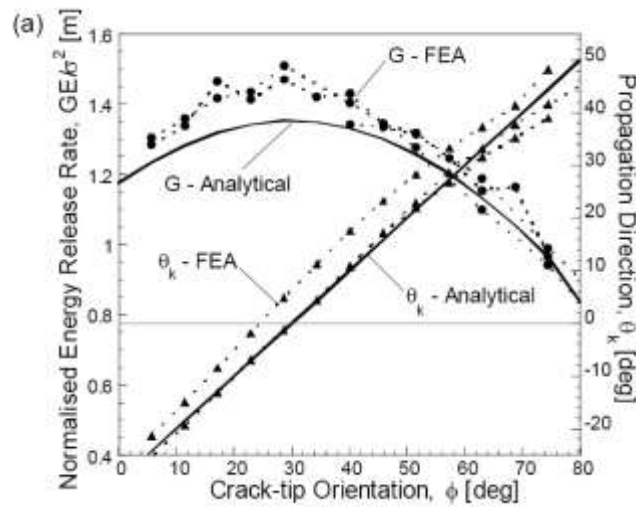


Fig. 9a Effect of crack-tip orientation on mechanical energy release rate and propagation direction under tensile loading($\eta=0^0$)

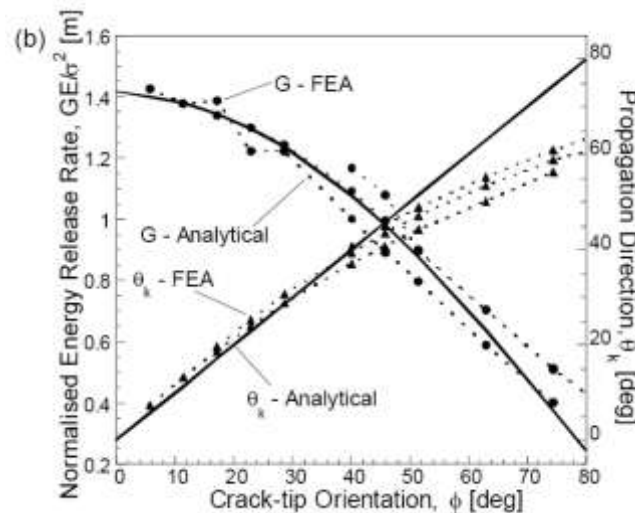


Fig. 9b Effect of crack-tip orientation on mechanical energy release rate and propagation direction under tensile loading($\eta=30^0$)

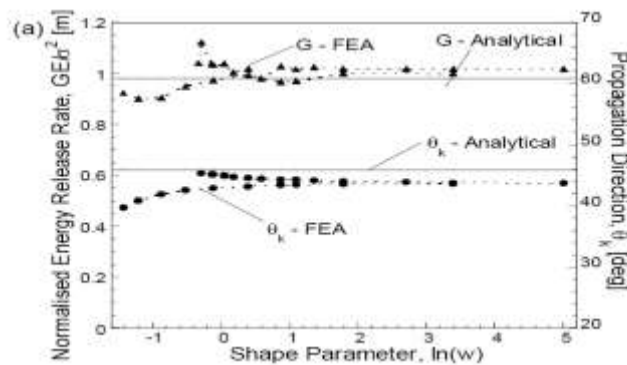


Fig 10a Effect of variation in radius of curvature at crack tip on mechanical energy release rate and propagation direction under tensile loading($\eta=0^0$)

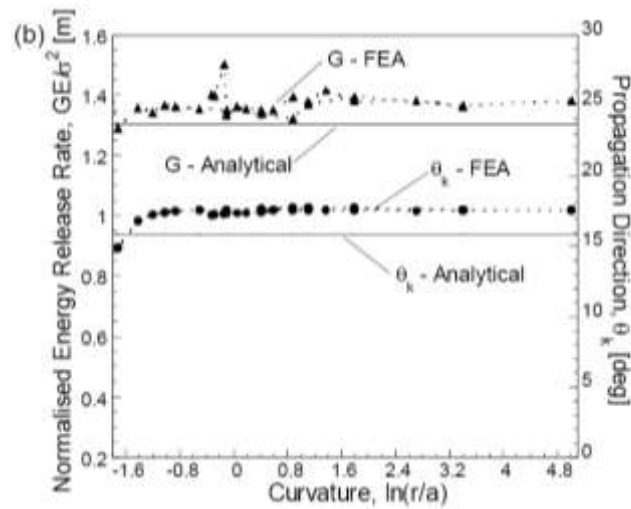


Fig 10 b Effect of variation in radius of curvature at crack tip on mechanical energy release rate and propagation direction under tensile loading($\eta=30^\circ$)

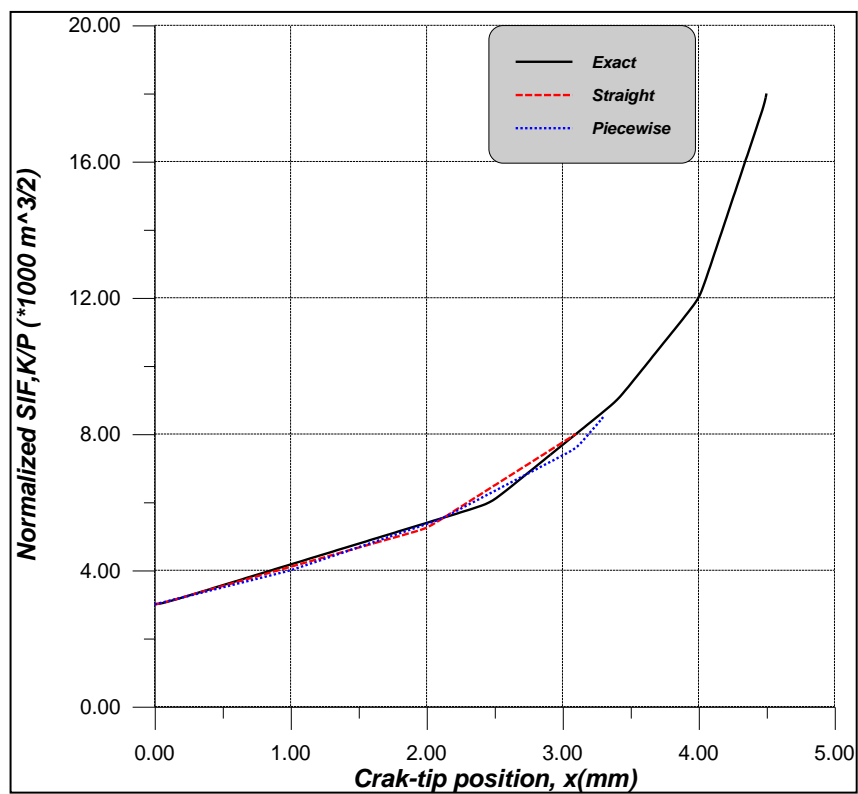


Fig. 11 Normalized stress intensity factor in homogeneous specimen for three cases of approximated cracks

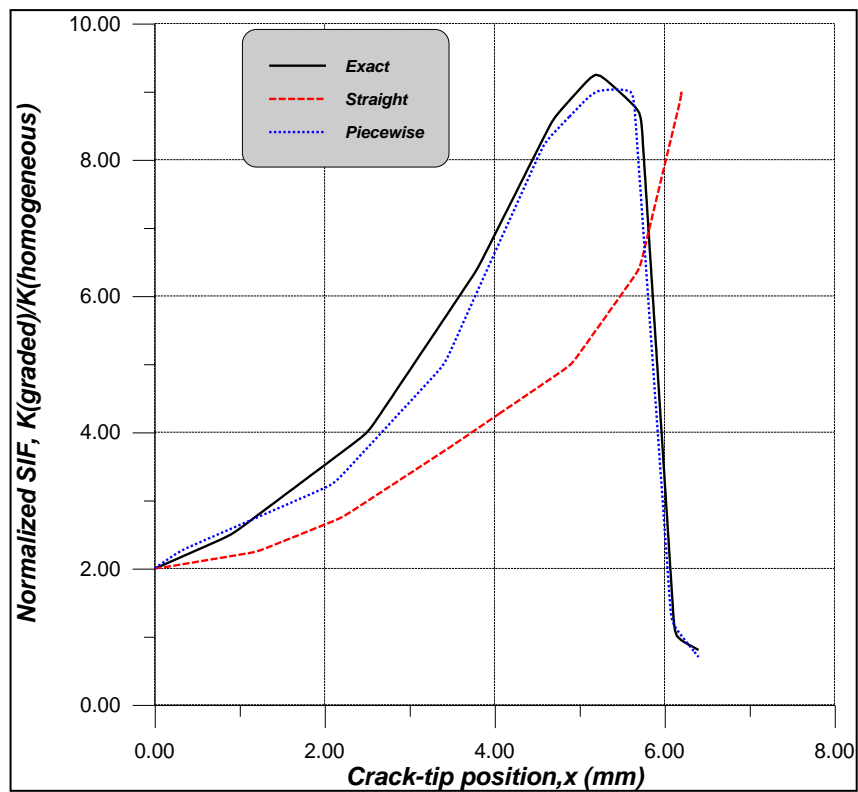


Fig. 11 Normalized stress intensity factor in bimaterial specimen for three cases of approximated cracks

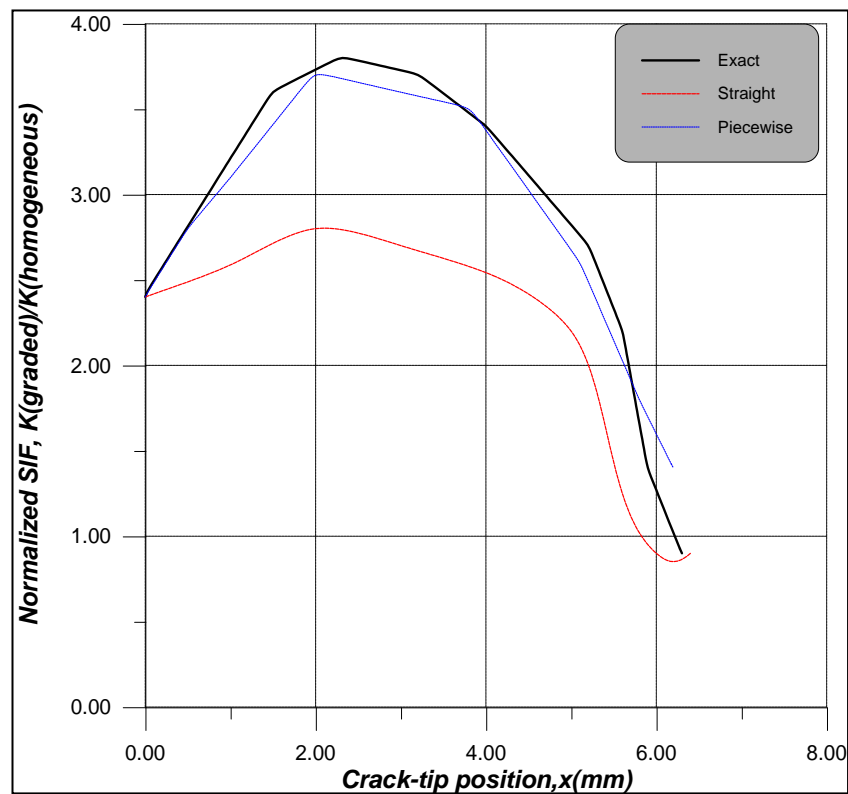


Fig. 13 Normalized stress intensity factor graded specimen (with linear variation in Young's modulus) for three cases of approximated cracks

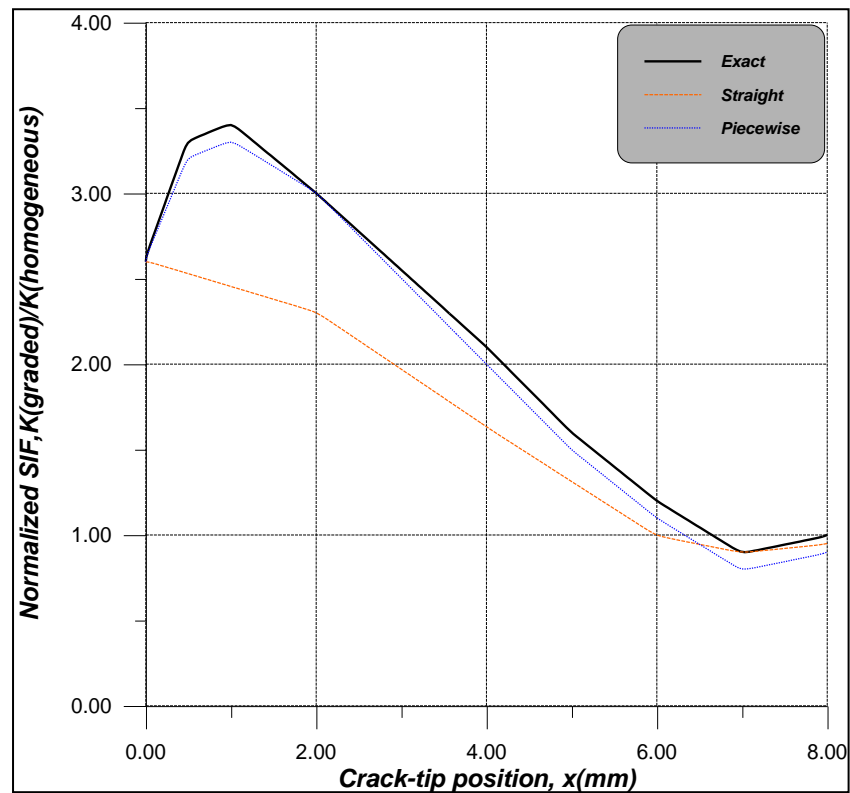


Fig. 14 Normalized stress intensity factor graded specimen (with parabolic variation in Young's modulus) for three cases of approximated cracks

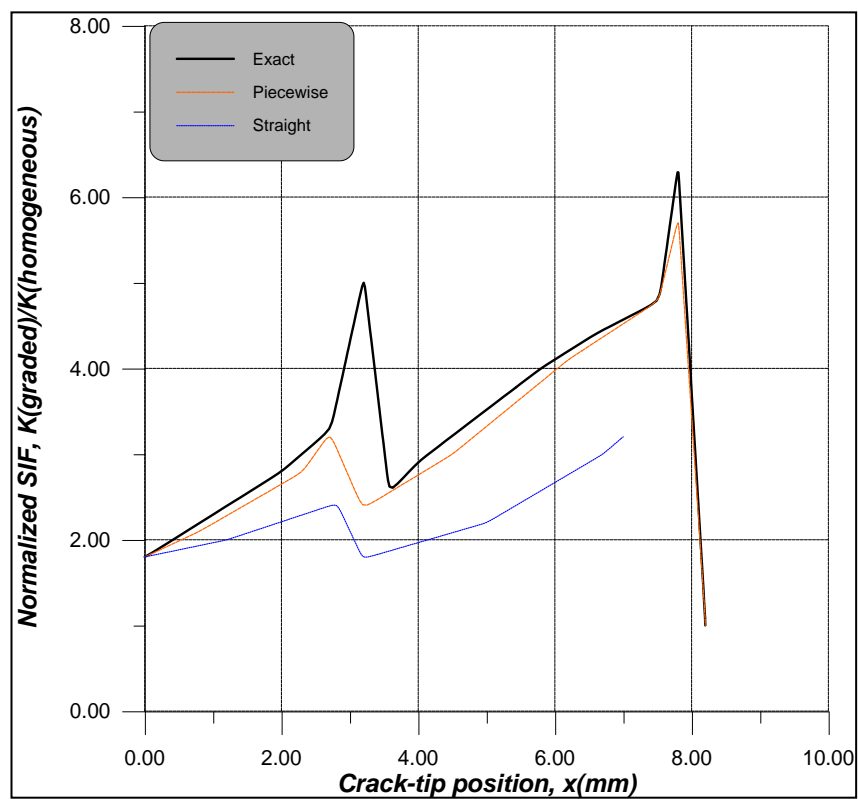


Fig. 15 Normalized stress intensity factor graded specimen (with stepped linear variation in Young's modulus) for three cases of approximated cracks



References

- ANSYS (2007) Version 11 Documentation, ANSYS Inc. Canonsburg,PA.
- Ashby MF, Jones DRH (1996), Engineering Materials 1: An introduction to their properties and applications, 2nd edition, Butterworth Heinemann.
- Broek (1991), Elementry Engineering Fructure Mechanics, 4th ed., Kluwer, Dordrecht.
- Chetterjee (2006), On The Elasic Moduli Of Some Heterogeneous, J Mech Phys Vol 13:223-227.
- Dag_, S., Kadio_lu, S. and Yahgi, O.S., 2004, “Circumferential Crack Problem for an FGM Cylinder Under Thermal Stresses”, *Journal of Thermal Stresses*, Vol. 22, pp. 659-687.
- Erdogan (2006), Fracture Mechanics of FGM, Vol. 12, pp. 112-122.
- Jin, Z.-H. and Paulino, G.H., 2001, “Transient Thermal Stress Analysis of an Edge Crack in a Functionally Graded Material”, *International Journal of Fracture*, Vol. 107, pp. 73-98.
- Jin & Batra(2007), Some Basic Fracture Mechanics Concepts On FGM, J Mech Phys Vol 45:20-27.
- Kitagawa H, Yurk R and Ohira T (1975) , Crack Morphological Aspects In Fracture Mechanics, Engineering Fract Mech : 515-29.
- Leever Ps, Radon JC and Cuvler LE (1980), Fracture Trajectories In A Biaxially Stressed Plate, J Mech Phys Vol. 24: 381-390.
- Mattew T. Tllboork (2005), Thermal Fatigue Of Heterogeneous Materials, Thesis.
- Noda N, Oda K and Ishi K(1994), Analysis Of Stress Intensity Factor For Curved Cracks, JSME Int vol.6: 360-365.
- Taya , Kfoury & Khan (2005), Functionally Graded Thermal Barrier Coating, Material Science Vol. 10: 102-114.

•

List of Symbols

- a: Crack length, mm
- d: Transverse deviation parallel to the edge, mm
- E': Effective young's modulus, Mpa
- G: Mechanical energy release rate, J/mm²
- h: Height of specimen, mm
- K: SIF, Mpa(\sqrt{mm})
- k: Aspect ratio of the relaxation volume
- w: Gradient width, mm
- R_E: Young's modulus ratio
- ϕ : Crack tip position relative to loading direction, degree
- γ : Gradient parameter
- η : Loading angle, degree
- θ : Crack angle, degree
- σ : Stress, Mpa
- ξ : Relative crack position

DEVELOPING A COMPUTER PROGRAM FOR MODELING THE STADIA MEASUREMENTS FOR TACHEOMETRY WORKS

Asma Th. Ibraheem
Nahrain University
College of Engineering
Department of Civil Engineering

Afrah M. Daham
Baghdad University
College of Engineering
Department of Surveying

ABSTRACT:

Tacheometry is used to measure the lengths of traverse sides, to check the more accurate taped distances in order to uncover gross errors or mistakes and to determine differences of elevation between points. It's most general use is found in the compilation of planimetric and topographic maps by field methods alone, by which distances, elevations and directions to points are to be determined from field control points whose positions have been established by a higher order of accuracy.

The principles of stadia measurement by use of the transit or theodolite or total station is one of the main method of tacheometry. This paper presents the principles of stadia measurement and a computer program **MSM** (**M**odeling the **S**tadia **M**easurements). The program is formulated and written by using the Visual Basic language, Version 6. This version of the language is objecting oriented provided with comprehensive tools to simplify the task of programming and to provide the programmer with wide range of options for design of the user interface system.

الخلاصة:

التاكيوميترية يستعمل لقياس اطوال اضلاع المضلع، لتدقيق المسافات المسجلة والاكثر دقة لكي تكشف الاخطاء الاجمالية وتعيين اختلاف الارتفاعات بين النقاط. ويعتبر استعمال عام جدا في تجميع الخرائط البلانومترية، الخرائط الطبوغرافية بواسطة طرق الحقل لوحدها، عن طريق قياس المسافات، والارتفاعات، وقياس الاتجاهات الى النقاط وذلك لتعيين نقاط الضبط الارضي التي اسست بدقة عالية.

ان مبادئ طريقة الستيديا والتي تتم باستخدام اجهزة الترانست او الثيودولايت او جهاز المحطة الكاملة (Total Station Instrument) هي واحدة من الطرق الرئيسية للتاكيوميترية. ان هذا البحث يعرض مبادئ طريقة الستيديا وتم عمل برنامج حاسوب اسمه ((**MSM**)) (**M**odeling the **S**tadia **M**easurements). تم اعداد البرنامج باستعمال لغة الفجوال بيسك، نسخة 6. هذه النسخة من اللغة موجهة ومجهزة بالأدوات الشاملة لتبسيط مهمة البرمجة ولتزويد المبرمج بتشكيلة واسعة من الخيارات لتصميم واجهات البرامج.

Keyword:

Stadia Measurements, Measurement by stadia horizontal sights, Stadia Leveling, Applications of Stadia Measurement, Stadia Surveying, Horizontal Measurements Distances and Tacheometry.

1. INTRODUCTION

The term tacheometry in surveying is used to denote the procedures for obtaining horizontal distances and difference in elevation by rapid indirect methods. The procedure is sometimes referred to as stadia, optical distance measurement or telemetry [4].

The stadia method is a rapid and efficient way to measure distances accurately enough for trigonometric leveling, some traverse, and the location of topographic details. Furthermore, a two-or three-man party can replace the three-or four-man party required in transit-tape surveys. The term stadia comes from the Greek word for a unit of length originally applied in measuring distances for athletic contests. The word denoted 600 Greek feet, or 606 ft 9 in. by present-day American standards.

The term "Stadia" is now applied to the cross wires and rod used in making measurements, as well as to the stadia method itself. Stadia reading can be taken with modern transits, theodolites, levels, and Total Station [1].

2. BASIC PRINCIPLE:

Stadia is based on similar triangles between the object, the focal point of lens, and the reticle of the instrument. The relationship is shown in Figure (1).

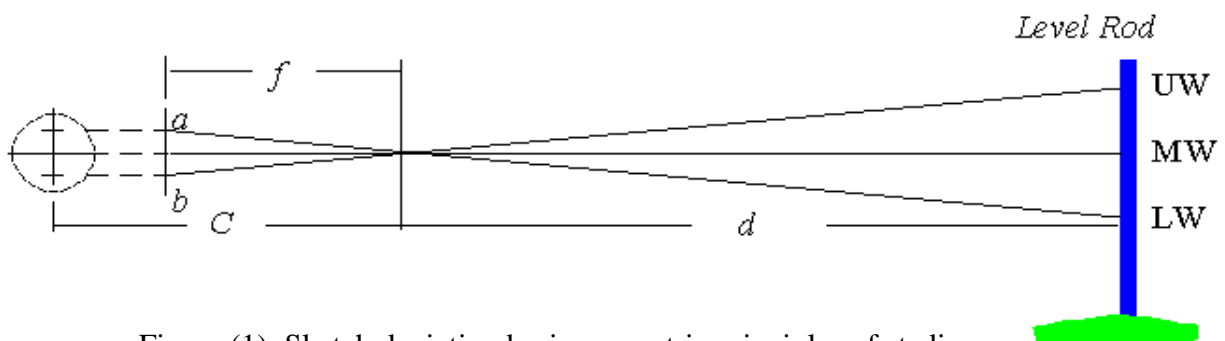


Figure (1): Sketch depicting basic geometric principles of stadia.

If we let

- $ab = i$, and
- $I = UW - LW$

$$\frac{f}{ab} = \frac{d}{I} \Rightarrow d = \frac{f}{ab} I \quad (1)$$

then

If $f/ab = K$, then $d = KI$ and the horizontal distance, D , from the instrument to the rod is:

$$D = KI + C \quad (2)$$

3. MEASUREMENT BY STADIA FOR HORIZONTAL SIGHTS

The stadia method is based upon the principle that in similar triangles homologous sides are proportional. Thus in Figure (2), which shows an external-focusing telescope, light rays from points A and B passing through the center of the lens the form a pair of similar triangles AmB

and amb . Here $Ab=R$ is the rod intercept (stadia interval) and ab is the interval between the stadia wires [4].

Standard symbols used in stadia measurements, and their definition, are as follows:

f = focal length of the lens (a constant for any particular compound objective lens). It can be determined by focusing upon a distant object and measuring the distance between the center (actually the *nodal point*) of the objective lens and the reticle.

f_1 = distance from the center (actually the nodal point) of the objective lens to the plane of the cross hairs when the telescope is focused on some definite point.

f_2 = distance from the center (actually the nodal point) of the objective lens to definite point when the telescope is focused on that point. When f_2 is infinite, or very large, $f_1=f_2$.

i = interval between the stadia wires (ab in figure (2)).

f/i = stadia interval factor, usually 100.

c = distance from the center of the instrument (spindle) to the center of the objective lens. It varies as the objective lens moves in and out for different sight lengths but is generally considered to be a constant [3].

$C=c+f$. C is called the stadia constant although it varies slightly with c .

d = distance from the focal point in front of the telescope to the face of the rod.

$D=C+d$ = distance from the center of the instrument to the face of the rod.

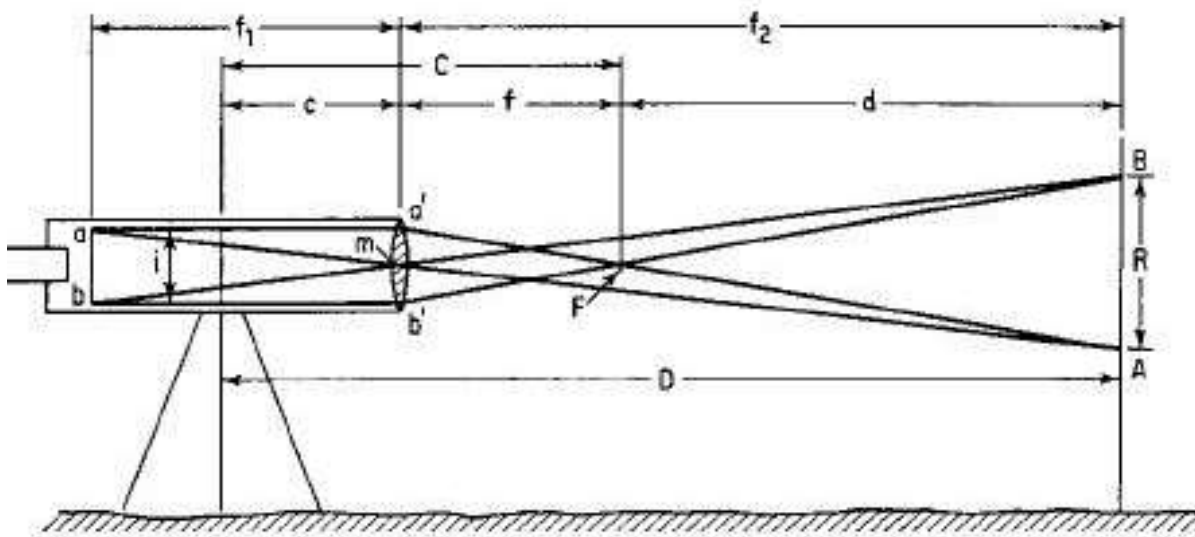


Figure (2): Principle of stadia, external-focusing telescope.

4. INCLINED MEASUREMENT

When collecting measurements using stadia as presented earlier, the requirement of having horizontal sights is limiting in normal terrain. Thus, the stadia formulas need to be developed for inclined measurements. In Figure (3), the geometric relationships of an inclined stadia measurement can be seen. In this figure, the desired position of the rod is perpendicular to the line of sight as shown by r' . Since it is impractical in the field to hold the rod in this manner, a correction to the readings on the level rod r must be determined. From simple geometric relationships, it can be shown that the altitude angle of the line of sight, α , is the same as the angle between positions of r' and r . For small vertical angles, we can make the assumption that the angle at the intersection of the upper wire line of sight and r' is 90° , and thus a simple right triangle relationship can be developed between the reading on the rod r and the corrected reading on the rod r' as :

$$I' = I \cos(\alpha) \dots\dots\dots (3)$$

Making this correction to Equation (1), the slope distance between the instrument and the rod is [4]:

$$S = KI \cos(\alpha) + C \dots\dots\dots (4)$$

The Equation (3) can now be used to compute the horizontal distance between the instrument and the rod as [5]:

$$H = KI \cos^2(\alpha) + C \dots\dots\dots (5)$$

Since theodolites and total stations read zenith angles, we can use the trigonometric relationships of $\sin(a) = \cos(90-a)$ to derive a similar equation for zenith angle reading instruments as:

$$H = KI \sin^2(z) + C \dots\dots\dots (6)$$

where z is the zenith angle of the line of sight. Similarly an equation for computing V is:

$$V = KI \cos(\alpha) \sin(\alpha) = KI \cos(z) \sin(z) \dots\dots\dots (7)$$

Note that in Equation (6), the term $C \sin(\alpha)$, or alternatively $C \cos(z)$ has been dropped since for small altitude angle or large zenith angles the value of the trigonometric functions is very small, and thus so is their product with C [4].

Using Equations (2) and (6), an expression for the elevation difference between ground at the instrument station and at the rod can be derived as [5]:

$$\Delta Elev = hi + V - MW \dots\dots\dots (8)$$

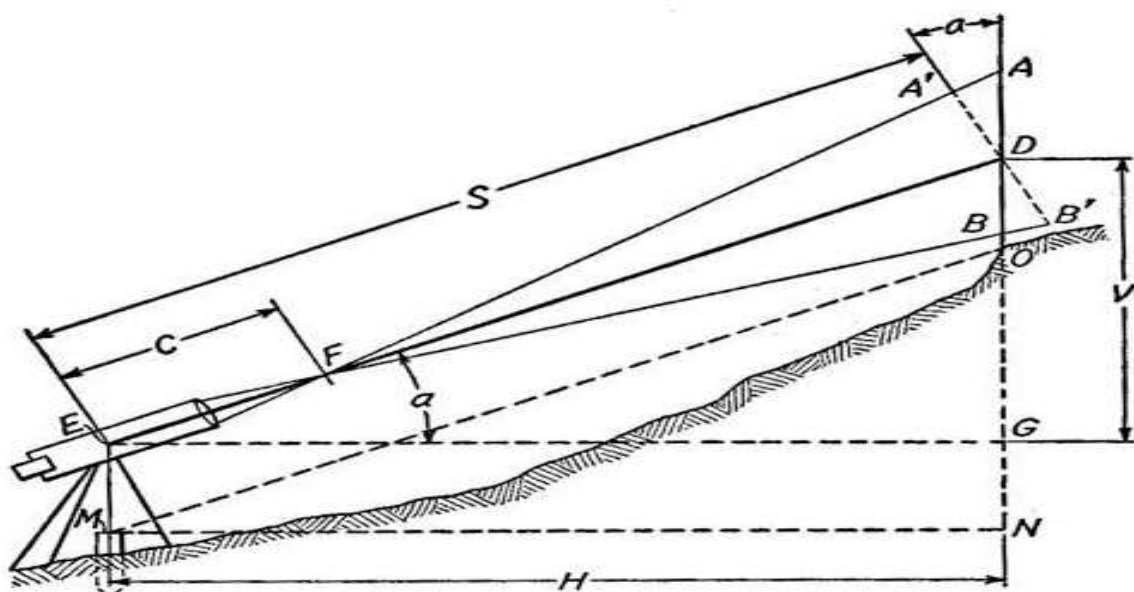


Figure (3): Inclined stadia measurement.

4.1 STADIA TRAVERSES

In a transit-stadia traverse, distances, horizontal angles, and vertical angles are measured at each corner. Reduction of stadia notes as the survey progresses provides elevations to be carried from hub to hub. Average values of stadia distances and differences in elevation are obtained from a foresight and a backsight on each line. An elevation check should be secured by closing on the initial point, or on bench marks near both ends for an open traverse [1].

4.2 TOPOGRAPHY

The stadia method is most useful in locating numerous topographic details, both horizontally and vertically, by transit or plane table. In urban areas, angle and distance readings can be taken faster than a notekeeper is able to record the measurements and prepare a sketch [4].

4.3 STADIA LEVELING

The stadia method is adaptable to trigonometric leveling. The h.i. is determined by sighting on a point of known elevation, or by setting the instrument over such a point and measuring the height of the horizontal axis above it with a stadia rod [2]. The elevation of any point can then be found by computation from the rod intercept and the vertical angle. If desirable a leveling circuit can be run to establish and check the elevations of two or more points [6].

5. PRECISION

A ratio of error of 1/500 can be obtained for a transit-stadia traverse run with ordinary care. Short sights, a long traverse, and careful work may give ratios up to 1/100. Errors in stadia work are usually the result of poor rod readings rather than incorrect angles. An error of 1 min in reading a vertical angle does not appreciably affect the horizontal distance. The same 1-min error produces a difference in elevation of less than 0.1 ft on a 300 ft sight for any vertical angle [4].

6. MODELING THE STADIA MEASUREMENT

The stadia measurement is modeled by Visual Basic language as software named **MSM** (**M**odeling the **S**tadia **M**easurements). The program is formulated and written by using Visual Basic, Version 6. This version of the language is object oriented provided with comprehensive tools to simplify the task of programming and to provide the programmer with wide range of options for design of the user interface system. Figure (4) shows the flowchart of this software.

The input data for each one of these forms and the link between these forms are described in the following sections with the aid of flowcharts, which provide description for the logic and the steps followed in the development of the program.

7. PROGRAM MENUS AND INPUT FORMS

In Visual Basic programming the term FORM is usually used to refer to the graphical area appeared on the screen, which is used to hold objects that may be fields or tables containing values, graphics or text boxes for input the required data values. The form interface is used because most people are familiar with paper form. These forms are written in such away to be user friendly and allow the data input to the program interactively. When the program (MSM) is run, the user presented with the form shown in figure (5).

This form displays program name and version, if the user select "Traverse and Leveling" from the main program menu interface displayed on the screen. The main Form of (MSM) also contains the cases of plotting the traverse and the cases of the plotting profile, as shown in figure (5).

The cases of plotting the traverse are classified into eight cases (number of sides = (3), number of sides = (4), number of sides = (5), number of sides = (6), number of sides = (7), number of sides = (8)), as it is clear in figure (5) and the cases of plotting profile classified into five cases (number of stations = (3), number of stations = (4), number of stations = (5), number of stations = (6), number of stations = (7),), as shown in figure (6).

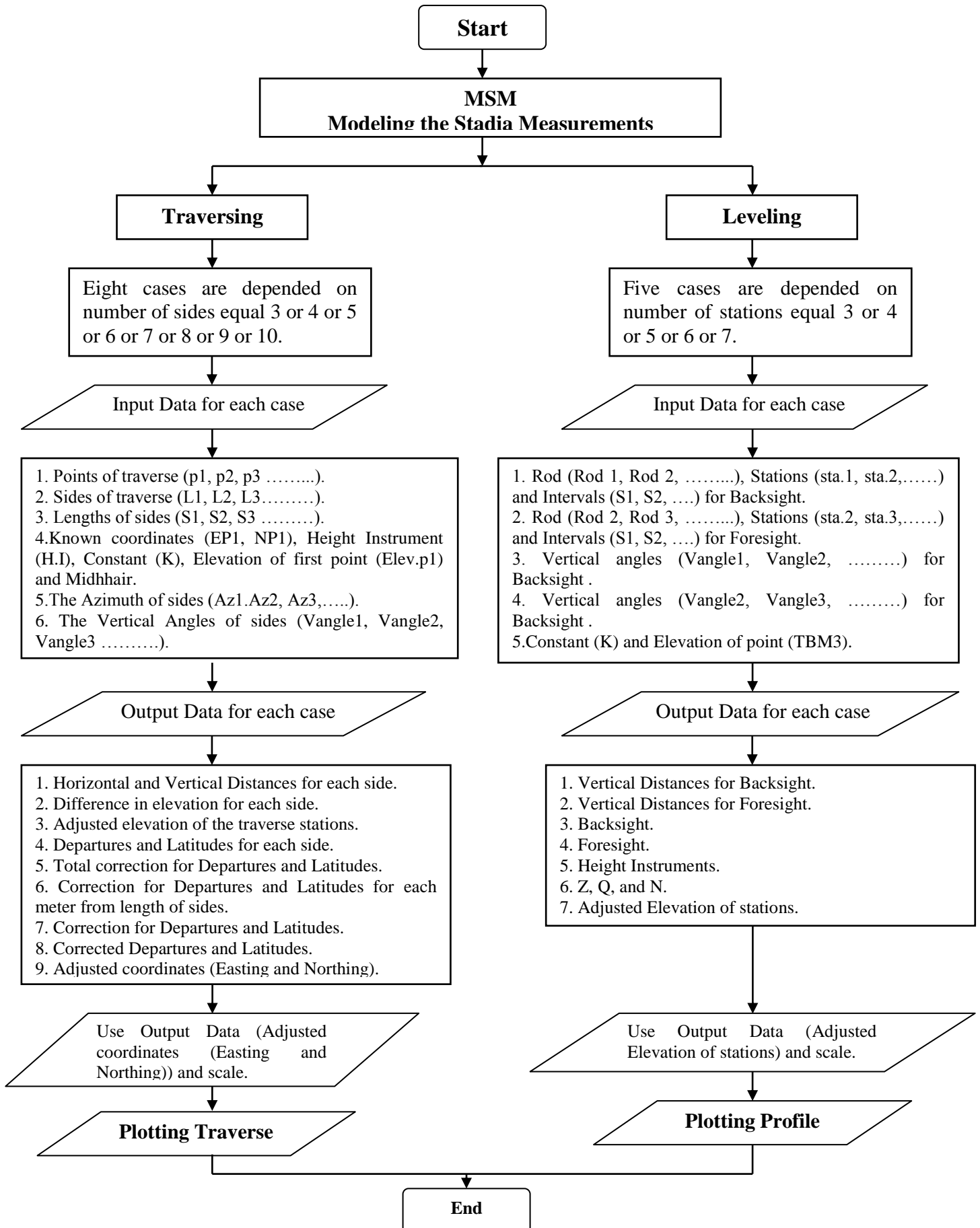


Figure (4): Flowchart of work steps.

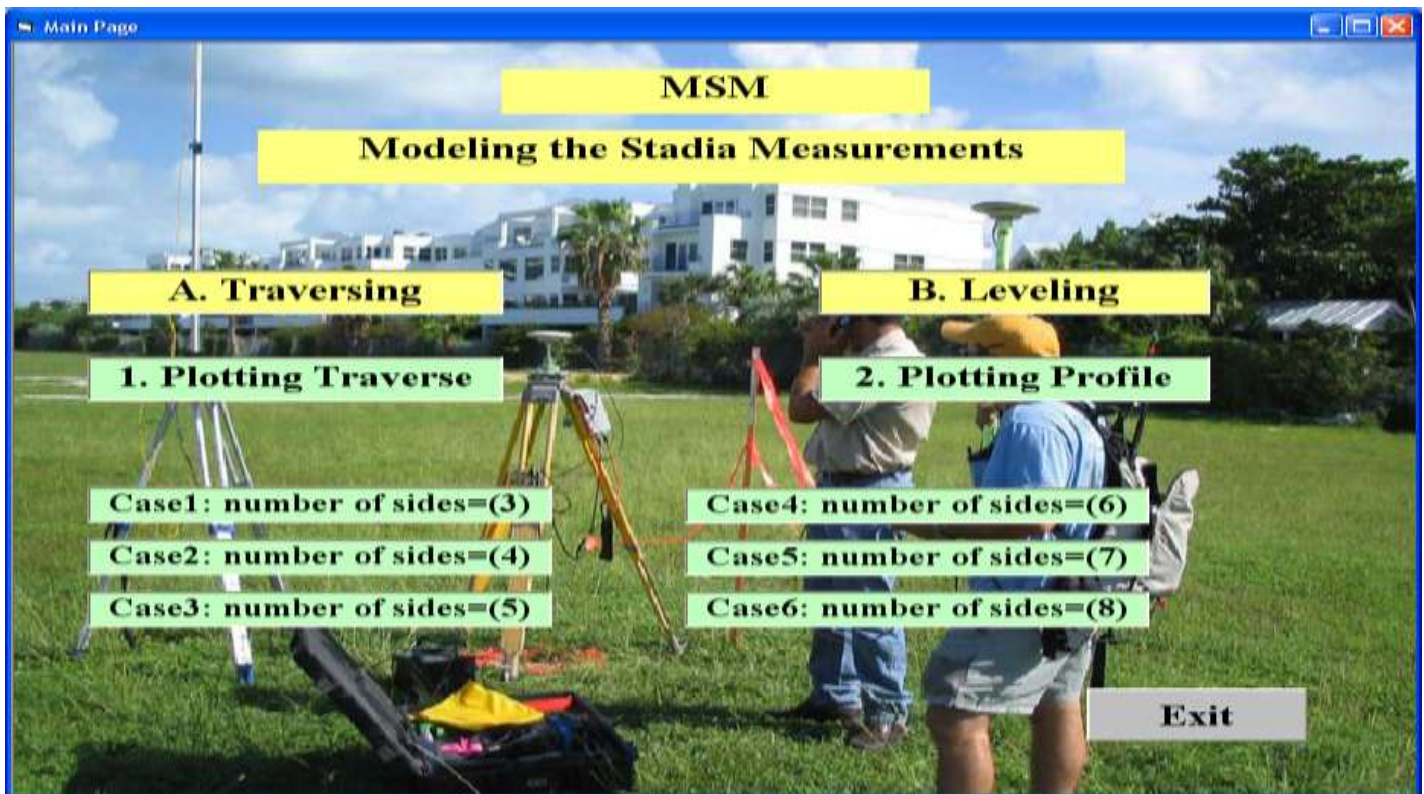


Figure (5): The main page of (MSM).

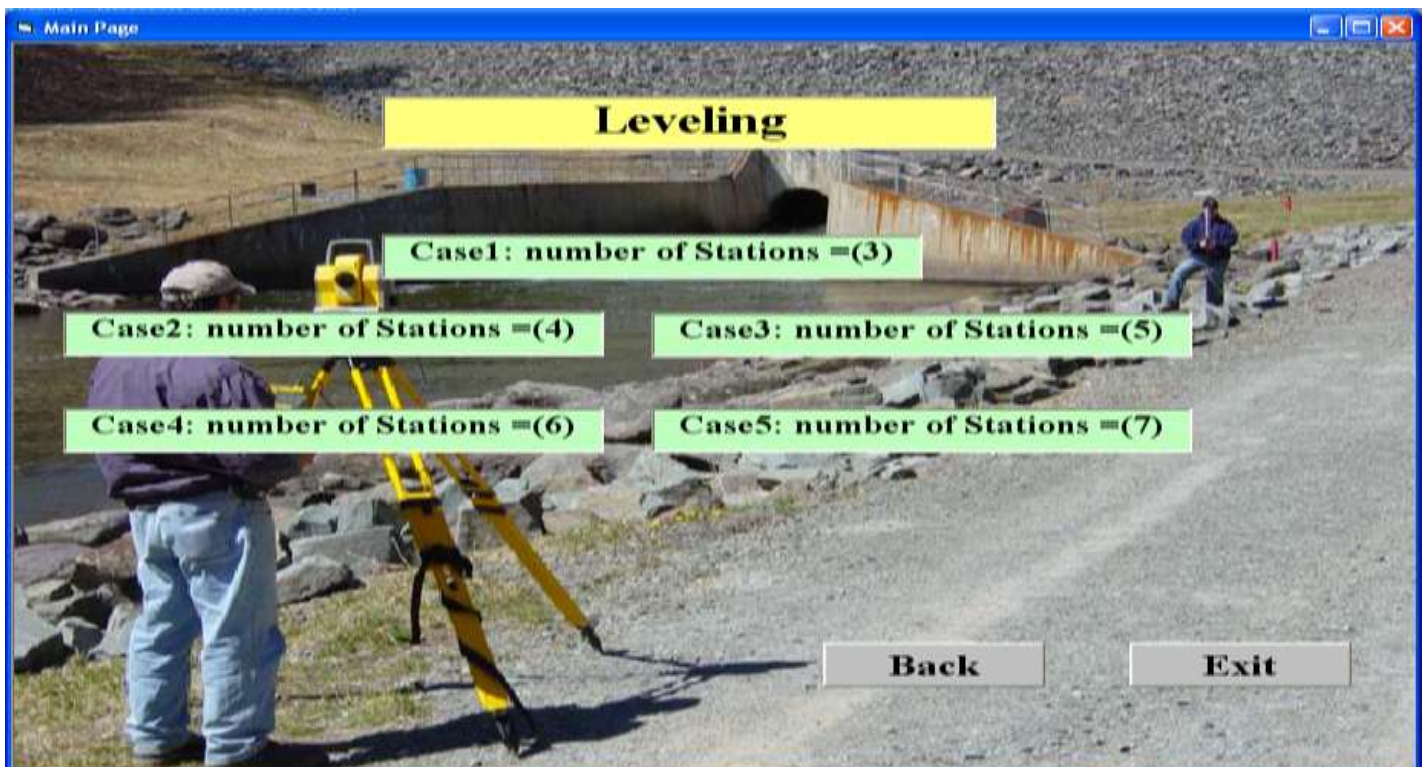


Figure (6): The main page of Leveling.

7.1 TRAVERSING

Traversing design is described in eight cases of the following:

1. Case1: number of sides = (3).
2. Case2: number of sides = (4).
3. Case3: number of sides = (5).
4. Case4: number of sides = (6).
5. Case5: number of sides = (7).
6. Case6: number of sides = (8).
7. Case7: number of sides = (9).
8. Case8: number of sides = (10).

These menu items are described in the following sections.

Case1: number of Sides = (3)

If the user selects this option, the form shown in figure (5) is displayed on the screen. First the user input information's the requirements of the first traverse and is listed below:

1. Points of traverse (P1, P2, P3,).
2. The sides of traverse (L1, L2, L3).
3. Lengths of sides (S1 S2, S3).
4. Known coordinates (EP1, NP1), Height Instrument (HI), Constant (K), Elevation of first point (Elev.p1) and Midhair.
5. The Azimuth of sides (Az1, Az2, Az3).
6. The Vertical angles (Vangle1, Vangle2, Vangle3)

When the user input the required data as displayed in figure (7/a), the program begins the calculation of the elements (Horizontal Distance for each side, Vertical Distance for each side, Difference in Elevation for each side, Adjusted Elevation of the Traverse Stations, Departure of Sides, Sum of Departures, Latitude of Sides, Sum of Latitudes, Total Correction for Departures and Latitudes, Correction for Departure and Latitude for each meter from Length of Sides, Correction for Departures, Correction for Latitudes, Sum Correction for Departures and Latitudes, Corrected Departures, Corrected Latitudes, Sum Corrected Departures, Sum Corrected Latitudes and Adjusted Coordinates (Easting and Northing of Points)) as shown in figure (7/b).

Figure (7/a): Traverse (3 Sides).



Traverse (3 sides)

Input

Points of Traverse

P1 A

P2 B

P3 C

The Sides of Traverse

L1 AB

L2 BC

L3 CA

Lengths of Sides

S1 3.27 m

S2 6.24 m

S3 5.09 m

Knowns

HI 1.52

K 100

Midhair 1.52

ElevP1 300 m

Known Coordinates

EPI 200

NP1 200

The Azimuth of Sides

Az1 89 deg 16 min 00 sec

Az2 14 deg 28 min 00 sec

Az3 269 deg 10 min 00 sec

The Vertical angles

Vangle1 +4 deg 32 min 00 sec

Vangle2 +3 deg 51 min 00 sec

Vangle3 -2 deg 10 min 00 sec

Calculation

Back **Next**

Plotting Traverse

Save

Output

Horizontal Distance for each side

Hdistance1 324.957174152038

Hdistance2 621.186758317448

Hdistance3 508.272472028533

SumHdistances 1454.41640449802

Vertical Distance for each side

Alpha1 25.76491635613

Alpha2 41.8036898030274

Alpha3 -19.2297280409172

Difference in Elevation for each side

DE1 25.76491635613

DE2 41.8036898030274

DE3 -19.2297280409172

Adjusted Elevation of the Traverse station

AdjElevP2 325.76491635613

AdjElevP3 367.568606159157

AdjElevP1 348 **Check**

Departure of Sides

Dep1 324.930557837925

Dep2 155.182835966232

Dep3 -508.21871298898

SumDeps -28.1053191848234

Latitude of Sides

Lat1 4.15904027550286

Lat2 601.490877844725

Lat3 -7.39226554045352

SumLats 598.257652579774

Total Correction for Departures and Latitudes

TCDEps 28.1053191848234

TCLats -598.257652579774

Correction for Departure and Latitude for each meter from Length of sides

KD 1.93241214124807E-01

KL -0.411338630896602

Correction for Departures

CorrforDep1 6.27951188717063

CorrforDep2 12.0038883375517

CorrforDep3 9.82191896010107

Correction for Latitudes

CorrforLat1 -133.667439115728

CorrforLat2 -255.518110697398

CorrforLat3 -209.072102766648

Corrected Departures

CorrDep1 331.210069725095

CorrDep2 167.186724303783

CorrDep3 -498.396794028879

SumCorrDeps 0

Corrected Latitudes

CorrLat1 -129.508398840225

CorrLat2 345.972767147327

CorrLat3 -216.464368307102

SumCorrLats 0

Adjusted Coordinates (Easting and Northing)

CorrEP2 531.210069725095

CorrEP3 698.396794028879

CorrEP1 200 **Check**

CorrNP2 70.4916011597747

CorrNP3 416.464368307102

CorrNP1 200 **Check**

Figure (7/b): Traverse (3 Sides) Input and Computation [4].

The results of all elements (Horizontal Distance for each side, Vertical Distance for each side, Difference in Elevation for each side, Adjusted Elevation of the Traverse Stations, Departure of Sides, Sum of Departures, Latitude of Sides, Sum of Latitudes, Total Correction for Departures and Latitudes, Correction for Departure and Latitude for each meter from Length of Sides, Correction for Departures, Correction for Latitudes, Sum Correction for Departures and Latitudes, Corrected Departures, Corrected Latitudes, Sum Corrected Departures, Sum Corrected Latitudes and Adjusted Coordinates (Easting and Northing of Points)) are saved in a text file as shown figure (7/c). Following that the transition traverse design process is considered completed the program enabled the user to go to the design of the next traverse in the alignment irrespective of its case (3 sides or 4sides or 5 sides or 6 sides or 7 sides or 8 sides or 9 sides or 10 sides) or can exit the traverse design if it is the last traverse in the alignment.

File Menu

The menu items available under the file menu are **Open**, **Save as**, **Save**, **Close**, **Print**, and **Exit**.

- When "**Open**" is selected, an existing design text file can be selected to open and made available to the user for seeing the calculated results or edit an existing file as shown in figure (7/d).

- When "Save As" is selected, a new file is created. The current file is then copied to the new file on the disk or location specified by the user.
- When "Save" is selected, an edited open file can be saved at any existing disk drive as shown in Figure (7/e).
- When "Close" is selected, to close opened text file.
- When "Print" is selected, to print text file.
- When "Exit" is selected, the program terminates, and the user is returned to the operating system level.

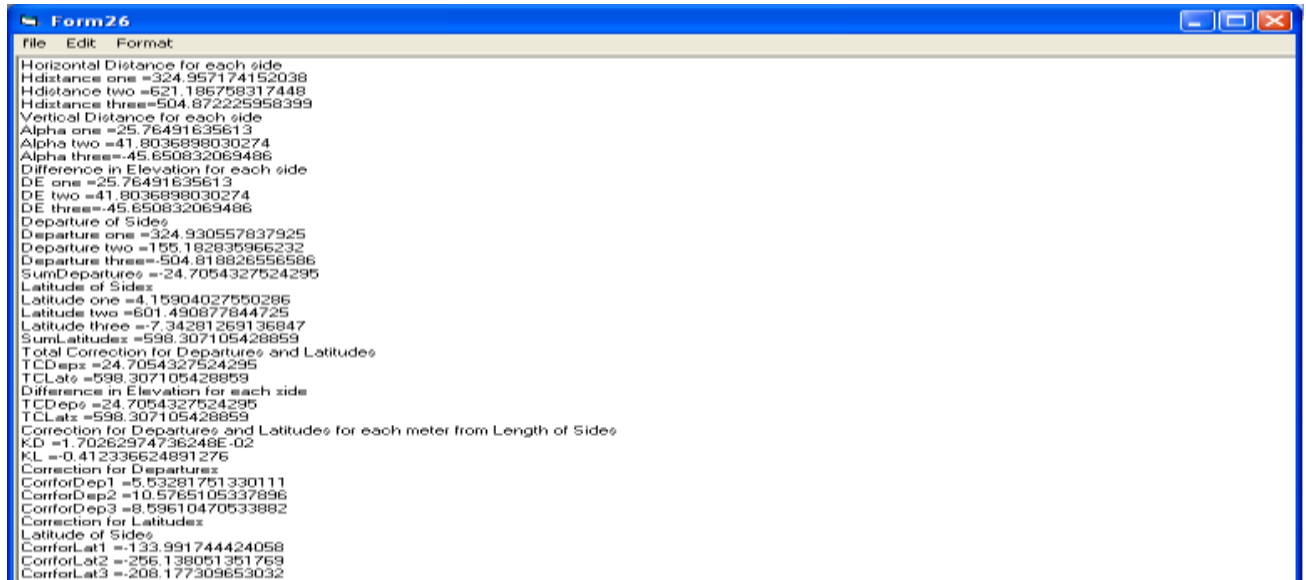


Figure (7/c): The Result of the Output.

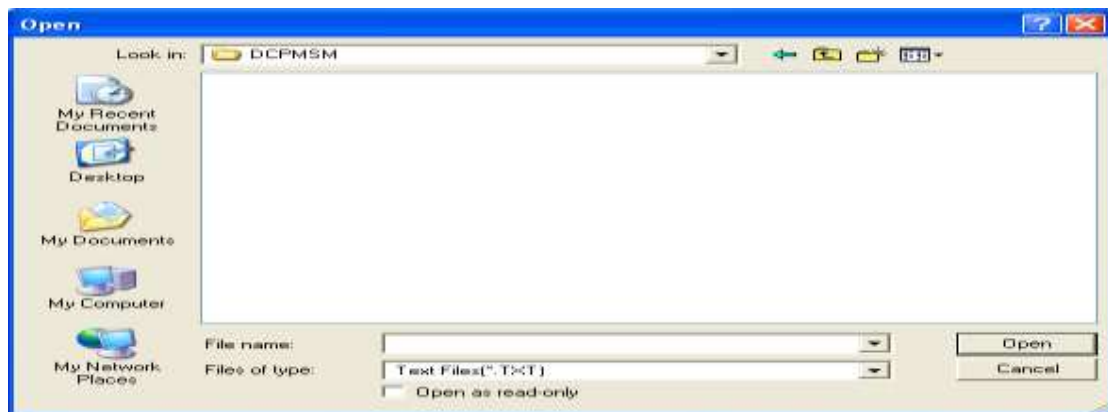


Figure (7/d): Open file dialog box.



Figure (7/e): Save file dialog box.

**Case2: number of Sides = (4)**

If the user selects this option, the form shown in figure (5) is displayed on the screen. First the user input information's the requirements of the second traverse and is listed below:

1. Points of traverse (P1, P2, P3, P4).
2. The Sides of traverse (L1, L2, L3, L4).
3. Lengths of sides (S1, S2, S3, S4).
4. Known coordinates (EP1, NP1), Height Instrument (HI), Constant (K), Elevation of first Point (Elev.p1), Midhair.
5. The Azimuth of sides (Az1, Az2, Az3, Az4).
6. The Vertical angles (Vangle1, Vangle2, Vangle3, Vangle4).

When the user input the required data as displayed in figure (8/a), the program begins the calculation of the elements (Horizontal Distance for each side, Vertical Distance for each side, Difference in Elevation for each side, Adjusted Elevation of the Traverse Stations, Departure of Sides, Sum of Departures, Latitude of Sides, Sum of Latitudes, Total Correction for Departures and Latitudes, Correction for Departure and Latitude for each meter from Length of Sides, Correction for Departures, Correction for Latitudes, Sum Correction for Departures and Latitudes, Corrected Departures, Corrected Latitudes, Sum Corrected Departures, Sum Corrected Latitudes and Adjusted Coordinates (Easting and Northing of Points)) as shown in figure (8/b).

Traverse (4 sides)

Input

Points of Traverse

P1 P2 P3 P4

The Sides of Traverse

L1 L2 L3 L4

Lengths of Sides

S1 m S2 m S3 m S4 m

Knowns

HI K Midhair ElevP1 m

Known Coordinates

EPI NP1

The Azimuth of Sides

Az1 deg min sec
Az2 deg min sec
Az3 deg min sec
Az4 deg min sec

The Vertical angles

Vangle1 deg min sec
Vangle2 deg min sec
Vangle3 deg min sec
Vangle4 deg min sec

Calculation

Back **Next**

Plotting Traverse

Output

Horizontal Distance for each side

Hdistance1 Hdistance2 Hdistance3 Hdistance4 SumHdistances

Vertical Distance for each side

Alpha1 Alpha2 Alpha3 Alpha4

Difference in Elevation for each side

DE1 DE2 DE3 DE4

Adjusted Elevation of the Traverse station

AdjElevP2 AdjElevP3 AdjElevP4 AdjElevP1 Check

Departure of Sides

Dep1 Dep2 Dep3 Dep4 SumDeps

Latitude of Sides

Lat1 Lat2 Lat3 Lat4 SumLats

Total Correction for Departures and Latitudes

TCDEps TCLats

Correction for Departure and Latitude for each meter from Length of sides

KD KL

Correction for Departures

CorrforDep1 CorrforDep2 CorrforDep3 CorrforDep4

Correction for Latitudes

CorrforLat1 CorrforLat2 CorrforLat3 CorrforLat4

Corrected Departures

CorrDep1 CorrDep2 CorrDep3

Corrected Latitudes

CorrLat1 CorrLat2 CorrLat3 CorrLat4 SumCorrLats

Adjusted Coordinates (Easting and Northing)

CorrEP2 CorrEP3 CorrEP4 CorrNP2 CorrNP3 CorrNP4 CorrNP1 Check

Save

Figure (8/a): Traverse (4 Sides).

The result of all elements (Horizontal Distance for each side, Vertical Distance for each side, Difference in Elevation for each side, Adjusted Elevation of the Traverse Stations, Departure

of Sides, Sum of Departures, Latitude of Sides, Sum of Latitudes, Total Correction for Departures and Latitudes, Correction for Departure and Latitude for each meter from Length of Sides, Correction for Departures, Correction for Latitudes, Sum Correction for Departures and Latitudes, Corrected Departures, Corrected Latitudes, Sum Corrected Departures, Sum Corrected Latitudes and Adjusted Coordinates (Easting and Northing of Points)) are saved in a text file. Following that the transition traverse design process is considered completed the program enabled the user to go to the design of the next traverse in the alignment irrespective of its case (3 sides or 4sides or 5 sides or 6 sides or 7 sides or 8 sides or 9 sides or 10 sides) or can exit the traverse design if it is the last traverse in the alignment.

Traverse (4 sides)

Input

Points of Traverse		The Sides of Traverse	
P1	A	L1	AB
P2	B	L2	BC
P3	C	L3	CD
P4	D	L4	DA

Lengths of Sides		Knowns	
S1	3.27 m	HI	1.52
S2	6.24 m	K	100
S3	5.09 m	Midhair	1.52
S4	6.11 m	ElevP1	300 m

Known Coordinates

EPI	200
NP1	200

The Azimuth of Sides

Az1	89 deg	16 min	00 sec
Az2	14 deg	28 min	00 sec
Az3	269 deg	10 min	00 sec
Az4	177 deg	14 min	00 sec

The Vertical angles

Vangle1	+4 deg	32 min	00 sec
Vangle2	+3 deg	51 min	00 sec
Vangle3	-5 deg	04 min	00 sec
Vangle4	-2 deg	10 min	00 sec

Calculation

Output

Horizontal Distance for each side		Latitude of Sides		CorrDep4	
Hdistance1	324.957174152038	Lat1	4.15904027550286	SumCorrDeps	0
Hdistance2	621.186758317448	Lat2	601.490877844725	Corrected Latitudes	
Hdistance3	505.03005174651	Lat3	-7.34510809432466	CorrLat1	5.91060497994983
Hdistance4	610.126680568631	Lat4	-609.415509456101	CorrLat2	604.839161518036
SumHdistances	2061.30066478463	SumLats	-11.1106994301981	CorrLat3	-4.62292534629787

Vertical Distance for each side		Total Correction for Departures and Latitudes		Adjusted Coordinates (Easting and Northing)	
Alpha1	25.76491635613	TCDEps	-4.58676963045401	CorrLa4	-606.126841151688
Alpha2	41.8036898030274	TCLats	11.1106994301981	SumCorrLats	0
Alpha3	-44.7765917851198	Correction for Departure and Latitude for each meter from Length of sides		Adjusted Coordinates (Easting and Northing)	
Alpha4	-23.0832295343819	KD	-2.22518223993939E-05	CorrEP2	524.207468905261

Difference in Elevation for each side		Correction for Departures		Correction for Latitudes	
DE1	25.76491635613	CorrforDep1	-0.723088932664006	CorrforLat1	1.75156470444698
DE2	41.8036898030274	CorrforDep2	-1.38225374229351	CorrforLat2	3.34828367331139
DE3	-44.7765917851198	CorrforDep3	-1.123783901782	CorrforLat3	2.72218274802679
DE4	-23.0832295343819	CorrforDep4	-1.35764305371449	CorrforLat4	3.28866830441295

Adjusted Elevation of the Traverse station		Corrected Departures	
AdjElevP2	325.76491635613	CorrDep1	324.207468905261
AdjElevP3	367.568606159157	CorrDep2	153.800582223938
AdjElevP4	322.792014374038	CorrDep3	-506.100419553536
AdjElevP1	300 Check		

Departure of Sides	
Dep1	324.930557837925
Dep2	155.182835966232
Dep3	-504.976635651754
Dep4	29.4500114780522
SumDeps	4.58676963045401

Save

Plotting Traverse

Figure (8/b): Traverse (4 Sides) Input and Computation [4].

Plotting Traverse

When this option is selected the figure shown in (8/b) presented to the user. The user has to input the following information:

- Corrected Easting of points (EP1, CorrEp2, and CorrEp3,.....).
- Corrected Northing of points (NP1, CorrNp2, and CorrNp3,.....).
- Scale (S).



When these data are input the computer program and when the user selects "**plotting traverse**" button to begin by drawing the points are illustrated in the below figures (9/a),(9/b),(9/c),(9/d),(9/e),(9/f),(9/g) and figure (9/h) . The program output result is saved for later use by the user in a text file.

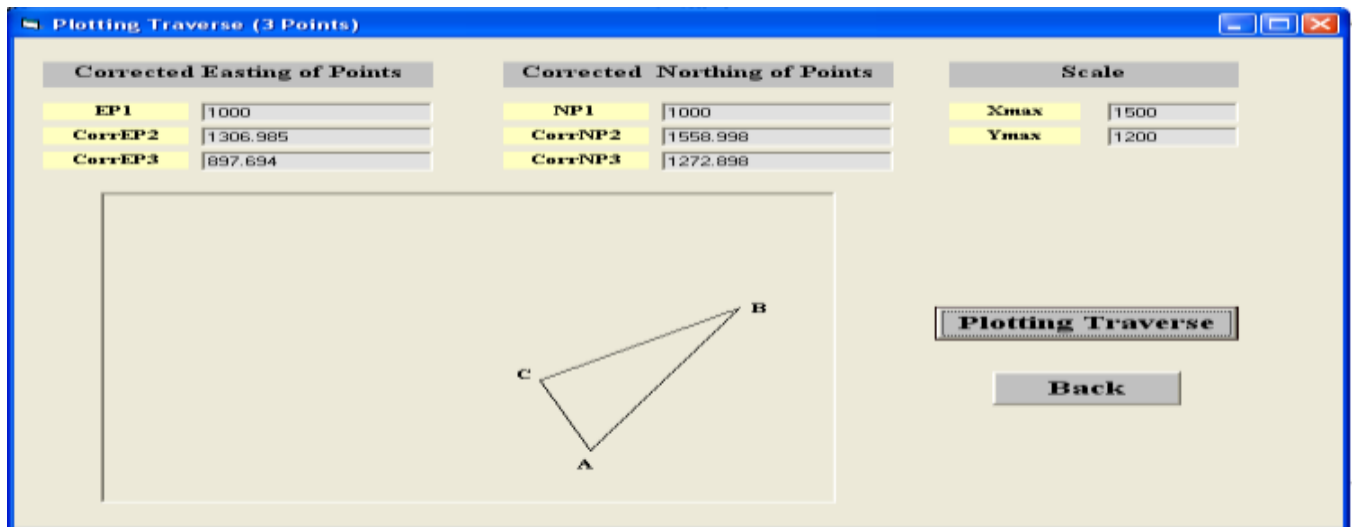


Figure (9/a): Plotting Traverse (3 points) Input and Plotting.

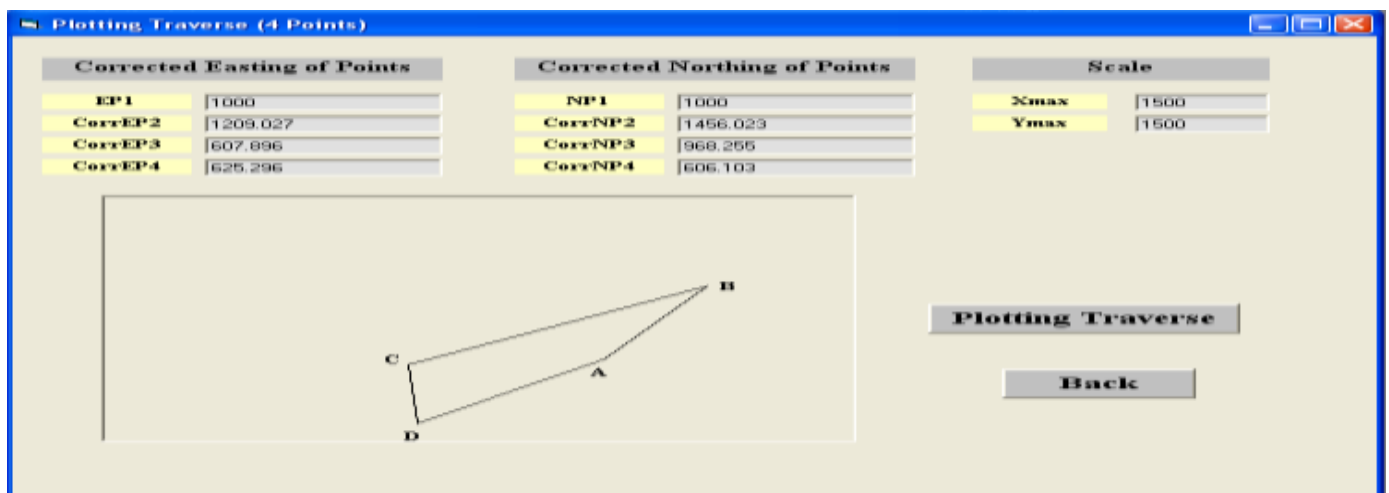


Figure (9/b): Plotting Traverse (4 points) Input and Plotting.

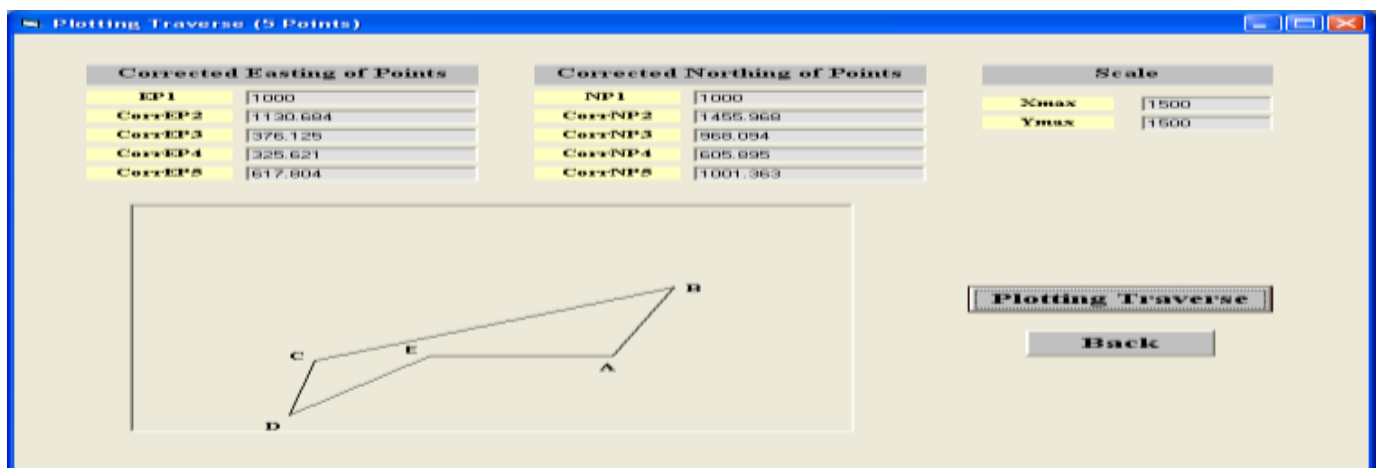


Figure (9/c): Plotting Traverse (5 points) Input and Plotting.

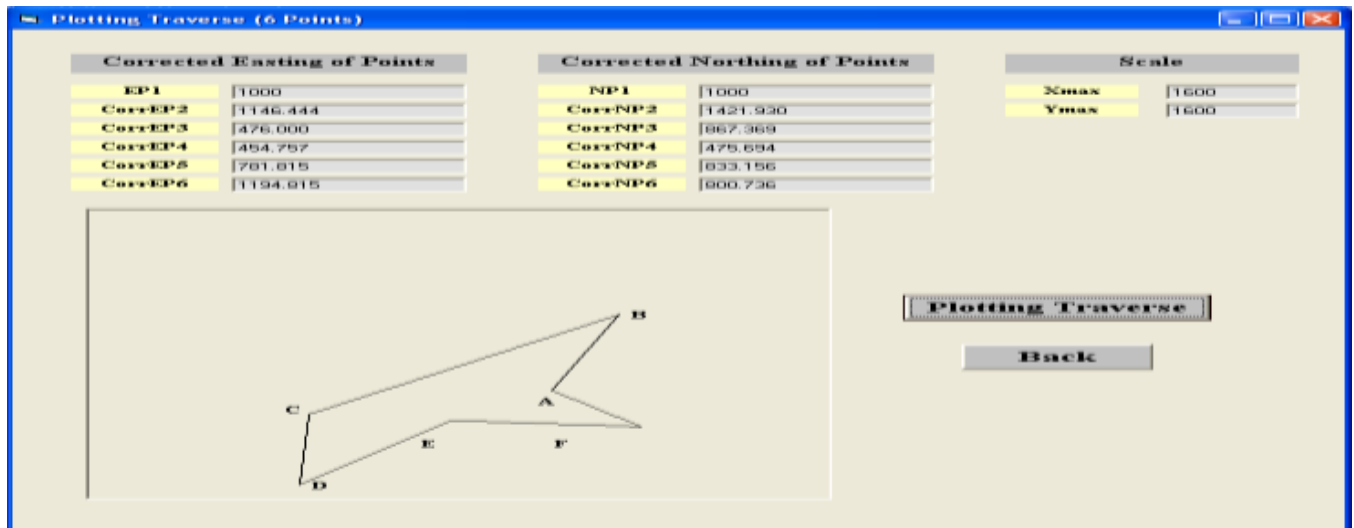


Figure (9/d): Plotting Traverse (6 points) Input and Plotting.

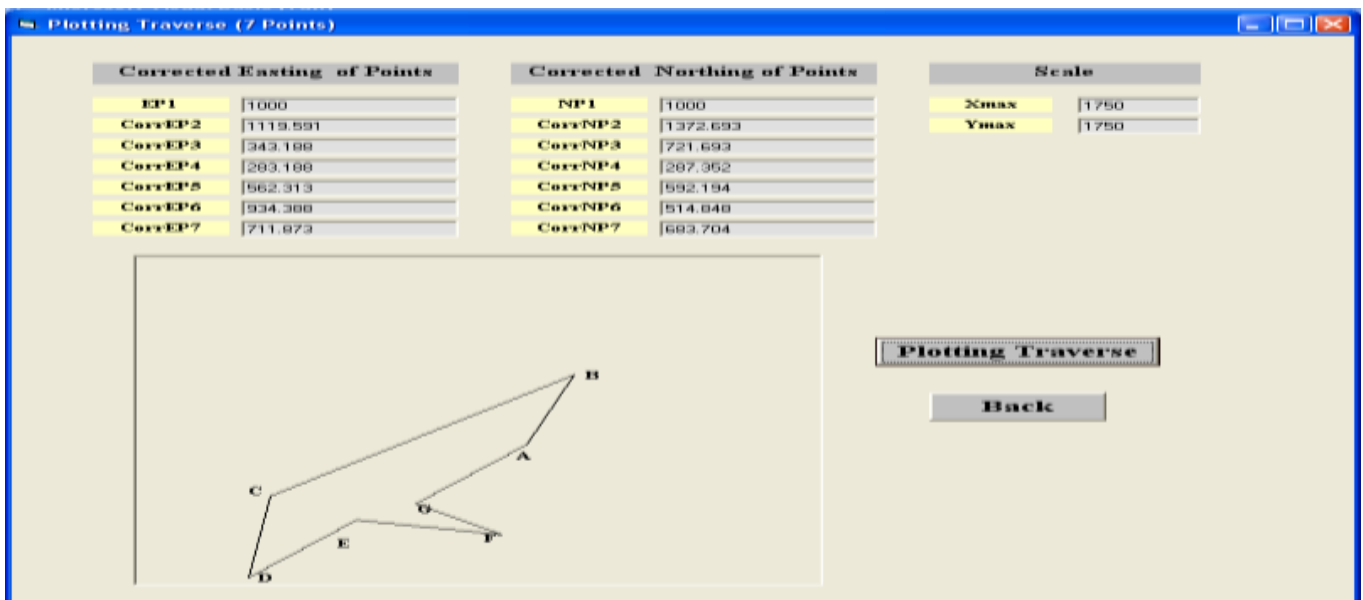


Figure (9/e): Plotting Traverse (7 points) Input and Plotting.

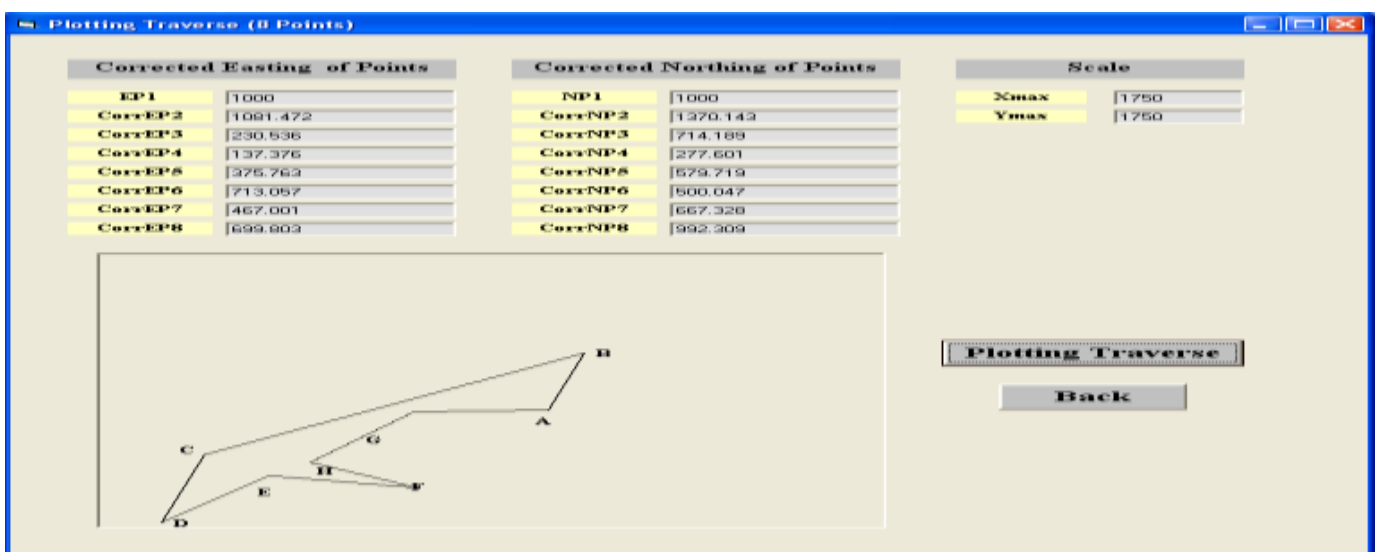


Figure (9/f): Plotting Traverse (8 points) Input and Plotting.

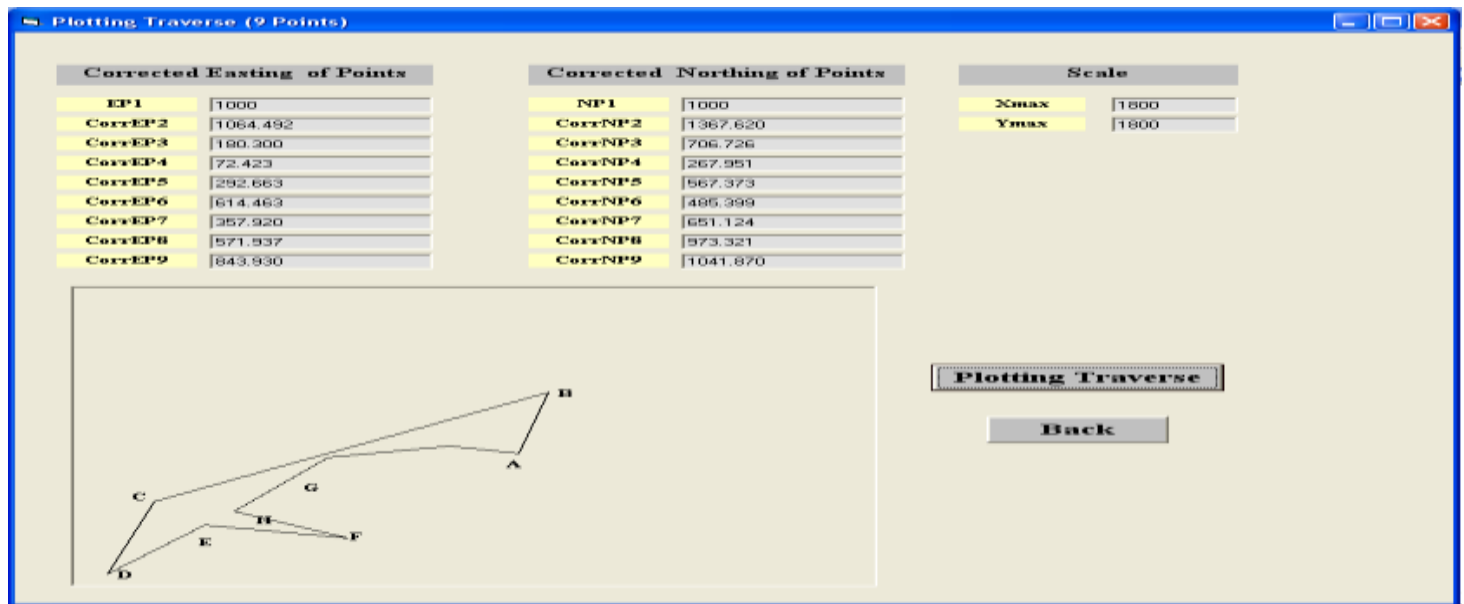


Figure (9/g): Plotting Traverse (9 points) Input and Plotting.

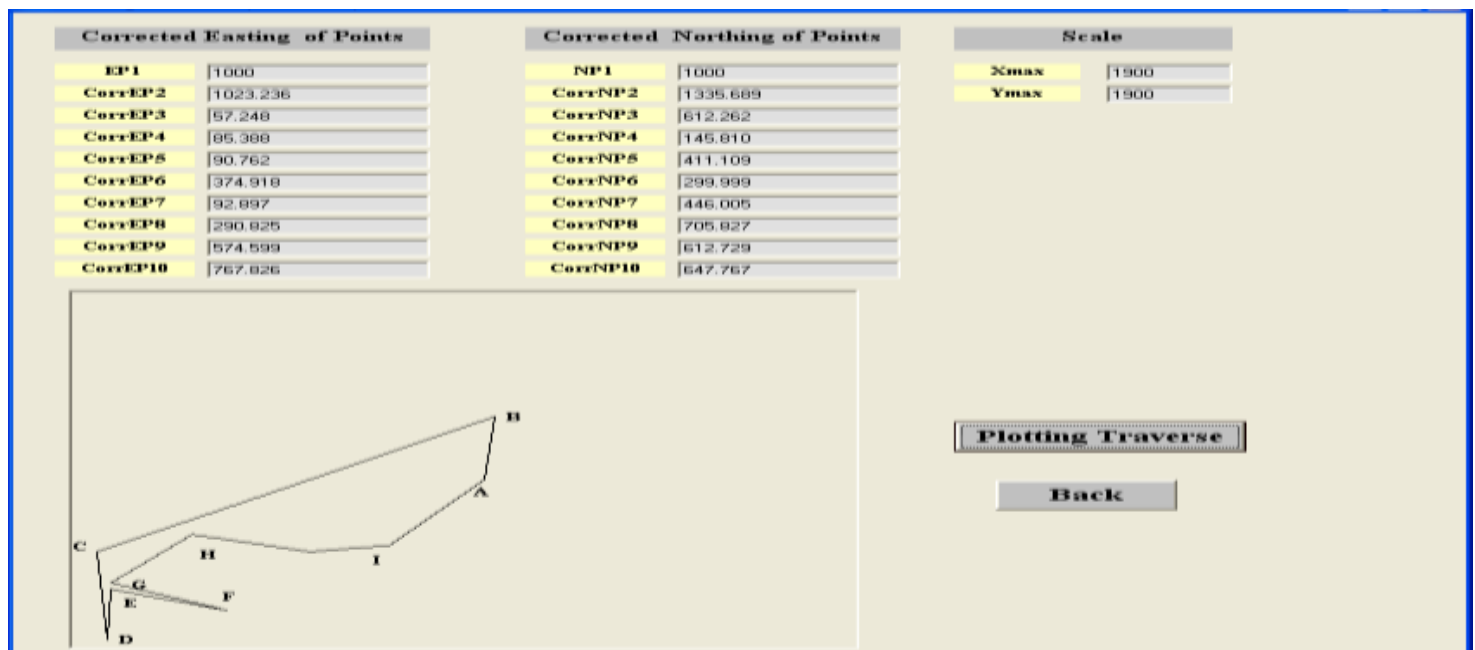


Figure (9/h): Plotting Traverse (10 points) Input and Plotting.

7.2 LEVELING

Leveling design is described in five cases of the following:

1. Case1: number of Stations = (3).
2. Case2: number of Stations = (4).
3. Case3: number of Stations = (5).
4. Case4: number of Stations = (6).
5. Case5: number of Stations = (7).

These menu items are described in the following sections.

Case1: number of Stations = (3)

If the user selects this option, the form shown in figure (6) is displayed on the screen. First the user input information's the requirements of the first leveling and is listed below:

1. Stations (Sta1, Sta2), Rod (Rod1, Rod2) and Interval (S1, S2) for Backsight.
2. The Vertical angles (Vangle1, Vangle2) for Backsight.
3. Stations (Sta2, Sta3), Rod (Rod2, Rod3) and Interval (S2, S3) for Foresight.
4. The Vertical angles (Vangle2, Vangle3) for Foresight.
5. Known Elevation of point (TBM2) and Constant (K).

When the user input the required data as displayed in figure (10/a), the program begins the calculation of the elements (Vertical Distances for Backsight, Vertical Distances for Foresight, Elevation of the Stations, Backsight and Sum of Backsight, Foresight and Sum of Foresight, Height Instrument, Z, Q and N) as shown in figure (10/b).

Leveling (3 Stations)

Input

Backsight

Station	Rod	Interval
Sta1	Rod1	S1
Sta2	Rod2	S2

The Vertical angles

Vangle1: deg min sec
Vangle2: deg min sec

Foresight

Station	Rod	Interval
Sta2	Rod2	S2
Sta3	Rod3	S3

The Vertical angles

Vangle2: deg min sec
Vangle3: deg min sec

Knowns

K:
ElevTBM2: ft

Calculation

Output

Vertical Distances for Backsight

Vd1: ft
Vd2: ft

Vertical Distances for Foresight

Vd2: ft
Vd3: ft

Height Instrument

HI1: ft
HI2: ft

Elevation of Stations

ElevTP1: ft
ElevTP2: ft

Backsight

BS1: ft
BS2: ft
Sum BS: Check

Foresight

FS2: ft
FS3: ft
Sum FS: Check

Summary Calculations

Z = (SumBS - SumFS) Check
Q = Elev Final point (TBM3) - Elev First Point (TBM2) Check
N = (Z - Q) Check

Buttons: Back, Next, Save, Plotting Profile

Figure (10/a): Leveling (3 Stations).

The results of all elements (Vertical Distances for Backsight, Vertical Distances for Foresight, Elevation of the Stations, Backsight and Sum of Backsight, Foresight and Sum of Foresight, Height Instrument, Z, Q and N) are saved in a text file. Following that the transition leveling design process is considered completed the program enabled the user to go to the design of the next leveling in the alignment irrespective of its case (3 stations or 4 stations or 5 stations or 6 stations or 7 stations) or can exit the leveling design if it is the last leveling in the alignment.



Leveling (3 Stations)

Input

Backsight							
Station	Rod	Interval					
Sta1	TBM2	Rod1	8.6	ft	S1	3.14	ft
Sta2	TP1	Rod2	4.5	ft	S2	6.32	ft

The Vertical angles

Vangle1: +0 deg 25 min 00 sec
Vangle2: +3 deg 15 min 00 sec

Foresight							
Station	Rod	Interval					
Sta2	TP1	Rod2	6.3	ft	S2	4.62	ft
Sta3	TBM3	Rod3	2.2	ft	S3	5.04	ft

The Vertical angles

Vangle2: -1 deg 52 min 00 sec
Vangle3: -6 deg 20 min 00 sec

Knowns

K: 100
ElevTBM2: 1416.8 ft

Calculation

Output

Vertical Distances for Backsight		Height Instrument	
Vd1	2.28339192868951 ft	HI1	1410.48339192869 ft
Vd2	35.7722155099583 ft	HI2	1463.09667832923 ft

Vertical Distances for Foresight		Elevation of Stations	
Vd2	-15.0410708905804 ft	ElevTP1	1431.82446281927 ft
Vd3	-55.258213233242 ft	ElevTP2	1520.55489156247 ft

Backsight		Foresight	
BS1	-6.31660807131049 ft	FS2	-21.3410708905804 ft
BS2	31.2722155099583 ft	FS3	-57.458213233242 ft
Sum BS	24.9556074386478 Check	Sum FS	-78.799284123822 Check

Z = (SumBS - SumFS) 103.75489156247 Check
Q = Elev Final point (TBM3) - Elev First Point (TBM2) 103.75489156247 Check
N = (Z - Q) 0 Check

Back **Next**

Save **Plotting Profile**

Figure (10/b): Leveling (3 Stations) Input and Computation [4].

Case2: number of Stations = (4)

If the user selects this option, the form shown in figure (6) is displayed on the screen. First the user input information's the requirements of the second leveling and is listed below:

1. Stations (Sta1, Sta2, Sta3), Rod (Rod1, Rod2, Rod3) and Interval (S1, S2, S3) for Backsight.
2. The Vertical angles (Vangle1, Vangle2, Vangle3) for Backsight.
3. Stations (Sta2, Sta3, Sta4), Rod (Rod2, Rod3, Rod4) and Interval (S2, S3, S4) for Foresight.
4. The Vertical angles (Vangle2, Vangle3, Vangle4) for Foresight.
5. Known Elevation of point (TBM2) and Constant (K).

When the user input the required data as displayed in figure (11/a), the program begins the calculation of the elements (Vertical Distances for Backsight, Vertical Distances for Foresight, Elevation of the Stations, Backsight and Sum of Backsight, Foresight and Sum of Foresight, Height Instrument, Z, Q and N) as shown in figure (11/b).

Leveling (4 Stations)

Input

Baksight				
Station	Rod	Interval		
Sta1	Rod1	S1		ft
Sta2	Rod2	S2		ft
Sta3	Rod3	S3		ft

The Vertical angles

Vangle1 deg min sec
Vangle2 deg min sec
Vangle3 deg min sec

Foresight				
Station	Rod	Interval		
Sta2	Rod2	S2		ft
Sta3	Rod3	S3		ft
Sta4	Rod4	S4		ft

The Vertical angles

Vangle2 deg min sec
Vangle3 deg min sec
Vangle4 deg min sec

Knowns

K
ElevTBM3 ft

Calculation

Output

Vertical Distances for Baksight

Vd1 ft
Vd2 ft
Vd3 ft

Vertical Distances for Foresight

Vd2 ft
Vd3 ft
Vd4 ft

Height Instrument

HI1 ft
HI2 ft
HI3 ft

Elevation of Stations

ElevTP1 ft
ElevTP2 ft
ElevTP3 ft

Baksight

BS1 ft
BS2 ft
BS3 ft
Sum BS Check

Foresight

FS2 ft
FS3 ft
FS4 ft
Sum FS Check

$Z = (SumBS - SumFS)$ Check
 $Q = Elev\ Final\ point\ (TBM4) - Elev\ First\ Point\ (TBM3)$ Check
 $N = (Z - Q)$ Check

Back **Next**

Plotting Profile

Save

Figure (11/a): Leveling (4 Stations).



Leveling (4 Stations)

Input

Backsight					
Station	Rod	Interval			
Sta1	TBM3	Rod1	8.6	S1	3.14 ft
Sta2	TP1	Rod2	4.5	S2	6.32 ft
Sta3	TP2	Rod3	10	S3	3.88 ft

The Vertical angles

Vangle1: +0 deg 25 min 00 sec
 Vangle2: +3 deg 15 min 00 sec
 Vangle3: -1 deg 02 min 00 sec

Foresight					
Station	Rod	Interval			
Sta2	TP1	Rod2	6.3	S2	4.62 ft
Sta3	TP2	Rod3	2.2	S3	5.04 ft
Sta4	TBM4	Rod4	5	S4	5.06 ft

The Vertical angles

Vangle2: -1 deg 52 min 00 sec
 Vangle3: -6 deg 20 min 00 sec
 Vangle4: -0 deg 13 min 00 sec

Knowns

K: 100
 ElevTBM3: 1416.8 ft

Calculation

Output

Vertical Distances for Backsight		Height Instrument	
Vd1	2.28339192868951 ft	HI1	1410.48339192869 ft
Vd2	35.7722155099583 ft	HI2	1463.09667832923 ft
Vd3	-6.99608946001652 ft	HI3	1503.55880210245 ft

Vertical Distances for Foresight		Elevation of Stations	
Vd2	-15.0410708905804 ft	ElevTP1	1431.82446281927 ft
Vd3	-55.258213233242 ft	ElevTP2	1520.55489156247 ft
Vd4	-1.91344439266989 ft	ElevTP3	1510.47224649512 ft

Backsight	
BS1	-6.31660807131049 ft
BS2	31.2722155099583 ft
BS3	-16.9960894600165 ft
Sum BS	7.9595179786313 Check

Foresight	
FS2	-21.3410708905804 ft
FS3	-57.458213233242 ft
FS4	-6.91344439266989 ft
Sum FS	-85.712728516492 Check

Z = (SumBS - SumFS) 93.6722464951236 Check
 Q = Elev Final point (TBM4) - Elev First Point (TBM3) 93.6722464951236 Check
 N = (Z - Q) 0 Check

Buttons: Save, Back, Next, Plotting Profile

Plotting Pro Figure (11/b): Leveling (4 Stations) Input and Computation [4].

When this option is selected the figure shown in figures (10/b) and (11/b) presented to the user. The user has to input the following information:

- Distances (D1, D2, and D3,.....).
- Elevation of Stations (ElevTBM2, ElevTP1, and ElevTP2,.....).
- Scale (S).

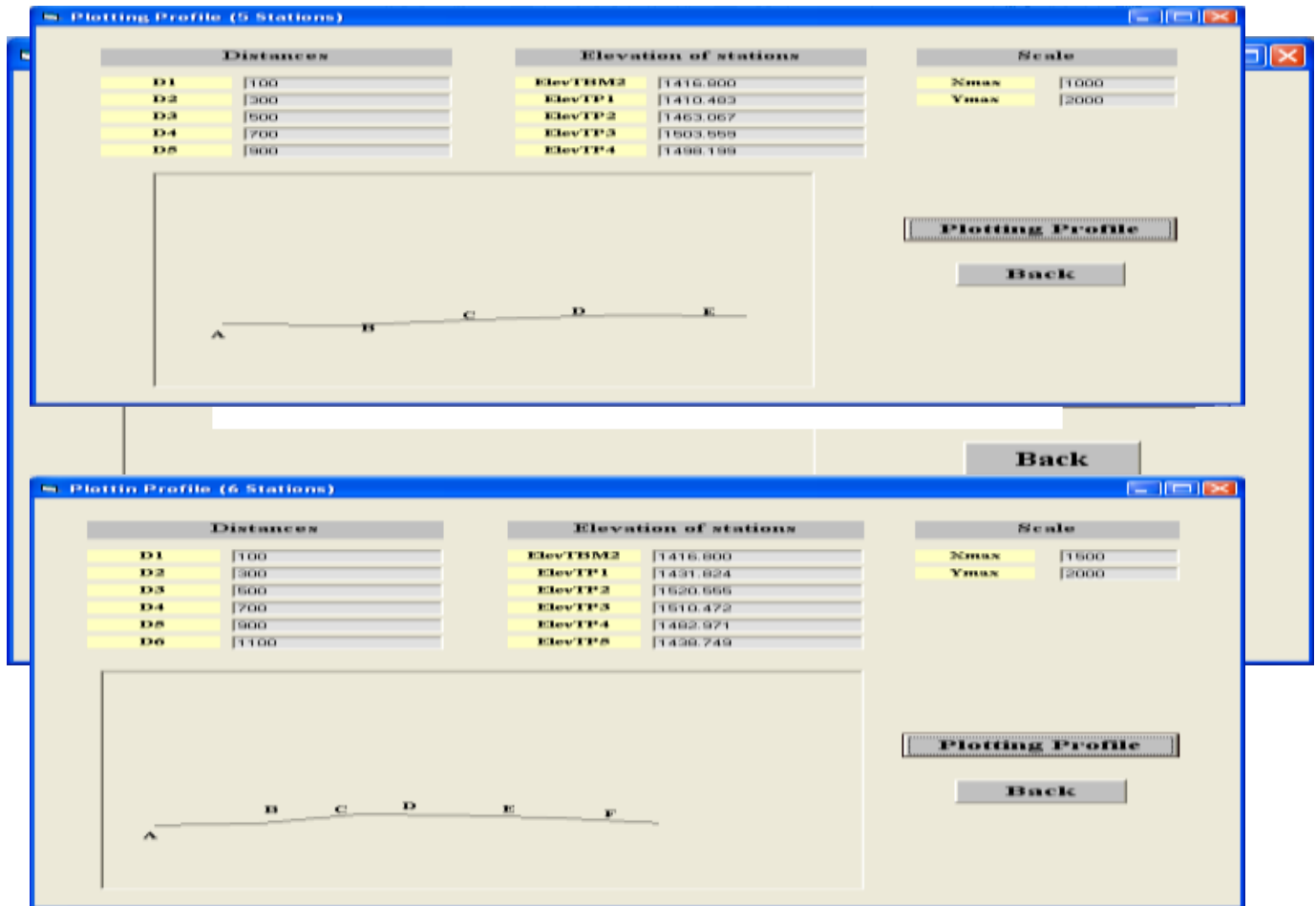
When these data are input the computer program and when the user selects "**plotting profile**" button to begin by drawing the points are illustrated in the below figures (12/a),(12/b),(12/c),and figure (12/d) . The program output result is saved for later use by the user in a text file.

Plotting Profile (3 Stations)

Distances		Elevation of stations		Scale	
D1	100	ElevTBM2	1416.800	Xmax	1000
D2	200	ElevTP1	1431.824	Ymax	2000
D3	300	ElevTP2	1520.555		

Plotting Profile

Back



Conclusions:

From the results obtained in research, the following conclusions can be made:-

1. The stadia measurement is modeled by Visual Basic language as software named **MSM** (**M**odeling the **S**tadia **M**easurements). The program is formulated and written by using Visual Basic, Version 6.
2. The software that were developed in this research has been tested by performing the stadia measurements method and proved to be efficient.
3. The solution problems of traversing and leveling in manual method is more complex if compared to Figure (12/c): Plotting Leveling (5 Stations) Input and Plotting.
4. The developed program (**MSM**) needs less time as compared to the manual method in order to solve the problem.

References Figure (12/d): Plotting Leveling (6 Stations) Input and Plotting.

- Davis R.E., et al. "*Surveying Theory and Practice*", 6th edition, New York, pp (296-375), (1981).



- Anderson J. M. and Mikhail E. M., "*Surveying Theory and Practice*", 7th edition, University of California Berkeley, (1998).
- Kennie, T.J.M. and Peterie, "*Engineering Surveying Technology*". John Wiley and Sons, New York, (1993).
- Francis H. Moffitt, "*Surveying*", 8th edition, University of Harry Bouchard, (1975).
- البكر زياد, "المسح الهندسي والكادسترائي", الطبعة الأولى, (1993), مطبعة الموصل, الصفحة (325-360).
- الخالصي فوزي, "المساحة المستوية", الطبعة الأولى, (1982), مطبعة جامعة الموصل, الصفحة (366-380).



THE USE OF DENTAL RADIOGRAPHIC IMAGE ANALYSIS IN IDENTIFICATION OF DECEASED INDIVIDUALS

Hana' S. Basheer* and Ahmed A.H. Hindy**

* Institute of Laser for Postgraduate Sstudies/ Baghdad University

** Oral and Maxillofacial Dept./College of Dentistry/ Babylon University

ABSTRACT:

Dental records recently used in forensic medicine to help in human identification, based mainly on radiograph images. The aim of our study is to automate this process, using image analysis and pattern recognition techniques.

Postmortem radiographs, including dental radiographs, with a database of ante mortem radiographs searching, in order to get the closest match with respect to some distinct features. Contours of teeth are used as the feature for matching, since they remain more invariant over time compared to some other features of the body. The work includes two stages: radiograph segmentation, with pixel classification, and contour matching.

Probability model is used to describe the distribution of object pixels in the image.

Results of retrievals on a database of over 40 images are encouraging.

استخدام نماذج تحليل صور اشعة الاسنان في التعرف على هوية الموتى

الخلاصة

تعتمد معلومات صور اشعة الاسنان من قبل الطبابة العدلية مؤخرًا للمساعدة على التعرف عن هوية الاشخاص البالغين الموتى، استنادًا على صور للاشعة تكون مثبتة ضمن قاعدة بيانات. الهدف من البحث جعل المقارنة ذاتية باستخدام تحليلات الصور وتقنية معالجة الصور. صور الاشعة مابعد الوفاة ومن ضمنها صور اشعة الاسنان تقارن مع صور لاشعات محفوظة في قاعدة بيانات للحصول على اقرب تطابق مع الاخذ بنظر الاعتبار بعض الخواص المنفصلة. محيط السن هو الميزة المستخدمة للتطابق وذلك لانها تبقى ثابتة مع الزمن بالمقارنة مع خواص اخرى للجسم. البحث هو من مرحلتين وهي اولا تقطيع الاشعة واستخدام التصنيف لمكون الصور الرقمية وثانيًا مقارنة المحيط الخارجي للسن. الموديل المقترح يستخدم لوصف توزيع مكون الصور الرقمية للجسم وهنا المقصود السن في صورة الاشعة، والنتائج طبقت على معلومات لقاعدة بيانات مكونة من 40 صورة لاشعة الاسنان

INTRODUCTION

The main purpose of forensic dentistry is to identify deceased individuals, for whom other cues of biometric identification (e.g., fingerprint, face, etc.) may not be available. In forensic dentistry, the postmortem (PM) dental record is compared against antemortem (AM) records pertaining to some presumed identity. A number of distinctive features are noted for each individual tooth. These features include properties of the teeth (e.g., tooth present/not present, crown and root morphology, pathology and dental restorations), periodontal tissue features, and anatomical features. Depending on the number of matches, the forensic expert rejects or confirms the tentative identity. There are several advantages for automating this procedure, such as automatic process will be able to compare the PM records against AM records pertaining to multiple identities in order to determine the closest match, and also, an automatic (or semi-automatic) system can perform *identification* on a large database (Jain and Chen, 2004), while a manual (non-automated) system is useful for *verification* on a small data set. For the automated identification, the dental records are usually available as dental radiographs. Different procedures had been used in this work to determine the best image analysis, such as using canny edge detector, with Gaussian smoothing operator for filtering to deal with problems for finding the true boundaries of objects in the image (Hoffman, 2007), and for the contour Extraction the self organizing map (SOM) based approach called the batch-SOM (BSOM) had been used (Kinouchi et al., 2002). Those to get the best image object to be matched with image objects saved early in a database

METHOD:

The method is to extract the shape or features of the tooth in the radiographic image, then try to use certain mathematical way for the purpose of matching the extracted features with other radiographic images. The feature extracted is the tooth contours. The feature extraction stage consists of the radiograph segmentation and the contour extraction. Since the image is available as radiograph, meaning that we are dealing with gray levels in the image. A probabilistic method is introduced to automatically find the contours of teeth. This automated dental identification system consists of two main stages; Feature extraction and Feature matching.

To reduce the images that have similar features, human experts must be taken into concern. The main stages for image processing used in our work shown in Fig.1.

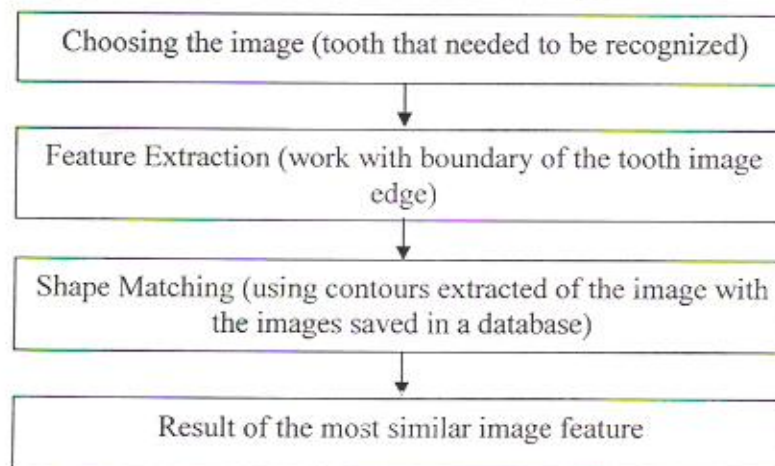


Fig.1: Procedure sequence of the image processing.

During feature extraction stage, certain information and type of mapping equation called intensity level slicing with many processing methods are considered:

- a) Image transformation, image segmentation method and edge detection (Umbaugh, 1998).
- b) The Use of morphological filter (Hoffman, 2007).

c) Contour extraction (tooth contour extraction) (Langlais and Kasle, 1985).

In this work we used morphological filter depending on Gaussian filter. Also the work with contour extraction had been done by using self organizing map (SOM).

At the feature matching stage, the query image is compared with that stored in our suggested database. A matching score is computed to measure the similarity between the two objects (the tooth) in the given radiographs (Jain and Chen, 2004).

- FEATURE EXTRACTION:

Radiographs are images consist of different gray levels histogram with different pixel intensities. The aim is to extract the Area of Interest (AOI). This can be done by extracting the boundary of the tooth image edge with an ordinary edge detection operation. The steps of image processing that had been chose to be used are shown in Fig.2.

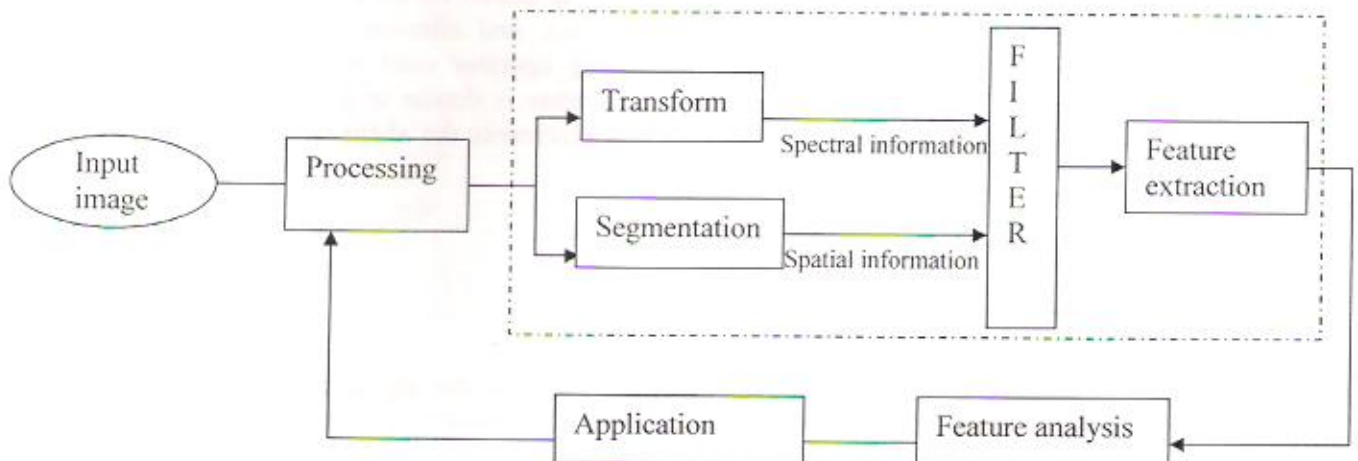


Fig.2: A frame work of image processing and analysis (Umbaugh, 1998).

A. Image Transformation, Image Segmentation and Edge Detection:

This is designed specifically to find lines. The line is a collection of edge points that are adjacent and have the same direction. *Hough Transform* is an algorithm that will take a collection of edges points that found by edge detector and find all the lines on which these edge points lie. The advantage of this method is reducing the search time in finding lines, In order to understand Hough transform; we consider the normal representation of a line. ρ is the distance from the origin to the line along a perpendicular line.

$$\rho = r \cos(\theta) + c \sin(\theta) \dots\dots\dots (1)$$

Where:

r : row, c : column, and θ is the angle between the r -axis and ρ -line. **Figure 3.** shows the line definition of ρ , r , θ , and c

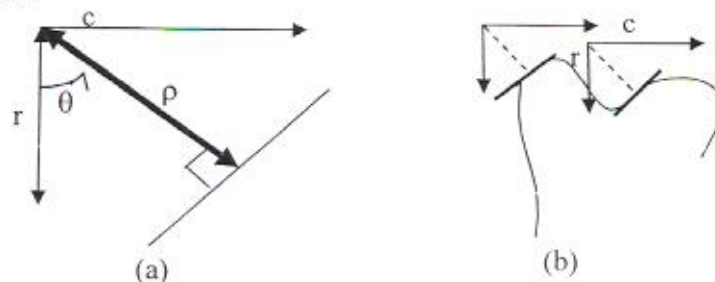


Fig.3: (a) Hough transform (Umbaugh, 1998), (b) Collection of edge points

The goal of image segmentation is to find the area that represents objects; our Area Of Interest (AOI) is the teeth in the radiographic image. Since we are dealing with gray levels image, we will use boundary detection segmentation, which means; finding of boundaries between object and the background in this work. Starting the work by marking points that may be part of the object edge using Hough transform algorithm, these points merge into line segmentation, where then merge into object boundaries. Here Canny edge detector was used (Deriche, 1987), threshold the results by considering the histogram of the image for the edge detection. We merge the existing edge segmentation into boundaries; this is done by edge linking (connecting the points that past the threshold test with maximum distance).

B. Morphological Filter:

This will simplify image segmentation facilitating the search for objects of interest; this is done by smoothing out object outlines, filling small holes, and eliminating small projections (Umbaugh, 1998). In this paper the Gaussian smoothing operator used is a 2-D convolution operator to remove detail and noise from the image. This sense is similar to the mean filter, but it uses a different convolution such as Kernel matrix that represents the shape of a Gaussian bell hump. (Hoffman, 2007)

In 2-D (circularly symmetric) Gaussian has the form

$$G(x, y) = 1 / (2\pi\sigma^2) * \exp \{ - (x^2 + y^2) / 2\sigma^2 \} \dots\dots\dots (2)$$

Where σ is the standard deviation of the distribution. In Fig.4 the signal flow for a general sharpening filter can be shown, where low-pass filter can be established by a Gaussian bell

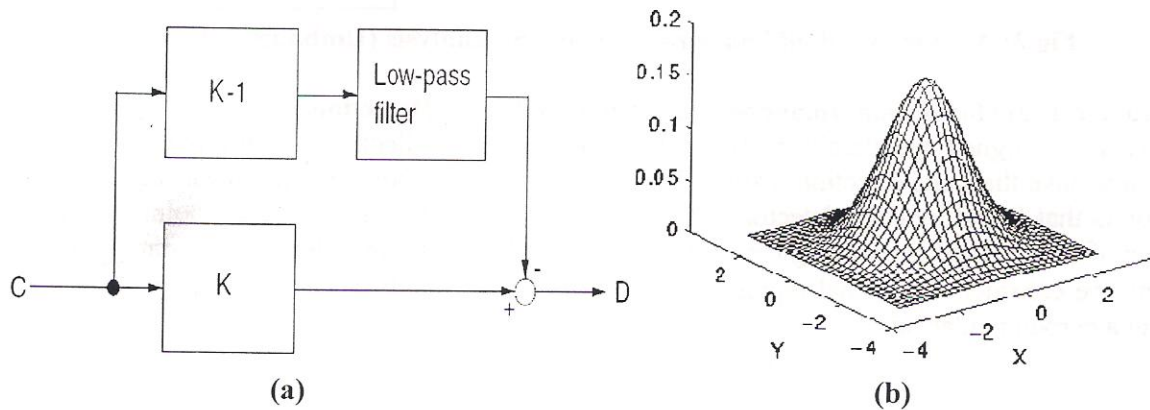


Fig. 4: (a) Frame work of using Gaussian distribution, (Hoffman, 2007).
(b) 2-D Gaussian distribution.

Where C is the input value in gray level, D is the sharpened value of the same input, and $D = [K - (K-1)G(x, y)]C$, the factor $K=1$ (no sharpening) or $K=2$ (sharpening) or $K=1.5$ (less sharpening), and $G(x, y)$ executes the averaging by Gaussian bell using the equation (2)

C. Contour Extraction:

Extraction of boundaries (or contours) of objects from the images are needed for shape description, leading to object localization and recognition, but the conventional edge extraction techniques, being sensitive to image noise and intensity variations, often do not give us the true

boundaries of objects in the image. In order to deal with such problems, a Gaussian filter (Hoffman, 2007) with the edge-linking techniques had been used.

In this work the object that had been deal with is a single tooth radiograph images. Our goal is to extract the tooth (object) from the background of the image which has different intensities.

The tooth has two main parts, the crown, which is above the gum line, and the root which is available in the bone below the gum see Fig. 5. Due to the over lap of the tooth root with the image of the jaws the root is not visible as the crown in the radiograph due to the difference in tissue density. The length of the tooth crown is ($L/3$) from the total length of the tooth, so we can have a crown extraction and root extraction. (Langlais and Kasle, 1985)



Fig. 5: Radiographic image of the tooth (two parts crown and root)

Based on the segmentation output, an enclosing rectangle that tightly fits the segmentation area (AOI) is constructed for the tooth, a point inside the rectangle, which will be used in shape extraction, is chosen and a mark is signed as the crown center C . This can be done since the distance of C to the top of the rectangle is one third the length of the (ROI), and the distance of C to the other two sides are equal ($W/2$) see Fig. 6 (Jain and Chen, 2004).

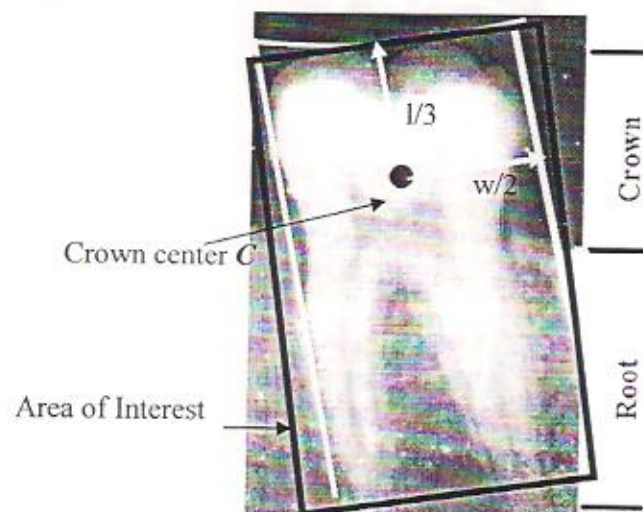


Fig. 6: describe of (RIO) and the crown center point

From Venkatesh (2006) self organizing map (SOM) had been used based approach called the batch-SOM (BSOM) (Kinouchi et al., 2002)

The used algorithm uses a two-layered neural architecture similar to that of the SOM-based for active contour modeling and the training of the network uses a scheme similar to kohonen's algorithm (Kinnebrock, 1995). The output of an edge detection algorithm as applied to the image provides the feature points for training the neural network. Consider the pair of points below:

$$P_a = w_i + ke^\perp ; \text{ and } P_b = w_i - ke^\perp \dots\dots\dots (3)$$

where $e^\perp = (-e_y, e_x)$ is the unit vector that is perpendicular to the contour, w_i is the weights of i^{th} neuron, in this algorithm uses the wrights of the neurons themselves as the new position of the control points, and hence of the contour, I is the image intensity function, and $k \in \{1, 2, \dots, N_r\}$ see Fig.7.

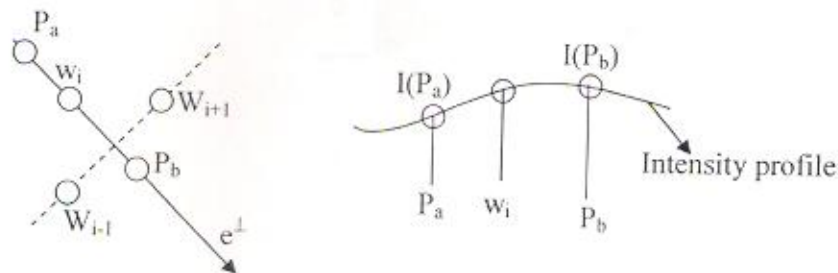


Fig.7: Region boundary, (Venkatesh 2006).

The feature vector in this algorithm uses the coordinate of edge points obtained from standard edge detection operations. In addition, the algorithm uses intensity variations and gradient information in a local region with crown center point C in order to guide the movement of the contour which we had them from the earlier steps of our work see Fig. 8.



Fig. 8: Final converged contour of an object (human teeth)
obtained using the present algorithm



-Feature Matching

The contours extracted from the query image result from the first step must be matched to the contours extracted from the proposed database images and that would be our consideration in the second step of our work. With the match step forensic medicine will be able to recognize the best matching images and with the help of personal observation, the goal would be reached to a good point of the best matching, and that means the forensic medicine identify deceased individuals. This matching can be done either manually or automatically. In this section an idea of Jain and Chen (2004) had been added to help to reduce the execution time, and which converted the work to match images automatically. All changes due to time passing and 2D images angles were insignificant. That means these variations would be omitted.

CONCLUSION

The dental radiograph based identification method has been applied to query radiographic images for the purpose of automated matching process, to be used in the deceased people identification in next future. The proposed work uses different techniques in its two stages, so that to get the most perfect result. This paper can be considered as a start point to initiate a data-base that helps the forensic medicine; this can be done by using collected radiograph images from private clinics and from governmental clinics as a starting point.

REFERENCES

- Deriche R., "Using Canny's Criteria to Derive an Optimal Edge Detector Recursively Implemented", *Int. J. Computer Vision*, Vol. 1, pp. 167-187, April 1987.
- Jain A. K., and Chen H., *J. Pattern Recognition Society*, 37(2004) 1519-1532, "Matching of dental X-ray images for human identification".
- Hoffman G., "Gaussian Filters", website, retrieved on (March/15/2007) from <http://www.fho-enden.de/~hoffmann/gauss25092001.pdf>
- Kinnebrock W., "Neural networks, fundamentals, applications, and examples", 2nd revised edition, R. Oldenbourg Publishing House Munich-Vienna, 1995.
- Kinouchi M., Kinouchi N. T., Kudo Y., and Ikemura T. "quick learning for batch-learning self-organizing map", *Genome Informatics* 13, pp. 266-267, 2002.
- Langlais R. P., and Kastle M. J., "Exercises in Oral Radiographic Interpretation", W. B. Saunders Company, p. 129, 1985
- Umbaugh S. E., Ph. D, "Computer vision and image processing: A practical approach using CVIP tools", Prentice Hall PTR Prentice-Hall, Inc., 1998
- Venkatesh Y. V., Raja S. K., and Ramya N., "Multiple contour extraction from gray level images using an artificial neural network". *IEEE transactions on image processing*, Vol., 15, No. 4, April, 2006

الأصالة و المعاصرة في المسكن الريفي العراقي

دراسة في مساكن قضاء عنة الجديدة

تغريد حامد علي*

المستخلص

تعد تصاميم المساكن التقليدية في ريفنا العراقي مدرسة رائدة في تقديم نماذج وحلول تصميمية ناجحة ، ذلك لأنها نابعة من بيئة مجتمعنا الريفي و المتمثلة بظروفه الطبيعية وعاداته وتقاليده . تقوم فرضية البحث على اساس ان تصميم المسكن الريفي التقليدي قد تغير نتيجة لعوامل وظروف متعددة أهمها التطورات الحضرية للمدن والزاحفة باتجاه أقاليمها الريفية والتي غالباً ما تكون سريعة وعشوائية غير خاضعة للتخطيط المسبق ، كما ان المسكن الريفي التقليدي قد قدم اساليب تحكم مناخي طبيعية ومتجانسة مع البيئة تلك البيئة القاسية حيث ارتفاع درجات الحرارة و تباينها اليومي وإشعاع شمسي يصاحبه هواء جاف ورياح حارة محملة بالأتربة ، يقابل ذلك شتاء بارد تنخفض فيه درجات الحرارة مع تساقط الامطار وارتفاع نسبة الرطوبة ، اضافة الى تجانسه مع البيئة الاجتماعية من حيث اعتماده الاسس الروحية العقائدية و الاعراف و العادات السائدة .

تكمن مشكلة البحث في ان هذا التغير قد ادى الى فقدان الهوية المميزة ، وتشويه المظهر العام للنسيج الريفي ككل وظهور التنافر و التناقض فيه. يهدف البحث الى بيان ان تصاميم المساكن الريفية التقليدية فيها من الافكار ما يمكن الاستلham منها وتحويلها بشكل يخدم متطلبات العصر للتغلب على الكثير من المشاكل التي تواجه مجتمعنا الريفي . علماً ان هذا البحث لا يدعو للعودة الى الاطار التقليدي البحث ، والابتعاد عن التطور الحضاري للإنسانية، وهو ايضاً لا يدعو للانفصال عن كل ماهو تقليدي وقبول ماهو عصري بل هو دعوة الى التواصل الحضاري بين الاصالة و المعاصرة في دعم خصوصيتنا المميزة .

Originality and Modernity of the Iraqi Rural House

A case study of the New Anna

ABSTRACT

Designs of the traditional rural houses of Iraq are considered as a school in presenting successful designs and solutions. This is because these designs are sourced from the environment of Iraqi rural community and its traditions and attitudes. The hypothesis of this research is that the traditional design of the rural house is in change. The problems of the research is that change leading to loosen the distinct identity, soiling the general view and appearance of conflict and opposition. this change can be contributed to several factors relating to the conditions of the urban development which are so speedy and are not under the prior planning. Results of this research indicated that the rural house natural environmental which consists with the hard, hot, daily deviation of temperature, hot wind and dust factors, and at the same time, cold winter, high rains and high level of humidity. in the other hand , the rural house is consistent with the social environment by depending on the common practices and traditions and attitudes. The research is aimed to return to the past , taking thoughts from it , manipulate these to use in solving the problems of our rural society. The recommendations are not a call to return back to the tradition from work of pure past and go away from modernity, and at the same time it is not a call to separate from all the tradition practices, and accepting all the modern and new practices, it is a call to matching the originality and modernity to support our distinct identity.

- منهجية البحث

تتكون منهجية البحث من محورين أساسيين هما :

- المحور الاول :المبحث النظري -التحليلي والذي اعتمد على الدراسة المكتبية وجمع المعلومات النظرية ومن ثم تحليلها .
- المحور الثاني :المبحث العملي حيث اعتمدت منطقة عنة(لاسباب سيرد ذكرها لاحقا)كدراسة ميدانية ، تم خلالها مسح المنطقة لغرض التعرف على تصاميم المساكن التقليدية و الحديثة الموجودة فيها ، وكذلك الاستفسار من عينة في احدى محلاتها

- المقدمة

ان الاصاله هي التاريخ ، التراث ، والمعاصرة هي الدعوة الى التحديث و التجديد والتي لا تستقيم الا اذا اتصل الماضي وتراثه بالحاضر والمستقبل . ان أهمية المحافظة على الأصالة في المسكن الريفي تتلّى من ان الموروث لم يكن وليد حقبة زمنية معينة بل وصل إلينا من أقدم الأزمنة حيث تراكمت الخبرات لتجعل المسكن ملبياً لجميع احتياجات افرادة ، ويتفق (كمونه،1990) مع ذلك ويؤكد ان العمران العراقي التقليدي رمزا لكيفية التعايش مع البيئة الطبيعية والاجتماعية حيث بحث الانسان منذ القدم عن الراحة و الحماية من التأثيرات السلبية للبيئة، ولكن من يزور ريفنا هذه الأيام قد يعجب بجمال الطبيعة و لكنه يندهش لنمط المساكن غير المنظم إذ يجد مساكن حديثة الطراز ملاصقة لآخرى تقليدية، ويتفق (البريدي،2004) مع ذلك بعد ان لاحظ هذه الظاهرة في ريف بلده سوريا ويضيف متسائلا أين المسكن الريفي النموذجي الذي يناسب مجتمعنا وظروفنا البيئية و الاقتصادية ، ويرجع (الشمرى،2006) هذه التغيرات الى التأثير بالافكار و المعايير الغربية كهدف يسعى المصمم والمالك الى بلوغه مما ادى الى تسارع عملية التغير العمراني للمدينة و اقليمها ، اما (الكناني،2006) فيشبه المدينة بالكائن الحي الذي يتأثر ويؤثر، فهي تتأثر بالتطورات و الافكار غربية كانت أم شرقية مما يؤدي الى تغير مستمر في انماطها العمرانية وبما ينسحب بالتاكيد على تغيير في انماط اقليمها الريفية، بينما يربط (الامارة،2001) المستوى الاقتصادي و الاجتماعي للفلاح بنمط الوحدات السكنية اذ ان الاخيرة ومساحتها عنده انعكاس للمستويين المذكورين للفلاح ضمن مجتمعه

-المبحث النظري - التحليلي

المسكن الريفي التقليدي

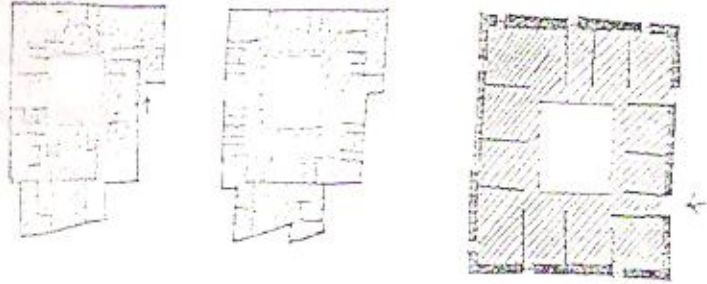
يؤكد العديد من الباحثين في مجال عمارة المناطق الحارة ان كل استراتيجيات البايو- مناخية ، يجب ان تأخذ بعين الاعتبار الفترة الحارة من مدار السنة (Croome,1990) ويؤكد اخرون ان حالة غياب الشمس في الشتاء في هذه المناطق تشكل حقبة قصيرة يمكن تجاهلها مقارنة بفصل الصيف الحار والطويل زمنياً (علي،2007)، فعند دراسة المسكن الريفي التقليدي نجد فيه نظم وأساليب تحكم مناخي طبيعية متجانسة مع البيئة القاسية التي تم ذكرها آنفاً، و يمكن تقسيم استراتيجيات التحكم المناخي للمسكن الريفي التقليدي الى :

- استراتيجيات تتجنب او تقلل الحمل الحراري (كالظليل، واستخدام مواد إنشائية ملائمة) .

- استراتيجيات التبريد الطبيعي (كإجلاء الهواء الحار الى الخارج ومنع دخوله للمسكن).
 - استراتيجيات تهدف الى زيادة رطوبة الهواء الداخلي للمسكن (كالتشجير و النافورات).
- ومن هنا ووفقاً للاستراتيجيات السابقة عمد المعمار التقليدي الى ابتكار عناصر تكيف ذاتية في المسكن الريفي التقليدي منبثقة من البيئة ومنسجمة معها وهي :

- الفناء الداخلي (الحوش)

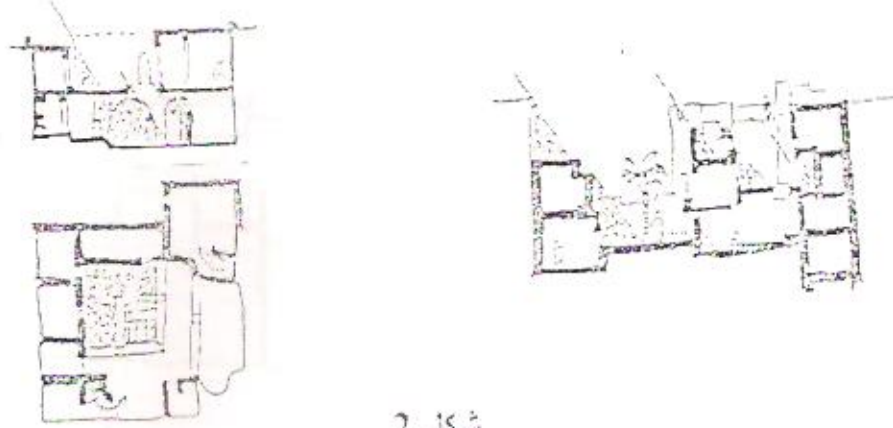
يعد الفناء عنصراً أساسياً للتكيف المناخي داخل المسكن التقليدي والمتحكم الاول بكافة الاستراتيجيات المذكورة آنفاً، أنه المنظم الحراري لجميع فضاءات المسكن، فضلاً عن كونه مصدر الإضاءة الطبيعية. شكل 1 .



شكل 1

الفناء الداخلي في المسكن الريفي التقليدي

- ويمكن ايجاز اثاره الايجابية من الناحية المناخية بما يلي :
- ان ارتفاع جدران الواجهات الداخلية لفضاءات المسكن و المظلة على الفناء الداخلي و استعمال البروزات فيها ،يؤدي الى تكسر اشعة الشمس الساقطة على هذه الجدران و تكوين الظل مما يقلل من الضغوط الحرارية على هذه الفضاءات. شكل 2.



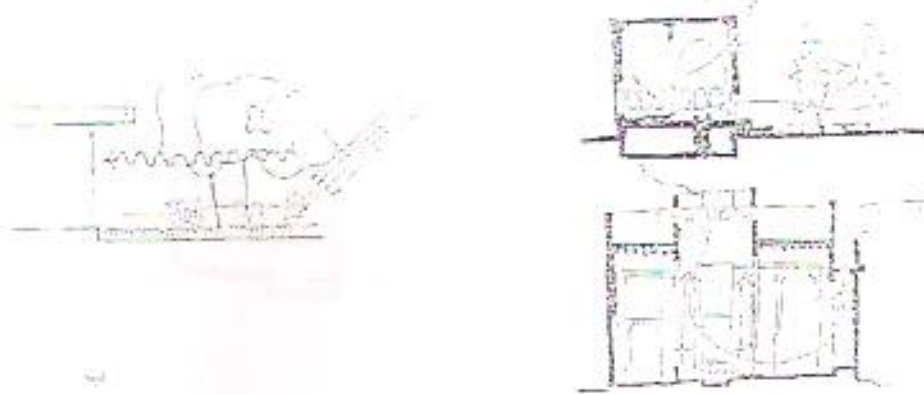
شكل 2

شكل 2

الظل في الفناء الداخلي

- بما ان الهواء البارد اثنل من الحار فانه يترسب اثناء الليل في داخل الفناء لارتفاع الهواء الحار وخروجه. كما ان الهواء البارد المتجمع في الفناء يبقى الى ساعة متأخرة من النهار لانه لا يتأثر بالهواء الحار الخارجي، والذي لا يستطيع الدخول نتيجة لانغلاق المسكن عن الخارج.

3- ترتبط التهوية الداخلية للمسكن بعدد وحجم الفتحات ومكان انفتاحها، و في المناطق الجافة الحارة حيث يكون الهواء الحار خارج المسكن خلال ساعات النهار مصدرا لارتفاع درجات الحرارة الداخلية، كما يكون الهواء البارد اثناء الليل سببا لانخفاضها لذلك كانت منافذ تهوية المسكن الريفي صغيرة ومقتصرة تقريبا على الفناء الداخلي. شكل 3-أ، ب.



شكل 3 - أ ، ب

شكل 3 - أ ، ب

الفناء كمنظم حراري

- جدران المسكن

تعد الجدران مستوى آخر للتكييف المناخي والتي تنظم الاشعاع الشمسي الواصل إلى المسكن عن طريق (المواد المكونة لها ، سمكها ، لونها وطبيعة ملمسها) ، فالجدران الخارجية تشكل قشرة المسكن الذي يعتبر الجزء المنظم لعملية التبادل الحراري بين المسكن والمحيط الخارجي ، فهي اولا عناصر اساسية في الحماية من أشعة الشمس إضافة إلى إن عناصر الواجهات تشكل الوسيلة الأكثر فاعلية في منع وصول هذه الاشعة الى سطوح الجدران حيث يتم اسقاط الظل عبر هذه العناصر . ونظراً لطبيعة بيئتنا التي تم ذكرها آنفاً كان من الضروري استخدام جدران ذات مقاومة للانتقال الحراري بين جانبيها ، ان استعمال مواد مثل الطين واللبن والخشب والتي تتمتع بتلك القابليات بالإضافة الى توفرها محلياً ، يعكس تفهم ابناء المنطقة لطبيعة بيئتهم . و بما ان الالوان تعكس او تمتص الاشعة الشمسية بحسب معامل انعكاسها ، فان انتهاء الجدران بمواد ذات الوان فاتحة يسمح بعكس نسبة عالية من الاشعة الشمسية مما يجنب الجدران الكثير من الاحمال الحرارية ، وهذا ما يفسر استخدام الالوان الفاتحة (الابيض ، الاصفر ، البيج) في المساكن الريفية التقليدية ، علماً ان مادة الجص التي يشيع استخدامها في إنهاء السطوح الخارجية لهذه المساكن تكون سطحاً بارداً لان معامل امتصاصها للاشعة الشمسية 12% كما ان معامل انبعاثها لهذه الاشعة عالي وقد يصل الى

95% (علي، 2007)، وهذه الخصائص تتجلب بشكل جيد مع مقتضيات التحكم المناخي للمناطق ذات الاشعاع الشمسي الشديد ، ويؤيد (شاهين ، 1990) ان طبيعة ونوعية وسمك الجدران ذات تأثير كبير على كمية الحرارة المتسربة داخل المسكن في الصيف والى خارجه في الشتاء ، وثبت ان خاصية الايصال البطيء للحرارة تقلل من الضغط الحراري في الصيف، لذلك استعملت الجدران الطينية السميكة و المعروفة كمادة انشائية ذات ايصال بطيء للحرارة من جهة وقابليتها الكبيرة على الاحتفاظ بها ، كما ان الطين يعمل على تأخير تسرب الحرارة الى داخل المسكن الى ان تبدأ درجات الحرارة بالتدني مابعد الظهيرة (الجمعة، 1998) .

- شكل المسكن وتوجيهه

يعتبر هذا العامل من العناصر المهمة في التكيف المناخي فيجب ان تتم بحسب الاعتبارات البنائية ومقتضيات السيطرة المناخية كحاجات التشميس او التظليل ، التهوية و الحماية من الرياح غير المرغوب فيها ، فالمسكن الريفي التقليدي عادة مايكون مستطيلاً (كمونه، 1993) و طوله يسير من الشرق الى الغرب ، أما عرضه فيكون باتجاه شمالي جنوبي وهذا يعني اطول واجهات المسكن تقابل اقل فترات ممكنة من الاشعاع الشمسي اثناء فترات النهار ، مما يقلل درجات الحرارة التي تمتصها الجدران الى اقل حد ممكن .

-المبحث العملي - الدراسة الميدانية

اختير قضاء عنة كموقع للدراسة الميدانية لخصوصيته المميزة في تغير انماط المساكن الريفية التقليدية، فكما هو معروف ان عنة القديمة قد تم اغراقها بسد حديثة وتم انشاء مدينة جديدة لسكانها من قبل شركة اجنبية (شركة S.A.E الفرنسية) تصميمها وتنفيذها كمرحلة أولى، فجاءت مساكنها خليط بين التقليدي والحديث، وتم توزيع اراضي على العوائل الجديدة كمرحلة ثانية لهذه المدينة ، فتم تشييدها وفق نمط غريب عن المنطقة متأثراً بالمساكن الحديثة الموجودة فيها حاملاً في عناصره بعضاً مما تبقى من التراث التقليدي، فكانت نموذجاً جديراً بالدراسة .

مدينة عنة - الموقع ، المساحة ، السكان

مدينة عنة هي إحدى المدن المهمة في إقليم الفرات الأوسط ، وإداريا هي إحدى الاقضية التابعة الى محافظة الانبار ، استحدث القضاء بموجب الارادة الملكية عام 1921 ، جدول 1 .

جدول 1. التقسيمات الادارية لقضاء عنة الجديدة

التقسيمات الإدارية	المساحة / كم ²	%
مركز قضاء عنة	5672	49.5
ناحية راوة	5772	50.5
مجموع مساحة القضاء	11444	100

المصدر: الدليل الاداري لجمهورية العراق، 1990 ، الجزء الاول ، محافظة الانبار ، ص 394 ، تقع مدينة عنة على امتداد نهر الفرات بطول 13 - 14 كم وعرض بحدود 300 م ، خارطة 4.



خارطة 4

خارطة تبين موقع مدينة عنة

يقع مركز قضاء عنة القديمة شمال مدينة الرمادي ويبعد عنها مسافة 220 كم ونتيجة لتنفيذ مشروع سد حديثة تم تعرض القضاء للانغمار وانتقل مركز القضاء الى مدينة عنة الجديدة ضمن منطقة الريحانة الى الجنوب الغربي من عنة القديمة. خارطة 5.



خارطة 5

موقع مدينة عنة الجديدة بالنسبة الى سد حديثة

بلغ عدد سكان مركز القضاء 12401 حسب نتائج التعداد لعام 1997 منهم 9021 نسمة سكان المناطق الحضرية و 2380 نسمة سكان المناطق الريفية (الجهاز المركزي للإحصاء، 1997) وحسب تعداد قامت به قائم مقامية قضاء عنة بلغ عدد السكان 20000 نسمة (قائم مقامية قضاء عنة 2000،

- الجانب التاريخي

ان هيكل وشوارع مدينة عنة القديمة وأزقتها وشكل المعالم المعمارية فيها ، ووجود بقايا أثرية تعود إلى العصور الإسلامية ما هي إلا شواهد على ان هذه المدينة تتميز بطابع تراثي يدل على انها احدى المدن القديمة في العراق ، علماً ان اسم عنة من الاسماء القديمة في التاريخ فقد ورد ذكره في المصادر البليدية بأسم خانات والذي يدل بهذه اللغة على القدسية (الدليل الاداري لجمهورية العراق 1990، ومن الآثار الباقية قلعة عنة القديمة والجامع الكبير وتتميز مدينة عنة بالنواير القديمة

الطراز لرفع المياه من النهر الى البساتين الواقعة على الضفتين اضافة الى الطواحين التي تعمل على قوة دفع الهواء .

فضاءات المسكن الريفي التقليدي

- غرف النوم

- تتبلين هذه الغرف من حيث العدد من مسكن الى آخر تبعاً لحجم الأسرة وعدد افرادها خصوصاً المتزوجين منهم ، وعادة ما تكون قابلة للزيادة نظراً لتوفر المساحة الكافية حول المسكن ، كما انها ذات مساحات متباينة وتختلف في تصميمها من حيث الموقع وارتفاع واحجام النوافذ واتجاهها.

• الفضاءات الخدمية

تشمل الحمام والمرافق الصحية والمخازن وعادة ما تحتوي على حمام واحد مشترك لا علاقة له بعدد افراد الأسرة وكذلك الحال بالنسبة للمطبخ، اما المرافق الصحية في الغالب خارج الوحدة السكنية لافتقارها الى الشروط الصحية الواجب توفرها مثل المجاري وتأسيسات الماء، اما المخازن فيعزل مخزن المواد الغذائية وغيرها من مخازن طعام الحيوانات والأعلاف.

• حظائر الحيوانات

هي من الفضاءات المهمة ، وقد تكون داخل المسكن بالنسبة للحيوانات الصغيرة مثل الدجاج والبط ، وخارجة في حاله الابقار والماشية ، وتسيج عادة بالأسلاك الشائكة والطين .

• المفتول

يستخدم هذا الفضاء للمراقبة وحراسة الحيوانات والمزارع ، وهو عبارة عن غرفة مربعة الشكل ابعادها لا تتجاوز 1.5×1.5 م مشيدة في احدى الزوايا العلوية للمسكن وفيها فتحات صغيرة يتم من خلالها الاشراف والمراقبة .

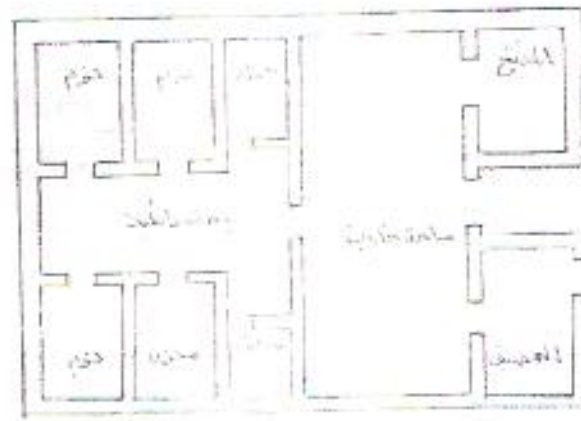
المضيف

يعتبر من الفضاءات المميزة للمسكن الريفي التقليدي ويقابل ما يعرف بالمناطق الحضرية بغرفة الاستقبال الخاصة بالضيوف ، وتأتي أهميته لأنه المعبر في هذه المناطق عن مدى أهمية العائلة ومستواها المعاشي مما يجعل السكان يتفاخرون بسعته وترتيبه ويكون عادة معزولا عن فضاءات المسكن الأخرى ، وملحقة به بعض الفضاءات الخدمية الخاصة مثل الحمام والمرافق الصحية ، ومدخله في اغلب الأحيان يكون منفصلا عن مدخل المسكن الرئيسي لتوفير الخصوصية العائلية ، تكون المضاييف على نوعين هما :

- مضاييف رؤساء وسادة الوحدات العشائرية وتكون واسعة ومبالغ في ترتيبها وأثاثها وعادة تحوي باحة امامية واسعة .

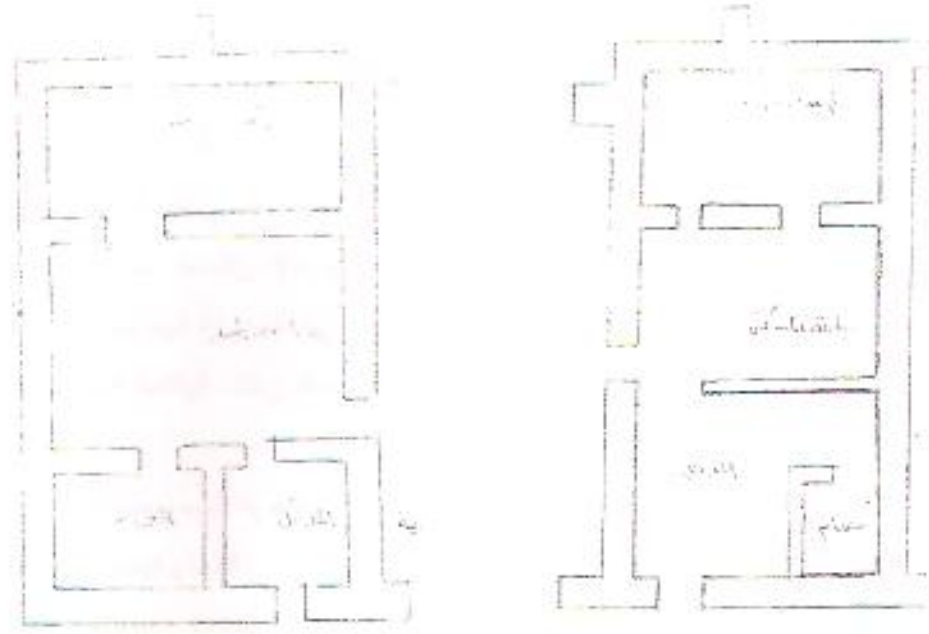
- مضاييف القرويين العاديين اذ يخصص صاحب المسكن فضاء (حجرة) منعزلا قدر المستطاع عن فضاءات المسكن الأخرى .

فضلا عن هذين النوعين فان القرويين ان لم يكن لديهم فضاء خاص للضيوف فانهم يحولون احدى حجرات المسكن للضيافة عند الحاجة فقط حيث تستخدم في الاوقات الأخرى لنام او جلوس العائلة. وتوضح الاشكال 8،7،6 نماذج من هذه المساكن .



شكل 6

نتائج المسح الميداني



شكل 8

شكل 7

مساكن ريفية تقليدية

المصدر : نتائج المسح الميداني

- مميزات المسكن الريفي التقليدي

- استعمال مواد البناء المتوفرة محلياً مثل قطع الطين التي توضع فوق بعضها وتسمى محلياً (بالطوف) واللبن والقصب التي لها قابلية العزل الحراري الجيد وفي بعض الاحيان يستعمل الطابوق والكلس كما هو الحال في مساكن ذوي الإمكانات العالية، اما السقوف فتكون عادة من جذوع النخيل وسعفها أو من بعض الاشجار المتوفرة والحصران وتغطيها بطبقة من الطين.
- أرضية اغلب المساكن غير مبلطة انما ترابية تفرش بالحصران ،اما في حالة تبلطها فتكون بطبقة من الطابوق الفرشي وهو ذو قابلية قليلة على امتصاص اشعة الشمس بالإضافة الى قابليته العالية على الاحتفاظ بالرطوبة .



- تصميم فضاءاته يتجه نحو الداخل فجميع المنافذ تفتح على الفناء الداخلي فيما عدا فتحات ضيقة في الواجهات الخارجية (واجهات تقريباً صماء) ، كان لتحديد استعمال الفتحات الخارجية وصغرها اثر بالغ في الحفاظ على درجة حرارة داخلية مناسبة دون تأثرها بارتفاع درجات الحرارة الخارجية نهائياً وتدنيتها ليلاً ، اضافة الى توفير خصوصية تامة لإفراد العائلة .

- المدخل الرئيسي غير مباشر الى المسكن وانما يؤدي الى جزء من الفناء الداخلي .
- ارتفاعه عادة طابق واحد ، وذلك انعكاساً لعادات اجتماعية تمنع بل تحرم الشرفية بين المساكن ، اضافة الى ان ذلك يعود لنوعية مواد البناء المستخدمة ومدى تحملها .
- استخدام الخشب في معظم التصميم الداخلي والابواب والشبابيك .
- زراعة مساحات خضراء حول المسكن ، ان وجود هذه المساحات يؤدي الى عدم وصول اشعة الشمس الى الجدران الخارجية للمسكن ، ويعتبر عاملاً أساسياً في التخفيف من الضغوط الحرارية التي يتعرض لها غلافه الخارجي.

- التصميم الاساسي لمدينة عنة الجديدة (محافظة الانبار، 1987)

- تم اعداد التصميم الاساسي للمدينة الجديدة حتى عام 2000 بحيث يتسع الى سكان 20000 عشرون الف نسمة .
 - تحتوي المدينة الجديدة على 3200 مسكن مع كافة مشاريع البنى التحتية الفنية والاجتماعية الخاصة بها اضافة الى انشاء المركز الرئيسي للمدينة .
 - يتكون التصميم الاساسي للمدينة الجديدة من اربعة محلات سكنية متماثلة الحجم ترتبط ببعضها بشريط من الارض تتجمع فيه العديد من الابنية العامة التي تشكل مركز المدينة .
- خارطة 9 .
- تحتوي المحطة السكنية الواحدة على مجموعة من الدور السكنية تبلغ 800 داراً مع مركز محلي يحتوي مبانى الخدمات الاجتماعية لسكان المحطة الواحدة .
 - تم تنفيذ عنة الجديدة على مرحلتين تحتوي المرحلة الاولى على انشاء 1600 وحدة سكنية مع خدماتها .



خارطة 9

التصميم الأساسي لمدينة عنة الجديدة

يحتوي التصميم الأساسي لمدينة عنة الجديدة على 3 نماذج للوحدات السكنية، جدول 2.

جدول 2 . تفاصيل الوحدات السكنية

نوع الوحدة السكنية	العدد	%	المساحة م ²	إبعاد القطعة م	مساحة البناء م ²
غرفتي النوم	704	22	300	30 × 10	126.5
ثلاث غرف نوم	1056	33	360	30 × 12	149
أربع غرف نوم	1440	45	600	30 × 20	192
المجموع	3200	100	—	—	—

المصدر: جمهورية العراق، 1987، وزارة الاسكان والتعمير (سابقاً)، المؤسسة العامة للإسكان، المختصر الفني لإنشاء المرحلة الأولى من مشروع عنة الجديدة، ص 7.

المسكن الريفي الحديث

استخدم في المسكن الريفي الحديث بعض الافكار العصرية المناقضة للتراث، فتصميم المسكن الريفي الحديث اذ لم يستند الى ملقى تراثنا من مقومات ايجابية يكون تصميماً فاشلاً، ذلك لان المسكن الريفي التقليدي قد وفق بين متطلبات الانسان الريفي الاجتماعية والدينية والنفسية مع الظروف البيئية التي يمتاز بها ريفنا العراقي اضافة الى المتطلبات الجمالية والفنية. وتوضح الجداول 3، 4، 5 تفاصيل الفضاءات التي تحتويها نماذج المساكن الحديثة في منطقة الدراسة (قضاء عنة الجديدة)

جدول 3. دار ذات 2 نوم - جدول 4. دار ذات 3 غرف نوم - جدول 5. دار ذات 4 غرف نوم

المساحة م ²	اسم الفضاء	المساحة م ²	اسم الفضاء	المساحة م ²	اسم الفضاء
15	1- نوم رئيسة	15	1- نوم رئيسة	15	1- نوم رئيسة
42	2- نوم عدد 3	24	2- نوم عدد 2	12	2- نوم
12.5	3- طعام	7.5	3- طعام	5	3- طعام
21	4- معيشة	18	4- معيشة	18	4- معيشة
17	5- استقبال	17	5- استقبال	17	5- استقبال
15.5	6- مطبخ	11.5	6- مطبخ	11	6- مطبخ
5	7- حمام	5	7- حمام	5	7- حمام
4	8- مرافق عدد 2	4	8- مرافق عدد 2	4	8- مرافق عدد 2
6	9- مخزن	4.5	9- مخزن	3	9- مخزن
22	10- ممرات	16.5	10- ممرات	14	10- ممرات
160	11- صافي المساحة	123	11- صافي المساحة	104.5	11- صافي المساحة
32	12- مساحة الجدران	26	12- مساحة الجدران	22	12- مساحة الجدران
192	13- المساحة الكلية	149	13- المساحة الكلية	126	13- المساحة الكلية
18	14- مساحة الكراج	18	14- مساحة الكراج	18	14- مساحة الكراج

المصدر: نتائج المسح الميداني

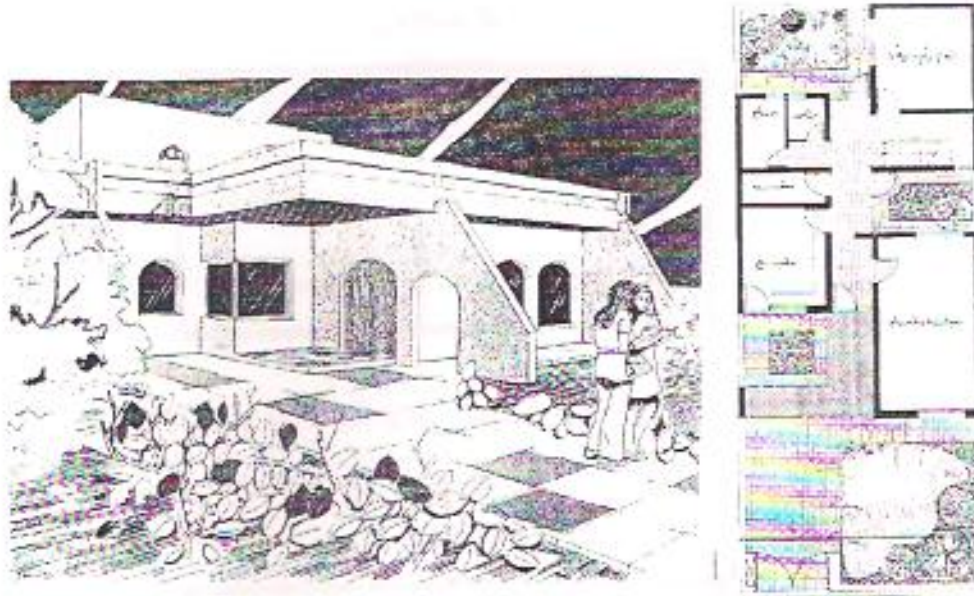
- مميزات المسكن الريفي الحديث

- نلاحظ في المسكن الريفي الحديث ان الاقواس لا تؤدي أي وظيفة انشائية او تصميمية وانما هي عناصر مرهقة للواجهات من حيث كثرتها واستخداماتها بشكل مختلف.
- فتحات الواجهات الخارجية كبيرة وبعيدة عن المعالجات المناخية والاجتماعية .
- الاعتماد الكلي على وسائل التكنولوجيا الحديثة لغراض التدفئة والتبريد حتى في حالة وجود الفناء الداخلي ، والذي غالبا ما يكون غير مدروس الابعاد والموقع ليؤدي الوظائف الذي وجد من اجلها .
- الابتعاد عن مواد البناء المحلية واستعمال الكونكريت والخرسانة والبلوك وهي من المواد الماصة والمشعة للحرارة .
- استخدام عناصر وتشكيلات في الواجهات او في الشكل الخارجي للمسكن دون التأثير بالمجاورات ولهذا تظهر هذه المساكن وكأنها اجسام مفروضة على بعضها البعض .
- المسكن الريفي الحديث بارتفاع طابقين او اكثر .
- عدم الدقة في اختيار الألوان وملامس وسطح الجدران خصوصا الخارجية منها.
- وتوضح الاشكال 10 و 11 بعض النماذج لمساكن ريفية حديثة ضمن منطقة الدراسة.



شكل 10

مسكن حديث في قضاء عنة الجديدة



شكل 11

مسكن حديث في قضاء عنة الجديدة

نتيجة لعملية المسح الميداني والاطلاع على النماذج الثلاثة للوحدات السكنية يتضح ان هذه الوحدات تحتوي على فناء داخلي مكشوف تحيط به فضاءات المسكن ، ولكن هذا الفناء قد يكون وسطياً او جانبياً ، وبما لا يتلاءم مع مناخ المنطقة الذي يتميز بالرياح الحارة الجافة صيفاً (رياح السموم) كما ذكرنا سابقاً ، ان فكرة الفناء هي امتداد للفناء في المسكن التقليدي لان التغير الجذري في النماذج الحديثة يمكن ان يسبب رفض او عدم تقبل الساكنين للعيش في المساكن الحديثة ، ولكن الفناء هنا ليس المتحكم المناخي لان معظم فتحات (الشبايك) الفضائات مفتوحة على الخارج مع تميزها بالاتساع خلافاً للنماذج التقليدية التي تم ذكرها سابقاً ، أي ان التصاميم الحديثة تبنت فكرة الانتقال التدريجي بوجود الفناء (رغم عدم أدائه للوظائف التقليدية) مع ترك حرية الانتقال لساكنين الدور في استعمال مختلف التقنيات لتحويل الفناء بما يتلاءم مع ظروفهم الخاصة . اما واجهات المساكن فقد استخدمت الأقواس فيها كلمة معمارية من تراثنا الزاخر . كما تم مراعاة إمكانية التوسع المستقبلي في جميع النماذج . ولمعرفة مدى ملائمة هذه المساكن لشاغلها تم الاستفسار عن ذلك من عينة عشوائية بلغت 10 % من وحدات المحلة المبحوثة فكان العدد 80 وحدة سكنية (تحتوي المحلة السكنية الواحدة على 800 وحدة سكنية).

جدول 6. مدى ملائمة الوحدة السكنية

نوع الإجابة	العدد	%
نعم	34	42.5
كلا	46	57.5
المجموع	80	100

من بيانات الجدول أعلاه يتضح إن النسبة الاعلى تعتقد إن المساكن غير ملائمة لبيئتهم الاجتماعية والطبيعية. وباستفسار آخر لنفس العينة عن إجراء تحويلات على مساكنهم، الجدولين 7، 8.

جدول 7. إجراء التحويلات

نوع الإجابة	العدد	%
نعم	49	61
كلا	31	39
المجموع	80	100

جدول 8 . نوع التحويل

المجموع	نوع التحويل والإضافة							
	إضافة غرفة أو أكثر مختلفة الاستعمال		تغير الواجهة		غلق النوافذ الخارجية		تسقيف الفناء	
	العدد	%	العدد	%	العدد	%	العدد	%
80	22	27.5	18	22.5	17	21	23	29

يتضح من بيانات الجدولين أعلاه ان الغالبية ونتيجة لعدم الشعور بالراحة من هذه المساكن تم تغييرها او تحويلها ، وان النسبة الاعلى قامت بتسقيف الفناء وهذا دليل على عدم قيامه بوظائفه التي كان يؤديها في المسكن الريفي التقليدي .

- الاستنتاجات

- ان المسكن الريفي التقليدي متلائم مع البيئة من الناحية المناخية والاجتماعية ويظهر وكأنه جزء من طبيعة المنطقة وليس مفروضاً عليه ، كما انه استطاع ان يجد الحلول لمعظم المشاكل التي كان سكان المنطقة يواجهونها في وقت لم تكن فيه التقنيات الحديثة موجودة وممهدة للكثير من الحلول السريعة والمريحة .
- استعمال المواد الانشائية المتوفرة محلياً مثل الطين واللين والخشب يدل على مدى التكيف مع البيئة المحلية وبراعة بنائي المنطقة في المسكن الريفي التقليدي ، اما المعاصر منه فاستعمال الكتل الكونكريتية و السقوف الحديدية ادى الى ضرورة استخدام اجهزة التكيف فيه .
- العناصر المعمارية في المسكن الريفي التقليدي لا تحتاج الى تعريف، كما انها تعد مثالا في الابتكار، بينما المعاصر منه جاءت الكثير من عناصره نقلاً لأنماط غربية عن بيئتنا.
- المسكن الريفي التقليدي جاء مكتمل الفكرة والحلول الكفيلة بالقناعة الوظيفية والجمالية بينما المعاصر لم يربط في اكثر الحالات المفردة المعمارية بوظيفتها.
- الاختلاف في ابحام وإعداد الفتحات الخارجية وارتفاعاتها وارتفاع المسكن ككل بين التقليدي والمعاصر يدل على ان الأول نابع من عادات المجتمع الموجود فيه، بينما الآخر ناقل لافكار غربية عنه.
- يمارس افراد العائلة معظم نشاطاتهم في الفناء الداخلي للمسكن اذ يوفر لهم الخصوصية التامة نظرا لانغلاقه عن الخارج، اذن للفناء الداخلي اثاره الاجتماعية اضافة الى اثاره الايجابية من الناحية المناخية.

- التوصيات

- يجب ان لا يرتبط تصميم المسكن الريفي الحديث بالاصالة فقط او بالمعاصرة، وانما يقوم على التعادل بينهما، اذ ان التصميم الحديث يجب ان لا يقف عند حدود الثوابت والا وقع في عملية تقليد الشكل القديم ، وكذلك لا يمكن ان يقوم على المتحولات فقط وبهذا ينقطع عن الجذور و يصبح دون هوية مميزة.
- التشجيع على إقامة المضاييف وخاصة الكبيرة منها لأنها من الفضاءات المميزة للمسكن الريفي التقليدي، فضلاً عن أثرها في العلاقات الاجتماعية والأنماط السلوكية .
- الاهتمام بتصميم المسكن الريفي وفق المتطلبات النفسية والاجتماعية و المناخية وخاصة من ناحية توفير الفناء الداخلي ، فيجب ان يكون الفضاء الذي يلي الاحتياجات السابقة وليس فناء موجودا محسوب .
- تقادي ارتفاع الوحدات السكنية والفتحات الواسعة في الواجهات لما لذلك من اثار سلبية كالتعرض لاشعة الشمس بالاضافة الى الجوانب الاجتماعية .
- استعمال المواد البنائية القديمة (طابوق والطابوق القرشي) والتقليل من استعمال المواد الحديثة كالسمنت والحديد.
- ان اختيار نمط المسكن حق من حقوق كل مواطن وفقا لإمكانياته ومتطلباته النفسية ، ولكن يجب ان يتم ذلك ضمن ضوابط محددة وملزمة موضوعة من قبل لجان وجهات معنية خدمه للصالح العام.



المصادر

- الإمارة، عماد، جريدة الصباح، 2001، www.Alsabah.com.
- البريدي، قاسم، مقالة منشورة بجريدة الثورة السورية 2004/8/13.
- www.alwehda.com
- الجمعة، احمد قاسم، 1998، "المعالجات البيئية لتصاميم المساكن التراثية"، مركز التراث العربي، دورة المعالجات البيئية لتصاميم المباني العربية، جامعة بغداد، ص ص 2-12.
- الجهاز المركزي للإحصاء، 1997، نتائج التعداد العام للسكان، محافظة الانبار، جداول وبيانات غير منشورة، (آخر تعداد رسمي معتمد).
- الدليل الإداري لجمهورية العراق، 1990، الجزء الأول، محافظة الانبار، ص ص 394 - 414، (لم يصدر آخر بعده).
- الثمري، د. ناصر صالح، 2006، "النمو السكاني والتطور العمراني"، مجلة المخطط والتنمية العدد 15، ص 52.
- الكنانى، د. كامل كاظم، 2006، تخطيط المدينة العربية الإسلامية - الخصوصية والحداثة، مجلة المخطط والتنمية، جامعة بغداد، العدد 15، ص 85.
- شاهين، بهجت رشاد، 1990، "الانتقال الحراري عبر القشور الخارجية للمباني"، دورة العمارة والمناخ في المناطق الحارة الجافة، جامعة بغداد، ص 1.
- علي، تركي حسن، 2007، "المرجع البيئي في المناطق العربية التقليدية"، رسالة ماجستير، كلية الهندسة، القسم المعماري، ص ص 22 - 54.
- قائم - مقامية قضاء عنة، 2000، جداول غير منشورة.
- كمونه، د. حيدر عبد الرزاق، 1990، "اثر المناخ في تخطيط المدينة العربية التقليدية"، الندوة القطرية السادسة لتاريخ العلوم عند العرب، مركز احياء التراث العلمي العربي، جامعة بغداد، ص 1.
- كمونه، د. حيدر، 1993، "الأسلوب الأمثل لربط الأصالة بالمعاصرة في تخطيط المدينة العربية"، مركز احياء التراث العلمي العربي، جامعة بغداد، ص 5.

- محافظة الانبار ، هيئة التخطيط العمراني ، المختصر الفني لإنشاء المرحلة الأولى من مشروع علة الجديدة ، ص 7 .

- Croome, Denary,1990," Environment and Human Development in the Arab World", auk, P12.

معامل الفعالية البوزولانية للفلدسبار المحلي

أ.م.ندى مهدي فوزي

أ.د. زين العابدين رؤوف

كلية الهندسة/جامعة بغداد

الخلاصة

يتناول هذا البحث دراسة معامل الفعالية البوزولانية للفلدسبار المحلي المتواجد في مقالع قرب بحر النجف ومقارنته مع معامل الفعالية لدقيق السليكا المستورد. تم استعمال الفلدسبار المطحون والمنعم الى (1200م²/كغم) بمقياس بلين (Blaine). وتم فحص الفعالية البوزولانية بموجب المواصفة الامريكية (ASTM C-311-02) حيث أظهرت النتيجة بان معامل الفعالية البوزولانية للفلدسبار (97%) مقارنة بـ (92%) لدقيق السليكا، والتي تشير الى إمكانية استخدام الفلدسبار المطحون كمادة بوزولانية نشطة في تحضير الخرسانة عالية الاداء والخرسانة عالية الرص.

Pozzolanic Activity Index of local Feldspar

ABSTRACT

The paper presents an experimental research on pozzolanic activity index of local feldspar obtained from quarries near Al- Najaf lake in comparison an imported microsilica.

The feldspar in ground to a very fine powder (1200m²/kg) on Blaine scale.

The experiments were made according to ASTM C-311-02. It is found that the pozzolanic activity index of local feldspar is (97%) compared to (92%)for microsilica, which indicates that feldspar can be used for making high performance or compact concrete..

الكلمات الرئيسية : البوزولانية، الفعالية البوزولانية، الفلدسبار، دقيق السليكا، الانسياب، درجة حرارة الحرق المثلى

-المقدمة-

إن مصطلح البوزولانا يطلق على المواد السليكية أو السليكية الألومينية والتي بحد ذاتها لا تمتلك الإمكانية السمنتية ولكنها عند إضافتها إلى السمنت أو النورة (وبوجود الماء) وبشكل مسحوق دقيق التجزئة فإنها تتفاعل كيميائياً مع هيدروكسيد الكالسيوم لتكوين مركبات تمتلك خصائص سمنتية. ويقصد بمعامل الفعالية النسبة بين مقاومة الانضغاط بعمر 28 يوم للنموذج الحاوي على المادة البوزولانية إلى مقاومة الانضغاط للخلطة المرجعية بدون إضافة البوزولانا وحسب المواصفات الأمريكية (ASTM C-311-02). ويجب أن يكون معامل الفعالية (Activity index) أكثر من 75 % عند استبدال جزء من السمنت وزناً ببوزولانا. وقد تم استخدام نوعين من البوزولانا في هذا البحث وهما دقيق السليكا وهي مادة بوزولانية فعالة وناتج عرضي لأفران إنتاج السليكون، والنوع الثاني الفلسبار المحلى . واجريت تجارب عديدة والتي دلت على أن معامل فعالية الفلسبار تكافئ معامل فعالية دقيق السليكا وأكثر منها بـ (5%).

- استعراض البحوث السابقة -

عرف الاتحاد الدولي لمختبرات فحوص المواد والبحوث المعروفة ب(RILEM) الاداء بكونه دالة تصف سلوكية وحدات أو مادة إنشائية يمكن متابعتها بمرور الزمن، وعلى هذا الاساس يمكن تعريف الخرسانة عالية الاداء بكونها خرسانة تمتلك الاداء المطلوب وضمن المدة المطلوبة. كما أن الحاجة إلى انتاج خرسانة ذات أداء متميز أدت بالباحثين إلى محاولة استغلال مواد طبيعية أو صناعية لتحسين أداء الخرسانة من هذه المواد دقيق السليكا (microsilica) ورماد قشور الرز وخبث الافران المطحون والمنعم.

حيث أجرى (Kakasoor 2000) بحثاً حول نوع جديد من المواد التركيبية السمنتية الحاوية على نوعين من البوزولانا النشطة هما رماد قشور الرز ودقيق السليكا المعروفة تجارياً باسم (Z - process) مع استخدام ملدنات متفوقة. وحصل على نوعية محسنة من المواد التركيبية ذات مقاومة عالية جداً وبين أن قشور الرز المحروقة بدرجة 500 مئوية والمنعمة إلى درجات نعومة عالية تزيد من المقاومة بمقدار 50 % مقارنة مع الخلطة المرجعية وكذلك تحسن خواص المادة التركيبية في حمل الشق الأول وقابلية انفعال الشد وقابلية العزم القصوى والمطيلية والجساءة.

كذلك بين (Bentur 2002) بأن البوزولانا مثل دقيق السليكا تحتوي على مركبات (SiO_2) و (Al_2O_3) ويتفاعل هذه المركبات مع $(Ca(OH)_2)$ تكون مركبات سمنتية تزيد من

مقاومة الخرسانة ونقل من مساميتها بسبب نعومتها العالية. كما درس (البديري 2002) تأثير فعالية دقيق السليكا ورماد فثور الرز وكانت أفضل نسبة اضافة للدقيق (2%) وافضل نسبة اضافة للرماد (3.5%) من وزن السمنت.

كما درس (حسين 2005) تأثير اضافة الفلدسبار غير المنشط فانه اعطى تحسن في خواص للخرسانة مقارنة مع الخرسانة غير المحتوية على دقيق الفلدسبار، كما تضمنت الدراسة على استخدام الفلدسبار المحروق بدرجة الحرارة المثلى وبين بان هذا النوع من البوزولانا يعطى تحسنا في خواص الخرسانة افضل من الفلدسبار غير المحروق. وقام (Nassif et al 2005) بعدة تجارب مخبرية بين فيها تأثير دقيق السليكا على خواص الخرسانة حيث تعمل على زيادة مقاومة الانضغاط ومعامل المرونة بعمر مكر.

خواص المواد المستعملة وطرق الفحص

السمنت

تم استخدام سمنت بورتلاندي اعتيادي من إنتاج معمل ترابة السبع اللبناني وأجريت له الفحوص الفيزيائية والكيميائية في مختبرات الجهاز المركزي للتقييس والسيطرة النوعية دائرة السيطرة النوعية وكانت النتائج كما موضحة في الجدولين (3 - 1) و (3 - 2). ويلاحظ بأن الخواص الفيزيائية والكيميائية مطابقة للمواصفة العراقية رقم (5) لسنة 1984.

الجدول (1-3) الخواص الفيزيائية للسمنت

الخواص	النتيجة	حدود المواصفة العراقية (1984/5)
النعومة بطريقة بلين (م/كغم)	340	لا تقل عن 230
زمن التجمد - الابتدائي (دقيقة) - النهائي (ساعة)	120 8	لا يقل عن 45 لا يزيد على 10
الثبات (بطريقة Autoclave) %	0.24	لا تزيد على 0.8
مقاومة الانضغاط (نت/ملم ²) عند عمر - ثلاثة أيام عند عمر - سبعة أيام	25 35	لا تقل عن 15 لا تقل عن 23

الجدول (2-3) الخواص الكيميائية للسمنت

الأكاسيد	المحتوى %	حدود المواصفة العراقية م.ق. ع (1984/5)
CaO	62.52	
SiO ₂	19.75	
Al ₂ O ₃	5.65	
Fe ₂ O ₃	3.63	
MgO	1.25	حد أعلى (5%)
SO ₃	2.73	حد أعلى (2.8%)
القلويات (Na ₂ O, K ₂ O)	0.48	
L.O.I.	2.35	حد أعلى (4%)
المواد غير الذاتية	0.75	حد أعلى (1.5%)
معامل الإشباع الجيري	0.85	(1.02-0.66)
المركبات % بموجب معادلات Bogue		
C ₃ S	53.42	
C ₂ S	16.41	
C ₃ A	8.84	
C ₄ AF	11.03	

الماء

تم استخدام ماء إسالة بغداد في جميع الخلطات الخرسانية المستخدمة في هذا البحث.

- الفلسبار

يعتبر الفلسبار من المعادن الرئيسية المكونة للصخور النارية كالبازلت. والصيغة الكيميائية للفلسبار هي $(Al_2O_3 \cdot ySiO_2 \cdot nMO)$ حيث أن (M) قد تكون K, Ca, أو Na. ويمكن أن يتحول هذا المعدن عبر العصور الجيولوجية وبفعل عوامل فيزيائية - كيميائية إلى معدن الكاؤولين. وتتكون كيميائياً من السليكات والألومينات وبين الجدول (3 - 3) التحليل الكيميائي للفلسبار العراقي ويوضح الشكل (3 - 1) تحليله المعدني باستخدام جهاز حيود الأشعة (X - Ray Defraction)، ويعتبر الفلسبار من مجموعة السليكات ثلاثية الهيكل (three dimensional structure).

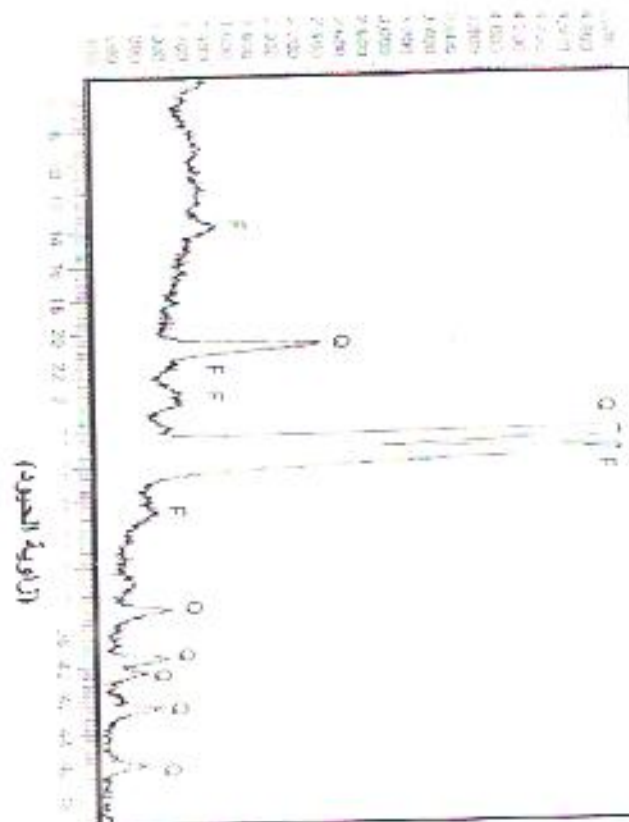
وقد استخدم الفلسبار المطحون والمنعم إلى نعومة عالية في الصين كمادة بوزولانية نشطة ويسمى تجارياً بالمسحوق السحري (magic powder) (Kelly 1996).

والفلدسبار المحلي المستخدم في هذا البحث جلب من بحر النجف ، واستخدم بعد طحنه وتنعيمه (باستخدام طاحونة كرات سيراميكية) وصولاً إلى نعومة (مقاسة بجهاز بلين) مقدارها 1200م²/كغم. ومن ثم حرقه حتى درجة 650م في فرن كهربائي مختبري، لأجل تنشيطه.

الجدول (3-3) التحليل الكيماوي لرمل للفلدسبار

المركبات	المحتوى %
SiO ₂	89.35
Al ₂ O ₃	5.5
CaO	0.5
MgO	0.11
SO ₃	0.1
Na ₂ O	0.94
K ₂ O	1.14
L.O.I.	0.64

I/Io



الشكل (1-3) حود الأشعة السينية للفلدسبار

دقيق السليكا

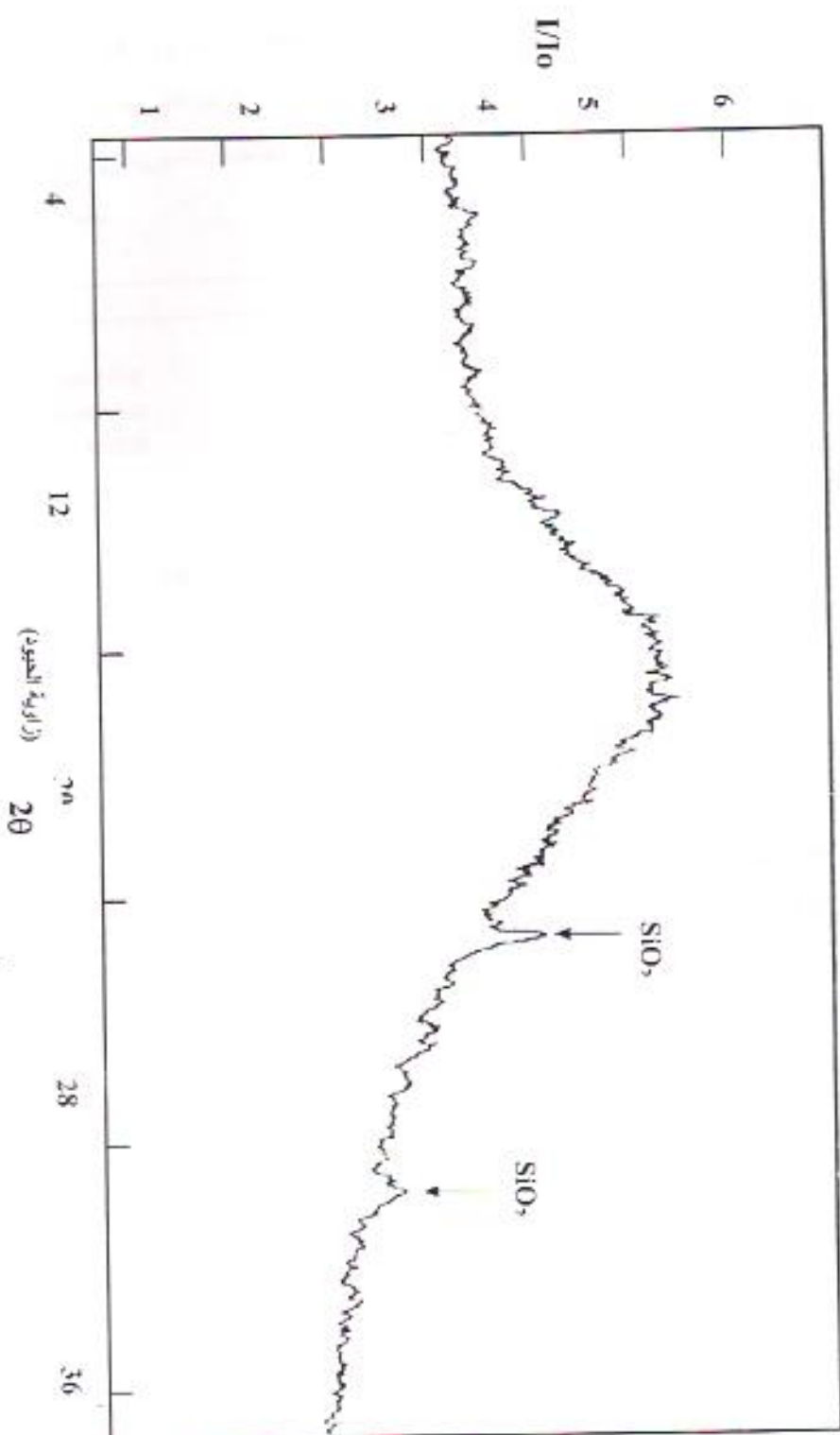
تم استخدام دقيق السليكا (Silica Fume) من شركة Fosrock وهي مادة دقيقة التجزئة ناعمة. وقد تم فحصها كيميائياً وثبت بأنها تحتوي على 95 % من السليكا. كما تم تحليلها باستخدام طريقة حيود الأشعة السينية كما في الشكل (3 - 2) وتبين بأن نوع السليكا غير متبلور (amorphous silica) والمعروفة بفعاليتها البوزولانية وهي ناتج عرضي لأفران إنتاج الحديد والمعادن الحديدية الحاوية على السليكون (Ferrosilicon alloys) حيث يتحول الكوارتز إلى سليكون بدرجات حرارية 2000 درجة مئوية وينتج أبخرة أكسيد السليكون SiO_2 وهذا بدوره يتجمع كحبيبات كروية عندما تقل درجة الحرارة. ويقدر معدل قطر هذه الحبيبة 0.1 مايكرون وتتراوح المساحة السطحية بين (15 - 25) m^2/gm (Mehta 1986). ويبين الجدول (3 - 4) التحليل الكيميائي لدقيق السليكا وفقاً لمعلومات الشركة المنتجة له وبموجب التحليل الكيميائي الفعلي.

الجدول (3 - 4) التحليل الكيميائي لدقيق السليكا

Fe ₂ O ₃	Na ₂ O	K ₂ O	Al ₂ O ₃	MgO	CaO	SiO ₂	المركبات الكيميائية
1.15	0.2	0.04	0.15	0.2	0.15	96.5	النسبة المئوية بموجب دليل الشركة
1.32	nil	nil	2.03	2.00	nil	94.0	النسبة المئوية بموجب التحليل الكيميائي



(نسبة شدة الانعكاس)

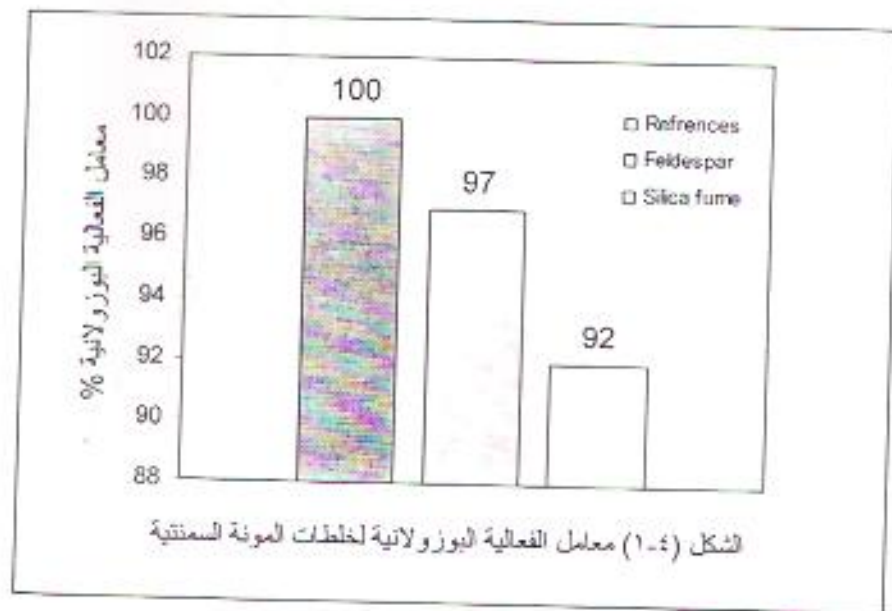


الشكل (2-3) منحنى حيود الانعكاس السطحية لأفريق السليكا

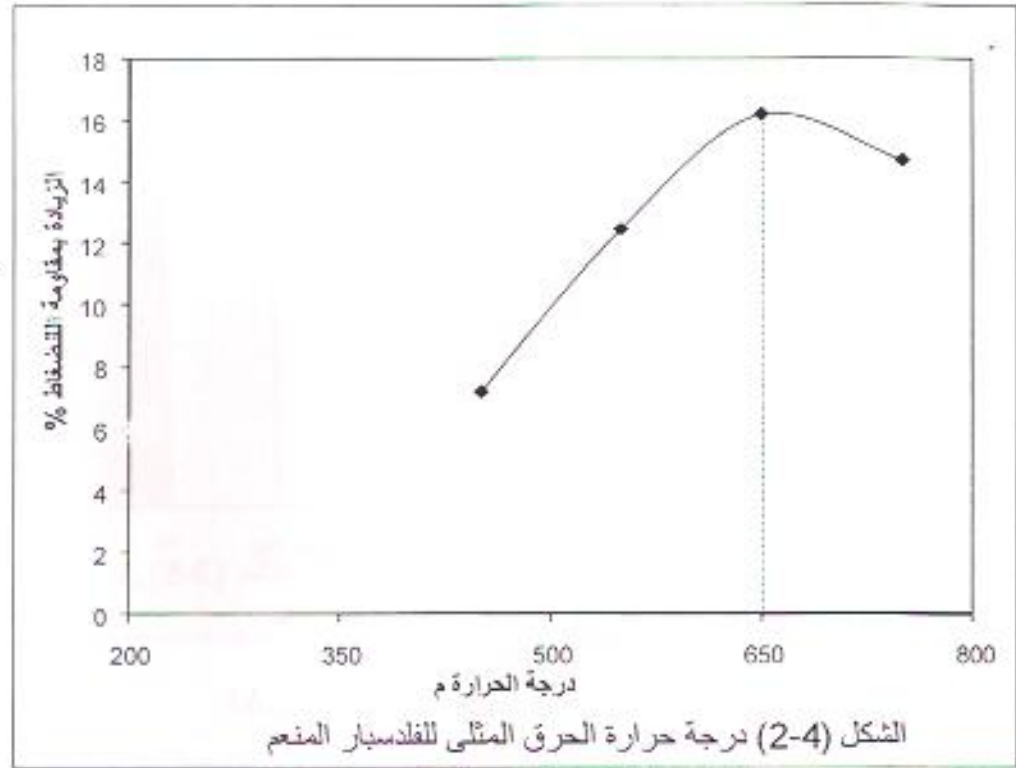
- النتائج ومناقشتها

- معامل الفعالية البوزولانية

بلاحظ من الشكل (4-1) معامل الفعالية البوزولانية لكل من دقيق السليكا والفلسبار المنعم والمحروق بدرجة حرارة 650 مئوية وقد حددت درجة الحرق هذه، بعد إجراء عدة تجارب حرق في درجات مختلفة إلى أن تم التوصل إلى الدرجة المثلى والتي تعطى أكبر مقاومة انضغاط.

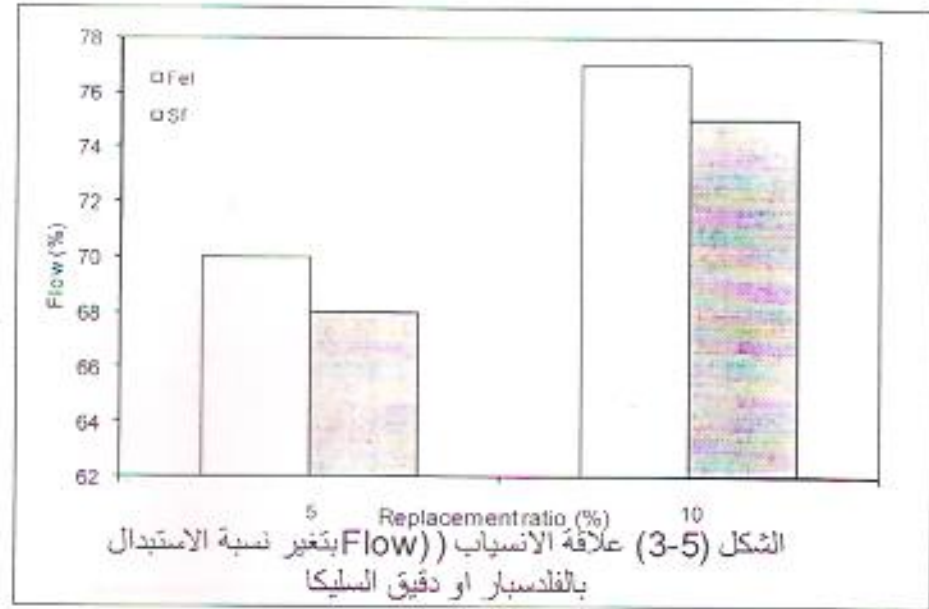


وبين الشكل (4-2) درجة حرارة الحرق المثلى للفلسبار المنعم بموجب المواصفة الأمريكية (ASTM C-311-2002) حيث استخدمت درجات حرارية بين (450-750) درجة مئوية في فرن مسيطر عليه ولمدة ساعتين ونصف ويلاحظ من الشكل (4-2) بأن أعلى زيادة في مقاومة الانضغاط حصلت عند درجة 650.



- الانسياب (Flow)

تم قياس الانسياب (Flow) للمونة السمنتية المستعملة في التجارب المختبرية بموجب المواصفة (ASTM C-230-97) ويشير الجدول (1-4) إلى نتائج فحص الانسياب للخلطات الحاوية على نسبة 1% من وزن السمنت من الملدن المتفوق مع تغير نسبة الاستبدال الجزئي للسمنت وكما موضح في الشكل (3-4).



الجدول (1-4) نتائج فحص الانسياب

رمز الخلطة	نسبة الاستبدال %	الانسياب %
1 Fel	5	70
2 Fel	10	77
3 Sf	5	68
4 Sf	10	75

- الاستنتاجات

تم في هذا البحث استخدام مواد بوزولانية محلية ومستوردة. وتم دراسة خواص هذه المواد وتأثيرها على المونة السمنتية بإجراء تجارب متعددة وعلى ضوء نتائج هذه التجارب يمكن التوصل إلى الاستنتاجات التالية:

- معامل الفعالية البوزولانية: من خلال نتائج فحوص معامل الفعالية البوزولانية لنوعين من البوزولانا احدهما محلية (دقيق الفلسبار المحروق) والاخرى مستوردة (دقيق السليكا) لوحظ بأن معامل فعالية الفلسبار المحروق يساوي (97%) مقارنة بـ (92%) لدقيق السليكا.
- 2- يمكن استخدام الفلسبار المحلي المطحون والمحروق في إنتاج مونة عالية الأداء بدلاً من دقيق السليكا المستورد.



REFERENCE

- American Society For Testing and Materials, C-311-02 "Sampling and testing Fly Ash or Natural Pozzolans for use in Portland – Cement Concrete". Vol.0402, 2002
- American Society For Testing and Materials, C-230/C230M - 98, "Flow Table for Use in Tests of Hydraulic Cement". Vol.0401, 1998
- Bentur, A., " Cementitious materials- nine millennia and a new century : past, present and future" Journal of Materials in Civil Engineering – January/February 2002.From Internet.
- Kakasoor, Dilshad, "Improvement of properties of Steel Fibre Reinforced cementitious composites", Ph.D Thesis, University of Baghdad July, 2001.
- Kelly S.J. "British Board of Agreement assessment report" Test ReportNo. 1279, NFG-1, paga 1-13, Feb.1996.
- Mehta, K.R. " Concrete: Structure, Properties and Material", Prentice-Hall, Inc. 1986.
- Nassif H. H., Husam Najm, Nakin Sukswamy "Effect of pozzazanic materials and curing methods on the elastic modulus of HPC" Cement and Concrete Composites 2005.From Internet

لمصادر العربية

- البدري، فراس فاضل "تقييم الخرسانة عالية الأداء بطرق غير إتلافية" أطروحة ماجستير، كلية الهندسة، جامعة بغداد 2001.
- حسين، جعفر "خواص الخرسانة عالية الاداء المسلحة بالاليف الفولاذنية وباستخدام دقيق الفلدسبار المحلي " أطروحة ماجستير، كلية الهندسة، جامعة بغداد 2005.